UNIVERSIDAD PERUANA
CAYETANO HEREDIA

COMPREHENSIVE ANALYSIS OF RESISTANCE TO RIFAMPICIN IN *Mycobacterium tuberculosis*: GENOMIC, FUNCTIONAL, AND STRUCTURAL INSIGHTS

THESIS FOR A DOCTORAL DEGREE IN LIFE SCIENCES

KATHERINE JAQUELINE
VALLEJOS SANCHEZ

LIMA-PERU

2024

UNIVERSIDAD PERUANA
CAYETANO HEREDIA

ANÁLISIS INTEGRAL DE LA RESISTENCIA A RIFAMPICINA EN *Mycobacterium tuberculosis*: PERSPECTIVAS GENÓMICAS, FUNCIONALES Y ESTRUCTURALES

TESIS PARA OPTAR EL GRADO DE DOCTOR EN CIENCIAS DE LA VIDA

KATHERINE JAQUELINE
VALLEJOS SANCHEZ

LIMA-PERÚ

2024

THESIS DIRECTORS

PERUVIAN DIRECTOR

Mirko Juan ZIMIC PERALTA, PhD. MSc.

Departamento de Ciencias Celulares y Moleculares
Laboratorio de Bioinformática Facultad de Ciencias y Filosofía
Universidad Peruana Cayetano Heredia (Lima-Perú)

PERUVIAN CO-DIRECTOR
Patricia SHEEN CORTAVARRIA, PhD. MSc.

Departamento de Ciencias Celulares y Moleculares
Laboratorio de Bioinformática Facultad de Ciencias y Filosofía
Universidad Peruana Cayetano Heredia (Lima-Perú)

FRENCH DIRECTOR

Martin COHEN-GONSAUD, PhD

Unité de recherche - Centre de Biochimie Structurale
CNRS UMR5048-Université de Montpellier-INSERM U1054 (Montpellier-France)

Jury members

Rachel Cerdan, PhD (Jury member-President)

Professeur, HDR, Université de Montpellier

Vanessa Karina Adaui Sicheri, PhD (Rapporteur et Jury member)

Professor, Universidad Peruana de Ciencias Aplicadas

Anthony D. Baughn, PhD (Jury member)
Associate Professor, University of Minnesota

Monica Jehnny Pajuelo Travezaño, PhD (Jury member)

Professor, Universidad Peruana Cayetano Heredia

Jean-Denis Pedelacq, PhD (Rapporteur)
Research Scientist (DR- CNRS). Institut de Pharmacologie et de Biologie Structurale

DEDICATION

To my dear family: Oscar, Flora and José, whose unwavering support and encouragement have been my constant strength throughout this journey.

This work is dedicated to you.

Acknowledgments

First and foremost, I would like to express my deepest gratitude to the members of my thesis jury: Dr. Jean-Denis Pedelacq, Dr. Vanessa Adaui, Dr. Rachel Cerdan, Dr. Anthony Baughn, and Dr. Monica Pajuelo. Thank you for your time, dedication, and invaluable feedback during the review and evaluation of my doctoral manuscript.

I am also immensely grateful to the Franco-Peruvian School of Life Sciences and Prociencia-Concytec for funding my doctoral studies, conducted in collaboration between the Université de Montpellier and the Universidad Peruana Cayetano Heredia, as part of a partnership between the Peruvian and French governments.

A special thanks goes to my thesis supervisors. To Dr. Mirko Zimic in Peru, for your unwavering academic and personal guidance, helping me generate knowledge that not only meets scientific rigor but also serves vulnerable populations. To Dr. Martin Cohen-Gonsaud, I offer my sincerest appreciation for your constant academic support and for fostering an environment that allowed me to grow technically and intellectually. Your mentorship has been instrumental to my development. I would also like to thank Dr. Patricia Sheen for her insightful advice, her teachings, and her meticulous project planning that supported me throughout this journey.

A special note of gratitude goes to Jerome Bonnet for welcoming me into his group, where I learned so much through interdisciplinary meetings, especially about group management and the dynamic nature of scientific research.

I am deeply thankful to the Synthetic Biology team: to Angélique De Visch for helping me implement methodologies for *in vitro* protein analysis, to Ana Zuñiga for her academic feedback and warm welcome, and to Julien Capin for generously sharing his expertise in synthetic biology, oligonucleotide design, and genetic manipulation. My thanks also extend to Pauline, Amanda, Peter, Paul, Elsa, Diego, Habib, Quentin, Chloé, and Estelle, whose collective knowledge and support contributed significantly to the success of this thesis.

To the members of the Centre de Biochimie Structurale, my heartfelt thanks for your academic support, your friendship, and the constant encouragement: Aurelie, Josephine, Nicolas, Mounia, Mouna, Charline, Nathalie, and all the post-docs with whom I shared wonderful experiences.

I am also deeply grateful to the Laboratory of Bioinformatics and Molecular Biology team for their guidance in bioinformatics analysis: Gustavo, Diego, Omar, Claudia, Ana Paula, Adiana, and Candy for their support in experimental analysis and strain management. I would also like to thank each of the members of the laboratory, where there is always a pleasant and collaborative environment.

Special thanks go to Dr. Louis Granjean, Dr. Arturo Torres, and Alice Osmaston for giving me the opportunity to work on the genomic analysis of clinical isolates from tuberculosis patients and for their commitment to both scientific research and humanitarian efforts.

I extend my heartfelt thanks to all those who provided academic and administrative support during my doctoral studies at CBS - Université de Montpellier and the Universidad Peruana Cayetano Heredia. Every contribution, no matter how small, played a vital role in my progress. In particular, I am deeply grateful to Rebeca Caldas and Aldo de la Torre, whose support throughout the entirety of my doctoral studies has been greatly appreciated.

I cannot forget to thank the team at the biosafety level 3 laboratory: Jorge, Walter, Eric, Nathaly, and Teresa, for their guidance, technical support, and patience during the long hours of meticulous work handling mycobacteria, as well as for their valuable contributions to the interpretation of results at every stage.

To my dear friends Dennise, Felix, Alba, and Céline, thank you for allowing me to explore interdisciplinary connections in science and for making every place feel like home. To my wonderful friends Nancy, Daniela, Elisa, Emily, Arnaud, Keny, Marilu, Tania, and Raquel, thank you for being my emotional pillars throughout this journey, always offering your wisdom and understanding.

In memory of those who supported me but are no longer here, my efforts have been, and always will be, in honor of you.

To my parents, Oscar Vallejos and Flora Sanchez, I cannot thank you enough for being my constant source of strength throughout this scientific adventure. To my brother, for being an unwavering support in my life. And finally, Ricardo Enrique, with whom I share not only this scientific journey but also the personal path that lies ahead.

FINANCIAL SUPPORT

This research was funded by Prociencia, contract number 450-2019, supporting the Franco Peruvian Ph.D. program in Life Sciences, and contract number PE501082878-2023, supporting the project <Desarrollo y evaluación de un protocolo basado en la secuenciación MinION (Nanopore) para determinar la heterorresistencia en pacientes con tuberculosis directamente de muestras de esputo=.

The research project was also supported by the project <Role of a metallochaperone in the mechanism of action and resistance to pyrazinamide in Mycobacterium tuberculosis= supported by ICGEB.

The CBS acknowledges support from the French Infrastructure for Integrated Structural Biology (FRISBI) ANR-10-INSB-05-01 and the GIS ChemBioFrance.

Abstract

Mycobacterium tuberculosis (Mtb) remains one of the deadliest pathogens worldwide, despite being a preventable disease. Tuberculosis (TB) is treated with a combination of four first-line antitubercular drugs: rifampicin (RIF), isoniazid, pyrazinamide, and ethambutol, in drug-susceptible cases. Among these, RIF is one of the most potent agents for controlling the disease. However, resistance to RIF results in the emergence of rifampicin-resistant (RR-TB) or multidrug-resistant tuberculosis (MDR-TB) cases. The primary mechanism of resistance involves mutations in the *rpoB* gene, which accounts for approximately 95% of cases. Nevertheless, other molecular mechanisms and conditions that could contribute to the spread of RR-TB and MDR-TB are still being identified.

This doctoral research first focuses on a retrospective analysis of whole-genome sequences from clinical isolates of TB patients. Through bioinformatic analysis, heteroresistant populations to RIF were detected and experimentally confirmed in a pilot study by reactivating primary culture. Key assays such as the agar proportion method (APM), test endpoint minimum inhibitory concentration (TEMA MIC), and microscopic-observation drug-susceptibility (MODS) indirect assay were employed for strain characterization. Additionally, for each primary culture, colonies grown in the absence and presence of RIF were isolated, followed by MIC determination and

rpoB gene sequencing. This approach confirmed that sequencing could successfully identify specific heteroresistant populations, underscoring the critical role of accurate diagnosis in ensuring effective treatment.

In the second part of the thesis, an *in silico* and *in vitro* study was conducted on the wild-type and mutant forms of the PonA1 protein, hypothesized to be involved in RIF resistance mechanisms. Recombinant wild-type and mutant proteins were cloned, expressed in *E. coli* Rosetta, and biophysically characterized. The affinity between PonA1 and RIF was evaluated using saturation transfer difference by Nuclear Magnetic Resonance spectroscopy (STD-NMR).

Moreover, a knockout of the *MMAR_0069* gene, the *ponA1* homolog, in *M. marinum* (Mmar), was generated using Oligo-mediated recombineering followed by BxB1 integrase targeting (ORBIT), with modifications in the payload plasmid. Complementation assays were performed by introducing the wild-type and mutant forms of *Mtb ponA1* into the Knock-out (KO) strains. MIC determination, morphological changes (cell length, width, and cell envelope thickness), and cell viability upon RIF exposure were evaluated in these complemented strains.

Lastly, this thesis presents a collaborative project undertaken during my stay at the Centre de Biochimie Structurale, where a bioinformatic tool called SecretoMyc was developed. This tool facilitates the prediction of secreted proteins in Mtb and provides homologous protein information for *M. bovis*, *M. smegmatis*, *M. marinum*, *M. abscessus*, and *M. avium* across three secretion systems: SEC, TAT, and T7SS.

In conclusion, this thesis contributes novel genetic manipulation techniques for mycobacteria and provides tools for the study and control of TB.

Key words: Tuberculosis, heteroresistance, ponA1, penicillin binding protein, rifampicin, ORBIT, genetic manipulation, secretome.

Résumé

Mycobacterium tuberculosis (Mtb) reste l'un des agents pathogènes les plus meurtriers au monde, malgré le fait qu'il s'agisse d'une maladie évitable. La tuberculose (TB) est traitée avec une combinaison de quatre médicaments antituberculeux de première ligne : la rifampicine (RIF), l'isoniazide, la pyrazinamide et l'éthambutol, dans les souches sensibles aux médicaments. Parmi ces médicaments, la RIF est l'un des agents les plus puissants pour contrôler la maladie. Cependant, la résistance à la RIF entraîne l'émergence de cas de tuberculose résistante à la rifampicine (RR-TB) ou multirésistante (MDR-TB). Le principal mécanisme de résistance implique des mutations dans le gène *rpoB,* responsable d'environ 95 % des cas. Néanmoins, d'autres mécanismes moléculaires et conditions pouvant contribuer à la propagation des populations RR-TB et MDR-TB sont encore en cours d'identification.

Cette recherche doctorale se concentre d'abord sur une analyse rétrospective des séquences génomiques complètes d'isolats cliniques de patients atteints de TB. Grâce à une analyse bio-informatique, des populations hétérorésistantes à la RIF ont été détectées et confirmées expérimentalement dans une étude pilote par réactivation des cultures primaires. Des tests clés tels que la méthode de proportion sur gélose, le test de concentration minimale inhibitrice (CMI) et le test indirect de sensibilité aux médicaments par observation microscopique ont été utilisés pour la caractérisation des

souches. En outre, pour chaque culture primaire, des colonies ont été isolées sur des milieux avec et sans RIF, suivies par la détermination de la CMI et le séquençage du gène *rpoB*. Cette approche a confirmé que le séquençage pouvait identifier avec succès des populations hétérorésistantes spécifiques, soulignant l'importance d'un diagnostic précis pour garantir un traitement efficace.

Dans la deuxième partie de la thèse, une étude *in silico* et *in vitro* a été réalisée sur les formes sauvage et mutante de la protéine PonA1, a protéine de liaison à la pénicilline que dont on suppose qu9elle est impliquée dans les mécanismes de résistance à la RIF. Les protéines recombinantes sauvage et mutantes ont été clonées, exprimées dans *E. coli* Rosetta, puis caractérisées biophysiquement. L'affinité entre PonA1 et la RIF a été évaluée à l'aide de la différence de transfert de saturation par spectroscopie de résonance magnétique nucléaire (STD-NMR, pour son acronyme en anglais).

De plus, un knockout du gène *MMAR_0069*, homologue de *ponA1*, chez *Mycobacterium marinum* (Mmar), a été réalisé à l'aide de la recombinaison médiée par oligos suivie du ciblage par intégrase BxB1 (ORBIT, pour son acronyme en anglais), avec des modifications dans le plasmide de charge utile. Des essais de complémentation ont été réalisés en introduisant les formes sauvage et mutante de *ponA1* de Mtb dans les souches KO. La détermination de la CMI, les changements morphologiques (longueur, largeur cellulaire et épaisseur de l'enveloppe cellulaire) et la viabilité cellulaire après exposition à la RIF ont été évalués dans ces souches complémentées.

Enfin, cette thèse présente un projet collaboratif réalisé lors de mon séjour au Centre de Biochimie Structurale, où un outil bio-informatique appelé SecretoMyc a été développé. Cet outil facilite la prédiction des protéines sécrétées chez Mtb et fournit des informations sur les protéines homologues chez *M. bovis*, *M. smegmatis*, Mmar, *M. abscessus* et *M. avium* dans trois systèmes de sécrétion : SEC, TAT et T7SS.

En conclusion, cette thèse apporte des techniques novatrices de manipulation génétique des mycobactéries et fournit des outils pour l'étude et le contrôle de la tuberculose.

Mots-clés : Tuberculose, hétéroresistance, *ponA1*, protéine de liaison à la pénicilline, rifampicine, ORBIT, manipulation génétique, sécrétome.

Resumen

Mycobacterium tuberculosis (Mtb) sigue siendo uno de los patógenos más mortales a nivel mundial, a pesar de ser una enfermedad prevenible. La tuberculosis (TB) se trata con una combinación de cuatro medicamentos antituberculosos de primera línea: rifampicina (RIF), isoniacida, pirazinamida y etambutol, para cepas sensibles a los medicamentos. Entre estos, la RIF es uno de los agentes más potentes para controlar la enfermedad. Sin embargo, la resistencia a la RIF conlleva la aparición de casos de TB resistente a la RIF (RR-TB) o multidrogo resistente (MDR-TB). El mecanismo principal de resistencia implica mutaciones en el gen *rpoB*, que es responsable de aproximadamente el 95% de los casos. No obstante, todavía se están identificando otros mecanismos moleculares y condiciones que podrían contribuir a la propagación de las poblaciones RR-TB y MDR-TB.

Esta investigación doctoral se centra inicialmente en un análisis retrospectivo de secuencias genómicas completas de aislados clínicos de pacientes con TB. A través del análisis bioinformático, se detectaron poblaciones heterorresistentes a la RIF y se confirmaron experimentalmente en un estudio piloto mediante la reactivación de los cultivos primarios. Se utilizaron ensayos clave como el método de proporciones en agar, el ensayo de punto final para la determinación de la concentración mínima inhibitoria (CMI) y el ensayo indirecto de susceptibilidad a los medicamentos por observación microscópica para la caracterización de las cepas. Además, por cada

cultivo primario, se aislaron colonias crecidas en ausencia y presencia de RIF, seguidas de la determinación del CMI y el secuenciamiento del gen *rpoB*. Este enfoque confirmó que el secuenciamiento podía identificar con éxito poblaciones heterorresistentes específicas, destacando el papel crucial de un diagnóstico preciso para garantizar un tratamiento eficaz.

En la segunda parte de la tesis, se realizó un estudio *in silico* e *in vitro* sobre las formas nativa y mutante de la proteína PonA1, una proteína de unión a penicilina que se hipotetiza por estar involucrada en los mecanismos de resistencia a la RIF. Las proteínas recombinantes nativa y mutantes se clonaron, expresaron en *E. coli* Rosetta y se caracterizaron biofísicamente. La afinidad entre PonA1 y la RIF se evaluó utilizando espectroscopía de resonancia magnética nuclear por diferencia de transferencia de saturación (STD-NMR).

Además, se generó un knockout del gen *MMAR_0069*, homólogo de *ponA1* en Mmar, mediante recombinación mediada por oligos seguida del direccionamiento de la integrasa BxB1 (por sus siglas en inglés ORBIT), con modificaciones en el plásmido de carga. Se realizaron ensayos de complementación introduciendo las formas nativa y mutante de *ponA1* de Mtb en las cepas KO. En estas cepas complementadas se evaluaron la determinación de la CMI, los cambios morfológicos (longitud celular, ancho y grosor de la envoltura celular) y la viabilidad celular tras la exposición a la RIF.

Finalmente, esta tesis presenta un proyecto colaborativo realizado durante mi estancia en el Centre de Biochimie Structurale, donde se desarrolló una herramienta bioinformática llamada SecretoMyc. Esta herramienta facilita la predicción de proteínas secretadas en Mtb y proporciona información sobre proteínas homólogas en *M. bovis*, *M. smegmatis*, Mmar, *M. abscessus* y *M. avium* en tres sistemas de secreción: SEC, TAT y T7SS.

En conclusión, esta tesis aporta nuevas técnicas de manipulación genética para micobacterias y ofrece herramientas para el estudio y control de la TB.

Palabras clave: Tuberculosis, heterorresistencia, ponA1, proteína de unión a penicilina, rifampicina, ORBIT, manipulación genética, secretoma.

Simplified thesis summary for the general public

This doctoral thesis examines key aspects of *Mycobacterium tuberculosis* and its resistance to rifampicin (RIF), a critical first-line antibiotic against TB. Analysis of 2,916 whole-genome sequences from Peru revealed that 0.79% of cases were RIF-heteroresistant, harboring both drug-susceptible and drug-resistant cells. Failure to detect these populations can undermine treatment and spread drug-resistant TB.

The research also explores the PonA1 protein9s role in RIF resistance mechanisms using *Mycobacterium marinum* as a model. PonA1 was found non-essential in both organisms, and gene complementation assays showed specific PonA1 mutations could contribute to antibiotic tolerance during the stationary phase.

Finally, the thesis presents SecretoMyc, a bioinformatic tool predicting secreted proteins in Mtb and related species, offering the potential for identifying novel therapeutic targets in future TB drug development.

Résumé de thèse vulgarisé pour le grand public

Cette thèse doctorale examine les aspects clés de *Mycobacterium tuberculosis* et de sa résistance à la rifampicine (RIF), un antibiotique de première ligne crucial contre la tuberculose (TB). L'analyse de 2 916 séquences de génomes complets provenant du Pérou a révélé que 0,79 % des cas présentaient une hétérorésistance à la RIF, abritant à la fois des bacteries sensibles et résistantes aux médicaments. L'incapacité à détecter ces populations peut compromettre les traitements et favoriser la propagation de la tuberculose résistante aux médicaments.

La recherche explore également le rôle de la protéine PonA1 dans les mécanismes de résistance à la RIF, en utilisant *Mycobacterium marinum* comme organisme modèle. Il a été démontré que PonA1 n'est pas essentielle dans les deux organismes, et les tests de complémentation génique ont montré que certaines mutations de PonA1 pourraient contribuer à la tolérance aux antibiotiques pendant la phase stationnaire.

Enfin, la thèse présente SecretoMyc, un outil bioinformatique qui prédit les protéines sécrétées chez *Mtb* et les espèces apparentées, offrant un potentiel prometteur pour identifier de nouvelles cibles thérapeutiques dans le cadre du développement futur de médicaments contre la tuberculose.

Resumen de tesis simplificado para el público en general

Esta tesis doctoral examina aspectos clave de *Mycobacterium tuberculosis* y su resistencia a la rifampicina (RIF), un antibiótico de primera línea crucial contra la tuberculosis (TB). El análisis de 2,916 secuencias de genomas completos de Perú reveló que el 0.79% de los casos eran RIF-heterorresistentes, albergando tanto células susceptibles como resistentes a los medicamentos. La falta de detección de estas poblaciones puede comprometer el tratamiento y favorecer la propagación de la TB resistente a los medicamentos.

La investigación también explora el papel de la proteína PonA1 en los mecanismos de resistencia a la RIF, utilizando *Mycobacterium marinum* como organismo modelo. Se encontró que PonA1 no es esencial en ambos organismos, y los ensayos de complementación genética mostraron que ciertas mutaciones en PonA1 podrían contribuir a la tolerancia a los antibióticos durante la fase estacionaria.

Finalmente, la tesis presenta SecretoMyc, una herramienta bioinformática que predice proteínas secretadas en *Mtb* y especies relacionadas, con un gran potencial para identificar nuevos objetivos terapéuticos en el desarrollo futuro de medicamentos contra la TB.

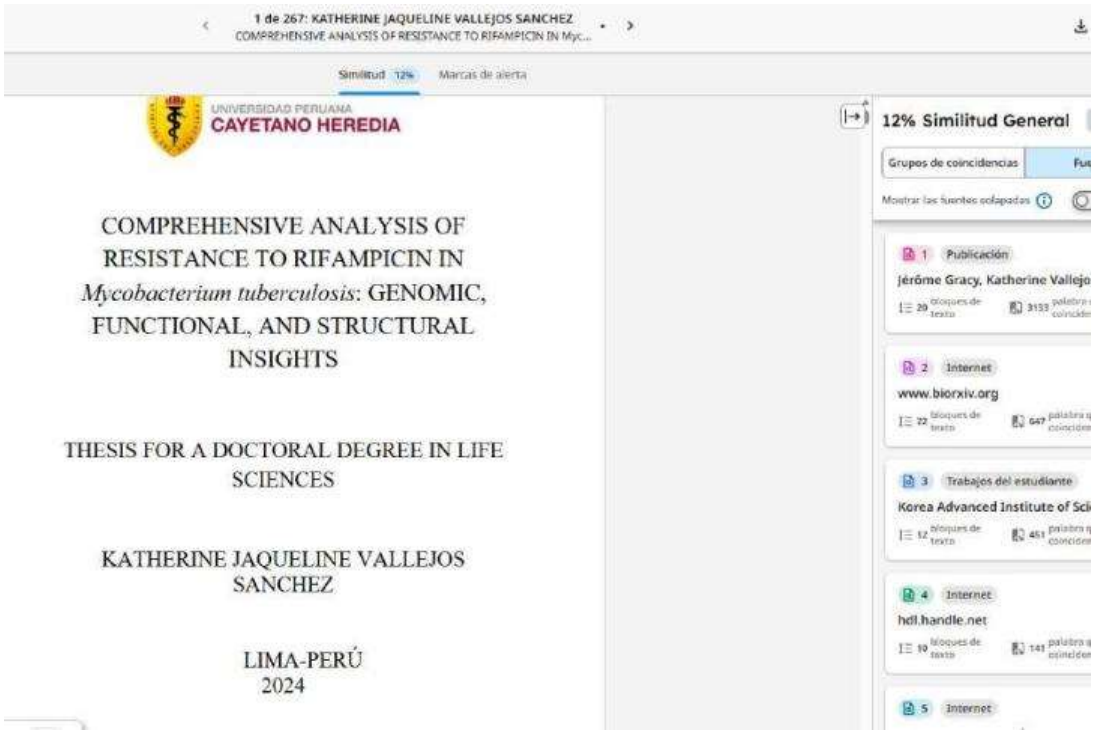
1 de 267: KATHERINE JAQUELINE VALLEJOS SANCHEZ
COMPREHENSIVE ANALYSIS OF RESISTANCE TO RIFAMPICIN IN Myc...
Similitud 12%
Marcas de alerta
UNIVERSIDAD PERUANA
CAYETANO HEREDIA
COMPREHENSIVE ANALYSIS OF RESISTANCE TO RIFAMPICIN IN Mycobacterium tuberculosis: GENOMIC, FUNCTIONAL, AND STRUCTURAL INSIGHTS
THESIS FOR A DOCTORAL DEGREE IN LIFE SCIENCES
KATHERINE JAQUELINE VALLEJOS SANCHEZ
LIMA-PERÚ
2024
12% Similitud General
Grupos de coincidencias
Mostrar las fuentes colapsadas
1 Publicación
Jérôme Gracy, Katherine Vallejo
2 Internet
www.biorxiv.org
3 Trabajos del estudiante
Korea Advanced Institute of Sci
4 Internet
hdl.handle.net
5 Internet

TABLE OF CONTENTS

Image index

Table index

ABBREVIATIONS LIST

TB	: Tuberculosis
WGS	: whole genome sequencing
Mtb	: *Mycobacterium tuberculosis*
Mmar	: *Mycobacterium marinum*
M.smegmatis	: *Mycobacterium smegmatis*
RIF	: Rifampicin
LB	: Luria Bertani medium
MDR-TB	: Multi-drug resistant strains of *Mycobacterium tuberculosis*
RR-TB	: rifampicin resistance-associated tuberculosis
rpoB	: gene encoding the β-subunit of RNA polymerase
rpoA	: gene encoding the α-subunit of RNA polymerase
rpoC	: gene encoding the β' subunit of RNA polymerase
Rv2629	: drug efflux pump gene
ponA1	: bifunctional transglycosylase/transpeptidase gene
MMAR_0069	: ponA1 homologue gen in *M. marinum*
PBP	: penicillin-binding proteins
PonA1	: PonA1 protein
RpoA	: RpoA protein
RpoB	: RpoB protein
RpoC	: RpoC protein
$PonA1_{234-820}$	: PonA1 recombinant protein covering residues 234 to 820
$PonA1_{234-820}$ _WT	: PonA1 protein wild type
$PonA1_{234-820}$ _Q365H	: PonA1 protein with substitution at residue Q 365 by H
$PonA1_{234-820}$ _P631S	: PonA1 protein with substitution at residue P631 by S
ponA1p	: ponA1 promotor from Mtb H37Rv
rpsTp	: *rpsT* promotor from Mmar

ΔMMAR0069::ponA1p-EGFP : *MMAR_0069* KO and insertion of ponA1 promoter with EGFP

ΔMMAR0069::*rpsTp*- EGFP : *MMAR_0069* KO and insertion of *rpsT* promoter with EGFP

ΔMMAR0069::*rpsTp*-ponA1 : *MMAR_0069* KO and insertion of *rpsT* promoter with ponA1 wt

ΔMMAR0069 : *MMAR_0069* KO with *rpsTp*-EGFP

ΔMMAR0069::L5-ponA1 : Δ*MMAR_0069* complemented with p*onA1* WT

ΔMMAR0069::L5-ponA1_T34A : Δ*MMAR_0069* complemented with *ponA1*-T34A

ΔMMAR0069::L5-ponA1 _T34D : Δ*MMAR_0069* complemented with *ponA1*-T34D

ΔMMAR0069::L5-ponA1_Q365H : Δ*MMAR_0069* complemented with *ponA1*-Q365H

ΔMMAR0069::L5-ponA1_A516T : Δ*MMAR_0069* complemented with *ponA1*-A516T

ΔMMAR0069::L5-ponA1_P631S : Δ*MMAR_0069* complemented with *ponA1*-P631S

ΔMMAR0069::L5-MMAR0069 : Δ*MMAR_0069* complemented with *MMAR_0069*

Chapter I

Integrated introduction

I.1. Tuberculosis overview: Tuberculosis and rifampicin resistance

Tuberculosis (TB), caused by *Mycobacterium tuberculosis* (Mtb), is easily transmitted through the air when individuals with active TB cough, sneeze, or spit. Despite being preventable and curable, TB remains a major global health issue. In 2022, approximately 10.6 million people contracted TB, leading to 1.3 million deaths. TB primarily affects vulnerable populations in low- and middle-income countries, with the highest incidence in the South-East Asian Region (46%), followed by the African Region (23%) and the Western Pacific (18%). Over 80% of TB cases and deaths occur in these regions (WHO, 2023b)

The drug susceptibility profile of Mtb allows its classification as either drug-susceptible, multidrug-resistant or rifampicin-resistant (MDR/RR-TB), or extremely drug-resistant (XDR-TB). Treatment for drug-susceptible strains typically involves a combination of first-line antibiotics4isoniazid (INH), rifampicin (RIF), pyrazinamide (PZA), ethambutol (EMB), and streptomycin (STM)4administered over a period of 6 to 9 months. However, inappropriate use of these first-line drugs, due to factors such as incorrect prescription practices, substandard drug quality, or patient non-adherence to treatment protocols, can drive the emergence of drug-resistant strains (WHO, 2020b, 2023b) MDR-TB develops as a consequence of resistance to INH and RIF, the most potent first-line therapies, while RR-TB is often associated with resistance to other anti-TB drugs, further complicating treatment and contributing to MDR-TB. XDR-TB arises when mycobacteria, already classified as MDR-TB, acquire additional resistance

to second-line drugs, significantly constraining available treatment options (WHO, 2023a).

TB control faces global challenges such as early case detection, effective treatment of both drug-susceptible and drug-resistant TB, prevention of drug-resistant strains, and managing risk factors like HIV infection, diabetes, and smoking (WHO, 2023b).

In Peru, the estimated incidence of TB cases for 2022 was 52,000, equating to 151 cases per 100,000 population, with MDR/RR-TB at 8.3 cases per 100,000. New MDR/RR-TB cases accounted for 4.9% of incidences, and 9.5% for previously treated cases. The treatment success rate for MDR/RR-TB, which involves second-line drugs, is 65% (WHO, 2020a, 2023b). These treatments last 9 to 20 months and are more expensive and toxic (Malenfant & Brewer, 2021).

I.1.1 *Mycobacterium tuberculosis*

Mtb is a small, rod-shaped, strictly aerobic, acid-fast bacillus, It is a slow-growing bacterium with a doubling time of approximately 16 hours (M. Zhu & Dai, 2018). This bacterium is metabolically flexible, having adapted to survive and persist in the human population due to its extraordinary stealth and adaptability throughout infection, making it a formidable and challenging pathogen to control (Cook et al., 2009).

Mtb is part of the Mycobacterium tuberculosis complex (MTBC), which includes several closely related species: *M. africanum, M. bovis, M. canettii, M. caprae, M.*

microti, M. mungi, M. orygis, M. pinnipedii, and *M. suricattae* (Bespiatykh et al., 2021). It is believed that mycobacteria evolved from a common ancestor of fast-growing mycobacteria, with genetic changes leading to speciation and variations in pathogenicity (Bachmann et al., 2020). This genus shows no evidence of horizontal gene transfer (Bespiatykh et al., 2021).

The genome size of Mtb H37Rv is 4.41million base pairs (Mbp) (Cole et al., 1998) and its genome comprises approximately 4,000 genes with a guanine and cytosine content of 65% (Bishai, 1998). The genome sizes of MTBC members are relatively similar: *M. africanum* has 4.4 Mbp (Bentley et al., 2012), *M. bovis* ranges from 4.34 to 4.37 Mbp (Garnier et al., 2003), *M. canettii* varies between 4.42 and 4.52 Mbp (Supply et al., 2013), *M. caprae* and *M. microti* both have a genome size of 4.4 Mbp (Orgeur et al., 2021; Romano et al., 2022). In non-tuberculosis mycobacteria, genome sizes are larger than in the MTBC. For example, *M. smegmatis* has 6.98 Mbp (Cook et al., 2009) and *M. marinum* (Mmar) ranges from 6.4 to 6.6 Mbp (Stinear et al., 2008; Yoshida et al., 2018). These species have retained genes enabling survival in various environmental conditions or preserving genes with functional redundancy. Despite their differences from MTBC, they are still valuable as model organisms for studying Mtb, albeit with certain limitations and technical advantages (Figure I.1) (Cook et al., 2009; Tobin & Ramakrishnan, 2008).

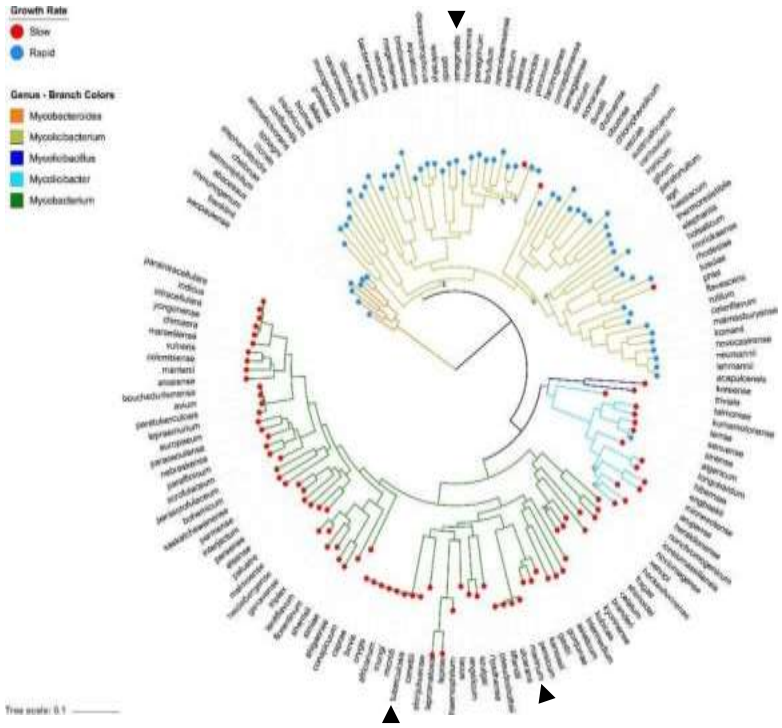

Figure I.1. The phylogenetic tree of Mycobacterium species. Based on the nucleotide alignment of 304 single-copy genes, it categorizes five distinct sub-genera and illustrates both slow and fast-growing species. Adapted from Bachmann et al. (2020). A black arrow indicates the position of *M. tuberculosis*, *M. marinum*, and *M. smegmatis* in the phylogenetic tree.

I.1.2 Tuberculosis infection

The infection process of TB involves a complex interaction between the human host and Mtb. TB primarily spreads through inhalation of respiratory droplets containing Mtb, released when an infected person with active TB coughs, sneezes, speaks, or sings (Figure I.2-a). Those in close contact with the infected individual are at the highest risk of exposure. Donald et al., (2018) reported the TB infectious dose to be as low as 1-2 bacilli in small droplets, underscoring Mtb's effectiveness. Once inhaled, the bacteria reach the alveoli of the lungs, where alveolar macrophages attempt

to engulf and destroy them. However, Mtb has evolved mechanisms to evade destruction and can survive within these macrophages (Chandra et al., 2022). If the immune response cannot completely clear the infection, the immune system recruits additional cells like dendritic cells, T cells, monocytes, and neutrophils to the infection site (Figure I.2- b) (Sia & Rengarajan, 2019). Infected macrophages present Mtb antigens, triggering a response that activates T and B lymphocytes. This phase may be asymptomatic or present mild symptoms (Sia & Rengarajan, 2019).

The formation of granulomas, primarily organized by macrophages, T-lymphocytes, and multinucleated giant cells, helps contain the infection and prevent bacterial spread (Chandra et al., 2022). Depending on the immunological status, the immune response may control but not completely eliminate the bacteria, leading to latent TB infection. Mtb persistence is linked to its survival in granulomatous lung lesions, creating microenvironments with conditions like hypoxia, acidic pH, and the presence of nitric oxide and carbon monoxide. These conditions are associated with the expression of dormancy genes and a basal metabolism (Barry et al., 2009). The dormant bacillus can remain in the granuloma for the host's lifetime, capable of reactivating under immunosuppressive conditions (Figure I.2-d; Ahmad, 2011; Chandra et al., 2022).

Nkatha Micheni et al., (2022) described a key aspect of TB infection, demonstrating that patients can be infected with multiple Mtb strains simultaneously, either as mixed infections or clonal diversity, accounting for about 6.4% of cases. The outcome of TB infection can vary depending on the involved Mtb strains.

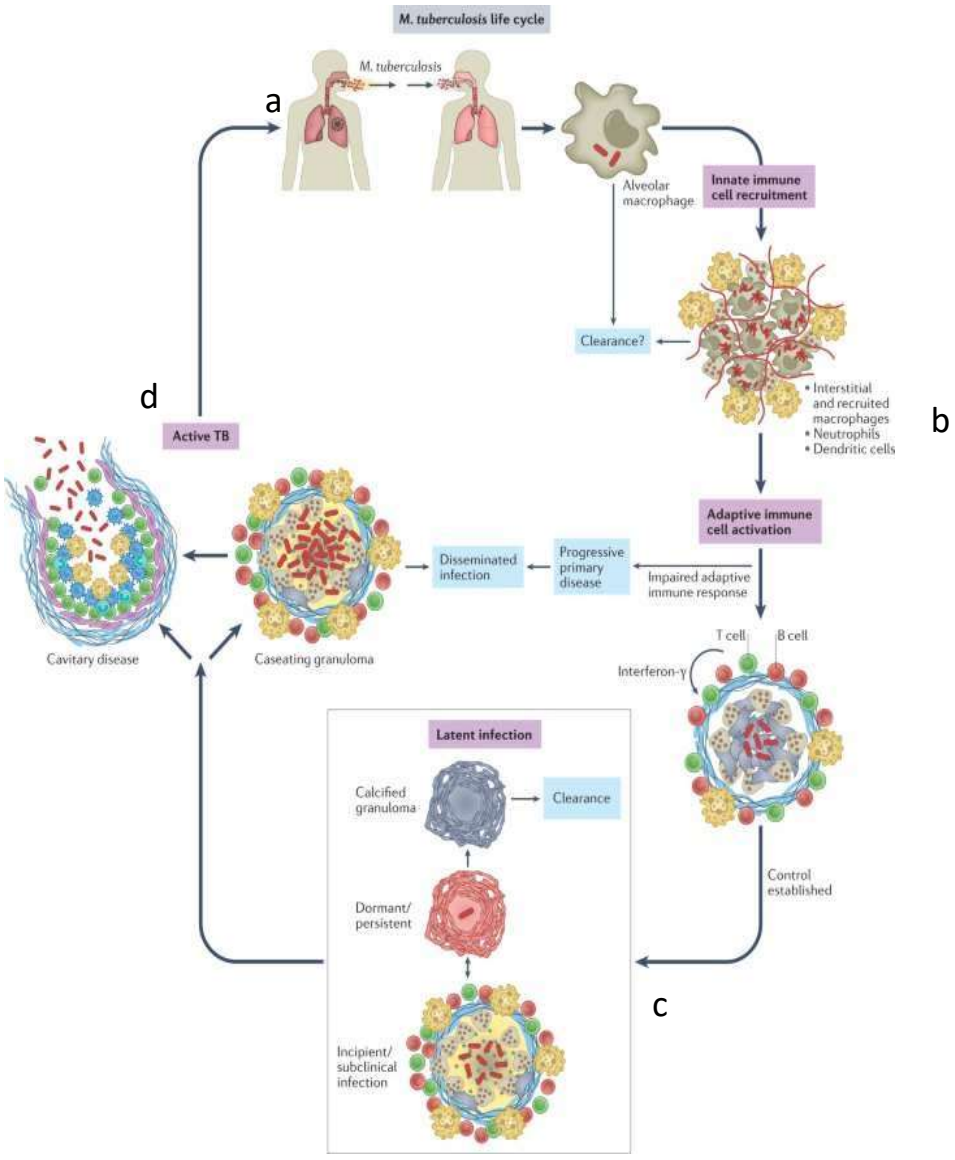

Figure I.2. Stages of *M. tuberculosis* infection. a. Exposure and entry of the bacillus. **b.** Innate-adaptive immune response. **c**. Control of latent infection. **d**. Granuloma formation and mycobacterial escape. Adapted from Chandra et al. (2022).

I.1.3 Types of tuberculosis drug-resistance

Drug-resistant TB presents a critical global health challenge, characterized by Mtb strains that exhibit resistance to standard anti-TB drugs. The WHO classifies drug-resistant TB in several distinct categories based on the patterns of resistance, each with

important implications for treatment strategies. The classification of TB includes the following categories (WHO, 2023b):

I.1.3.1. Drug-Susceptible tuberculosis

This involves TB bacteria susceptible to primary first-line anti-TB drugs: INH, RIF, PZA, and EMB. This form of TB is the most common and the least complicated to treat, provided that the patient follows the prescribed treatment regimen correctly. These drugs are typically administered over a 6-month regimen, divided in two phases: one intensive phase where a combination of all four drugs is given to rapidly reduce the bacterial load and minimize the risk of developing drug resistance. and a second phase where the INH and RIF are continued to eliminate any remaining bacteria and prevent relapse.

I.1.3.2. Mono-resistant tuberculosis

Mono-resistance refers to the resistance of Mtb to a single first-line anti-TB drug, while remaining susceptible to the others. Mono-resistant strains may still respond to alternative first-line agents, making early detection and appropriate treatment adjustments essential. The most frequent case of mono-resistance is related to INH.

I.1.3.3. Multidrug-Resistant tuberculosis

MDR-TB is a form of TB caused by Mtb strains resistant to at least INH and RIF, the two most potent first-line anti-TB drugs. Despite this resistance, MDR-TB strains may remain susceptible to other medications. Treatment for MDR-TB is significantly

more complex than for drug-susceptible TB, typically requiring second-line drugs such as fluoroquinolones (e.g., levofloxacin, moxifloxacin, or ofloxacin) and injectable agents like amikacin, kanamycin, or capreomycin. The treatment duration ranges from 18-24 months, requiring close monitoring due to potential adverse effects. Recently, a change in the therapeutic scheme has been proposed, which includes a purely oral scheme for 6 months, this treatment includes bedaquiline, pretomanid, linezolid and moxifloxacin (WHO, 2020b) and it depend of the drug-resistant profile of each Mtb strain.

I.1.3.4. Pre-Extensively Drug-Resistant tuberculosis (Pre-XDR-TB)

Pre-XDR-TB refers to disease caused by Mtb strains resistant to INH, RIF, and either a fluoroquinolone or an injectable second-line drug. Treatment is similar to XDR-TB and may offer a slightly better prognosis. It is crucial to base the treatment of drug-resistant TB (MDR-TB, XDR-TB, and Pre-XDR-TB) on drug susceptibility testing, patient history, and regional drug availability. These treatments are complex, requiring careful management and close patient monitoring to ensure success and minimize further complete drug resistance.

I.1.3.5. Extensively Drug-Resistant tuberculosis (XDR-TB)

XDR-TB represents a more advanced and severe form of drug-resistant TB, caused by Mtb strains resistant to INH, RIF, at least one fluoroquinolone, and one injectable second-line drug. Treating XDR-TB is particularly challenging, often requiring the use of novel or less accessible drugs, with treatment durations typically

longer than those for MDR-TB. This leads to increased treatment costs and a significantly higher risk of treatment failure or relapse.

I.1.4. Rifampicin and mycobacteria

I.1.4.1. Rifampicin and mechanism of action

RIF is a semi-synthetic drug 3-(4-metil-1- piperazinil-iminometil) rifamicina SV, with the chemical formula is $C_{43}H_{58}N_4O_{12}$ and a molecular weight of 822.9402 g/mol (Figure I.3), is highly liposoluble. It is derived from rifamycins, naturally produced by *Amycolatopsis mediterranei* (Lechevalier et al., 1986). Since its discovery in 1957, RIF has been a primary drug in the first-line treatment of TB (Sensi, 1983).

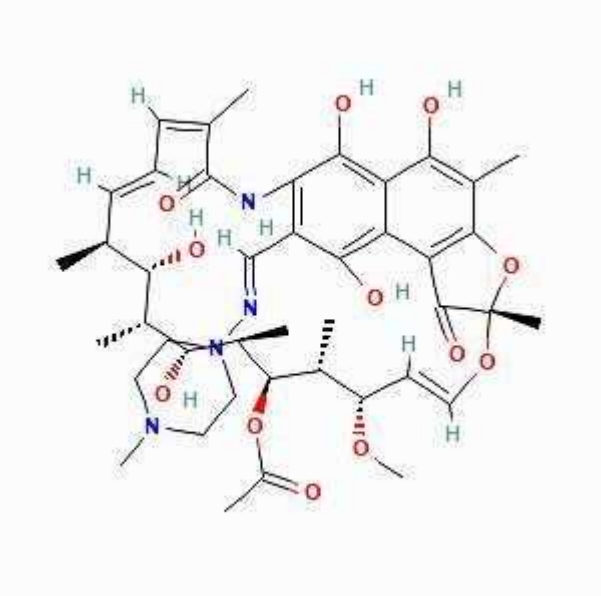

Figure I.3. Structure of rifampicin. Pubchem CID 135398735.

RIF is effective against a variety of bacteria, including Gram-positive bacteria such as *Staphylococcus aureus* and *Staphylococcus epidermidis*, mycobacteria like Mtb, *M. bovis*, *M. leprae*, *M. kansasii* and Mmar and certain Gram-negative bacteria,

including *Brucella sp., Neisseria gonorrhoeae, N. meningitidis, and Legionella pneumophila*. MICs generally range from 0.002 to 0.5 ¼g/mL for Gram-positive bacteria, 0.005 to 2 ¼g/mL for mycobacteria, and 1 to 10 ¼g/mL for Gram-negative bacteria (Merrell, 2023).

In *E. coli*, the mechanism of action of RIF involves its specific binding to the β-subunit of the bacterial DNA-dependent RNA polymerase (RpoB), which has an approximate molecular weight of 150 kDa. RIF forms a 1:1 enzyme-drug complex with a binding constant of 10{y M at low concentrations (approximately 0.01 µg/mL, the 50% effective dose) at 37°C (Wehrli, 1983). RIF can bind to either the free enzyme or the binary rpoB-DNA complex; however, the enzyme becomes resistant to inhibition once a ternary complex with RNA is formed (Schulz & Zillig, 1981). RIF exerts its inhibitory effect by sterically blocking elongation at the 5' end of nascent RNA or by reducing RpoB9s affinity for short RNA transcripts (Campbell et al., 2001; McClure & Cech, 1978).

Kinetic studies indicate that the dissociation constant (K_D) of the RIF-RpoB complex follows first-order kinetics, with a half-life of 12 hours at 0°C, decreasing to 9 minutes at 37°C (Wehrli, 1983). The association constant (Ka) follows second-order kinetics, with a rate of 6 x 10^4 M{¹s{¹ at 0°C, increasing to 1.2 x 10^6 M{¹s{¹ at 37°C. The equilibrium constant (K_D/Ka) is estimated at 3.5 x 10{¹⁰ M at 0°C and 10{y M at 37°C, explaining RIF9s effectiveness at low concentrations, as a single RIF molecule can inactivate RpoB.

Approximately 90% of drug resistance in *E. coli* is attributed to mutations in the rifampicin resistance-determining region (RRDR) of the β-subunit. This region is divided in three key areas based on amino acid location: region I (507-533), region II (563-572), and region III (687) (Goldstein, 2014).

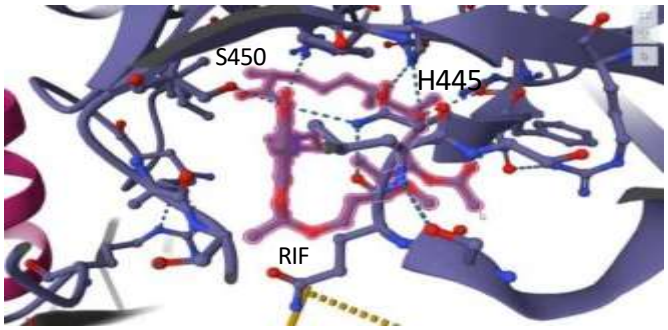

Figure I.4. Interactions between *M. tuberculosis* RpoB and rifampicin. Crystal 5UHB - adapted from Lin et al. (2017)**.**

Lin et al., (2017) resolved the crystal structure of Mtb RpoB at a resolution of 3.8-4.4 Å, revealing interaction sites with RIF that closely resemble those observed in previous studies on *Thermus aquaticus* (Campbell et al., 2001), *Thermus thermophilus* (Artsimovitch et al., 2005), and *E. coli* (Molodtsov et al., 2013). In the Mtb RpoB-RIF interaction, residues H445 and S450 form direct contacts with RIF through hydrogen-bonded bridges (Figure I.4), while D435 makes contact through van der Waals interactions (Lin et al., 2017). RIF inhibits Mtb transcription by sterically blocking the elongation of RNA, preventing the extension of 2- to 3-nucleotide products in longer RNA chains.

I.1.4.2. Rifampicin resistance determining region in mycobacteria

In the Mtb genome, a region equivalent to RRDR of *E. coli*, spanning codons 426 to 452 (equivalent to 507 to 533 in the *E coli*), has been aligned (Andre et al., 2017 , Figure I.5), This analysis reveals that the majority of mutations occur in region I, predominantly at codons 435, Ser450Leu and His445Asp (Ohno et al., 1996; Pang et al., 2013a; Taniguchi et al., 1996; Yang, 1998), with one notable mutation in region II at Ile491Phe (Siu et al., 2011).

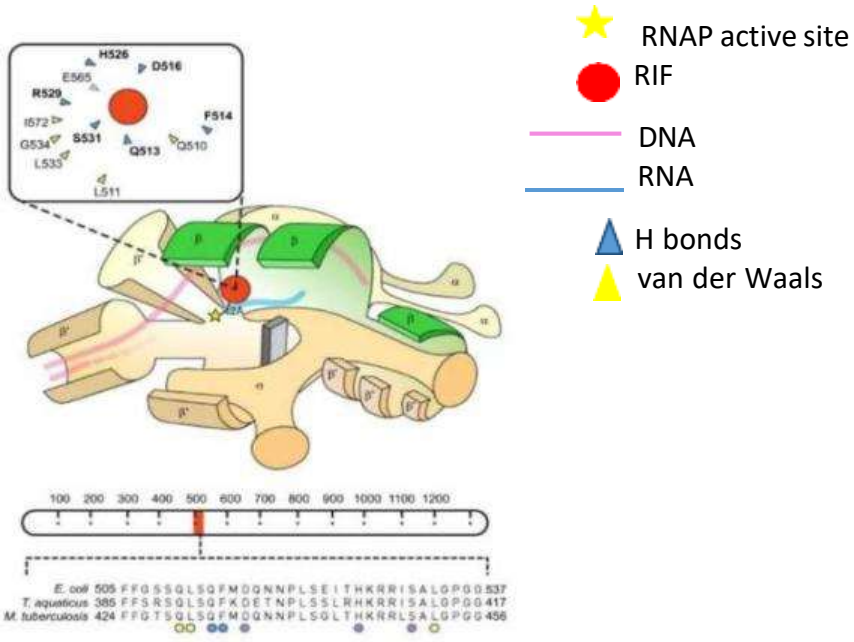

Figure I.5. Representation of the RNA polymerase holoenzyme from *E. coli* and the rifampicin resistance-determining region (RRDR). Subunit β is highlighted in green, with circles indicating amino acids that directly interact with rifampicin. Residues frequently associated with rifampicin resistance in RR-TB isolates are marked in red. Amino acids involved in hydrogen bond-mediated interactions are shown in blue, those interacting via van der Waals forces are depicted in yellow, and residues in gray are not associated with rifampicin resistance but are located near the rifampicin binding pocket. Adapted from Koch et al. (2014).

Additionally, a mutation at the N-terminal end, corresponding to residue 170 of the β-subunit, has also been associated with RIF resistance (Taniguchi et al., 1996). Due to Mtb's slow replication and growth process (M. Zhu & Dai, 2018), disrupting protein synthesis significantly impacts its ability to maintain infection and replicate. Mutations in the RRDR, such as the prevalent Ser450Leu and His445Asp, exhibit high-level drug resistance and a loss of fitness. Other frequent mutations, summarized in Figure I.6 (Shea et al., 2021; Xu et al., 2021) are used for predicting RIF resistance from sequencing data (https://tbdr.lshtm.ac.uk/).

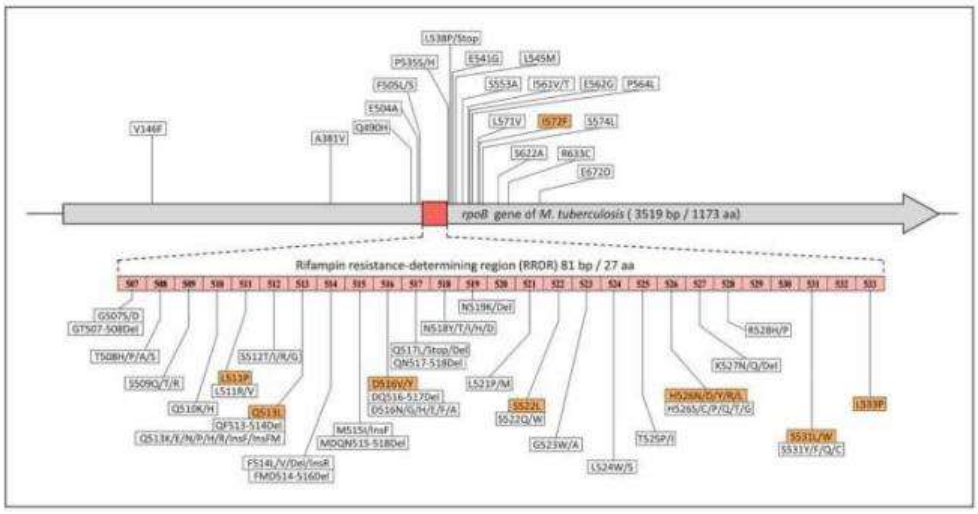

Figure I.6. Mutations in the *rpoB* gene and the rifampicin resistance-determining region in *M. tuberculosis*, using the *E. coli rpoB* nomenclature for numbering. Mutations with high correlation in RIF resistance are marked in orange. These mutations were acquired from the Tuberculosis Drug Resistance Mutation Database. Taken from Xu et al. (2021).

I.1.4.3. Other mechanisms involved in mycobacterial rifampicin resistance

RIF-resistant Mtb strains often show some *in vitro* fitness loss compared to native strains. However, strains with frequent mutations in RpoB (S450L) may not exhibit performance deficiencies, possibly due to compensatory mutations in the *rpoA* and *rpoC* genes (Comas et al., 2012). *rpoB* gene mutations outside of the RRDR have been described to confer RIF resistance, Ile491, described in 30% of MDR-TB isolates (Sanchez-Padilla et al., 2015). Additionally, other RIF resistance mechanisms, such as efflux pumps (Figure I.7), have been identified. These pumps can export RIF from cells, reducing intracellular drug concentration and accounting for about 5% of RIF resistance (Li et al., 2015; Pang et al., 2013b; Xu et al., 2021). In strains with mono-resistance to RIF but without *rpoB* mutations, efflux pumps like Rv0783, Rv2936, and Rv0933 were identified at the transcriptional level as contributors to RIF-mono-resistance (Louw et al., 2009; Pang et al., 2013). Another study showed that RIF exposure could induce overexpression of putative efflux pump genes: *Rv2333*, *drrB*, *drrC*, *Rv0842*, *bacA*, and *efpA* and they can have a contribution in the level of RIF resistance in addition to classical *rpoB* mutations (Li et al., 2015).

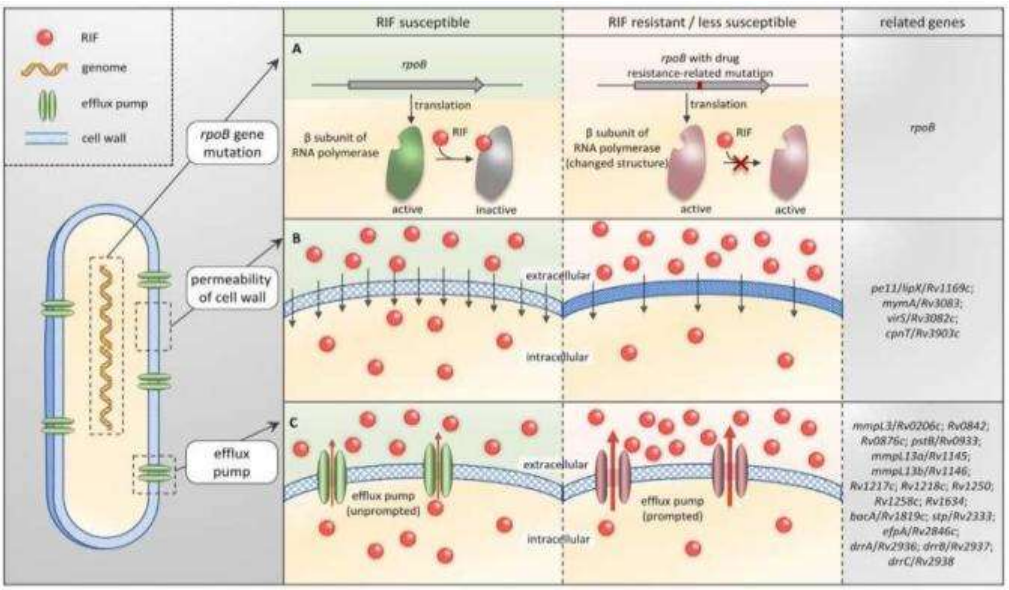

Figure I.7. Genes and mechanisms associated with rifampicin resistance.
Taken from Xu et al. (2021).

Reprogramming of macrophage metabolism, potentially caused by the RpoB polymorphism (H445Y), confers drug resistance, and leads to the overexpression of cell wall lipids, such as phthiocerol dimycocerates (PDIMs). This alteration helps evade the interleukin-1 receptor signaling pathway and induces interferon β (Gleeson et al., 2016; Howard et al., 2018)..

Sebastian *et al.* observed that Mtb strains grown in the presence of RIF develop a thicker outer coat compared to a control group (Sebastian & Swaminath, 2019), suggesting the existence of unknown mechanisms. Moreover, it's proposed that RpoB substitutions, specifically H445N and S450L, even in the absence of RIF, can affect the proteome and metabolome. These mutations lead to the up-regulation of polypeptide synthase (PKS) genes *ppsA-ppsE* and the *drrA* operon related to PDIM biosynthesis (Bisson et al., 2012). This evidence suggests that mutations in *rpoB* not

only confer RIF resistance but also induce compensatory transcriptional changes (Alifano et al., 2015; Bisson et al., 2012).

Another mechanism contributing to RIF resistance involves heterogeneous populations with varied drug resistances, arising from errors in protein translation that enable mycobacteria to adapt to changing environments (Meyerovich et al., 2010). For instance, in *M. smegmatis*, different environmental conditions, with or without drug exposure, induce *rpoB* gene expression via distinct promoters. This leads to the emergence of phenotypically RIF-resistant bacteria due to translation errors (Zhu et al., 2018).

I.2. Identifying heteroresistant tuberculosis infection from whole genome analysis of peruvian isolates

I.2.1. Mixed infections and heteroresistance

The management of TB has grown more complex with the emergence of drug-resistant strains, highlighting two challenges: mixed infections and heteroresistance. Mixed infection in TB means a single patient harbors multiple genetically distinct strains of Mtb (Mankiewicz & Liivak, 1975). This can lead to heteroresistance, where both drug-susceptible and drug-resistant subpopulations coexist in a single clinical sample (Hofmann-Thiel et al., 2008).

Dickman et al., (2010), observed that patients with mixed infections showed similar proportions of Mtb smear-positive cultures after two and five months of treatment. Another study, showed about 22.9% of mixed infections

experienced treatment failures after 6 months, and 24% exhibited heteroresistance, indicating a significant link between treatment failure and heteroresistance (Kargarpour Kamakoli et al., 2017). Later, Tarashi et al., (2017) noted that mixed infection rates vary by geographic prevalence, ranging from 0.4% to 57% in areas of low and high TB dissemination, respectively. A 2010-2020 systematic review by Nkatha Micheni et al. (2022)in the Sub-Saharan region, a high TB prevalence area, found mixed infection rates between 2.8% and 21.1%. To mitigate the global TB burden and limit the spread of drug resistance, accurately detecting strains within a mixed infection and identifying their specific resistance patterns are crucial. Various molecular typing methods, such as IS6110-restriction fragment length polymorphism (IS6110-RFLP), spoligotyping, and Mycobacterial Interspersed Repetitive Unit-Variable Number Tandem Repeat (MIRU-VNTR) genotyping, have provided insights in the presence of multiple Mtb strains in a single infection. However, these methods mainly reveal the strain lineages within a sample without pinpointing intra-lineage infections.

In recent years, whole genome sequencing (WGS) has become more accessible, providing a comprehensive analysis of a sample's genetic composition. It is increasingly used to identify mixed infections, although certain limitations are being studied for improvement. Wang et al. (2023) analyzed WGS data of main L1-L4 Mtb lineages worldwide, finding that 1% of isolates were potential mixed infections, including RR-TB, isoniazid-resistant TB (HR-TB), and MDR-TB. Countries with more than 5% mixed infections

included Colombia, Malawi, Turkmenistan, Russia, Brazil, Algeria, and India (Wang et al., 2023, Figure I.8). These findings underscore the significance of understanding mixed infections in TB for both epidemiological research and treatment strategies.

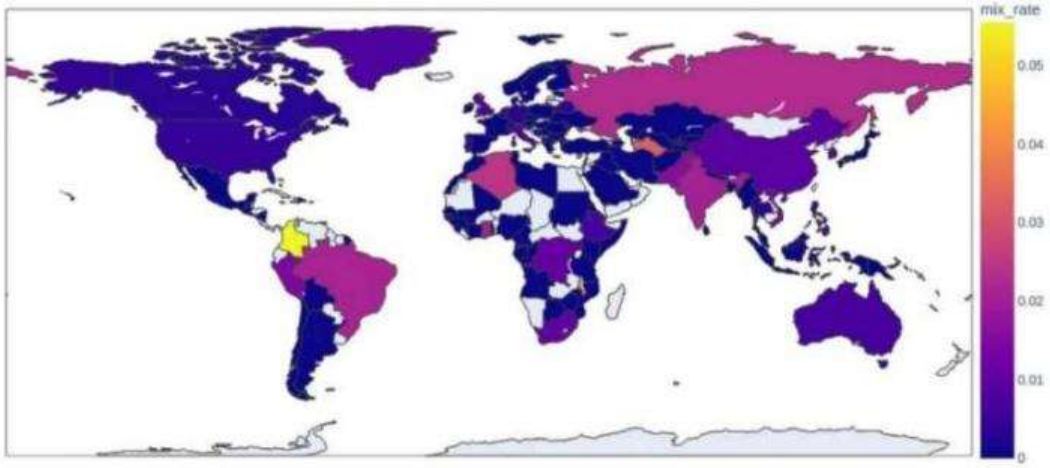

Figure I.8. Global map of reported heteroresistance proportions. Countries lacking data are shaded in light gray. Percentage of isolates with a multiple strain infection, ranging from purple (lower values) to yellow (higher values). Taken from Wang et al. (2023).

I.2.2. Heteroresistance

Heteroresistance refers to the presence of a heterogeneous bacterial population where one or several subpopulations exhibit increased levels of antibiotic resistance compared to the main population. The presence of resistant subpopulations at a proportion of 1% or more is defined as heteroresistance in the context of mixed infections (Canetti et al., 1963) or may arise from an existing resistant clonal subpopulation (Ng et al., 2019). Heteroresistance is a

critical stage that can lead to the development of fully drug-resistant TB, representing challenges for treatment outcomes (Abakur et al., 2020).

Key factors to consider in addressing heteroresistance include clonality, level of resistance, and the stability of heteroresistance (Andersson et al., 2019).

a) In Mtb, polyclonal heteroresistance has been observed in cases of mixed infections, which may arise from successive infections with different resistance levels (Figure I.9.A).

b) Some studies recommend establishing the level of resistance to clarify ambiguities at the borderline of the minimum inhibitory concentration (MIC), with resistance levels quantified as 2X, 4X, 8X, or higher compared to the major population.

c) Finally, the stability of heteroresistance influenced by exposure to antibiotics, concerns whether a strain maintains or loses its resistance profile in an antibiotic-free medium (Figure I.9.B). This aspect of heteroresistance has been documented in *E. coli*, K. *pneumoniae*, and S. *enterica* subsp. enterica serovar Typhimurium (Andersson et al., 2019; Manjunath et al., 2021). In Mtb it was registered the <unfixed resistance= and precedes full resistance because of increased selection for resistance under treatment (Folkvardsen et al., 2013).

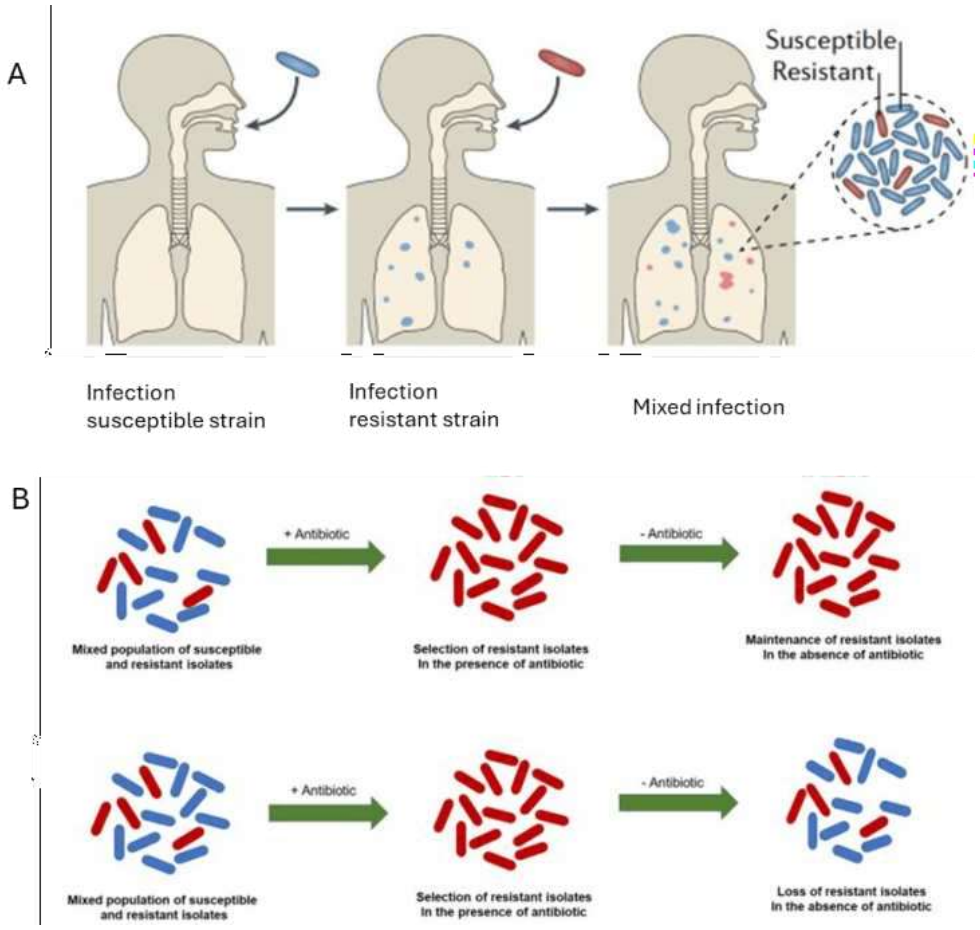

Figure I.9. Mixed Infections and Heteroresistance. A. Heteroresistance arising from mixed tuberculosis infections. Adapted from Andersson et al. (2019). B. Stability of heteroresistance can vary: it may be stable (upper), where resistance is maintained even in the absence of antibiotics, or unstable (lower), where susceptibility is restored once the antibiotic is removed. Adapted from Manjunath et al. (2021).

Risk factors for the development of heteroresistance in TB include:

- Interactions between different Mtb strains within a host can elevate the risk for poor treatment outcomes. For instance, a new infection triggering the reactivation of a latent infection can lead to mixed-strain infections (Kargarpour Kamakoli et al., 2017; Shin et al., 2018).

- Microevolution: Heteroresistance can arise when a single drug-susceptible Mtb strain evolves in a mix of susceptible and resistant organisms through microevolution (Sonnenkalb et al., 2021). This evolution within an infection can complicate treatment strategies (Shin et al., 2018).

- High TB burden areas: In regions with high rates of TB infection, such as sub-Saharan Africa, mixed infections and drug resistance are more common, posing challenges for diagnosis and treatment. Delayed diagnosis of mixed infections and heteroresistance in these high-burden areas can increase the risk of treatment failure and transmission of resistant strains (Nkatha Micheni et al., 2022).

- Socioeconomic status: Lower socioeconomic status can increase the risk of repeated exposure to Mtb, leading to mixed-strain infections and poor treatment outcomes. This repeated exposure may contribute to the development of mixed infections with drug-resistant and drug-susceptible strains (Shin et al., 2018).

- Diagnostic challenges: Detecting heteroresistance can be challenging using routine laboratory tests, such as GeneXpert Cepheid tests, which may have low sensitivity in detecting mixed infections and resistance patterns accurately. This diagnostic challenge can lead to missed detection of resistant strains and impact treatment outcomes (Chengalroyen et al., 2022; Nkatha Micheni et al., 2022).

I.2.3. Tuberculosis diagnosis and drug susceptibility testing

TB diagnosis involves detecting Mtb bacteria or their genes in a clinical specimen, typically sputum, though other biological exudates can be used. The drug susceptibility classification for TB treatment, based on drug susceptibility testing (DST), is crucial. DST, a key part of TB management, identifies effective drugs against the specific Mtb strain causing the infection. This classification is vital for tailoring treatment regimens to each individual, ensuring successful treatment, and preventing the development of drug-resistant TB.

I.2.3.1. Acid fast bacilli (AFB) (sputum smear) microscopy

The technique is based on the direct observation of a stained sample under a microscope, commonly using the Ziehl-Neelsen stain. A positive result for TB is indicated by the presence of acid-fast bacilli. This practical, simple, and rapid method can be performed in most health services. It detects patients with high bacilli counts, who are likely to spread the infection in the community. AFB is widely used for confirming TB, monitoring the evolution of infectious cases, confirming cure in successfully treated cases, identifying treatment failures, and monitoring drug-resistant TB patients. It is a primary medical procedure for diagnosing TB, typically conducted when a patient shows symptoms of the disease (Beltrame S et al., 2014; Sardiñas et al., 2016).

I.2.3.2. Microbiological culture

Mtb culture, a laboratory test for diagnosing TB, involves culturing a sample of body fluid or tissue on media like Löwenstein-Jensen or 7H10 supplemented with 10% OADC (oleic acid, albumin, dextrose, and catalase), and observing for bacterial growth for up to 6 weeks. It is the gold standard for sensitivity, specificity, species identification, DST, and genotyping. Additionally, it monitors patient response to treatment and is widely used for confirming TB, evaluating infectious case progression, confirming successful treatment, and identifying treatment failures, as well as monitoring patients with drug-resistant TB (Beltrame S et al., 2014; Oxford University Hospitals, 2024). A drawback of this method is the extended time required due to the slow growth rate of the mycobacterium.

I.2.3.3. Microscopic observation drug susceptibility (MODS)

MODS assay is a rapid, cost-effective method for diagnosing TB and determining resistance to INH and RIF. It detects the growth of Mtb through cordon formation with a characteristic pattern described by Caviedes et al., (2000), using an inverted microscope. Employed by Peru's National Network of Public Health Laboratories, MODS is effective for the rapid detection of TB and MDR-TB (Instituto Nacional de Salud [INS], 2011), which could be positive from the seventh or tenth day of culture (Caviedes et al., 2000). It is particularly valuable in resource-limited settings for diagnosing TB and identifying drug resistance. The assay has been standardized and is increasingly recognized as an important tool in the global effort to control TB.

I.2.3.4. Minimal inhibitory concentration (MIC)

MIC is the lowest concentration of an antibiotic that completely inhibits bacterial growth. It guides the selection of optimal antibiotics for treating mycobacterial infections, significantly impacting therapeutic strategy and treatment efficacy. MIC determination involves preparing a dilution series of antibiotics, adding agar or broth, inoculating with mycobacteria, and incubating at a suitable temperature (Kowalska-Krochmal & Dudek-Wicher, 2021). On solid Middlebrook medium, methods like the agar proportion, absolute concentration, and resistance ratio require 21 days of incubation at 37°C (Sirgel et al., 2009). Additionally, another important technique, the Direct Tetrazolium Microplate Assay (TEMA) is a rapid, cost-effective colorimetric method. After 5-15 days of incubation, the growth of Mtb is indicated by a color change in the tetrazolium solution, resulting from the formation of formazan as a consequence of the of the tetrazolium salts reduction, allowing determination of MICs for each tested antibiotic (Berridge et al., 2005; Caviedes et al., 2002; Wan Nor Amilah et al., 2016).

I.2.3.5. Molecular methods

In high TB burden countries, efficient and scalable approaches are essential for rapid detection. Molecular techniques offer a viable alternative, delivering results in just 2 to 5 hours, compared to the 21 to 30 days required for culture-based methods. Depending on the technology, these methods can also identify drug resistance types, thus accelerating diagnosis, guiding the most effective therapeutic scheme for the patient, and preventing exposure to ineffective toxic drugs (Table I.1) (Global Tuberculosis Programme [GTB], 2021, MacLean et al., 2020). This methodology has

been proposed to replace smear microscopy, especially when bacterial load is low or paucibacillary, making detection challenging (GTB, 2022).

Finally, WGS is another valuable and increasingly affordable molecular tool for studying TB. It enables the identification of genetic markers associated with treatment outcomes, infection prognosis, and bacterial microevolution (Nurwidya et al., 2018). However, in developing countries, the cost of WGS remains a significant barrier, highlighting the need to enhance national TB management strategies.

Table I.1. WHO-recommended molecular diagnostic tests for tuberculosis and drug susceptibility.

Technology	Method principle	Resistance detected	Description	Sensitivity (%)	Specificity (%)	Reference
Initial TB diagnosis						
FluoroType MTB	PCR, hybridization	None	Automated NAAT	92 (MTB detection)	94 (MTB detection)	Dippenaar et al., 2021.
Loopamp MTBC assay	Loop−mediated isothermal amplification	None	Manual or automated NAAT	78 (pooled)	98 (MTB detection)	WHO, 2016
Truenat MTB plus	Micro RT−PCR	MTB diagnosis	Automated NAAT	80 (pooled)	96 (MTB detection)	GTB, 2021; MacLean et al., 2020; Nurwidya et al., 2018.
Initial TB diagnosis with drug-resistance detection						
Xpert MTB/RIF	qPCR	RIF	Automated NAAT	85 (pooled), 96 (RIF resistance)	99 (MTB detection) 98 (RIF resistance)	GTB, 2021, 2022.
Xpert MTB/RIF ultra	qPCR/melting temperature analysis	RIF	Automated NAAT	90 (pooled), 94 (RIF)	96 (MTB detection), 98 (RIF)	GTB, 2021, 2022; MacLean et al., 2020.
Truenat MTB-RIF Dx	Micro RT−PCR	RIF	Automated NAAT	84 (RIF)	97 (RIF)	GTB, 2021, 2022; MacLean et al., 2020.
FluoroType MTBDR	PCR, hybridization	MTB diagnosis and INH−RIF resistance detection	Automated NAAT	90	98	Dippenaar et al., 2021.

RIF, rifampicin; INH, isoniazid; FLQ, fluoroquinolone, AMK, amikacin, KAN, Kanamycin, CAP, capreomycin, ETH, ethambutol, ETO, ethionamide; PZA, pyrazinamide; LVX, levofloxacin LAMP, loop-mediated isothermal amplification; NAAT, nucleic acid amplification test; RT-PCR, reverse transcriptase PCR; WHO, World Health Organization.

Table I.1. (... continuation). WHO-recommended molecular diagnostic tests for tuberculosis and drug susceptibility.

Technology	Method principle	Resistance detected	Description	Sensitivity (%)	Specificity (%)	Reference
Follow-on diagnostic test for drug -resistance detection						
Second-line probe assays (e.g., GenoType MTBDRsl)	PCR, hybridization	Diagnosis of FLQ and KAN, CAP, AMK, ETH resistance	Manual reverse hybridization assay	87 (FLQ), 77 (KAN), 80 (CAP), 100 (AMK), 57 (ETH)	96 (FLQ), 100 (KAN), 98 (CAP), 100 (AMK), 92 (ETH)	GTB, 2021; Nurwidya et al., 2018.
Xpert MTB/XDR	qPCR/melting temperature analysis	INH, RIF, FQ, AMK, KAN, CAP	Automated NAAT	98.3−98.9 (RIF), 94.2 (INH), 93.3 (FLQ), 98 (ETO), 86,1 (AMK)	22.5−100 (RIF), 98.5 (INH), 98 (FLQ), 99,7 (ETO), 98.9 (AMK)	Pillay et al., 2022.
GenoTypeMTBDRplus	PCR, hybridization	RIF, INH, ETO	Manual reverse hybridization assay	91 (INH), 96 (RIF)	99 (INH), 98 (RIF)	GTB, 2021, 2022; Nurwidya et al., 2018.
Genoscholar NTM+MDRTB detection kit	PCR, hybridization	RIF−INH	Manual reverse hybridization assay	98.9 (RIF), 90,6 (INH), 89,7 (PZA), 93 (LVX)	97.3 (RIF), 100 (INH), 96 (PZA), 100 (LVX)	Mitarai et al., 2012.

RIF, rifampicin; INH, isoniazid; FLQ, fluoroquinolone, AMK, amikacin, KAN, Kanamycin, CAP, capreomycin, ETH, ethambutol, ETO, ethionamide; PZA, pyrazinamide; LVX, levofloxacin LAMP, loop-mediated isothermal amplification; NAAT, nucleic acid amplification test; RT-PCR, reverse transcriptase PCR; WHO, World Health Organization.

I.2.4. Detection of mixed infections and heteroresistance

Currently, the WHO does not mandate the detection of mixed TB infections as part of routine TB diagnosis. However, mixed infections can complicate TB treatment and impact disease transmission, making their detection relevant for comprehensive management, especially in research and clinical trials. Below is a brief description of some methods used to detect mixed infections and heteroresistance. These techniques have been applied in research settings and for generating epidemiological data, contributing to the understanding of TB transmission dynamics and resistance development until now.

I.2.4.1. Agar proportion test

It is a phenotypic method used for testing the susceptibility of MTBC to antimicrobial drugs. This test has been considered the gold standard for drug susceptibility testing in the U.S. and Europe. The agar proportion method involves inoculating a drug-containing quadrant of an agar plate with a diluted inoculum of the test specimen and comparing the growth in this quadrant to a drug-free control quadrant. The interpretation of the test is based on the proportion of mutant colonies resistant to a drug, with a threshold of greater than 1% resistance indicating resistance. The agar proportion test typically takes about three weeks to determine susceptibility, although resistance may be detected earlier (Canetti et al., 1963).

I.2.4.2. Genotyping methods

Various genotyping methods and molecular approaches require a primary culture of mycobacteria to be employed effectively for the detection of mixed infections.

- **MIRU-VNTR** (Mycobacterial Interspersed Repetitive Units-Variable Number Tandem Repeats) is a molecular typing technique that analyzes the number and arrangement of genetic elements named MIRU in the Mtb genome. Unlike IS*6110* RFLP, this technique can obtain fingerprints directly from clinical specimens (Mazars et al., 2001). It requires a low DNA concentration to perform PCR with specific primers for MIRU-VNTR loci. The resulting fragments are analyzed by electrophoresis, and their sizes determined to generate fingerprints for each isolate, which are then compared with reference strains (Mazars et al., 2001; Scott et al., 2005). Mixed infections are identified by the presence of varying MIRU-VNTR patterns at two or more loci in the same clinical sample, while clonal heterogeneity refers to variations at a single locus (Cohen et al., 2011; Tarashi et al., 2017).

- **Xpert MTB/RIF** assay is an automated test that performs DNA extraction and real-time PCR to simultaneously detect Mtb and resistance to RIF (Cepheid, 2020) in less than two hours. It is recommended for populations where the prevalence of RIF resistance exceeds 2% (Vallejo et al., 2015). The Xpert assay has a sensitivity of 98% in smear positive samples (Boehme et al., 2011) for detecting RIF resistance. However, its sensitivity drops to 72.5 %- 77% in smear negative samples and 80.0% in patients with mixed MTBC

infections (Zetola et al., 2014). It detects mutation S450L only in mixtures with at least 20-40% resistant bacilli, mutation H445D need to be present in the sample around 40-60% and mutation D435V with at least 70-80% mutant bacilli (Ng et al., 2018).

- **Xpert MTB/ultra**, is the most updated version of Xpert MTB/RIF, which is more sensitive in smear-negative TB or paucibacillary cases; as well as in HIV patients (Cepheid, 2024; Dorman et al., 2018). It has also been reported to be better able to discriminate the presence of mixed infections and RIF heteroresistance through <mixed patterns= denotation (Ng et al., 2018). Ng *et al*, reported for mutation S450L a minimum of 20 to 30% resistant bacilli needs to be present in the population, 40 to 50% for D435V, 40 to 60% for H445D and 60-70% for H445Y.

- **The line probe assay (LPA),** utilizes DNA strip technologies for the rapid detection of drug-resistant Mtb (GTB), 2022). DNA can be extracted from cultures, direct smear-positive, and smear-negative sputum specimens and the process involves PCR amplification of target genes, followed by reverse hybridization with specific probes on a strip. Mutations are identified by the binding of amplicons to probes or by the absence of hybridization to wild-type probes, revealing specific patterns post-hybridization (WHO, 2022). In a study by Ng et al. (2018), the techniques GenoType MTBDRplus v2.0 and Genoscholar NTM+MDR TB II were shown to detect RIF heteroresistance in populations containing 1-10% resistant bacilli, with sensitivity varying depending on the mutation evaluated.

- **Deeplex-MycTB**, is directly applicable to clinical samples and predicts resistance to 15 anti-TB drugs through multiplex PCR and targeted deep sequencing. It provides information about sublineages and offers quantitative results, enabling the detection of heteroresistance in a range between 1-3% (GenoSreen, 2023) and up to 5% as reported by Ng *et al*. (2018).

I.2.4.3. Whole genome sequencing

WGS has become a crucial tool for detecting mixed infections, offering high sensitivity and discriminatory power. This technique enables the simultaneous identification of different Mtb strains, providing comprehensive insights in the genetic makeup of mixed infections (Sobkowiak et al., 2018). Furthermore, it has been reported that WGS's capability can be enhanced by incorporating statistical models to accurately determine the sub-lineage and assign drug profiles for each strain, significantly improving diagnostic precision and treatment strategies (Wang et al., 2023). WGS can be useful to follow transmission chains and it was reported as well to distinguish relapses from exogenous reinfections, based on the single nucleotide variation (Fernandez Do Porto et al., 2021).

I.3. PonA1 of *M. tuberculosis*: *In vitro* study and genomic integration in *M. marinum*, insights in rifampicin resistance.

I.3.1. Mycobacterium cell envelope

Mtb cell wall has a complex architecture comprising three main components: long-chain mycolic acids, highly branched arabinogalactans polysaccharides, and cross-linked peptidoglycan (PG).

In most bacteria, PG consists of repeated disaccharide units of N-acetylmuramic acid and N-acetylglucosamine type β-(1,4) bonds. However, in Mtb, muramic acid molecules are N-glycolylated and not N-acetylated (Raymond et al., 2005). Consequently, Mtb9s PG is constituted by a skeleton of N-acetylglucosamine (GlcNAc) and N-glycolylmuramic acid (MurNGlyc). PG in Mtb has side chains of L-alanyl-D-isoglutaminyl-meso-diaminopimelic-D-alanyl-D-alanyl-D-alanine pentapeptides, forming a mesh-like structure. This structure emerges from bonds between meso-diaminopimelic acid (m-DAP) and D-alanine (4 →3) across adjacent glycan chains, catalyzed by D, D -transpeptidases of penicillin-binding proteins (PBPs) during the exponential growth phase. Additionally, bonds between m-DAP and m-DAP (3→3) are formed by the activity of L,D-transpeptidases throughout all growth (P. Kumar et al., 2012; Lavollay et al., 2008). PG formation in Mtb is a complex process involving several enzymes, including ligases, flippases, transglycosidases and transpeptidases (Figure I.10). MurA (*Rv1315*) is an enoylpyruvyl transferase activity that adds phosphoenol pyruvate to UDP-GlcNAc to form UDP-eneylpyruvyl-GlcNAc (Kim et

al., 1996), MurB (*Rv 0482*) reduces the product generated by MurA using NADPH to form UDP-MurNAc (Benson et al., 1996). NamH (*Rv3808*) forms UDP-MurNGlyc by hydroxylation of UDP-MurNAc, thereby generating two types of UDP-MurNAc/Glyc substrate (Raymond et al., 2005). The action of MurC (*Rv 2151c*) (Mahapatra et al., 2000), MurD (*Rv2155c*), MurE (*Rv2158c*) (Basavannacharya et al., 2010), MurF (*Rv2157c*) ligate L-alanine, D-isoglutamate, m-DAP and D-alanyl-D-alanine, respectively, to form the muramyl pentapeptide (Jankute et al., 2015). MurX (*Rv2156c*) catalyzes the transfer of muramyl pentapeptide to decaprenyl phosphate, creating the first lipid intermediate (Lipid I) in PG formation (Bouhss et al., 1999). MurG (*Rv2153c*) then binds GlcNAc to Lipid I, forming Lipid II, via a β 1→4 linkage between GlcNAc and MurNAc/Glyc (Trunkfield et al., 2010). Lipid II is translocated across the plasma membrane by a flippase, possibly MurJ (*Rv3910*) (Ruiz, 2008) or FtsW (*Rv2154c*) (Mohammadi et al., 2011).

The bifunctional proteins PonA1 (*Rv0050*) and PonA2 (*Rv3682*) transglycosylate lipid II monomers by binding GlcNAc and the muramyl group of the growing chain (Hett et al., 2010). Likewise, PonA1 and PonA2 proteins have transpeptidase activity, forming 4→3 bonds between m-DAP and D-ala (Chang et al., 1990).

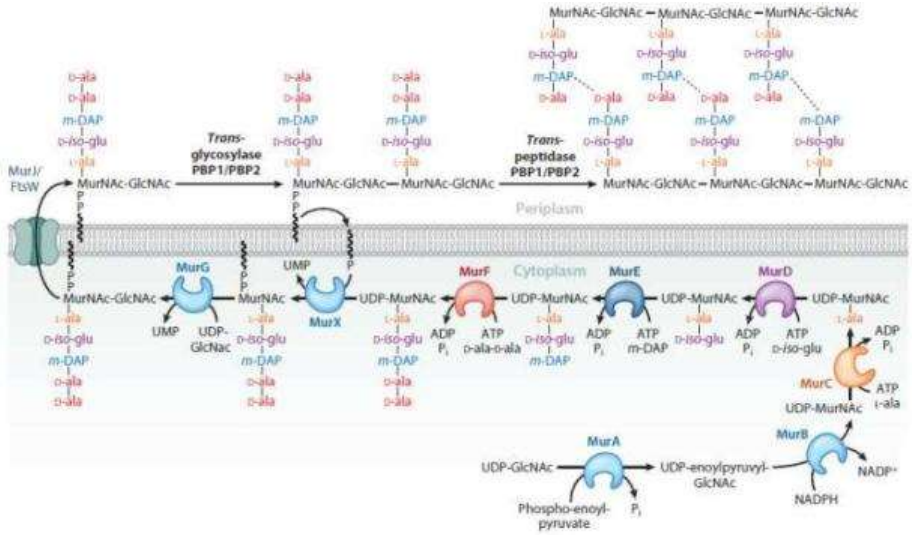

Figure I.10. **Biosynthesis of peptidoglycan in *M. tuberculosis***
Taken from Jankute et al. (2015).

I.3.2. Cell wall biosynthesis and *M. tuberculosis* drug resistance mechanisms

The cell wall in Mtb contributes to RIF resistance by affecting the permeability barrier to the antibiotic. Studies indicate that Mtb cells exposed to continuous bactericidal concentrations of RIF develop a negatively charged, thickened capsular outer layer, which limits antibiotic permeability (Sebastian et al., 2020). Furthermore, inhibitors targeting cell wall biosynthesis, such as MmpL3, Pks13, EMB, and even INH at concentrations above the MIC, have been shown to enhance RIF accumulation in Mtb, underscoring the cell wall's role in the antibiotic's effectiveness (McNeil et al., 2019).

In a genomic study, Farhat et al. (2013) identified 39 genes or intergenic regions associated with drug resistance in Mtb, including 11 previously known drug resistance genes and 5 new ones involved in cell wall biogenesis or remodeling (Figure I.11). The genes *ppsA, pks12* and *pks3* are related to the biosynthesis and translocation of PDIM, while *murD* and *ponA1* are associated with PG biosynthesis and homeostasis.

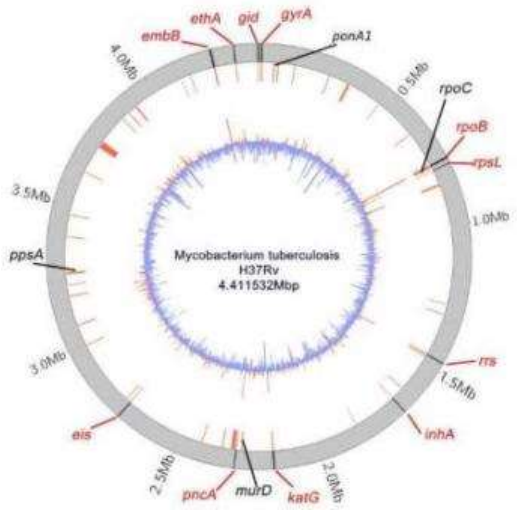

Figure I.11. PonA1 as a candidate gene under selection for antibiotic resistance in *M.tuberculosis*. Previously identified drug resistance genes are highlighted in red, while four independent mutation targets are displayed in black. Taken from Farhat et al. (2013).

I.3.3. Penicillin binding protein, structure and function

PBPs are membrane-associated proteins crucial in PG biosynthesis, the main component of bacterial cell wall. Functionally, they are categorized in three classes based on their molecular weight, Class I, II and III (Sauvage et al., 2008). Class I, the High Molecular Weight PBPs, includes Class A PBPs, which are bifunctional for transglycosylation and transpeptidation, and Class B PBPs with only transpeptidation

functions (Shaku et al., 2020). Class II and III, includes low molecular weight PBPs related with transpeptidation, carboxypeptidation and endopeptidation involved in the biosynthesis of PG to ensure the proper formation and maintenance of the bacterial cell wall (Shaku et al., 2020).

The diversity of PBPs is linked to various processes in cell wall formation and composition. It's important to note the differences in cell wall composition between Gram-positive and Gram-negative bacteria, particularly in the amount of PG. For instance, Gram-negative bacteria like *E. coli* have a thin PG layer covering the outer membrane, while Gram-positive bacteria possess a much thicker or multilayered PG layer (Figure I.12; Shaku et al., 2020).

E. coli has three Class A PBPs (PBP1a, PBP1b and PBP1c) and two class B PBPs (PBP2 and PB3/FtsI), among other 36 enzymes involved in PG synthesis ((Shaku et al., 2020). The adaptation of *E. coli* to different environmental conditions, including pH changes, is partly due to PBPs activity, with PBP1a and PBP1b maintaining viability under alkaline or acidic conditions, respectively (Mueller et al., 2019).

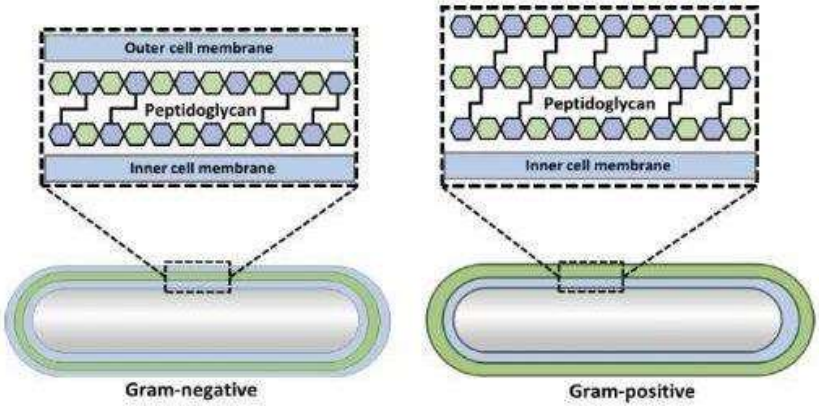

Figure I.12. Peptidoglycan disposition in the cell wall of Gram-positives and Gram-negatives bacteria. Taken from Shaku et al. (2020).

The cell wall structure of mycobacteria is comparable to that of Gram-positive bacteria. Mtb has two PBP functional proteins, PonA1 and PonA2. Although they have similar functions, they are not redundant (Kieser, Baranowski, et al., 2015). PonA1 is involved in PG synthesis at the poles and septum. While Mtb with a deleted (Δ) *ponA1* can grow in culture, its replication is less robust during infection (Kieser, Boutte, et al., 2015). In contrast, *M. smegmatis*, has three bifunctional PBPs: PonA1, PonA2 and PonA3 (Patru & Pavelka, 2010). It is shown that *ponA1* is essential in *M. smegmatis*, and ΔponA1 affects cell proliferation and shape (Kieser, Boutte, et al., 2015).

I.3.4. PonA1 and rifampicin resistance

In vitro assays showed the deletion in the *ponA1* gene led to higher survival rates in the presence of RIF. Mutations in this gene, specifically G1095T (non-synonymous change Q365H) conferred a 4 to 6-fold survival advantage in the presence of the drug (Figure I.13). This mutation, situated near the catalytic site of the transpeptidase domain, suggests that the single nucleotide polymorphism (SNP) might inactivate PonA19s enzymatic activity (Farhat et al., 2013).

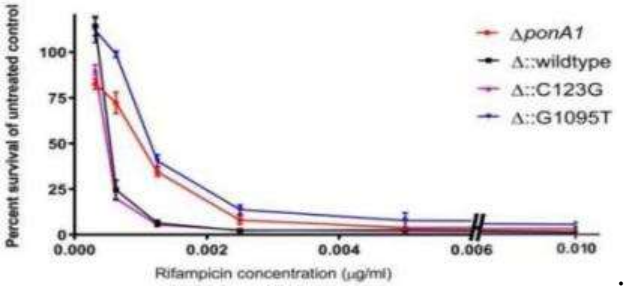

Figure I.13. Survival of *M. tuberculosis* PonA1 mutant at various rifampicin concentrations. Taken from Farhat et al. (2013).

In a study performed by Rabanal (2020), 914 genomes were analyzed and their drug resistance profiles were associated, identifying specific SNPs in the *ponA1* gene, such as A516T and P631S, as potential contributors to alterations in RIF resistance susceptibility. The presence of at least one SNP in *ponA1*, particularly P631S, appears to act as a protective factor against RIF resistance. In contrast, the A516T SNP has been linked to an increased risk of RIF resistance, underscoring the complex role of *ponA1* variants in influencing drug susceptibility.

Additionally, the P631S mutation is located in a proline-rich region at the C-terminal end, which has been reported to mediate the interaction between PonA1 and RipA (Hett et al., 2010). The effects of this mutation in *M. smegmatis* have been described as altering cell morphology, leading to deregulation in cell size and resulting in a more dispersed population (Gao et al., 2019).

I.3.5. PonA1 structure

In Mtb, the *ponA1* gene, located at the Rv0050 locus, encodes a Class A PBP with a molecular weight of 71 kDa (Sauvage et al., 2008). The PBP domain spans residues 420 to 820, and the protein includes a signal peptide at its N-terminal end and a transmembrane helix between positions 139 and 159. The transglycosylase (TG) domain (EC: 2.4.1.129) is positioned between residues 180 and 360, with its active site at position 213, where it functions as a proton donor. Additionally, the DD-transpeptidase (TP) domain (EC: 3.4.16.4) is located between residues 453 and 743, with the active site at position 487 acting as an acyl-ester intermediate (Accession

number: YP_177687.1). These structural elements are essential for the protein's role in PG synthesis (Figure I.14.A).

Filippova et al. (2016) resolved the crystal structure of the transpeptidase (TP) domain of Mtb, spanning residues 234-818 in the full protein (corresponding to 92-676 in the crystal structure 5CRF). This domain consists of two distinct subdomains, separated by a cleft that houses the active site serine. The first subdomain includes α1 (428-444), β1 (449-458), β2 (463-468), β1(483-485), β5′ (615-617), β6′ (645-647), α8 (662-667), β3 (679-687), β4 (692-702), β5 (705-714), and α9 (732-747). The second subdomain contains α2 (491-500), α3 (533-539), α4 (541-552), α5 (555-567), α6 (600-613), α7 (649-661), β2′ (506-510), β3′ (513-515), β4′ (518-520), and a disulfide bridge between Cys528 and Cys531 (Figure I.14.B).

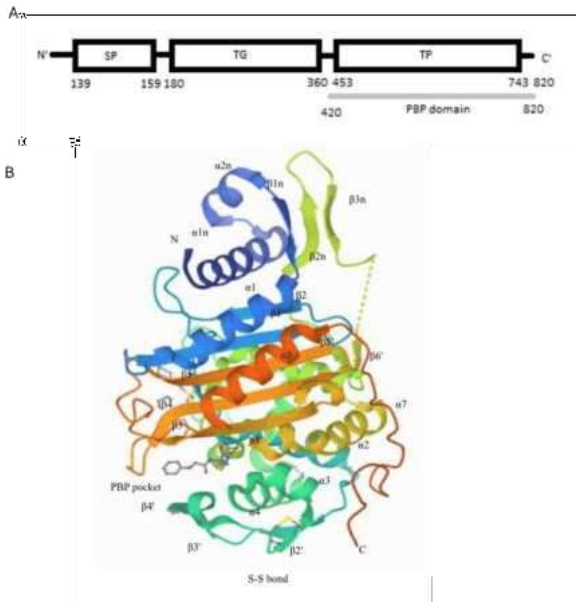

Figure I.14. PonA1 structure and crystal representation from *M. tuberculosis* H37Rv. A. Schematic representation of PonA1 domains. B. Crystal structure of the TP domain resolved by X-ray diffraction at 1.80Å resolution (PDB: 5CXW, Filippova et al., 2016). SP= Signal Peptide, TG= Transglycosylase domain, TP= Transpeptidase domain, PBP= Penicillin Binding Protein domain.

The PBP domain, conserved across different species, comprises two subdomains. In the first subdomain, the serine active site is located at the start of the α2 helix, followed by a lysine in the SxxK motif (Ser487, Ser488, Phe489, Lys490) located at the N-terminal end of α2. Another motif, SxN (Ser540, Leu541, Asn542) is positioned in a loop-like region between helices α3 and α4. The third motif, KTG(T/S), involves residues Lys681, Thr682 and Gly683 located in the β3-sheet (Filippova et al., 2016; Sauvage et al., 2008). This domain can interact with penicillin V (Filippova et al., 2016) and has been shown to interact with a RipA, an endopeptidase, in the terminal region (561-820 aa), playing a role in PG hydrolysis regulation (Hett et al., 2010).

I.3.6. D-D transpeptidase mechanism of action

The TP domain cross-links the nascent chains produced by the -cis-TG domain, however studies in *M. smegmatis* show that the activities of these domains are independent (Kieser, Boutte, et al., 2015) with TP functioning without active -cis-TG. This cross-linking performed by TP is crucial for maintaining normal cell length in Mtb, as its absence can reduce cell length by 6 to 11 %, indicating the role of TP in proper cell length maintenance (Kieser, Boutte, et al., 2015). This process adds rigidity to the bacterial cell wall by replacing one amide bond with another, thus forming the cell wall.

The transpeptidation of PonA1 involves three steps: first, the rapid and reversible formation of a non-covalent Henri-Michaelis complex between the enzyme and the muramyl pentapeptide (donor strand). This is followed by the acylation of the active site serine by the PG and the release of the D-ala from the C-terminus. The final step

is diacylation, where the crosslink is formed with a second peptide from the PG arm, known as the acceptor strand (Lee et al., 2003; Sauvage et al., 2008- Figure I.15).

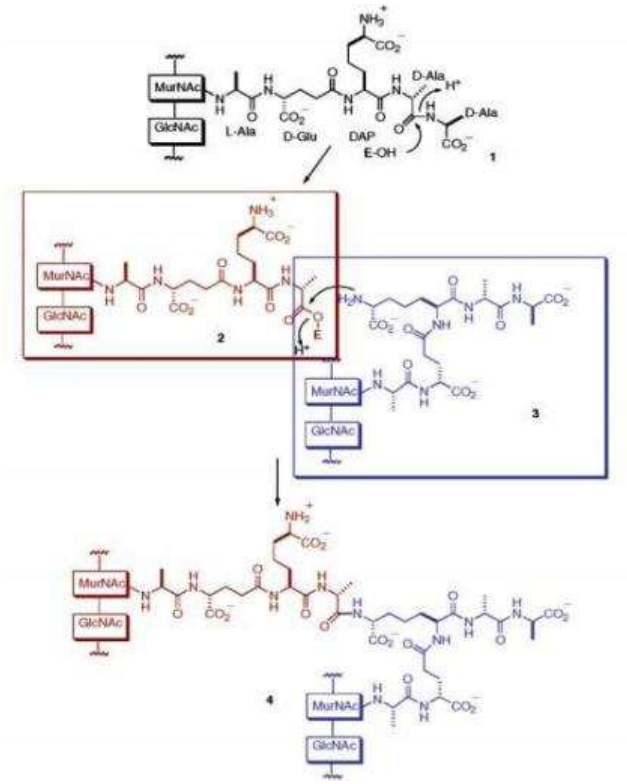

Figure I.15. Mechanism of cell wall cross-linking by DD-transpeptidases. Taken from Lee et al. (2003).

I.3.7. β-lactams, PBPs and their utility in structural studies

An important point to develop this part of the study was the information related with the PBP-like domain in the C-terminal of PonA1. Tipper & Strominger (1965) proposed that the structure of β-lactams could mimic the acyl-D-Ala-D-Ala portion of the PG structure (Figure I.16). The β-lactams act as suicide substrates of TP, in contrast to PG which acylates the active site and allows the terminal D-ala to serve as the leaving group, acylation of the active site by β-lactams results in opening of the β-lactam ring

and leaves the leaving group covalently bound to the enzyme-acylated species. Thus, the enzyme is irreversibly inactivated by β-lactam ring strain (Edoo et al., 2017).

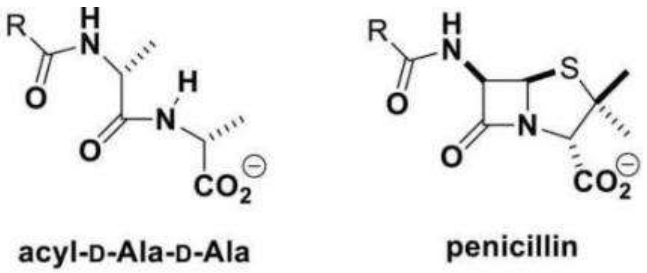

Figure I.16. Chemical structure of D-alanyl-D-alanine and penicillin. Taken from Fishovitz et al. (2014)**.**

Under *in vitro* conditions, this domain can be exploited to evaluate the interaction between PBPs and molecules presenting synthetic β -lactam rings, such as Bocillin-FL (Golemi-Kotra et al., 2003; Zhao et al., 1999). It is a fluorescent analog of penicillin V (Figure I.17), which covalently interacts with the active serine site in the TP domain (Figure II.4; Kieser, Boutte, et al., 2015). If a protein does not bind Bocillin-FL, it indicates that the PBP domain is either absent or non-functional. Kieser et al. (2015) demonstrated that *M. smegmatis* PonA1 isoforms lacking the transpeptidase TP domain were unable to bind Bocillin-FL, a fluorescent analog of penicillin V.

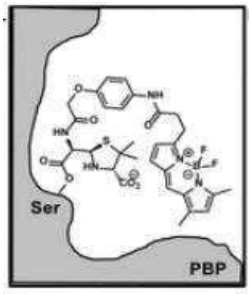

Figure I.17. PBP -Bocillin FL interaction. Taken from Levine & Beatty 2021).

I.4. Objectives and thesis organization

RIF resistance is a critical issue in TB treatment, as it often indicates resistance to other drugs. The mechanism of resistance to RIF at the molecular level is explained by mutations that can occur in the *rpoB* gene, which is responsible for protein translation. It has been demonstrated that *rpoB*9s mutations can alter the cellular fitness of mycobacteria to varying degrees, contributing to a diverse cellular response. In this study, we have explored additional mechanisms that may influence the maintenance of RR-TB populations. Additionally, we explored the use of a new methodology for studying genes that may be related to RR-TB, employing ORBIT technique in the Mmar model.

Chapter I provides a comprehensive overview of TB, beginning with a description of the state-of-the-art of TB in the world, the techniques for detecting the disease and categorizing the different types of TB based on drug resistance profiles. It discusses the general biology of Mtb and the complex host-pathogen interactions that lead to infection and disease progression, detailing the background of each topic covered in the thesis. A significant focus is placed on the molecular mechanisms of resistance to RIF, a key antibiotic in TB treatment, highlighting the specific genetic mutations and cellular adaptations that enable the bacterium to survive antibiotic exposure. In addition to these established resistance mechanisms, the chapter explores lesser-known pathways that may represent novel therapeutic targets, providing insights in new strategies for managing resistant strains.

Chapter II provides a detailed analysis of WGS of clinical isolates from TB patients, focusing on the main antibiotic resistance genes, with particular emphasis on the *rpoB* gene. The chapter also delves deeper in isolates identified as heteroresistant. Through *in vitro* evaluation of some of these isolates, it was possible to compare the data obtained from WGS with the presence of *rpoB* SNPs in isolated subpopulations of Mtb and their susceptibility profile to RIF. Finally, this study highlights the role of mixed bacterial populations in TB diagnosis and treatment selection, focusing on RIF susceptibility.

Chapter III addresses the PonA1 protein characterization, the effect of the most frequent mutations found in clinical strains on the morphology of the mycobacterium and investigates the potential role of the *ponA1* gene in RIF resistance. Current evidence suggests statistically significant correlations between PonA1 mutations and RIF resistance, indicating these mutations, related to PG maintenance and regeneration, may enhance bacterial survival against the antibiotic. On another hand, in this chapter we used Mmar as a model organism to study RIF resistance, offering a closer phylogenetic relationship with lower-risk genetic manipulation capabilities.

Chapter IV introduces a web tool aggregating genetic and protein information from six mycobacterial species. This tool facilitates data retrieval and comparison of identity, homology, and protein structure prediction, linking hypothetical proteins to various secretion systems crucial in mycobacterial pathogenesis.

Chapter V, an integrated discussion is presented, synthesizing all the topics explored throughout the study. This section offers a cohesive analysis that connects the molecular mechanisms of RIF resistance, the role of *rpoB* and *ponA1* mutations, and

the importance of secreted proteins in Mtb pathogenesis. It also addresses the application of novel methodologies, such as the modified ORBIT technique, and the use of Mmar as a model organism. Furthermore, the discussion emphasizes how these findings contribute to the broader understanding of TB biology, resistance mechanisms, and the potential for identifying new therapeutic targets, providing a comprehensive conclusion to the research.

Finally, chapter V provides an overview of the study through an integrated discussion, limitations and perspectives based on the findings obtained as a result of this research.

Chapter II

Identifying rifampicin heteroresistant tuberculosis infection from whole genome analysis of peruvian isolates

Identification of rifampicin heteroresistant tuberculosis infection through whole genome analysis of peruvian isolates

Katherine Vallejos-Sánchez[a,b], Diego A. Taquiri-Díaz[a], Omar A. Romero-Rodriguez[a], Ana Paula Vargas[a], Jorge Coronel[a], Arturo Torres[c], Jose L. Perez[a], Adiana Ochoa[a], Robert H. Gilman[d], Louis Grandjean[c]; Martin Cohen-Gonsaud[b], Mirko Zimic[a*], Patricia Sheen[a*]

[a]Laboratorio de Bioinformática, Biología Molecular y Desarrollos Tecnológicos. Laboratorios de Investigación y Desarrollo. Facultad de Ciencias e Ingeniería. Universidad Peruana Cayetano Heredia, Av. Honorio Delgado 430, San Martín de Porres 15102, Peru.

[b]Centre de Biologie Structurale, CNRS, INSERM, 29 rue de Navacelles, 34090 Montpellier, France.

[c] Department of Infection, Immunity and Inflammation, Institute of Child Health, University College London, WC1N 1EH, London, UK.

[d] International Health Department. Johns Hopkins School of Public Health, 615 N. Wolfe Street, Baltimore, MD 21205, USA

This manuscript was submitted for peer-review to the Journal of Medical Microbiology. Minor changes have been introduced in the chapter below.

Author Contributions

Conceptualization, MZ, PS and KV ; methodology, KV and MZ, PS; investigation, KV, DT, OR, AO and JC; formal analysis, MZ, PS, DT, OR and KV; resources MZ and PS; data curation KV, DT, OR, AT, JP writing4original draft preparation, KV; writing4review and editing MZ, LG, MCG, AT, RHG and PS. All authors have read and agreed to the published version of the manuscript.

Funding

This research was funded by Prociencia, contract number 450-2019, supporting the Franco Peruvian Ph.D. program in Life Sciences and contract number PE501082878-2023, supporting the project <Desarrollo y evaluación de un protocolo basado en la secuenciación MinION (Nanopore) para determinar la heterorresistencia en pacientes con tuberculosis directamente de muestras de esputo=.

Institutional Review Board Statement

This study was approved by the Ethic Committee CAREG-ORVEI-004-23 from the Universidad ¨Peruana Cayetano Heredia.

Abstract

Introduction: This study underscores the critical role of identifying heteroresistant infections of *Mycobacterium tuberculosis* (Mtb) in enhancing the diagnostics of tuberculosis (TB). These conditions complicate diagnostics and treatment, underlining the need for advanced techniques to detect and characterize resistant populations effectively.

Hypothesis/ Gap statement: Current diagnostics may fail to identify heteroresistance and mixed infections, limiting the understanding of their impact on treatment outcomes.

Aim: This pilot study aimed to phenotypically and genotypically characterize rifampicin-heteroresistant clinical isolates and assess their genetic diversity and resistance patterns.

Methodology: A retrospective analysis of 2,917 Mtb genomes from Peru (1999-2020) was conducted using MTBseq and TBprofiler. Techniques included microscopic-observation drug-susceptibility indirect (MODS indirect), minimum inhibitory concentration (MIC) determination via tetrazolium microplate assay (TEMA), agar proportion method (APM) and sequencing. From each clinical isolate, three colonies were isolated from both RIF-supplemented (1 µg/mL) and drug-free media for subsequent phenotypic and genotypic characterization, including *rpoB* sequencing.

Results: Of the 2,917 genomes analyzed, 14.6% were classified as mixed infections, 3.8% exhibited heteroresistance to at least one drug between 21 antibiotics analyzed, and 0.79% were rifampicin-heteroresistant. Colonies from rifampicin-supplemented media displayed high resistance (MIC >1 µg/mL) with mutations such as S450L in the *rpoB* gene. In contrast, those from drug-free media exhibited sensitivity to rifampicin (MIC<1 µg/mL), harboring other *rpoB* mutations including D435Y, L452P, and L430P. Notably, some colonies retained wild-type *rpoB* sequences, suggesting a diversity of subpopulations within isolates.

Conclusion: WGS and phenotypic analysis confirmed the coexistence of rifampicin-susceptible and rifampicin-resistant Mtb populations within single clinical isolates. Subculturing in drug-free media favored the selection of sensitive strains, emphasizing the critical need for advanced diagnostic tools to accurately detect and characterize heteroresistant and mixed infections. These findings pave the way for more targeted treatment strategies to combat antimicrobial resistance in TB.

Keywords: Rifampicin, heteroresistance, mixed populations, tuberculosis, WGS.

II.1. Introduction

Tuberculosis (TB), caused by *Mycobacterium tuberculosis* (Mtb), remains a leading global health challenge and a significant contributor to antimicrobial resistance [1]. Efforts to control the disease are further complicated by the presence of mixed infections and heteroresistance, phenomena that reflect the pathogen9s genetic diversity and adaptative capabilities [2].

Mixed infections, defined as the simultaneous presence of multiple distinct Mtb strains within a single patient, represent a significant obstacle in TB management. These infections may arise through simultaneous transmission of multiple strains during a single infection event, sequential infections over time, or within-host diversification after a single infection [335]

Microbiological heterogeneity within a single patient has become an important item to study, due to its relationship with drug tolerance or drug resistance [3]. Mixed infections often lead to heteroresistance4a condition characterized by the coexistence of drug-susceptible and drug-resistant Mtb populations within the same clinical sample [6].This phenomenon complicates treatment, as resistant strains can thrive and proliferate under selective pressure while susceptible strains are suppressed [7,8]. The global presence of such complex infections represents a critical barrier to eradicating TB [9].

The clinical implications of mixed infections are profound. Patients with multiple Mtb strains are at a higher risk of poor treatment outcomes. Dickman *et al.* [10] reported that patients with multiple Mtb strains showed similar proportions of Mtb

smear-positive cultures after two and five months of treatment. Approximately 22.9% of patients with mixed infections experienced treatment failures after six months, and 24% demonstrated heteroresistance, suggesting a strong link between these phenomena and treatment failure [11]. These findings emphasize the need for advanced diagnostic tools capable of detecting mixed infections and profiling their resistance patterns.

Whole genome sequencing (WGS) has emerged as a transformative tool in TB research, enabling detailed genetic analysis to identify mixed infections and provides comprehensive resistance profiles. Recent studies have revealed that mixed infections, including those resistant to rifampicin (RIF) and isoniazid (INH), constitute approximately 1% of isolates globally, with rates exceeding 5% in certain countries [12]. This variability underscores the need for region-specific strategies to address the challenges posed by mixed infections.

In Peru, the incidence of multidrug-resistant TB (MDR-TB) increased markedly between 1999 and 2020, rising from 50 to 200-300 cases per 100,000 population [13]. This alarming trend underscores the urgent need for improved diagnostic and treatment strategies. Moreover, Peru9s high MDR/RR-TB burden highlights the critical importance of addressing mixed infections and heteroresistance.

This study aims to deepen the understanding of the genotypic and phenotypic diversity in Mtb within individual patients, focusing on primary cultures identified as heteroresistant to RIF based on their WGS and drug susceptibility tests (DST). By characterizing these diversities, we can enhance diagnostic accuracy and tailor treatment strategies more effectively, ultimately improving treatment outcomes and reducing the transmission of resistant TB strains.

II.2. Methodology

II.2.1. *M. tuberculosis* genome data analysis, mixed infections and *in-silico* RIF heteroresistance determination

WGS data from 2945 Mtb clinical isolates processed by the Peruvian Tuberculosis group were assembled and analyzed using the reference strain H37Rv (NC_000962.3) with the MTBseq [14] and TBprofiler pipelines (https://tbdr.lshtm.ac.uk/) [15]. These isolates were sequenced as part of previous studies conducted by the Peruvian Tuberculosis Group, and sequencing data have been made publicly available in the European Nucleotide Archive (ENA) under the project accessions PRJEB5280, PRJEB32234, PRJEB23245, and PRJEB39837, with detailed accession numbers listed in the supplementary material.

The genomes were filtered based on the percentage of mapped reads (using a cutoff of 90%), and an average depth greater than 40X. The genotypic profiles derived from MTBseq and TBprofiler analyses were compared to gain comprehensive insights into drug resistance. A single nucleotide polymorphisms (SNPs) database was also compiled and cross-referenced with the MODS test, which provided phenotypic information from our databases and health centers to determine the RIF susceptibility profile.

For lineage classification, TBprofiler uses the SNP database consistent with the gold-standard regions of difference classification system proposed by Coll et al. [16] and the SNP barcode refined by Napier et al. [17] which consider 90 SNP in the analysis.

Heteroresistance analysis was performed by the TB-profiler pipeline [15] in its command-line version 4.4.2 with default settings. This software used variant calling on candidate antibiotic resistance genes in TB using its built-in database, TBDB [18]. We required a minimum depth of 10 reads for identifying polymorphisms and set the minimum allele frequency for calling a variant at 0.1. Reads cleanup was conducted using Trimmomatic version 0.39, mapping with Burrows-Wheeler Aligner (BWA) version 0.7.17, and variant calling with FreeBayes version 1.3.5.

II.2.2. Reactivation of primary cultures of *M. tuberculosis* for drug susceptibility testing.

Two groups of four primary cultures, previously characterized by WGS and drug susceptibility profiles determined by microscopic-observation drug-susceptibility (MODS), were processed: one classified as rifampicin-heteroresistant and the other classified as susceptible to RIF. These isolates were randomly selected.

The rifampicin-heteroresistant group includes different drug susceptibility profiles determined by MODS in the sputum sample: one isolate was reported as susceptible (1R), one as RR-TB (4R) and two as MDR-TB (2R-3R). The second group included susceptible strains identified through genomic analysis and MODS (codification name CA-1012 (1S), CA0957 (2S), 28832_3#219 (3S), 28889_1#17 (4S)). These samples were requested from the Peruvian Tuberculosis group as they are part of the collection for the period 1999-2020.

For the re-activation, an aliquot of the glycerol stock was cultured in 2 mL of Middlebrook 7H9 (DB Difco, USA) liquid medium, supplemented with 10% OADC

(oleic acid, albumin, dextrose, catalase) and 0.5% glycerol (7H9-OADC), they were incubated for 7-10 days at 37°C. Subsequently, 100 µL of this culture was transferred to Middlebrook 7H10 (DB Difco, USA) solid medium, also supplemented with 10% OADC and 0.5% glycerol (7H10-OADC), and then incubated for 21-30 days at 37°C, these isolates are henceforth referred to as secondary cultures. Mtb H37Rv (pan-susceptible) and DM97 (MDR clinical isolate) were used as control strains.

For each isolate the susceptibility was determined by MODS indirect, MIC determination by Tetrazolium Microplate Assay (TEMA) and Agar Proportion Method (APM). All procedures were performed at a P3 security level facility. A graphical summary for all procedures is shown in Figure II.1.

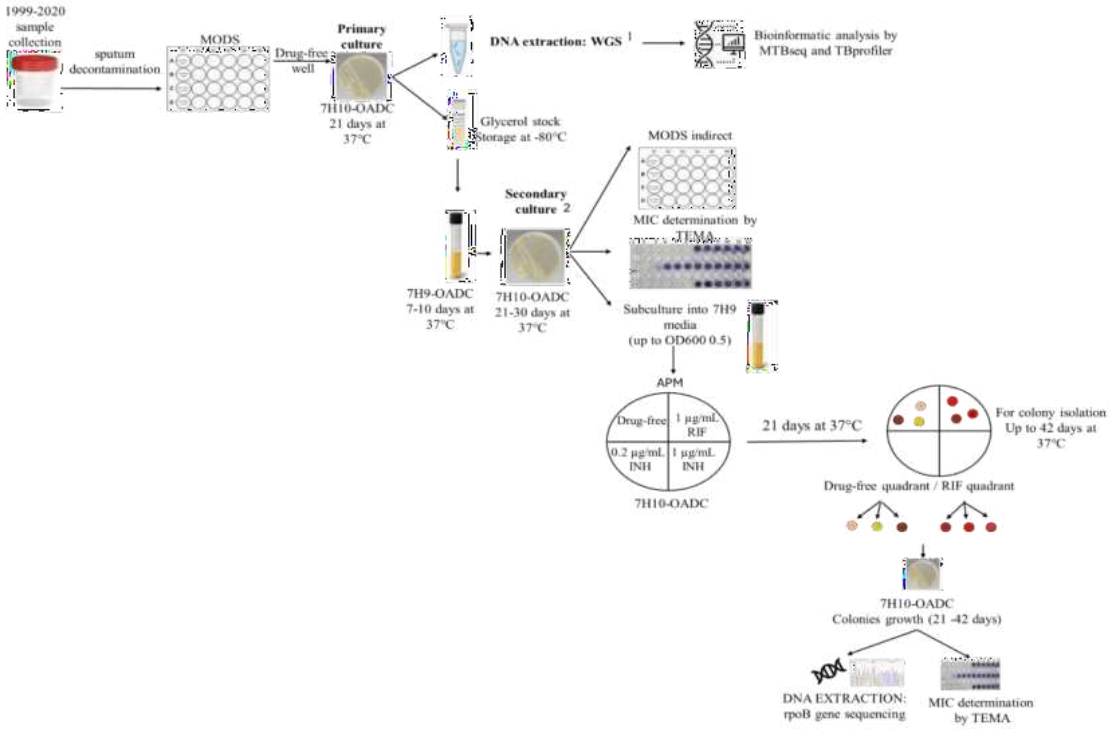

[1] WGS analyzed in this study.
[2] Starting point of cultivations after RIF heteroresistant strains selection

Figure II.1. Graphical summary of methodology in the analysis of *M. tuberculosis* heteroresistant/susceptible isolates.

II.2.3. Microscopic-observation drug-susceptibility indirect (MODS indirect)

The protocol developed by Caviedes et al. [19] was adapted for use with clinical isolates. Briefly, from a 21-day Mtb secondary culture, a suspension equivalent to the McFarland 1 scale was prepared by resuspending approximately two loops of the culture in a mix solution (200 µL tween 80 10% into 50 mL of sterile distilled water). Then, 5 µL of this suspension was inoculated into a total volume of 5 mL of 7H9-OADC. 900 µL of this dilution was placed into each well of a 24-well plate containing 100 µL of 7H9-OADC, 7H9-OADC with 1µg/mL RIF and 7H9-OADC with 0.4 µg/mL INH. The plates were incubated at 37°C, with the first examination under an inverted microscope on day 6, followed by monitoring until 21 days.

II.2.4. Minimal inhibitory concentration determined by tetrazolium microplate assay (TEMA)

To determine the MIC for RIF, TEMA test, which uses 3-(4,5-dimethylthiazol-2-yl)-2,5 diphenyl-tetrazolium bromide was performed following the previous protocol standardized by our group [20].

Briefly, 96-well plates (Corning REF 3599) were prepared with final antibiotic concentrations as follows: 32 µg/mL for INH, 16 µg/mL for RIF, 32 µg/mL for streptomycin (SM), 128 µg/mL for ethambutol (EMB), 8 µg/mL for capreomycin (CAP) and 16 µg/mL for ciprofloxacin (CIP) [21] and put them in column 2. Serial dilutions were performed in 100 µL Middlebrook 7H9 - OADC from column 3 to 10. Column 11 was used as a control well without antibiotics.

From a 21 to 30 day Mtb culture, a suspension equivalent to McFarland 1 scale was prepared by resuspending approximately two loops of the culture in a mix solution (200 µL tween 80 10% into 50 mL of sterile distilled water). A 1:25 dilution was made in 7H9-OADC. Then, 100 µL of this dilution was inoculated onto the plate, which was incubated at 37°C.

On the day 5 of incubation, 50 µL of a fresh mixture of 0.1% tetrazolium diluted in absolute ethanol and 10% tween 80 (1:1) was added to the control well and incubated at 37°C for 24 h. If the well remains yellow, the incubation was extended for another 24 h at 37°C. If the well remains yellow, the plate is further incubated for up to 20 days. However, if the well-turned purple due to formazan formation, the tetrazolium-tween 80 was added to all the wells and the color was assessed after 24 hours.

II.2.5. Determination of the percentage of rifampicin-resistant *M. tuberculosis* population by agar proportion method (APM)

APM determines the proportion of mutants within a mycobacterial population that are resistant to a specific drug. After 21 days of secondary culture on 7H10-OADC, strains were grown in 7H9-OADC to reach log phase, in the absence of antibiotics. Cultures were then adjusted to a 0.5 McFarland standard using physiological saline solution and serially diluted (10^-2 and 10^-4). Approximately 100 µL from each dilution was inoculated in triplicated on 7H10-OADC, across quadrants with varying conditions: (1) drug-free, (2) 1 µg/mL INH, (3) 0.2 µg/mL INH and (4) 1 µg/mL RIF. Cultures were incubated at 37°C for 3 weeks and the colony-forming units (CFUs) were counted. Resistance proportion was calculated by comparing colony numbers in

antibiotic-supplemented media quadrants to those in the drug-free media quadrant. Clinical isolates were deemed resistant if this percentage was over 1% [22,23], according to CLSI guidelines. Clinical isolates previously registered as susceptible to INH and RIF were evaluated under the same conditions. Mtb H37Rv (pan-susceptible) and DM97 (MDR clinical isolate) were used as a control.

II.2.6. Colonies isolation from the secondary culture

It was performed on six colonies per isolate: three from the drug-free quadrant and three from the RIF-exposed (1 µg/mL) quadrant, corresponding the inoculum with 10^-4 dilution (Figure II.2). They were replicated on 7H10-OADC and incubated for 21-42 days at 37°C and a subculture to obtain a full plate was performed under the same conditions. DNA extraction for *rpoB* gene sequencing and MIC determination by TEMA were performed for each colony.

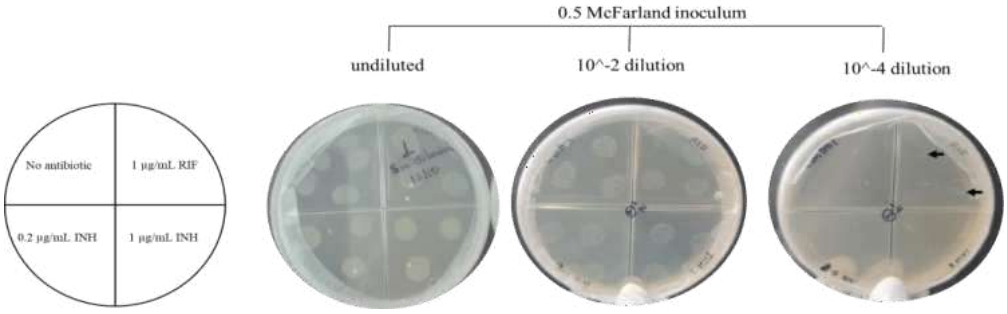

Figure II.2. Agar proportion method for *M. tuberculosis* strain. Arrows indicate isolated colonies.

II.2.7. DNA genomic extraction

Mtb DNA was extracted using the proteinase K digestion method. Briefly, Mtb culture was resuspended in 500 µL TE buffer and inactivated at 100°C for 30 minutes.

50 µL of lysozyme (Sigma, USA) (10 mg/mL) was added to the inactivated bacteria and incubated overnight at 37°C. Subsequently, 75 µL of 10 % SDS (J.T.Baker, USA) and 20 µL of proteinase K (Ambion, Life Technologies, USA) (20 mg/mL) were added, followed by incubation at 65°C for 3 hours with homogenization every 20 minutes for 20 seconds. After incubation, 100 µL of 5M NaCl (Merck, USA) and 100 µL of pre-heated CTAB/NaCl at 65°C were added, mixed and incubated at 65°C for 10 minutes. Then, 750 µL of phenol-chloroform-isoamyl alcohol (EMD Millipore, USA) (25:24:1) was added, mixed, and centrifuged for 5 minutes at 10,000 rpm. The supernatant was recovered in a new tube. To this, 750 µL of chloroform-isoamyl alcohol (24:1) was added, homogenized, and centrifuged for 5 minutes at 10,000 rpm, with the supernatant again transferred to a new tube. DNA was precipitated using 1 mL of cold (-20°C) absolute ethanol (EMD Millipore, USA) and washed with 1 mL of cold (-20°C) 70% ethanol. The supernatant was discarded, the pellet dried and DNA resuspended in 50 µL of the elution buffer, then incubated at 55°C for 15 minutes to dissolve the pellet. DNA quantification was performed using a spectrophotometer (Nanodrop 2000c).

II.2.8. *rpoB* gene amplification and sequencing

The PCR mixture included 100 ng of genomic DNA, 2X Phusion Flash High Fidelity PCR Master Mix (Thermo Scientific), and 0.5 µM of each primer F-ext-rpoB (59-GACAAAATTATCGCGGCGAACG-39) and R-ext-rpoB (59TCGCCATAGGACCATTGCCTGA-39). The cycling conditions were set at 98°C for 30 seconds for initial denaturation, followed by 30 cycles of 98°C for 10 seconds, 68°C for 30 seconds, and 72°C for 2 minutes (Biorad).

The amplicons were purified with a DNA clean and concentrator kit following the manufacturer9s instructions (Zymo research). DNA quantification was measured by spectrophotometer (Nanodrop 2000c) and quality by Qubit® dsDNA HS Assay Kit (Thermo Fisher Scientific, Waltham, MA, USA). Then, it was normalized at a final concentration of 50 ng for each sample.

Samples were prepared for sequencing in the Laboratorio de Bioinformatica y Biologia Molecular - LID-UPCH-Peru, following the manufacturer instructions for Oxford nanopore technologies. Then, R10.4.1 flow cells were utilized for sequencing on a GridION (ONT, Oxford, UK) for a duration of 72 hours. Finally, an analysis for variant calling was performed with the pipeline EPI2ME/wf-amplicon Bioinformatics resources from Oxford Nanopore Technologies Plc (https://github.com/epi2me-labs/wf-amplicon).

II.3. Results

II.3.1. *M. tuberculosis* genome data analysis, mixed infections and *in-silico* RIF heteroresistance determination

RIF susceptibility analysis classified 76.35% for MTBseq and 76.24% for TBprofiler as sensitive strains, indicating similar prediction accuracies by both pipelines. 20.05% and 20.26% strains were classified as genetically and phenotypically RR-TB isolates with MTBseq and TBprofiler, respectively (agreement percentage 96.4 and 96.5%; Coefficient Kappa 0.895 and 0.899, respectively) (Table II.1).

The discordance rate between genotypic resistance (presence of SNPs associated with RR-TB) and phenotypic susceptibility (susceptible to RIF in negative MODS) for both pipelines was 2.57 - 2.67%. Discordance for strains lacking SNPs (related to RIF susceptible) but testing as RIF resistance in MODS ranged between 1.03 and 0.82% (Table II.1).

Table II.1. Percentage concordance between phenotypic susceptibility determined by MODS and genotypic susceptibility from WGS for rifampicin, analyzed by MTBseq and TBprofiler.

N=2917	MTBseq		TBprofiler	
MODS	Resistant (%)	Sensitive (%)	Resistant (%)	Sensitive (%)
Resistant (%)	20.05	1.03	20.26	0.82
Sensitive (%)	2.57	76.35	2.67	76.24
Agreement (%)	96.4		96.5	
Coef. Kappa	0.895		0.898	

The results showed that the frequency of some SNPs in *rpoB* did not represent 100%, so this information opens the possibility that other SNPs are present in lower abundance. To evaluate this, 2945 genomes were evaluated and quality filtering was applied. After the quality filtering, 2917 isolates were analyzed by TBprofiler and various subpopulations were categorized as follows: isolates resistant to at least one drug (39.5%), MDR (18.8%), mixed infections (14.6%), heteroresistant to at least one drug (3.8%), and specifically rifampicin-heteroresistant (0.79%). Additionally, 9,5% of the isolates were identified as heteroresistant and MDR at the same time (Figure II.3).

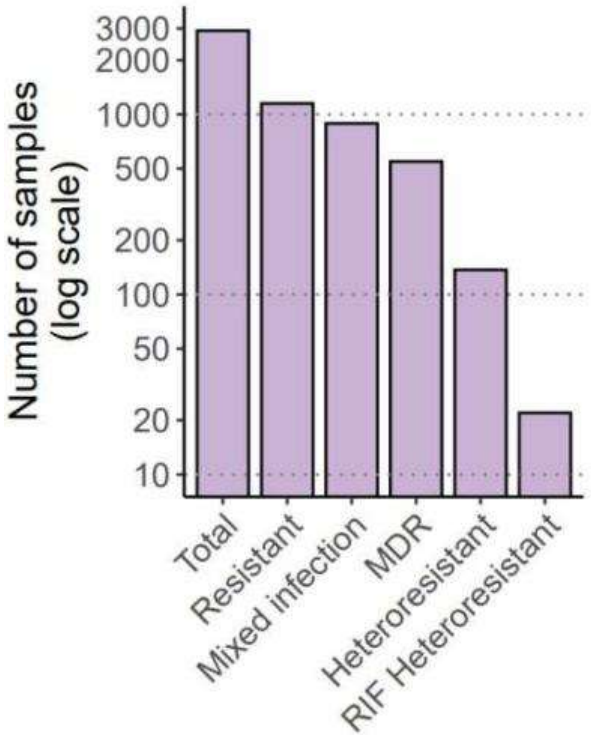

Figure II.3. Genotypic resistance profile of 2917 Mtb clinical isolates from Peru collected between 1999-2020. Strains were filtered with over 90% of reads mapped and an average depth exceeding 40X. MDR= Multi drug-resistant, RIF= rifampicin

23 isolates were detected as rifampicin-heteroresistant, and it is noteworthy that these isolates have between one to three SNPs in the *rpoB* gene and the SNP frequency varies from 11 to 85%, as detailed in Table II.2. It is important to note that in this analysis, some isolates contain a single sublineage, while others have up to two Mycobacterial sublineages per isolate.

II.3.2. Microscopic-observation drug-susceptibility indirect (MODS indirect)

In the rifampicin-heteroresistant group, resistance to RIF was observed in 2 out of 4 samples by day 6, increasing to 3 out of 4 by day 14 post-inoculation (Appendix II.2). One of them, the isolate 3R exhibited slower growth compared to other isolates by day 14, while isolate 1R showed growth by day 21 (data not shown).

In the susceptible isolates group, all were sensitive in the same period. Our H37Rv pan-sensitive control strain showed no growth in the well containing RIF until day 14, while the MDR control strain demonstrated growth by day 6 in the presence of RIF. Results for INH (0.4 µg/mL) are also shown in Appendix II.2, thus we determined the MDR-TB phenotype for clinical isolates 1R, 2R, and 3R; while clinical isolate 4R is RR-TB.

II.3.3. Minimal inhibitory concentration determined by tetrazolium microplate assay (TEMA)

TEMA assay was performed in our study and strains with a discrepant phenotype in the Rifampicin-heteroresistant group were found as shown in appendix II.3. In the rifampicin-heteroresistant group, isolate 1R maintained a susceptibility profile, isolate 2R was reported as RR-TB (MIC >16 µg/mL), while isolates 3R and 4R, discrepant to the primary culture, were reported as susceptible (MIC =0.063 µg/mL).

None of the susceptible strains were reported as RR-TB, consistent with their initial profile. Pan-sensitive H37Rv and clinical MDR DM97 maintained their profile.

II.3.4. Determination of the percentage of rifampicin-resistant *M. tuberculosis* population by agar proportion method (APM)

The genotypically rifampicin-heteroresistant group had a resistant proportion from 2.5 to 85%. All susceptible clinical isolates keep the susceptible profile (Appendix II.4). The pan-sensitive H37Rv strain grew only in the drug-free quadrant, while the DM97 MDR strain exhibited consistent growth in quadrants containing RIF (1 µg/mL) and INH (0.2 µg/mL and 1 µg/mL).

Table II.2. Genotypic characteristics of clinical isolates characterized as rifampicin-heteroresistant by genomic analysis by TB profiler and MTBseq.

Clinical isolate ID**	MODS*	MTBseq	TB PROFILER				
		RIF_rpoB allele proportion	RIF_rpoB allele proportion	Main lineage***	Sub lineage	Number of sub lineages	DR type
LI2174109	RR	S450L (0.8)	S450L (0.80)	4	4.3.3	1	MDR
PLE-0891	RR	S450L (1.0)	T400A (0.18), S450L (1.00)	4	4.3.2	1	MDR
PMFR-0719	RR	M434I (0.84), D435G (0.83), P454L (0.88)	M434I (0.84), D435G (0.85)	4	4.9; 4.3.4.1	2	MDR
PMFR-0732	MDR	D435Y (1.0), V695L (0.99)	D435Y (1.00), A451V (0.20)	4	4	1	MDR
PMFR-0737 4R	RR	--	L430P (0.11), H445D (0.64), L452P (0.17)	2	2.2.1	1	RR
PMOP-0526	MDR	S450L (0.85)	S450L (0.85)	4	4.3.3	1	MDR
PMOP-0618	MDR	S450L (1.0)	S450L (1.00), I480V (0.41)	4	4.1.2.1	1	Pre-XDR
PSLM-0811	MDR	S450A (0.75), S450L (1.0), V695L (1.0)	S450V (0.74)	4	4	1	Pre-XDR
PSLM-0843	MDR	S450L (0.78)	S450L (0.79)	4	4.3.3	1	MDR
PTAN-0241	MDR	S450L (1.0)	S450L (1.00), E761D (0.69)	4	4.3.4.1	1	MDR
28832_3#257	MDR	--	S450L (0.71)	4	4.3.3; 4.3.2	2	MDR
CA-0116 1R	Sus	D435Y (0.8)	D435Y(0.79), L452P (0.16)	1	1.2.1.2.1	1	MDR
28832_4#246	Sus	V695L (0.76)	S450L (0.32)	4	4.3.4.2	1	MDR
28832_4#250	MDR	--	S450L (0.70)	4	4.3.4.2	1	MDR
28832_4#318	Sus	D435V (0.84)	D435V (0.82)	4	4.4.1.1; 4.3.3	2	MDR
28889_1#38	MDR	S450L (1.0), I480V (0.8)	S450L (1.00), I480V (0.77), R552C (0.17)	4	4.1.1	1	MDR
28889_1#95	MDR	D435Y (1.0), V695L (1.0)	D435Y (1.00), L452Q (0.25)	4	4	1	MDR
29544_1#13 3R	MDR	--	S450L (0.24)	4	4.3.4.2; 4.1.2.1	2	MDR
29544_1#232 2R	MDR	S450L (0.81)	S450F (0.83)	4	4.1.2.1; 4.1.1	2	Pre-XDR
29544_1#316	Sus	--	D435V (0.42)	4	4.3.3; 4.3.2	2	MDR
29544_1#337	MDR	--	D435V (0.45)	4	4.3.3; 4.3.2	2	MDR
29544_1#6	MDR	--	D435V (0.26)	4	4.3.3; 4.1.2.1	2	MDR
28832_3#91	RR	S441L (0.81)	S441L (0.82), L452P (0.18)	4	4.8	1	RR-TB

*MODS: Susceptibility profile as determined by MODS for the Peruvian tuberculosis group or primary health centers, Sus= susceptible; RR= Rifampicin resistant, MDR= multidrug resistant, Pre−XDR= Pre−extensively drug resistant. **Isolates randomly selected for experimental analysis are codified as 1R, 2R, 3R and 4R and they are shown in bold type. *** Lineage 1= Indo-Oceanic, Lineage 2= East-Asian, Lineage 4= Euro-american.

Table II.3. Minimum inhibitory concentration determined by TEMA in selected *M. tuberculosis* clinical isolates.

Strain ID*	Mtb clinical isolates**		Colonies					
	DR Genotypic status	MIC TEMA RIF (µg/mL)	Colony ID Free-drug quadrant	MIC TEMA RIF (µg/mL)	Phenotypic status	Colony ID RIF quadrant	MIC TEMA RIF (µg/mL)	Phenotypic status
1R	RIF-heteroresistant	0.125	1	<0.063	Sus	1	0.125	Sus
			2	<0.063	Sus	2	0.125	Sus
			3	<0.063	Sus	3	0.125	Sus
R	RIF-heteroresistant	>16	1	>16	Res	1	>16	Res
			2	>16	Res	2	>16	Res
			3	>16	Res	3	>16	Res
3R	RIF-heteroresistant	0.063	1	0.063	Sus	1	>16	Res
			2	0.063	Sus	2	>16	Res
			3	0.063	Sus	3	>16	Res
4R	RIF-heteroresistant	0.063	1	0.125	Sus	1	>16	Res
			2	0.125	Sus	2	>16	Res
			3	0.125	Sus	3	>16	Res
1S	Susceptible	0.063	1	0.125	Sus	-	-	
			2	0.063	Sus	-	-	
			3	0.063	Sus	-	-	
2S	Susceptible	0.063	1	0.125	Sus	-	-	
			2	0.063	Sus	-	-	
			3	0.063	Sus	-	-	
3S	Susceptible	0.25	1	0.125	Sus	-	-	
			2	0.125	Sus	-	-	
			3	0.125	Sus	-	-	
4S	Susceptible	0.063	1	0.063	Sus	-	-	
			2	0.063	Sus	-	-	
			3	0.063	Sus	-	-	
H37Rv	pan-susceptible	0.063	1	<0.063	Sus	-	-	
			2	<0.063	Sus	-	-	
			3	<0.063	Sus	-	-	

*Isolates 1R, 2R, 3R, and 4R were randomly chosen from Table 2, while isolates 1S, 2S, 3S, and 4S were selected from those classified as susceptible by TBprofiler and MODS. ** Among the isolates classified by TBprofiler as heteroresistant to RIF based on genomic analysis, one susceptible isolate, one RR-TB, and two MDR-TB isolates4determined by MODS from sputum samples4were randomly selected for evaluation. Sus= susceptible; Res= resistant.

II.3.5. Drug susceptibility test for colonies isolates from secondary culture

Upon colony isolation, it was observed that 50% exhibited strong phenotype differences between colonies from the antibiotic-free quadrant and those from the RIF-exposed (1 µg/mL) quadrant (Table II.3). In the isolates, 3R and 4R, colonies from the drug-free quadrant were susceptible (MIC < 1 µg/mL), whereas colonies from the RIF-exposed quadrant showed resistance (MIC >16 µg/mL). Colonies from both quadrants of isolate 2R displayed identical resistance patterns to RIF (MIC >16 µg/mL). In contrast, isolated 1R showed varied RIF susceptibility profiles, but with a slight difference between colonies isolated from the drug-free quadrant (MIC< 0.063 µg/mL) and those isolated from the RIF-exposed quadrant (MIC=0.125 µg/mL). Susceptible strains keep the same drug profile including the pan-sensitive H37Rv.

II.3.6. DNA extraction, *rpoB* amplification, and sequencing

DNA concentrations ranged from 50 to 200 ng/¼L with purity ratios of 260/280 and 260/230 both between 1.8 to 2.0. For PCR, concentrations between 10 to 100 ng of DNA per sample were used, amplifying a 3728 bp product covering a full-length *rpoB* gene. Synonymous *rpoB* mutations, including A1075A (T3225C), A36A (T108C), D103D (C309T), and P483P (T1449C), are not shown. Table II.4 summarizes all the analyses performed for this study, where considering the initial DST for the primary culture, the genomic analysis based on WGS with two softwares: MTBseq and TBprofiler, this table included as well the phenotypic analysis for secondary culture after cryopreservation considering MODS indirect, DST determined by TEMA and the APM. Finally, a

characterization phenotypically for RIF susceptibility by TEMA and *rpoB* sequencing was performed for colonies obtained from the isolates belonging to secondary cultures of Mtb clinical strains.

Isolate 1R, initially in the sputum sample it was identified as susceptible by MODS, was classified as resistant by MTBseq due to the D435Y mutation at 80% and heteroresistant by TBprofiler with the same mutation at 79% and L452P at 16 %. WGS analysis identified this isolate as belonging to the Indo-Oceanic lineage and the sublinage 1.2.1.2.1. In the secondary culture, both APM and MODS indirect tests identified it as RR-TB, while the TEMA showed a susceptible profile. APM analysis indicated that a small portion of the population (2.5%) was resistant and notably, this isolate exhibited slower growth in MODS indirect testing compared to other isolates. Colonies from the drug-free quadrant harbored both WT and D435Y *rpoB* mutations with a RIF-susceptible phenotype, and colonies from the RIF quadrant also maintained a RIF-susceptible phenotype with the D435Y mutation.

Isolate 2R analyzed by MTBseq and TBprofiler showed the S450L and S450F *rpoB* mutations, respectively, both with abundances over 80%. Two sublineages, 4.1.2.1 and 4.1.1, were predicted to harbor in this isolate. Experimentally, the evaluation of this isolate showed consistency as RR-TB across all tests. Colonies from both quadrants, drug-free, and RIF-supplemented, maintained the RR-TB profile with the S450F mutation in the *rpoB*. This mutation appears to be fixed within the population, as only bacilli carrying this mutation could be recovered from the colonies, regardless of drug exposure at the time of isolation.

Isolate 3R revealed the S450L mutation at 24% via TBprofiler, with no mutations detected by MTBseq, and two sublineages were found in the sample sublineage 4.3.4.2 and sublineage 4.1.2.1. TEMA classified this isolate as RIF susceptible but colonies from RIF quadrants harbored the S450L mutation and exhibited a RR-TB phenotype, while those from drug-free quadrants showed RIF susceptibility.

4R was identified to harbor a single lineage 2.2.1 analyzed by TBprofiler, which showed L430P, H445D, and L452P mutations, undetected by MTBseq. In secondary culture, MODS indirect, and APM indicated RR-TB, yet TEMA showed susceptibility to RIF. Drug-free quadrant colonies had L452P and L430P mutations and were susceptible to RIF by TEMA, while RIF-exposed colonies with the S450L mutation showed resistance. Clinical isolates identified as RIF-susceptible in primary culture remained susceptible in subsequent DST, with no colonies obtained in the APM. No mutations related to RIF resistance were reported for these strains. The pan-sensitive H37Rv strain maintained a RIF-susceptible profile throughout all tests performed, similar to the clinical isolates.

Table II.4. Genotype and phenotype comparison involved primary culture, secondary culture and colonies from selected clinical isolates.

Sus= susceptible, Res= resistant; RIF cut off : 1µg/mL; Heterores= Heteroresistant. L430P, D435Y, H445D and L452P substitutions in RpoB are considered borderline mutations that confer low-level RIF resistance WHO (2021).

Isolate ID	Analysis from primary cultures				RIF susceptibility from secondary cultures			Colony isolation from secondary cultures					
								Drug-free quadrant			RIF quadrant		
	MODS RIF	*rpoB* MTBseq (%)	*rpoB* TBprofiler (%)	Genotypic status TBprofiler	MODS reverse	TEMA	APM (% Resistance)	Colony ID	TEMA	*rpoB* sequence	Colony ID	TEMA	*rpoB* sequence
1R	Sus	D435Y (80) WT (20)	D435Y (79), L452P (16) WT (5)	RIF heterores	Res	Sus	Res (2.5)	1	Sus	D435Y	1	Sus	D435Y
								2	Sus	WT	2	Sus	D435Y
								3	Sus	WT	3	Sus	D435Y
2R	Res	S450L (81) WT (19)	S450F (83) WT (17)	RIF heterores	Res	Res	Res (85)	1	Res	S450F	1	Res	S450F
								2	Res	S450F	2	Res	S450F
								3	Res	S450F	3	Res	S450F
3R	Res	-	S450L (24) WT(76)	RIF heterores	Res	Sus	Res (1.8)	1	Sus	WT	1	Res	S450L
								2	Sus	WT	2	Res	S450L
								3	Sus	WT	3	Res	S450L
4R	Res	-	L430P (11), H445D (64), L452P (17) WT (8)	RIF heterores	Res	Sus	Res (53)	1	Sus	L452P	1	Res	S450L
								2	Sus	L430P	2	Res	S450L
								3	Sus	L452P	3	Res	S450L
1S	Sus	-	-	Sus	Sus	Sus	Sus	1	Sus	WT	-	-	-
								2	Sus	WT	-	-	-
								3	Sus	WT	-	-	-
2S	Sus	-	-	Sus	Sus	Sus	Sus	1	Sus	WT	-	-	-
								2	Sus	WT	-	-	-
								3	Sus	WT	-	-	-
3S	Sus	-	-	Sus	Sus	Sus	Sus	1	Sus	WT	-	-	-
								2	Sus	WT	-	-	-
								3	Sus	WT	-	-	-
4S	Sus	-	-	Sus	Sus	Sus	Sus	1	Sus	V695L	-	-	-
								2	Sus	V695L	-	-	-
								3	Sus	V695L	-	-	-
H37Rv	Sus	-	-	pan-S	Sus	Sus	Sus	1	Sus	WT	-	-	-
								2	Sus	WT	-	-	-
								3	Sus	WT	-	-	-

II.4. Discussion

Globally, although the proportion of MDR/RR-TB cases has declined, our findings highlight the persistent and escalating challenge in regions like Peru, where RR-TB cases have increased significantly by 80.7% from 2021 to 2022 according to the latest statistics [24]. Our comprehensive study underscores the significant prevalence and complexity of heteroresistance in TB, particularly in RIF resistance.

For RIF, a potent anti-TB drug, resistance is primarily due to mutations in the *rpoB* gene's RIF resistance determining region, with frequencies ranging from 85.2 to 90% [25,26], in our study, this accounted for 96.1% of the RR-TB population. Conversely, Zheng et al. [27] found that 3.8% of RR-TB clinical isolates had no mutations in the *rpoB* gene, similarly to our study, which identified 3.9% of such strains. In the RIF-susceptible population, Su et al. [25] reported that 9% of TB strains had *rpoB* mutations, compared to 3.4% in our study when analyzed with the MODS test. In addition, Aung et al. [28] found a *rpoB* mutation rate of 10.1% in clinical isolates prior to RIF treatment, indicating the complexity of the genetic landscape.

This genetic complexity is also evident in mixed infections, which cannot always be detected by traditional clinical diagnostic methodologies. For example, in Peruvian samples, where the percentage of mixed infections was 1.4%, determined by spoligotyping and 15-locus MIRU-VNTR analysis, however, 23.5% of the MDR isolates analyzed in that study could not be assigned to a lineage [29]. The prevalence of mixed infections varies greatly by geographic location, ranging from as low as 0.4% to as high as 57%, with higher rates generally observed in regions with intensive TB

transmission [30,31], being more important in regions where prevalence is high and especially when related to heteroresistance. Sobkowiak et al. [32] used WGS to identify mixed infections *in silico* when the minor strain exceeded 10%, finding a frequency of approximately 10% for this population. In our study, using the same threshold, 14.6% were involved in mixed infections and 3.8% of the Peruvian clinical isolates analyzed displayed heteroresistance to at least one drug between 21 drugs evaluated, underscoring the complexity of TB infections and the need for advanced bioinformatic tools to identify these variations. Moreover, 23 isolates (23/2917= 0.79%) were identified as rifampicin-heteroresistant by TBprofiler; of these, 91,3% (21/23 isolates) belonged to Lineage 4 (Euro-American), while 4.35% (1/23) belonged to Lineages 1 (Indo-Oceanic) and 2 (East-Asian) each. Among the Lineage 4 isolates, 65.2% had a single sublineage and 34.8% had two sublineages. This is particularly critical given the geographic and lineage-specific variability in drug resistance and transmissibility of Mtb strains, with certain lineages such as Lineage 2 and Lineage 4 showing higher risks of drug resistance and widespread distribution, respectively [33-36]. Our results are consistent with Hofmann-Thiel S et al. [6], who proposed two mechanisms for heteroresistance: superinfection by two different lineages or diversification of a single lineage into susceptible and resistant strains, the latter being more likely to relapse.

Additionally, our results reflect the most prevalent tuberculosis lineages circulating in Perú, as reported by Barletta et al., [29] and Grandjean et al., [37]. Lineage 4 accounts for 58.5 to 68% of cases, while lineage 2, the second most common, represents 9 to 16.4% of cases. These lineages also dominate among isolates with extensively drug-resistant profiles [38].

Among the isolates analyzed we have the isolate 1R, it belongs to sublineage 1.2.1.2.2.1, which is associated with Southeast Asia [39] and has low prevalence in Peru. It is important to remark because in secondary culture for MODS indirect, this isolate exhibited delayed growth by day 21, unlike other isolates. In the APM, isolate 1R showed a ratio of 2.5%, while isolate 3R, which also had a low proportion (1.8%), grew in MODS indirect by day 14. This indicates that isolate 1R contains slow-growing strains and possesses *rpoB* mutations categorized as borderline [26], complicating the accurate identification of its resistance profile due to partial resistance to RIF. Mutations in the *rpoB* gene may affect the growth rate and vary the relative fitness [40,41], these mutations can also be influenced by the genetic background and affect the potential transmission [42]. However, the reason why some strains grow later than others remain unclear.

In the analysis of colonies from isolate 3R, two distinct populations were identified: one with wild-type *rpoB* exhibiting a susceptible RIF phenotype, and the other with the S450L mutation displaying RR-TB. This mutation was present at 24% in the WGS analysis from the primary culture and dropped to 1.8% in secondary culture when quantified by the APM, indicating a significant decrease in the population harboring the mutation. This phenomenon of predominant populations outgrowing minority ones in culture, which may obscure mixed infections, was also noted by Martin et al. [43] in conventional liquid cultures and by Metcalfe et al. [44] in subcultures carried out in the absence of drugs. It is expected that changes in population ratios can be influenced by *in vitro* sample processing [45]. Additionally, Metcalfe et al. [44] categorized heteroresistant samples into macroheteroresistance (5-95% of the

total population) and microheteroresistance (less than 5% of the total population), noting that the diversity of heteroresistant subpopulations decreases with serial cultures, especially when it is less than 1%.

In the case of isolate 4R, the genomic analysis performed by TBprofiler identified three mutations in the *rpoB*: L430P, H445D, and L452P, with proportions of 11%, 64%, and 17%, respectively. In secondary culture, 53% of the population displayed heteroresistance to RIF determined by APM. Subsequent analysis of colonies identified mutations S450L, L452P, L430P, and H445D (data not shown). The L452P and L430P mutation, isolated from colonies grown in a drug-free medium, showed a susceptible RIF phenotype, while the other mutations, isolated from a drug-supplemented medium, showed a RIF resistant phenotype. This diversity aligns with characteristics attributed to lineage 2, which is known for higher mutation rates [46-48]. Jamieson et al. [49] also found the L430P mutation to be susceptible to RIF, as well as the H445L, H445N, and D435G-S441L mutations with the same phenotype. Meanwhile, Salaam-Dreyer et al. [50] found this mutation, L430P, in 13.9% of RR-TB isolates compared to 1.1% in MDR isolates, indicating it confers low-level resistance. In the same study, in 10 clinical isolates with the L430P mutation, 7 were phenotypically susceptible at a critical concentration of 0.5 ¼g/mL.

Moreover, Hofmann-Thiel et al. [6] later corroborated by Nimmo et al. [48] evaluated the nucleotide diversity in patients who completed treatment without mixed infections in a longitudinal study. They observed the emergence of heteroresistant populations that either became fixed or persisted over time. In the same study, they noted the presence of two resistant subpopulations, whose frequencies fluctuated

during treatment. Significant SNPs identified included D435V, S450L, L430P, H445Y, H445D, L452P, and H445R, which coexisted for weeks or months within the same patient. Despite this, no association was found between mixed infections and unfavorable outcomes, but opposite findings were found by Shin et al. [51] and Cohen et al. [52]. The mutations S450L, L430P, H445D, and L452P were also identified in our isolates, suggesting their implications in the generation of heteroresistant populations.

Remarkably, the MIC for colonies with the D435Y mutation ranged from <0.063 to 0.125 µg/mL in our study, compared to Jeon et al. [53], who reported a range of 0.5 to 16 µg/mL. For the L452P mutation, we observed an MIC of 0.125 µg/mL, while Jeon et al. found it varied from 1 to 16 µg/mL. These mutations are categorized as borderline by WHO (2023) [26] due to their phenotypic variability, depending on the MIC test applied.

Additionally, our study identified a nonsynonymous T187P mutation in the RpoA and several mutations in the RpoC protein, including H525Q, G594E, R741S, H767P, I832V, E1033K, P1040A, and T1230I (see supplementary data 1 for details). The H525Q and P1040A mutations, previously associated with the transmission of RR- TB isolates, are believed to mitigate minor fitness defects caused by the primary S450L mutation in the RpoB [54,55]. However, the WHO's 2023 catalog of <mutations in MTBC and their association with drug resistance= did not find an association with RR-TB for some RpoA and RpoC mutations, including G594E found in this study. Furthermore, the impact of other previously proposed compensatory mutations in the

rpoA or rpoC genes remains to be clarified [54,56,57], leaving their effects on RIF resistance and their role in transmission uncertain.

Ultimately, the persistence and tolerance of bacterial populations, as shown in our study, suggest that some mutations may confer a survival advantage without altering MICs, complicating the eradication of these populations [58], which emphasizes the importance of considering growth rate differences between strains and proportions, which may contribute to the establishment of drug-tolerant populations [3,59-63]. These observations underline the critical importance of early diagnosis to prevent the development of drug-resistant strains [64,65]. Genotyping in clinical samples is recommended to reveal the clonal complexity of Mtb infection as was performed by Aung et al. [28], who detected 5% heteroresistance to RIF in sputum using droplet digital PCR. The proportion of mutant strains showing *rpoB* gene heteroresistance ranged from 20 to 80%, while nearly all strains in RR-TB populations were 85 to 100% mutant and almost completely resistant to RIF.

Our analysis confirms the complex interplay between genetic mutations and phenotypic expression. It underscores the necessity for enhanced diagnostic techniques that can accurately detect and characterize heteroresistant and mixed infections. Future research should focus on integrating detailed genomic data with clinical outcomes to develop targeted treatment strategies that address both dominant and minor resistant populations, thereby improving patient outcomes and contributing to the global effort to control and eliminate TB.

II.5. Conclusion

WGS revealed the presence of multiple Mtb strains in the sputum samples, which was further validated through colony isolation. During the isolation process, we identified colonies harboring mutations in the *rpoB* gene with high levels of RIF resistance. These colonies were isolated from RIF-supplemented media, highlighting that subculturing in drug-free media may preferentially select for drug-sensitive strains over resistant ones.

These findings emphasize the critical need for advanced techniques capable of accurately detecting and characterizing heteroresistant and mixed infections. Such tools are essential to improve treatment outcomes and combat the challenges posed by antimicrobial resistance in TB.

II.6. References

1. World Health Organization. Global tuberculosis report 2024 [Internet]. Geneva; 2024 [cited 2025 Jan 15]. Available from: https://www.who.int/teams/global-tuberculosis-programme/tb-reports/global-tuberculosis-report-2024
2. Ye M, Yuan W, Molaeipour L, Azizian K, Ahmadi A, Kouhsari E. Antibiotic heteroresistance in *Mycobacterium tuberculosis* isolates: a systematic review and meta-analysis. Ann Clin Microbiol Antimicrob. 2021 Dec 13;20(1):73.
3. McIvor A, Koornhof H, Kana BD. Relapse, re-infection and mixed infections in tuberculosis disease. Pathog Dis. 2017 Apr 1;75(3).
4. Baik Y, Modongo C, Moonan PK, Click ES, Tobias JL, Boyd R, et al. Possible transmission mechanisms of mixed *Mycobacterium tuberculosis* infection in high HIV prevalence country, Botswana. Emerg Infect Dis. 2020 May;26(5):953360.

5. Cohen T, Wilson D, Wallengren K, Samuel EY, Murray M. Mixed-strain *Mycobacterium tuberculosis* infections among patients dying in a hospital in KwaZulu-Natal, South Africa. J Clin Microbiol. 2011 Jan;49(1):38538.
6. Hofmann-Thiel S, van Ingen J, Feldmann K, Turaev L, Uzakova GT, Murmusaeva G, et al. Mechanisms of heteroresistance to isoniazid and rifampin of *Mycobacterium tuberculosis* in Tashkent, Uzbekistan. European Respiratory Journal. 2008 Sep 17;33(2):368374.
7. Abakur EHA, Alnour TMS, Abuduhier F, Albalawi FMA, Alfifi KAS. Emergence of heteroresistance *Mycobacterium tuberculosis* in Saudi Arabia. Infect Disord Drug Targets. 2020 Oct 16;20(4):49134.
8. Werngren J, Mansjö M, Glader M, Hoffner S, Davies Forsman L. Detection of pyrazinamide heteroresistance in *Mycobacterium tuberculosis.* Antimicrob Agents Chemother. 2021 Aug 17;65(9).
9. Asare-Baah M, Séraphin MN, Salmon LAT, Lauzardo M. Effect of mixed strain infections on clinical and epidemiological features of tuberculosis in Florida. Infection, Genetics and Evolution. 2021 Jan;87:104659.
10. Dickman KR, Nabyonga L, Kateete DP, Katabazi FA, Asiimwe BB, Mayanja HK, et al. Detection of multiple strains of *Mycobacterium tuberculosis* using MIRU-VNTR in patients with pulmonary tuberculosis in Kampala, Uganda. BMC Infect Dis. 2010 Dec 10;10(1):349.
11. Kargarpour Kamakoli M, Sadegh HR, Farmanfarmaei G, Masoumi M, Fateh A, Javadi G, et al. Evaluation of the impact of polyclonal infection and heteroresistance on treatment of tuberculosis patients. Sci Rep. 2017 Jan 25;7(1):41410.
12. Wang L, Campino S, Phelan J, Clark TG. Mixed infections in genotypic drug-resistant *Mycobacterium tuberculosis*. Sci Rep. 2023 Oct 10;13(1):17100.
13. MINSA. Situación actual-Estrategias de prevención y control de TBC en el Perú [Internet]. 2021 [cited 2024 Apr 30]. Available from: https://www.dge.gob.pe/portal/docs/tools/teleconferencia/2021/SE422021/04.pdf

14. Kohl TA, Utpatel C, Schleusener V, De Filippo MR, Beckert P, Cirillo DM, et al. MTBseq: a comprehensive pipeline for whole genome sequence analysis of *Mycobacterium tuberculosis* complex isolates. PeerJ. 2018 Nov 13;6:e5895.
15. Phelan JE, O9Sullivan DM, Machado D, Ramos J, Oppong YEA, Campino S, et al. Integrating informatics tools and portable sequencing technology for rapid detection of resistance to anti-tuberculous drugs. Genome Med. 2019 Dec 24;11(1):41.
16. Coll F, McNerney R, Guerra-Assunção JA, Glynn JR, Perdigão J, Viveiros M, et al. A robust SNP barcode for typing *Mycobacterium tuberculosis* complex strains. Nat Commun. 2014 Sep 1;5(1):4812.
17. Napier G, Campino S, Merid Y, Abebe M, Woldeamanuel Y, Aseffa A, et al. Robust barcoding and identification of *Mycobacterium tuberculosis* lineages for epidemiological and clinical studies. Genome Med. 2020 Dec 14;12(1):114.
18. Phelan J. TBDB: Standard database for the TBProfiler tool [Internet]. 2022 [cited 2024 Sep 12]. Available from: https://github.com/jodyphelan/TBProfiler
19. Caviedes L, Lee TS, Gilman RH, Sheen P, Spellman E, Lee EH, et al. Rapid, efficient detection and drug susceptibility testing of *Mycobacterium tuberculosis* in sputum by microscopic observation of broth cultures. The Tuberculosis Working Group in Peru. J Clin Microbiol [Internet]. 2000 Mar;38(3):120338. Available from: http://www.ncbi.nlm.nih.gov/pubmed/10699023
20. Caviedes L, Delgado J, Gilman RH. Tetrazolium Microplate Assay as a rapid and inexpensive colorimetric method for determination of antibiotic susceptibility of *Mycobacterium tuberculosis*. J Clin Microbiol [Internet]. 2002 May 1;40(5):187334. Available from: http://jcm.asm.org/cgi/doi/10.1128/JCM.40.5.1873-1874.2002
21. Franzblau SG, Witzig RS, McLaughlin JC, Torres P, Madico G, Hernandez A, et al. Rapid, low-technology MIC determination with Clinical *Mycobacterium tuberculosis* isolates by using the Microplate Alamar Blue Assay. J Clin Microbiol [Internet]. 1998;36(2):36236. Available from: https://jcm.asm.org/content/36/2/362
22. Canetti G, Rist N, Grosset J. [Measurement of sensitivity of the tuberculous bacillus to antibacillary drugs by the method of proportions. Methodology, resistance criteria, results and interpretation]. Rev Tuberc Pneumol (Paris). 1963;27:217372.

23. Danchuk SN, Solomon OE, Kohl TA, Dreyer V, Barilar I, Utpatel C, et al. Challenging the gold standard: the limitations of molecular assays for detection of *Mycobacterium tuberculosis* heteroresistance. Thorax. 2024 Jan 29;thorax-2023-220202.
24. CDC MINSA. Boletin epidemiológico [Internet]. 2023 [cited 2024 Jul 17]. Available from: https://www.dge.gob.pe/epipublic/uploads/boletin/boletin_202320_28_163316.pdf
25. Su F, Cao L, Ren X, Hu J, Tavengana G, Wu H, et al. The mutation rate of *rpoB* gene showed an upward trend with the increase of MIRU10, MIRU39 and QUB4156 repetitive number. BMC Genomics. 2023 Jan 16;24(1):26.
26. World Health Organization. Catalogue of mutations in Mycobacterium tuberculosis complex and their association with drug resistance, 2 nd ed [Internet]. 2023 [cited 2025 Jan 15]. Available from: https://iris.who.int/handle/10665/374061
27. Zheng C, Li S, Luo Z, Pi R, Sun H, He Q, et al. Mixed Infections and rifampin heteroresistance among *Mycobacterium tuberculosis* Clinical isolates. J Clin Microbiol. 2015 Jul;53(7):2138347.
28. Aung YW, Faksri K, Sangka A, Tomanakan K, Namwat W. Heteroresistance of *Mycobacterium tuberculosis* in the sputum detected by droplet digital PCR. Biology (Basel). 2023 Mar 30;12(4):525.
29. Barletta F, Otero L, de Jong BC, Iwamoto T, Arikawa K, Van der Stuyft P, et al. Predominant *Mycobacterium tuberculosis* families and high rates of recent transmission among new cases are not associated with primary multidrug resistance in Lima, Peru. J Clin Microbiol. 2015 Jun;53(6):1854363.
30. Tarashi S, Fateh A, Mirsaeidi M, Siadat SD, Vaziri F. Mixed infections in tuberculosis: The missing part in a puzzle. Tuberculosis. 2017 Dec;107:168374.
31. Nkatha Micheni L, Deyno S, Bazira J. *Mycobacterium tuberculosis* mixed infections and drug resistance in sub-Saharan Africa: a systematic review. Afr Health Sci. 2022 Apr 29;22(1):560372.

32. Sobkowiak B, Glynn JR, Houben RMGJ, Mallard K, Phelan JE, Guerra-Assunção JA, et al. Identifying mixed *Mycobacterium tuberculosis* infections from whole genome sequence data. BMC Genomics. 2018 Dec 14;19(1):613.
33. Phyu AN, Aung ST, Palittapongarnpim P, Htet KKK, Mahasirimongkol S, Aung HL, et al. Distribution of *Mycobacterium tuberculosis* lineages and drug resistance in upper Myanmar. Trop Med Infect Dis. 2022 Dec 19;7(12):448.
34. Merker M, Blin C, Mona S, Duforet-Frebourg N, Lecher S, Willery E, et al. Evolutionary history and global spread of the *Mycobacterium tuberculosis* Beijing lineage. Nat Genet. 2015 Mar 19;47(3):24239.
35. Freschi L, Vargas R, Husain A, Kamal SMM, Skrahina A, Tahseen S, et al. Population structure, biogeography and transmissibility of *Mycobacterium tuberculosis.* Nat Commun. 2021 Oct 20;12(1):6099.
36. Gagneux S. Ecology and evolution of *Mycobacterium tuberculosis*. Nat Rev Microbiol. 2018 Apr 19;16(4):202313.
37. Grandjean L, Iwamoto T, Lithgow A, Gilman RH, Arikawa K, Nakanishi N, et al. The Association between *Mycobacterium tuberculosis* genotype and drug resistance in Peru. PLoS One. 2015 May 18;10(5):e0126271.
38. Santos L, Medeiros MA, Santos S, Costa MC, Tavares R, Curto MJM. NMR studies of some rifamycins. J Mol Struct [Internet]. 2001 May;5633564:61378. Available from: https://linkinghub.elsevier.com/retrieve/pii/S0022286000008711
39. Netikul T, Thawornwattana Y, Mahasirimongkol S, Yanai H, Maung HMW, Chongsuvivatwong V, et al. Whole-genome single nucleotide variant phylogenetic analysis of *Mycobacterium tuberculosis* Lineage 1 in endemic regions of Asia and Africa. Sci Rep. 2022 Jan 28;12(1):1565.
40. Billington OJ, McHugh TD, Gillespie SH. Physiological cost of rifampin resistance induced in vitro in *Mycobacterium tuberculosis*. Antimicrob Agents Chemother. 1999 Aug;43(8):186639.
41. Mariam DH, Mengistu Y, Hoffner SE, Andersson DI. Effect of *rpoB* mutations conferring rifampin resistance on fitness of *Mycobacterium tuberculosis*. Antimicrob Agents Chemother. 2004 Apr;48(4):1289394.

42. Loiseau C, Windels EM, Gygli SM, Jugheli L, Maghradze N, Brites D, et al. The relative transmission fitness of multidrug-resistant *Mycobacterium tuberculosis* in a drug resistance hotspot. Nat Commun. 2023 Apr 8;14(1):1988.
43. Martín A, Herranz M, Ruiz Serrano MJ, Bouza E, García de Viedma D. The clonal composition of *Mycobacterium tuberculosis* in clinical specimens could be modified by culture. Tuberculosis. 2010 May;90(3):20137.
44. Metcalfe JZ, Streicher E, Theron G, Colman RE, Penaloza R, Allender C, et al. *Mycobacterium tuberculosis* subculture results in loss of potentially clinically relevant heteroresistance. Antimicrob Agents Chemother. 2017 Nov;61(11).
45. Chengalroyen, M. D., Beukes, G. M., Otwombe, K., Gordhan, B. G., Martinson, N., & Kana, B. (2022). The detection of mixed tuberculosis infections using culture filtrate and resuscitation promoting factor deficient filtrate. *Frontiers in Cellular and Infection Microbiology*, *12*. https://doi.org/10.3389/fcimb.2022.1072073
46. Ford CB, Shah RR, Maeda MK, Gagneux S, Murray MB, Cohen T, et al. *Mycobacterium tuberculosis* mutation rate estimates from different lineages predict substantial differences in the emergence of drug-resistant tuberculosis. Nat Genet. 2013 Jul 9;45(7):784390.
47. Eldholm V, Pettersson JHO, Brynildsrud OB, Kitchen A, Rasmussen EM, Lillebaek T, et al. Armed conflict and population displacement as drivers of the evolution and dispersal of *Mycobacterium tuberculosis*. Proceedings of the National Academy of Sciences. 2016 Nov 29;113(48):1388136.
48. Nimmo C, Brien K, Millard J, Grant AD, Padayatchi N, Pym AS, et al. Dynamics of within-host *Mycobacterium tuberculosis* diversity and heteroresistance during treatment. EBioMedicine. 2020 May;55:102747.
49. Jamieson FB, Guthrie JL, Neemuchwala A, Lastovetska O, Melano RG, Mehaffy C. Profiling of *rpoB* mutations and MICs for rifampin and rifabutin in *Mycobacterium tuberculosis.* J Clin Microbiol. 2014 Jun;52(6):2157362.
50. Salaam-Dreyer Z, Streicher EM, Sirgel FA, Menardo F, Borrell S, Reinhard M, et al. Rifampicin-monoresistant tuberculosis is not the same as multidrug-resistant

tuberculosis: a descriptive study from Khayelitsha, South Africa. Antimicrob Agents Chemother. 2021 Oct 18;65(11).

51. Shin SS, Modongo C, Baik Y, Allender C, Lemmer D, Colman RE, et al. Mixed *Mycobacterium tuberculosis*3strain infections are associated with poor treatment outcomes among patients with newly diagnosed tuberculosis, independent of pretreatment heteroresistance. J Infect Dis. 2018 Aug 4;
52. Cohen T, Chindelevitch L, Misra R, Kempner ME, Galea J, Moodley P, et al. Within-host heterogeneity of *Mycobacterium tuberculosis* infection is associated with poor early treatment response: a prospective cohort study. Journal of Infectious Diseases. 2016 Jun 1;213(11):179639.
53. Jeon SM, Park S, Lim NR, Lee N, Jung J, Sung N, et al. Molecular analysis of anti-tuberculosis drug resistance of *Mycobacterium tuberculosis* isolated in the Republic of Korea. Antibiotics. 2023 Aug 17;12(8):1324.
54. de Vos M, Müller B, Borrell S, Black PA, van Helden PD, Warren RM, et al. Putative compensatory mutations in the *rpoC* gene of rifampin-resistant *Mycobacterium tuberculosis* are associated with ongoing transmission. Antimicrob Agents Chemother. 2013 Feb;57(2):827332.
55. Gagneux S. The Competitive Cost of antibiotic resistance in *Mycobacterium tuberculosis*. Science (1979) [Internet]. 2006 Jun 30;312(5782):194436. Available from: https://www.sciencemag.org/lookup/doi/10.1126/science.1124410
56. Comas I, Borrell S, Roetzer A, Rose G, Malla B, Kato-Maeda M, et al. Whole-genome sequencing of rifampicin-resistant *Mycobacterium tuberculosis* strains identifies compensatory mutations in RNA polymerase genes. Nat Genet [Internet]. 2012 Jan 18;44(1):106310. Available from: http://www.nature.com/articles/ng.1038
57. Vargas A, Rios A, Grandjean L, Kirwan D, Gilman R, Sheen P, et al. Determination of potentially novel compensatory mutations in *rpoC* associated with rifampin resistance and *rpoB* mutations in *Mycobacterium tuberculosis* clinical isolates from Peru. Int J Mycobacteriol. 2020;9(2):121.

58. Brauner A, Fridman O, Gefen O, Balaban NQ. Distinguishing between resistance, tolerance and persistence to antibiotic treatment. Nat Rev Microbiol. 2016 May 15;14(5):320330.
59. Zumla A, Nahid P, Cole ST. Advances in the development of new tuberculosis drugs and treatment regimens. Nat Rev Drug Discov. 2013 May 30;12(5):3883404.
60. Kana BD, Karakousis PC, Parish T, Dick T. Future target-based drug discovery for tuberculosis? Tuberculosis. 2014 Dec;94(6):55136.
61. Mukamolova G V., Turapov O, Malkin J, Woltmann G, Barer MR. Resuscitation-promoting factors reveal an occult population of tubercle bacilli in sputum. Am J Respir Crit Care Med. 2010 Jan 15;181(2):174380.
62. Chengalroyen MD, Beukes GM, Gordhan BG, Streicher EM, Churchyard G, Hafner R, et al. Detection and quantification of differentially culturable tubercle bacteria in sputum from patients with tuberculosis. Am J Respir Crit Care Med. 2016 Dec 15;194(12):1532340.
63. Loraine J, Pu F, Turapov O, Mukamolova G V. Development of an *in vitro* assay for detection of drug-induced resuscitation-promoting-factor-dependent Mycobacteria. Antimicrob Agents Chemother. 2016 Oct;60(10):6227333.
64. Sun G, Luo T, Yang C, Dong X, Li J, Zhu Y, et al. Dynamic population changes in *Mycobacterium tuberculosis* during acquisition and fixation of drug resistance in patients. J Infect Dis. 2012 Dec 1;206(11):1724333.
65. Ley SD, de Vos M, Van Rie A, Warren RM. Deciphering within-host microevolution of *Mycobacterium tuberculosis* through whole-genome sequencing: the phenotypic impact and way forward. Microbiology and Molecular Biology Reviews. 2019 May 15;83(2).

Chapter III

PonA1 of *Mycobacterium tuberculosis*: *In vitro* study and genomic integration in *Mycobacterium marinum*, insights in rifampicin resistance

Abstract

PonA1 is a penicillin binding protein (PBP), and it is a promising candidate for antibiotic development due to its essential role in maintaining cell wall integrity in *Mycobacterium tuberculosis* (Mtb) through peptidoglycan synthesis. In the first part of this chapter, we investigated the functional and structural implications of PonA1 mutations, specifically Q365H and P631S, using *in silico* modeling and *in vitro* experiments. The AlphaFold and ESMFold algorithms were employed to model the complete protein, and the transpeptidase crystal structure was used as part of the model validation process. Structurally, these mutations did not induce significant changes in the PBP domain. Molecular docking analyses using the DiffDock algorithm, combined with NMR spectroscopy, revealed a reduced binding affinity between rifampicin (RIF) and both wild-type and mutant PonA1, suggesting a non-specific, transient interaction.

In the second part of this chapter, we evaluated the phenotypic effects of deleting the *ponA1* homologue, *MMAR_0069*, in *Mycobacterium marinum* (Mmar), as well as integrating *ponA1* from Mtb H37Rv into its genome. While the deletion did not significantly affect cell growth, it resulted in notable morphological changes *in vitro* and increased resistance to RIF at subinhibitory concentrations of 0.5 µg/mL. Furthermore, Mmar strains complemented with wild-type Mtb *ponA1* and the T34D mutation exhibited enhanced resistance during the logarithmic phase at the same level. While, during the stationary phase, the A516T, and P631S mutations provided a survival advantage during RIF exposure, coinciding with cellular morphological changes, particularly for A516T and P631S, further demonstrating the contribution of PonA1 in drug resistance mechanisms.

This study also highlights the successful application of the modified ORBIT technique for simultaneous gene knockout and complementation, offering a rapid and efficient method for evaluating promoter libraries and gene function in mycobacterial genomes.

Key words: PonA1, penicillin binding protein, AlphaFold, ESMfold, Diffdock, ORBIT, rifampicin, tuberculosis.

III.1. Introduction

The PonA1 protein is involved in cell wall synthesis and regeneration through its role in peptidoglycan (PG) synthesis in many bacterial species (Dörr et al., 2014; Kieser, Baranowski, et al., 2015; McPherson & Popham, 2003; Paradis-Bleau et al., 2010; Valbuena et al., 2007). It contains two functional domains: a transglycosylase (TG) domain and a transpeptidase (TP) domain, as well as a PBP domain located in the TP domain. The PBP domain enables PonA1 to interact with β-lactam antibiotics, which mimic the acyl-D-Ala-D-Ala structure of the PG, thereby inhibiting cell wall synthesis (Tipper & Strominger, 1965).

This protein has attracted attention for its potential role in conferring a growth advantage in the presence of rifampicin (RIF). Notably, both the knockout (KO) of the *ponA1* gene and the Q365H substitution have been shown to influence antibiotic tolerance to RIF (Farhat et al., 2013). In addition, the P631S mutation in PonA1, located in a proline-rich region, mediates its interaction with RipA, a peptidoglycan endopeptidase involved in regulating the cell cycle through cell elongation and division (Hett et al., 2010). Gao et al. (2019) further demonstrated that reducing the number of prolines in this region enhances the interaction between PonA1 and RipA, leading to cell length deregulation. The P631S mutation was found to be statistically associated with RIF resistance, alongside the A516T mutation (Rabanal et al., 2020). The A516T mutation was primarily associated with resistant strains, while the P631S mutation was more commonly found in susceptible strains, based on an analysis of 914 Mtb complete genomes from Peru.

Given the association of *ponA1* mutations with RIF resistance and the structural differences between RIF and penicillin, this study aims to evaluate the potential molecular interactions between PonA1 and RIF, and to assess the impact of *ponA1* mutations on RIF resistance. This chapter explores these interactions using a combination of *in silico* and *in vitro* analyses. Additionally, Mmar was employed to assess the effects of both wild-type and mutated *ponA1* through gene KO and complementation with the *ponA1* gene from Mtb H37Rv.

In this sense, the chapter is divided in two parts. The first part focuses on *in silico* and *in vitro* analyses of PonA1-RIF interactions. Structurally, we predicted the complete PonA1 protein using AlphaFold and ESMFold, comparing these models with the crystal structure of PonA1 residues 391-785 (Filippova et al., 2016). Molecular docking was then performed to assess the interaction between RIF and both wild-type and mutant PonA1 proteins. Subsequently, molecular dynamics simulations were conducted to evaluate the temporal evolution and stability of these interactions. *In vitro* analysis involved the recombinant production of PonA1 proteins (residues 234-820) from wild-type Mtb H37Rv, as well as the Q365H and P631S mutants. These mutations were selected based on their reported association with resistance and susceptibility to RIF, respectively (Farhat et al., 2013; B. Gao et al., 2019; Rabanal J, 2020). The recombinant proteins were subsequently subjected to biophysical and conformational studies to assess their structural and functional properties. The interactions between these recombinant proteins and RIF were analyzed using 1D nuclear magnetic

resonance (NMR) spectroscopy and affinity was calculated using saturation transfer difference-nuclear magnetic resonance (STD-NMR).

The second part of this study examines the effects of *ponA1* mutations from Mtb in Mmar, aiming to understand the impact of these mutations on bacterial behavior, cell wall morphology, and RIF resistance, and to draw parallels between the responses of Mmar and Mtb.

Mmar is a slow-growing, photochromogenic mycobacterium that causes skin and soft tissue infections in humans, as well as TB-like infections in fish, known as mycobacteriosis. It has a doubling time of about 839 hours and is phylogenetically close to Mtb (Biet et al., 2005). Due to its phylogenetic position and pathogenic similarities to Mtb, Mmar is commonly used as a model system in studies related to Mtb, its ease of manipulation further supports its use in research, helping to study TB pathogenesis in its natural host species (Aubry et al., 2017; Broussard & Ennis, 2007; Clay et al., 2007; Das et al., 2018; Davis et al., 2002; Gao & Manoranjan, 2006; Hashish et al., 2018; Swaim et al., 2006; Volkman et al., 2004).

Mmar infections can be effectively treated with anti-TB agents such as RIF, EMB, clarithromycin, doxycycline, and quinolones (Aubry et al., 2000; Stinear et al., 2008). The organisms share virulence determinants, with Mtb virulence genes able to complement orthologous Mmar genes with mutations (Cosma et al., 2006; Gao et al., 2004; Tobin & Ramakrishnan, 2008; Volkman et al., 2004).

Optimal growth of Mmar occurs between 30- 35°C in Middlebrook 7H9 broth, and it grows poorly at 37°C (Clark & Shepard, 1963; Gao & Manoranjan, 2006). Like

Mtb, it is a facultative anaerobe however, unlike Mtb, it cannot reduce nitrate and produces bright yellow carotenoid pigments when exposed to light, which protect it from UV damage (Stinear et al., 2008; Tsukamura, 1983). The Mmar genome includes a 6,636,827-bp circular chromosome with a G/C content of 65.73%, 5424 coding sequences (CDS), 10 prophages, and a 23-kb mercury-resistance plasmid (Stinear et al., 2008). Genome comparisons with Mtb reveal a close genetic relationship, sharing 3000 orthologs with an average amino acid identity of 85% (Table III.1).

The annotated *ponA1* sequence from Mtb H37Rv shares 82.82% nucleotide identity with the homologous *MMAR_0069* gene from Mmar, and 91% protein homology (Appendix III.1-2), Additionally, *MMAR_0069* has a 79.62% identity to the *ponA1* gene and an 84.39 % protein homology based on the -426 transcription start site proposed by Kieser et al. (2015) (Appendix III.334). For the KO of the *MMAR_0069* gene, we employed oligonucleotide-mediated recombineering followed by Bxb1 integrase targeting (ORBIT), a method previously used in Mtb and *M. smegmatis* (Murphy et al., 2018) and recently used in Mmar (Saelens et al., 2022).

Given Mmar's closer phylogenetic relationship to Mtb, its slower growth rate, and more manageable handling requirements, developing ORBIT in Mmar presents significant potential for advancing Mtb research. Additionally, we initiated exploratory studies on promoter analysis using ORBIT to enable simultaneous knockout and gene complementation in one step.

Table III.1. Chromosome features of *M. marinum* strain M compared with *M. tuberculosis*. Adapted from Stinear et al. (2008).

Feature	*M. marinum* M	*M. tuberculosis* H37Rv
Chromosome size (bp)	6,636,827	4,411,532
GC content %	65.73	65.61
Base Pairs per gene	1223	1110
Average CDS length	1101	1009
Protein-coding sequences	5424	3974
Conserved with assigned function	3987 (74%)	3049 (77%)
Conserved with unknown function	1254 (23%)	907 (22.5%)
Pseudogenes	65	17
rRNA	1	1
tRNA	46	45

Objective

The primary objective of this study was to investigate the association between mutations in the PonA1 protein and resistance to RIF. Specifically, it aimed to characterize the effect of these mutations on PonA1's affinity for RIF, both *in silico* and *in vitro*. In addition, a *MMAR_0069* gene KO (ΔMMAR0069) strain of Mmar was generated, this KO strain was then complemented with various mutated *ponA1* genes

from the reference strain Mtb H37Rv. The phenotypic traits and RIF susceptibility of these modified strains were subsequently assessed.

III.2. Experimental section

III.2.1. *In silico* interaction between the PonA1 and rifampicin

This section was developed at the Laboratorio de Bioinformatica y Biologia Molecular, UPCH, Lima- Peru, with the collaboration of Gustavo Olivos, Diego Taquiri and Omar Romero.

III.2.1.1. PonA1 full-length structural modeling compared to the PonA1 transpeptidase crystal structure

The complete structural model of PonA1 was constructed by two methodologies: AlphaFold v.2 (Jumper et al., 2021) and Evolutionary Scale Modeling (ESMFold) (Lin et al., 2023).

We used the full-length sequence of PonA1 (Uniprot ID: P71707) alongside the crystal structure of PonA1 complexed with its ligand penicillin, available in the Protein Data Bank (PDB ID 5CXW), featuring a single chain. The nomenclature of the residues studied in the crystal structure4Q365, A516, and P6314was used consistently for both *in silico* and *in vitro* analyses. These correspond to residues Q507, A658, and P773, respectively, in models generated based on the full-length proteins, depending on the assay performed.

For the modeling of the PonA1 protein, the structure with ID AF-P71707-F1 from the AlphaFold database was utilized. For mutants modeling, we modified single

amino acids in the AlphaFold model and used the AlphaFold algorithm locally to predict the structures of the mutated proteins. The parameters set for our modeling included the use of the MonomerPTM model preset. This approach allowed us to investigate both the wild-type structure of PonA1 and its mutations. Specifically, the mutations modeled in the PonA1 protein using AlphaFold were Q365H and P631S. A structural alignment was then performed to assess deviations between the mutant models and the wild-type PonA1 (PonA1_WT_AF).

Furthermore, for the structural prediction of PonA1 -wild type and mutants, we also employed ESMfold v1, a deep learning-based model. This was operated locally with a chunk size of 128, appropriate for the protein's length.

III.2.1.2. Molecular docking between variants of PonA1 and RIF

To assess the impact of mutations on RIF binding affinity, blind molecular docking assays were performed. For these assays, we utilized both the available PDB structure of the PonA1 protein (PDB ID: 5CXW) and the full-length model predicted by ESMFold. The PDB structure comprises only 394 residues, corresponding to positions 390-785 of the protein, whereas the ESMFold models represent the complete sequence, spanning residues 0-820. This allowed for a comprehensive comparison between the truncated crystal structure and the full-length predicted model.

To model ligand binding, we employed RIF with the PubChem CID 135398735 (https://doi.org/10.1093/nar/gkac956), and penicillin V in its open form, as seen in the crystal structure, with the PubChem CID 137348124.

For the molecular docking studies, we employed two software tools: GNINA and DiffDock. GNINA (McNutt et al., 2021) utilized an automatic selection based on the *penicillin.pdb* file, with most parameters set to default. Specifically, an additional 4 Å was added to all six sides of the automatically generated binding box (--autobox_add +4). The exhaustiveness level was set to 64 (--exhaustiveness 64) to ensure comprehensive sampling of potential binding modes. By default, GNINA generates up to 9 binding poses (--num_modes 9) and applies a root mean square deviation (RMSD) filter of 1 Å (--min_rmsd_filter 1) to eliminate redundant poses. The default convolutional neural network (CNN) scoring function is set to rescore the poses (--cnn_scoring 1), with a grid resolution of 0.5 Å (--cnn_resolution 0.5), which enhances the accuracy and detail in modeling molecular interactions.

DiffDock (Corso et al., 2022) was utilized with a default box size covering the entire input protein and was executed with standard parameters. The inference process involved 20 steps (--inference_steps 20) and processed 40 samples per complex (--samples_per_complex 40), with a batch size of 6 (--batch_size 6). This approach enabled a detailed exploration of the binding interactions between the ligands and PonA1, providing comprehensive insights into the potential docking poses and molecular interactions.

The best docking modes were ranked based on the most favorable interaction energies, considering the ΔG (kcal/mol) for GNINA and the top DiffDock confidence score (DCS). The optimal binding poses for each model, including both PonA1 wild-type and its mutants, were further analyzed using the Protein-Ligand Interaction

Profiler (PLIP, (Salentin et al., 2015) to identify key molecular interactions. These selected poses were subsequently used for molecular dynamics simulations to further evaluate the stability and dynamics of the protein-ligand interactions.

III.2.1.3. Molecular dynamics evaluation of PonA1-RIF complex stability

We conducted molecular dynamics simulation using GROMACS 2023.3 to assess the stability of the interaction between RIF and PonA1 wild-type and its mutants. The simulations were initiated with the docked structures of PonA1_WT_ESM, PonA1_Q365H_ESM, and PonA1_P631S_ESM, each selected based on the highest DiffDock scores from the models predicted by ESMfold. Prior to the simulations, the topologies of both the protein and ligand were separately generated using Antechamber (Wang et al., 2000; https://ambermd.org/antechamber/ac.html), after which they were combined to form the protein-ligand complex. Given the size of the protein (820 residues), the complex was placed in a cubic simulation box with 1.5 Å of padding on each side to ensure sufficient space for interactions. The system was solvated using the SPC216 water model, and NaCl was added to achieve an ionic concentration of 0.154 mM for Naz and 20 mM for Cl{ to maintain electrostatic balance. Following solvation and ionization, the system underwent energy minimization using the steepest descent algorithm (Meza, 2010) for 5000 steps to eliminate steric clashes and ensure system stability before proceeding with molecular dynamics.

For the equilibration phase, restrictions were applied specifically to the ligand and the backbone of the protein. Both temperature and pressure were equilibrated over a period of 100 ns to achieve a steady state for the subsequent molecular dynamic simulations. We used the NVT (300 K) and NPT (1 bar) ensemble, respectively. The

molecular dynamics simulation was then carried out for 100 ns, using the LINCS algorithm (Hess et al., 1997) to restrict all joint particles; while the Ewald Mesh algorithm (PME) (Petersen, 1995) was used to approximate the long-range interactions. Drug stability in the protein active site was analyzed by Root Mean Square Deviation (RMSD) and Root Mean Square Fluctuation (RMSF) of the molecules. Additionally, the trajectory data were visualized using VMD (Visual Molecular Dynamics) software (https://www.ks.uiuc.edu/Research/vmd/), and protein-ligand interaction analysis was performed with the PLIP package (Salentin et al., 2015), to identify key interactions occurring with a frequency greater than 2% of the simulation time.

III.2.2. Cloning, expression and purification of recombinant PonA1 variants and RpoB

This part of the experiment was developed in the Centre de Biologie Structurale (CBS) -Montpellier-France, with the support of PhD. Martin Cohen-Gonsaud and Angelique De-Visch.

The $PonA1_{234\text{-}820}$ design was performed taking the sequence used by Filippova *et al*. covering residues 234-820 (NCBI accession number NC_000962.3 - YP_177687.1). This sequence was cloned in the plasmid pET28a-TEV (Genscript), which includes a His-tag and contains a TEV protein cleavage site at the N-terminal (Appendix III.5-7). RpoB was cloned as a full-length sequence (NCBI accession number NC_000962.3) with a His-tag at the N terminal (Appendix III.8).

The plasmids were transformed in *E. coli* Rosetta cells using heat shock, grown on Luria Bertani (LB) agar with 40 ¼g/mL Kanamycin (KAN) at 37°C for 24 hours. A single colony was then cultured in 10 mL of LB broth with KAN at 37°C overnight at 250 rpm. The next day, 10 mL was added to 500 mL of ZYM-5052 media (Appendix III.9), incubated at 37°C for 4 hours then at 25°C overnight. Cells were harvested by centrifugation at 6000 rpm for 25 min at 4°C, resuspended in buffer containing 50 mM Tris pH 8, 150 mM NaCl, 2 mM dithiothreitol (DTT) and 0.08% N-Dodecyl-beta-Maltoside (DDM) with 1 µl/mL of lysozyme (1 mg/mL) and stored at -40°C. After thawing, sonication (parameters were 50 amplitude for 5 minutes at 2 pulse) and centrifugation (18000 rpm at 8°C for 25 minutes) was performed.

For $PonA1_{234\text{-}820}$_WT and its mutants, the pellet was resuspended in buffer containing 8M urea, 50 mM Tris pH 8, 150 mM NaCl and 2 mM DTT, centrifugation at 20000 rpm, 20°C for 20 minutes was performed and the supernatant was recovered.

All PonA19s recombinant proteins were purified by affinity chromatography, using imidazole gradients between 10 mM to 500 mM, in 50 mM Tris-HCl buffer, 150mM NaCl, pH 8 urea 8M. Then, dialysis was performed in buffer 50 mM Tris-HCl pH 8, 150 mM NaCl, 2 mM DTT without urea at 4°C overnight. An additional step was performed, size exclusion chromatography by gel filtration in 50 mM Tris-HCl pH 8, 150 mM NaCl and 2 mM DTT in a Superdex 200 26/60 column.

For RpoB protein, one colony was subcultured in 10 mL of LB media with KAN, it was incubated at 37°C overnight at 250 rpm. The next day, 10 mL of the culture was added to 500 mL of ZYM 50-52 media cultured at 37°C for 4 hours and 25°C overnight at 250 rpm. A step of centrifugation to collect the pellet at 6000 rpm at

25 min 4°C, the supernatant was discarded and buffer containing 50 mM Tris-HCl pH 8, 150 mM NaCl, 2 mM DTT was used to resuspend the pellet cellular, 1 µl of lysozyme per mL (1 mg/mL) was added. The suspension was stored at -40°C and warmed at room temperature for 20 minutes. Sonication parameters were 50 amplitude for 5 minutes at 2 pulses, centrifugation step at 18000 rpm at 8°C for 25 minutes was performed. The supernatant after centrifugation was collected. Buffer 50 mM Tris pH 8, 150 mM NaCl and 2 mM DTT was used for affinity purification using imidazole gradients between 10 mM to 500 mM, in 20 mM Tris-HCl buffer, 300mM NaCl, pH 8. Dialysis was performed in buffer 50 mM Tris pH 8, 150 mM NaCl, 2 mM DTT at 4°C overnight and gel filtration was performed in Superdex 200 26/60 column in the same buffer.

The purity of the proteins was confirmed by SDS-PAGE and Coomassie blue staining. Concentrations were performed with centrifugal filter (Amicon ® ultra 10K 3 Merck Millipore) and quantified by UV spectroscopy at 280 nm with parameters obtained from Expasy ProtParam tool (https://web.expasy.org/cgi-bin/protparam/protparam). PonA1 (ε=66810 M^{-1} cm^{-1}, MW= 63 222 Da), RpoB (ε=85260 M^{-1} cm^{-1}, MW= 129 349 Da).

III.2.3. Biophysical characterization of PonA1$_{234-820}$ variants, and RpoB

Stability and protein folding of purified recombinant proteins were evaluated using Tycho NT.6 (Breitsprecher et al., 2018; Mohamadi M, 2017), circular dichroism (CD), and molecular exclusion chromatography coupled with multiple angle light scattering (SEC-MALS) (Some et al., 2019). For each evaluation, the protocols described by the manufacturer were followed.

The thermal stability of $PonA1_{234\text{-}820}$_ WT and its mutant proteins was evaluated using a protein thermal shift assay with Tycho NT.6 (Nanotemper), capillaries (TY-C001) were used and 10 µL of each protein (1 mg/mL) per capillary to prevent sample loss due to excessive brightness. All proteins were maintained in a buffer consisting of 50 mM Tris-HCl, 150 mM NaCl, and 2 mM DTT; tryptophan fluorescence was followed during a ramp of temperature of 35-95°C.

To evaluate the effect of RIF addition on protein stability, it was performed protein buffer exchange with 20 mM potassium phosphate pH 6.8, 100 mM NaCl, 0.5 mM DTT (Zeba Spin Desalting Columns, 7K MWCO, 2mL). Each protein, at a concentration of 40 µM, was analyzed under three conditions: alone, with the addition of dimethyl sulfoxide (DMSO) at final concentration of 20%, and with 2 mM RIF dissolved in DMSO.

SEC-MALS analysis was performed after purification from the insoluble fraction for PonA1 and the soluble fraction for RpoB, using 100 µL of native PonA1, refolded PonA1, and RpoB protein. All proteins were evaluated following the manufacturer9s instructions (Wyatt technology), column Superdex^{TM} 200 increase 10/300 GL with Agilent 1260 Infinity II. All the proteins were evaluated in Tris-HCl 50 mM, NaCl 150 mM, and 2 mM DTT. The MiliQ water, buffers and 20% ethanol were filtered 0,2 µm and equilibrated. The sample was incorporated through the exclusion column connected to the MALS detector and UV detector. After the sample was eluted from the column, SEC-MALS data collection commenced. The data were analyzed using ASTRA software (Wyatt Technology), which allows for the

determination of molecular weight and other relevant biophysical properties of the protein samples.

For CD, 40 µL of each protein was placed in the chamber, following the manufacturer9s protocol (Chirascan- Applied photophysics), in precision cells 106-QS 0,1 mm light path (Hellma Analytics).

III.2.4. Transpeptidase enzyme activity of PonA1

The C-terminal TP domain of PonA1 contains the PBP domain, which has active sites that recognize the β-lactam ring of antibiotics such as penicillin, which mimic the acyl-D-Ala-D-Ala portion of the PG . Upon interaction between the PBP and penicillin, an irreversible covalent bond is formed with a serine residue in the active site. This interaction was exploited using a fluorescent analog of penicillin V, Bocillin-FL, to confirm the enzymatic activity of the protein and to assess whether mutations in PonA1 preserve this activity.

$PonA1_{234\text{-}820}$ _WT and its mutants (20-480 ng) were incubated in a total volume reaction of 10 µL containing 20 mM potassium phosphate buffer pH 6,8, 0.1 M NaCl and 0.5 mM DTT with 10 µM of Bocillin-FL (Lee et al., 2003), and was incubated for 30 min at 25°C. The samples were prepared with loading buffer without bromophenol blue (1.25 mL Tris pH 6.8 1M, 2mL SDS 20%, 4 ml glycerol 50%, 2 ml DTT 1 M up to 10 mL final volume). The marker and the samples were resolved by SDS-PAGE on a 10% gel (Kieser, Boutte, et al., 2015; Zhao et al., 1999). The gel was rinsed with water, the marker in the first lane was cut, and to visualize the labeled PBPs, the gels

were scanned using a TyphoonFLA 9500 with excitation at 504 nm and emission at 511 nm.

III.2.5. PonA1$_{234-820}$-RIF interaction measured by Nuclear Magnetic Resonance (NMR) spectroscopy

To experimentally detect the affinity between PonA1 and RIF, NMR experiments were performed with the support of Dr. Phillippe Barthe at CBS-Montpellier-France.

The following protein-ligand complexes were evaluated: RpoB_WT + RIF, PonA1$_{234-820}$_WT + RIF, PonA1$_{234-820}$ _Q365H + RIF, PonA1$_{234-820}$_P631S + RIF, and Rv1813c Mtb H37Rv+RIF. The RpoB protein was used as a positive binding control and the Rv1813c protein, generously provided by Dr. Cohen-Gonsaud, was used as a negative binding control.

III.2.5.1. Sample preparation

All experiments were performed using 3 mm New Era NMR tubes. RpoB and PonA1$_{234-820}$9s proteins were expressed as described in section III.2.2. Rv1813c protein, supplied by PhD. Cohen-Gonsaud of the CBS, was evaluated as a negative control.

Protein buffer exchange was carried out using 20 mM potassium phosphate pH 6.8, 100 mM NaCl, 0.5 mM DTT (Zeba Spin Desalting Columns, cat # 89890, 7K MWCO, 2mL). RIF was resuspended in DMSO-d6 (Sigma-Aldrich), and all reagents were purchased from Sigma 3 Aldrich.

Protein-ligand gradient samples were prepared by placing homogeneous solutions of buffer, protein, and RIF at the bottom of the NMR tube, spinning the solution down on a Hettich 1011 hand-wound centrifuge to ensure removal of any residual protein from the tube walls.

For 1D NMR analysis, to perform binding specificity assays, a concentration of 40 µM was used for all proteins ($PonA1_{234-820}$_WT, $PonA1_{234-820}$_Q365H, $PonA1_{234-820}$_P631S) and 2 mM for RIF. RpoB was used as a positive control, and Rv1813c as negative control for binding.

For the STD-NMR analysis, the same conditions used for 1D-NMR sample preparation were followed, and five serial dilutions of RIF concentrations were performed.

III.2.5.2. NMR analysis to measure PonA1 and RIF affinity

All NMR spectroscopy experiments were performed on a Bruker Avance III 800 MHz spectrometer equipped with a cryoprobe at a temperature of 293 K. The data acquisition parameters were as follows: spectral width of 20 ppm, 32K points in the time domain (16K real, 16K complex), resolution of 0.98 Hz. Each measurement began by calibrating the frequency of the transmitted pulse O1 on resonance with the water protons (4.697 ppm), and optimizing the 90° proton pulse P1, calibrated at 7 ¼s.

- 1D ^{1}H NMR: the classical 1D proton sequence (zgesgp) uses gradient excitation sculpting as a water suppression technique.

- **STD-NMR:** The STD-NMR sequence employs a 30° pulse to maximize saturation transfer efficiency, and a water suppression using excitation sculpting with gradients. A pseudo-2D version of the STD-NMR sequence (stddiffesgp.2) was used for the interleaved acquisition of on- and off-resonance spectra. The on-resonance frequency was adjusted to 8.9 ppm whereas the off-resonance frequency was 40 ppm. The experiments were based on the methodology described by Angulo & Nieto, 2011. Saturation times to obtain the STD buildup curves were 0.5, 0.75, 1, 1.5, 2, 2.5, 3 and 4 s, and the number of scans was 64. The total duration of each experiment was 6 s, following the protocols of Angulo & Nieto (2011) and Walpole et al. (2019).

III.2.6. *MMAR_0069* gene knockout in *M. marinum* by ORBIT

The experiments were carried out at CBS-Montpellier-France, for the experiments with Mmar strain M, the BSL-2 security area was required.

To perform the ΔMMAR0069, the steps described by Murphy et al. (2018) were followed to use the Oligo-mediated recombineering followed by BxB1 Integrase Targeting (ORBIT). In brief, this system utilizes three main components: a plasmid that expresses Che9c RecT and Bxb1 integrase, an oligonucleotide, and a payload plasmid, also referred to as the ORBIT plasmid. The Che9c RecT annealase protects single-stranded DNA (ssDNA) and promotes its annealing to a complementary ssDNA target within the cell. Its expression is essential for recombineering with an ssDNA oligo substrate, and it is controlled by the inducible Ptet promoter. The Bxb1 integrase is one of the most efficient enzymes for DNA recombination, surpassing many other integrases in its recombination efficiency (Wang et al., 2017). The oligonucleotide

provides recognition of the target sequence, flanked by 70 bp upstream and 70 bp downstream, with an *attP* site located in the middle. The payload or ORBIT plasmid carries the *attB* site (Figure III.1.A), allowing site-specific integration. Depending on the desired genetic manipulation, the plasmid design can vary. Upon integration, the entire plasmid is incorporated into the genome at the lagging strand, with the system additionally incorporating an antibiotic resistance marker into the modified cells. This approach enhances the efficiency and precision of genetic modifications (Armianinova et al., 2022).

Two rounds of electroporation were performed, the first one to insert pKM444 plasmid, this plasmid express Che9c phage, RecT and Bxb1 phage integrase under PTet promoter control inducible with anhydrotetracycline (ATc). The second electroporation, to do the gene KO through the insertion of the payload ORBIT plasmid mediated by the oligonucleotide (Figure III.1.B), it was constructed based on pKM464 ORBIT plasmid.

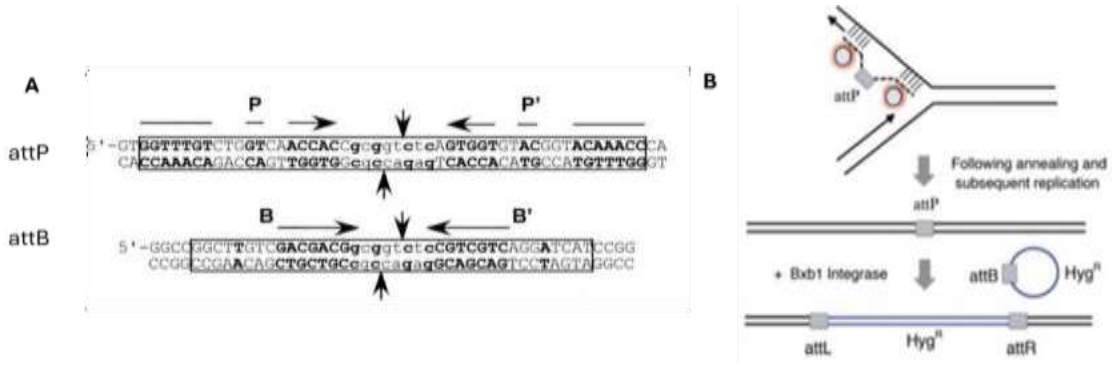

Figure III.1. Oligo-mediated recombineering followed by BxB1 Integrase Targeting (ORBIT) elements and scheme. A Phage » recombination mediated by *attP* and *attB* site (Taken from Ghosh et al., 2003). B. ORBIT mechanism overview (Taken from Murphy et al., 2018).

III.2.6.1. Oligonucleotide design

For the oligonucleotides design, the protocol described by Murphy *et al* (2018) was followed, using the CP000854.1 Mmar strain M chromosome as a template. The targeted genome region for removal spanned from 68,539-71,016.

Oligonucleotide was designed with 70 bp towards the upstream end (68,469-68,538) and 70 bp towards the downstream end (71,017- 71,086) of *MMAR_0069* gene (Figure III.2), comprising the *attP* site between both sequences, highlighted in bold.

ssDNA-BOTTOM-INV_5-3_Mmarinum_ORBIT (oligonucleotide), had the sequence: 59

GGTTCGGGCGAGGTGGCGCAACGTGGTGTCCGTGCGTCCGTCACGGTGGC
GGATTGTCGGCGGGTGGCGCG**GTTTGTACCGTACACCACTGAGACCGC**
GGTGGTTGACCAGACAAACCCGGCTGGTGGTGGCGCCCTTCGTTACTCA
CTGGCAGTGCGGGCTCCATTGCGCGCCGTGCGCTTGCCACC 39.

This oligonucleotide was ordered as ultramer from IDT (Integrated DNA technologies). The stock concentration was 100 µM, and the working solution was diluted to 10 µM in the Tris-EDTA buffer (pH 8.0). The concentration was quantified by spectrophotometry at 260 nm with 1 µg used for each transformation.

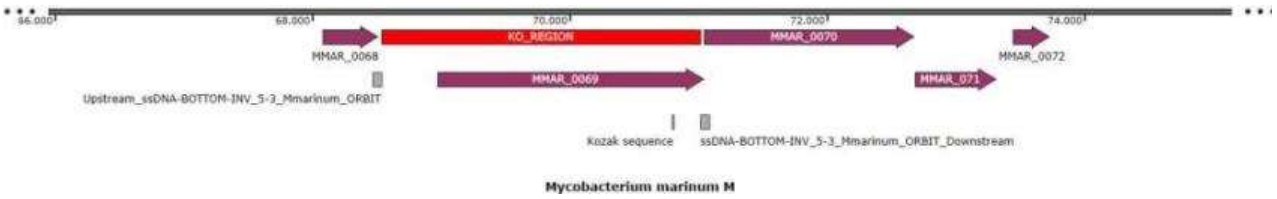

Figure III.2. Scheme for the design of oligonucleotide targeting the *MMAR_0069* gene knockout in *M. marinum*.

III.2.6.2. ORBIT payload plasmid modification for *MMAR_0069* gene knockout

The aim was to use the ORBIT plasmid to perform the gene KO while simultaneously inserting a reporter system with the EGFP gene to evaluate the activity of two promoters: *ponA1* promotor (*ponA1p*) from Mtb H37Rv and *rpsT* promotor from Mmar (*rpsTp*). *ponA1p* has been proposed by Kiesser but has not been previously evaluated experimentally (Kieser et al, 2015). *rpsTp* from Mmar evaluated by DaSilva A, DeVish A and Cohen-Gonsaud M 2022 (direct communication) had a good performance for the green fluorescent protein (GFP) expression after integration of pMV361 in *M. smegmatis* genome (Appendix III.10).

A. pKM464-ponA1p-EGFP construction

Plasmid pKM464-ponA1p-ponA1 (constructed in this study, appendix III.11-12), served as a template for constructing pKM464-ponA1p-EGFP. The plasmid was linearized using primers: F-EGFP-pKM464 59-TGGACGAGCTGTACAAGTAACCGGCGCGCTGTCCCAAAGC-39 and R-EGFP-pKM464 59- TCCTCGCCCTTCGACACCATTGGCCGTGCGGGCCCCGTTG-39.

The reaction employed Q5 High-Fidelity 2X Master Mix, 10 µM of each primer, and 10 ng of pKM464-ponA1p-ponA1 as a template. PCR conditions included an initial denaturation at 98°C for 30 seconds, followed by thirty cycles of 98°C for 10 seconds, 70°C for 20 seconds, and 72°C for 2 minutes with 24 seconds, with a final extension at 72°C for 2 minutes and a hold at 12°C. Gel purification was performed (Monarch DNA Gel Extraction kit-NEB).

EGFP was amplified with the primers F-EGFP 59-ATGGTGTCGAAGGGCGAGGAG-39 and R-EGFP 59-TTACTTGTACAGCTCGTCCATGC-39 (Appendix III.13). The reaction employed Q5 High-Fidelity 2X Master Mix, 10 µM of each primer, and 10 ng of pKM468 (Addgene-plasmid #108434) as the template. PCR conditions included an initial denaturation at 98°C for 30 seconds, followed by thirty cycles of 98°C for 10 seconds, 62°C for 20 seconds, and 72°C for 24 seconds, with a final extension at 72°C for 2 minutes and a hold at 12°C.

B. pKM464-*rpsTp*-EGFP construction

rpsTp locus_tag MMRN_39890 (GenBank: AP018496.1) (Appendix III.15-16), which was evaluated for regulation of GFP expression in *M. smegmatis* by Cohen-Gonsaud (personal communication). It was amplified with primers: F-pKM464-rpsT 59- CCAGCAGGCCGGTCAGCCTCACGTCTTTTGGGTGAAAACG-39 and R-EGFP-rpsT 59- CTCCTCGCCCTTCGACACCATGCTGTTGGTGCGGTTGCGCT-39. The reaction employed Q5 High-Fidelity 2X Master Mix, 10 µM of each primer, and 10 ng of synthetic *rpsTp* as a template. PCR conditions included an initial

denaturation at 98°C for 30 seconds, followed by thirty cycles of 98°C for 10 seconds, 62°C for 20 seconds, and 72°C for 6 seconds, with a final extension at 72°C for 2 minutes and a hold at 12°C.

pKM464 plasmid was opened with F-EGFP-pKM464 59-TGGACGAGCTGTACAAGTAACCGGCGCGCTGTCCCAAAGC-39 and R-pKM464 59- GAGGCTGACCGGCCTGCTGG-39. The reaction employed Q5 High-Fidelity 2X Master Mix, 10 µM of each primer, and 10 ng of pKM464 as a template. PCR conditions included an initial denaturation at 98°C for 30 seconds, followed by thirty cycles of 98°C for 10 seconds, 68°C for 20 seconds, and 72°C for 1 minute with 36 seconds, with a final extension at 72°C for 2 minutes and a hold at 12°C. Gel purification was performed (Monarch DNA Gel Extraction kit-NEB).

EGFP was amplified following the same steps described in the construction of pKM464-ponA1p-EGFP in section III.2.6.2.A. *in silico* representation is provided in Appendix III.14.

III.2.6.3. Cloning and transformation in *E. coli*

For all cloning procedures Gibson assembly (GA) was performed (Protocol standardized by the Synthetic biology group-CBS-Montpellier-France), DH5α cells were employed for heat-shock transformation (Appendix III.17 and 18). Clone selection was verified by sequencing with F-pKM464-int and R-pKM464-int primers (Appendix III.34). Sequencing service was performed by Eurofins (https://eurofinsgenomics.eu/). All plasmids were propagated in *E. coli* DH5α cells,

and plasmid extraction was performed using the Monarch® Plasmid Miniprep Kit, following the manufacturer's instructions.

III.2.6.4. *M. marinum* strains and media

This technique was developed at the BLS-2 facilities of CBS-Montpellier-France using the Mmar strain M, generously provided by A. Blanc-Potard, LPHI. The logistics and protocols were implemented with this thesis for its application.

Mmar (wild type) was cultured at 30-32°C in darkness, for liquid culture Middlebrook 7H9 broth supplemented with 5% OADC (comprising 5 g/L albumin, 2 g/L dextrose, 3 g/L catalase, oleic acid), 0,2% glycerol and 0.05% tween80 (7H9). Solid cultures were grown on Middlebrook 7H10 medium, similarly supplemented with 5% OADC and 0.5% glycerol (7H10). The growth and purity of these strains were monitored under an inverted microscope (Invitrogen TM EVOS TM FL).

III.2.6.5. *MMAR_0069* gene knockout in *M. marinum* by ORBIT

To achieve the gene KO, the first requirement was to obtain cells that have already incorporated a plasmid capable of expressing the Che9c phage, RecT and Bxb1 phage integrase under the control of the PTet promoter, which is inducible with ATc. To achieve this, the initial step was to prepare competent cells from the Mmar wild-type, briefly described in sections A-B, below. Once the cells containing the plasmid were obtained, they were cultivated to prepare a new batch of competent cells, into which the ORBIT plasmid was introduced for integration mediated by the oligonucleotide, as described in sections C-D.

A. Electro-competent cells preparation for pKM444 insertion

A wild-type Mmar colony was cultured in 5 mL of 7H9 for 2-3 days at 30°C. Subsequently, 0.5 mL of this culture was transferred to 50 mL of 7H9, achieving a 1:100 dilution, and grown for 3-4 days until an OD_{600} of 0.8-1 was reached. At this point, 5 mL of 2M glycine was added, and the culture was incubated for 16-24 hours. The culture was then centrifuged at 3500 rpm for 10 minutes at 17°C. The resulting pellet was washed three times with 20, 10, and 5 mL of sterile 10% glycerol containing 0.05% Tween 80, preheated to 30-32°C. Finally, the pellet was resuspended in 1 mL of 10% glycerol-Tween 80 (0.05%) and divided into 400 µL aliquots for immediate use.

B. First electroporation of *M. marinum*

Between 0.5-1 µg (less than 5 µL) of the pKM444 plasmid (Addgene Plasmid #108319) was mixed with 400 µL of competent cells and transferred to an electroporation cuvette with a 0.2 cm electrode gap. Electroporation was conducted at 2.5 kV, 25 µF, with a pulse-controller resistor at 1000Ω. The cuvette was then subjected to a single pulse, and if the time constant was outside the optimal range, the procedure was repeated, targeting pulse times between 15 and 25 ms. Immediately after electroporation, the cell suspension was transferred to 5 mL of 7H9 medium (without antibiotics) and incubated at 32°C for 3-4 hours to allow cell recovery. The culture was then homogenized by pipetting, and 100 µL of the suspension was plated onto 7H10 agar plates containing 20 µg/mL KAN. The remaining cell suspension was

concentrated and plated on a second agar plate. The plates were covered with aluminum foil and incubated at 30-32°C until colonies formed, typically within 7-14 days.

C. Preparation of electro-competent cells and electroporation for gene knockout by ORBIT

Once the strains had acquired the pKM444 plasmid, competent cells were prepared for the insertion of the payload plasmid (pKM464, Addgene Plasmid #108322) and the oligonucleotide. The addition of ATc induced the expression of RecT, facilitating the plasmid insertion, which was mediated by the oligonucleotide.

Mmar containing the pKM444 plasmid was cultured in 5 mL of 7H9 supplemented with 20 µg/mL KAN for 2-3 days at 30°C. Following this, 0.5 mL of the culture was transferred to 50 mL of 7H9 with 20 µg/mL KAN, grown for 3-4 days until reaching an OD_{600} of 0.8-1. At this point, ATc was added to a final concentration of 500 ng/mL, and the culture was incubated for 8 hours at 30-32°C to induce RecT expression. Subsequently, 5 mL of 2M glycine was added, and the culture was incubated for 16-24 hours. After incubation, the culture was centrifuged at 3500 rpm for 10 minutes at 17°C, and the pellet was washed three times with pre-heated 10% glycerol-Tween 80 (0.05%), then resuspended in 1 mL of the same solution.

For electroporation, 1 µg of oligonucleotide and 200 ng of either pKM464-ponA1p-EGFP /pKM464-*rpsTp*-EGFP plasmid (total volume of 5 µL) were mixed with 400 µL of competent cells. The mixture was placed in an electroporation cuvette with a 0.2 cm electrode gap and subjected to electroporation at 2.5 kV, 25 ¼F, with a

pulse-controller resistor set to 1000Ω. Transformation controls without the oligonucleotide and negative controls without the plasmid were also included for comparison.

The cell suspension was immediately transferred to 5 mL of enriched 7H9 (without antibiotic) and incubated at 30-32°C for 16-24 hours to allow cell recovery. Subsequently, 500 µL of the cell suspension was plated on 7H10 containing 50 µg/mL hygromycin (HYG) and 20 µg/mL KAN and incubated at 30-32°C until colonies appeared, usually within 10-14 days.

D. Colonies selection and verification of integration of the payload ORBIT plasmid

For colony selection, 1 mL of 7H9 was distributed in 24 plate-well, with one colony cultivated per well at 30°C in darkness for 7 days. Verification of contamination was controlled after 24 hours of incubation. After 7 days, 20 µL of each culture was transferred to screw cap tubes containing 20 µL of TE buffer and inactivated at 80°C for 30 minutes. PCR was conducted to verify plasmid insertion, using primers F-Mmar-Rv0050-orbit 59- CGCACCTGCAGTTGGAATCACCTG-39 and R-Mmar-Rv0050-orbit 59- CGATCAGCGCGTGGCGG-39. The PCR mix included One Taq 2x polymerase (New Englands Biolabs), 10 µM of each primer, and between 2 - 4 µL of supernatant containing Mmar DNA_g as the template. The PCR cycle consisted of an initial denaturation at 94°C for 5 minutes, followed by thirty cycles of 94°C for 30 seconds, 64°C for 30 seconds, and 68°C for 3 minutes 30 seconds, with a final

extension at 68°C for 5 minutes and storage at 12°C. Electrophoresis in agarose gel at 0.8 - 1% was performed to visualize the results, run in buffer TAE 1X.

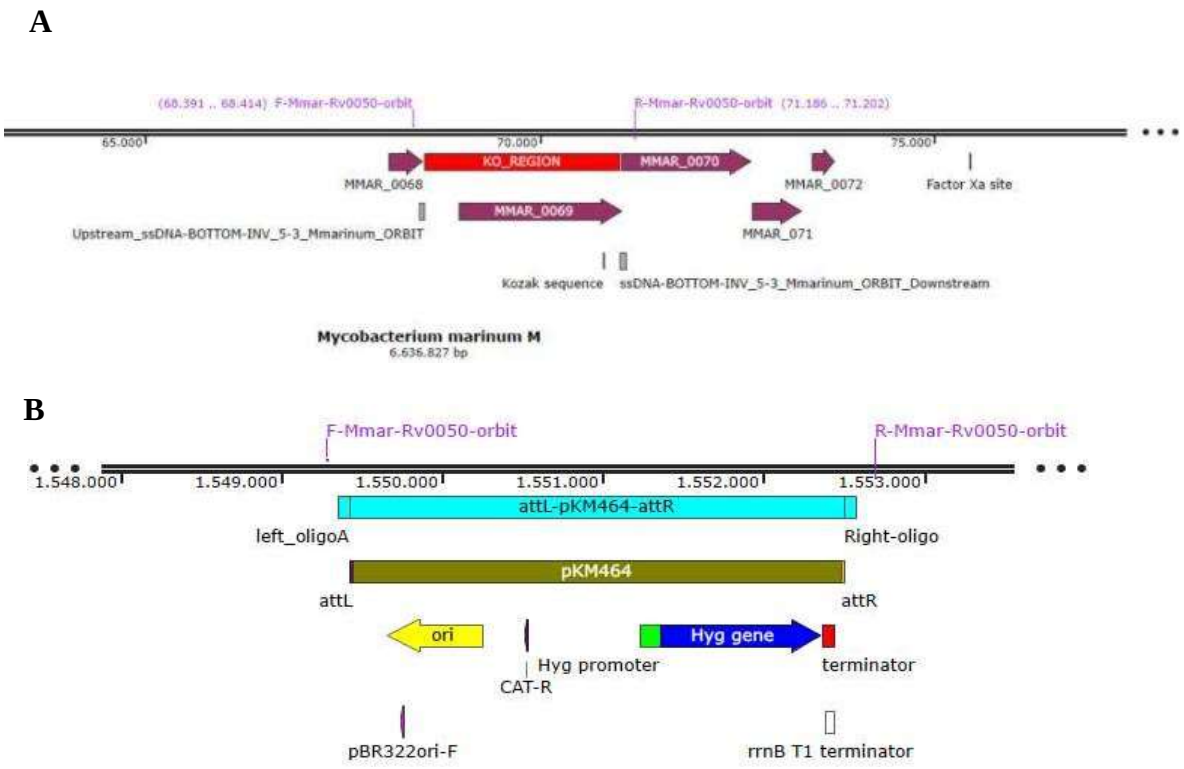

Figure III.3. ***MMAR_0069*** **gene knockout in the** ***M. marinum*** **genome.** A. Locus of the *MMAR_0069* gene. B**.** Disposition of the plasmid pKM464 after gene knockout on the lagging strand using an oligonucleotide.

E. Sequencing and cryopreservation

The PCR product was purified using a gel extraction kit (Monarch Gel extraction kit-NEB), and quantified by nanodrop. Eurofins (https://eurofinsgenomics.eu) performed the sequencing with the same primers used for the amplification. The sequence analysis was performed with SnapGene ® 6.1.2.

To confirm that the plasmid was correctly integrated into the chromosomal DNA, long-read sequencing was conducted at the Laboratorio de Bioinformática y Biología Molecular, UPCH, Peru. DNA extraction was performed using the ZymoBIOMICS™ DNA Miniprep kit, following the manufacturer's instructions. Genomic DNA was quantified using fluorescence with a Qubit 1x dsDNA kit. For sequencing, the manufacturer's protocol was followed: library preparation was carried out using a rapid kit and loaded onto a GridION flow cell R9 (Oxford Nanopore Technologies). For the bioinformatic analysis, we mapped the assembled contigs against the constructed reference genome of Mmar, which included the plasmid inserts, using Minimap2 (Li, 2018). The origin of replication was set to the *DNA A1* gene. The alignment was visualized using the Integrative Genomics Viewer (IGV). Annotation was performed with Bakta to confirm that the plasmid sequence mapped accurately to the intended location and to verify that the upstream and downstream genes were positioned as expected.

For cryopreservation, 50 µL of the verified clone was cultured in 7H10 and incubated at 30°C for 5-7 days in darkness. The solid culture was collected with a loop, resuspended in 1200 µL of 7H9 mixed with 300 µL of 50% glycerol, and stored at -70°C.

III.2.6.6. Assessment of promoter function via EGFP reporter expression in *M. marinum*

Cells in the logarithmic phase were adjusted to a McFarland scale of 1 and diluted 1:25 in 7H9. They were placed in 96-well plates (Costar 96 clear bottom black

side with lid) and monitored every 12 hours for OD_{600} and fluorescence, with excitation at 485 nm and emission at 528 nm, and a gain setting of 100 read from the bottom. The experiment was conducted at a constant temperature of 30°C for 122 h.

III.2.7. *ponA1* gene complementation in *M. marinum MMAR_0069* gene knockout strains

Two techniques were tested for *ponA1* gene complementation: the first involved cloning the *rpsTp* and the *ponA1* gene from Mtb H37Rv into the ORBIT payload plasmid, enabling both gene knockout and complementation mediated by ORBIT. The second method utilized L5-phage site integration in strains with the ΔMMAR0069, where the plasmid pMV361, containing *ponA1* cloned under *hsp60* regulation, was integrated into the genome.

III.2.7.1. *MMAR_0069* gene knockout and *ponA1* gene complementation in one step mediated by ORBIT

The ORBIT technique enabled the KO of the *MMAR_0069* gene through the insertion of the pKM464 plasmid (Murphy, 2018), as described in section III.2.6.5. Our objective was to further modify this plasmid by incorporating a promoter (*rpsTp*) and a gene of interest (*ponA1* from Mtb H37Rv). If successful, this modified plasmid could facilitate both gene KO and gene complementation simultaneously in a single step.

A. ORBIT payload plasmid modification for one-step gene knockout and complementation and transformation in *E. coli*

Based on the evaluation performed in section III.2.6 the *ponA1* gene was cloned under the control of the *rpsTp* and the process is detailed below:

For the construction of pKM464-*rpsTp*-ponA1 plasmid (Appendix III.19), primers: F-pKM464-rpsT 59-CCAGCAGGCCGGTCAGCCTCACGTCTTTTGGGTGAAAACG-39 and R-ponA1-rpsT 59- GTGACGCCCGTCGCTATTCACGCTGTTGGTGCGGTTGCGCT-39 were used to amplify the *rpsTp*. The reaction employed Q5 High-Fidelity 2X Master Mix, 10 µM of each primer, and 10 ng of *rpsT* synthetic promoter as a template. PCR conditions included an initial denaturation at 98°C for 30 seconds, followed by thirty cycles of 98°C for 10 seconds, 62°C for 20 seconds, and 72°C for 6 seconds, with a final extension at 72°C for 2 minutes and a hold at 12°C.

For amplification of the pKM464-ponA1g, primers F-ponA1-gene-H37Rv 59-GTGAATAGCGACGGGCGTCAC-39 and R-pKM464 59-GAGGCTGACCGGCCTGCTGG-39 were used. The reaction employed Q5 High-Fidelity 2X Master Mix, 10 µM of each primer, and 10 ng of pKM464-ponA1p-ponA1g plasmid as a template. PCR conditions included an initial denaturation at 98°C for 30 seconds, followed by thirty cycles of 98°C for 10 seconds, 67,7°C for 20 seconds, and 72°C for 2 minutes 45 seconds, with a final extension at 72°C for 2 minutes and a hold at 12°C. Gel purification was performed (Monarch DNA Gel Extraction kit-NEB). For assembling the PCR fragments, GA was utilized.

Transformations in *E. coli* DH5α were conducted as previously described in Section III.2.6.3. Colony PCR and sequencing were carried out using appropriate primers.

B. ORBIT for *MMAR_0069* gene knockout and *ponA1* gene complementation in one step

Mmar harboring pKM444 plasmid was reactivated in 5 mL of 7H9 for 2-3 days at 30 °C. 0.5 mL culture was transferred to 50 mL 7H9 (1:100 dilution). For this procedure, the same steps were followed as in section III.2.6.5.C, electroporated with the modified pKM464-*rpsTp*-ponA1 plasmid. 500 µL cells were plated on 7H10 plates containing 50 µg/mL HYG plus 20 µg/mL KAN. The plates were incubated at 32°C until the colonies appeared (around 7-10 days). Colonies screening and verification was performed (Section III.2.6.5.D-E). Long read sequencing was performed to evaluate gene KO and verification of site-specific integration, described in section III.2.6.5.E.

III.2.7.2. *ponA1* gene complementation mediated by pMV361 integration via L5 phage site in *M. marinum*

Mmar strains carrying the ΔMMAR0069::*rpsTp*-EGFP construct (hereafter referred to as ΔMMAR0069) were cultivated and subjected to electroporation for gene complementation via pMV361 integration at the L5 phage site. The resulting strain, in which *MMAR_0069* gene was reintroduced is referred to as the isogenic wild-type strain. This approach allow as for the evaluation of whether the mutant phenotype can be restored to a wild type gene add-back cell line is meant to assess that the mutant phenotype can be reverted to a 8wild-type9 status due to the introduced transgene as was previously used by Kieser et al. (2015).

The steps followed for this process are described below.

A. *ponA1* cloning in pMV361

ponA1 gene from Mtb H37Rv (NCBI Reference Sequence:WP_031651598), spanning residue 53237-55699 and containing 820 residues, was cloned in the pMV361 vector under the control of the *hsp60* promoter. The gene was amplified using primers F-pMV361-ponA1-H37Rv 59-GATCCAGCTGCAGAATTCGAGTGAATAGCGACGGGCGTCA-39 and R-pMV361-ponA1-H37Rv 59-CTACGTCGACATCGATAAGCTTCACGGCGGCGGCGTGGGAG-39 (Appendix III.20). The reaction employed Q5 High-Fidelity 2X Master Mix, 10 µ M of each primer, and 10 ng pKM464-ponA1p-ponA1g (generated in this study, for details see Appendix III.12) as a template. PCR conditions included an initial denaturation at 98°C for 30 seconds, followed by thirty cycles of 98°C for 10 seconds, and 72°C for 2 minutes 10 seconds, with a final extension at 72°C for 2 minutes and a hold at 12°C.

pMV361 plasmid was linearized with F-pMV361 59-AGCTTATCGATGTCGACGTAG-39 and R-pMV361 59-TCGAATTCTGCAGCTGGATC-39. The reaction employed Q5 High-Fidelity 2X Master Mix, 10 µM of each primer, and 10 ng pMV361 plasmid as a template. PCR conditions included an initial denaturation at 98°C for 30 seconds, followed by thirty cycles of 98°C for 10 seconds, 60 °C for 20 seconds and 72°C for 2 minutes 30 seconds, with a final extension at 72°C for 2 minutes and a hold at 12°C.

B. Antibiotic cassette replacement in pMV361-ponA1

The goal of this section was to modify the antibiotic resistance cassette of pMV361-ponA1 to create pMV361$_{zeo}$-ponA1 with Zeocin (ZEO) resistance as a selection marker. This modification was necessary because the pMV361 plasmid contains a KAN resistance marker, the same as the pKM444 plasmid, which was introduced during the first electroporation to achieve the gene KO. To do this, the BleoR gene was introduced in the integrative plasmid pMV361 for replacing the KAN resistance cassette. The EM7 promoter and BleoR gene (Appendix III.21.A-B) were amplified using primers F-EM7promoter-BleoR 5'- GCCCGTCATCGTCAACGCCT-3' and R-BleoR 5'- TTCGCAACGTTCAAATCCGC-3' from plasmid pKM496 (Addgene Plasmid #109301). The reaction employed Q5 High-Fidelity 2X Master Mix, 10 µM of each primer, and 10-20 ng of template DNA. PCR conditions included an initial denaturation at 98°C for 30 seconds, followed by thirty cycles of 98°C for 10 seconds, 68°C for 20 seconds, and 72°C for 21 seconds, with a final extension at 72°C for 2 minutes and a hold at 12°C.

For amplifying pMV361-ponA1, primers F-BleoR-pMV361 59-GCGGATTTGAACGTTGCGAACCAACCGTGGCTCCCTCACT-39 and R-EM7promoter-pMV361 59-CAGGCGTTGACGATGACGGGCAGGTGGCTAGCTGATCACCG-39 were used. The reaction employed Q5 High-Fidelity 2X Master Mix, 10 µM of each primer, and 10-20 ng of template DNA. PCR conditions included an initial denaturation at 98°C for 30 seconds, followed by thirty cycles of 98°C for 10 seconds and 72°C for 3 minutes 10 seconds, with a final extension at 72°C for 2 minutes and a hold at 12°C. This

approach was integral to generating pMV361$_{zeo}$-ponA1, as detailed in appendix III.21.C.

C. Cloning and transformation in *E. coli*

The same protocol described in section III.2.6.3 was followed.

D. *ponA1* gene complementation mediated by pMV361 via L5-site: electroporation in *M. marinum*

The ΔMMAR0069 strain was re-activated in 5 mL of 7H9 for 2-3 days at 30 °C. A 0.5 mL culture was diluted 1:100 in 50 mL 7H9. Following the protocol outlined in section III.2.6.5.B, this culture was electroporated with the modified pMV361$_{zeo}$-ponA1 plasmid. Subsequently, 100 µL cells were plated on 7H10 plates containing 30 µg/mL ZEO and incubated at 32°C until the colonies developed, typically within 7-10 days.

III.2.7.3. Cloning of *ponA1* mutants in pMV361$_{zeo}$ in *E. coli*

Mutations in the *ponA1* gene, including T34A (A376G), T34D (A376G, C377A), Q365H (G1521T), A516T (G1546A), and P631S (C2317T) from Mtb H37Rv, were introduced by PCR. The nucleotide point mutations are based on the -426 transcription start site for *ponA1*. The reaction employed Q5 High-Fidelity 2X Master Mix, 10 µM of each primer, and 10 ng pKM464-*rpsTp*-ponA1 plasmid as a template for the generation of *ponA1* mutants. For this purpose, two pairs of primers were used to introduce the mutation, designed according to the specific mutation being targeted. The generation of *ponA1* mutants typically involves an initial denaturation step at 98°C for 30 seconds, followed by thirty cycles under specific conditions outlined in Table III.2. This is then followed by a final extension at 72°c for 2 minutes

and a hold at 1C. The *in silico* representation of primer localization for all mutants is detailed in Appendix III.22 to 26. Additionally, the procedure for subcloning these mutated genes in the pMV361$_{ZEO}$ plasmid is also included.

Table III.2. Primers used for site directed mutagenesis in *ponA1* of *M. tuberculosis.*

PonA1 mutants	Description	Primers for cloning in pKM464	Primers sequence	PCR conditions (Thirty cycles)
T34A	Fragment I	F-T34-ponA1	59- GCGATCCTCCCGCCGGTGAC-39	98°C for 10 seconds
		R-H37Rv_ponA1_promoter	59- AGATGTTGCTGCTTTGGGACAG-39	69°C for 20 seconds 72°C for 1 minute 20 seconds
	Fragment II	R-T34A-ponA1	59-GTCACCGGCGGGAGGATCGCGGcCAGTCTGTCGTCGGGTG-39	98°C for 10 seconds
		F_pKM464-ponA1	59-GTCCCAAAGCAGCAACATCTTGCGGCCGCTAGCGGTACCAG-39	72°C for 2 minutes 10 seconds
T34D	Fragment I	F-T34-ponA1	59- GCGATCCTCCCGCCGGTGAC-39	98°C for 10 seconds,
		R-H37Rv_ponA1_promoter	59- AGATGTTGCTGCTTTGGGACAG-39	69°C for 20 seconds 72°C for 1 minute 20 seconds
	Fragment II	R-T34D-ponA1	59-GTCACCGGCGGGAGGATCGCGtcCAGTCTGTCGTCGGGTG-39	98°C for 10 seconds
		F_pKM464-ponA1	59-GTCCCAAAGCAGCAACATCTTGCGGCCGCTAGCGGTACCAG-39	72°C for 2 minutes

Table III.2 (…continuation). Primers used for site directed mutagenesis in *ponA1* of *M. tuberculosis.*

PonA1 mutants	Description	PRIMERS for cloning in pKM464	Sequence	PCR conditions (Thirty cycles)
Q365H	Fragment I	F-H37Rv_ponA1_promoter	59-CCAGCAGGCCGGTCAGCCTC-39	98°C for 10 seconds
		R-Q365H-ponA1	59-GTCAACGGAGAGCTGTCTACaTGGTAGCCCAGGCCGATCC-39	69°C for 20 seconds 72°C for 50 seconds
	Fragment II	F-Q365H-ponA1	59- GTAGACAGCTCTCCGTTGAC-39	98°C for 10 seconds, and
		R_pKM464-ponA1	59-GAGGCTGACCGGCCTGCTGGactagtgcatgctctagactc-39	66°C for 20 seconds 72°C for 2 minutes 3 seconds
A516T	Fragment I	F-A516T-ponA1	59- GCGATGGAGCCGATCGCAGG-39	98°C for 10 seconds, and
		R_pKM464-ponA1	59-GAGGCTGACCGGCCTGCTGGACTAGTGCATGCTCTAGACTC-39.	72°C for 2 minutes 10 seconds
	Fragment II	F-H37Rv_ponA1_promoter	59- CCAGCAGGCCGGTCAGCCTC-39	98°C for 10 seconds
		R-A516T-ponA1	59-CCTGCGATCGGCTCCATCGCCGtAGTCACGTTGTCGGCTA-39	72°C for 1 minute 30 seconds
P631S	Fragment I	F-H37Rv_ponA1_promoter	59- CCAGCAGGCCGGTCAGCCTC-39	98°C for 10 seconds,
		R-P631S-ponA1	59-GTCTCCGAAGGTGGTACCTCCGaCGGCGGCGGCGGCGGCGGCACACC -39	69°C for 20 seconds 72°C for 1 minute 18 seconds
	Fragment II	F-P630-P631-ponA1	59- GAGGTACCACCTTCGGAGAC-39	98°C for 10 seconds
		R_pKM464-ponA1	59-GAGGCTGACCGGCCTGCTGGACTAGTGCATGCTCTAGACTC-39	69°C for 20 seconds 72°C for 1 minute 40 seconds

The generated *ponA1* genes were verified by sequencing and subsequently subcloned in the pMV361 plasmid. For this purpose, *ponA1* with any mutation was amplified with primers F-pMV361-ponA1-H37Rv 59-GATCCAGCTGCAGAATTCGAGTGAATAGCGACGGGCGTCA-39 and R-pMV361-ponA1-H37Rv 59-CTACGTCGACATCGATAAGCTTCACGGCGGCGGCGTGGGAG-39. The reaction employed Q5 High-Fidelity 2X Master Mix, 10 µM of each primer, and 10 ng pKM464-*rpsTp*-ponA1-mut plasmid as a template. PCR conditions included an initial denaturation at 98°C for 30 seconds, followed by thirty cycles of 98°C for 10 seconds, and 72°C for 2 minutes 10 seconds, with a final extension at 72°C for 2 minutes and a hold at 12°C.

For all mutations, the plasmid $pMV361_{zeo}$, was linearized to create an opening for the insertion of mutated genes. Primers F-pMV361 59-AGCTTATCGATGTCGACGTAG-39 and R-pMV361 59-TCGAATTCTGCAGCTGGATC-39 were used. The reaction employed Q5 High-Fidelity 2X Master Mix, 10 µM of each primer, and 10 ng $pMV361_{zeo}$-ponA1 plasmid as a template. PCR conditions included an initial denaturation at 98°C for 30 seconds, followed by thirty cycles of 98°C for 10 seconds, 60°C for 20 seconds and 72°C for 2 minutes 30 seconds, with a final extension at 72°C for 2 minutes and a hold at 12°C (Appendix III.27-31).

III.2.7.4. *MMAR_0069* gene cloning in pMV361

To construct the isogenic wild-type strain, the *MMAR_0069* gene, which had been previously knocked out, was amplified and cloned to enable gene complementation, allowing the strain to serve as a control.

A. Cloning of *MMAR_0069* gene in pKM44 under *rpsTp* regulation

The *MMAR_0069* gene was amplified with primers F-MrcB-Mmar 59-GTGAGTAACGAAGGGCGCCA-39 and R-MrcB-Mmar 59-TCACGGTGGCGGATTGTCGG-39. The reaction employed Q5 High-Fidelity 2X Master Mix (New England Biolabs), 10 µM of each primer, and 10 ng genomic DNA from Mmar as a template. PCR conditions included an initial denaturation at 98°C for 30 seconds, followed by thirty cycles of 98°C for 10 seconds, 71°C for 20 seconds and 72°C for 1 minute 20 seconds, with a final extension at 72°C for 2 minutes and a hold at 12°C.

The plasmid was amplified with primers F-MrcB-pKM464 59-CCGACAATCCGCCACCGTGACCGGCGCGCTGTCCCAAAGC-39 and R-MrcB-rpsT-Mmar 59-TGGCGCCCTTCGTTACTCACGCTGTTGGTGCGGTTGCGCT-39 were used. The reaction employed Q5 High-Fidelity 2X Master Mix, 10 µM of each primer, and 10 ng pKM464-*rpsTp*-ponA1 as a template. PCR conditions included an initial denaturation at 98°C for 30 seconds, followed by thirty cycles of 98°C for 10 seconds, and 72°C for 1 minute 39 seconds, with a final extension at 72°C for 2 minutes and a hold at 12°C (Appendix III.32).

B. *MMAR_0069* gene subcloning in pMV361zeo

pMV36$_{ZEO}$ was amplified with primers F-pMV361-MMAR0069 59-GATCCAGCTGCAGAATTCGAGTGAGTAACGAAGGGCGCCAC-39 and R-pMV361-Mmar0069 59-TACGTCGACATCGATAAGCTTCACGGTGGCGGATTGTCGG-39. The reaction employed Q5 High-Fidelity 2X Master Mix, 10 µM of each primer, and 10 ng pKM464-*rpsTp*-MMAR0069 as a template. PCR conditions included an initial denaturation at 98°C for 30 seconds, followed by thirty cycles of 98°C for 10 seconds, and 72°C for 2 minutes 55 seconds, with a final extension at 72°C for 2 minutes and a hold at 12°C.

Primers F-MrcB-Mmar 59-GTGAGTAACGAAGGGCGCCA-39 R-MrcB-Mmar 59-TCACGGTGGCGGATTGTCGG-39 were used to amplify the *MMAR_0069* gene. The reaction employed Q5 High-Fidelity 2X Master Mix, 10 µM of each primer, and 10 ng pKM464-*rpsTp*-MMAR0069 as a template. PCR conditions described previously (Appendix III.33).

C. Cloning, transformation in *E. coli* and verification

The same protocol described in Section III.2.6.3 was followed. Sequencing was performed by Eurofins (https://eurofinsgenomics.eu/). Primers for sequencing are described in appendix III.34, Verif_GgPMV_Rv and Verif_Gg_PMV_Fw. All plasmids were propagated in *E. coli* DH5α cells, and plasmid extraction was performed using the Monarch® Plasmid Miniprep Kit, following the manufacturer's instructions.

D. ponA1-mutants gene complementation mediated by pMV361 plasmid for integration in *M. marinum* genome

The ΔMMAR0069 strain was reactivated in 5 mL of 7H9 for 2-3 days at 30 °C. A 0.5 ml culture was diluted 1:100 in 50 mL 7H9. Following the protocol outlined in section III.2.6.5.B, this culture was electroporated with the modified $pMV361_{zeo}$-ponA1-mutants plasmid. Subsequently, 100 µL cells were plated on 7H10 plates containing 30 µg/mL ZEO and incubated at 32°C until the colonies developed, typically within 7-10 days.

E. PCR colony, verification of plasmid integration, sequencing and cryopreservation

Protocols described in III.2.6.5.D and III.2.6.5.E sections were followed. Primers for verification of integration were Verif_Gg_PMV_Fw 59-GACCATTTACGGGTCTTGTTGT-39 and Verif_GgPMV_Rv 59-TGGCAGTCGATCGTACGCTA-39. The PCR mix included One Taq 2x polymerase, 10 µM of each primer, and between 2 - 4 µL of Mmar genomic DNA as the template. The PCR cycle consisted of an initial denaturation at 94°C for 5 minutes, followed by thirty cycles of 94°C for 30 seconds, 51°C for 30 seconds, and 68°C for 2 minutes 45 seconds, with a final extension at 68°C for 5 minutes and storage at 12°C. Electrophoresis in agarose gel at 1% was performed to visualize the results, run in buffer TAE 1X.

III.2.8. Drugs susceptibility test by TEMA

The Tetrazolium Microplate Assay (TEMA), using 3-(4,5-dimethylthiazol-2-yl)-2,5 diphenyl-tetrazolium bromide, was performed as described by Caviedes et al. (2002). The methodology is briefly outlined below.

For plate preparation, 96-well plates (Corning REF 3599) were set up with a final RIF concentration of 16 µg/mL in column 2. Serial dilutions were made in 100 µL of 7H9 medium from column 3 to 10. Column 11 served as the control well, containing no antibiotics.

The inoculum was prepared from a 10 to 14-day-old Mmar solid culture. A suspension equivalent to McFarland standard 1 was made by resuspending approximately two loops of culture in a mixture of 200 µL of 10% Tween 80 in 50 mL of sterile distilled water. A 1:25 dilution was then prepared in 7H9 medium without Tween 80, and 100 µL of this dilution was inoculated into each well. The plate was incubated at 30°C.

On day 5, 50 µL of a freshly prepared solution of 0.1% tetrazolium in absolute ethanol and 10% Tween 80 (1:1) was added to the control well and incubated at 30°C for 24 hours. If the control well remained yellow, the incubation was extended for another 24 hours. If the well remained yellow after 48 hours, the plate was incubated for up to 15 days. If the well-turned purple due to formazan formation, the tetrazolium solution was added to all wells, and color development was assessed after 24 hours. Formazan is produced as a result of the reduction of tetrazolium salts by the activity of dehydrogenase enzymes in viable cells (Berridge et al., 2005).

III.2.9. Morphology by light microscopy

Selected strains were grown in 7H9 at 30-32°C to log phase, then homogenized by vortexing and centrifuged at 3000 xg for 10 minutes. Within a biological safety cabinet level 2, 10 ¼L of each culture was placed on a polysine-treated microscope slide (VWR Cat No 631-0107) and incubated at room temperature for 5 minutes. Then, 5 ¼L of PBS 1x was added. A coverslip was applied, avoiding bubble formation, and the edges were sealed with transparent enamel.

Images were acquired using the Invitrogen EVOS FL system equipped with a 60X oil immersion objective (PLAPON60XOSC2, EVOS Floid Imaging System, Thermo Scientific) and a 10X ocular, providing a total magnification of 600X. This setup allowed for high-resolution imaging necessary for detailed cellular analysis.

100 cell-length and cell-width measurements were carried out using ImageJ2 software (Rueden et al., 2017), individual cell lengths were measured manually by tracking along the cell, from cell pole to the opposite cell pole. To evaluate the cell size heterogeneity of Mmar strains, values of mean, standard deviation (SD), and coefficient of variation were employed.

III.2.10. Cell wall thickness measurements by cryoEM microscopy

This technique was performed in collaboration with PhD. Josephine Lai Kee Him and Aurelie Ancelin from CryoEM- CBS-Montpellier- France.

Selected strains were grown in 7H9 and tween 80 0,05%, at 32 °C to achieve log phase, and then 1 mL of each culture was passed through a 5 mL syringe and 26G

needle 5 times, then centrifuged at 1500 rpm for 10 minutes, resuspended in 1 mL of 1X PBS, centrifuged again for 40 minutes at 800xg. The supernatant was discarded and resuspended in 25-100 µL of 1X PBS to reach an OD between 5-6.

For the preparation of the sample, the copper grids with a carbon filament perforated at regular intervals (quantifoil) were used; they were ionized by a Glow discharge before use. 1-2 µL of the sample concentrated was put on the grid and the freezing was performed on a cryo plunger (Leica). The samples were evaluated in the Jeol 1400 fs with 120kV HT, a Lab 6 filament with a direct detection camera. Cell wall thickness was measured manually by tracking along the cell wall, using InteredgeDistance_v1.4_ImageJMacro in the ImageJ2 software (Rueden et al., 2017).

III.2.11. Effect of rifampicin exposure on the viability of *M. marinum* harboring the *ponA1* gene from *M. tuberculosis* H37Rv

From a logarithmic-phase Mmar culture, a suspension equivalent to McFarland 1 scale was prepared by resuspending the culture in a mix solution (200 µL of 10% Tween 80 in 50 mL of sterile distilled water). This suspension was diluted 1:25 in 7H9 medium, and 100 µL of the dilution was inoculated into a 96-well plate (Costar 3599, Corning Incorporated). Plates were prepared with 100 µL of 7H9 medium with and without RIF, achieving a final concentration of 0.5 µg/mL RIF. OD_{600} was measured at 48 and 72 hours, the values from the RIF wells were normalized with the untreated control wells (Kieser, Boutte, et al., 2015).

After 6 days of incubation, when the cells had reached the stationary phase, samples were collected for analysis to assess cell viability on 7H10 plates without RIF, and CFU/mL was counted in triplicate. The experiment was conducted in duplicate, with CFU/mL values transformed to log scale.

III.2.12. Membrane fluidity test

From 10 to 14 day different Mmar cultures, 50 µ L was inoculated in 5 mL of 7H9 and allowed to incubate until reach an OD_{600} of 0.25, each culture was processed for the evaluation of membrane fluidity (kit Ab189819), following the manufacturer's instructions. Briefly, 0.5 mL of the culture was centrifuged at 3000xg for 10 minutes, 50µL of labelling solution was added, incubated at 25 °C at 220 rpm for one hour in the darkness. Cells were washed with 1X PBS and centrifuged 3000xg 10 minutes at room temperature. Washing was repeated once more and then the supernatant was discarded. 50 µL of 7H9 was added and read on the Fluoreader with excitation at 350 nm and emission at 400 nm and 450 nm.

The ratio of the maximum emission from the excimer (450 nm) to that of the monomer (400 nm) was calculated to quantify relative membrane fluidity. This method relies on the behavior of pyrene within the membrane, where it can exist either as a monomer (single pyrene molecule) or as an excimer (formed when two pyrene molecules come into close proximity). The balance between these two states reflects the fluidity of the membrane, with a higher excimer-to-monomer ratio indicating increased membrane fluidity (Galla & Hartmann, 1980).

III.2.13. Statistical analysis

Prism 6.0 software (GraphPad Software, La Jolla, CA) was used to analyze and graph numerical data. Statistical tests in the Prism software were used to calculate mean, SD, CV, normality test, ANOVA, Kruskal-Wallis test and multiple comparisons depending on the analysis required for each experiment.

Additionally, for the analysis of cell envelope thickness, means were compared using linear regression after confirming the normality of the data with the Shapiro-Wilk test. An indicator variable was employed as a predictor to account for the specific groups being compared, and the inverse of the standard deviation was used as an analytical weight to adjust for variability across groups. The analysis was conducted using Stata 14 software, with a significance level set at 5%.

III.3. Results

III.3.1. *In silico* interaction between PonA1 and rifampicin

III.3.1.1. PonA1 full-length structural modeling compared to the PonA1 transpeptidase crystal structure

We predicted the full-length structure, including the significant TG domain, using the AlphaFold (PonA1_WT_AF) and ESMFold (PonA1_WT_ESM) approaches. We first verified the models' accuracy for the well-characterized TP domain. The results were promising, showing RMSDs of 0.471 Å for AlphaFold and 1.874 Å for ESMFold (Figure III.4). Our computational analysis provided Local Distance Difference Test (lDDT) scores for all 820 residues. Both, AlphaFold and ESMFold models closely matched the experimental structure of the transpeptidase domain, with lDDT scores of 91 and 94, respectively; thereby validating their accuracy.

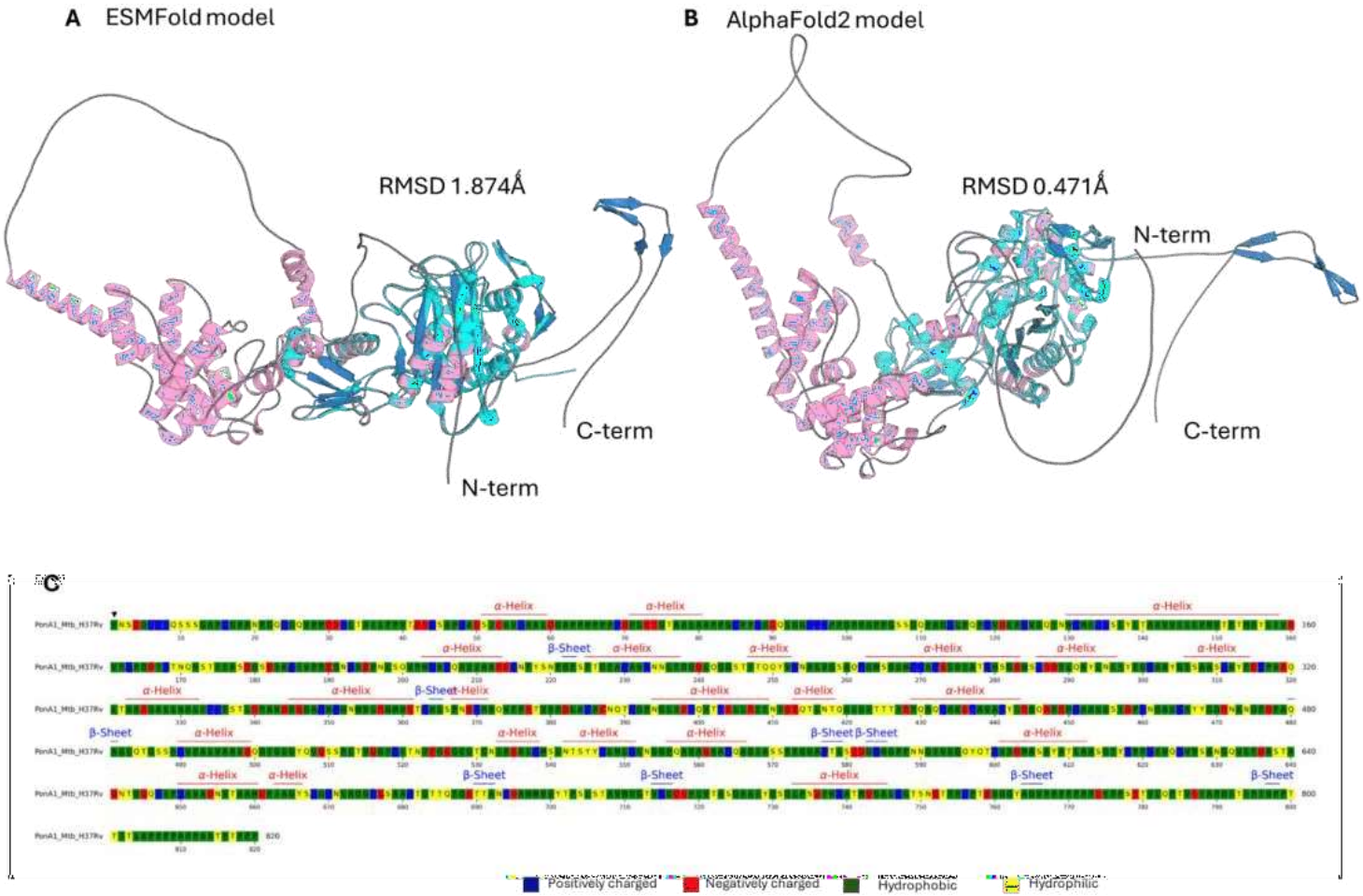

Figure III.4. Comparison of *M. tuberculosis* H37Rv PonA1 models and crystal structure. A. PonA1-WT-ESM model, B. PonA1_WT_AF model, and transpeptidase domain crystal structure (PDB 5CXW). C. The primary amino acid sequence of PonA1 is shown.

Further evaluation of the TG domain, for which no crystal structure exists, also indicated robust predictive performance from both models. While there was a slight discrepancy in accuracy compared to the experimentally determined domain, both ESMFold and AlphaFold offered credible structural predictions with minimal differences between them, as illustrated in Figure III.5. Importantly, regions marked as disordered by Uniprot were predicted with low lDDT scores by both models.

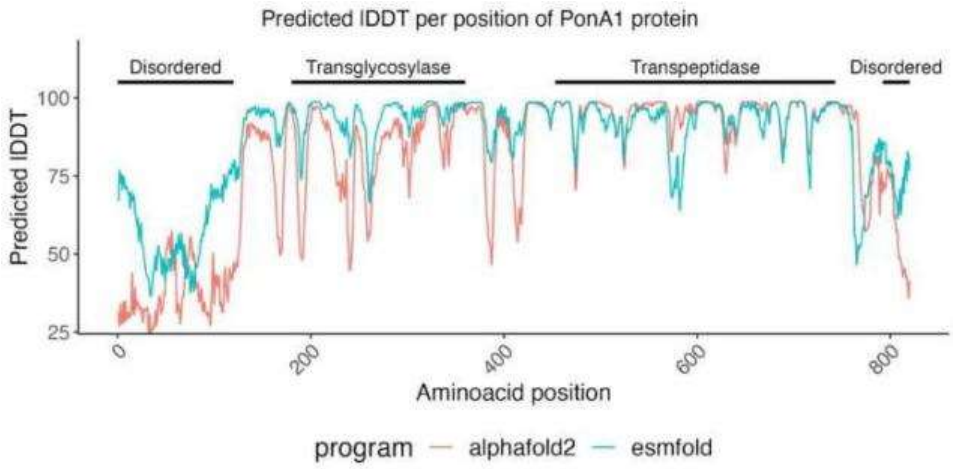

Figure III.5. Comparative analysis of AlphaFold and ESMFold predictions for PonA1 protein structure. Prediction of Local Distance Difference Test (LDDT) per position of PonA1 protein.

A. Modeling of AlphaFold mutations

Using the AlphaFold model, we extended our modeling to include two mutations, Q365H and P631S, in the PonA1_WT_AF protein.

The atomic positions in the full-length models of both the WT and Q365H (PonA1_Q365H_AF) vary primarily in regions surrounded by loops. This variation is reflected by a high RMSD value of 20.168 Å, attributed to the high flexibility of these

regions (Figure III.6.A). Another scenario is observed when comparing the PonA1_WT_crystal (5CXW) with the PonA1_Q365H_AF mutation, the tertiary structures appear identical (RMSD 0.477Å, Figure III.6.B), suggesting that this mutation does not significantly alter the protein's tertiary structure. Additionally, the comparison shows no changes in the PBP pocket (Figure III.6.D).

Similarly, the atomic positions in both the PonA1 WT and P631S (PonA1_P631S_AF) mutant models, as shown in Figure III.7.A (RMSD 15.094 Å), differ primarily due to the spatial displacement of the loops. However, the comparison between 5CXW and PonA1_P631S_AF shows no changes in the pocket (RMSD 0.460Å), indicating that the P631S mutation, as modeled by AlphaFold, does not significantly alter the structure of the PBP pocket where the substrate binds. This suggests the mutation has a minimal functional impact (Figure III.7.B-D).

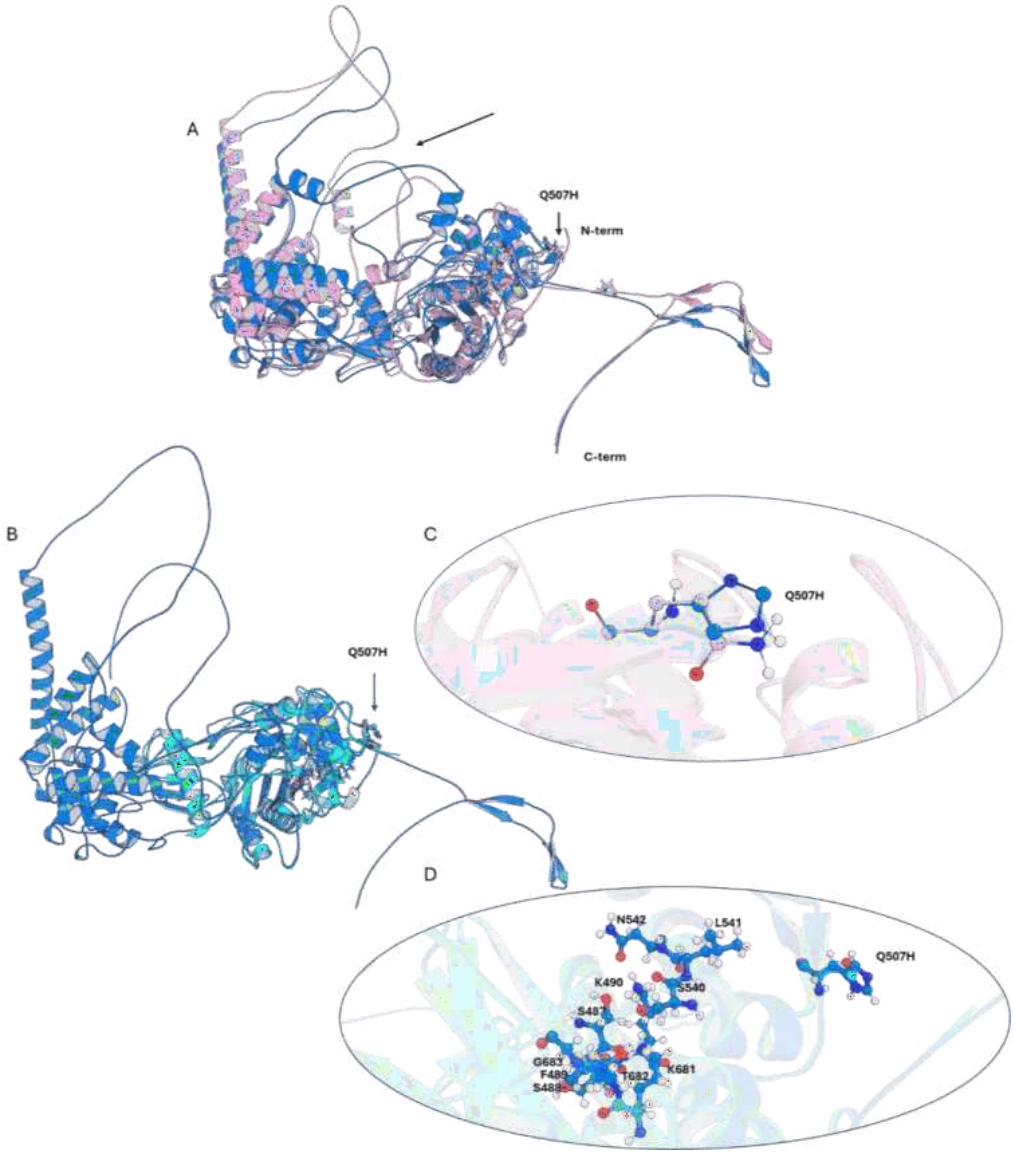

Figure III.6. Structural comparison of PonA1 wild type and Q365H modeled by AlphaFold. A. PonA1_WT_AF (pink) versus PonA1_Q365H_AF (blue). B. PonA1_Q365H_AF compared to PonA1 crystal 5CXW (cyan). C. Residues Q365H (pink) and H507 (blue) are visualized in the model. D. Detailed view of the transpeptidase catalytic center showing the Q365H localization; mutation Q365H in the crystal corresponds to Q570H in the model. An arrow indicates the region displaced by loops in the models.

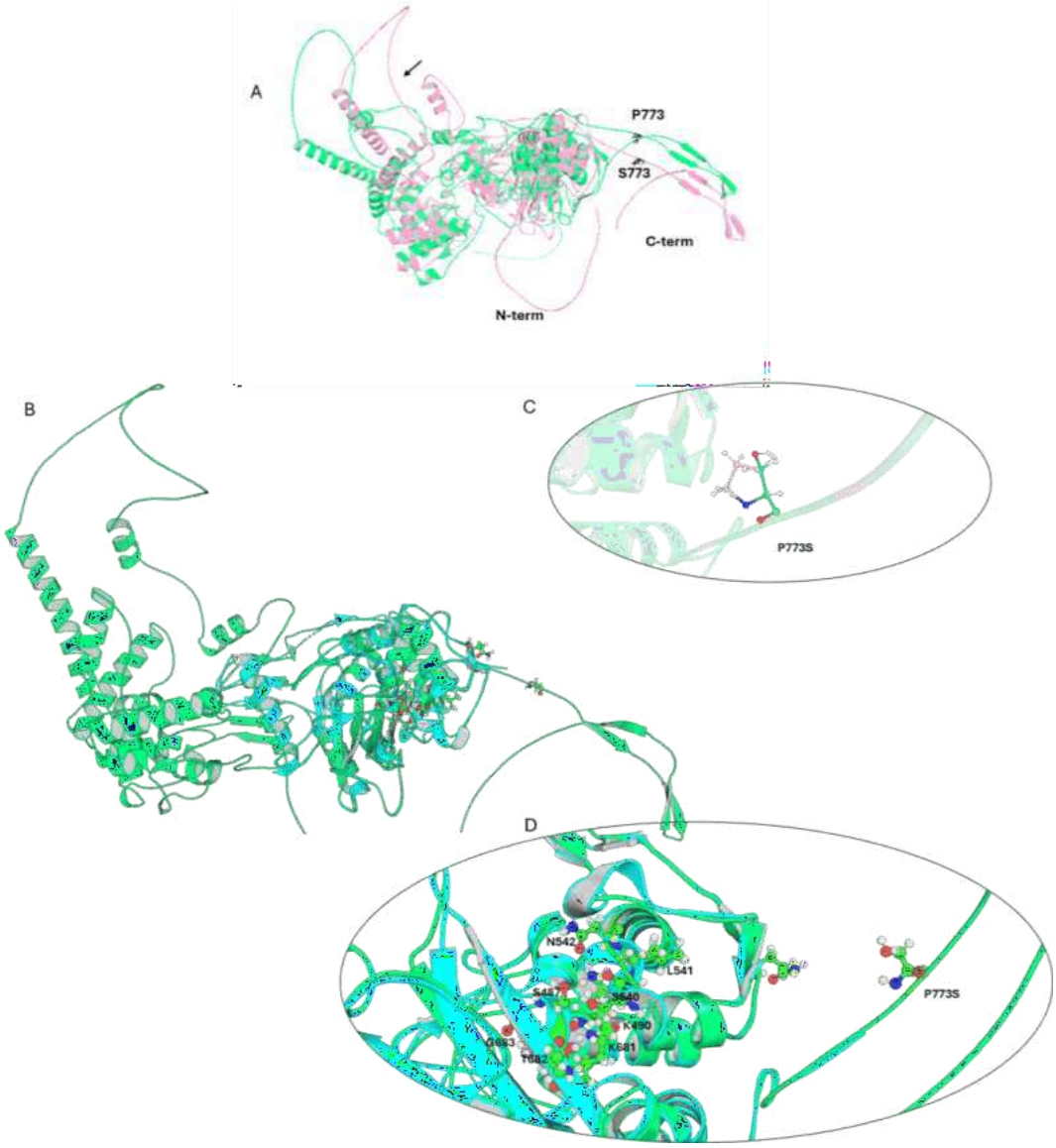

Figure III.7. Structural comparison of PonA1 wild type and P631S modeled by AlphaFold. A. PonA1_WT_AF (pink) versus PonA1_P631S_AF (green). B. PonA1_P631S_AF compared to PonA1 crystal 5CXW (cyan). C. Residues P631 (pink) and S631 (green) visualized in the model. D. Close-up of the transpeptidase catalytic center highlighting P631S localization; P631S corresponds to P773S in the model.

B. Modeling of ESMFold mutations

An alignment of the three-dimensional structures was performed using ESMFold to measure structural deviations between the WT protein, the mutated protein, and the partially crystallized structure of PonA1. The analysis revealed subtle variations for the protein with PonA1_Q365H_ESM mutation when it is compared with the PonA1_WT_ESM (RMSD 1.953 Å, Figure III.8.A), and the model is even more similar when it is compared with the crystal (RMSD 0.815 Å, Figure III.8.B). In this case, no variations in the spatial arrangement of the loops were observed.

Conversely, a significant modification was observed in the loop region (alpha helix) of PonA1_P631S_ESM protein, which exhibited a rotational displacement when it is compared with PonA1_WT_ESM (RMSD 4.151Å, Figure III.9.A). Besides, to compare against a ground truth, PonA1_P631S_ESM was aligned against the partial crystallized structure for PonA1 (5CXW), but no major variations were observed at least in the folded region (RMSD= 1.998 Å) (Figure III.9.B).

Based on the smaller variations in RMSD, it was decided to proceed with the following tests using the model generated by ESMFold, both for the wild-type protein and the mutants.

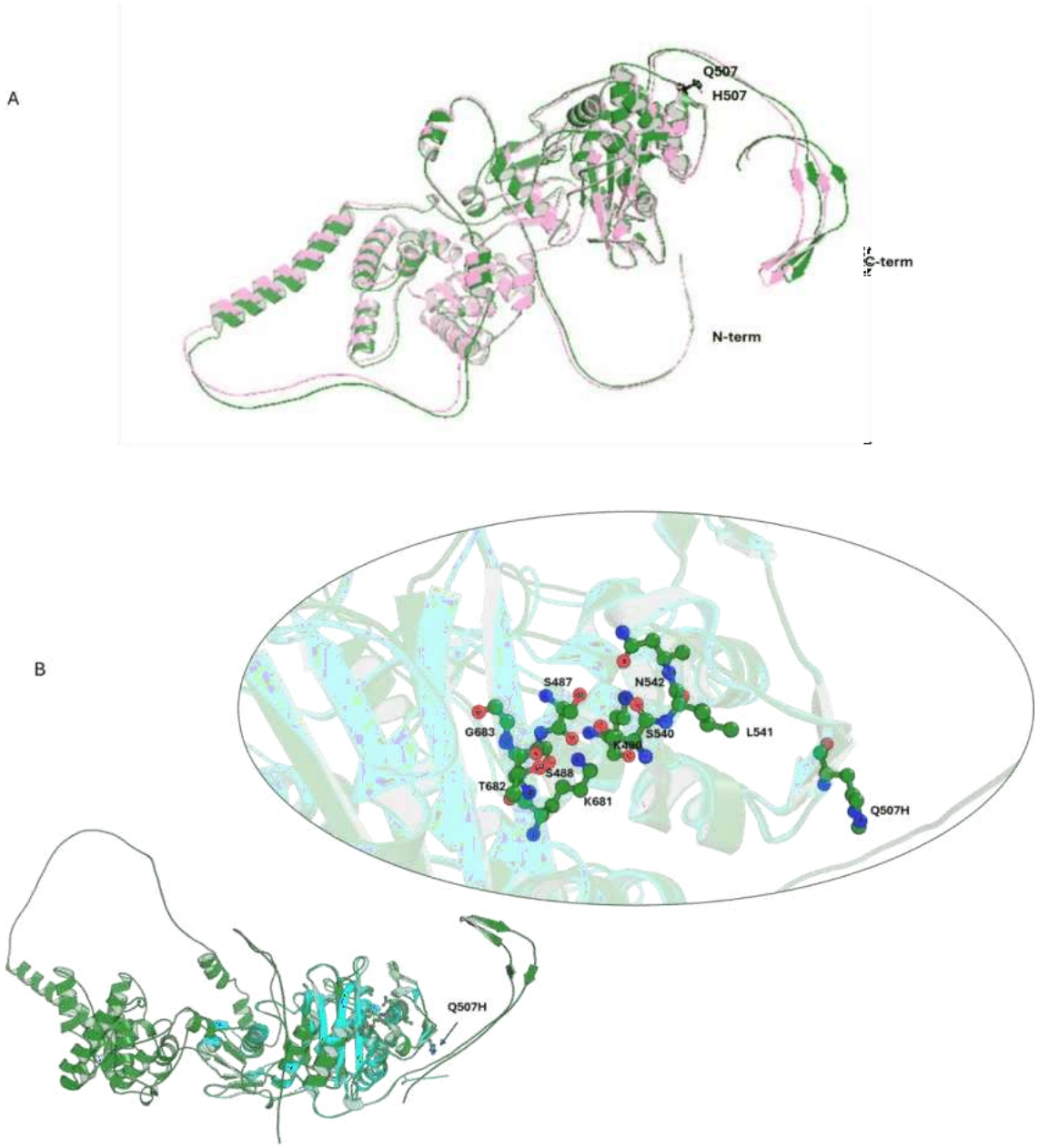

Figure III.8. Structural comparison between PonA1 wild type and Q365H modeled by ESMFold. A. PonA1_WT_ESM (pink) versus PonA1_Q365H_ESM (green). B. PonA1_Q365H_ESM compared to PonA1 crystal 5CXW (cyan); mutation Q365H in the crystal corresponds to Q570H in the model.

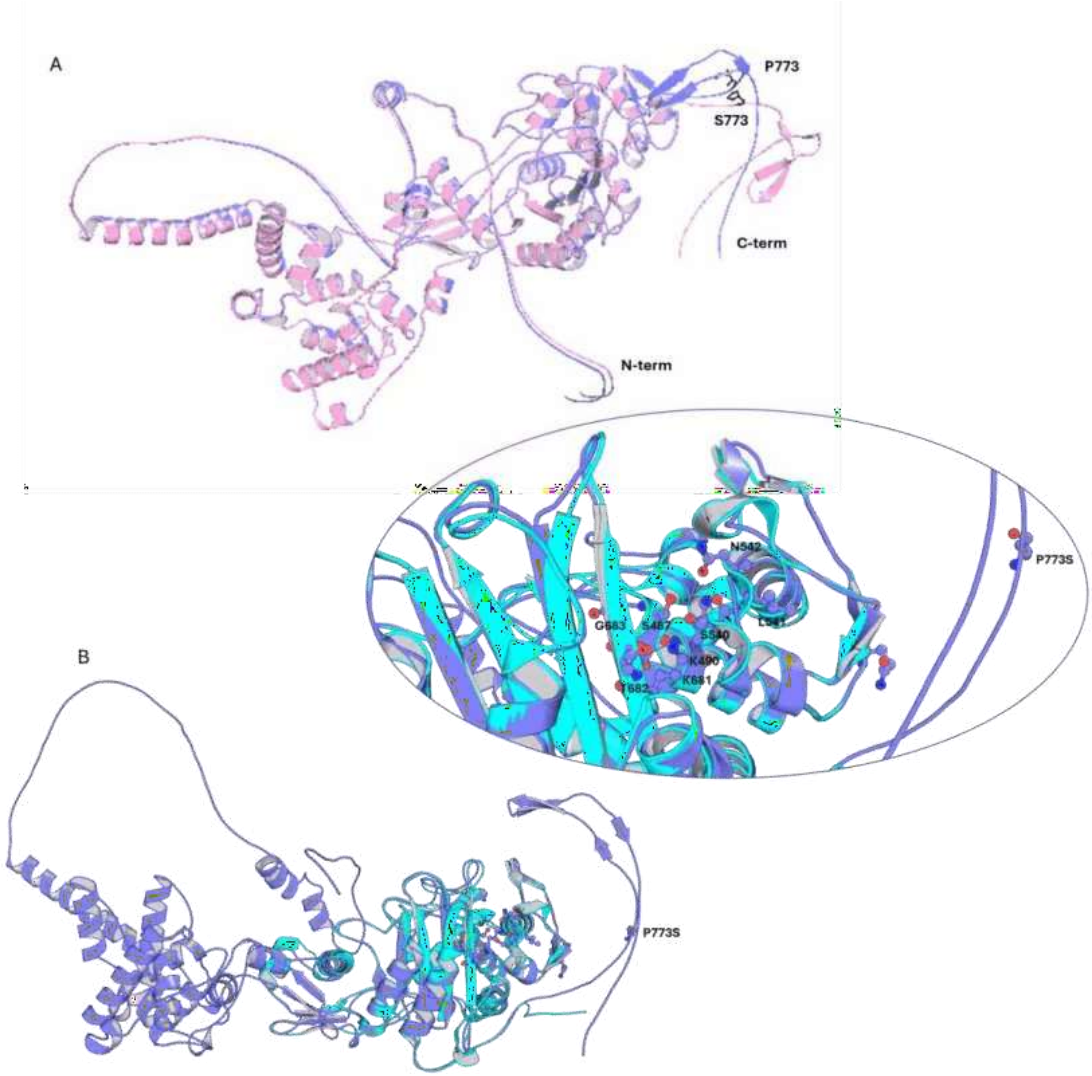

Figure III.9 Structural comparison between PonA1 wild type and P631S modeled by ESMFold. A. Comparison of PonA1_WT_ESM (pink) with PonA1_P631S_ESM (purple). B. Comparison of PonA1_P631S_ESM with PonA1 Crystal 5CXW (cyan); P631S in the crystal corresponds to P773S in the model.

III.3.1.2. Molecular docking between variants of PonA1 and RIF

A. Docking crystal structure of PonA1 against penicillin

In our study, we initially employed GNINA for molecular docking, using the crystal structure of PonA1 (5CXW) against its known ligand, penicillin V, in its open form. This approach served as a benchmark to measure successful docking in our system, with the advantage of having the crystal structure data of PonA1 and penicillin V bound together. In addition, it provides us with a referential binding energy or confidence scores to compare with the mutant structures.

Using GNINA, we set up a docking scenario with a docking box representing the penicillin9s binding pockets. GNINA aimed to identify the correct pose of penicillin V, yielding RMSDs of 3.6 Å and 4.3 Å, and the top nine poses were under 10 Å RMSD. The highest affinity achieved was -8.58 kcal/mol (Figure III.10.A; Appendix III.35).

Subsequently, we tested the same scenario with DiffDock, which operates without a specific docking box in a blind dock scenario, considering the entire protein as the docking area. DiffDock showed superior results, with the top two poses having RMSDs under 2 Å and the remaining top nine poses under 3.1 Å RMSD, achieving a DCS between 0.13 to -0.4 (Figure III.10.B). These results suggested a successful docking pose, even without a specified docking box (Appendix III.37). It is important to note that DSC values above 0 indicate high confidence, values ranging between -1.5 and 0 suggest moderate confidence in the predicted models, while more negative values suggest lower confidence in the model predictions (https://github.com/gcorso/DiffDock?tab=readme-ov-file#inference).

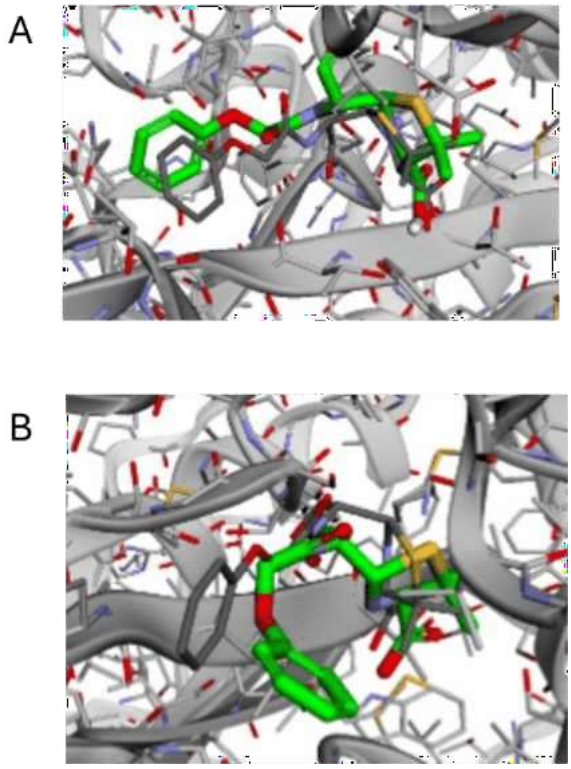

Figure III.10. Molecular docking of PonA1 crystal with penicillin V was performed using GNINA and DiffDock. A. Docking results from GNINA showed the highest RMSD of 3.6 Å and energy of interaction of -8.58 kcal/mol. B. Docking results from DiffDock, highest RMSD of 2 Å with DSC 0.13. In the figure, penicillin V co- crystallized with PonA1 is shown in gray, while the penicillin V docked by both algorithms is displayed in green.

B. Docking full-length PonA1_WT modeled against penicillin

PonA_WT_ESM was docked with penicillin V using the DiffDock algorithm, given the already known pocket of the penicillin in the PBP pocket, we evaluated how many of the poses docked in the same pocket or in another. Here, the ligand binds to 3 main domains: 1) TP, 2) TG, and 3) transmembrane (TM) domains (Figure III.11-A).

From 40 penicillin binding modes generated 33 docked to the ground truth pocket in the TP domain (Figure III.11-B, Appendix III.38), where the highest DCS was -0.28

generating interactions that involves residue Q596 establishing hydrophobic interactions, while S487, N542, T682, T684, G730, and S731 form hydrogen bonds. Additionally, K681 forms a salt bridge with penicillin V (Figure III.11-C). In the TG domain, 6 out of 40 binding modes docked, the best DCS was -1.86 while in the TM domain 1 out of 40 binding modes was observed with DCS= -3.19.

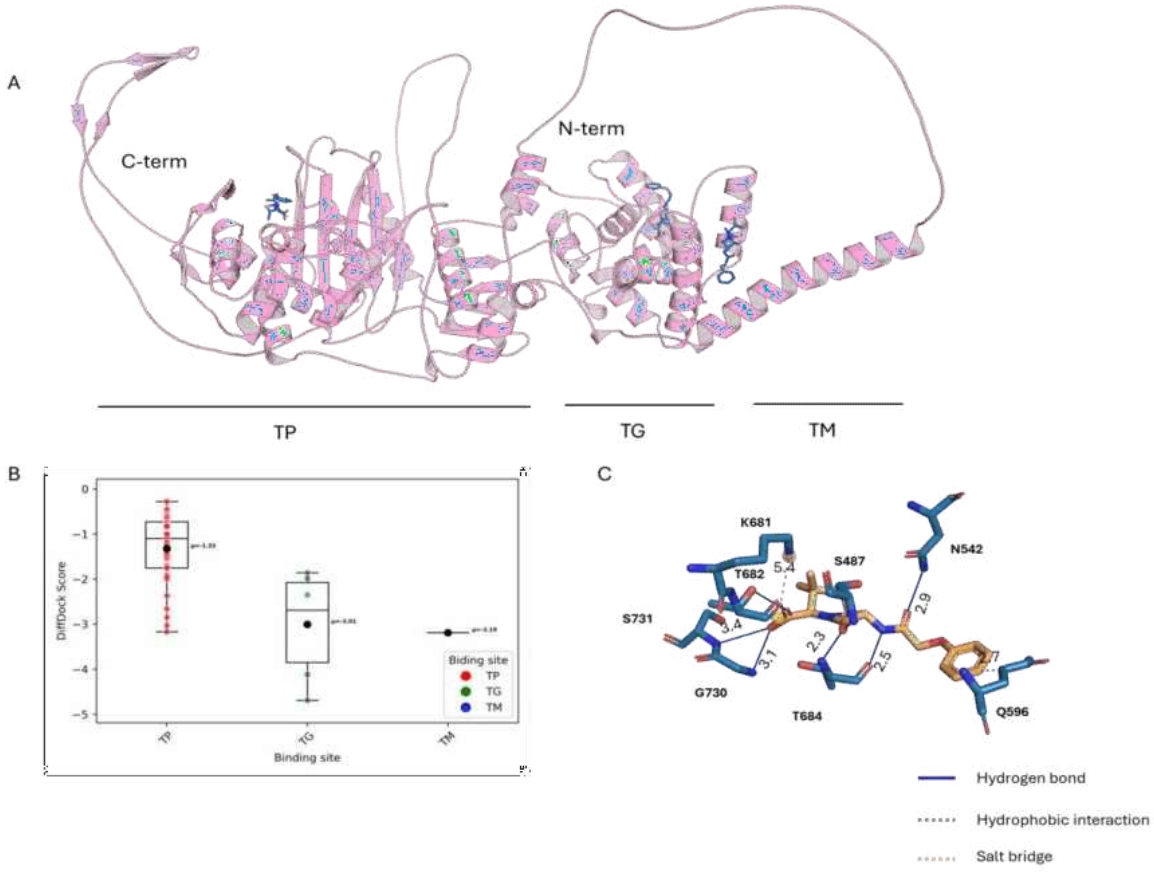

Figure III.11. **Molecular docking between PonA1 wild type and penicillin V by DiffDock.** A. PonA1_WT modeled with ESMFold (pink) showing docking sites with penicillin V (blue). B. DiffDock confidence score rankings and localization of penicillin V binding sites. C. Interactions between PonA1 and penicillin V. This figure was created using PLIP. Abbreviations: TP = transpeptidase domain, TG = transglycosylase domain, TM = transmembrane domain.

C. Docking full-length PonA1_WT modeled against rifampicin

The DiffDock algorithm identified potential interaction sites between the PonA1 protein (WT modeled by ESMFold) and RIF through blind docking, performing 40 dockings and identifying three possible interaction sites (Figure III.12.A-B). The interactions with the highest DCS between the full-length PonA1 and RIF were selected for each analysis.

In the TP domain, we observed a convergence of 31 out of 40 docking (DCS = -1.78 for the top score, mean DSC was -3.32, Appendix III.38 detailed DSC for the top 9 poses) involving residues V523, E524, Y666, T682, T684, Q686 and Y729 through hydrophobic interactions, and V523, N542, R668, T684 through hydrogen bonds, plus K490 forming a pi-Cation interaction with RIF (Figure III.12.C). While in the TG domain, there were 7 out of 40 docking (DCS= -2.5), featuring hydrophobic interactions with residues L241, I297, Y298, P336, and hydrogen bonds with G243 and K253 (Figure III.12.D). Moreover, in the TM domain, there were 2 out of 40 docking were observed (DCS=-1.92), here the RIF interacts with residues P148, T151, F228, W264 through hydrophobic interactions, and P148 and F152 through hydrogen bonds (Figure III.12.E).

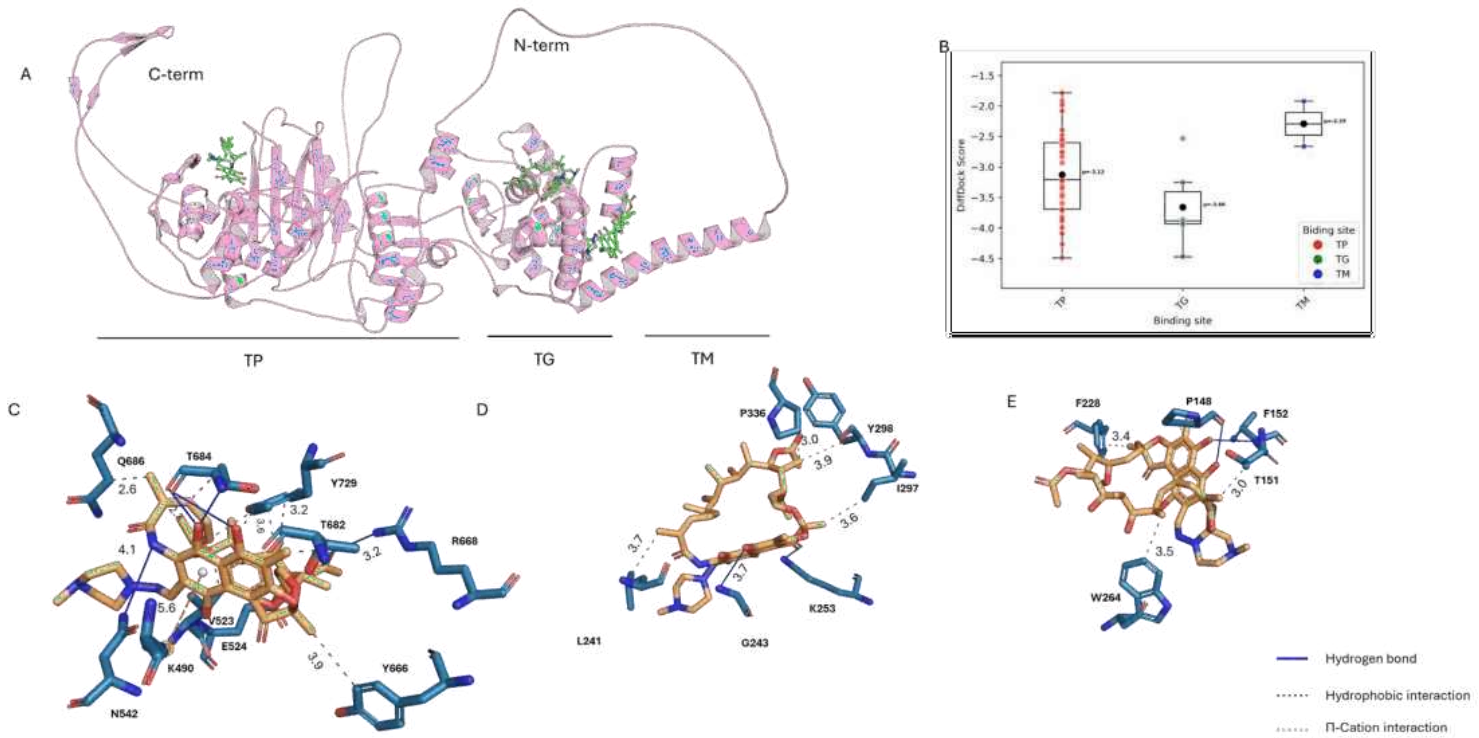

Figure III.12. Molecular docking between PonA1 wild type and rifampicin using DiffDock. A.PonA1_WT_ESM model displaying three potential rifampicin (green) interaction sites . B. Diffdock score ranking and localization of rifampicin interaction sites. C. Interaction of rifampicin with the transpeptidase domain. D. Interaction within the transglycosylase domain. E. Interaction within the transmembrane domain. This figure was generated using PLIP. Abbreviations: TP = transpeptidase domain, TG = transglycosylase domain, TM = transmembrane domain.

D. Docking full-length PonA1_mutants modeled against rifampicin

For the PonA1_Q365H_ESM mutation, the DCS ranged from -2.36 to -4.34. In the TP domain, there were a convergence of 25 out of 40 binding modes with the most probable interactions (DCS = -2.43) involving hydrophobic interactions with residues V523, E524, L594, T684 and Y729, and hydrogen bonds with residues S487, K490, S540, N542, T684, Q686, N693 and Y729 with RIF (Figure III.13.C). While in the TG domain, there were 13 out of 40 docking (DCS = -2.39), featuring hydrophobic interactions with residues K253 and hydrogen bonds with residues N235, G243 and K253 (Figure III.13.D). Moreover, in the TM domain, only 2 out of 40 binding modes were observed, with a lower DCS of -2.95, where the RIF interacts with residues T151, W264, A271, and V275 through hydrophobic interactions, and T151 through hydrogen bonds (Figure III.13.E). All these DSC for Q365H suggest that the predicted poses have low confidence, as the score is lower than that of the wild-type model when comparing the top scores.

For the PonA1_P631S_ESM mutations, the DCS ranged from -2.08 to -4.45. In the TP domain, 28 out of 40 docking converged, showing the most probable interactions (DCS = -2.08) involving hydrophobic interactions with residues V523, E524, Y666, T682, T684, Q686 and Y729, and hydrogen bonds with T521, V523, T682, G683, T684 and G730, along with pi-cation interaction between K490, K681 and RIF (Figure III.14.C). In the TG domain, 10 out of 40 docking were observed almost in the same site, the highest DCS of the position was -2.11, featuring hydrophobic interactions with P336, hydrogen bonds with Y298 and Y304, and salt

bridges with E190 and R385 (Figure III.14.D). Moreover, in the TM domain, only 2 out of 40 binding modes were observed (DCS =-2.99), where the ligand interacts with residues P148, F152, A155, W264, L267, M268, A271 through hydrophobic interactions and T151 hydrogen bonds (Figure III.14.E). Similar to Q365H, the DSC are lower than that of the wild-type model when comparing the top scores.

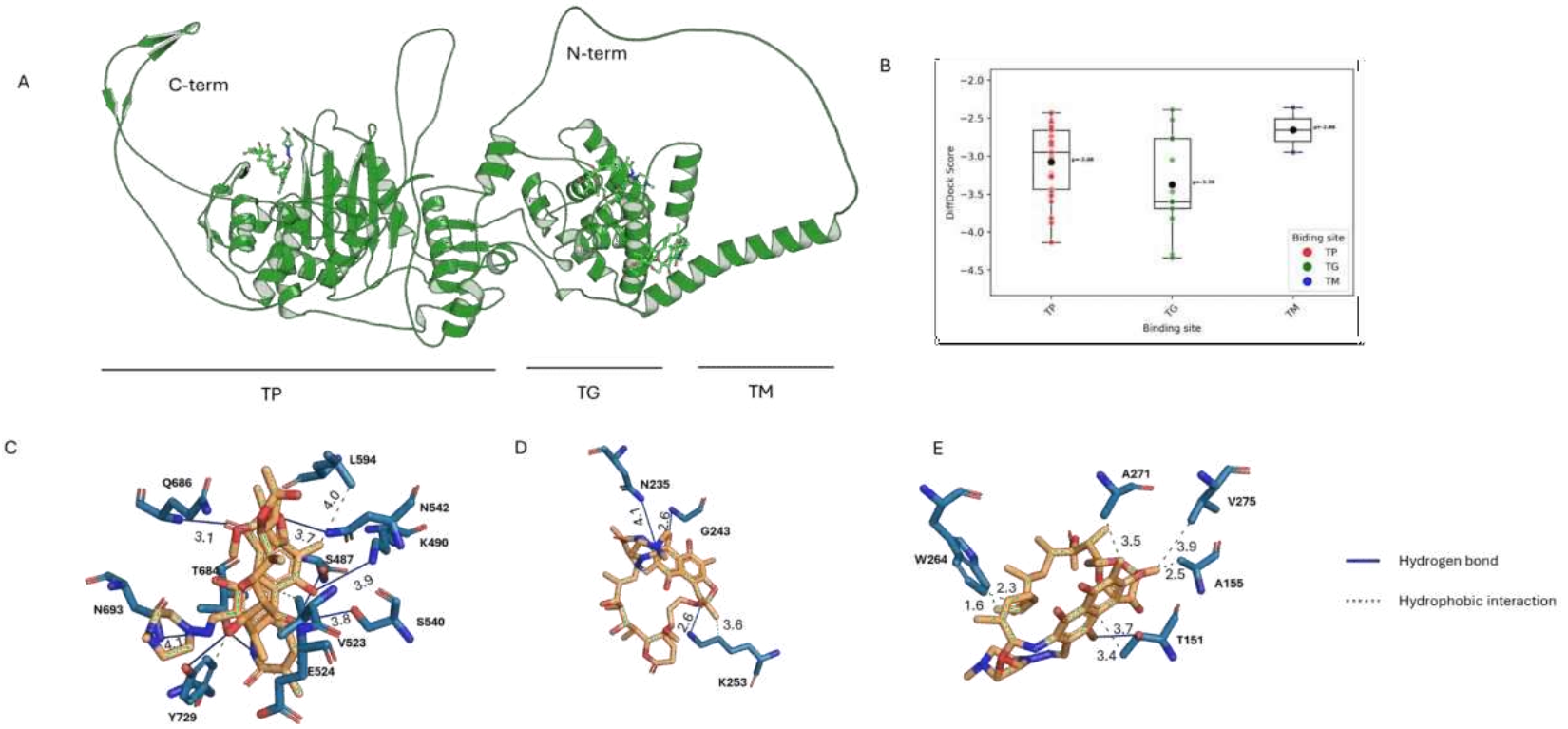

Figure III.13. Molecular docking of PonA1 Q365H and rifampicin using DiffDock. A. Full-length PonA1_Q365H_ESM protein showcasing three potential rifampicin (green) interaction sites. B. DiffDock score rankings and localization of rifampicin binding sites. C. Interaction of rifampicin with the transpeptidase domain. D. Transglycosylase domain interactions. E. Transmembrane domain interactions. This figure was generated using PLIP. Abbreviations: TP = transpeptidase domain, TG = transglycosylase domain, TM = transmembrane domain.

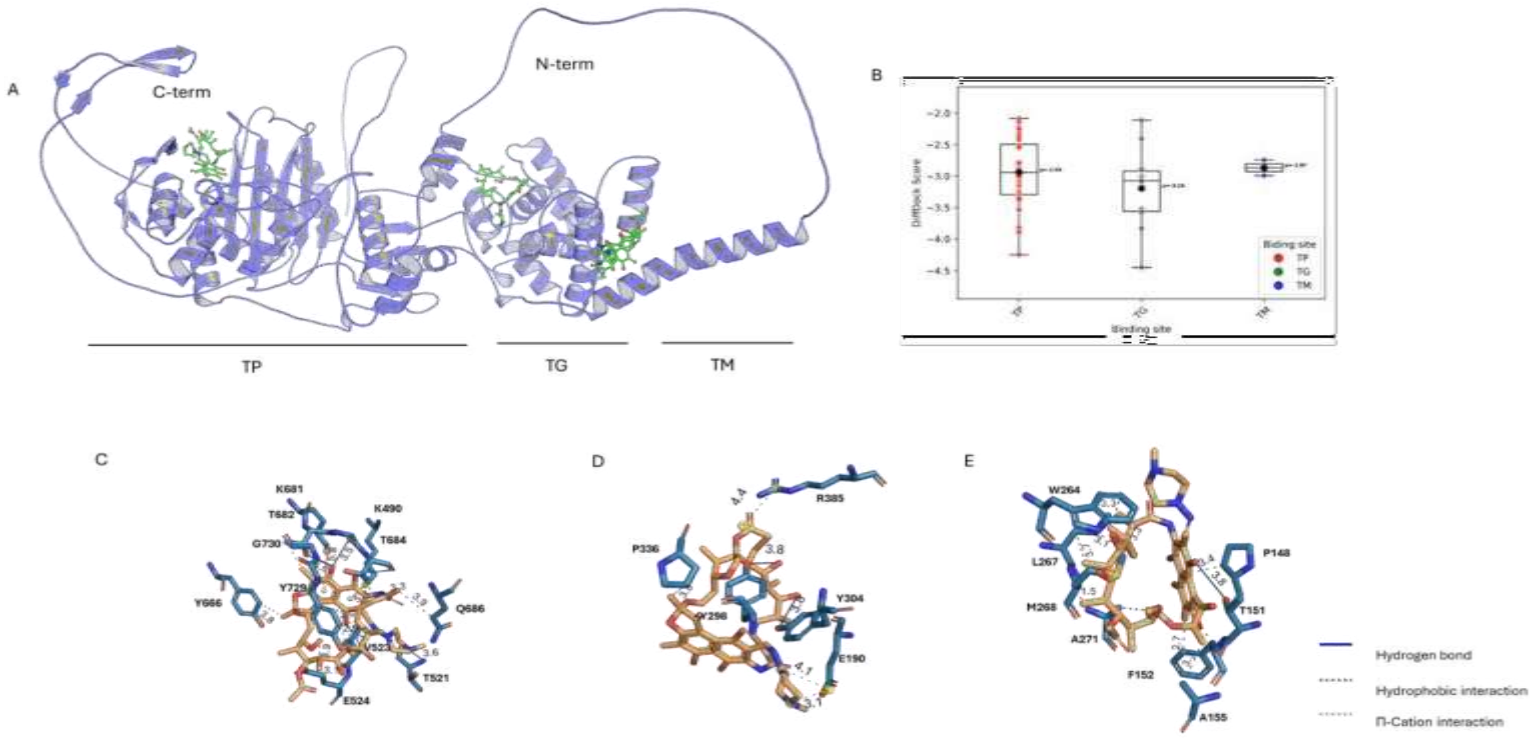

Figure III.14. Molecular docking of PonA1 P631S and rifampicin using DiffDock. A. Full-length PonA1_P631S_ESM displaying three potential rifampicin (green) interaction sites. B. DiffDock score rankings and rifampicin binding site localization. C. Interaction of rifampicin with the transpeptidase domain. D. Transglycosylase domain interactions. E. Transmembrane domain interactions. This figure was created using PLIP. Abbreviations: TP = transpeptidase domain, TG = transglycosylase domain, TM = transmembrane domain.

Table III.3. Summary of interactions between PonA1_WT, PonA1_Q365H, PonA1_P631S and rifampicin.

Residue*	Interaction Type	PonA1_
SER 487	Hydrogen bridge	Q365H
LYS 490	Hydrogen bridge, pi-Cation	WT, Q365H, P631S
THR 521	Hydrogen bridge	P631S
VAL 523	Hydrophobic, Hydrogen bridge	WT, Q365H, P631S
GLU 524	Hydrophobic	WT, Q365H, P631S
SER 540	Hydrogen bridge	Q365H
ASN 542	Hydrogen bridge	WT, Q365H
LEU 594	Hydrophobic	Q365H
TYR 666	Hydrophobic	WT, P631S
ARG 668	Hydrogen bridge	WT
LYS 681	pi-Cation	P631S
THR 682	Hydrophobic, Hydrogen bridge	WT, P631S
GLY 683	Hydrogen bridge	P631S
THR 684	Hydrophobic, Hydrogen bridge	WT, Q365H, P631S
GLN 686	Hydrophobic, Hydrogen bridge	WT, Q365H, P631S
ASN 693	Hydrogen bridge	Q365H
TYR 729	Hydrophobic, Hydrogen bridge	WT, Q365H, P631S
Gly 730	Hydrogen bridge	P631S

*Residues in bold are related to conserved sites in the PBP domain (Kieser et al, 2015).

Table III.3 displays the residues interacting with the TP domain, which were selected due to the majority of simulations (albeit with low confidence) suggesting that RIF could bind to this region in the WT, Q365H, and P631S variants. Specifically, over 70% of the simulations indicated binding within the PBP domain for both PonA1-WT and the P631S mutant. In contrast, for the PonA1 Q365H mutant, the percentage of simulations showing binding in this domain was 62.5%. Among the residues identified in the potential interaction between PonA1 and RIF, S487 and K490 belong to the conserved SXXK motif, S540 and N542 to the SXN motif, and K681, T682, G683, and

T684 to the KTG(T/S) motif. All these residues are part of the conserved domain of PBP, which is also integral to the TP domain.

It is noteworthy that among the residues interacting with RIF, some are common across all three proteins, while others are shared between two or unique to one type. This indicates variations in protein conformation, potentially due to mutations, which could affect RIF interactions. To assess the temporal evolution and stability of the interaction, molecular dynamics simulations were performed using the top poses with the highest DSC from each interaction.

III.3.1.3. Molecular dynamics evaluation of PonA1-RIF complex stability

In the molecular dynamics (MD) timeline of the three complexes4 PonA1_WT_ESM, PonA1_Q365H_ESM, and PonA1_P631S_ESM 4the ligand (RIF) remains bound at the interaction site throughout the simulation. Notably, in PonA1_WT, the binding pocket shows slight closure between 75 and 100 ns of the simulation, a behavior that is not observed in the Q365H and P631S mutants. This suggests that the wild-type form of PonA1 exhibits a dynamic conformational adjustment that stabilizes RIF binding, whereas the mutant proteins lack this pocket closure, potentially influencing the overall binding stability and affinity (Figure III-15-A).

The RMSD values stabilize after approximately 10 nanoseconds (ns) (Figure III-15-B-D), a typical pattern as the protein structure adjusts from its initial configuration to a more energetically favorable conformation. For PonA1_WT, the

RMSD stabilizes between 1.2 nm and 1.6 nm after an initial increase, while PonA1_P631S shows similar fluctuations between 1.2 nm and 1.5 nm. In contrast, PonA1_Q365H exhibits greater variability, with RMSD fluctuating between 1.5 nm and 1.7 nm. Notably, after 50 nanoseconds, PonA1_Q365H demonstrates regions of enhanced stability, where the RMSD remains more consistent, indicating structural convergence. Despite these differences, the RMSD fluctuations for PonA1_WT and PonA1_P631S are comparable on average, whereas PonA1_Q365H shows deviations of approximately 2 Å, suggesting a less stable conformational adjustment.

In addition, the RMSF analysis highlighted key regions of flexibility throughout the proteins, as summarized in Figure III.15-E. Notably, both the N-terminal (residues 1 to 150) and C-terminal (residues 750 to 820) regions exhibited significant fluctuations, indicating areas of high flexibility in both the wild-type and mutant structures. These fluctuations suggest that these terminal regions, which are distant from the active site, may contribute to the overall structural dynamics and stability of the PonA1 protein complexes.

The PonA1_Q365H and PonA1_P631S fluctuations show N-terminal more compact than PonA1_WT, while in the C-terminal, PonA1_P631S becomes more flexible, and PonA1_Q365H more compact in the same region. In addition, in the most structured regions (with lower RMSF values), slight variations have been seen in the TP region compared to the TG region; thus, it could be inferred that these mutations could have an effect on the stability of the protein. However, mutations have not been shown to make the drug less stable in the complex.

The dynamics interactions predominantly occur through hydrophobic interactions and hydrogen bonds, as demonstrated by residue interaction analysis (Figure III.16). For PonA1_WT, we identified 11 hydrophobic interactions involving residues V523, Q526, M539, L541, L594, Y666, T684, Q686, T691, Y729, and A814; besides, 7 hydrogen bonds with residues S487, V523, S540, N542, T684, and N693. Meanwhile, the PonA1_Q365H protein forms 7 hydrophobic interactions with residues T521, V523, E524, Q686, T691, Y729, T815, and P816; and 5 hydrogen bonds with residues T521, E524, T691, Y729, and T815. PonA1-P631S forms 6 hydrophobic interactions with residues V523, E524, N542, Y666, Q686, and T691; and 6 hydrogen bonds with residues V523, M539, S540, T684, N693, and Y729 (Figure III.16).

It should be noted that important residues (hotspots) for the interaction fluctuate slightly between the mutated structures. Residues V523, Q686, T691, and Y729 interact with RIF in all three proteins (PonA1_WT, PonA1_Q365H, and PonA1_P631S) through hydrophobic contacts. In addition, we found hydrogen bond interactions shared exclusively between PonA1_WT and PonA1_Q365H: T521, E524, T691, Y729, and T815; while hydrogen bond interactions shared exclusively between PonA1_WT and PonA1_P631S: V523, S540, T684, and N693.

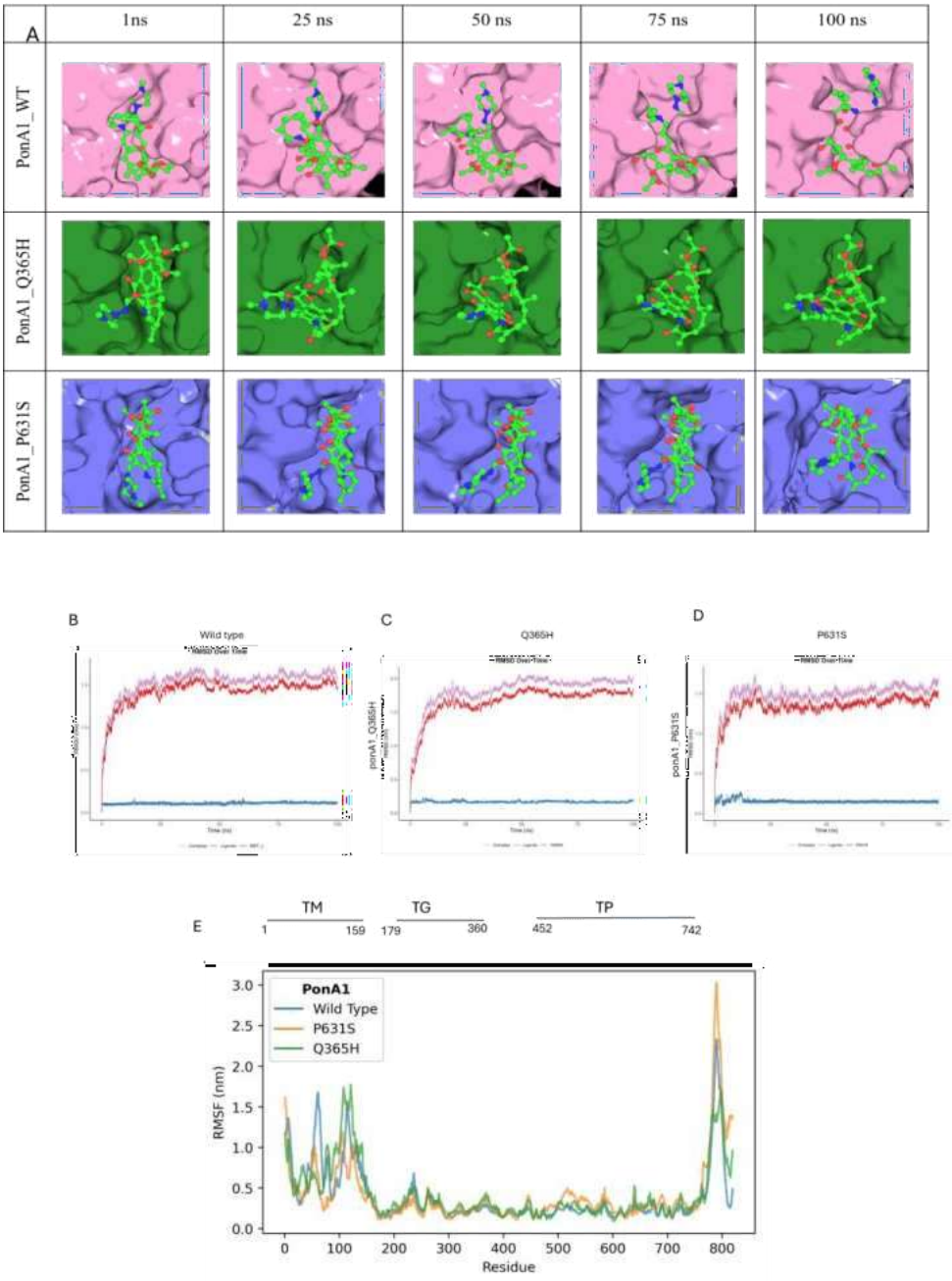

Figure III.15. **Molecular dynamic simulations between PonA1 from *M. tuberculosis* H37Rv (both wild-type and mutant forms) and rifampicin.** A.Timeline of molecular dynamics for PonA1_WT, Q365H and P631S at 1, 25, 50, 75 and 100 ns. B. RMSD values for PonA1_WT_ESM. C. RMSD for PonA1_Q365H_ESM. D. RMSD for PonA1_P631S_ESM. alone (red), in complex with rifampicin (purple), and rifampicin alone (blue) E. RMSF values for all protein variants in interaction with rifampicin, evaluated over 100 ns.

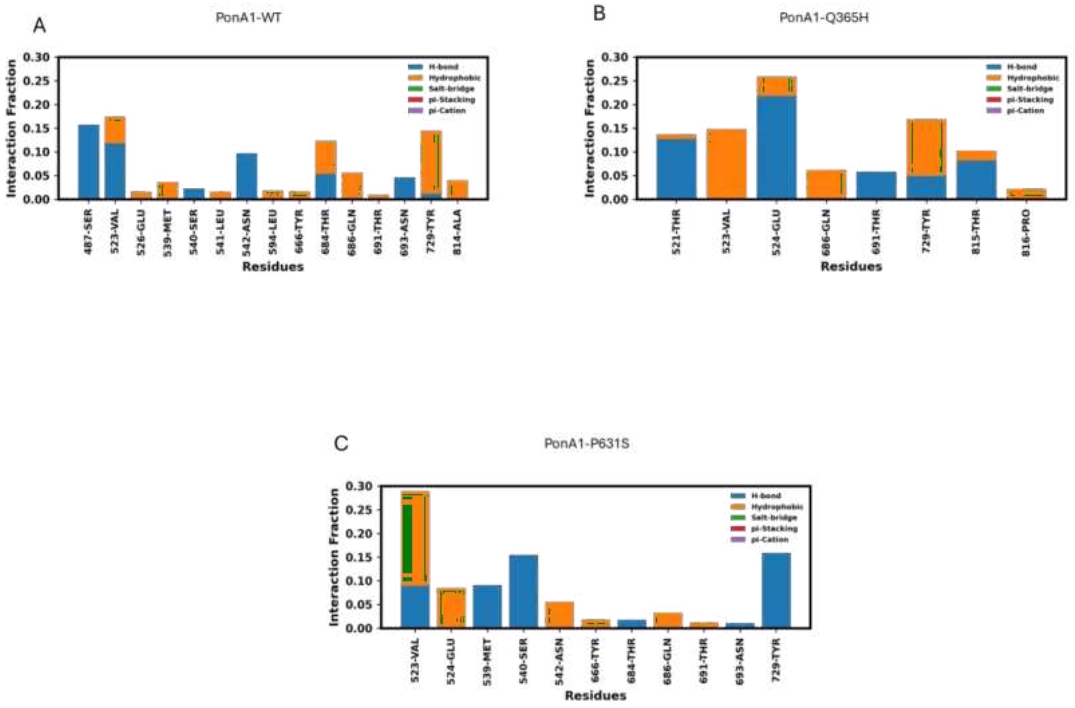

Figure III.16. **Interaction fraction analysis between PonA1 proteins and rifampicin.** A. Residue interactions of PonA1_WT with rifampicin. B. Residue interactions of PonA1_Q365H with rifampicin. C. Residue interactions of PonA1_P631S with rifampicin (Analysis generated using PLIP).

III.3.2. Cloning, expression and purification of recombinant PonA1 variants and RpoB

To assess *in silico* predictions, PonA1$_{234-820}$_WT, PonA1$_{234-820}$_Q365H, PonA1$_{234-820}$_P631S, were expressed in *E. coli* Rosetta. All of them were expressed as an insoluble protein and refolded slowly by dialysis. RpoB was expressed as a soluble protein and used as a control in the interaction studies, serving as a reference for binding and interaction assays. Protein molecular weight and purity were evaluated by SDS-PAGE and Coomassie blue staining (Figure III.17), obtaining approximately 90% purity.

The pattern of migration showed us bands corresponding to molecular weight of 63 KDa for PonA1$_{234-820}$_WT and mutants and 129 KDa for RpoB (marker PageRuler prestained Thermo Scientific #26616). The proteins were concentrated up to 1 -2 mL and, a concentration around 3-7 mg/mL for PonA1$_{234-820}$ and 4-9 mg/mL for RpoB were obtained, respectively. They were aliquoted in fractions of 100 or 200 µL and stored at -20°C until their use.

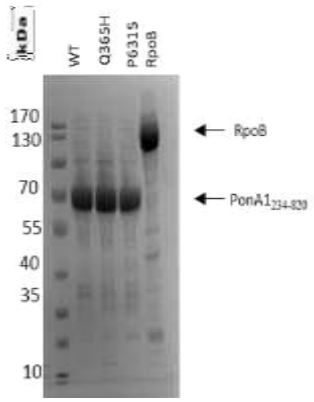

Figure III.17. SDS-PAGE of PonA1 and RpoB proteins from *M. tuberculosis* H37Rv expressed in *E. coli* purified and concentrated. Line 1: Marker PageRuler prestained, Line 2: PonA $_{234-820}$ _WT, Line 3: PonA1$_{234-820}$ _Q365H, Line 4: PonA1$_{234-820}$ _P631S and Line 5: RpoB. Acrylamide gel 15%, 200A-25 min**.**

III.3.3. Biophysical characterization of PonA1$_{234-820}$ variants, and RpoB

The purified recombinant proteins were evaluated for stability, homogeneity, purity, and proper folding. To achieve this, thermal stability, size-exclusion chromatography coupled with multi-angle light scattering (SEC-MALS), and circular dichroism (CD) techniques were employed.

III.3.3.1. Thermal stability

The thermal stability of the proteins was assessed by monitoring the exposure of hydrophobic regions during protein unfolding under a thermal gradient. The analysis was performed on PonA1$_{234-820}$_WT and mutant variants (Figure III.18), as well as RpoB (Figure III.19).

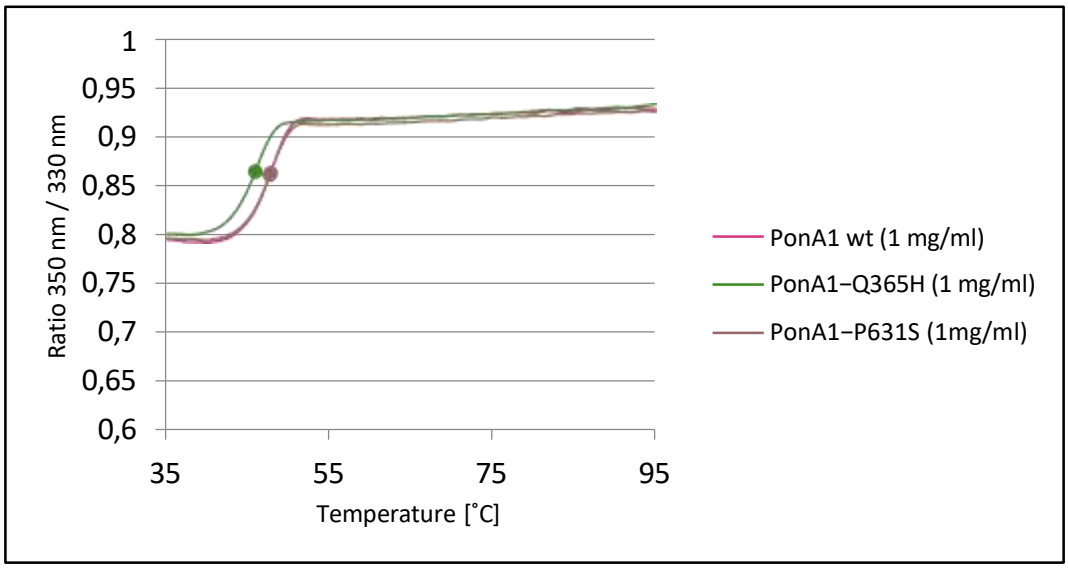

Figure III.18. Thermal stability characterization of PonA1 wild type and mutant variants from *M. tuberculosis* H37Rv using Tycho NT.6. PonA1$_{234-820}$_WT (pink), PonA1$_{234-820}$_Q365H (green) and PonA1$_{234-820}$_P631S (brown).

The inflexion temperature (T_i) was 47,8 +/- 0.12 for $PonA1_{234-820}$_WT, 45,9 +/- 0,1 for $PonA1_{234-820}$_Q365H and 47,7 +/- 0,3 °C for $PonA1_{234-820}$_P631S, all measured at a protein concentration of 1 mg/mL (Figure III.18). There are no differences in the inflection point values between the proteins, $PonA1_{234-820}$_WT and $PonA1_{234-820}$_P631S, suggesting that this mutation does not significantly alter the thermal stability of the protein. The $PonA1_{234-820}$_Q365H shows the lower Ti, suggesting that the mutation leads to a slight reduction in thermal stability. In the case of the RpoB protein of Mtb H37Rv, the most significant T_i is 49 +/- 0,45 °C, among three observed points (Figure III.19).

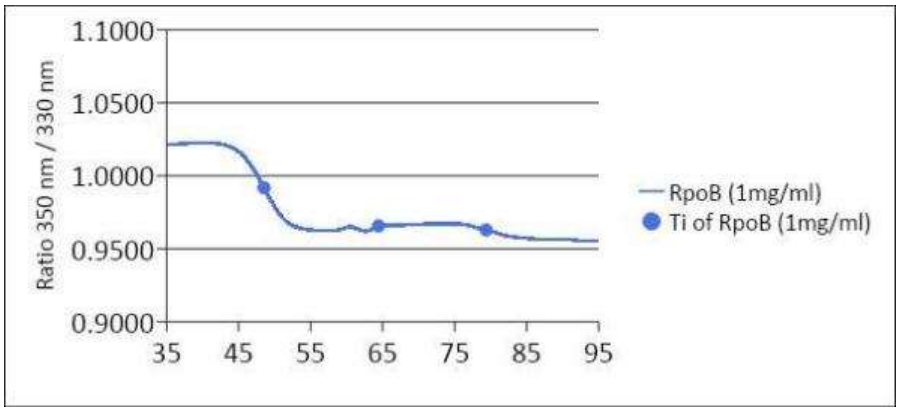

Figure III.19. **Thermal stability characterization of RpoB full-lenght from *M. tuberculosis* H37Rv using Tycho NT.6.**

Since RIF was to be evaluated for its interaction with PonA1, the impact of DMSO, the solvent used for RIF, on the thermal stability of the recombinant proteins was assessed (Figure III.20). The thermal stability analysis of $PonA1_{234-820}$_WT revealed a shift in the Ti upon the addition of DMSO, decreasing from Ti $PonA1_{234-820}$

at 47.7°C to T_i $PonA1_{234\text{-}820\text{-}DMSO}$ at 44.3°C. However, the addition of RIF resulted in a Ti change, from Ti $PonA1_{234\text{-}820}$ at 47.7°C to T_i $PonA1_{234\text{-}820\text{-}DMSO\text{-}RIF}$ at 48.5°C.

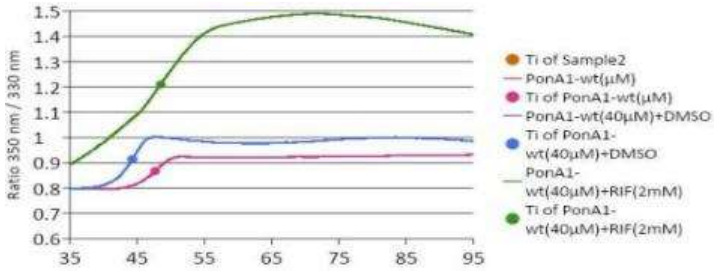

Figure III.20. Thermal stability characterization of $PonA1_{234\text{-}820}$_WT from *M. tuberculosis* H37Rv with and without DMSO using Tycho NT.6. $PonA1_{234\text{-}820}$_WT (pink), $PonA1_{234\text{-}820}$ with DMSO (blue) and $PonA1_{234\text{-}820}$ with DMSO and RIF (green).

For $PonA1_{234\text{-}820}$_Q365H, the addition of DMSO resulted in a significant decrease in the Ti, from 45.8°C to 42.3°C. Prior to the addition of RIF, the Ti could not be accurately determined. However, based on the analysis of the graph, the T_i after RIF addition appears to be comparable to that of the protein alone, albeit with a different 350/330 nm ratio (Figure III.21).

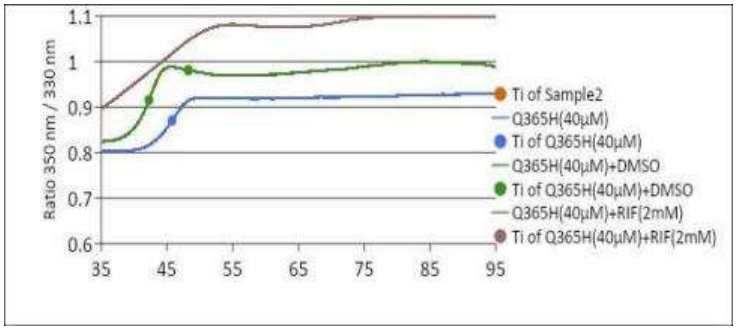

Figure III.21. Thermal stability characterization of $PonA1_{234\text{-}820}$_Q365H with and without DMSO using Tycho NT.6. $PonA1_{234\text{-}820}$_Q365H (blue), $PonA1_{234\text{-}820}$_Q365H with DMSO (green) and $PonA1_{234\text{-}820}$_Q365H with DMSO and RIF (brown).

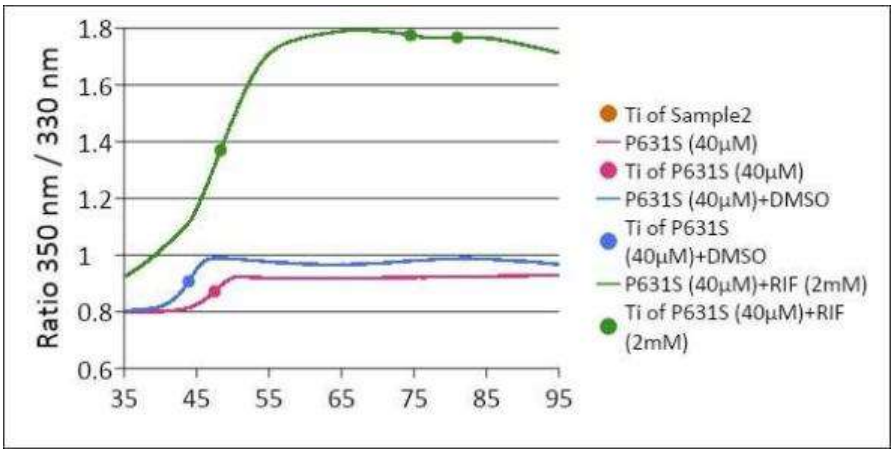

Figure III.22. Thermal stability characterization of PonA1$_{234-820}$_ P631S with and without DMSO using Tycho NT.6. PonA1$_{234-820}$_P631S (pink), PonA1$_{234-820}$_P631S with DMSO (blue) and PonA1$_{234-820}$_P631S with DMSO and RIF (green).

In figure III.22, the thermal stability of PonA1$_{234-820}$_P631S showed a change in the Ti with DMSO addition, from 47.5°C for PonA1$_{234-820}$ to 43.9°C for PonA1$_{234-820-DMSO}$. The addition of RIF altered the T_i from 47.5°C for PonA1$_{234-820}$ to 48.3°C for PonA1$_{234-820-DMSO-RIF}$. RIF notably impacted the profile of the protein unfolding curve.

The information is summarized in Table III.4. The Ti is similar between PonA1$_{234-820}$_WT and PonA1$_{234-820}$_P631S but differs from PonA1$_{234-820}$_Q365H. The addition of DMSO to the solution decreased the Ti by an average of 3.5°C for all evaluated proteins, while the addition of RIF caused an approximate increase of 0.8°C in the Ti of both PonA1$_{234-820}$_WT and PonA1$_{234-820}$_P631S compared to the protein alone. For PonA1$_{234-820}$_Q365H, the Ti could not be accurately determined. There are not notable changes in the thermal stability of the proteins after the RIF addition.

Table III. 4. Inflection temperature for PonA1$_{234-820}$ recombinant proteins evaluated in this study.

Sample	WT (Ti °C)	Q365H (Ti °C)	P631S (Ti °C)
PonA1$_{234-820_}$	47.7	45.8	47.5
PonA1$_{234-820-DMSO}$	44.3	42.3	43.9
PonA1$_{234-820-DMSO-RIF}$	48.5	~45	48.3

III.3.3.2. Molecular exclusion chromatography and multiple angle light scattering (SEC MALS)

In our study, the molar mass and size in solution were determined using SEC MALS. PonA1$_{234-820}$ was evaluated under two conditions: native, after purification from the insoluble fraction, and after refolding. In the native sample, three different peaks were observed at 82.1, 120.3, and 160.2 kDa, suggesting the presence of protein mixtures or with missfolding, with only a small fraction likely corresponding to our target protein (Figure III.23.A). In contrast, after slow refolding, a single peak at 64.34 KDa was observed (Figure III.23.B), which closely matches the predicted molar mass of 63.57 KDa from1 *in silico* analysis. This suggests that the refolding sample is homogeneous, monomeric, and pure.

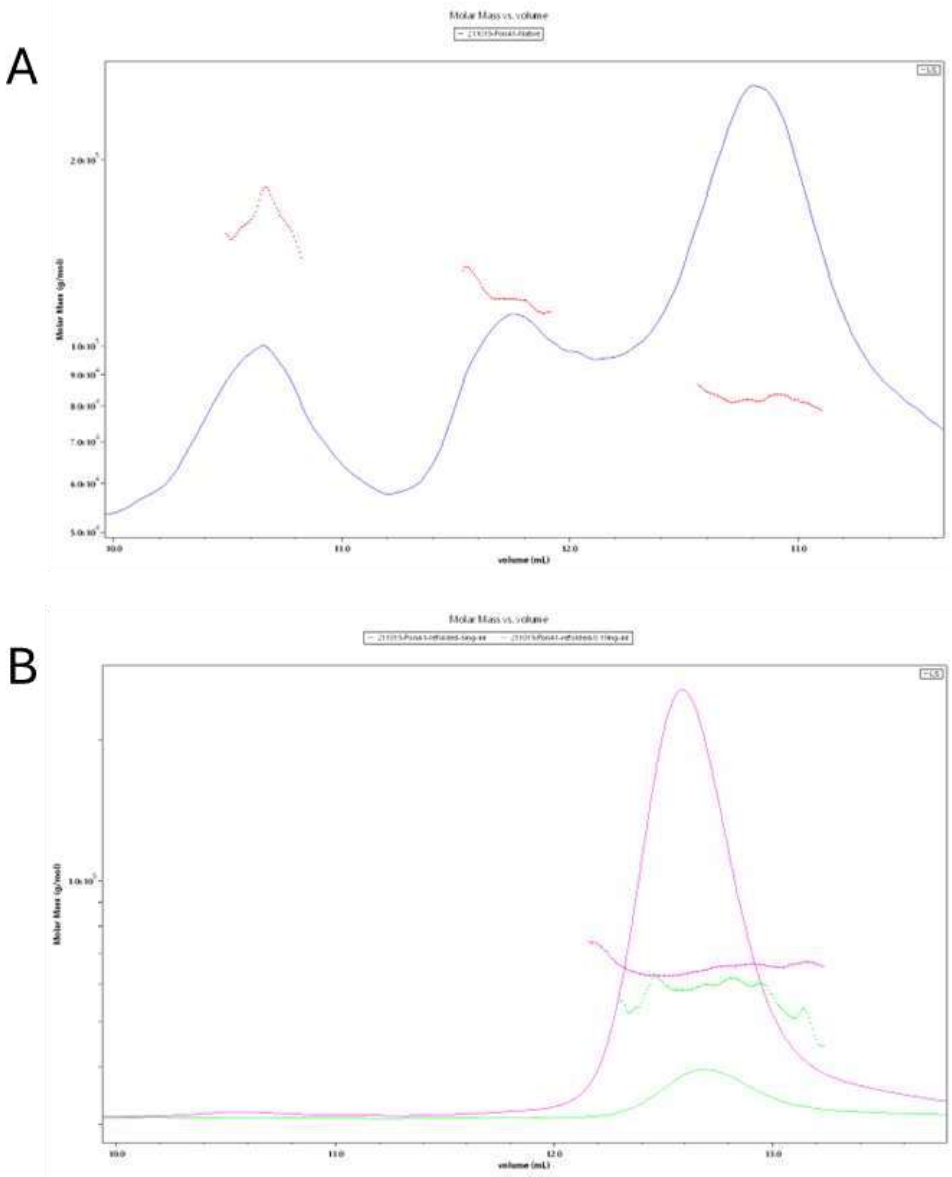

Figure III.23. SEC MALS analysis of PonA1$_{234-820}$_WT recombinant protein from *M. tuberculosis* H37Rv expressed in *E. coli.* A. native and B. refolded protein from the insoluble fraction.

RpoB was expressed as soluble protein, and the SEC-MALS analysis shows a peak corresponding to 111.9 KDa (Figure III.24). Similarly, the predicted molecular weight based on the *in silico* linear amino acid sequence is 129.35KDa. This result indicates that the protein is monomeric, homogeneous and of high purity.

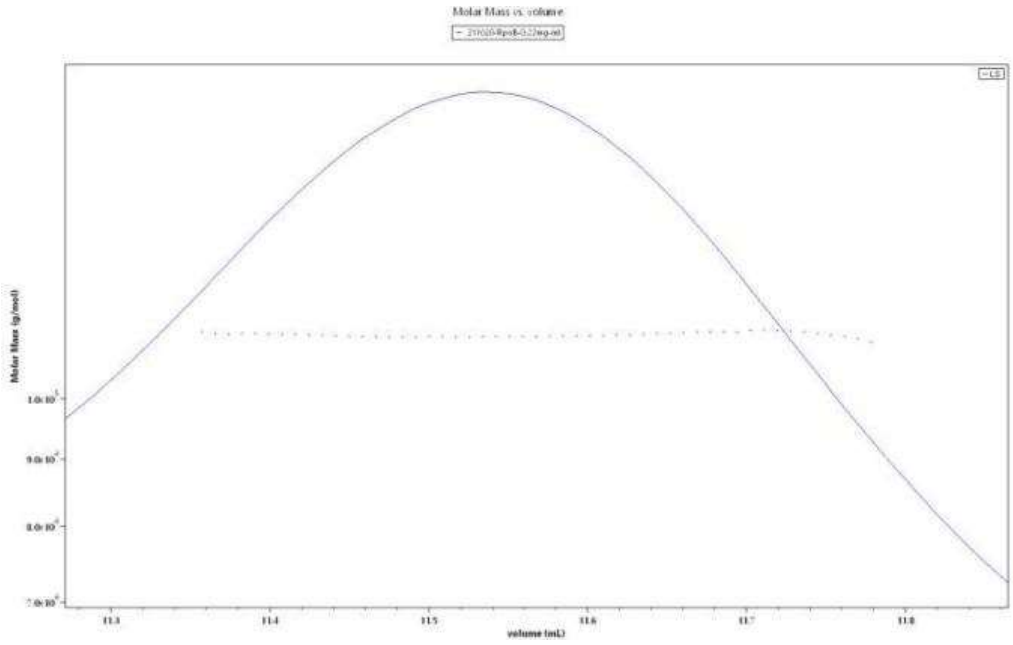

Figure III.24. **SEC MALS analysis of RpoB recombinant protein from *M. tuberculosis* H37Rv expressed in *E. coli.***

III.3.3.3. Circular dichroism (CD)

From the CD spectra of PonA1$_{234\text{-}820}$ (Figure III.25) and RpoB (Figure III.26), we can infer that both proteins are properly folded and suitable for use in subsequent assays. This assessment was particularly crucial for PonA1$_{234\text{-}820}$, which underwent a refolding process after affinity purification.

Negative bands were observed around 208 nm and 222 nm and a positive band around 190 nm indicating the predominant presence of α-helices, no negative band spectra are observed near 195 nm, so there is no indication of disordered or spun structures for both proteins.

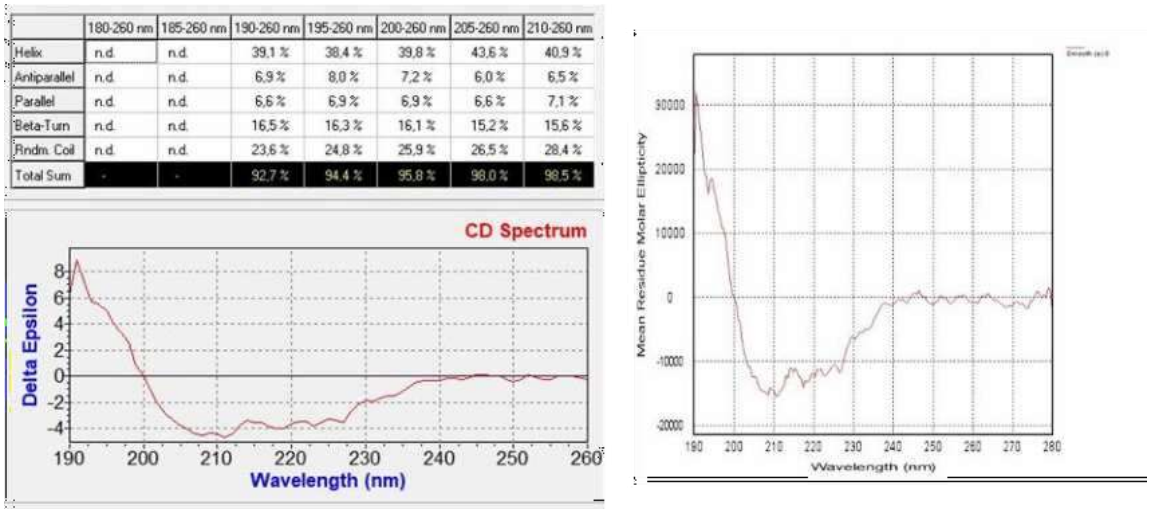

	180-260 nm	185-260 nm	190-260 nm	195-260 nm	200-260 nm	205-260 nm	210-260 nm
Helix	n.d.	n.d.	39,1 %	38,4 %	39,8 %	43,6 %	40,9 %
Antiparallel	n.d.	n.d.	6,9 %	8,0 %	7,2 %	6,0 %	6,5 %
Parallel	n.d.	n.d.	6,6 %	6,9 %	6,9 %	6,6 %	7,1 %
Beta-Turn	n.d.	n.d.	16,5 %	16,3 %	16,1 %	15,2 %	15,6 %
Rndm. Coil	n.d.	n.d.	23,6 %	24,8 %	25,9 %	26,5 %	28,4 %
Total Sum	-	-	92,7 %	94,4 %	95,8 %	98,0 %	98,5 %

Figure III.25. Circular dichroism analysis of PonA1$_{234-820}$ from *M. tuberculosis* H37Rv. The protein was resuspended in buffer Tris-HCl 50 mM, NaCl 150 mM, and 2 mM DTT with DDM 0.08%.

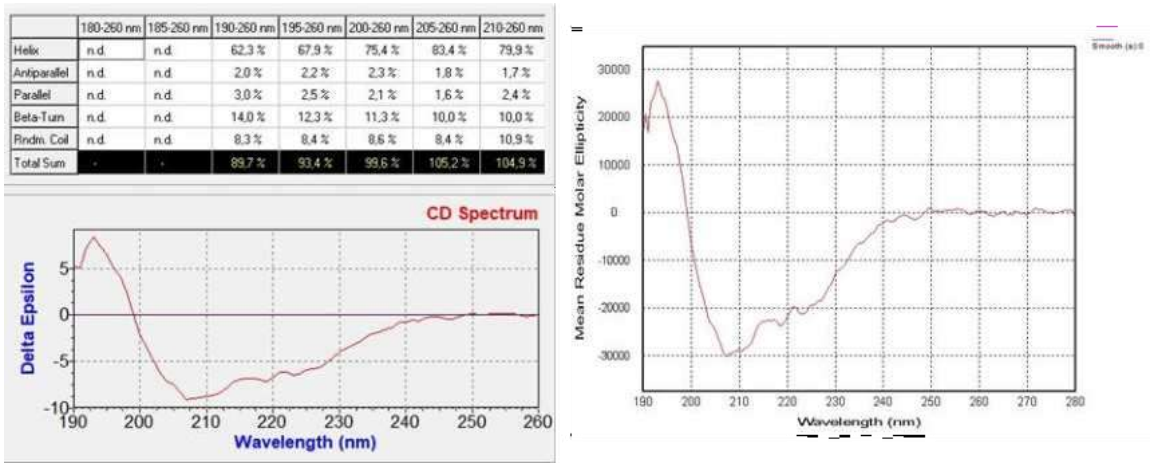

Figure III.26. **Circular dichroism analysis of RpoB from *M. tuberculosis* H37Rv.** The protein was resuspended in buffer Tris-HCl 50 mM, NaCl 150 mM, and 2 mM DTT.

III.3.4. Transpeptidase enzyme activity of PonA1

PBPs are inactivated by covalent modification at a catalytic serine by β-lactam antibiotics, such as Bocillin-FL, a fluorescent analog of penicillin V. Figure III.27 illustrates the interaction between $PonA1_{234-820}$_WT and Bocillin-FL through twin gels. Panel A shows the gel under UV exposure at 500 V, while Panel B is stained with Coomassie Blue, displaying the experiment with 0.1 µM $PonA1_{234-820}$_WT across a range of Bocillin-FL concentrations (40, 20, 10, 5, 2.5, 1.25, 0.625, 0.3125, 0.156 µM). The experiment9s goal was to determine the Bocillin-FL concentration needed to adequately detect the protein signal. Notably, the signal intensity was consistent from 40 µM to 10 µM Bocillin-FL with 0.1 µM of protein.

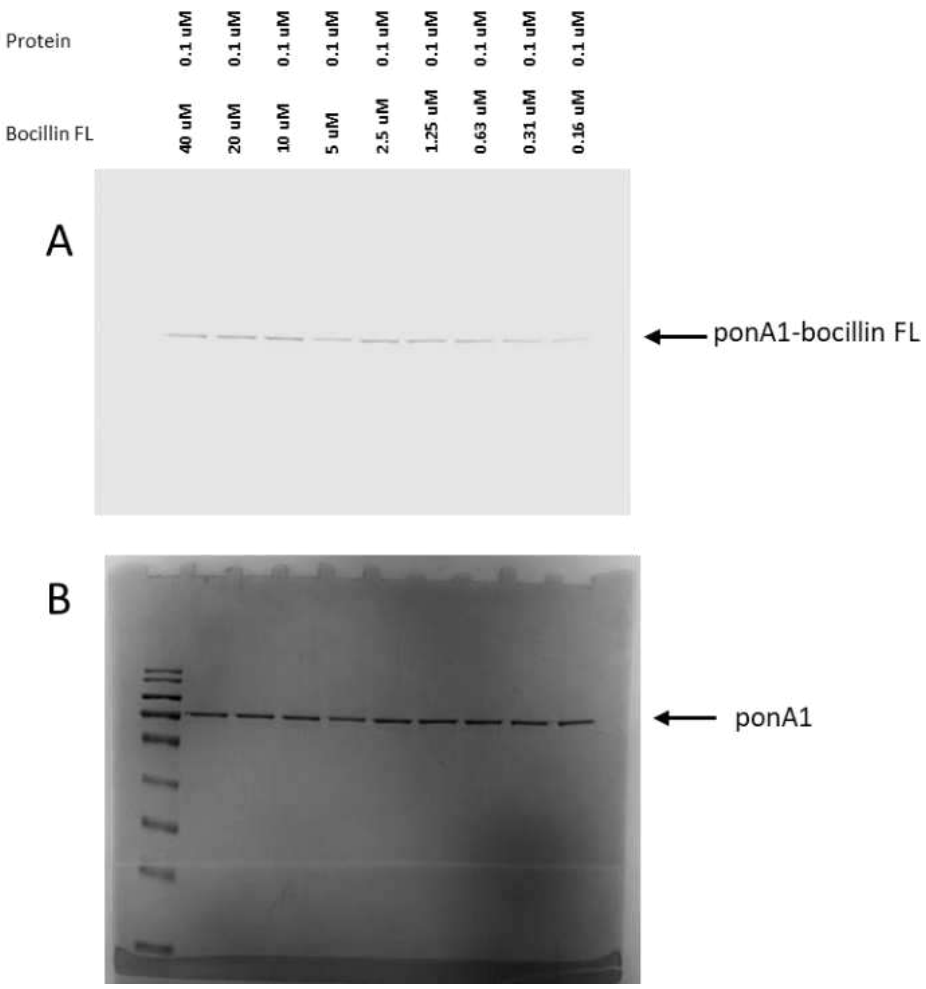

Figure III.27. **Transpeptidase enzyme activity evaluation between PonA1 recombinant protein and different concentrations of Bocillin-FL.** $PonA1_{234-820}$_WT and different Bocillin-FL concentrations (40, 20, 10, 5, 2.5, 1.25, 0.63, 0.31, 0.16 µM) - twin gels. A. Cuan exposition 500 V. B. Coomasie blue stain. Marker PageRuler prestained. Acrylamide gel 15%, 200A-25 min.

The following different protein concentrations under saturating Bocillin-FL conditions were assessed and observed that complex formations were proportional to the added protein concentration in the reaction (Figure III.28).

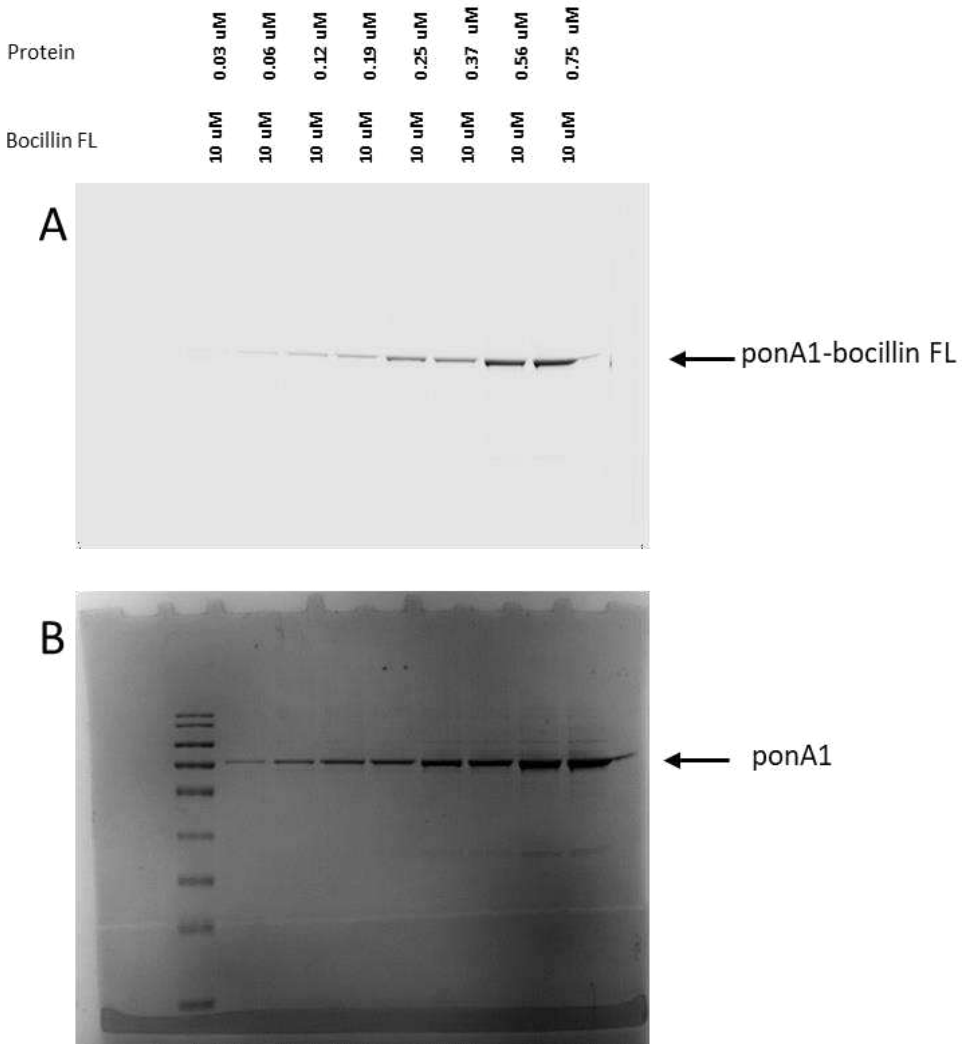

Figure III.28. **Transpeptidase enzyme activity evaluation between different concentrations of between PonA1$_{234\text{-}820}$ recombinant protein and Bocillin-FL.** Twin gels were run with PonA1$_{234\text{-}820}$_WT at different concentrations, in the presence of 10 µM Bocillin-FL. A. Cuan exposition 500 V. B. Coomassie blue stain. Marker PageRuler prestained, Acrylamide gel 15%, 200A-25 min.

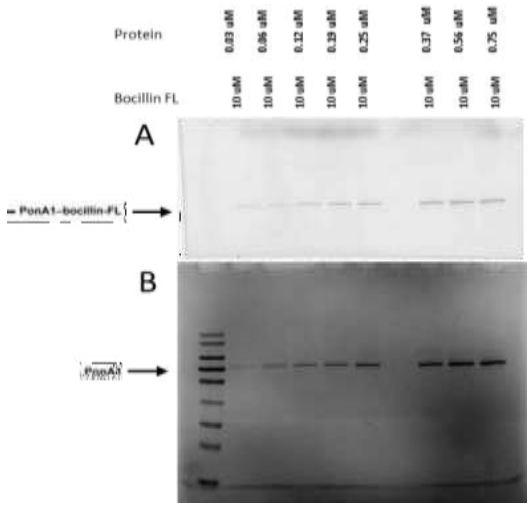

Figure III.29. Transpeptidase enzyme activity evaluation between PonA1$_{234-820}$_Q365H and Bocillin-FL. A. Cyan exposition 500V. B. Coomasie blue stain. Different protein concentrations were tested with 10 µM Bocillin-FL. Marker PageRuler prestained, Acrylamide gel 15%, 200A-25 min.

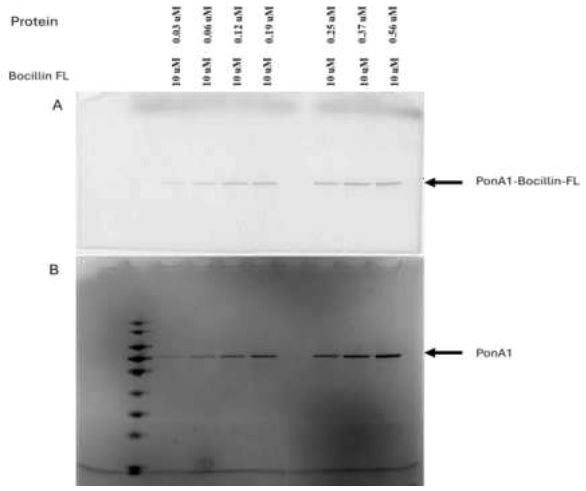

Figure III.30. Transpeptidase enzyme activity evaluation between PonA1$_{234-820}$_P631S and Bocillin-FL interaction. A. Cyan exposition 500V. B. Coomasie blue stain. Different protein concentrations were evaluated with 10 µM Bocillin- FL. Marker PageRuler prestained, Acrylamide gel 15%, 200A-25 min.

PonA1$_{234\text{-}820}$_WT, PonA1$_{234\text{-}820}$_Q365H, PonA1$_{234\text{-}820}$_P631S were able to form complexes with Bocillin-FL in concentrations greater than 0.06 µM in a similar way. Based on the results obtained, we suggest that enzymatic activity remains intact for both the wild-type protein and the proteins with Q365H and P631S mutations. This suggests that these mutations do not impair enzymatic activity (Figure III.29-30).

III.3.5. PonA1- RIF interaction measured by nuclear magnetic resonance (STD-NMR) spectroscopy

Each reaction has 2 mM RIF as a ligand with 40 µM of each protein in 20 mM potassium phosphate pH 6.8, 100 mM NaCl, 0.5 mM DTT. The on-resonance pulse was calibrated based on RIF at 8.9 ppm to obtain a flat difference spectrum (Figure III.31.A). In the presence of RpoB protein, the natural ligand for RIF, peaks appear in the difference spectrum between 8 to -0.5 ppm indicating the protons involved in the interaction (Figure III.31.B).

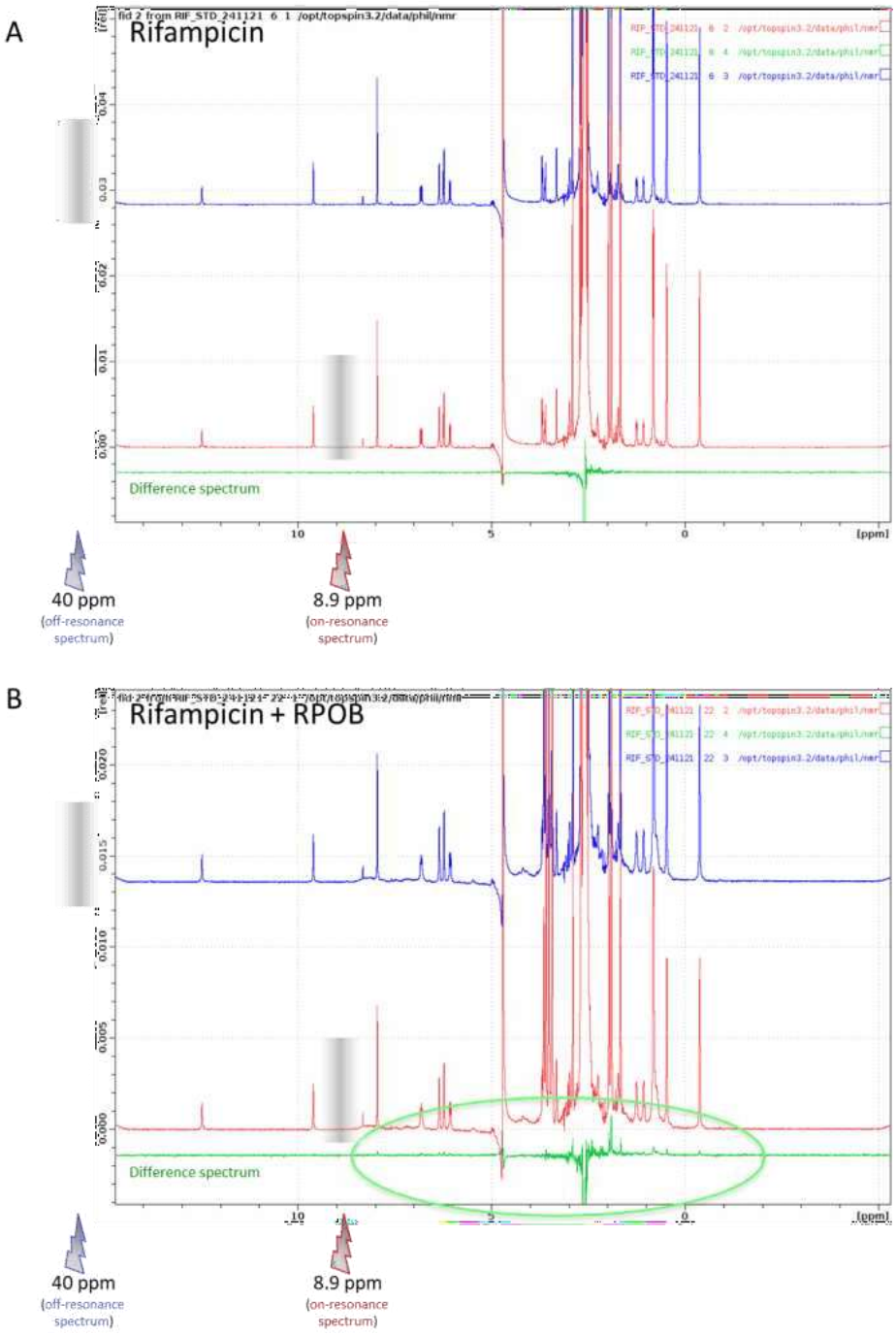

Figure III.31. **1D NMR spectra of rifampicin and RpoB protein.** (A) 1D NMR spectra of 2 mM rifampicin. (B) 1D NMR spectra of rifampicin with 40 µ M RpoB in 20 mM potassium phosphate pH 6,8; 100 mM NaCl, 0.5 mM DTT; 293 K, 800 MHz, 3 min. Off resonance spectrum (blue), on resonance spectrum (red) and STD spectrum (green).

The second step was to check the interaction of RIF with other proteins. To do this, we performed 1D NMR spectra of RIF alone, to which we added small quantities of the $PonA1_{234\text{-}820}$_WT protein, $PonA1_{234\text{-}820}$ mutants, and RpoB (as a positive control for interaction with RIF). In addition, the Rv1813c protein, supplied by Dr. Cohen-Gonsaud of the CBS, was used as a negative control for the interaction. The interaction of RIF with a large protein should result in a modification of the 1D NMR spectrum, either by chemical shifts or by variations in peak intensity, as the fraction of free RIF decreases.

The RIF spectra (Figure III.32.A), in the range of about 0.9 to -0.5 ppm, are arbitrarily shifted relative to each other for clarity, as no variation in the chemical shift of the peaks is observed. Figure III.32. B-C shows decrease in intensity with the addition of $PonA1_{234\text{-}820}$ proteins (WT and mutants), as well as RpoB, whereas the intensity of the RIF peaks does not decrease with the addition of Rv1813c. It should be noted that RIF peak intensities were greatly reduced with the addition of the $PonA1_{234\text{-}820}$_Q365H mutant.

Based on the observed spectral changes, we investigated the impact of time on these changes, comparing the evolution of the spectra over time (Figure III.33.A-B). After 8 hours, we noted a significant decrease in the intensity of the peaks with the $PonA1_{234\text{-}820}$_Q365H protein, which prompted us to ask whether this shift resulted from a change in the affinity of the protein for RIF or a change in the viscosity of the medium over time.

To assess behavior and identify differences in interaction magnitude between PonA1$_{234\text{-}820}$_WT, PonA1$_{234\text{-}820}$_Q365H and RIF we estimated the dissociation constant (K_D).

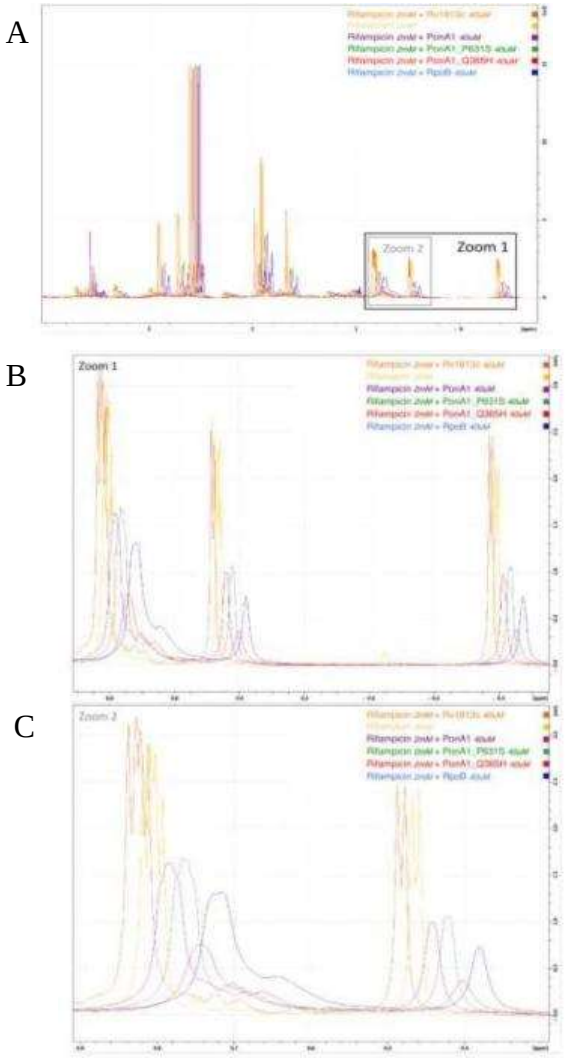

Figure III.32. 1D NMR spectra for rifampicin with or without addition of recombinant proteins. A. Total 1D-NMR spectra of rifampicin 2 mM in 20 mM potassium phosphate pH 6,8; 100 mM NaCl, 0.5 mM DTT (yellow), with PonA1$_{234\text{-}820}$_WT (purple), PonA1$_{234\text{-}820}$_Q365H (red), PonA1$_{234\text{-}820}$_P631S (green), Rv1813 (mustard) and RpoB (blue) at 293 K, 800 MHz. The spectra are arbitrarily shifted for better clarity. B. Magnification of the 0.9 to -0.6 ppm spectra. C. Magnification of the 0.9 to 0.3 ppm spectra.

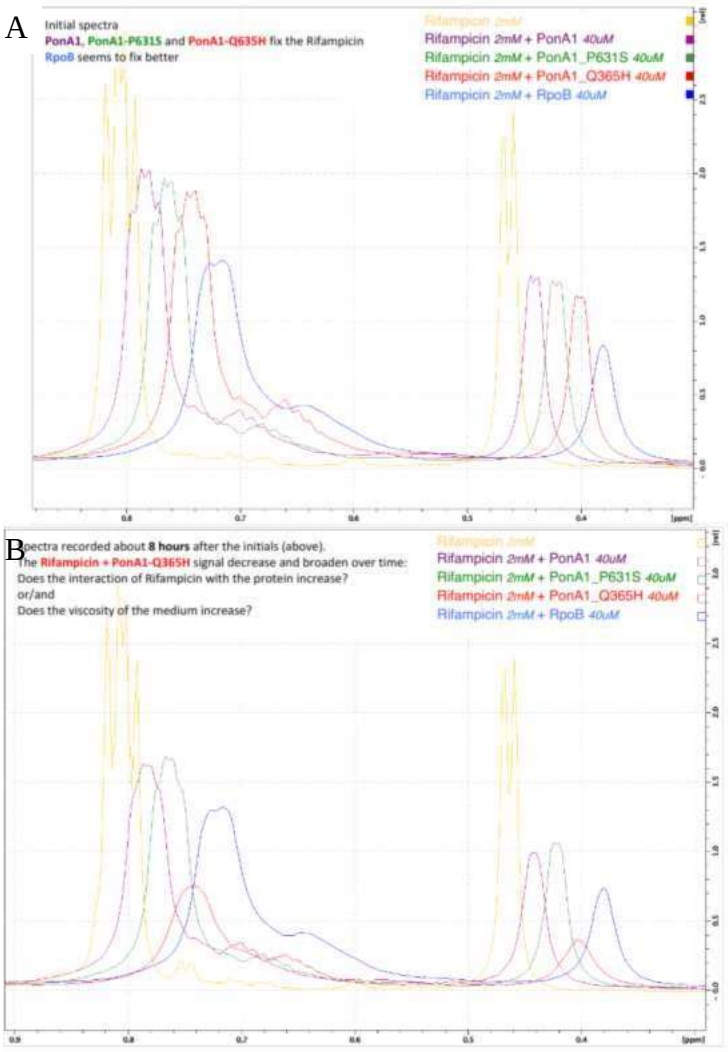

Figure III.33. Evolution of 1D NMR spectra of rifampicin and recombinant proteins varying at different times. 2 mM rifampicin in 20 mM potassium phosphate pH 6,8; 100 mM NaCl, 0.5 mM DTT (yellow), with PonA1$_{234\text{-}820}$_WT (purple), PonA1 $_{TP}$_ Q365H(red), PonA1 $_{TP}$_ P631S(green), Rv1813 (mustard), RpoB (blue) at 293 K, 800 MHz, 3 min (A) and 8 hours after (B).

The K_D determination for PonA1$_{234\text{-}820}$-RIF complex involved titrations with RIF concentrations ranging from 1.2 and 0.075 mM and 38.3 µM of each protein, following protocols described (Angulo & Nieto, 2011; Walpole et al., 2019). The K_D values for PonA1$_{234\text{-}820}$_WT, PonA1$_{234\text{-}820}$_Q365H and PonA1$_{234\text{-}820}$_P631S were estimated at 1.8 (Figure III.34), 2.1 mM (Figure III.35) and 6,41 mM (Figure III.36) respectively. Given

that all K_D values are in the millimolar range, the binding between $PonA1_{234-820}$ and RIF suggests low affinity and non-specific interaction regardless of whether the protein is in the form wild type or mutated.

Tabulated data for the binding isotherms, including STD-NMR build-up curves at various depths of the tube corresponding to increasing ligand concentrations, are reported in the Appendix III.39-41.

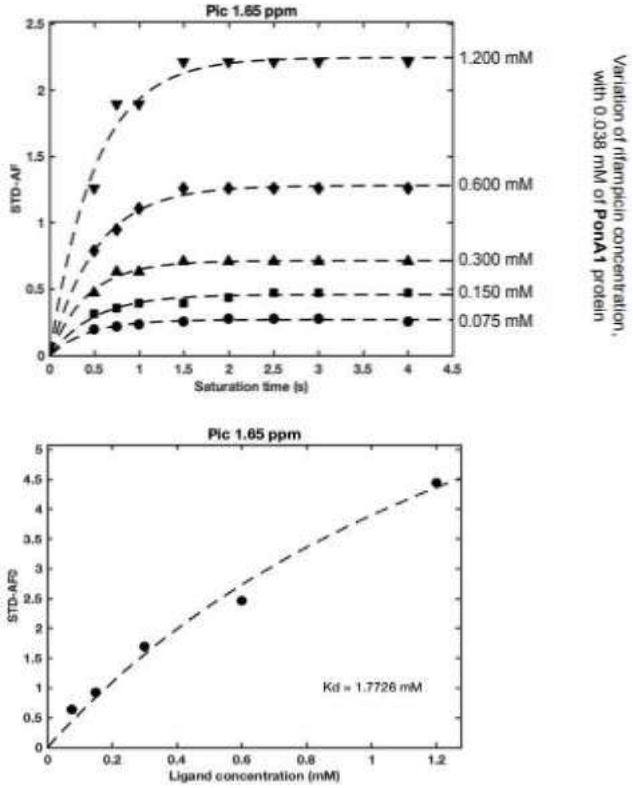

Figure III.34. Determination of K_D between $PonA1_{234-820}$_WT and rifampicin by STD-NMR. Using 20 mM potassium phosphate buffer (pH 6,8); 100 mM NaCl, 0.5 mM DTT; 1.65 ppm. The assay was conducted with protein concentrations of 38 µM $PonA1_{234-820}$_WT and rifampicin concentrations ranging from 1.2 mM, 0.6 mM, 0.3 mM, 0.150 mM, 0.075 mM in deuterated DMSO. Data was collected at 1.65 ppm.

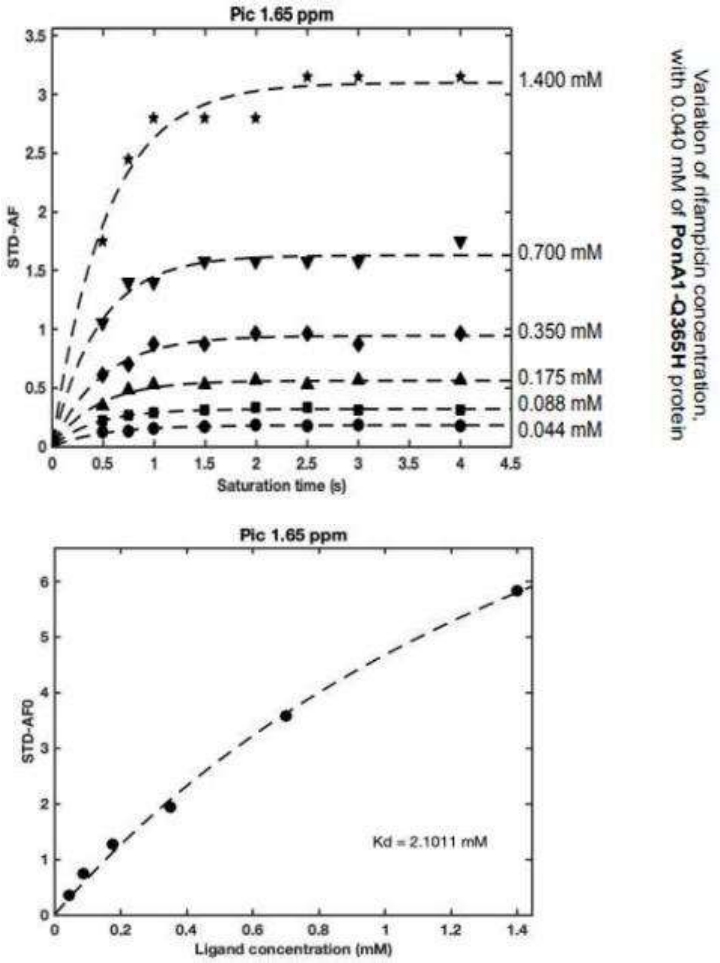

Figure III.35. Determination of K_D between PonA1$_{234\text{-}820}$_Q365H and rifampicin by STD-NMR. Using 20 mM potassium phosphate buffer (pH 6,8); 100 mM NaCl, 0.5 mM DTT. The assay was conducted with protein concentrations of 40 µM PonA1$_{234\text{-}820}$_Q365H and rifampicin concentrations ranging from 1.4 mM, 0.7 mM, 0.35 mM, 0.175 mM, 0.088 mM, 0.044 mM in deuterated DMSO. Data was collected at 1.65 ppm.

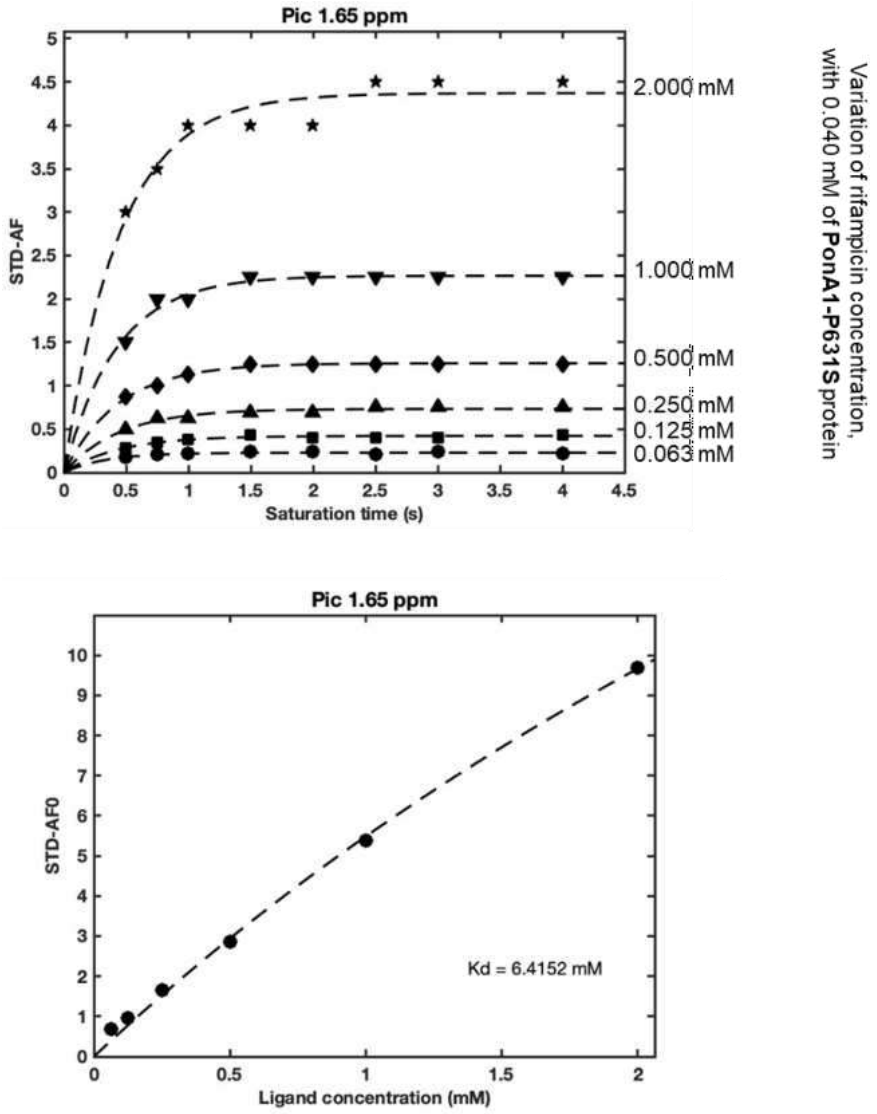

Figure III.36. Determination of K_D between PonA1$_{234-820}$_P631S and rifampicin by STD-NMR. Using 20 mM potassium phosphate buffer (pH 6,8); 100 mM NaCl, 0.5 mM DTT. The assay was conducted with protein concentrations of 40 µM PonA1$_{234-820}$_P631S and rifampicin concentrations ranging from 2 mM, 1 mM, 0.5 mM, 0.25 mM, 0.125 mM and 0.063 mM in deuterated DMSO. Data was collected at 1.65 ppm.

III.3.6. *MMAR_0069* knockout in *M. marinum* by ORBIT

MMAR_0069 is identified as the *ponA1* gene homologue in Mmar. The KO of the *MMAR_0069* gene was achieved by integrating one modified ORBIT plasmid: pKM464-ponA1p-EGFP or pKM464-*rpsTp*-EGFP; facilitated by one oligonucleotide as described in section III.2.6.1. The following sections provide a detailed description of the procedure.

III.3.6.1. pKM464-ponA1p-EGFP plasmid construction, transformation in *E. coli* and *MMAR_0069* knockout in *M. marinum* by ORBIT

This process was completed in two stages: first, the construction, ligation, and transformation of the plasmids in *E. coli* were carried out, followed by verification through sequencing. In the second stage, the KO of the gene in Mmar was performed, with the final step involving confirmation by sequencing.

A. pKM464-ponA1p-EGFP plasmid construction and transformation in *E. coli*

A fragment of pKM464 containing the *ponA1p* was amplified (Figure III.37.A), along with the EGFP gene at 717 bp (Figure III.37.B). Both fragments were verified by electrophoresis, and gel purification was performed. GA and *E. coli* DH5α transformants exhibited growth after 24 hours (Figure III.37.C), with 105 CFU resulting from the assembly of the two fragments and 45 from recircularization. Three colonies were assessed by PCR colony using primers F-pKM464-int and R-pKM464-

int, producing a 2896 bp PCR product (Figure III.37.D), compared to pKM464 without any insert (Line 1- Figure III.37.D). Clone 1 was confirmed correct by sequencing.

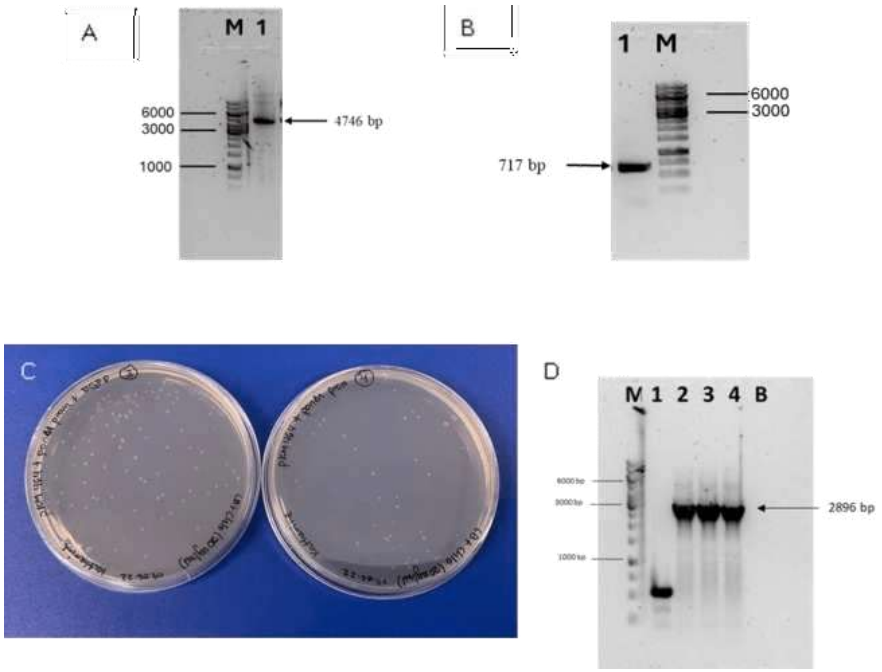

Figure III.37. Cloning of pKM464-ponA1p-EGFP and transformation in *E. coli*. A. Electrophoresis in agarose gel of pKM6464 plasmid and *ponA1p* obtained by PCR amplification. B. Electrophoresis in agarose gel of EGFP obtained by PCR amplification. C. LB agar plate with Chlo (25 µg/mL) for selection of transformants with both fragments assembled by GA (left). Negative control of auto assembling (right). D. Electrophoresis in agarose gel for PCR colony screening. Line 1: pKM464 plasmid, line 2 to 4: *E. coli* clones screening. B Blank. M marker 1 kb GeneRuler. Agarose electrophoresis 0.8 %, TAE 1X. Chlo=chloramphenicol.

B. ORBIT with pKM464-ponA1p-EGFP in *M. marinum* for *MMAR_0069* knockout

The first requirement for the ORBIT system was to obtain cells containing the pKM444 plasmid. For this, Mmar was electroporated with 1 µg of pKM444, followed by incubation at 30°C in darkness. Colonies began to appear on day 13, yielding 2,4x 10^4 CFU/µg of pKM444.

Therefore, in a second electroporation with the pKM464 plasmid containing a promoter regulating EGFP expression was evaluated. This approach enabled both gene KO and simultaneous tracking of EGFP expression in Mmar.

ponA1p was evaluated, to do this a second electroporation was performed with the pKM464-ponA1p-EGFP plasmid (5426 bp) mediated by oligonucleotide designed in this study. After 12 days, it resulted in 100 CFU, while 2 CFU were obtained without the oligonucleotide (Figure III.38.A). PCR on 6 colonies with primers F-Mmar-Rv0050-orbit and R-Mmar-Rv0050-orbit produced a 5761 bp product in three of them (Figure III.38.B). The insertion of the plasmid in the flanking region of the *MMAR_0069* gene was verified by sequencing. At this stage, the results indicate that the viability of Mmar was not significantly impacted by the deletion of the *MMAR_0069* gene.

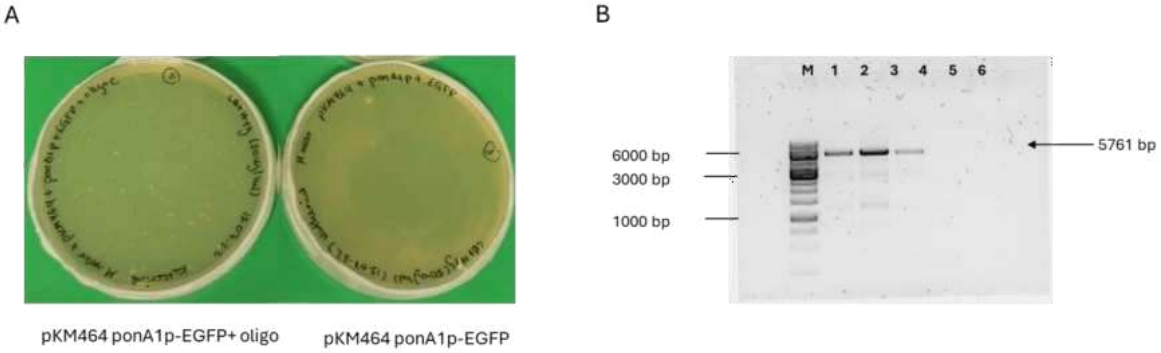

Figure III.38. *MMAR_0069* knockout using pKM464-*ponA1p*-EGFP payload plasmid integration in *M. marinum* genome by ORBIT. A. 7H10 plates with HYG (50 µg/mL) for selection of Mmar strains electroporated with pKM464-ponA1p-EGFP with (left)/without (right) oligonucleotide generating the strain Mmar ΔMMAR0069::ponA1p_EGFP. B. Electrophoresis in agarose gel for PCR colony verification of ΔMMAR0069 and insertion of pKM464-ponA1p-EGFP. Lines 1-6: *M. marinum* transformants colonies evaluated. M marker 1 kb GeneRuler. Agarose electrophoresis 0.8 % TAE 1X. HYG= Hygromycin.

III.3.6.2. pKM464-*rpsTp*-EGFP plasmid construction, transformation in *E. coli* and *MMAR_0069* knockout in *M. marinum* by ORBIT

A. pKM464-*rpsTp*-EGFP plasmid construction and transformation in *E. coli*

Three fragments were amplified for the construction of this plasmid, plasmid pKM464 linearized (Figure III.39.A), the EGFP gene (Figure III.39.B) and the Mmar *rpsTp* (Figure III.39.C), with 3152, 717 and 148 bp, respectively. The GA and transformation process resulted in 46 colonies with the three assembled fragments and no colonies when only the fragment corresponding to the pKM464 plasmid was used (Figure III.39.D). Three colonies were selected for verification generating a 1470 bp fragment for the colonies with the *rpsTp*-EGFP assembled in pKM464 as opposed to 148 bp corresponding to *rpsTp* alone (Figure III.39.E).

Verification by sequencing was performed on the three colonies and all harbored the C79T mutation in the *rpsTp*, clone 1C1 was used for the next steps.

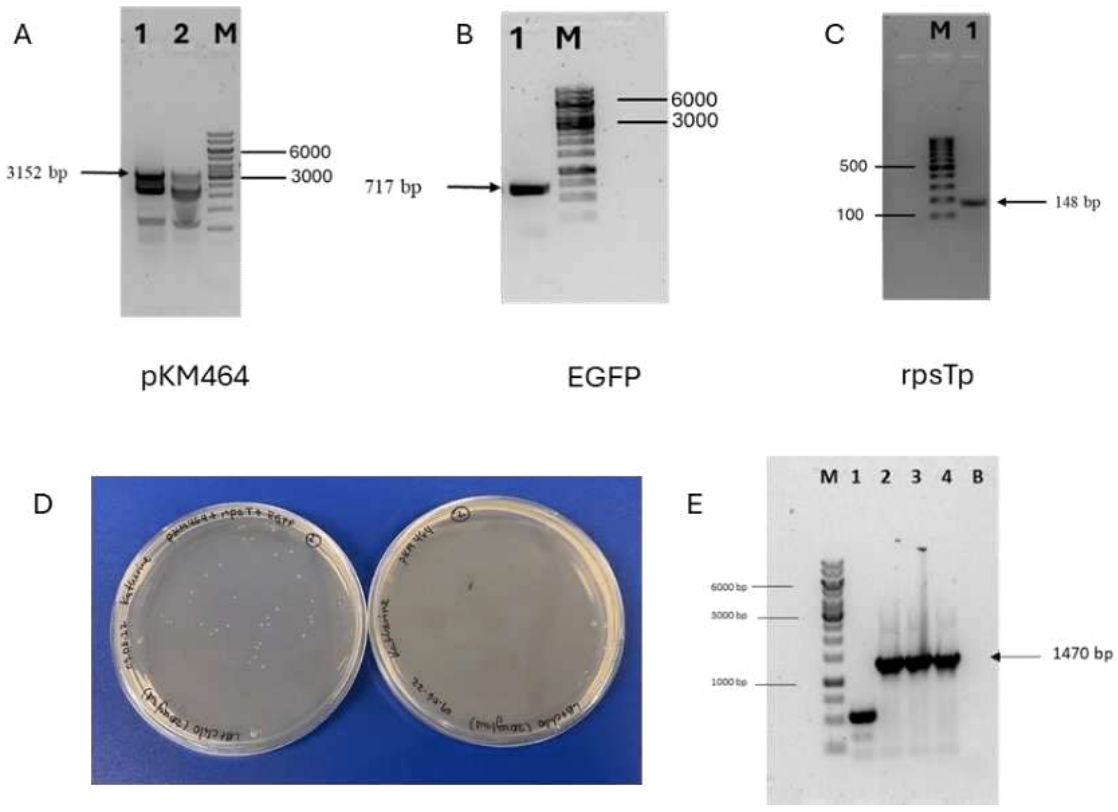

Figure III.39. Cloning of pKM464-*rpsTp*-EGFP and transformation in *E. coli*. A. Electrophoresis in agarose gel of pKM464 plasmid PCR amplification B. Electrophoresis in agarose gel of EGFP gene PCR amplification. C. Electrophoresis in agarose gel of *rpsTp* amplification D. LB agar plate with Chlo (25 µg/mL) for selection of *E. coli* DH5α transformants with all fragments assembled (left). Negative control of auto assembling (right). E. Electrophoresis in agarose gel for PCR colony screening. Line 1: pKM464 plasmid, line 2-4: *E. coli* DH5α clones evaluated. B Blank. M marker 1 kb GeneRuler. Agarose electrophoresis 0.8 % TAE 1X. Chlo=chloramphenicol.

B. ORBIT with pKM464-*rpsTp*-EGFP in *M. marinum* for *MMAR_0069* knockout

By applying ORBIT with pKM464-*rpsTp*-EGFP plasmid, we achieved the ΔMMAR0069 and simultaneously track the expression of EGFP under the regulation of *rpsTp* of Mmar. The integration of pKM464-*rpsTp*-EGFP plasmid (4000 bp) mediated by oligonucleotide resulted in 103 CFU, while none CFU were obtained when the oligonucleotide was not present (Figure III.40.A). PCR was performed on 6 colonies with primers F-Mmar-Rv0050-orbit and R-Mmar-Rv0050-orbit and a product of 4379 bp was obtained for all of them (Figure III.40.B). Long-read sequencing was performed using nanopore technology at the Laboratorio de Bioinformática y Biología Molecular, UPCH - Peru. The neighboring upstream and downstream genes of *MMAR_0069* were identified, confirming the precise integration of the pKM464-*rpsTp*-EGFP plasmid at the *MMAR_0069* locus (Figure III.40.C). Similar to the observations in section III.6.1.b, the KO of the *MMAR_0069* gene generated with the pKM464-*rpsTp*-EGFP plasmid did not have a lethal effect on the survival of the strain.

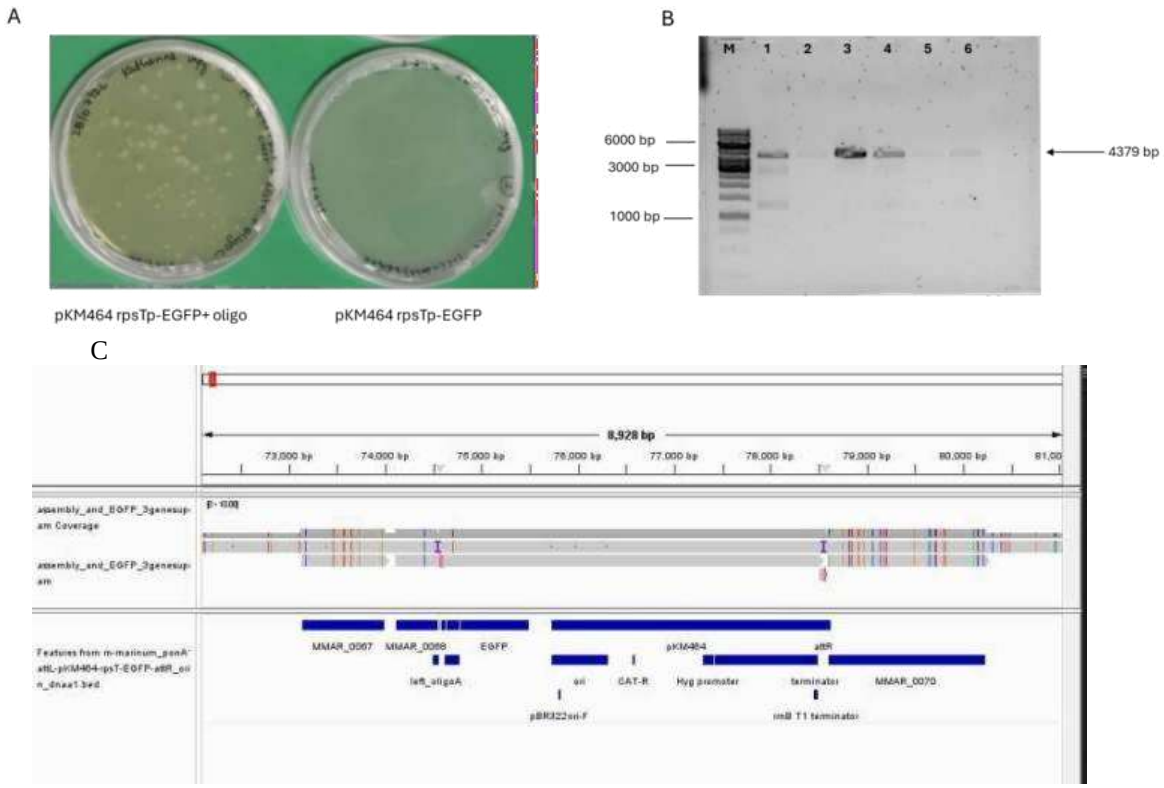

Figure III. 40. *MMAR_0069* knockout using pKM464-*rpsTp*-EGFP payload plasmid integration in *M. marinum* genome by ORBIT. A. 7H10 plates with HYG (50 µg/mL) for selection of Mmar strains electroporated with pKM464-*rpsTp*-EGFP with (left)/without (right) oligonucleotide generating the strain ΔMMAR0069::*rpsTp*_EGFP. B. Electrophoresis in agarose gel for PCR colony verification of ΔMMAR0069 and insertion of pKM464-*rpsTp*-EGFP. Lines 1-6: *M. marinum* transformants colonies evaluated. M marker 1 kb GeneRuler. Agarose electrophoresis 0.8 % TAE 1X. C. Long read sequencing in the strain ΔMMAR0069::*rpsTp*_EGFP, shows the vicinity of genes upstream and downstream of *MMAR_0069*. HYG= Hygromycin.

III.3.6.3. Assessment of promoter function via EGFP reporter expression in *M. marinum*

The ΔMMAR0069 strains carrying EGFP reporter under the regulation of two promoters-*ponA1p* and *rpsTp*- were generated in a single step using the ORBIT system. This approach enabled the simultaneous assessment of the promoters9 capacity to regulate EGFP expression. Fluorescence levels were measured with an excitation wavelength of 485 nm and an emission wavelength of 528 nm, and the results were normalized based on OD_{600}, the experiments were carried out in triplicate. The *rpsT* promoter effectively regulated EGFP expression, while no significant EGFP levels were observed under the regulation of the *ponA1p* ($p<0.0001$, Kruskal-Wallis Test; Dunn9s multiple comparison; Figure III.41.A). This demonstrates that, in this system, only *rpsT* was capable of driving EGFP expression.

In addition, no significant differences in growth rate were observed between wild type and ΔMMAR0069 strains with the inserted promoters and EGFP ($p>0.05$, ANOVA Test - Figure III.41.B). The growth rate for Mmar was 0.0987 with a generation time of 7 hours, while for ΔMMAR0069::ponA1p-EGFP it was 0.072 with 9.6 hours, and for ΔMMAR0069::*rpsTp*-EGFP it was 0.084 with 8.3 hours.

A

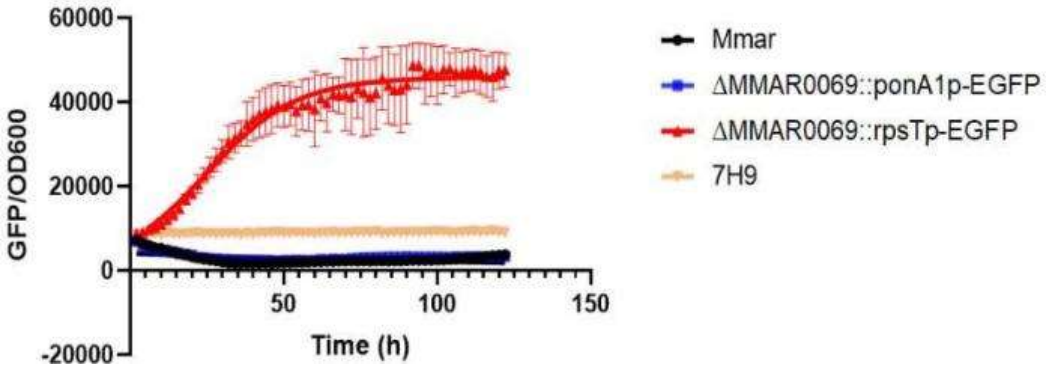

B

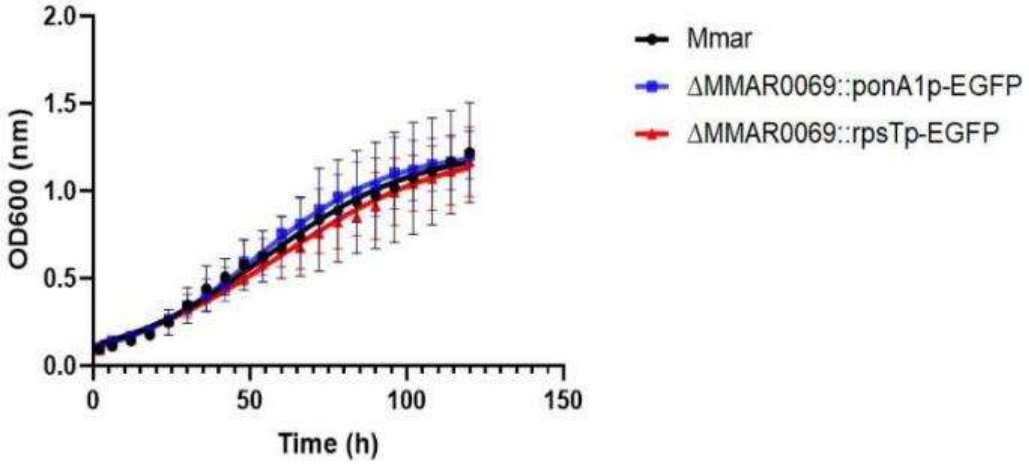

Figure III.41. Evaluation of EGFP expression and growth in *M. marinum* wild type and *M. marinum* ΔMMAR0069. A. Evaluation of EGFP expression regulated by the *ponA1p* (*M. tuberculosis* H37Rv) and *rpsTp* (*M. marinum*) promoters, quantified by fluorescence/OD_{600}. B. Growth curve analysis. Three independent experiments were performed.

III.3.7. *ponA1* gene complementation in *M. marinum*

As described in the methodology section, two approaches were developed to achieve gene complementation. The first approach was based on the results presented in section III.6.3, where the *rpsTp* successfully regulated the expression of the EGFP reporter gene. The second approach utilized the integrative plasmid pMV361, which mediates integration through the L5 site of the mycobacterial genome. The results of each stage, along with the final outcomes in obtaining strains complemented with the genes of interest (*ponA1* wild type or mutants, and *MMAR_0069*), are described below.

III.3.7.1. Payload plasmid's ORBIT modification for knockout and gene complementation in one step

A. pKM464-*rpsTp*-ponA1 plasmid construction and transformation in *E. coli*

Gene complementation with Mtb H37Rv *ponA1* was performed using a modified ORBIT plasmid under the control of the *rpsTp*, previously evaluated in this study for its capacity to regulate EGFP expression.

To do this, the pKM464-ponA1p-ponA1g plasmid was opened and a fragment of 5595 bp was amplified (Figure III.42.A), in addition the *rpsTp* was amplified obtaining a fragment of 148 bp (Figure III.42.B). Both fragments were assembled, obtaining 344 CFU positive and 37 CFU with auto circularization used as a control (Figure III.42.C). PCR colony was performed on three clones obtaining a 3213 bp fragment and verified by sequencing. Clone 3 was cryopreserved.

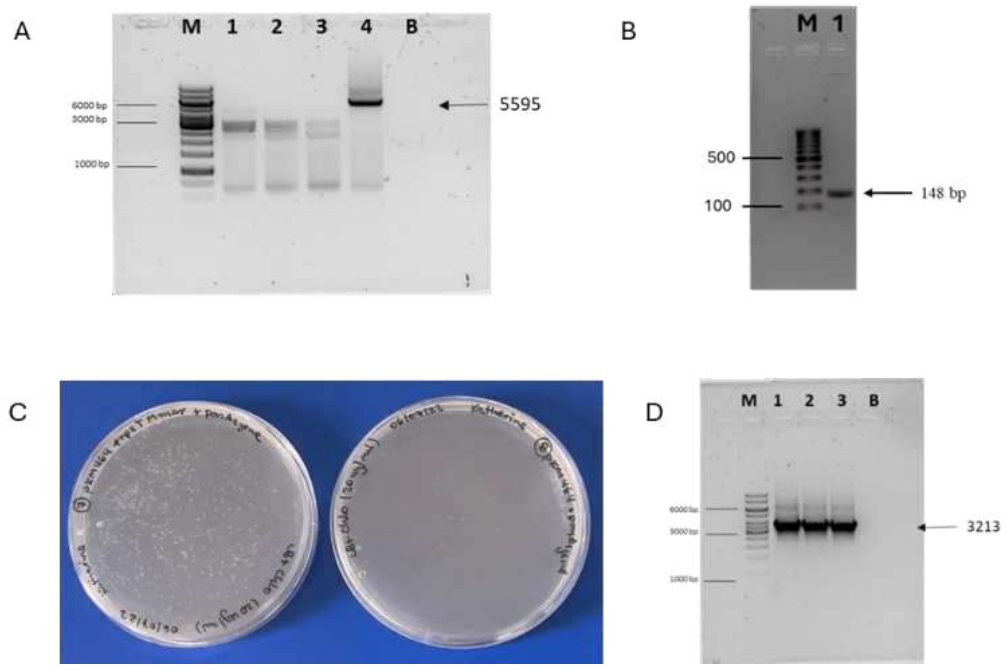

Figure III.42. Cloning of pKM464-*rpsTp*-ponA1 and transformation in *E. coli*. A. Electrophoresis in agarose gel - Temperature gradient for the amplification of pKM464-ponA1g. Line 1-4: correspond to PCR amplification at 60.9, 62.8, 65.5 and 67.7 °C, respectively. B. Electrophoresis in agarose gel of *rpsTp* PCR amplification. C. LB agar plate with Chlo (25 µg/mL) for selection of transformants with all fragments assembled (left), control of auto assembling (right). D. Electrophoresis in agarose gel of PCR colony verification. Line 1 -3: *E. coli* DH5α colonies evaluated. B Blank. M Marker 1 kb GeneRuler. Agarose electrophoresis 0.8 % TAE 1X. Chlo=chloramphenicol.

B. ORBIT with pKM464-*rpsTp*-ponA1 in *M. marinum* for *MMAR_0069* knockout and *ponA1* gene complementation in one step

Using ORBIT-mediated insertion, we aimed to create the ΔMMAR0069 mutant and simultaneously insert the Mtb H37Rv *ponA1* gene under the control of the *rpsTp*. The pKM464-*rpsTp*-ponA1 plasmid (5743 bp) mediated by the oligonucleotide resulted in 12 CFU, while 1 CFU was obtained when the oligonucleotide was not present (Figure III.43.A). PCR was performed on 6 colonies with primers F-Mmar-Rv0050-orbit and R-Mmar-Rv0050-orbit and a product of 6122 bp was obtained for all of them (Figure III.43.B). The insertion of the plasmid in the flanking region of the *MMAR_0069* gene was verified by sequencing in two clones. In addition, long-read sequencing was performed on clone two to confirm the deletion of *MMAR_0069* and insertion of *rpsTp*-ponA1 into pKM464 plasmid (Figure III.43.C), and the results were as expected. Simultaneously, through this sequencing, we verified the absence of gene duplication.

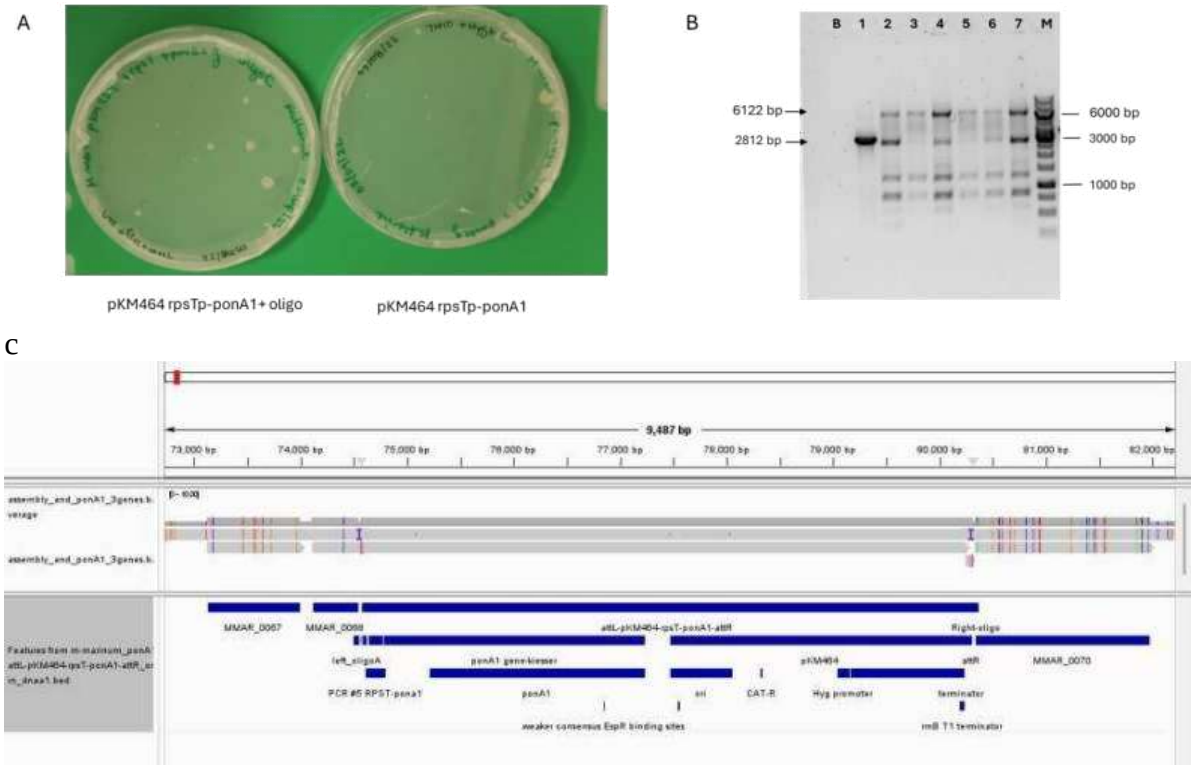

Figure III.43. ***MMAR_0069*** **knockout and** ***ponA1*** **gene insertion from** ***M. tuberculosis*** **H37Rv in the** ***M. marinum*** **genome using ORBIT in one step. A.** 7H10 plates with HYG (50 µg/mL) and KAN (20 µg/mL) for Mmar strains electroporated with pKM464-*rpsTp*-ponA1 with (left)/without (right) oligonucleotide generating the strain ΔMMAR0069::*rpsTp*-ponA1. **B.** Electrophoresis in agarose gel for PCR colony verification of ΔMMAR0069 and insertion of pKM464-*rpsTp*-ponA1. Line 1: *M. marinum* wild type. Lines 2-6: *M. marinum* transformants colonies evaluated. B Blank. M Marker 1 kb GeneRuler. Agarose electrophoresis 0.8 % TAE 1X. **C.** Long read sequencing on the clone two to confirm the ΔMMAR0069 and *rpsTp*-ponA1-containing plasmid insertion between the *MMAR_0068* and *MMAR_0070* genes. HYG= Hygromycin, KAN= Kanamycin.

III.3.7.2. *ponA1* gene complementation mediated by pMV361 integration via L5 phage site in *M. marinum*

A. pMV361- *hsp60*-ponA1 cloning and transformation in *E. coli*

The *ponA1* gene from Mtb H37Rv was cloned in the integrative plasmid pMV361 under the control of the strong promoter *hsp60,* integrated in the plasmid. *ponA1* and pMV361 were amplified, obtaining fragments of 2463 and 4446 bp, respectively (Figure III.44.A-B). Assembly was performed by GA and transformation in *E. coli* DH5α (Figure III.44.C), and PCR colony for the *ponA1* gene was evaluated for 14 samples, obtaining 4 positives, colonies 4,5,10 and 14 (Figure III.44.D). Colony 4 was verified for sequencing.

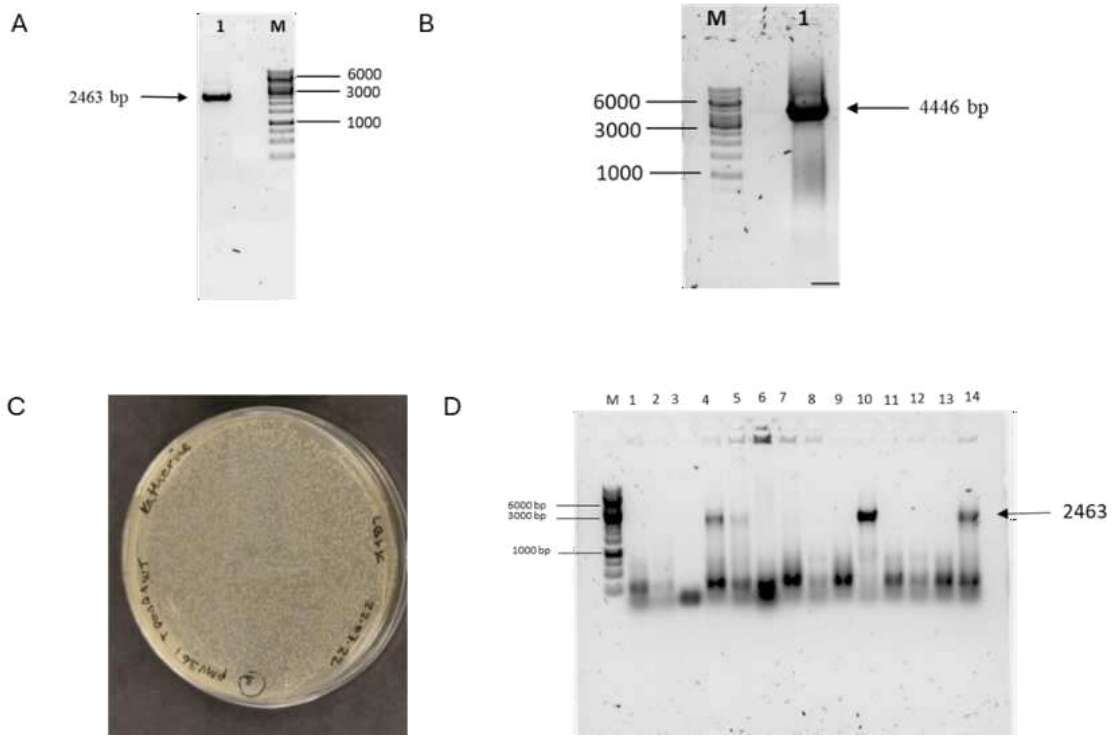

Figure III.44. Cloning of the *ponA1* gene from Mtb H37Rv in pMV361 plasmid and transformation in *E. coli*. A. Electrophoresis in agarose gel of *ponA1* gene PCR amplification. B. Electrophoresis in agarose gel of pMV361 plasmid PCR amplification. C. LB agar plate with KAN (50 µg/mL) for selection of *E. coli* DH5α with the pMV361-ponA1 ligated vía Gibson assembly. D. Electrophoresis in agarose gel of PCR colony screening. Lines 1-14 colonies evaluated. M Marker 1 kb GeneRuler. Agarose electrophoresis 0.8 % TAE 1X. KAN= Kanamycin.

B. Antibiotic cassette replacement in pMV361-ponA1

The cells carrying the ΔMMAR0069 maintained the plasmid pKM444 with a KAN resistance cassette. Therefore, the plasmid pMV361, to be incorporated in the next step, was modified by replacing its KAN cassette with a ZEO resistance marker to facilitate the selection of transformed clones.

The plasmid pMV361-ponA1 generated in the previous step was opened with the primers F-BleoR-pMV361 and R-EM7promoter-pMV361 obtaining a fragment of 5815 bp (Figure III.45.A), and the BleoR gene coding for resistance to ZEO was amplified together with the EM7 promoter with F-EM7 promotor-BleoR and R-BleoR primers obtaining a product of 628 bp (Figure III.45.B). As a result of the transformation in *E. coli* DH5α cells, 22 candidate CFU were obtained (Figure III.45.C) and 11 colonies were evaluated by PCR colony to verify the insertion of the BleoR gene. Clone 1 was sequenced with the correct sequence inserted in pMV361.

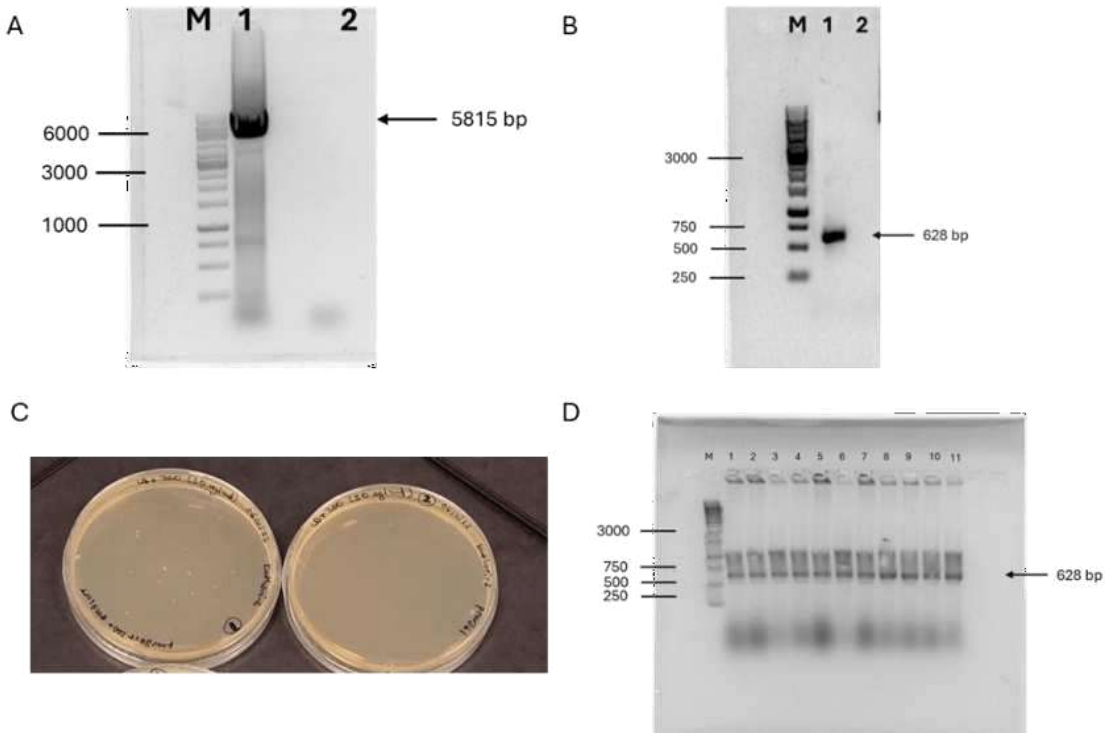

Figure III.45. Zeocyn resistance cassette cloned in pMV361-ponA1. A. Electrophoresis in agarose gel for PCR amplification of pMV361-ponA1 plasmid without kanamycin cassette. B. Electrophoresis in agarose gel for BleoR gene PCR product. C. LB agar plate with ZEO (50 µg/mL) for selection of *E. coli* DH5α transformed with plasmid closed (left) and only plasmid opened (right). D. Electrophoresis in agarose gel for *E. coli* DH5α colonies screening. Line 1-11: *E. coli* DH5α colonies verification for BleoR gene insertion in plasmid. M Marker 1 kb GeneRuler. Agarose electrophoresis 0.8 % TAE 1X. ZEO= Zeocyn.

C. pMV361zeo -ponA1 electroporation in *M. marinum*

The Mmar ΔMMAR0069 was electroporated with pMV361$_{ZEO}$-ponA1 plasmid; after 10 days the cells grew, obtaining a transformation efficiency of 8.6x10^3 CFU/µg. This contrasts with the results obtained from the one-step complementation described in Section III.3.7.1.B, where the efficiency was low but yielded similar outcomes.

At this point, the cells present two plasmids inserted in their genome and their location would be as follows: the plasmid pKM464-*rpsTp*-EGFP is located at position 68 582 - 72540 bp (Figure III.46.A), between genes *MMAR_0068* and *MMAR_0070*. The plasmid pMV361$_{ZEO}$-ponA1 is located between genes *MMAR_3809* and *MMAR_3010* as shown in Figure III.46.B.

Therefore, colonies were isolated, inactivated, and genome integration was verified by PCR colony screening. Eight colonies were confirmed to harbor the pMV361$_{ZEO}$-ponA1 plasmid in their genome through sequencing. For PCR, the pMV361$_{ZEO}$-ponA1 plasmid was used as a positive control, while Mmar wild-type genomic DNA served as a negative control. Colony six was further verified by sanger sequencing. Additionally, long-read sequencing was performed on clone two to confirm the *MMAR_0069* gene deletion and the insertion of the pMV361-ponA1-containing plasmid between the *MMAR_0068* and *MMAR_0070* genes, and between *MMAR_3809* and *MMAR_3010*, respectively. Simultaneously, this sequencing verified the absence of gene duplication (Figure III.46.E).

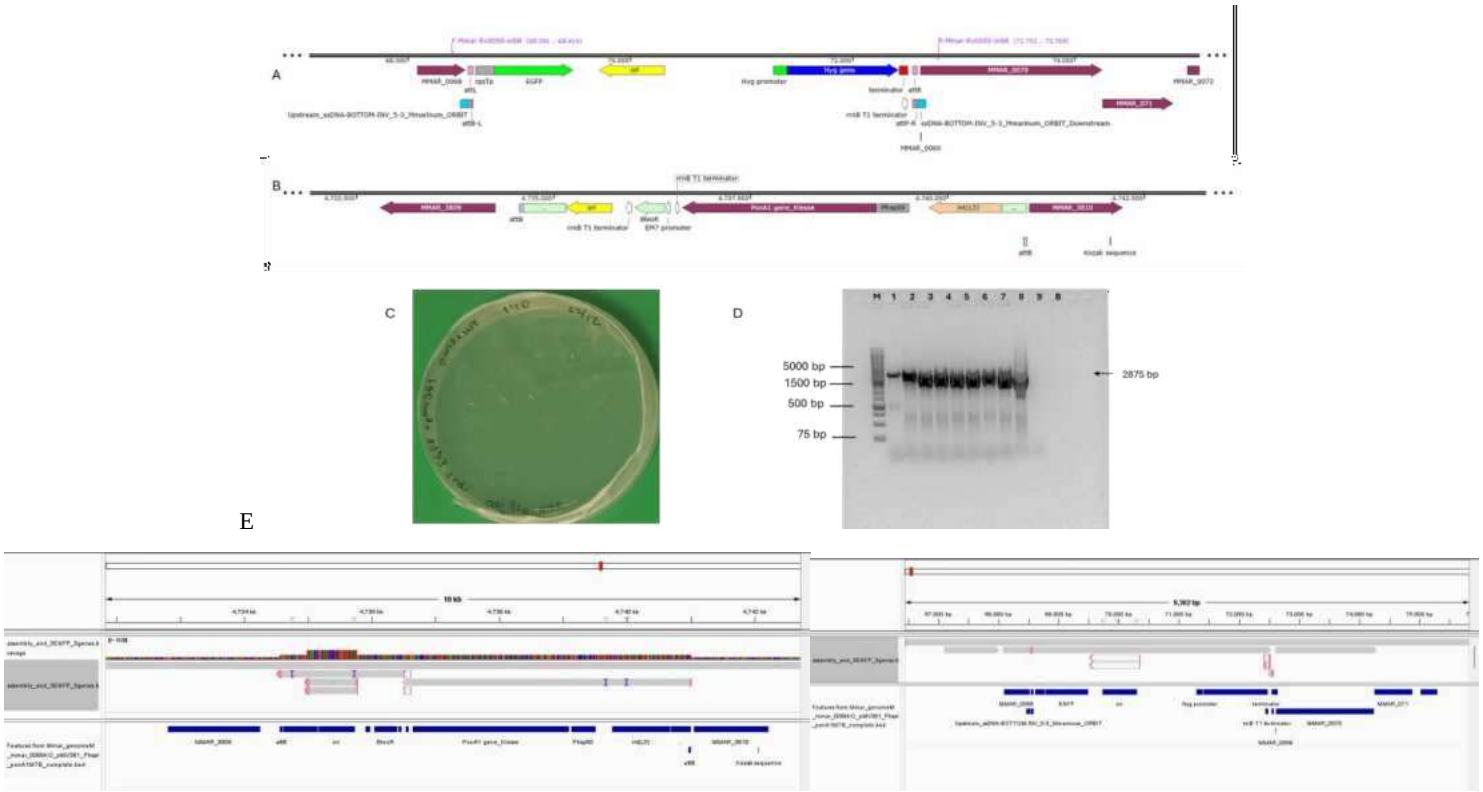

Figure III.46. *ponA1* gene complementation in *M. marinum* ΔMMAR0069 mediated by L5-site integration. Scheme of two plasmid insertions for the strain generation. A. pKM464-*rpsTp*-EGFP integrated in *MMAR_0069* locus. B. pMV361$_{zeo}$-ponA1 integrated between genes *MMAR_3809* and *MMAR_3010*. C. 7H10 agar plate with HYG (50 µg/mL) and ZEO (30 µg/mL) for selection of *M. marinum.* ΔMMAR0069::*rpsTp*-EGFP::L5-ponA1. D. Electrophoresis in agarose gel for PCR colony verification of pMV361$_{zeo}$-ponA1 plasmid integration. Line 1-pMV361zeo-ponA1 plasmid, Line 2-8, colonies evaluated. Line 9- Mmar wild type. B Blank.

III.3.7.3. Cloning of *ponA1* mutants in pMV361$_{ZEO}$ in *E. coli*

Point mutations for *ponA1* (T34A, T34D, Q365H, A516T, P631S) were introduced using primers carrying the specific mutations via GA, as described in the methodology section (Table III.2). The plasmid pKM464-*rpsTp-ponA1* was used as the template, and the results are detailed below.

A. Site mutagenesis directed for *ponA1* T34A

Two PCR fragments with 3392 and 2391 bp were generated to introduce the T34A mutation in *ponA1* gene (Figure III.47.A). $3x10^4$ CFU transformants of *E. coli* DH5α grown and screening of 7 colonies were performed (Figure III.47.B-C). Verification with primers F-pKM464-int and R_pKM464-int showed that 4 out of 7 colonies had the expected 3213 bp PCR product, whose amplification includes the *rpsTp* and the *ponA1* T34A (Figure III.47.C). Colony number one was corroborated to harbor the T34A mutation in *ponA1* by sequencing.

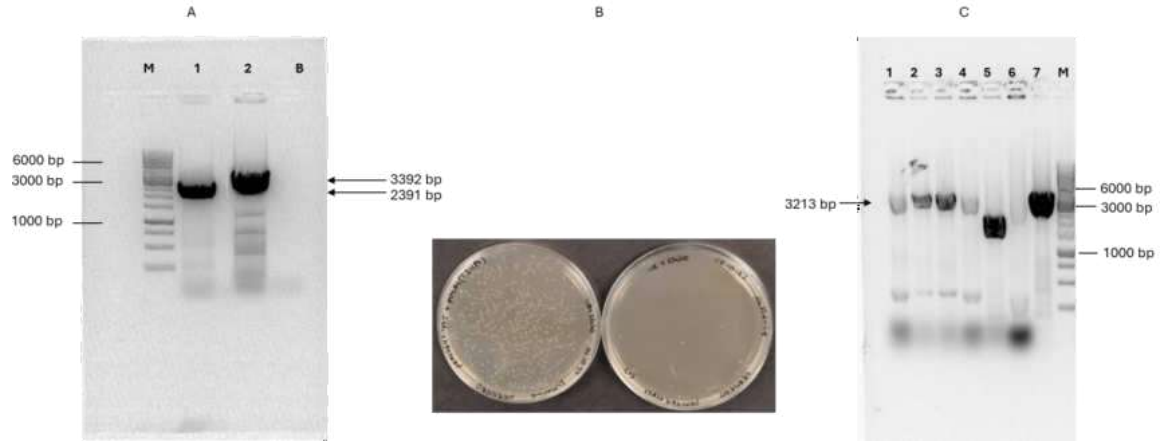

Figure III.47. Site directed mutagenesis for generation of *ponA1* T34A via Gibson assembly in the pKM464-ponA1 plasmid and transformation in *E. coli*. A. Electrophoresis in agarose gel for two PCR fragments that introduce the T34A mutation in *ponA1* gene. Line 1 PCR fragment with primers F-T34-ponA1 and R-H37Rv_ponA1_promoter. Line 2 PCR fragment with primers R-T34A-ponA1 and F_pKM464-ponA1. B Blank, B. LB agar plate with Chlo (25 µg/mL) for selection of *E. coli* DH5α transformants with two fragments assembled (left) and one fragment auto assembled (right) used as a control. C. PCR colony for selection of *E. coli* recombinant colonies Lines 1-7. M Marker 1 Kb plus. Agarose electrophoresis 0.8 % TAE 1X. Chlo= chloramphenicol.

B. Site mutagenesis directed for *ponA1* T34D

Similar to the generation of the T34A mutation in *ponA1*, the T34D mutation was generated, with fragments of 3392 and 2391 bp (Figure III.48.A). $6x10^4$ CFU transformants of *E. coli* NEB Turbo grown, and a screening of 6 colonies was performed, getting all the colonies with the PCR product expected (3213 bp) (Figure III.48.B-C). Colony number nine was verified by sequencing.

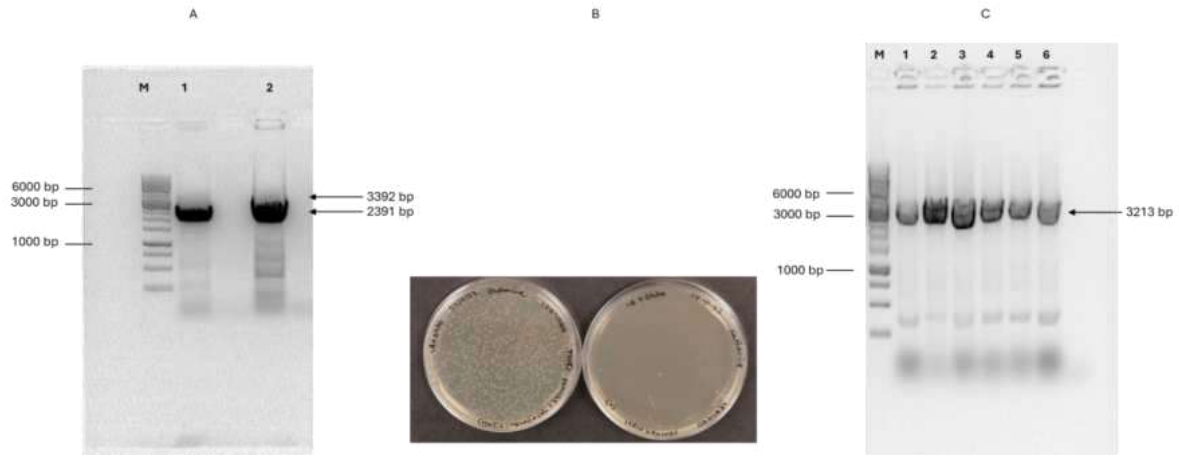

Figure III.48. Site directed mutagenesis for generation of *ponA1* T34D via Gibson assembly in the pKM464-ponA1 plasmid and transformation in *E. coli*. A. Electrophoresis in agarose gel for two PCR fragments that harbor T34D mutation. Line 1: PCR fragments with primers F-T34-ponA1 and R-H37Rv_ponA1_promoter. Line 2: PCR fragment with primers R-T34D-ponA1 and F_pKM464-ponA1. B. LB agar plate with Chlo (25 µg/mL) for selection of *E. coli* NEB turbo transformants with two fragments (left) and one fragment (right) assembled. C. PCR colony for selection of *E. coli* recombinant strains. Verification with primers F-pKM464-int and R_pKM464-int. Marker 1 Kb plus. Agarose electrophoresis 0.8 % TAE 1X. Chlo= chloramphenicol.

C. Site mutagenesis directed for *ponA1* Q365H

Two fragments of 4074 and 1709 bp were amplified to introduce the Q365H mutation (Figure III.49.A), which were assembled by GA and transformed in *E. coli* DH5α competent cells (Figure III.49.B). $4.2x10^4$ CFU transformants were obtained and six colonies were selected for the screening, PCR colony with F-pKM464-int and R-pKM464-int primers was performed, obtaining a 3213 bp fragment indicating the presence of the complete *ponA1* gene (Figure III.49.C). Clones 2 and 4 were verified for sequencing with primers F-H37Rv-ponA1-gen-2-2360, R-H37Rv-ponA1-gen-2687, F-H37Rv-PonA1-gen-3-3460, R_pKM464-int and F-pKM464-int.

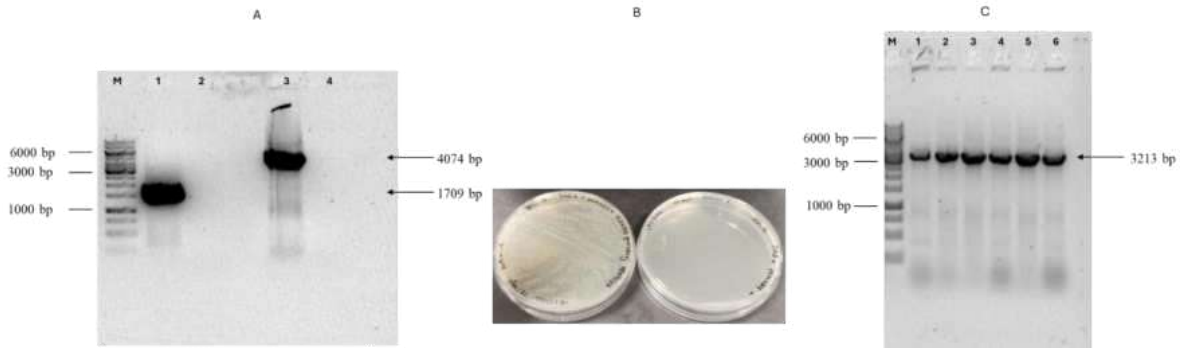

Figure III.49. Site directed mutagenesis for generation of *ponA1* Q365H via Gibson assembly in the pKM464-ponA1 plasmid and transformation in *E. coli*. A. Electrophoresis in agarose gel for PCR fragments Line 1 PCR fragment with primers F-H37Rv_ponA1_promoter and R-Q365H-ponA1. Line 3 PCR fragment with primers F-Q365H-ponA1 and R_pKM464-ponA1. Line 2 and 4 are blank for each reaction, respectively. **B**. LB agar plate with Chlo (25 µg/mL) for selection of *E. coli* transformants with two fragments (left) and one fragment (right) assembled. **C.** Electrophoresis in agarose gel of PCR colony for selection of *E. coli* recombinant strains. Line 1-6. Clones screening. Primers F-pKM464-int and R-pKM464-int were used for amplification. Marker 1 Kb plus. Agarose electrophoresis 0.8 % TAE 1X. Chlo= chloramphenicol.

D. Site mutagenesis directed for *ponA1* A516T

Two fragments of 3581 bp and 2162 bp were amplified to introduce the A516T mutation in the *ponA1*. Fifty CFU transformants were obtained when both fragments were successfully assembled, whereas no growth was observed in the negative control used to evaluate fragment recircularization (Figure III.50.A and B). Eleven colonies were evaluated, and nine displayed the desired 3213 bp amplification product (Figure III.50.C). Clones 4 and 6 were confirmed by sequencing.

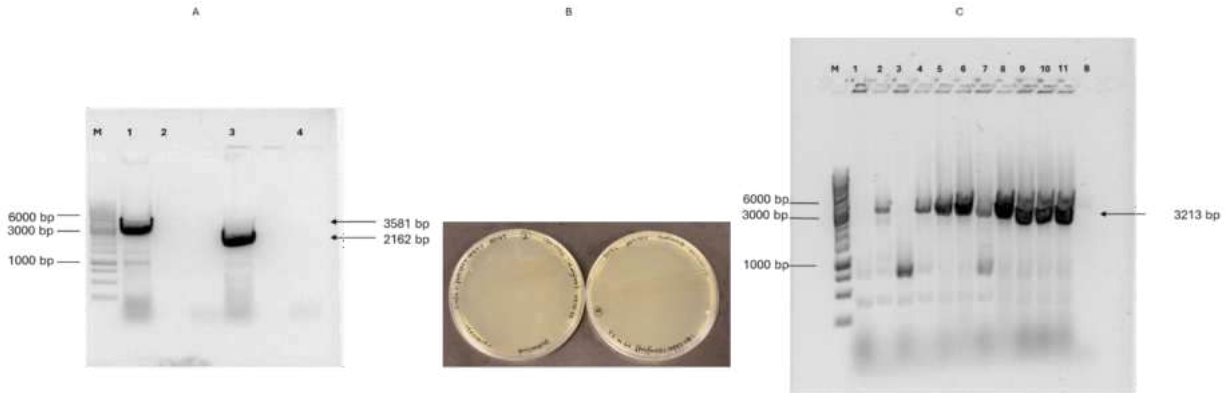

Figure III.50. Site directed mutagenesis for generation of *ponA1* A516T via Gibson assembly in the pKM464-ponA1 plasmid and transformation in *E. coli*. A. Electrophoresis in agarose gel for PCR fragments. Line 1 PCR fragment with primers F-A516T-ponA1 and R_pKM464-ponA1. Line 3 PCR fragment with primers F-H37Rv_ponA1_promoter and R-A516T-ponA1. Lines 2-4 are blank for each reaction, respectively. B. LB agar plate with Chlo (25 µg/mL) for selection of *E. coli* transformants with two fragments (left) and one fragment (right) assembled. C. PCR colony for selection of *E. coli* recombinant strains. Line 1-11. Clones screening. Verification with primers F-pKM464-int and R-pKM464-int. Marker 1 Kb plus. Agarose electrophoresis 0.8 % TAE 1X. Chlo= chloramphenicol.

E. Site mutagenesis directed for *ponA1* P631S

Two fragments were amplified for the generation of the P631S mutation in the *ponA1*, with sizes of 3276 and 2507 bp (Figure III.51.A). Both were purified by gel extraction and assembled by GA (Figure III.51.B). Seven out of eight colonies were PCR-positive, and colony one was further verified by sequencing.

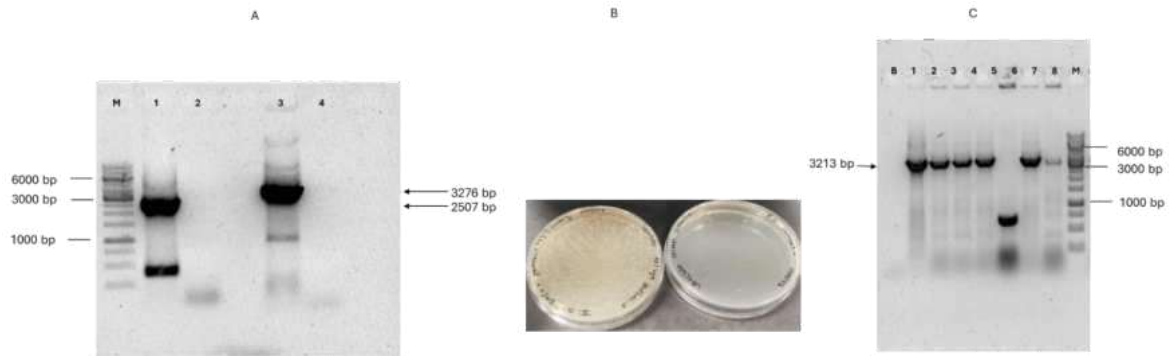

Figure III.51. Site directed mutagenesis for generation of *ponA1* P631S via Gibson assembly in the pKM464-ponA1 plasmid and transformation in *E. coli*. A. Electrophoresis in agarose gel for PCR fragments. Line 1 PCR fragment with primers F-H37Rv_ponA1_promoter and R-P631S-ponA1. Line 3 PCR fragment with primers F-P630-P631-ponA1 and R_pKM464-ponA1. Lines 2-4 are blank for each reaction, respectively. B. LB agar plate with Chlo (25 µg/mL) for selection of *E. coli* transformants with two fragments (left) and one fragment (right) assembled. C. Electrophoresis in agarose gel for PCR colony selection of *E. coli* recombinant strains. Line 1-8. Colonies screening. Verification with primers F-pKM464-int and R-pKM464-int. M Marker 1 Kb plus. Agarose electrophoresis 0.8 % TAE 1X. Chlo= chloramphenicol.

F. *ponA1* mutants amplification for subcloning in pMV361$_{ZEO}$ and transformation

For the *ponA1* gene complementation process in Mmar ΔMMAR0069, and to assess mutations in this gene, we subcloned the wild type and mutant *ponA1* genes from plasmid pKM464 to pMV361$_{ZEO}$, an integrative mycobacterial vector.

ponA1 genes with the punctual mutations were amplified with primers F-pMV361-ponA1-H37Rv and R-pMV361-ponA1-H37Rv and a fragment of 2504 bp was obtained (Figure III.52.A-B), all these fragments were purified by gel extraction and cloned in pMV361$_{ZEO}$ (4446 bp) (Figure III.52.B) by GA. *E. coli* transformants for all *ponA1* mutants are shown in Figure III.52.C. Colonies were evaluated to harbor the

ponA1 gene (2463 bp) and different colonies were verified to harbor the *ponA1* mutation desired. Colony one and two were verified for ponA1-Q365H and T34D, colony two for T34A, A516T and P631S (Figure III.53).

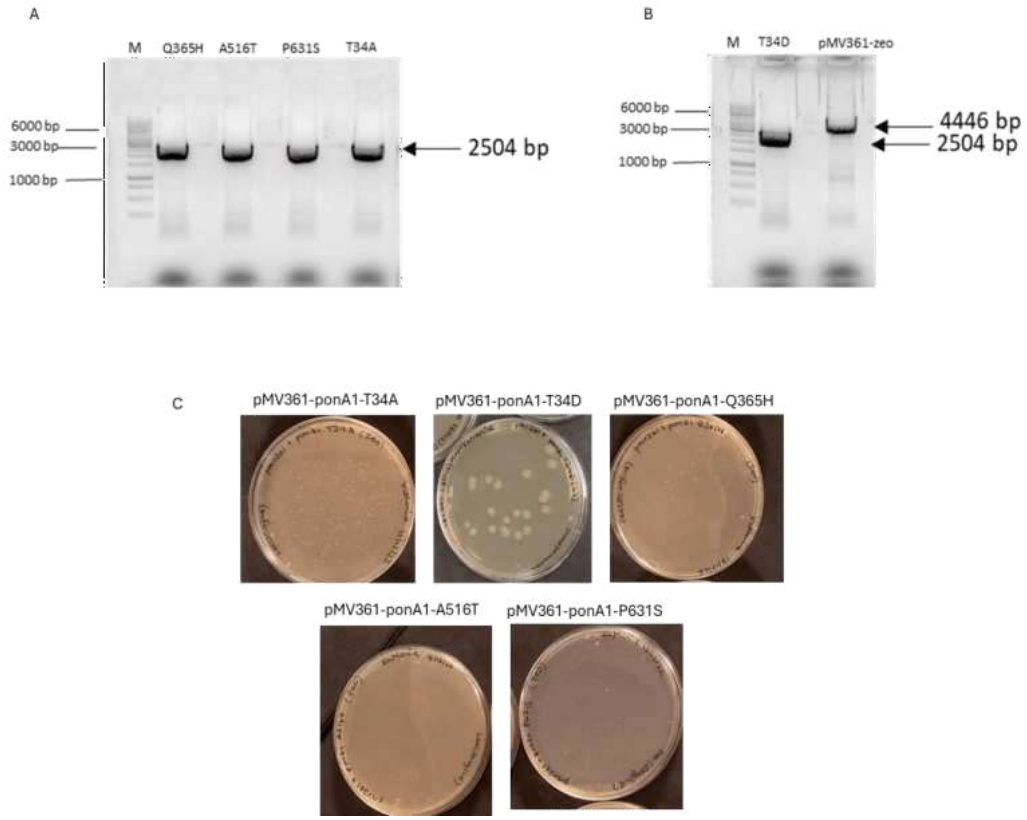

Figure III.52. Subcloning of *ponA1* mutant genes from *M. tuberculosis* H37Rv in pMV361$_{ZEO}$ transformed in *E. coli*. A. Electrophoresis in agarose gel for PCR amplification with *ponA1* mutants Q365H, A516T, P631S, T34A. B. Electrophoresis in agarose gel for *ponA1* T34D gene and pMV361$_{ZEO}$ plasmid amplification. C. LB agar plate with ZEO (50 µg/mL) for selection of *E. coli* transformants harboring plasmid pMV361$_{ZEO}$-ponA1 mutants. M Marker 1 Kb plus. Agarose electrophoresis 0.8 % TAE 1X. ZEO =Zeocin.

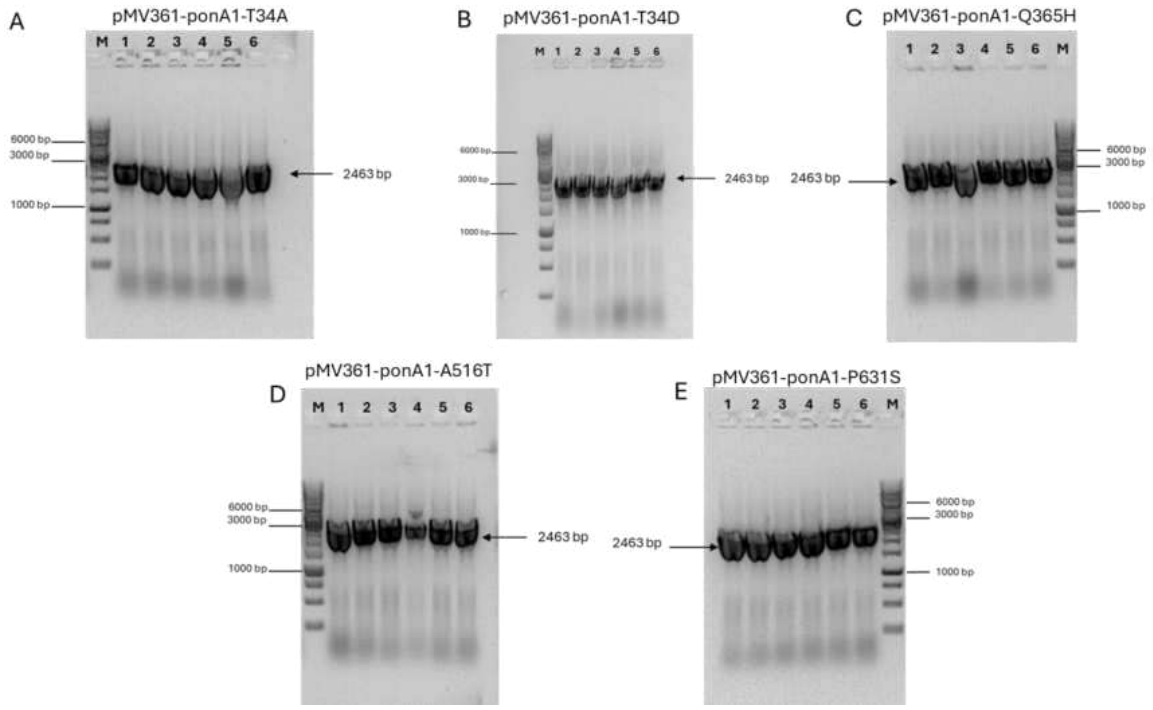

Figure III.53. PCR colony for selection of *E. coli* transformants harboring *ponA1* mutants cloned in pMV361$_{ZEO}$. Electrophoresis in agarose gel for amplification of A. pMV361$_{ZEO}$- ponA1-T34A. B.pMV361$_{ZEO}$- ponA1-T34D. C. pMV361$_{ZEO}$- ponA1-Q365H. D. pMV361$_{ZEO}$- ponA1-A516T. E. pMV361$_{ZEO}$- ponA1-P631S. M Marker 1 Kb plus. Agarose electrophoresis 0.8 % TAE 1X.

III.3.7.4. *MMAR_0069* cloning in pMV361

A. Cloning of *MMAR_0069* in pKM464 under *rpsTp* regulation and transformation in *E. coli*

MMAR_0069 gene was amplified from the gDNA of Mmar strain M obtaining a fragment of 2538 bp (Figure III.54.A) and was cloned in the plasmid pKM464-*rpsTp* (Figure III.54.B). GA was performed and *E. coli* transformants were obtained (Figure III.54.C). Twelve colonies were evaluated using F-MrcB-Mmar and R-MrcB-Mmar

primers, and a PCR fragment of 2528 bp was obtained in all colonies (Figure III.54.D). Clones 7 and 8 were confirmed by sequencing.

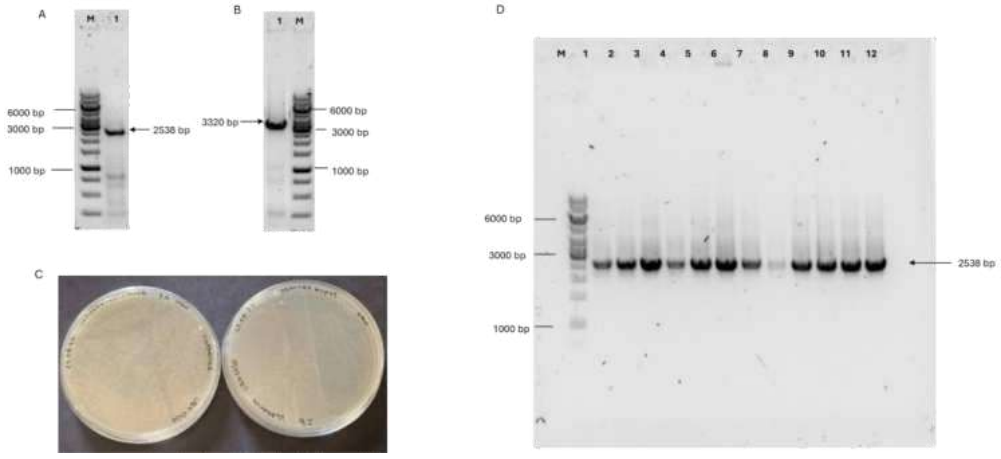

Figure III.54. *MMAR_0069* gene cloned in pKM464 plasmid and transformed in *E. coli*. A. Electrophoresis in agarose gel for *MMAR_0069* gene. B. Electrophoresis in agarose gel for pKM464-*rpsTp* plasmid. C. LB agar plate with Chlo (25 µg/mL) for selection of *E. coli* transformants with two fragments (left) and one fragment (right) assembled. D. Electrophoresis in agarose gel for PCR colony selection of recombinant strains. Line 1-12. Clones screening. M Marker 1 Kb plus. Agarose electrophoresis 0.8 % TAE 1X.

B. pMV361-MMAR0069 subcloning and transformation in *E. coli*

To generate the isogenic wild type, the *MMAR_0069* gene was subcloned in the plasmid pMV361$_{ZEO}$, from the plasmid pKM464-MMAR0069, obtaining a fragment of 2538 bp. The fragments were assembled by GA and the transformation was carried out in competent *E. coli* DH5α cells, few colonies grew in the plate, they were verified by PCR, from 7 colonies evaluated 5 had the expected product of 2875 bp (Figure III.55).

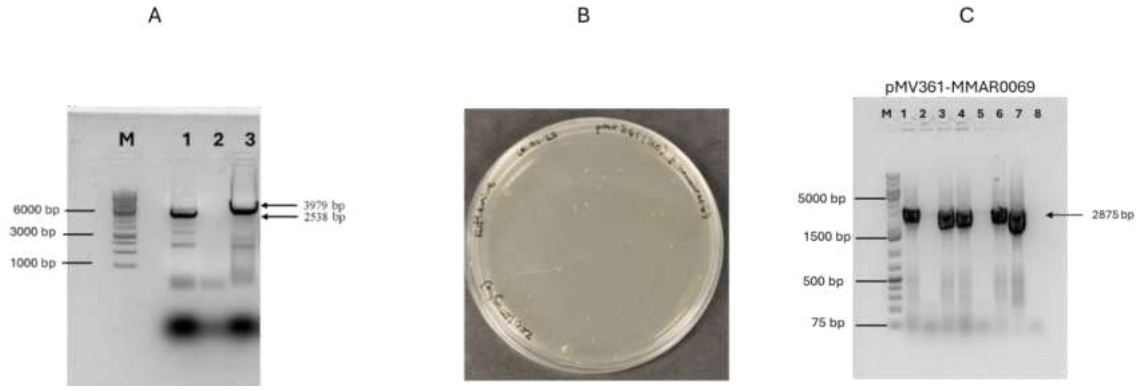

Figure III.55. *MMAR_0069* gene from *M. marinum* subcloning in pMV361$_{ZEO}$ and transformation in *E. coli*. A. Electrophoresis in agarose gel for PCR fragments. Line 1 *MMAR_0069* gene PCR fragment. Line 2 blank, Line 3 pMV361zeo plasmid PCR fragment. B. LB agar plate with ZEO (50 µg/mL) for selection of *E. coli* transformants with two fragments (left) assembled. C. Electrophoresis in agarose gel for PCR colony selection of recombinant strains. Line 1-7. Colonies screening. Line 8 blank. Agarose electrophoresis 0.8 % TAE 1X. ZEO=Zeocin.

C. *ponA1*-mutants gene complementation using pMV361$_{ZEO}$ plasmid in *M. marinum*

Cells with ΔMMAR0069 were complemented with *ponA1* genes containing the mutations under study, being inserted between the *MMAR_3809* and *MMAR_3810* genes, using the *attP* L5 site. Transformation efficiency was $3.5x10^3$, $3.9x10^3$, $6.3x10^3$, $5.1x10^3$, $5.6x10^3$, $6.6x10^3$ CFU/µg of pMV361$_{ZEO}$-ponA1 for each strain harboring the T34A, T34D, Q365H, A516T, P631S, *ponA1's* mutation, and *MMAR_0069* complementation (Figure III.56.A), respectively. PCR colony was performed with Verif_Gg_PMV_Fw and Verif_GgPMV_Rv primers, for all constructs generated. A fragment size of 2875 bp was expected for *ponA1* mutants and 2950 bp for *MMAR_0069* gene complementation (Figure III.56.B). For the strains ΔMMAR0069::L5-ponA1-T34A, ΔMMAR0069::L5-ponA1-Q365H,

ΔMMAR0069::L5-ponA1-A516T, and ΔMMAR0069::L5-ponA1-P631S, clone one was verified by sequencing. For the ΔMMAR0069::L5-ponA1-T34D strains, sequencing of clones one and six confirmed the correct insertion. Finally, for the ΔMMAR0069::L5-MMAR0069 strain (isogenic wild type), clone two was verified for the insertion.

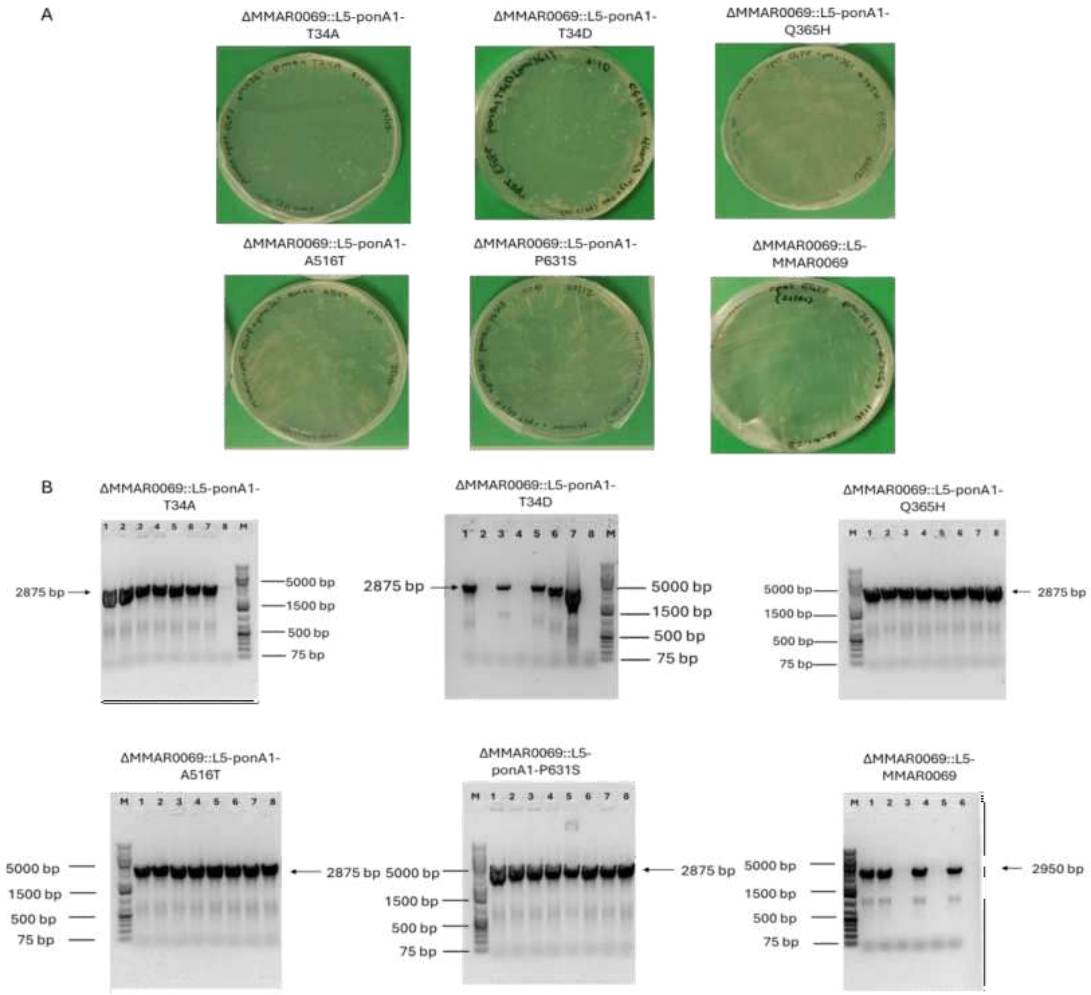

Figure III.56. *ponA1*'s wild type and mutants from *M. tuberculosis* integrated in *M. marinum* ΔMMAR0069 genome via L5-mycobacteriphage site. A. 7H10 agar plate with ZEO (50 µg/mL) and HYG (50 µg/mL) with *M. marinum* transformants harboring *ponA1* mutations integrated via L5-site. B. Electrophoresis in agarose gel for PCR colony verification of pMV361$_{ZEO}$-gene insertion in *M. marinum* ΔMMAR0069 genome.

III.3.8. Drugs susceptibility test by TEMA

The MIC for RIF was evaluated for all strains: ΔMMAR0069, the strain complemented with *ponA1* under the control of the *rpsTp* in a single step using the modified ORBIT system (ΔMMAR0069::*rpsTp*-ponA1), and those complemented in two steps via the integrative plasmid pMV361$_{ZEO}$, mediated by the L5 site. This group includes the isogenic wild-type strain (ΔMMAR0069::L5-MMAR0069), as well as the *ponA1* wild-type and mutant strains (ΔMMAR0069::L5-ponA1).

The Mmar wild-type strain had an MIC of 2 µg/mL, while the ΔMMAR0069 strains generated in this study using ORBIT4either ΔMMAR0069::*rpsTp*-EGFP or ΔMMAR0069::ponA1p-EGFP4exhibited increased sensitivity to RIF, with MICs of 1 µg/mL and 0.5 µg/mL, respectively. This suggests that the absence of the *MMAR_0069* gene in the Mmar genome increases the strains' susceptibility to RIF.

On the other hand, both the Mmar wild-type strain and the isogenic wild-type strain exhibited an MIC of 2 µg/mL, restoring their RIF resistance phenotype. The same MIC of 2 µg/mL was observed in strains complemented with Mtb H37Rv *ponA1*, whether in its wild-type form or with mutations. This suggests that the complementation technique using the Mmar gene under the regulation of the *hsp60* promoter was effective in restoring RIF resistance. Furthermore, these results indicate that the *ponA1* gene from Mtb H37Rv is capable of complementing and restoring the RIF resistance profile in the absence of *MMAR_0069* in Mmar. Moreover, the *ponA1* mutations evaluated here, T34A, T34D, Q365H, A516T and P631S, did not alter the RIF susceptibility profile, as assessed using this technique.

Notably, the strains complemented with *ponA1* inserted via the ORBIT plasmid under regulation of *rpsTp* (ΔMMAR0069::*rpsTp*-ponA1) exhibited an MIC of 0.5 µg/mL, which failed to restore the RIF resistance profile compared to the wild-type strain, instead increasing susceptibility to RIF by 4-fold and 2-fold relative to the ΔMMAR0069 strain (Figure III.57). This could indicate that the *rpsTp* was not sufficiently strong to drive adequate *ponA1* expression, or that the regulatory mechanism under this promoter was insufficient to restore the RIF resistance phenotype. Further characterization of this promoter is recommended to better understand its regulatory capacity in this context, or other promoters can be evaluated using this system.

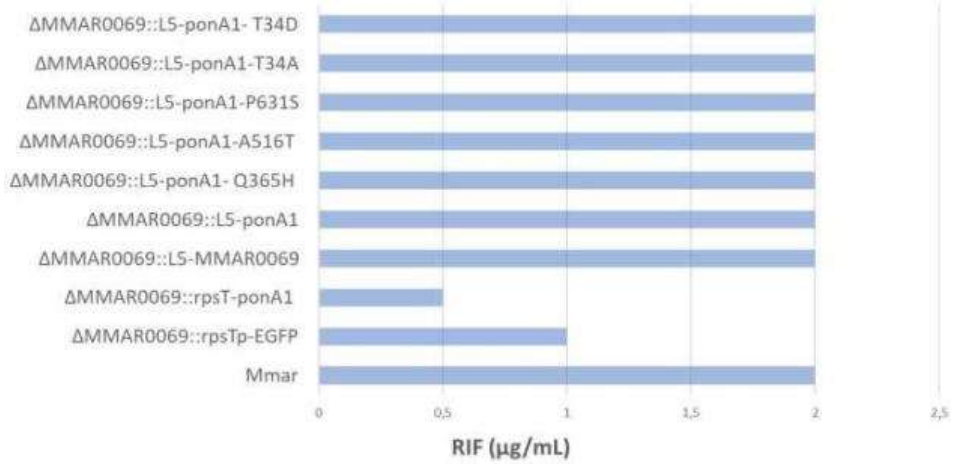

Figure III.57. Drug susceptibility test to determine the minimum inhibitory concentration of rifampicin for *M. marinum* strains generated in this study and *M. marinum* wild type strain M. Three independent MIC measures were performed for each strain. ΔMMAR0069 = knockout in the gene *MMAR_0069* ΔMMAR0069::L5-ponA1= knockout in the gene *MMAR_0069* and complemented with *ponA1* gene wild type or mutant under regulation of *hsp60*. . ΔMMAR0069::L5-MMAR0069= knockout in the gene *MMAR_0069* and complemented with *MMAR_0069* under regulation of *hsp60*, ΔMMAR0069::*rpsTp*-ponA1= knockout in the gene *MMAR_0069* and complemented with *ponA1* gene wild type under regulation of *rpsT* promoter from *M.marinum.*

III.3.9. Morphology by light microscopy

Based on the primary function of PonA1 in PG synthesis and regulation, this study evaluated the effects of *MMAR_0069* deletion and its complementation with wild-type *ponA1* from Mtb H37Rv, along with the mutants evaluated in this study.

To evaluate the cell-length, several fields were captured where the cells were isolated with a magnification of 600X (as shown in Figure III.58). One hundred measurements per strain were recorded.

The cell-length of the ΔMMAR0069 was 2.807 ± 0.657 µm, showing an increase of 7.3% compared to wild type strain ($p = 0.0497$-Figure III.59.A). Among the strains complemented with *ponA1*, the one regulated by the *rpsTp* had a mean length of 2.676 ± 0.52 µm ($p=0.3417$ compared to isogenic wild type), while the one regulated under the *hsp60* had a mean of 3.284 ± 0.792 µm, marking a 17.8 % increase in mean length ($p<0.0001$). In this assay, the presence of *ponA1* from *Mtb* H37Rv significantly increased cell size in Mmar, with this enlargement consistently observed in strains carrying the Q365H ($p = 0.0027$), A516T ($p < 0.0001$), and T34D ($p < 0.0001$) mutations, representing increases of 14%, 17.7%, and 26.5%, respectively, compared to the isogenic wild-type strain.

Among strains harboring the *ponA1* gene, significant differences were observed between the wild-type strain and those carrying the P631S ($p < 0.0001$), T34A ($p < 0.0001$), and T34D ($p = 0.0189$) mutations. The P631S and T34A mutations resulted in size reductions of 19.46% and 15.56%, respectively, while the T34D mutation

caused a 7.4% increase in size. These differences in length were determined using the Mann-Whitney test (Table III.5, Figure III.59.B).

The mean cell width of Δ*MMAR0069* was 0.4873 ± 0.1126 µm, showing a reduction of 14% compared to the wild type strain ($p<0.0001$, T-test and Welch correction). Among the strains complemented with *ponA1*, the one regulated by the *rpsTp* had a mean width of 0.5130 ± 0.1016 µm ($p=0.0017$, T-test and Welch correction, compared to isogenic wild type), marking a 9.7 % increase in mean width. No significant variations were found between isogenic wild type and the Δ*MMAR0069* complemented with *ponA1* from Mtb H37Rv ($p=0.3127$, Mann-Whitney test -Figure III.59.C). Significant differences were observed when *ponA1* presented the Q365H ($p = 0.0280$, t-test with Welch's correction), A516T ($p < 0.00019$, Mann-Whitney test), P631S ($p = 0.0144$, t-test with Welch's correction), and T34A ($p < 0.0001$, t-test with Welch's correction) mutations, resulting in a 6.18% reduction and increases of 26.24%, 7.3%, and 16.9%, respectively, compared to the isogenic wild-type strain.

Among strains harboring the *ponA1* gene, the wild-type strain significantly differed from those carrying the A516T ($p < 0.0001$), P631S ($p = 0.0002$), T34A ($p < 0.0001$), and T34D ($p = 0.0264$) mutations, with observed increases in cell width of 30%, 10.5%, 20.4%, and 6.47%, respectively (Mann-Whitney test was used to compare each mutated strain with the *ponA1* wild-type strain, Table III.6, Figure III.59.D). In contrast, no significant differences were found for the Q365H mutation ($p = 0.3168$, Mann-Whitney test).

Based on these results, it is important to highlight that the deletion of the *ponA1* homolog in Mmar, the *MMAR_0069* gene, has a significant impact on the regulation

of both cell length and width. These changes were also observed when the *MMAR_0069* KO strain was complemented with *ponA1* from Mtb H37Rv, showing notable alterations in cell length. The magnitude of these changes varied depending on the specific *ponA1* mutation integrated into the Mmar genome.

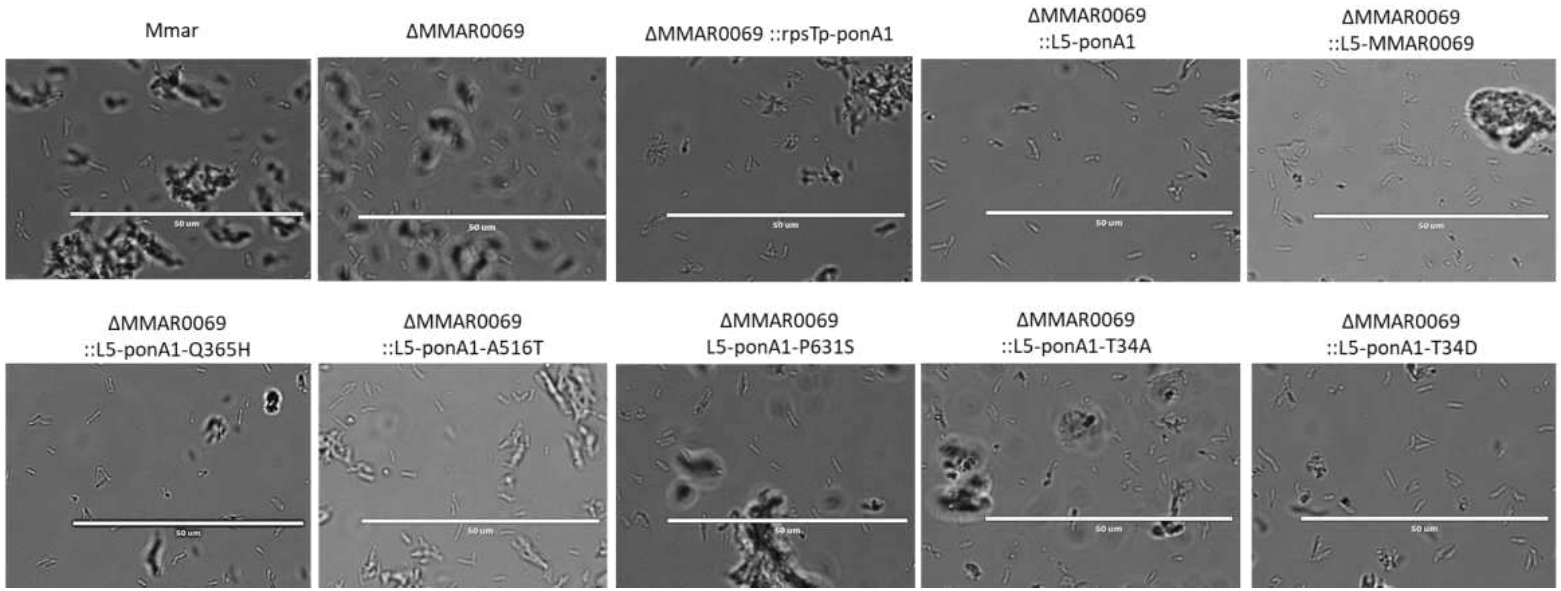

Figure III.58. *M. marinum* strains generated in this study and *M. marinum* wild type strain M, morphology evaluated by light microscopy with polysine fixation (600X magnification). ΔMMAR0069 = knockout in the gene *MMAR_0069* . ΔMMAR0069::L5-ponA1= knockout in the gene *MMAR_0069* and complemented with *ponA1* gene wild type or mutant under regulation of *hsp60*. ΔMMAR0069::L5-MMAR0069= knockout in the gen *MMAR_0069* and complemented with *MMAR_0069* under regulation of *hsp60* promoter, ΔMMAR0069::*rpsTp*-ponA1= knockout in the gene *MMAR_006*9 and complemented with *ponA1* gene wild type under regulation of *rpsT* promoter from *M.marinum.*

Table III.5. Length measurements of wild type, *MMAR_0069* knockout strain, and gene complemented with *ponA1* from *M. tuberculosis* H37Rv wild type and mutants integrated in *M. marinum* genome.

	Mmar	ΔMMAR0069	ΔMMAR0069:: rpsTp-ponA1	ΔMMAR0069 ::L5-MMAR0069	ΔMMAR0069::L5-ponA1	ΔMMAR0069:: L5-ponA1-Q365H	ΔMMAR0069 :: L5-ponA1-A516T	ΔMMAR0069: : L5-ponA1-P631S	ΔMMAR0069 :: L5-ponA1-T34A	ΔMMAR0069: : L5-ponA1-T34D
Number of values	100	100	100	100	100	100	100	100	100	100
Minimum	1,523	1,608	1,669	1,493	1,824	1,669	1,846	1,440	1,549	1,931
Median	2,589	2,685	2,639	2,690	3,172	3,120	3,243	2,615	2,669	3,451
Maximum	3,979	4,340	5,024	5,239	5,617	5,696	6,426	4,100	4,440	5,570
Mean	2,616	2,807	2,676	2,787	3,284	3,177	3,281	2,645	2,773	3,526
Std. Deviation	0,506	0,657	0,52	0,709	0,792	0,907	0,732	0,595	0,624	0,776
Std. Error of Mean	0,051	0,066	0,052	0,071	0,079	0,091	0,073	0,059	0,062	0,078
Coefficient of variation	19,33%	23,41%	19,41%	25,43%	24,11%	28,53%	22,30%	22,49%	22,49%	22,02%
p-value*	REF	**0.0497**	-	-	-	-	-	-	-	-
p-value**	-	-	0.3417	REF	**<0.0001**	**0.0027**	**<0.0001**	0.2630	0.9344	**<0.0001**
p-value***	-	-	-	-	REF	0.2894	0.7787	**<0.0001**	**<0.0001**	**0.0189**

* Comparison with wild type strain (Mann-Whitney test) . **comparison with ΔMMAR0069::L5-MMAR0069 (Mann-Whitney test). *** Comparison ΔMMAR0069::L5-ponA1(Mann-Whitney test). REF= reference strain used for analysis. ΔMMAR0069 = strains with knockout in the gene *MMAR_0069* . ΔMMAR0069 = knockout in the gene *MMAR_0069*. ΔMMAR0069::L5-ponA1= knockout in the gene *MMAR_0069* and complemented with *ponA1* gene wild type or mutant under regulation of *hsp60*. ΔMMAR0069::L5-MMAR0069= knockout in the gen *MMAR_0069* and complemented with *MMAR_0069* under regulation of *hsp60* promoter , ΔMMAR0069::*rpsTp*-ponA1= knockout in the gene *MMAR_0069* and complemented with *ponA1* gene wild type under regulation of *rpsT* promoter from *M.marinum.* Significant values are marked in **bold**.

Table III. 6. Width measurements of wild type, *MMAR_0069* knockout strains, and gene complemented with *ponA1* from *M. tuberculosis* H37Rv wild type and mutants integrated in *M. marinum* genome.

	Mmar	ΔMMAR0069	ΔMMAR0069::rpsTp-ponA1	ΔMMAR0069::L5-MMAR0069	ΔMMAR0069::L5-ponA1	ΔMMAR0069::L5-ponA1 Q365H	ΔMMAR0069::L5-ponA1-A516T	ΔMMAR0069::L5-ponA1-P631S	ΔMMAR0069::L5-ponA1-T34A	ΔMMAR0069::L5-ponA1-T34D
Number of values	100	100	100	100	100	100	100	100	100	100
Minimum	0,2980	0,1880	0,2660	0,2150	0,2820	0,2380	0,2660	0,1880	0,3040	0,3100
Median	0,5650	0,4780	0,5180	0,4705	0,4465	0,4440	0,5680	0,5090	0,5295	0,4790
Maximum	0,7990	0,8520	0,8520	0,7740	0,7720	0,7380	0,9660	0,7530	0,8380	0,8090
Mean	0.5671	0,4873	0,5130	0,4676	0,4541	0,4387	0,5903	0,5016	0,5467	0,4835
Std. Deviation	0.1002	0,1126	0,1016	0,1003	0,08729	0,08334	0,1677	0,09413	0,1128	0,09460
Std. Error of Mean	0.01002	0,01126	0,01016	0,01003	0,008729	0,008334	0,01677	0,009413	0,01128	0,009460
Coefficient of variation	17.67%	23,11%	19,80%	21,46%	19,22%	19,00%	28,41%	18,77%	20,63%	19,57%
p-value*	REF	**<0.0001**	-	-	-	-	-	-	-	-
p-value**	-	-	**0.0017**	REF	0.3127	**0.0280**	**<0.0001**	**0.0144**	**<0.0001**	0.2512
p-value***	-	-	-	-	REF	0.3168	**<0.0001**	**0.0002**	**<0.0001**	**0.0264**

*Comparison with wild type strain (T Test, two -tailed Welch9s correction). ** comparison with ΔMMAR0069::L5-MMAR0069 (T Test, two -tailed Welch9s correction/Mann-Whitney test). *** comparison with ΔMMAR0069::L5-ponA1 (Mann-Whitney test). REF= reference strain used for analysis. ΔMMAR0069 = knockout in the gene *MMAR_0069*. ΔMMAR0069::L5-ponA1= knockout in the gene *MMAR_0069* and complemented with *ponA1* gene wild type or mutant under regulation of *hsp60*. ΔMMAR0069::L5-MMAR0069= knockout in the gene *MMAR_0069* and complemented with *MMAR_0069* under regulation of *hsp60*, ΔMMAR0069::*rpsTp*-ponA1= knockout in the gene *MMAR_006*9 and complemented with *ponA1* gene wild type under regulation of *rpsT* promoter from *M.marinum.* Significant values are marked in **bold**.

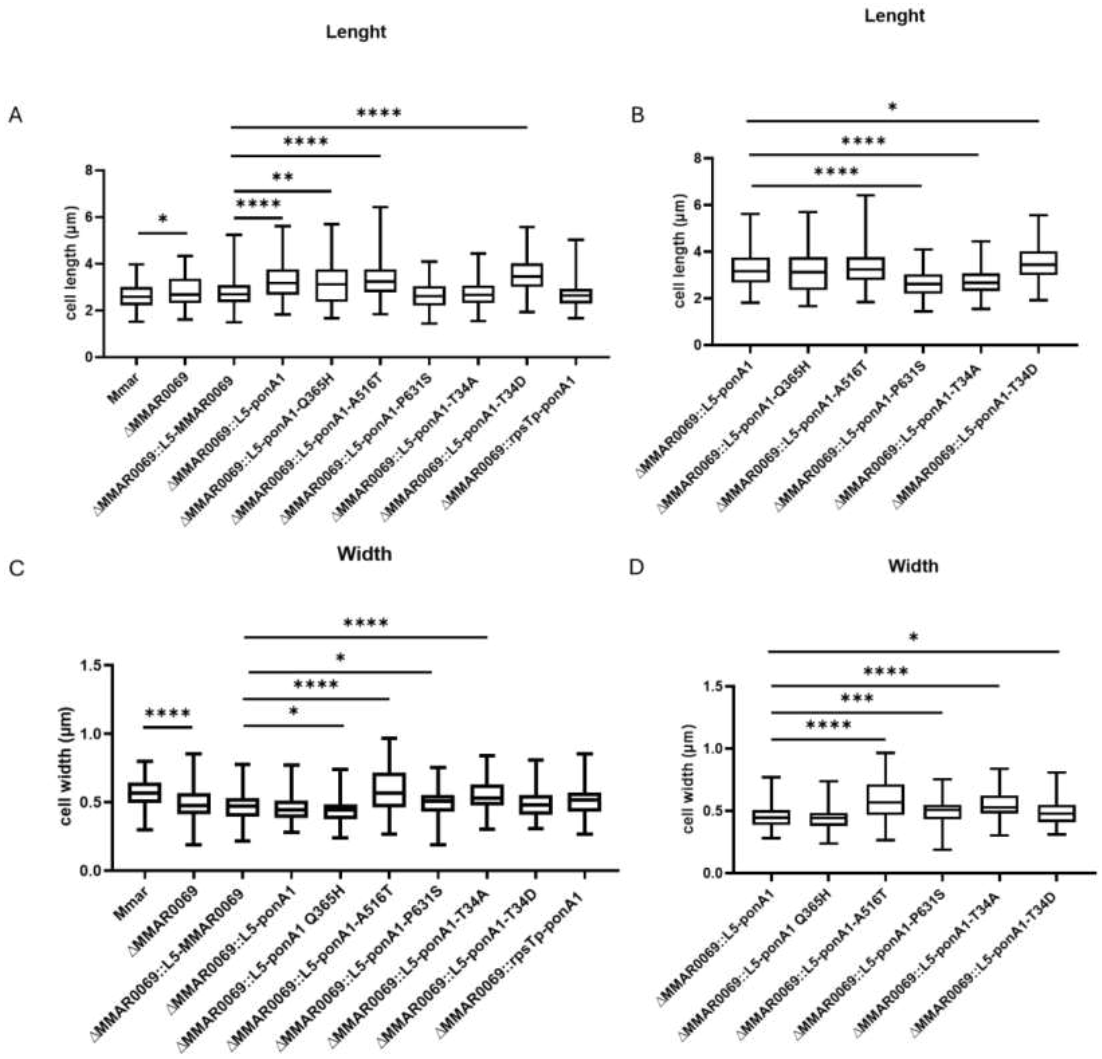

Figure III.59. Length and width measurements of *M. marinum* strains, including *MMAR_0069* knockout, and strains complemented with *ponA1* from *M. tuberculosis* H37Rv integrated in their genome. Min to max values for **A**. Length comparison using wild type and isogenic wild type as controls. **B.** Length comparison using the *ponA1* wild type from *M. tuberculosis* H37Rv as a control. **C.** Width comparison using wild type and isogenic wild type as controls. **D.** Width comparison using the *ponA1* wild type from *M. tuberculosis* H37Rv as a control. ΔMMAR0069 = knockout in the gene *MMAR_0069*. ΔMMAR0069::L5-ponA1= knockout in the gene *MMAR_0069* and complemented with *ponA1* gene wild type or mutant under regulation of *hsp60* promoter. ΔMMAR0069::L5-MMAR0069= knockout in the gene *MMAR_0069* and complemented with *MMAR_0069* under regulation of *hsp60*, ΔMMAR0069::*rpsTp*-ponA1= knockout in the gene *MMAR_0069* and complemented with *ponA1* gene wild type under regulation of *rpsT* promoter from *M.marinum.*

III.3.10. Cell envelope thickness measurements by cryoEM microscopy

Given that the PG layer is a critical component of the cell wall, changes in PonA1 function4such as those evaluated in this study (gene knockout and *ponA1* mutations)4may affect the cell9s ability to maintain a robust and well-regulated envelope. To assess this, the cell envelope thickness was measured. For each strain, a total of ten cells were analyzed at 30 000x magnification by CryoEM, with fifteen measurements taken per cell, resulting in a total of 150 measurements per strain (Figure III.60-A). Measurements were made considering the inner and outer edges of the cell envelope, providing detailed insights into structural variations across different groups (Figure III.60-B).

Linear regression was applied for statistical analysis, using 1/SD as an analytic weight to account for variability. This approach was employed for pairwise comparisons between groups. Significant differences in cell wall thickness were observed between the wild-type strain and the ΔMMAR0069 mutant, with the mutant showing a 7.41% increase ($p < 0.0001$). Additionally, strains complemented with *ponA1* from *Mtb* H37Rv under the regulation of the *hsp60* promoter exhibited a 6.98% increase in thickness ($p = 0.026$), while regulation by the *rpsTp* resulted in a 5.7% increase ($p = 0.031$), both compared to the isogenic wild-type strain. Further significant differences were also found in strains carrying the P631S ($p = 0.049$) and T34A ($p = 0.044$) mutations, with increases of 3.5% and 6.4% in thickness, respectively.

Another important observation emerged when comparing strains carrying *ponA1* mutations with the wild-type strain. Notably, the T34D mutation resulted in a significant 7.9% reduction in cell wall thickness ($p < 0.0001$), distinguishing it from

the other *ponA1* mutants, which exhibited increased thickness. These findings underscore the importance of species-specific variations in *ponA1* and their impact on cell wall integrity and thickness regulation.

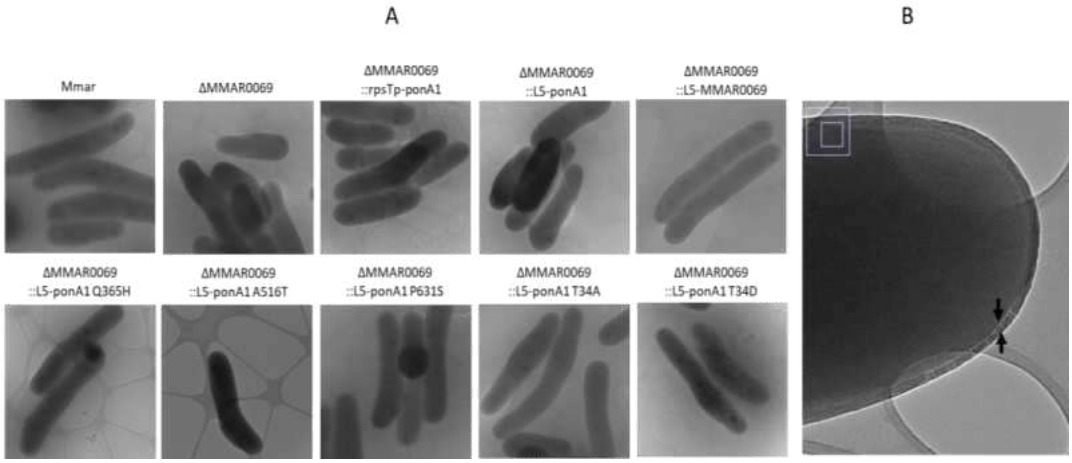

Figure III.60. Cell envelope thickness measurements of *M. marinum* evaluated by CryoEM. A. Magnification 12000X. B. Magnification 30000X, inner and outer edges of the cell envelope are marked by arrows . ΔMMAR0069 = knockout in the gene *MMAR_0069*. ΔMMAR0069::L5-ponA1= knockout in the gene *MMAR_0069* and complemented with *ponA1* gene wild type or mutant under regulation of *hsp60*. ΔMMAR0069::L5-MMAR0069= knockout in the gene *MMAR_0069* and complemented with *MMAR_0069* under regulation of *hsp60*, ΔMMAR0069::*rpsTp*-ponA1= knockout in the gene *MMAR_006*9 and complemented with *ponA1* gene wild type under regulation of *rpsT* promoter from *M.marinum.*

Table III.7. Cell envelope thickness measurements of *M. marinum* wild type, *MMAR_0069* knockout strains, and gene complementation with *ponA1* from *M. tuberculosis* H37Rv wild type and mutants evaluated by CryoEM.

	Mmar	ΔMMAR0069	ΔMMAR0069::rpsTp–ponA1	ΔMMAR0069::L5–MMAR0069	ΔMMAR0069::L5–ponA1	ΔMMAR0069::L5–ponA1–Q365H	ΔMMAR0069::L5–ponA1–A516T	ΔMMAR0069::L5–ponA1–P631S	ΔMMAR0069::L5–ponA1–T34A	ΔMMAR0069::L5–ponA1–T34D
Number of values	150	150	150	150	150	150	150	150	150	150
Minimum	77	78,20	78,70	71,40	80,40	77,50	72,90	76,20	79,70	74,70
Maximum	86,60	92,40	92,60	91,30	91,90	112,8	95,80	92,50	93,70	84,40
Range	9,6	14,20	13,90	19,90	11,50	35,30	22,90	16,30	14,00	9,700
Mean (pixel units)	81,21	87,23	86,19	81,54	87,25	86,75	85,10	84,41	86,72	80,37
Std. Deviation	2,951	4,417	4,443	6,184	3,371	9,971	6,706	5,486	4,424	2,962
Std. Error of Mean	0,9333	1,397	1,405	1,955	1,066	3,153	2,121	1,735	1,399	0,9367
Coefficient of variation	3,634%	5,064%	5,154%	7,584%	3,863%	11,49%	7,880%	6,500%	5,101%	3,685%
p-value	REF	**0.0025**	-	-	-	-	-	-	-	-
p-value 1/SD	REF	**0.0001**	-	-	-	-	-	-	-	-
p-value	-	-	**0.0069**	REF	**0.0020**	0.177	0.233	0.287	**0.045**	0.596
p-value 1/SD			**0.0031**	REF	**0.026**	0.182	0.144	**0.049**	**0.044**	0.887
p-value	-	-	-	-	REF	0.882	0.377	0.180	0.767	**0.0001**
p-value 1/SD	-	-	-	-	REF	0.854	0.711	0.937	0.867	**0.0001**

Linear regression was applied for the statistical analysis, with an additional p-value determined using 1/SD as an analytic weight. This approach was employed for pairwise comparisons between the groups. REF= The reference strain used as a strain of comparison.
ΔMMAR0069 = knockout in the gene *MMAR_0069*. ΔMMAR0069::L5-ponA1= knockout in the gene *MMAR_0069* and complemented with *ponA1* gene wild type or mutant under regulation of *hsp60*. ΔMMAR0069::L5-MMAR0069= knockout in the gene *MMAR_0069* and complemented with *MMAR_0069* under regulation of *hsp60*, ΔMMAR0069::*rpsTp*-ponA1= knockout in the gene *MMAR_006*9 and complemented with *ponA1* gene wild type under regulation of *rpsT* promoter from *M.marinum.* Significant values are marked in **bold**.

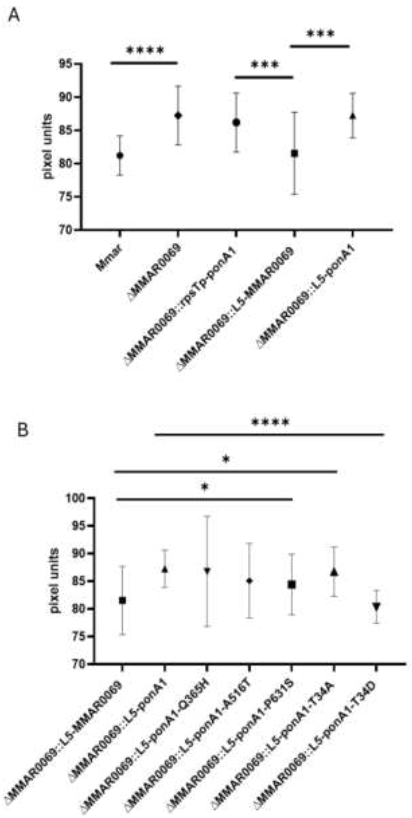

Figure III.61. Cell envelope thickness measurements of *M. marinum* strains with *MMAR_0069* gene knockout and complemented with *ponA1* variants genes from *M. tuberculosis* H37Rv evaluated by CryoEM. Mean and standard deviation for the A. Comparison of cellular thickness using the wild-type and isogenic wild-type strains as control references. B. Comparison of *ponA1* mutants and their control strains. ΔMMAR0069 = knockout in the gene *MMAR_0069*. ΔMMAR0069::L5-ponA1= knockout in the gene *MMAR_0069* and complemented with *ponA1* gene wild type or mutant under regulation of *hsp60*. ΔMMAR0069::L5-MMAR0069= knockout in the gene *MMAR_0069* and complemented with *MMAR_0069* under regulation of *hsp60*, ΔMMAR0069::*rpsTp*-ponA1= knockout in the gene *MMAR_006*9 and complemented with *ponA1* gene wild type under regulation of *rpsT* promoter from *M. marinum.*

III.3.11. Effect of *ponA1* from *M. tuberculosis* H37Rv on *M. marinum* growth upon RIF exposure

In this section, we evaluated the effect of RIF on the growth and viability of the different strains generated in this study during both the logarithmic and stationary phases of Mmar growth. The impact of RIF was assessed to determine whether genetic modifications, such as *MMAR_0069* deletion and *ponA1* Mtb H37Rv complementation, influence the strain9s response to antibiotic stress across different growth stages: logarithmic and stationary phases.

Bacterial survival was evaluated at two points in the logarithmic phase, 48 and 72 hours, by measuring OD_{600} in the presence of 0.5 ¼g/mL RIF, with values normalized to antibiotic-free controls.

At 48 hours, a statistically significant difference was found between the ΔMMAR0069 strain and the wild type strain (p=0.0089, t-test, two tailed, Welch9s test), exhibiting around 20% survival advantage after 48 hours (Figure III.62-A). This advantage becomes greater after 72 h, showing 54 % higher survival in the presence of RIF (p = 0.0058, T-test, Welch correction).

At 48 hours, the strain complemented with *ponA1* under the regulation of the *rpsTp* exhibited approximately 10% greater susceptibility compared to the isogenic wild-type strain (p = 0.0004, T-test, Welch correction). A similar trend was observed in the strain carrying the Q365H mutation, which also showed increased susceptibility (p = 0.0242, Mann-Whitney test). At 72 hours, a significant survival advantage was observed in the

strain complemented with Mtb H37Rv *ponA1*, showing a 54% increase compared to the isogenic wild-type strain ($p = 0.0009$, T-test, Welch correction). A similar advantage was noted for the *ponA1*-P631S mutant, with a 40% increase in survival ($p = 0.0105$, T-test, Welch correction), and the *ponA1*-T34D mutant, which demonstrated a 67% advantage ($p = 0.0001$, T-test, Welch correction), suggesting that this mutant behaves similarly to the wild-type Mtb *ponA1* (Figure III.62-B). No significant differences were found between other *ponA1* mutants and the wild-type strain.

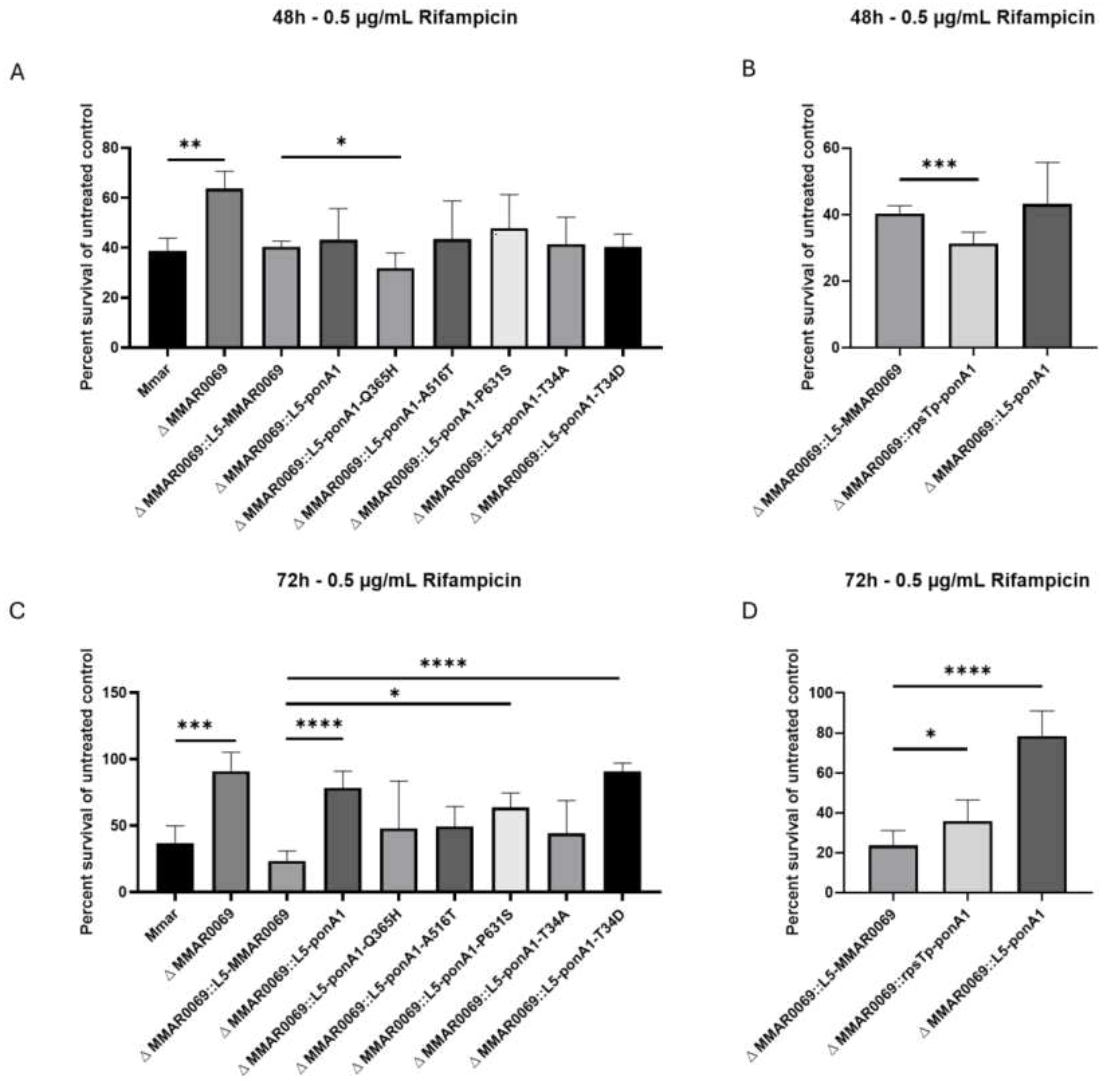

Figure III.62. Survival of *M. marinum* strains with *ponA1* knockout, carrying either wild-type or mutant *ponA1* from *M. tuberculosis* H37Rv, after exposure to rifampicin. Mean and SD are shown for bacterial survival cultivated in the presence of 0.5 µg/mL RIF, OD_{600} values were quantified and data is expressed as the percent of treated strains by untreated control. **A-B.** After 48 hours, **C-D.** After 72 hours of RIF exposure. ΔMMAR0069 = knockout in the gene *MMAR_0069.* ΔMMAR0069::L5-ponA1= knockout in the gene *MMAR_0069* and complemented with *ponA1* gene wild type or mutant under regulation of *hsp60*. ΔMMAR0069::L5-MMAR0069=isogenic wild type. Three independent assays were performed.

The same culture was maintained in the presence of RIF for up to 144 hours, allowing the cells to reach the stationary phase. After six days of incubation at 30°C and darkness, colony counting was performed in duplicate. In absence of RIF, no significant differences in the number of UFC/mL were observed between the wild-type and ΔMMAR0069 strains (p=0.3664, T-test, Welch correction). Similarly, no differences were found between the isogenic wild-type strain and those complemented with either wild type or mutant *ponA1* from Mtb H37Rv (p>0.9999, Kruskal-Wallis test, Dunn9s test for multiple comparisons).

In terms of survival in the presence of RIF, all strains exhibited significant effects from RIF exposure compared to their untreated controls ($p < 0.0001$, t-test or Mann-Whitney test). The ΔMMAR0069 strain demonstrated higher resistance than the wild-type strain ($p < 0.0001$, Mann-Whitney test), consistent with observations at 48 and 72 hours as quantified by OD_{600} . Furthermore, ΔMMAR0069 complemented wit *ponA1* -wild type and mutant - showed a significant viability advantage compared to the isogenic wild-type strain: wild-type ($p < 0.0001$, T-test, Welch correction), Q365H ($p = 0.0022$, Mann-Whitney test), A516T ($p = 0.0001$, Mann-Whitney test), P631S ($p < 0.0001$, T-test, Welch correction), T34A ($p < 0.0001$, T-test, Welch correction), and T34D ($p = 0.0004$, Mann-Whitney test).

Moreover, when strains with the *MMAR_0069* knockout carrying *ponA1* mutants were compared to the *ponA1* wild-type strain, the A516T mutation exhibited significantly increased resistance to RIF ($p < 0.0001$, Mann-Whitney test), as did the

P631S mutation (p = 0.0086, T-test, Welch correction). The other mutant strains showed similar responses to the *ponA1* wild-type strain upon exposure to rifampicin

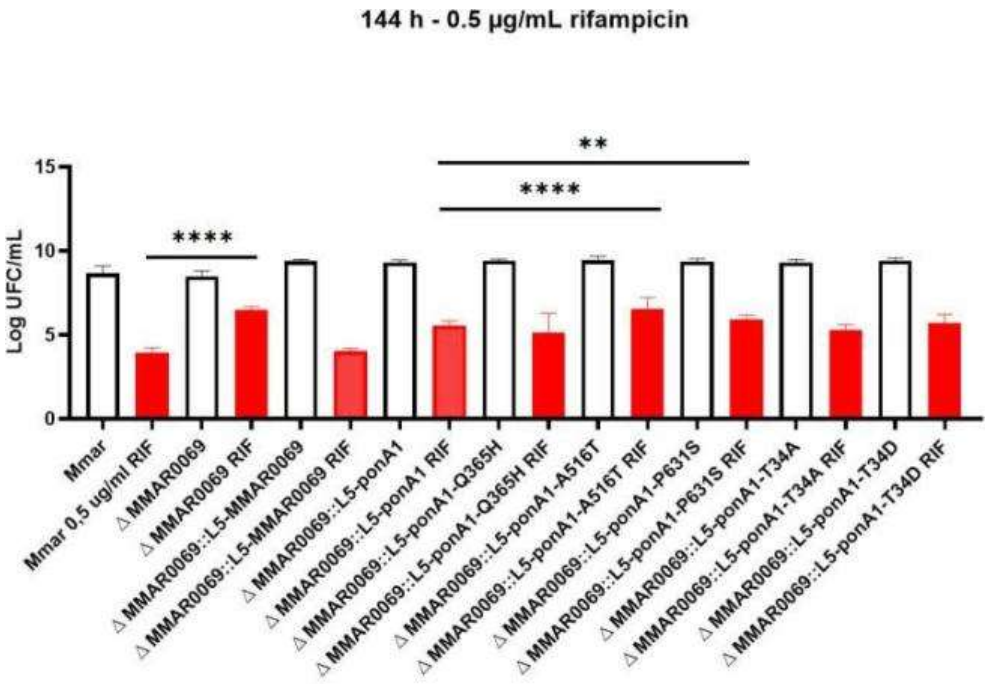

Figure III.63. Viability assay of *M. marinum* strains and their response to rifampicin after 144 hours of exposure. Mean and SD are shown for bacterial growth quantification on 7H10 medium, before (white box) and after rifampicin (0.5 µg/mL) exposure over six days (red box). ΔMMAR0069 strains showed higher resistance than wild type ($p<0.0001$, T-test, Welch correction), All the strains with *ponA1* MtbH37Rv were significantly different to isogenic wild type strain: wild type, Q365H, A516T, P631S, T34A, T34D ($p<0.0001$, $p=0.0022$, $p=0.0001$, $p<0.0001$, $p<0.0001$ and $p=0.0004$, respectively. T-test and Welch correction or Mann Withnney were performed for each pair). After rifampicin exposition mutations A516T ($p<0.0001$, Mann-Whitney test), and P631S ($p=0.0086$) were significantly different compared with *ponA1* wild type. ΔMMAR0069 = knockout in the gene *MMAR_0069*. ΔMMAR0069::L5-ponA1= knockout in *MMAR_0069* and complemented with *ponA1* wild type or mutant under regulation of *hsp60*. ΔMMAR0069::L5-MMAR0069= knockout in *MMAR_0069* and complemented with *MMAR_0069* under regulation of *hsp60*. RIF=rifampicin. Duplicate assays independently were performed. All the strains grew up similarly without antibiotic ($p>0.9999$, Kruskal-Wallis test, Dunn9s test for multiple comparison).

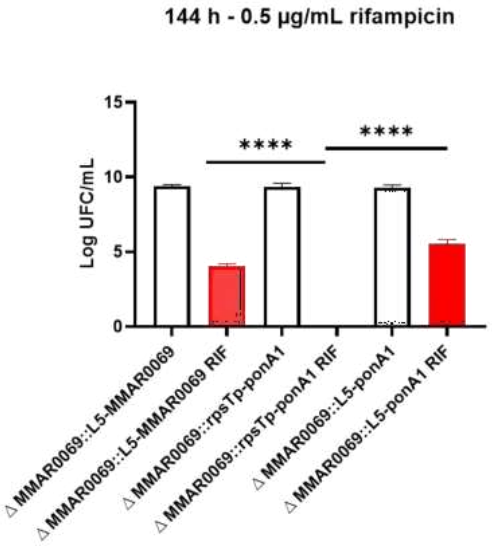

Figure III.64. Cell viability assay of *M. marinum* strains carrying *ponA1* from *M.tuberculosis* H37Rv under two different promoter regulation: *rpsTp* and *hsp60p*, and their response to rifampicin after 144 hours of exposure. No differences in viability were observed, between isogenic wild type and *ponA1* complemented strains, without drug exposure (p=0.4950, Mann-Whitney test). However, after rifampicin exposition, a significant increase in sensitivity was detected for the strain complemented with ponA1 under *rpsTp* regulation (p<0.0001, Mann-Whitney test). ΔMMAR0069::L5-MMAR0069= isogenic wild type. ΔMMAR0069::rpsT-ponA1= knockout in *MMAR_0069* and complemented with *ponA1* gene wild type under regulation of *rpsTp* from *M.marinum.* ΔMMAR0069::L5-MMAR0069= knockout in *MMAR_0069* and complemented with *MMAR_0069* under regulation of *hsp60*. RIF=rifampicin.

Strains complemented with *ponA1* under the regulation of the *rpsTp* showed no significant differences in growth under normal conditions without antibiotic exposure (p = 0.587, Mann-Whitney test). However, in the presence of antibiotics, they exhibited significantly increased susceptibility compared to the isogenic wild-type strain (p < 0.0001, Mann-Whitney test), with this effect being more pronounced during the stationary phase. This suggests that further characterization of *rpsTp* regulation during the stationary phase is necessary, as the regulation of *ponA1* across different growth

phases may play a critical role under stress conditions, such as antibiotic exposure (Figure III.64).

From these findings, we determined that *MMAR_0069* KO conferred increased resistance to RIF during both the logarithmic and stationary phases.

The presence of *ponA1* from Mtb H37Rv confers a survival advantage to strains exposed to RIF, which progressively increases as the cells transition into the stationary phase, with the A516T and P631S mutations showing significant effects. Notably, the T34D mutation also became significant after 72 hours of RIF exposure, exhibiting a level of resistance comparable to that observed in the KO strain.

Additionally, a notable observation was the response of cells expressing *ponA1* under the regulation of *rpsTp*. While these cells exhibited similar behavior during the logarithmic phase with and without RIF exposition (48 and 72 hours), their survival dropped severely after 144 hours, with no recovery from RIF exposure, suggesting that proper regulation of *ponA1* is critical during stress conditions. Ultimately, the experiment demonstrated that, after six days of RIF exposure, the mycobacteria remained viable and capable of proliferation at 0.5 µg/mL RIF.

III.3.12. Membrane fluidity test

With this assay, we aimed to explore whether alterations in *ponA1*, through either deletion or the insertion of mutated variants, could directly or indirectly influence membrane fluidity. This approach helps us assess the potential physiological consequences of these genetic modifications on the overall structure and behavior of the cell membrane.

Under the conditions analyzed in this study, no significant differences were found in the membrane fluidity between the Mmar wild type strain and the strain complemented with *MMAR_0069* (One-way ANOVA, p=0.3061). Similarly, no significant differences in membrane fluidity were observed between strains with ΔMMAR0069 or those ΔMMAR0069 complemented with *ponA1* from H37Rv WT and its mutants (One-way ANOVA, p=0.3099) (Figure III.65). However, a trend is observed in the means of the wild-type and isogenic wild-type strains, which are quite similar, while those strains harboring the *ponA1* gene from Mtb H37Rv display a different pattern. This experiment was conducted in duplicate.

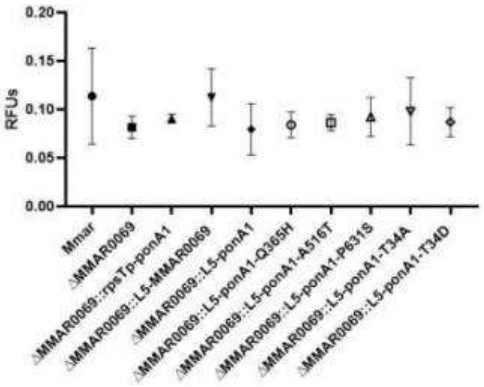

Figure III.65. Excimer/monomer fluorescence ratio (450nm/400 nm) in *M. marinum* strains with ΔMMAR0069 and ponA1 from *M. tuberculosis* H37Rv wild type and mutated. ΔMMAR0069 = *MMAR_0069* knockout. ΔMMAR0069::L5-ponA1= *MMAR_0069* knockout and *ponA1* complementation with wild type or mutant under regulation of *hsp60*. ΔMMAR0069::L5-MMAR0069= *MMAR_0069* knockout and complemented with *MMAR_0069* under regulation of *hsp60*, ΔMMAR0069::*rpsTp*-ponA1= strain with knockout in the gene *MMAR_0069* and complemented with *ponA1* gene wild type under regulation of *rpsTp* from *M. marinum.*

A table summarizing the main results of the work is presented below (Table III. 8-9).

Table III.8. Summary of morphological changes and rifampicin susceptibility profile in *M. marinum* strains with *MMAR_0069* knockout and integration of the wild-type *ponA1* gene from *M. tuberculosis* H37Rv. Comparison with wild type and isogenic wild type strains.

Strains	ΔMMAR0069 MIC: 1 µg/mL	ΔMMAR0069:: *rpsTp*-ponA1 MIC: 0.5 µg/mL	ΔMMAR0069::L5-ponA1 MIC: 2 µg/mL
Mmar MIC: 2 µg/mL	**L: ↑ 7.3%** **W:↓ 14 %** **T: ↑ 7.41%** **48h: 20% RES** **72h: 54 % RES** **144h: RES**	-	-
ΔMMAR0069::L5-MMAR0069 MIC: 2 µg/mL	-	L: ns **A: ↑9.7%** **T: ↑ 5.7%** 48h: 10 % SUS 72h: 10% RES 144h:SUS	**L: ↑ 17.8%** W: ns T: ↑ 6.98% 48h: ns **72h: 54% RES** **144h: RES**

L:length, W: width, T: thickness, Percent survival at 48 and 72 hours after RIF exposition compared with wild type or isogenic wild type. Viability at 144 hours post exposition of RIF compared with wild type or isogenic wild type. RES= resistant, ns= similar to isogenic wild type, SUS= susceptible compared to isogenic wild type. ns =non-significative change.

Table III.9. Summary of morphological changes and rifampicin susceptibility profile in *M. marinum* strains with *MMAR_0069* knockout and integration of the mutants in *ponA1* gene from *M. tuberculosis* H37Rv. Comparison with wild type and isogenic wild type strains.

	ΔMMAR0069:: L5-ponA1- Q365H MIC: 2 µg/mL	ΔMMAR0069:: L5-ponA1- A516T MIC: 2 µg/mL	ΔMMAR0069:: L5-ponA1- P631S	ΔMMAR0069:: L5-ponA1- T34A	ΔMMAR0069:: L5-ponA1- T34D
ΔMMAR0069::L5-MMAR0069 MIC: 2 µg/mL	**L: ↑14 %** **W: ↓ 6.18%** T: ns **48h:10% SEN** 72h: ns **144h: RES**	**L: ↑17,7 %** **W:↑26.24 %** T: ns 48h: ns 72h: ns **144h:RES**	L: ns W:**↑7.3 %** **T: ↑3.5 %** 48h: ns **72h: 40% RES** **144h:RES**	L: ns **W:↑16.9 %** **T: ↑ 6.4%** 48h: ns 72h: ns **144h:RES**	**L: 26.5↑ %** W: ns T: ns 48h: ns **72h: 67% RES** **144h:RES**
ΔMMAR0069::L5-ponA1 MIC: 2 µg/mL	L: ns W:ns T: ns 48h: ns 72h: ns 144h:ns	L: ns **W:↑30 %** T: ns 48h: ns 72h: ns **144h:RES**	**L: ↓ 19.5%** **W:↑10.5 %** T: ns 48h: ns **72h:RES** **144h:RES**	**L: ↓15.56 %** **W:↑20.4 %** T: ns 48h: ns 72h: ns 144h:ns	L: **↑7.4 %** W: **↑6.47%** **T: ↓7.9 %** 48h: ns 72h: ns 144h:ns

L: length, W: width, T: thickness, Percent survival at 48 and 72 hours after RIF exposition compared with wild type or isogenic wild type. Viability at 144 hours post exposition of RIF compared with wild type or isogenic wild type. RES= resistant, ns= similar to isogenic wild type, SUS= susceptible compared to isogenic wild type.

III.4. Discussion

PonA1 is a protein involved in the synthesis and regeneration of PG and has two critical domains: a transglycosylase (TG) domain and a transpeptidase (TP) domain, the latter of which includes the penicillin-binding protein (PBP) domain. PBP-type proteins are widely distributed among bacterial species, and in some cases, their function can be compensated by other genes (Kieser, Baranowski, et al., 2015; McPherson & Popham, 2003; Paradis-Bleau et al., 2010) and some of them are been related with antibiotic resistance.

Previous studies in PonA1 from Mtb have demonstrated that the TP domain interacts with several β-lactam antibiotics, including penicillin V, carbenicillin, cefotaxime, and dicloxacillin (Bhakta & Basu, 2002; Filippova et al., 2016). Additionally, PonA1 has been implicated in contributing to RIF resistance, with mutations in this protein reported to be associated with reduced susceptibility to the drug (Farhat et al., 2013; Rabanal J, 2020). It is crucial to note that RIF resistance in Mtb is primarily (90-95%) driven by mutations in the *rpoB* gene, which encodes the RNA polymerase β subunit (Miotto et al., 2017). However, resistance mechanisms can be multifaceted, involving both direct and compensatory mutations in essential targets such as *rpoB.*

In this chapter, we aimed to explore the functional and structural implications of PonA1 mutations through *in silico* modeling and *in vitro* experiments, contributing further to the understanding of its role in Mtb9s cell wall synthesis and potential

involvement in RIF resistance. In addittion, we evaluated the phenotypic effects of deleting the homologous *ponA1* gene (*MMAR_0069*) and assessed the impact of the genomic integration of *ponA1* from Mtb H37Rv, both the wild-type and its variants, in the Mmar model.

In silico structural modelling of PonA1 WT and mutants

The complete PonA1 protein4wild type, Q365H, and P631S4was modeled using two algorithms: AlphaFold (Jumper et al., 2021) and ESMFold (Lin et al., 2023).

When comparing the AlphaFold models of the PonA1 mutant proteins to the wild type, larger RMSD deviations were observed, with most mutants exceeding 15 Å. This outcome is linked to AlphaFold's algorithm, which incorporates energy minimization to generate a single, energetically stable conformer. While this reliance on multiple sequence alignments (MSA) enhances structural accuracy, it also introduces flexibility that can lead to significant conformational changes in response to mutations, as seen in the PonA1 Q365H and P631S models. This flexibility is considered a limitation, as it can result in large conformational shifts that are not always reflective of protein stability (Pak et al., 2023).

In contrast, PonA1 models generated by ESMFold displayed more stable RMSD values between the mutant and wild-type proteins, ranging from 0.8 Å for Q365H to 4 Å for P631S. The differences in performance are attributed to the fact that ESMFold bypasses MSA and provides more consistent results for this specific analysis.

Importantly, based on the comparison between models generated by AlphaFold and ESMFold for specific point mutations, the only significant change observed between the wild-type protein and the P631S mutant was a shift in the C-terminal region. Additionally, the crystallized structure of the TP domain (Filippova et al., 2016) was used for comparison with the generated models, revealing minimal structural differences in the TP active site, despite the mutations being located within this region.

In silico and *in vitro* analysis of the interaction between rifampicin and PonA1

Our molecular docking analysis, using the DiffDock algorithm (Corso et al., 2022), provided key insights into the interaction between PonA1 protein and two ligands: penicillin V and RIF.

For comparison, we used the crystallized TP domain of PonA1. Penicillin V (a confirmed ligand of PonA1 (Filippova et al., 2016), was used as control for the molecular docking, giving a DiffDock-Confidence Score (DSC) of 0.13, which is considered of high confidence, suggesting a high affinity. However, for the full-length PonA13Penicillin V interaction, the top DSC was -0.28, which is considered as moderate confidence. In addition, the mean DSC for the full-length PonA13Penicillin V interaction was -1.33, indicating also a moderate confidence. It is important to note that DSC values ranging between -1.5 and 0 suggest moderate confidence in the predicted models, while more negative values suggest lower confidence in the model predictions (https://github.com/gcorso/DiffDock?tab=readme-ov-file#inference).

Our analysis of the interaction between PonA1 and RIF revealed a top DSC of -1.78. The docking analysis for PonA1 mutants Q365H and P631S produced DSC values of -2.43 and -2.08 respectively. These scores are considered as of low confidence, suggesting that the predicted affinity between PonA1 (WT and its variants) and RIF are considered to be modest and marginal. Interestingly, the docking model shows RIF binding to the same interaction site as the corresponding Penicillin V to in the majority of simulations (77.5% for the wild type, 62.5% for Q365H, and 70% for P631S).

Importantly, the interaction between RIF and PonA1 (WT and its mutated variants) determined by molecular docking, involves critical residues from the conserved motifs in the PBP domain, notably S487, K490, S540, N542, and others (Table III.4), previously identified by Filippova et al. (2015) in the interaction with penicillin V. Our analysis of structure/binding stability through MD simulations over 100 ns supported these findings and showed that residues V523, Q686, and Y729 consistently maintained hydrophobic interactions with RIF throughout the simulations in both WT and mutant PonA1 variants. Interestingly, the stability analysis confirmed that the catalytic-site residues (S540 and N542 (from the SxN motif) and T684 (from the KTG(T/S)) site, which is the region to where Penicillin V and RIF binds, are structurally conserved in all the PonA1 variants.

Although the *in-silico* binding analysis suggest a modest interaction between PonA1 and RIF, we decided to continue with further evaluations, first because we believed that RIF-PonA1 may contributed modestly to the RIF resistance mechanism,

where the major role is played by RpoB, acting as a modulator. And second, because previous studies (Farhat et al., 2013; Kieser, Baranowski, et al., 2015; Rabanal et al., 2020) showed partial evidence of PonA1-RIF interactions as well.

To further investigate PonA19s affinity for RIF, we performed a binding assay using 1D NMR. The resulting spectrum demonstrated an interaction between RIF and PonA1, displaying a pattern similar to the spectrum observed for RIF/RpoB (Figure III.32), which was used as a control. Notably, the spectrum of PonA1-Q365H mutation shifted over time (Figure III.33), suggesting changes in the interaction dynamics with RIF. Based on the observed spectral changes, we investigated the impact of time on these changes, comparing the evolution of the spectra over time (Figure III.33.A-B). After 8 hours, we noted a significant decrease in the intensity of the peaks with the $PonA1_{234\text{-}820}$_Q365H protein, which prompted us to ask whether this shift resulted from a change in the affinity of the protein for RIF or a change in the viscosity of the medium over time? Indeed, it appears that the concentration of free RIF in solution has significantly decreased. This could be explained by several factors: (i) There may be a time-dependent increase in the affinity of $PonA1_{234\text{-}820}$_Q365H for RIF. This could occur through an allosteric mechanism that activates new interaction sites for RIF or through the aggregation of $PonA1_{234\text{-}820}$_Q365H, which would provide additional binding sites. In both cases, the K_D would be expected to decrease. (ii) An increase in the viscosity of the medium could also explain the broadening of the NMR peaks of RIF. In NMR, the width of the peaks is inversely proportional to the transverse relaxation time (T2). The higher the viscosity of the medium, the slower the molecular

motion, leading to faster transverse relaxation (reduction in T2) and, consequently, broader NMR peaks.

To measure the T2 of RIF, it is necessary to conduct experiments using carbon-13 resonance, which is naturally present in low abundance (approximately 1.1%). This results in very long acquisition times since more experiments need to be accumulated to obtain a sufficiently clear signal. An alternative would be to use carbon-13 enriched RIF, which would reduce the acquisition times required to obtain a quality signal but would incur significant additional costs, as carbon-13 enriched molecules are quite expensive.

Consequently, STD-NMR experiments were conducted to determine the K_D values, which were 1.8 mM for $PonA1_{234\text{-}820}$_WT, 2.1 mM for $PonA1_{234\text{-}820}$_Q365H, and 6.4 mM for $PonA1_{234\text{-}820}$_P631S. These values indicate a modest binding affinity in the millimolar range. These values highlight that, while the mutations may further reduce the affinity for RIF, the overall interaction between PonA1 and RIF is relatively weak compared to the well-established RIF-RpoB interaction, which has a K_D in the nanomolar range (2-4 nM) (Kurepina et al., 2022)(Kurepina et al., 2022). This stark contrast illustrates that RIF binds much more tightly to RpoB than to PonA1, further confirming that PonA1 is not a primary target of RIF. Despite the modest affinity between PonA1 and RIF, we believe that it is still possible that RIF/PonA1 may contribute to a modulatory approach in RIF-resistance, in contrast to the strong effect of RIF/RpoB interaction. As Bagheri et al. (2020) explain, when K_D values are in the mM range, higher ligand concentrations are necessary for binding, and the resulting

complexes tend to be transient and less stable. Interestingly, in other studies *in silico*, Maurya et al., (2023) identified that RIF could also interact with the ribonuclease VapC2 with a binding energy of approximately -8.8 kcal/mol, similar to the value we measured for the interaction between PonA1 and penicillin V (-8.58 kcal/mol). This suggests that RIF may not only have specificity for the β subunit of RNA polymerase but could also potentially target other proteins with varying affinities. Further experimental evaluation is necessary to confirm these interactions

PonA1 recombinant protein expression and biophysical characterization

While Filippova et al. (2015) expressed PonA1 in the pMCSG73 vector in BL21(DE3) Magic cells and observed protein degradation via SDS/PAGE, in our study, we cloned the same *ponA1* gene sequence into the pET28A-TEV vector and expressed it in Rosetta cells. Initially, we encountered issues with insoluble protein formation, however, by employing a slow refolding process, we successfully obtained monomeric, homogeneous and of high purity proteins as confirmed by SEC-MALS, CD, and thermal stability analysis.

For the evaluation of our proteins' functionality, we utilized the PBP domain of PonA1. We used Bocillin-FL, similar to the approach by Kieser et al. (2015), who successfully labeled PBPs, enabling the detection of TP activity in mycobacterial proteins. Our results showed that both wild-type and mutant $PonA1_{234\text{-}820}$ proteins bound Bocillin-FL with a molar ratio of 1.6 molecules per protein, confirming functional PBP activity across all variants.

Interestingly, the characterization of the Q365H mutation revealed that, compared to the wild-type and P631S mutant, Q365H affects only a few aspects of the protein, such as long-term stability, as evidenced by a slight decrease in the inflection temperature of 1.8°C. However, it does not significantly impair the protein9s enzymatic activity, contrary to the previous hypothesis proposed by Farhat et al. (2013).

MMAR_0069 essentiality in *M. marinum*

The essentiality of *ponA1* among the different mycobacterial species has been studied, revealing that for *M.smegmatis* it is essential for proliferation, and its depletion leads to severe growth defects and abnormal cell morphology (Hett et al., 2010; Kieser, Boutte, et al., 2015). In *M. tuberculosis* (Mtb), while *ponA1* is not essential *under in vitro* conditions (Bosch et al., 2021), it plays a crucial role in replication and dissemination during and after infection in mice (Kieser, Boutte, et al., 2015; Zhang et al., 2013). Likewise, our results demonstrate that deleting the *MMAR_0069* gene (which is the homologue of *ponA1*) in Mmar, does not result in significant changes in growth capacity. Since *MMAR_0069* is not essential in Mmar, this suggests that another gene, possibly *MMAR_5171*, which is the *ponA2* homologue, may be compensating for the loss of *ponA1* function, as has been observed in Mtb (Cole et al., 1998; Kieser, Baranowski, et al., 2015).

Evaluation of promoter activity by EGFP expression

In our study, in addition to performing the ΔMMAR0069, we also evaluated the action of two promoters, *ponA1p and rpsTp*, from Mtb and Mmar, respectively,

inserted through the ORBIT plasmid to regulate the constitutive expression of the EGFP gene. No variation in cell viability or cell growth was observed.

The native putative promoter of *ponA1p* proposed by (Kieser, Baranowski, et al., 2015); which includes the genes *Rv0047c, Rv0048c, Rv0049* (51,663-53,236) in Mtb, failed to express EGFP under the integration conditions used here. In contrast, using the same conditions, this reporter gene was successfully expressed with Mmar's *rpsTp*, previously tested in the pMV361 expression system in *M. smegmatis* (Cohen-Gonsaud et al., direct communication). These findings present new opportunities to evaluate promoter libraries and reduce the steps required for genetic manipulation in mycobacteria, enhancing the study of mycobacterial gene regulation.

Morphology

In our study, the deletion of *MMAR_0069* in Mmar resulted in an average 7.3% increase in cell length, along with a regulated reduction of approximately 14% in cell width, compared to the wild-type strain. In contrast, Kieser, Baranowski, et al. (2015) demonstrated that deletion of *ponA1* in Mtb through whole-genome transposon mutagenesis led to cells that were 14% shorter compared to their isogenic wild-type counterparts. Notably, we also observed a statistically significant 7.4% increase in cell envelope thickness in the ΔMMAR0069 mutant, distinguishing it from the wild-type strain. Morphology variation has also been observed in other studies. In Mtb, deletion of *ponA2 in vitro* results increased cell width, whereas deletion of *ldtB*, a L,D-transpeptidase, increases cell width and decreases length, highlighting the pivotal role

of these proteins in regulating cell morphology (Kieser et al., 2015a). Complementing the ΔMMAR0069 strains (Mmar) with *ponA1* from Mtb H37Rv resulted in a 17.8% increase in cell length. This regulation has previously been described in Mtb and *M. smegmatis* for the *ponA1* and *ponA2* genes (Kieser et al., 2015), and is now corroborated in Mmar, where *ponA1* also plays a role in length regulation. Additionally, among the *ponA1* mutations studied, the P631S mutation resulted in shorter and wider cells, consistent with the findings of Gao et al. (2019). In that study, it was observed that a reduction in the number of prolines in the proline-rich region at the C-terminal end increases the interaction with RipA, endopeptidase, leading to greater variation in cell size.

In addition, the *ponA1* A516T mutant led to a 30% increase in cell width compared to the *MMAR_0069* knockout strain complemented with wild-type *ponA1*.

All these findings suggest that mutations in *ponA1* affect both cell length and width, underscoring the critical role of this gene in cellular morphology. The A516T which was identified in Mtb strains from Peruvian clinical isolates, are reported here for the first time in relation to their impact on mycobacterial morphology.

Phosphorylation-mediated regulatory site of PonA1

While the NCBI lists PonA1 to comprise residues 234-820 (NC_000962.3), this designation has been recently modified by Kieser, Boutte, et al. (2015); Prisic et al. (2010) and Schubert et al. (2013), who proposed an adjustment, suggesting that the actual starting point of *ponA1* should be residue -426 from the initial transcription site,

contrasting from the current annotation. In our study, for the *ponA1* integration in the Mmar genome, we used the -426 start site relative to the annotated *ponA1* in the Mtb H37Rv genome. T34 is identified as a regulatory residue potentially regulated through PknB-associated phosphorylation.

In Mtb, Kieser, Boutte, et al. (2015) found that the T34A substitution resulted in a 5% increase in cell length. Similarly, in *M. smegmatis* a homologous T50A mutation led to an 11% increase in cell size compared to the wild type, further supporting this hypothesis. Conversely, in our study using the Mmar model (ΔMMAR0069 with *ponA1* from Mtb H37Rv), this mutation reduced cell length by approximately 15% and increased cell width by 20.4% compared to the wild-type *ponA1*. Additionally, the T34D mutation, which may mimic phosphorylation due to its physicochemical properties, resulted in a 7.4% increase in cell length and a 6.5% increase in cell width compared to the ΔMMAR0069 strain complemented with wild-type *ponA1*. These changes were smaller compared to those observed with the T34A mutation. Conversely, in Mtb, this mutation (T34D) generated cells that were 11% shorter than the isogenic wild-type strains, while in *M. smegmatis*, it resulted in a 9% reduction in cell length Kieser, Boutte, et al. (2015). These opposing effects caused by T34 mutations on cell morphology may be attributable to the heterologous Mtb gene introduced into Mmar, suggesting that *ponA1* regulation could also occur through phosphorylation. Overall, these significant changes indicate a regulatory role at this residue, potentially serving as a phosphorylation site in Mmar as well, making it critical for controlling the enzymatic activity of PonA1 and the rate of cell elongation.

Notably, the T34D mutation reduced the thickness of the cell envelope by 7.9% compared to the wild-type *ponA1*, but remained similar to the isogenic wild-type Mmar strain. These findings highlight the complexity of cellular responses to mutations across different mycobacterial species and underscore the need for further investigation into their regulatory mechanisms under stress conditions.

PonA1 and RIF exposure

Mmar, a model organism for TB studies, is susceptible to several antituberculosis drugs including RIF, a critical first-line drug for TB treatment. The RIF9s MIC for Mtb resistant strains, can change depending on the methodology used. Some studies suggest a more sensitive breakpoint of 0.5 ¼g/mL to detect borderline resistance, and the Clinical Laboratory Standards Institute (Clinical and Laboratory Standards Institute [CLSI], 2018) sets breakpoints for RIF resistance at greater than 1.0 ¼g/mL.

RIF's MIC in Mmar typically ranges from 0.03 to 4 µg/mL, determined by the agar dilution method, though this can vary depending on the method used (Aubry et al., 2017; Getahun et al., 2022). Our study found that deleting the *MMAR_0069* gene halved the MIC compared to the wild-type strain, making it more sensitive to the RIF and suggesting a link in the resistance mechanism to RIF mediated by Mmar9s *ponA1*-like gene. MIC values were restored upon complementation with *MMAR_0069* gene or Mtb H37Rv *ponA1*, provided gene expression was regulated by the strong *hsp60*. Farhat et al. (2013) reported that a strain with the Q365H mutation in *ponA1* exhibited a RIF MIC of 0.0025 µg/mL4twice that of its reference strain at 0.00125 µg/mL. This

contrasts with the results obtained in our study, in which the presence of Mtb H37Rv PonA1 mutations in the Mmar model did not significantly affect the MIC against RIF.

Survival assays for exposure to RIF demonstrated that the Δ*MMAR0069* strain exhibited approximately 20% greater cell survival after 48 hours and 67% after 72 hours of RIF exposure compared to the wild-type strain. This assay was conducted at a concentration of 0.5 µg/mL, which is close to the MIC for RIF in Mmar strains. Similarly, Farhat et al., despite using a much lower concentration, observed comparable results, with approximately a 30% survival advantage for the Δ*ponA1* strain after 6 days in Mtb and highlighted the role of *ponA1* in cell growth at subinhibitory concentrations.

At 72 hours under *hsp60* promoter regulation, strains carrying the *ponA1* gene from Mtb exhibited a greater survival advantage compared to the isogenic wild-type strain. This increase was significant for both the wild-type, P631S and T34D variants compared with isogenic wild type. Similarly, in Mtb, strains with the T34D allele showed a fourfold increase in tolerance to RIF (Kieser, Boutte, et al., 2015). This advantage persisted up to 144 hours, indicating that the cells were tolerant to 0.5 µg/mL of RIF and were capable of forming colonies post-exposure. In Mtb, this mutation at the phosphorylation site mimics threonine and likely facilitates interaction with PknB at the cytoplasmic level (Kieser, Boutte, et al., 2015) and based on the results obtained, it could have similar behavior as Mmar.

After 144 hours of exposure to 0.5 µg/mL of RIF, a subinhibitory concentration for most strains, altered their response. The *ponA1* mutations A516T, and P631S conferred a slightly higher advantage in the Mmar viability compared to wild type *ponA1* strain. These results suggest that mutations in *ponA1* may contribute to RIF tolerance, as previously reported by Farhat et al. (2013), and support the hypotheses proposed by Rabanal et al. (2020) based on their analysis of Mtb genomes from Peruvian clinical strains.

It is still unclear whether these variations in cell size generated by *ponA1* mutations contribute to RIF resistance. However, (Richardson et al., 2016) suggested that changes in cell length could influence susceptibility and tolerance to RIF in different mycobacterial subpopulations. They highlighted those factors like asymmetric cell division and the inheritance of cell length, along with mature growth poles contributing to increased cell size in the later stages of the cell cycle, contrast with those seen in earlier stages. This observation highlights the complex intrinsic mechanisms of RIF tolerance, which may be linked to the cell size differences observed in this study.

On the other hand, during our essays, another important point was noted. The gene complementation with *ponA1* (H37Rv Mtb) under the regulation of the Mmar *rpsTp*, maintained cell viability, and no significant differences in cell length were observed compared to the isogenic wild-type strain. Similarly, after 48 or 72 hours of RIF exposure, the response mirrored that of the isogenic wild-type strain. However, after 6 days of exposure to 0.5 µg/mL RIF, a severe reduction in survival was observed,

indicating the impact of RIF at different bacterial growth stages. This is consistent with the MIC evaluation findings, where the *ponA1*-complemented strain regulated by the *rpsTp* failed to restore RIF resistance to the level observed in the isogenic wild-type strain. Its susceptibility was four times higher than the isogenic wild-type strain and two times higher than the KO strain, raising questions about the expression levels of *ponA1* under the regulation of this promoter, particularly during the stationary phase.

Dörr et al., (2014) demonstrated that *Vibrio cholerae* cells in the stationary phase show competitive disadvantages compared to those in the exponential phase when the PBP1a gene is deleted. In an *in vivo* assay, it was found that cells in the exponential phase could overcome the competitive defects observed *in vitro*. This suggests that the growth phase can significantly modulate infectivity. Based on this information, we hypothesize that the differential response in RIF susceptibility could be attributed to the relatively moderate activity of the *rpsTp* compared to the hsp60 promoter. It is important to mention that, *rpsTp* controls the expression of the S20 ribosomal protein and is constitutively active, its activity fluctuates with the cell9s growth phase (Burgos et al., 2017). In contrast, the *hsp60* promoter is known for its robust induction of high levels of gene expression (Kumar et al., 1998; Stover et al., 1991) making it probably more potent than *rpsTp*.

Finally, other studies in mycobacteria highlight the variability present in each cell division (Santi et al., 2013). Rego et al. (2017) found that deleting *lamA*, a gene involved in the cell division complex, reduces population heterogeneity. This reduction increases susceptibility to antibiotics, as more homogeneous populations are eliminated

more quickly when exposed to RIF and other cell wall-targeting drugs. Additionally, the *ponA1* mutations identified in clinical strains evaluated in this study have caused morphological changes in the cells, either increasing or decreasing their length and width. These morphologic changes may align with the response to antibiotic exposure, suggesting that mutations in *ponA1* could confer increased fitness under antibiotic pressure, as reported by (Gao et al., 2019).

PonA1 putative promoter from H37Rv

Notably, the *ponA1* promoter (proposed by Kieser et al., 2015) evaluated in our studied, was unable to induce expression of the EGFP reporter gene, as previously mentioned. However, interestingly, the insertion of *ponA*1's putative promoter caused a change in the MIC of RIF. We hypothesize that this may be due to alterations in gene architecture, either related to the size of the inserted sequence or its composition/secondary-structure, as it includes three consensus (atttgcgac, atttgctca, and ctttgctcc) and three weaker (cttcgccac and gttcgcggt) EspR binding sites. EspR binding sites have been found clustered in different regions, not limited to promoters, suggesting that EspR protein also functions as a nucleoid-associated protein, playing architectural and regulatory roles that influence cell wall structure and pathogenesis (Blasco et al., 2012; Jin et al., 2019; Rosenberg et al., 2011; Santoshi et al., 2024). Hypothetically, the integration of more EspR binding sites in the Mmar genome could have generated new binding sites for the EspR protein, generating a change in the response to exposure to RIF. The *Rv3849* gene in Mtb H37Rv encodes the EspR protein and its homolog in Mmar is *MMAR_5399* (https://secretomyc.cbs.cnrs.fr/), located

towards position 6, 533 101 in the Mmar strain M genome. Additionally, this sequence was found in the *MMAR_0068* gene, located near the KO *MMAR_0069* gene. In this sense, future studies on EspR protein activity or EspR binding sites may provide insights in its potential contribution to the stress response induced by RIF exposure.

III.5. Conclusion of the chapter

In conclusion, this chapter highlights several key findings regarding the function and role of *ponA1* in Mtb H37Rv and Mmar.

In silico and *in vitro* analyses revealed a non-specific, transient interaction between RIF and PonA1 from Mtb H37Rv, showing low binding affinity (K_D in the millimolar range).

The ΔMMAR0069 gene in Mmar demonstrated that this gene is not essential for mycobacterial survival and conferred increased resistance to RIF at subinhibitory concentrations, highlighting its potential role in antibiotic resistance. We observed that this had a significant impact on cell morphology, which could be a potential mechanism through which *ponA1* contributes to RIF resistance.

The T34A mutation induced significant morphological changes compared to the T34D mutation, both relative to the strain complemented with wild-type *ponA1*, suggesting that this site may regulate cell morphology through phosphorylation in Mmar.

Strains carrying the P631S and T34D mutations in *ponA1* exhibited significantly higher viability compared to the isogenic wild-type strain 72 hours after exposure to RIF. Additionally, both the A516T and P631S mutations in *ponA1* appeared to confer survival advantages during the stationary phase when exposed to RIF.

Based on the methodologies used in this chapter, we can conclude that:

Recombinant PonA1 proteins from Mtb H37Rv, both wild-type and mutants, were successfully produced in their native form, with the Q365H and P631S mutations preserving the active site9s function, as indicated by their ability to bind to Bocillin-FL, an analog fluorescent of penicillin.

ponA1 gene from Mtb H37Rv under *hsp60* regulation is capable of complementing and restoring the RIF resistance profile in the absence of *MMAR_0069* in Mmar.

Furthermore, the modified ORBIT approach enabled simultaneous gene KO and complementation in one step, showing the *rpsTp* successfully regulated EGFP expression in Mmar, in contrast to the non-functional *ponA1* promoter. This method presents a promising tool for the evaluation of integrated promoter libraries within mycobacterial genomes.

Our studies showed ORBIT as a potent tool for genetic manipulation, 83% of the strains showed successful plasmid integration, and long-fragment sequencing confirmed correct gene KO at the targeted genomic site.

Chapter IV

SecretoMyc, a web-based database on mycobacteria secreted proteins and structure-based homology identification using bio-informatics tools.

SecretoMyc, a web-based database on mycobacteria secreted proteins and structure-based homology identification using bio-informatics tools

This project was conducted in parallel with the development of the thesis, during the period that I was working at CBS, in collaboration with PhD. Jérôme Gracy and PhD. Martin Cohen-Gonsaud. The first part of this chapter includes a brief literature review on the types of secretion systems in Mtb. The second part of the chapter contains the submitted manuscript with minor changes.

Abstract

To better understand the interaction between the host and the *Mycobacterium tuberculosis* pathogen, it is critical to identify its potential secreted proteins. While various experimental methods have been successful in identifying proteins under specific culture conditions, they have not provided a comprehensive characterization of the secreted proteome. We utilized a combination of bioinformatics servers and in-house software to identify all potentially secreted proteins from six mycobacterial genomes through the three secretion systems: SEC, TAT, and T7SS. The results are presented in a database that can be crossed referenced to selected proteomics and transcriptomics studies (https://secretomyc.cbs.cnrs.fr). In addition, thanks to the recent availability of Alphafold models, we developed a tool in order to identify the structural homologues among the mycobacterial genomes.

Keywords: Secretion, Host-pathogen Mycobacteria Alphafold.

IV.1. Secretion system in *M. tuberculosis*

The secretion system in Mtb is composed by three secretion systems: general secretion (SEC), Twin-arginine translocation (TAT) and type seven secretion system (T7SS) known as ESX (Figure V.1, Roy et al., 2020; Sankey et al., 2023). This system is essential for the bacterium's survivability and pathogenesis, playing a crucial role in the export of proteins through the mycobacterial membrane, enabling interaction with the host, manipulating immune responses, and ensure survival within hostile environments such as macrophages (Pal et al., 2022).

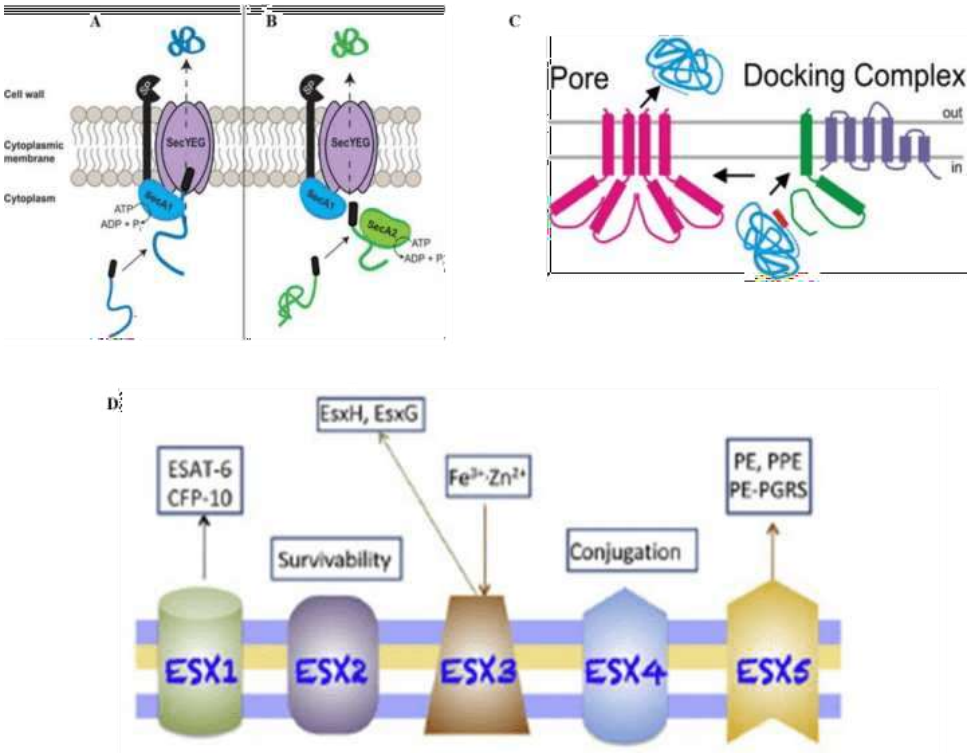

Figure IV.1. Secretion system types in *M. tuberculosis*. A, B. General secretion system featuring SecA1 and SecA2, respectively. C. Twin-arginine protein translocation system. D. Early Secretory Antigenic Target (ESAT) or Type VII Secretion System (Adapted from Goosens et al., 2014; Miller et al., 2017; Roy et al., 2020).

IV.1.1. General secretion system (Sec)

The Sec system, essential and conserved across all bacteria, is responsible for the export of most proteins, within this group, there are two secretion systems: SecA1, which is essential for Mtb viability and virulence, and SecA2, which, while not essential, transports a small group of proteins critical for Mtb virulence, latency, and immunomodulation.

Proteins transported by the SecA1 system, whether remaining in the cell envelope or fully exported to the extracellular space. These proteins are synthesized as preproteins with a signal peptide at the N-terminal end. This signal peptide features a positively charged N-terminal, a hydrophobic central domain, and uncharged polar amino acids with a cleavage site at the C-terminal end (von Heijne, 1990).

Proteins destined for the periplasm have a sequence that will be recognized by SecB, which will act as a chaperone to prevent the folding of the proteins, keeping them in an unfolded state, and then interact with the protein SecA, and pass through the SecYEG membrane channel (Randall & Hardy, 2002). SecA recognizes this signal peptide, which is removed by signal peptidases on the extracytoplasmic side of the membrane during export using ATP (Catipovic et al., 2019), facilitating the protein's folding process (Paetzel et al., 2002).

The proteins exported by this system include those involved in cell wall synthesis during cell division and remodeling factors (Miller et al., 2017) such as PBPs that are crucial for PG synthesis, in Mtb are eight PBPs annotated and all were predicted to have Sec type export signals (Machowski et al., 2014). Other proteins that have been reported to be secreted by this pathway are the L,D-transpeptidases: LdtMt2, PBPA

and Rv1433 that together with PonA2 could be important during the dormancy stage due to their ability to regulate PG formation and transition from an active growth to a dormant state (Dutta et al., 2010; Patru & Pavelka, 2010). Another important group is composed of lipoproteins, which may contribute to Mtb virulence and have been evaluated in some cases in macrophages and mice as models of infection, determining that mutants of these lipoproteins generate attenuation despite not being essentials (Sander et al., 2004). Notably, lipoproteins exported by this pathway contain a lipobox motif at the C-terminal end of the signal peptide (Nakayama et al., 2012).

SecA2-dependent proteins may either have a signal peptide at the N-terminal end or lack it. This system secretes various proteins, including solute-binding proteins (SBP) (Feltcher et al., 2015), superoxide dismutase (SodA), and catalase-peroxidase (KatG), which are important for their antioxidant activity in macrophages, as well as serine-threonine kinase PknG (van der Woude et al., 2014). All these proteins have been reported to lack a signal peptide (Braunstein et al., 2003; Cowley et al., 2004). Additionally, multiple DosR-regulated proteins have been found to be transported by SecA2 (Feltcher et al., 2015).

IV.1.2. Twin-arginine translocation pathway

Unlike the general secretion system, this system can transport folded proteins and those containing cofactors (Goosens et al., 2014). It utilizes a signal peptide containing twin-arginine residues, characterized by the motif S/T-RRxFLK. This hydrophobic region is larger but less hydrophobic than those of proteins transported by the Sec system (Cristobal, 1999; Robinson et al., 2011). The system includes TatC, the largest

protein, and TatA, which may also be identified as TatB or TatE. Proteins with the twin-arginine signal peptide interact with TatC and TatA-like proteins, with TatC inserting the proteins in the membrane. This docking complex recruits the pore-forming TatA-like proteins, and translocation occurs through protonic force (Goosens et al., 2014).

The proteins secreted by this system often have globular domains and a single transmembrane helix at either the N- or C-terminal end (Gallego-Parrilla et al., 2024). They also undergo a substrate quality control system before export, involving a chaperone-like recognition that monitors each protein's conformational state (Taw et al., 2022). In Mtb, this secretion system, composed of TatA, TatB, and TatC, is essential for survival (Posey et al., 2006; Saint-Joanis et al., 2006). Proteins such as β-lactamase BlaC and phospholipase C PlcA and PlcB, which play significant roles in the pathogenesis of Mtb, are exported by this pathway (McDonough et al., 2005; Raynaud et al., 2002).

IV.1.3. Type seven secretion system (T7SS)

The proteins secreted by this system are involved in nutrient uptake for mycobacterial maintenance, as well as in interactions with the host and modulation of the immune system response (Famelis et al., 2023; Tufariello et al., 2016). There are five type VII or ESX pathways, known as early secretory antigenic target systems, where proteins secreted have homology with the ESAT6 protein. Five *esx* loci have been described named *esx1* to *esx-5*, they contain genes encoding proteins with the WXG motif forming a helix-turn-helix structure (Renshaw et al., 2005) and genes for

transmembrane proteins of the FtsK-SpoIIIE ATPase family (Abdallah et al., 2007; Pallen, 2002), which lack Sec or Tat signal peptides. This system encodes its own components for membrane transporters and secretory substrates, along with other proteins specific to each secretory system, which are not functionally redundant (Gray et al., 2016).

ESX-1, located at the RD1 loci (regions of difference 1), was deleted in *M. bovis* BCG to create the Mtb vaccination strain. This region is crucial for Mtb cell function and virulence, encoding the cellular antigens ESAT-6 and CFP-10 found in the supernatant (Pym et al., 2002). This secretion system also facilitates Mtb escape from phagosomes to the cytosol by producing pore-forming toxins that can disrupt the phagosome membrane, plasma membrane, and cellular organelles (Los et al., 2013). Additionally, the ESX-1 locus encodes mycosin 1, a serine protease like subtilisin, which regulates the ESX-1 secretion system and substrate processing (Ohol et al., 2010). Granuloma formation, typically associated with host defense, may also be a pathogen-induced mechanism via the ESX-1 system; as these environments become replicating niches, defects in the *espL* gene at the ESX-1 loci were linked to reduced granuloma formation (Stoop et al., 2011). In the Mmar model, this system is linked to macrophage hemolysis and cytolysis through the secretion of the species-specific MMAR_2894 (Bosserman et al., 2019), which is not found in Mtb.

ESX-3 is known for its role in regulating mycobactin-mediated iron homeostasis and zinc incorporation. This system secretes the EsxG-EsxH heterodimer, which not only regulates iron acquisition but also controls the secretion of the PE-PPE family of proteins (Ilghari et al., 2011). EsxH was identified to interacts with human hepatocyte

growth factor-regulated tyrosine kinase substrate, a component of the Endosomal Sorting Complex Required for transport, which cause the inhibition of phagosome maduration (Mehra et al., 2013). Additionally, EsxH strongly induce IFN**γ** secretion in T cells from TB patients, as well as in CD4+ and CD8+ cells from Mtb-infected mice (Hervas-Stubbs et al., 2006; Majlessi et al., 2003). Tufariello et al. (2016) discovered that PE5-PPE4 are crucial for ESX-3 siderophore-mediated iron acquisition and that process is host genotype-dependent, underscoring the system9s significance in combating host defense mechanisms that limit iron availability. The presence of ESX-3 is critical for all mycobacteria, whether pathogenic or environmental (Roy et al., 2020).

ESX-5 is a crucial secretion system in the pathogenesis of mycobacteria, involved in the secretion of proteins containing Proline-Glutamic acid (PE) motifs, polymorphic GC-rich sequences (PGRS), and Pro-Pro-Glu (PPE) motifs. These motifs, located towards the N-terminal end, act as cell surface antigens associated with virulence (Abdallah et al., 2007; Bottai & Brosch, 2009). For instance, the PPE10 protein, essential for capsule maintenance (Ates et al., 2016), can modulate the innate immune response. Additionally, point mutations in the *eccC5* loci, found in clinical strains, have been linked to the development of resistance to ofloxacin (Eilertson et al., 2016), which would imply that these systems may also participate in the resistance to different drugs.

ESX-2 and ESX-5 are specific to slow-growing mycobacteria (Gröschel et al., 2016; Roy et al., 2020), whereas ESX-4, found at the esx-4 locus, contains the fewest genes among the *esx* loci and is considered the ancestral origin of other ESX systems,

with orthologous systems identified in other species (Dumas et al., 2016). Gray et al. (2016) observed that ESX-1 mutations in a donor can hyperinduce a transcriptional response in the recipient of *esx4*, suggesting a correlation between ESX-1 and *esx-4* in enhancing DNA transfer efficiency and promoting conjugation between mycobacteria. Additionally, ESX-4 has been linked to the export of the CpnT protein, whose carboxyl-terminal end carries the TB necrotizing toxin, a major cytotoxicity factor of Mtb in macrophages. Both ESX-2 and ESX-4 have been described as contributing to the permeabilization of the phagosomal membrane, similar to ESX-1 (Pajuelo et al., 2021).

IV.1.4. Importance of the study of secretory proteins

Upon entering the host and interacting with macrophages, Mtb has developed various strategies for evasion, virulence, and immunomodulation, utilizing its diverse secretion systems which target many proteins as key factors in these processes. While many of these secreted proteins have been well-described and studied, others remain uncharacterized experimentally. Comparative membrane proteome studies between Mtb H37Rv and *M. bovis* BCG have revealed the overexpression of ESX-3 genes in the virulent strain, suggesting their involvement in virulence-associated mechanisms (Gunawardena et al., 2013). Additionally, a quantitative proteomic analysis comparing sensitive and resistant Mtb strains identified downregulation of genes like *eccA3*, *eccB3*, and *tatA* in RIF-resistant and XDR strains; *esxL* and *esxN* in RIF-resistant and MDR strains; and *espB*, *esxK*, and *espL* in RIF-resistant, MDR, and XDR strains. Furthermore, *esxA*, *esxB*, PPE18, and PPE36 were downregulated between MDR and

XDR strains when compared to H37Rv (Ullah et al., 2021). This study also found that genes such as PPE58 and PPE59, which are not detected in resistant strains but are present in sensitive strains.

Wang et al. (2022) discovered that they could restore growth functions and virulence in strains lacking the ESX-3 system by overexpressing an ESX-3 paralog, which appears to compensate for the loss of other secretory proteins. More recently, Chen et al., (2024), found that proteins such as Rv3899c, CFP10, Mce1F, and DnaK interact with pathways related to the mitochondrial membrane, glycolysis, the respirasome, and translation in mitochondria-associated pathways. Additionally, proteins like ANXA1 and S100A11 may facilitate cell adhesion and interact with G-protein complexes, while DnaK could enhance glucan metabolism in the host. These findings underscore the complex interactions between Mtb and host biological and metabolic processes and emphasize the importance of conducting studies on the different mycobacterial secretion systems.

IV.2. Article: SecretoMyc, a web-based database on mycobacteria secreted proteins and structure-based homology identification using bio-informatics tools

Jérôme Gracy [a,1], Katherine Vallejos-Sanchez [a,b,1], Martin Cohen-Gonsaud [a,*]
[a] Centre de Biologie Structurale, CNRS, INSERM, Universit´e de Montpellier, France
[b] Laboratorios de Investigación y Desarrollo, Facultad de Ciencias y Filosofía, Universidad Peruana Cayetano Heredia, Lima, Peru
https://doi.org/10.1016/j.tube.2023.102375
Received 16 May 2023; Received in revised form 4 July 2023; Accepted 5 July 2023. Journal of Tuberculosis.
Available online 6 July 2023.

Minor changes have been introduced in the chapter below.

Author contributions

Jérôme Gracy developed the software and tools for the analysis.

Katherine Vallejos-Sanchez developed the website and analysed the data.

Martin Cohen-Gonsaud designed the study and analysed the data. All the authors wrote the paper.

Acknowledgement

The CBS acknowledges support from the French Infrastructure for Integrated Structural Biology (FRISBI) ANR-10-INSB-05-01 and the GIS ChemBioFrance.

IV.2.1. Main text

Mycobacterial infection relies on perturbation of multiple immune responses like phagosome maturation to cytokine secretion. These mycobacteria-driven modifications of the host-cell response can be mediated by either lipidic or protein effectors [1]. It is estimated that over 20% of bacterial proteins have functions outside the bacterial cytoplasm and are exported to their designated locations by protein export systems [2].

The functions of the exported proteins are essential for physiological processes (*i.e.* the cell-wall maintenance) but also, in the case of pathogenic bacteria they are crucial for virulence. To comprehend the interplay between host and pathogens, it is essential to identify the putative secreted proteins. Biochemical, genetic and imaging tools have been developed to evaluate protein secretion [3]. While reporter-based assays [4] and functional screens [5] have been used, mass spectrometry has been the most commonly employed technique used to identify secreted or cell-wall associated proteins in various strains and under different culture conditions. These proteomics studies have demonstrated their ability to identify proteins in specific growth conditions [638]. Although these studies can uncover the secretion patterns in specific growth conditions, they are not designed to capture the complete bacterial secretome. For example, the secretion pattern will differ when bacteria are grown under anaerobic conditions compared to normoxic conditions or in a laboratory culture medium compared to an infection. As a consequence, it is unsurprising to observe variations in secretion patterns across different bacterial experiments. As a consequence, data from various proteomic studies on secreted mycobacterial proteins have shown a weak overlap for proteins identified as secreted. Furthermore, the host cell environment also plays an important role, as recently revealed by two studies focusing on the identification of secreted proteins during infection [4,9].

M. tuberculosis possesses three different secretion systems [10]. The general secretion (Sec) and the twin-arginine translocation (Tat) path- ways perform the bulk of protein export and are both essential. Proteins exported by the Sec pathway are distinguished by the presence of an N-terminal signal recognized by the SecA protein

before translocation [11]. The Tat pathway exports preproteins containing N-terminal signal peptides with a twin-arginine motif for binding to the TatC protein [12, 13]. *M. tuberculosis* has also specialized export pathways that transport specific subsets of proteins. Five specialized ESX export systems (ESX-1 to ESX-5) are present in *M. tuberculosis* with some of them essential for virulence [14]. Although the ESX systems were first discovered in

M. tuberculosis, they also exist in a few other Gram-positive bacteria. The ESX systems are also referred to as Type VII secretion systems (T7SS). Proteins secreted by T7SS lack Sec or Tat signal peptides, instead secretion relies on a combination of sequence and structural motifs. Based on the identification of various T7SS secreted proteins, two secretion motifs (YxxxD/E and WxG) included in a flexible loop that participates in a helix-turn-helix structure [15,16] were identified. Two proteins, one containing the YxxxD/E motif and the other containing the WxG motif interact and are exported as dimers after binding to the cytosolic chaperone EspG [17].

Here we use and combine multiple bioinformatics servers and in- house tools in order to identify all the putative secreted mycobacterial proteins (Figure IV.2). We analysed the 3906 *M. tuberculosis* H37Rv sequences using an in-house pipelining tool for large-scale integrative bioinfor- matics [18] (PAT pipeline). First, known signal peptides and/or struc- tural features necessary for secretion were predicted using dedicated available software [19,20] (*i.e.* SignalP v4.1 and PredTAT). In addition, transmembrane segments were inferred using either Uniprot annota- tions or the TmHMM prediction software [21], then we also looked at the number of predicted transmembrane segments and the position of the last transmembrane segment to identify

signals potentially missed by the various servers and to avoid confusion with membrane proteins. For the T7SS, based on previous work we aim to identified the combination of sequence and structural motifs. We selected the *M. tuberculosis* pro- teins whose Alphafold models obtained from the EBI database (https://a lphafold.ebi.ac.uk/) had at least 70 residues in helical conformation in the 100 first positions, and whose sequences had a WxG motif between positions 30 and 79 or a YxxxD/E motif between positions 80 and 99. This Alphafold-based selection method detected 108 putative T7SS proteins in *M. tuberculosis* (alignments available at https://secretomyc. cbs.cnrs.fr/myctu_H70-99_PE0-19_Wxg30-79_or_YDE80-99.html).

These data were crossed with various data from proteomics and transcriptomics studies and five additional mycobacterial genomes (*M. marinum, M. bovis, M. abscessus, M. avium and M. smegmatis*) un- derwent the same process to compare predictions between various mycobacterial species, specifically in regards to their ability to survive within infected cells. Thus, we identified 176 T7SS, 79 Tat, and 462 Sec M. tuberculosis proteins with characteristic secretion signals. The data are presented in web-page at this address: https://secretomyc.cbs.cnrs. fr.

Next, we first applied the homology modeling procedure to identify distant homologues of the proteins, and the resulting information was used to exclude false positive proteins. For instance, some proteins belonging to the TerR cytoplasmic transcriptional regulator family possess sequence and structural features matching the T7SS secretion motif but are not secreted, and as consequence excluded from our secretome. We took advantages of the breakthrough brought by AlphaFold [22] to insert in our database the generated models. Those models can be used to detect structural

homologues and then correct and/or complement the current genomic annotations as well as it pro- vides information on domain delimitation. Here, we used the models to identify homologues within the genome. We first collected a structure database including all Alphafold models of the *M. tuberculosis* proteome in the EBI database (https://alphafold.ebi.ac.uk/) and a representative set of protein domain structures obtained from the SCOP classification database [23]. Structure pairs were structurally aligned using TMalign [24] and the pairs sharing a TM-score above 0.55 were then hierarchically aggregated yielding structural clusters which we called AlphaClans. When a *M. tuberculosis* Alphafold model belongs to an AlphaClan, its member structures are listed at the bottom of the corre- sponding *M. tuberculosis* report, with pairwise TM-scores, RMSD, and sequence identity percentages. The secretion scores which are also listed for each AlphaClan member can help to better assess if the considered *M. tuberculosis* protein is secreted or not.

The home page of the web server provides access to the SecretoMyc database through a global table where information on all *M. tuberculosis* proteins is synthetized: database cross-references, homology searches, secretion predictions, structural models, domain families and prote- omics experiments (Figure IV.3). The display of table columns can be customized using the left panel with toggle buttons. Column data can be sorted or searched using simple or advanced query form.

Clicking on a table line opens a new window with a detailed report of all cross-references, homologues, predictions, and classifications ob- tained on the corresponding protein (Figure IV.4). This report provides many important information for analyzing the

protein: alignment with orthologs from close

genomes, synthetic table with transmembrane and secretion predictors, list of similar Pfam families, PDB structures or Alphafold models.

In summary, the database provides a convenient way for users to determine whether a protein of interest may be secreted, and to identify homologues among six mycobacterial proteomes, as well as more distant structural homologues using the available Alphafold models and AlphaClan classification. Each individual page presents all the required information for evaluating the results. Furthermore, the database facilitates the integration of data from proteomics and transcriptomics studies, allowing users to set thresholds for selecting putatively secreted proteins based on their corresponding RNA expression levels. While the database currently includes only a few selected studies, more can be incorporated upon request from users.

IV.2.2. Material and methods

Six mycobacteria proteomes (*M. tuberculosis, M. bovis, M. avium, M. marinum, M. smegmatis* and *M. abcessus*) were retrieved using the <Proteome= server of the Uniprot database [25]. Secretion pathways, structural predictions, domain architectures, proteomics and transcriptomics data were predicted or collected for each of these proteins. The resulting information was summarized in individual entries describing each *M. tuberculosis* protein. The whole SecretoMyc database is accessible through an interactive web table whose columns can be customized, sorted and queried.

For proteins associated with the General Secretion Pathway (SEC), the program SignalP version 4.1 [19] was utilized. The model used for prediction was trained on

Gram-positive bacteria and set with a D-cutoff of 0.45. Peptide signals indicative of the Twin-arginine Secretion Pathway (TAT) were predicted using the web server PRED-TAT [20] available at http://www.compgen.org/tools/PRED-TAT.

The proteins related to the Type VII Secretion Pathway (T7SS) were detected using a refined detection method based on iterated HMMER search. First, a sequence database was constructed using fragments of *M. tuberculosis* proteins. Each fragment consisted of the first 110 residues of the respective *M. tuberculosis* protein. To generate the identifier for each protein fragment, the Tuberculist identifier [26], the gene name, the first PFAM domain [27], the number of residues in helix conformations, and the starting positions of the identified motifs WxG and YxxxD/E (when present) were concatenated. The database of these protein fragments was searched using seven iterations of HMMER [28] with an E-value cutoff of 1 and a 50% query overlap cutoff. The input query for this search was the alignment of all ESX proteins known to belong to T7SS. The full sequences corresponding to the hits detected by HMMER were then aligned using MAFFT, resulting in 183 aligned T7S proteins with gene names, PFAM domains, helix counts, and PPE, WxG, YxxxD/E annotations. The multiple sequence alignment of these 183 proteins is accessible from the home page (https://secretomyc.cbs.cnrs.fr/myctu_t7s_color_string.htm). For each aligned protein hit, all interacting proteins were gathered if their combined score in the STRING database exceeded 800 [25]. These possible interactions are listed after the sequence of each hit in the above alignment.

Transmembrane proteins were predicted using the TmHMM software. The transmembrane features were also retrieved from the Uniprot database [25]. The number of predicted or featured transmembrane segments were stored in the SecretoMyc

database for each *M. tuberculosis* protein.

Alphafold 3D models computed for the whole *M. tuberculosis* proteome were obtained from the EBI web server (https://alphafold.ebi.ac. uk). A database of 3D structures was then built by merging these 3D

M. tuberculosis models with a list of representative experimental domain structures obtained from the SCOP database filtered at 40% maximum sequence identity. All these 3D structures were hierarchically aggregated according to a similarity score combining the BLOSUM62 substitution score [29] of their aligned sequences and the similarity of their secondary structure composition. This initial classification step resulted in a binary tree whose nodes were checked following a bottom-up tree scan. For each node, a protein pair representative of its 2 descending branches was selected and compared using the structural alignment program TM-align [24]. Each branch representative was the protein closest to the consensus sequence of the protein cluster under the considered node branch. If the structural TM score was above 0.55, the checked node was validated and its father node was further inspected. Otherwise, the leaf cluster under each branch of the non-validated node was saved as an Alphafold clan of similar protein structures sharing Tm-scores above 0.55. The tree traversal was then skipped to the next non checked tree-bottom leaf.

3D domains were obtained from the PFAM database and up to 3 domains were stored in our database for each *M. tuberculosis* protein. Furthermore, we added data proteomics research to enable the user to compare our findings with proteomics studies. *M. tuberculosis* culture filtrated protein identify after mass spectrometry analysis focused

pI range 4.034.7 and the Mr range 6320 kDa of the 2-DE pattern were added [30] (33 proteins identified), as well two previous studies and more general characterisation after short and long culture from the same group that were previously available on MPIIB web-page (138 and 33 proteins identified). Similar studies with different results were also added [6] (159 and 254 proteins identified). Data from a specific bioinformatics study focused on T7SS was also added [16] (92 proteins identified).

In the context of the host pathogen interaction and immune response perturbation, it is also interesting for the user to be able to compare our data with transcriptomics data obtained during infection. We added two sets of data of genes expressed differentially as a consequence of intraphagosomal residence [31] (compared to broth culture) with or without activation at three time points (4, 24 and 48 h post infection) (Schnappinger2003) and transcription profile of genes expressed during the course of early tuberculosis in immune-competent (BALB/c) and severe combined immune-deficient (SCID) hosts in comparison with growth in medium at three time points (7, 14 and 21 days post infection).

All this computed information was compiled in a global database called SecretoMyc. It is accessible through a web server (http://secretomyc.cbs.cnrs.fr) with a Javascript interface based on W2UI (htt ps://w2ui.com/web/). For easier use, the displayed columns of the global table shown in the server home page can be selected using the dedicated left panel. The protein entries can also be sorted according to each column and a searching form permits the construction of composite queries for selecting protein subsets.

For each *M. tuberculosis* protein, an individual entry was stored in the SecretoMyc

database by compiling the following information:

- Uniprot identifier and accession number, gene name, species name, sequence length, amino acid sequence.

- Links to complementary databases Uniprot (https://www.uniprot. org/), TBDB (http://tbdb.bu.edu/), Mycobrowser (https://mycobr owser.epfl.ch/), AlphaFold (https://alphafold.ebi.ac.uk/), GO (http://geneontology.org/), EggNog (http://eggnog5.embl.de/), 3Did (https://3did.irbbarcelona.org/), Domine (https://manticore. niehs.nih.gov/cgi-bin/Domine) and String (https://string-db.org/).

- Orthologous proteins detected in the 5 close mycobacteria genomes (*M. bovis*, *M. avium*, *M. marinum*, *M. smegmatis* and *M. abcessus*). The ortholog groups were clustered using the Kclust program [32].

- Alignment of all orthologs built using the multiple sequence alignment program MAFFT [33].

- Secretion pathway and transmembrane annotations are summarized in global <Location= table listing all ortholog predictions.

- Similar SCOP domains and Alphafold models detected for each protein as explained above. The detected pairwise 3D similarities are assessed using the various scores provided by the structural alignment program TM-align (TM-score, RMS deviation, Sequence identity percentage, Alignment length).

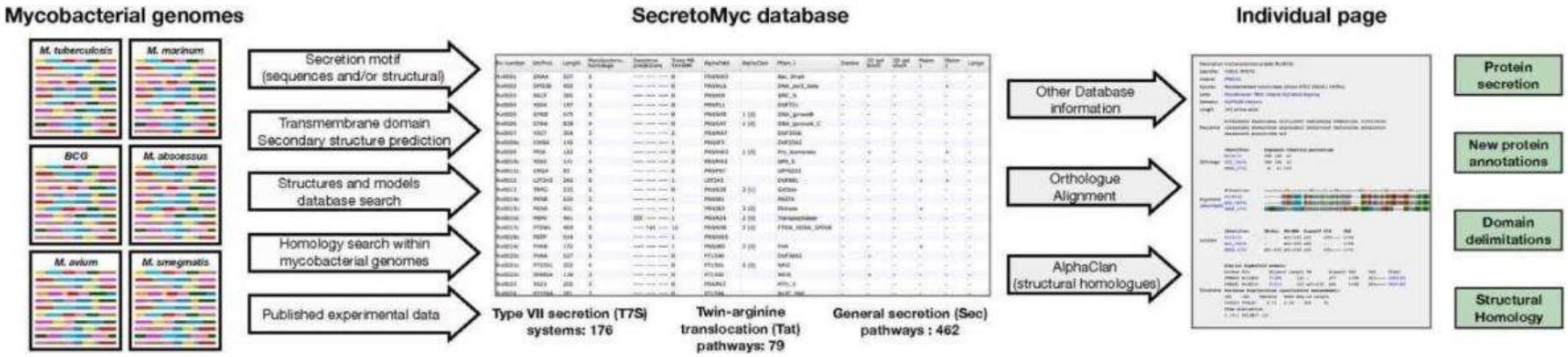

Figure IV.2. Flowchart of the workflow used to generate the SecretoMyc database.

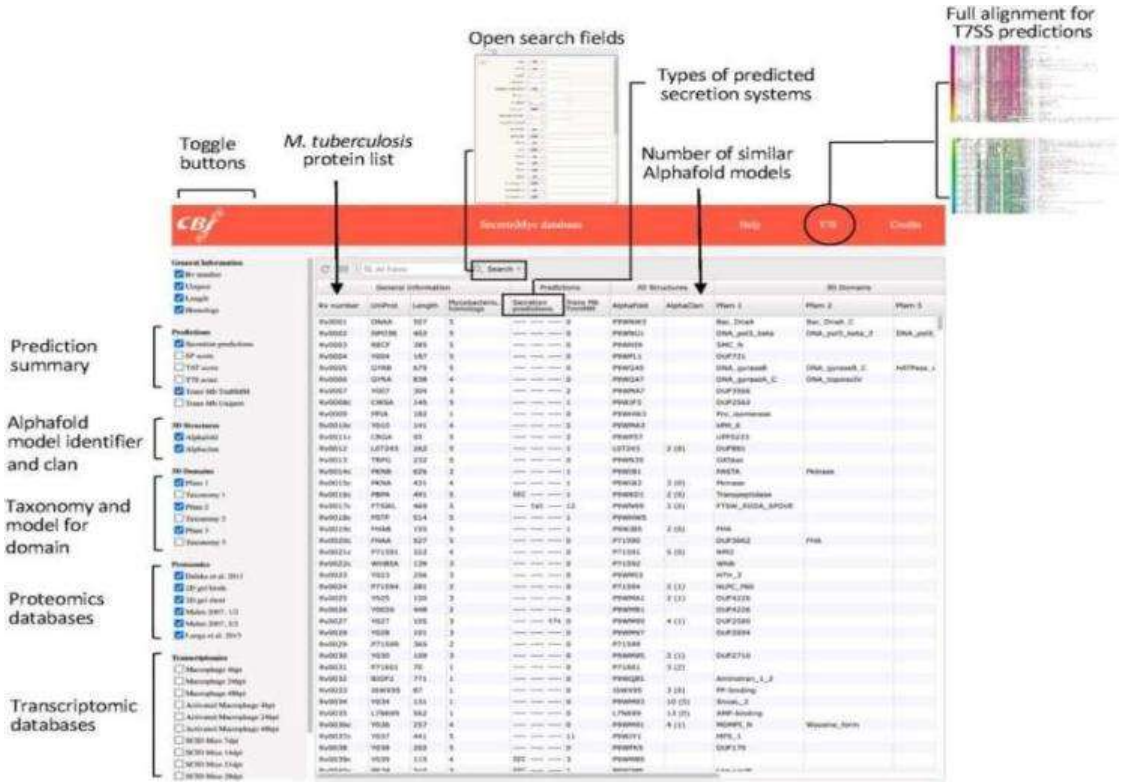

Figure IV.3. The home page of the web server that provides access to the SecretoMyc prediction database is an interactive analysis toolkit. The home page displays the all *M. tuberculosis* proteome with quick access to essentials information: Secretion prediction, taxonomy and domain identification, structural homolog using the AlphaClan tool and homologues within other mycobacterial genomes (*M.Marinum, M.bovis, M.abscessus, M.avium, and M.smegmatis*) as well as results from proteomics and transcriptomics studies. The columns are sortable, and the user can utilize an open search field to select a portion of the secretome based on one or multiple criteria from the available cross-referenced information. The categorization of secretion predictions is as follows: SEC = probable signal peptide predicted by SignalP4.1(score>50); sec = possible signal peptide predicted by SignalP4.1 (score>45); TAT = probable twin arginine signal predicted by PredTAT server (score>90); tat = possible twin arginine signal predicted by PredTAT server (score>0); T7S = probable T7S pathway, t7s = possible T7S pathway.

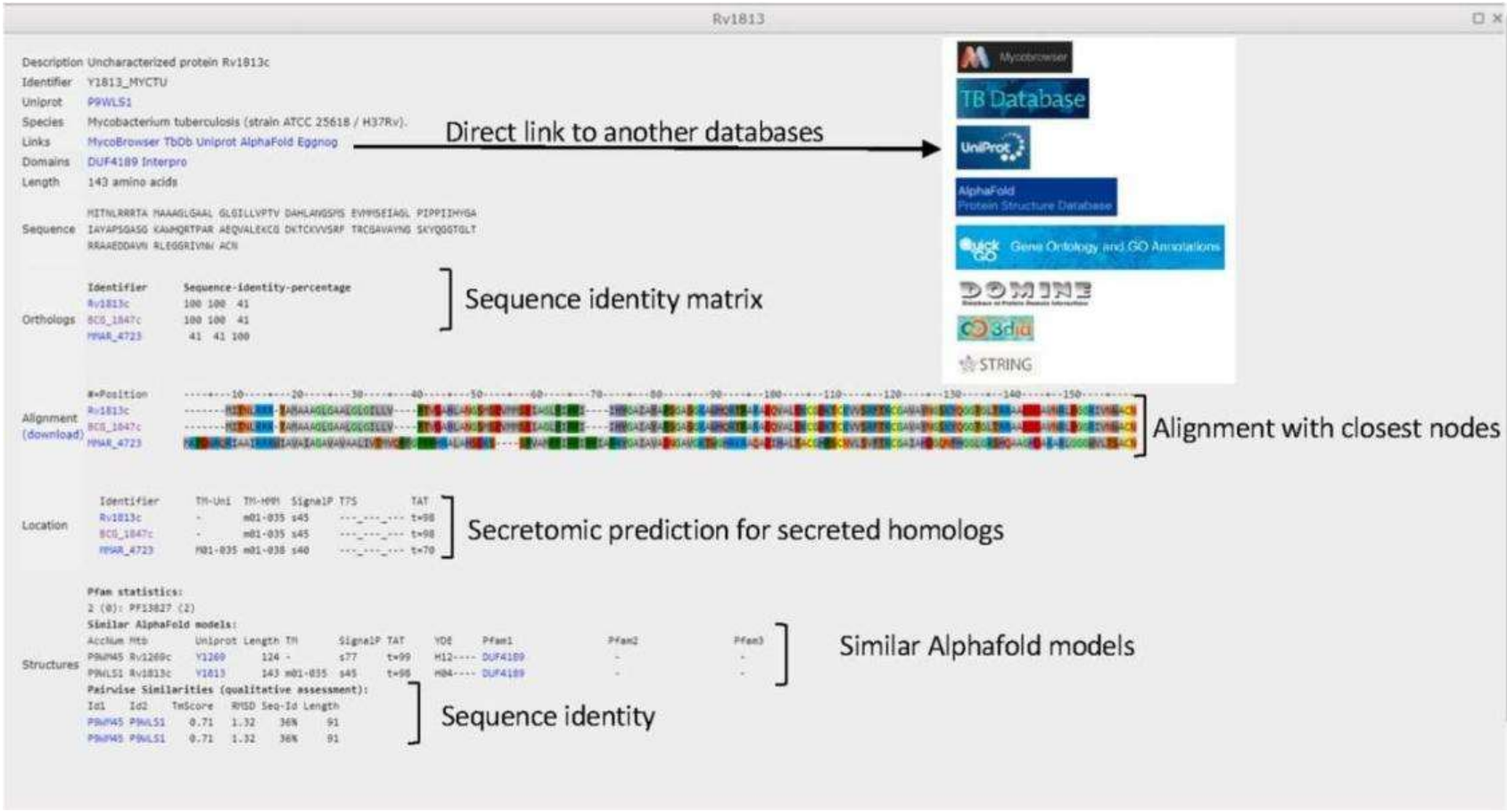

Figure IV.4. Clicking on a corresponding line from the homepage will lead to a protein page that contains all available information about the protein, including a description and direct links to major protein databases, protein sequence, protein homolog identity matrix and alignments, secretion predictions for all homologues, and structural homology prediction using Alphaclan

IV.2.3. References of the article

[1] Pai M, Behr MA, Dowdy D, Dheda K, Divangahi M, Boehme CC, Ginsberg A, Swaminathan S, Spigelman M, Getahun H, et al. Tuberculosis. Nat Rev Dis Primers 2016;2:1323. https://doi.org/10.1038/nrdp.2016.76.

[2] Kostakioti M, Newman CL, Thanassi DG, Stathopoulos C. Mechanisms of protein export across the bacterial outer membrane. J Bacteriol 2005;187:43063 14. https://doi.org/10.1128/JB.187.13.4306-4314.2005.

[3] Maffei B, Francetic O, Subtil A. Tracking proteins secreted by bacteria: what9s in the toolbox? Front Cell Infect Microbiol 2017;7:221. https://doi.org/10.3389/ fcimb.2017.00221.

[4] Perkowski EF, Zulauf KE, Weerakoon D, Hayden JD, Ioerger TR, Oreper D, Gomez SM, Sacchettini JC, Braunstein M. The EXIT strategy: an approach for identifying bacterial proteins exported during host infection. mBio 2017;8. https:// doi.org/10.1128/mBio.00333-17.

[5] Heidtman M, Chen EJ, Moy M-Y, Isberg RR. Large scale identification of Legionella pneumophila Dot/Icm substrates that modulate host cell vesicle trafficking pathways. Cell Microbiol 2009;11:230348. https://doi.org/10.1111/j.1462- 5822.2008.01249.x.

[6] Målen H, Berven FS, Fladmark KE, Wiker HG. Comprehensive analysis of exported proteins from Mycobacterium tuberculosis H37Rv. Proteomics 2007;7:1702318. https://doi.org/10.1002/pmic.200600853.

[7] de Souza GA, Leversen NA, Målen H, Wiker HG. Bacterial proteins with cleaved or uncleaved signal peptides of the general secretory pathway. J Proteonomics 2011; 75:502310. https://doi.org/10.1016/j.jprot.2011.08.016.

[8] Albrethsen J, Agner J, Piersma SR, Højrup P, Pham TV, Weldingh K, Jimenez CR, Andersen P, Rosenkrands I. Proteomic profiling of Mycobacterium tuberculosis identifies nutrient-starvation-responsive toxin-antitoxin systems. Mol Cell Proteomics 2013;12:1180391. https://doi.org/10.1074/mcp.M112.018846.

[9] Penn BH, Netter Z, Johnson JR, Von Dollen J, Jang GM, Johnson T, Ohol YM, Maher C, Bell SL, Geiger K, et al. An mtb-human protein-protein interaction map identifies a switch between host antiviral and antibacterial responses. Mol Cell 2018;71:637348. https://doi.org/10.1016/j.molcel.2018.07.010. e5.

[10] Feltcher ME, Sullivan JT, Braunstein M. Protein export systems of Mycobacterium tuberculosis: novel targets for drug development? Future Microbiol 2010;5: 1581397. https://doi.org/10.2217/fmb.10.112.

[11] McDonough JA, Hacker KE, Flores AR, Pavelka Jr MS, Braunstein M. The twin-arginine translocation pathway of *Mycobacterium smegmatis* is functional and

required for the export of mycobacterial beta-lactamases. J Bacteriol 2005 Nov;187 (22):7667379. https://doi.org/10.1128/JB.187.22.7667-7679.2005.

[12] Saint-Joanis B, Demangel C, Jackson M, Brodin P, Marsollier L, Boshoff H, Cole ST. Inactivation of Rv2525c, a substrate of the twin arginine translocation (Tat) system of *Mycobacterium tuberculosis*, increases beta-lactam susceptibility and virulence. J Bacteriol 2006 Sep;188(18):6669379. https://doi.org/10.1128/JB.00631-.

[13] Braunstein M, Brown AM, Kurtz S, Jacobs Jr WR. Two nonredundant SecA homologues function in mycobacteria. J Bacteriol 2001 Dec;183(24):6979390. 0.1128/JB.183.24.6979-6990.2001.

[14] Vaziri F, Brosch R. ESX/Type VII secretion systems-an important way out for mycobacterial proteins. Microbiol Spectr 2019;7. https://doi.org/10.1128/microbiolspec.PSIB-0029-2019.

[15] Pallen MJ, Chaudhuri RR, Henderson IR. Genomic analysis of secretion systems. Curr Opin Microbiol 2003;6:519327. https://doi.org/10.1016/j.mib.2003.09.005.

[16] Daleke MH, Ummels R, Bawono P, Heringa J, Vandenbroucke-Grauls CMJE, Luirink J, Bitter W. General secretion signal for the mycobacterial type VII secretion pathway. Proc Natl Acad Sci U S A 2012;109:1134237. https://doi.org/10.1073/pnas.1119453109.

[17] Crosskey TD, Beckham KSH, Wilmanns M. The ATPases of the mycobacterial type VII secretion system: structural and mechanistic insights in secretion. Prog Biophys Mol Biol 2020;152:25334. https://doi.org/10.1016/j.pbiomolbio.2019.11.008.

[18] Gracy J, Chiche L. PAT: a protein analysis toolkit for integrated biocomputing on the web. Nucleic Acids Res 2005;33:W65371. https://doi.org/10.1093/nar/gki455.

[19] Nielsen H. Predicting secretory proteins with SignalP. Methods Mol Biol 2017; 1611:59373. https://doi.org/10.1007/978-1-4939-7015-5_6.

[20] Bagos PG, Nikolaou EP, Liakopoulos TD, Tsirigos KD. Combined prediction of Tat and Sec signal peptides with hidden Markov models. Bioinformatics 2010;26: 281137. https://doi.org/10.1093/bioinformatics/btq530.

[21] Krogh A, Larsson B, von Heijne G, Sonnhammer EL. Predicting transmembrane protein topology with a hidden Markov model: application to complete genomes. J Mol Biol 2001;305:567380. https://doi.org/10.1006/jmbi.2000.4315.

[22] Jumper J, Evans R, Pritzel A, Green T, Figurnov M, Ronneberger O, Tunyasuvunakool K, Bates R, Zˇídek A, Potapenko A, et al. Highly accurate protein

structure prediction with AlphaFold. Nature 2021;596:58339. https://doi.org/10.1038/s41586-021-03819-2.

[23] Andreeva A, Howorth D, Chothia C, Kulesha E, Murzin AG. SCOP2 prototype: a new approach to protein structure mining. Nucleic Acids Res 2014;42:D3103 4. https://doi.org/10.1093/nar/gkt1242.

[24] Zhang Y, Skolnick J. TM-align: a protein structure alignment algorithm based on the TM-score. Nucleic Acids Res 2005;33:230239. https://doi.org/10.1093/nar/ gki524.

[25] Consortium UniProt. UniProt: the universal protein knowledgebase in 2021. Nucleic Acids Res 2021;49:D48039. https://doi.org/10.1093/nar/gkaa1100.

[26] Lew JM, Kapopoulou A, Jones LM, Cole ST. TubercuList310 years after. Tuberculosis 2011;91:137. https://doi.org/10.1016/j.tube.2010.09.008.

[27] Pfam: the protein families database in 2021 - PubMed. https://pubmed.ncbi.nlm.nih.gov/33125078/.

[28] Szklarczyk D, Gable AL, Nastou KC, Lyon D, Kirsch R, Pyysalo S, Doncheva NT, Legeay M, Fang T, Bork P, et al. The STRING database in 2021: customizable protein-protein networks, and functional characterization of user-uploaded gene/ measurement sets. Nucleic Acids Res 2021;49:D605312. https://doi.org/10.1093/ nar/gkaa1074.

[29] Anoosha P, Sakthivel R, Gromiha MM. Prediction of protein disorder on amino acid substitutions. Anal Biochem 2015;491:18322. https://doi.org/10.1016/j.ab.2015.08.028.

[30] Lange S, Rosenkrands I, Stein R, Andersen P, Kaufmann SHE, Jungblut PR. Analysis of protein species differentiation among mycobacterial low-Mr-secreted proteins by narrow pH range Immobiline gel 2-DE-MALDI-MS. J Proteonomics 2014;97: 235344. https://doi.org/10.1016/j.jprot.2013.06.036.

[31] Talaat AM, Lyons R, Howard ST, Johnston SA. The temporal expression profile of Mycobacterium tuberculosis infection in mice. Proc Natl Acad Sci USA 2004;101: 460237. https://doi.org/10.1073/pnas.0306023101.

[32] Hauser M, Mayer CE, So¨ding J. kClust: fast and sensitive clustering of large protein sequence databases. BMC Bioinf 2013;14:248. https://doi.org/10.1186/1471- 2105-14-248.

[33] MAFFT: a novel method for rapid multiple sequence alignment based on fast Fourier transform - PubMed. https://pubmed.ncbi.nlm.nih.gov/12136088/.

Chapter V

Integrated discussion

V.1. Discussion and conclusions

Mtb remains a critical public health challenge, particularly in regions with high rates of drug-resistant TB such as Peru, where cases of RR-TB increased by 80.7% between 2021 and 2022 (CDC MINSA, 2023). Despite the global reduction in MDR-TB, resistance to RIF 4a cornerstone of TB treatment4remains alarmingly prevalent, with the *rpoB* gene mutations accounting for 96.1% of RR-TB cases in this study. This is notably higher than global estimates (Su et al., 2023; Walker et al., 2022) and highlights the need for a comprehensive understanding of both canonical and alternative mechanisms of resistance in order to refine treatment strategies.

Genomic complexity of heteroresistance and mixed infections

Our findings underscore the genomic complexity inherent in heteroresistance, where diverse subpopulations within a single host can exhibit varying levels of drug susceptibility. Heteroresistance complicates both the diagnosis and treatment of TB, as traditional phenotypic tests may fail to detect minor resistant subpopulations, especially in high-burden areas. In our study, we observed heteroresistance in 3.8% of isolates, consistent with global reports that range widely from 0.4% to 57% (Nkatha Micheni et al., 2022; Tarashi et al., 2017). This phenomenon was particularly prevalent in Lineage 4 (Euro-American) strains, which represented 91.3% of RIF-heteroresistant cases. Given the high mutation rates observed in Lineage 2 (East Asian), these findings emphasize the need for a lineage-specific approach to TB management, where understanding the genetic and phenotypic nuances within Mtb lineages can help tailor

effective therapies (Merker et al., 2015; Phyu et al., 2022).

Furthermore, mixed infections present additional challenges, as they may contribute to treatment failures when resistant subpopulations go undetected. Our study demonstrates that traditional diagnostic methods often fall short in identifying mixed infections, necessitating the use of advanced bioinformatic tools capable of deconvoluting these complex genomic landscapes (Barletta et al., 2015). Detecting heteroresistant strains and mixed infections with high precision is crucial for improving TB treatment outcomes and limiting the spread of drug resistance.

For future studies, it would be important to consider the complexity of TB infections, which is further exacerbated by phenotypic variations within bacterial populations, such as persistence and tolerance. These phenomena can contribute to treatment failure and the emergence of drug resistance. While mixed infections involve genetically distinct subpopulations, phenotypic resistance mechanisms arise within clonal populations, allowing certain bacteria to survive antibiotic exposure without acquiring genetic mutations. These transient, non-heritable adaptations can prolong bacterial survival during treatment, complicating disease management. A comprehensive understanding of these mechanisms, alongside genetic resistance, is essential for optimizing TB treatment strategies.

Standard methods for assessing Mtb antibiotic susceptibility, such as the MIC or the determination of the minimum duration required to eliminate 99% of the bacterial population, assume homogeneous bacterial populations. However, when heterogeneity

is present, these parameters may not accurately reflect bacterial growth and death dynamics, as subpopulations can respond differentially to antibiotics (Balaban et al., 2019). Beyond heteroresistance, persistent and tolerant bacterial populations present additional challenges to TB treatment. These phenomena not only hinder complete bacterial clearance but may also drive the emergence of MDR strains through mechanisms similar to those of heteroresistance.

Bacterial persistence is characterized by the presence of a subpopulation within a clonal culture that is not eliminated at the same rate as the majority of the cells due to a transiently increased tolerance to antibiotics (Boldrin et al., 2020). A key feature of persistent cells is that once they resume growth in the absence of antibiotics, their progeny exhibits susceptibility similar that of the original population. This contrasts with resistant cells, which continue to replicate in the presence of the drug (Balaban et al., 2019). Similarly, bacterial tolerance, which- like persistence-does not increase the MIC, depends on both genetic and environmental factors (Balaban et al., 2019; Brauner et al., 2016). The molecular mechanism underlying tolerance includes metabolic changes (Torrey et al., 2016) and processes that promote population heterogeneity (Ackermann, 2015).

Furthermore, RIF exposure has been shown to induce RpoB expression in subpopulations, though this phenotype is transient and disappears after prolonged cultivation (16 hours or more) in the absence of the drug (Zhu et al., 2018). Given these factors, it is crucial to recognize that heritable resistance, phenotypic resistance, and tolerance all contribute to RIF treatment failure. Understanding the interplay

between these mechanisms could inform the development of more effective therapeutic strategies, ultimately improving antibiotic efficacy and reducing treatment duration (Adams et al., 2021).

Structural insights into ponA1 and the utility of *M. marinum* as a model system.

PonA1, a bifunctional enzyme with TG and TP domains, plays an essential role in the synthesis of PG and is known to influence cell morphology in mycobacteria. The utility of Mmar as a model organism for studying Mtb pathogenesis is underscored by its phylogenetic proximity to Mtb, sharing approximately 3000 orthologous genes with an average amino acid identity of 85% (Stinear et al., 2008; Zhu & Dai, 2018). Mmar's slower growth rate and capacity to aggregate *in vitro* provide a viable alternative for investigating TB-related mechanisms without the need for biosafety level 3 containment facilities (El-Etr et al., 2004; Tobin & Ramakrishnan, 2008).

In our study, the structural and functional implications of wild-type PonA1 and its mutants were explored using Mmar. Notably, our findings reveal that PonA1 mutants such as Q365H and P631S did not exhibit significant binding affinity to RIF, as demonstrated through molecular docking and dynamics studies with DiffDock (Corso et al., 2022). These results suggest that PonA19s influence on RIF resistance is likely indirect, potentially altering cell wall properties or compensating for fitness losses associated with other resistance mechanisms (Filippova et al., 2016; Kurepina et al., 2022).

Additionally, the deletion of the homologous *MMAR_0069* gene in Mmar did not

significantly impair cell growth, suggesting functional redundancy where other PBPs, such as PonA2, might compensate for the loss of PonA1 (Kieser, Baranowski, et al., 2015). The integration of Mtb H37Rv PonA1 into Mmar resulted in a marked increase in cell length, pointing to its role in regulating cell morphology and potential contributions to antibiotic tolerance under selective pressure (Hett et al., 2010). While PonA1 interactions with RIF appear weak, mutations in PonA1 may impact RIF tolerance, warranting further investigation into its role in heteroresistance and its regulatory mechanisms.

The secretome of *M. tuberculosis* and host-pathogen interactions

A comprehensive understanding of Mtb's secretome is essential for elucidating its pathogenicity, as secreted proteins are integral to host immune modulation and bacterial virulence. By leveraging bioinformatics tools, our study mapped Mtb9s secretome across three major secretion pathways (SEC, TAT, and T7SS), identifying 176 T7SS, 79 TAT, and 462 SEC proteins that likely contribute to the bacterium's ability to evade host immune responses and sustain long-term infections. This secretome data is now available in the SecretoMyc database, which serves as a resource for linking genomic data with functional and structural protein predictions (https://secretomyc.cbs.cnrs.fr).

The integration of AlphaFold models into our analysis enabled us to identify structural homologues among mycobacterial proteins, providing insights into how these proteins may contribute to Mtb's virulence. In particular, proteins secreted

through the T7SS pathway are implicated in immune evasion and modulation of host cell responses, emphasizing their potential as targets for vaccine and drug development (Sauvage et al., 2008). These findings underscore the importance of structural biology in understanding the functional implications of Mtb9s secreted proteins, which are critical to the pathogen's survival and persistence within the host.

Integrating findings across the thesis

This thesis highlights the complex interplay between Mtb's genetic diversity, structural protein functionality, and its interactions with the host. The identification of heteroresistant subpopulations and their varying resistance mechanisms illustrate the adaptive resilience of Mtb to antibiotic pressure. Additionally, our work with PonA1 highlights how structural mutations at the protein level can influence antibiotic interactions and bacterial morphology, while our exploration of Mtb9s secretome reveals the extensive network of secreted proteins involved in modulating host-pathogen interactions.

The insights gained from this integrated approach underscore the importance of addressing TB treatment from multiple angles, including genomic, structural, and functional perspectives. By combining these elements, we can better understand the pathways through which Mtb develops drug resistance and how it manipulates the host immune environment to enhance its survival. These findings not only provide valuable information for developing targeted therapies but also open new avenues for diagnostic and vaccine strategies that address the multifaceted challenges posed by this pathogen.

V.2. Limitations

In Chapter Two, our study focused on detecting heteroresistant populations using the agar proportion method, which is recognized as the gold standard for identifying even 1% of a population with distinct drug susceptibility profiles. While WGS provides valuable data more quickly and across a broader range of antibiotics, it is limited by bioinformatic techniques that cannot reliably detect subpopulations constituting less than 10% of the total bacterial population. This limitation suggests that some primary isolates with lower abundance heteroresistant populations may go undetected, potentially leading to an underestimation of the actual percentage of heteroresistance. Additionally, the current approach excludes microheteroresistance populations, defined as those comprising less than 5% of the total population. Advancing bioinformatic pipelines to detect such low-abundance populations would be critical for improving diagnostic accuracy and, consequently, for optimizing treatment strategies and limiting the spread of multi-drug-resistant strains.

In Chapter Three, the *in silico* analysis could be expanded by including additional replicates to capture a more diverse range of conformational states. This would enable a more thorough representation of the protein-ligand interaction dynamics, potentially yielding a more accurate consensus on binding affinities and conformational stability. Additionally, the Q365H mutation in *ponA1* has been reported to confer RIF resistance at subinhibitory concentrations (0.00125 µg/mL), which are significantly lower than those employed in this study (0.5 µg/mL). Future experiments at varying drug concentrations could offer insight into whether *ponA1* mutations confer resistance

differentially across a range of RIF levels, potentially elucidating threshold effects relevant to treatment efficacy.

Further research into the differential expression of *ponA1* across various growth stages is essential for understanding its possible relationship to antibiotic resistance, specifically RIF resistance. Analyzing *ponA1* expression during different growth phases, such as the exponential and stationary phases, could identify periods of upregulated expression in response to subinhibitory RIF concentrations or other stress conditions. This analysis could determine whether *ponA1* contributes to resistance mechanisms either through its role in cell wall synthesis or through indirect interactions with RIF. Additionally, it could reveal whether morphological changes, such as increases in cell length and thickness, correlate with elevated *ponA1* expression levels in response to antibiotic exposure, as suggested by previous studies on mutations like A516T and P631S. Techniques such as RT-qPCR or RNA-Seq could be employed to quantify *ponA1* transcription throughout the growth cycle and under various antibiotic stress conditions, offering a deeper understanding of its regulatory dynamics.

Finally, while this thesis provides significant insights into the complex interactions between Mtb proteins and RIF, there are inherent limitations related to the choice of the Mmar model, which, although phylogenetically similar, may not fully replicate the pathophysiological conditions of Mtb infections in humans. Future studies could benefit from complementing Mmar data with studies on human-derived cell lines or *in vivo* models, allowing for a more comprehensive evaluation of PonA19s role in RIF resistance. Furthermore, additional structural and biochemical analyses focusing

on other cell wall-associated proteins could provide a broader understanding of Mtb9s resistance mechanisms and the potential interplay between various PBPs.

V.3. Perspectives

In Chapter Two, our whole-genome analysis of primary isolates from TB patients revealed the presence of heteroresistant populations to RIF, with variable proportions of *rpoB* SNPs identified in each sample. This discovery was further supported by a pilot study that isolated up to four distinct strains from a single sample, indicating that both resistant and sensitive populations can coexist within the same patient. This finding underscores the urgent need for diagnostic methods capable of detecting these heteroresistant populations directly from sputum samples or within a minimal timeframe to ensure precise diagnosis and effective treatment. Future research could explore the development of rapid, point-of-care diagnostic tools that detect such mixed infections in clinical samples, leveraging next-generation sequencing or single-cell technologies to enhance early detection.

Chapter Three revealed that the deletion of *MMAR_0069* in Mmar did not significantly affect cell growth under *in vitro* conditions, aligning with previous findings regarding *ponA1* deletion in Mtb. However, it remains to be determined whether, similar to what has been observed in *Mtb*, this deletion might lead to attenuation in a murine infection model, as noted by Kieser et al. (2015). This opens up the potential for using Mmar as a model to study pathogenicity and host-pathogen interactions associated with cell wall modifications resulting from gene deletions,

offering a controlled and safer experimental environment. Further *in vivo* studies could help determine whether these cell wall alterations impact virulence, which could inform the development of new therapeutic targets aimed at disrupting cell wall synthesis in pathogenic mycobacteria.

Additionally, with the rising incidence of MDR-TB, strains complemented with *ponA1* from *Mtb* H37Rv could be used to evaluate β-lactam antibiotics in conjunction with BlaC inhibitors, potentially expanding the arsenal of effective drugs against TB, as suggested by Filippova et al. (2015). Moreover, the protocol established for recombinant PonA1 expression could be employed in *in vitro* assays to screen new antibiotic candidates, assessing their antimicrobial efficacy and binding energies through advanced biophysical techniques like Surface Plasmon Resonance (SPR) and Isothermal Titration Calorimetry (ITC).

Our successful use of the ORBIT system for gene KO and complementation via the *pMV361* plasmid at the L5 mycobacteriophage integration site illustrates a highly specific and efficient approach to generating mycobacterial mutants. This methodology significantly streamlines genetic studies in mycobacteria, allowing for rapid generation of KO strains and gene complementation. Future work could refine this process further, exploring the potential of multiplexed ORBIT systems to KO multiple genes simultaneously, facilitating comprehensive studies of gene interactions and compensatory mechanisms in mycobacterial pathogenesis.

Expanding upon this, future research could also explore the potential of

combining ORBIT with CRISPR interference (CRISPRi) systems to achieve gene silencing in a reversible manner. This approach would enable temporal control of gene expression, allowing for a deeper investigation into the dynamic roles of key genes like *ponA1* throughout various stages of mycobacterial growth and infection. Furthermore, the development of inducible KO systems could facilitate the study of essential genes, which are difficult to analyze using conventional gene KO methods.

In terms of exploring the mycobacterial secretome, there is significant potential for expanding the bioinformatics pipeline to include predictive modeling of protein-protein interactions within the host. By integrating proteomics data with host immune response profiles, future studies could identify novel vaccine candidates and drug targets that disrupt critical interactions between secreted proteins and host cells. Additionally, future work could involve the application of machine learning algorithms to analyze large-scale transcriptomic and proteomic data, potentially uncovering new regulatory networks that govern protein secretion and virulence in Mtb.

Finally, as we continue to identify and characterize the role of heteroresistant and mixed infections in TB treatment outcomes, expanding our understanding of how these populations evolve in response to different drug regimens would be highly beneficial. Longitudinal studies following patients over the course of treatment could provide insights into the dynamics of heteroresistant populations and their potential to acquire further mutations, which could inform the design of more adaptive and personalized treatment protocols.

In summary, the findings from this thesis prepare the way for several promising avenues of research, from refining diagnostic tools and exploring alternative models for studying mycobacterial pathogenicity to advancing genetic manipulation techniques and leveraging bioinformatics for therapeutic discovery. By addressing these perspectives, future studies could significantly enhance our ability to diagnose, treat, and ultimately prevent TB.

Bibliography

1. Abakur, E. H. A., Alnour, T. M. S., Abuduhier, F., Albalawi, F. M. A., & Alfifi, K. A. S. (2020). Emergence of Heteroresistance Mycobacterium Tuberculosis in Saudi Arabia. *Infectious Disorders - Drug Targets*, *20*(4), 4913494. https://doi.org/10.2174/1871526519666190326141550
2. Abdallah, A. M., Gey van Pittius, N. C., DiGiuseppe Champion, P. A., Cox, J., Luirink, J., Vandenbroucke-Grauls, C. M. J. E., Appelmelk, B. J., & Bitter, W. (2007). Type VII secretion 4 mycobacteria show the way. *Nature Reviews Microbiology*, *5*(11), 8833891. https://doi.org/10.1038/nrmicro1773
3. Ackermann, M. (2015). A functional perspective on phenotypic heterogeneity in microorganisms. *Nature Reviews Microbiology*, *13*(8), 4973508. https://doi.org/10.1038/nrmicro3491
4. Adams, R.A., Leon, G., Miller, N.M. et al. Rifamycin antibiotics and the mechanisms of their failure. J Antibiot 74, 7863798 (2021). https://doi.org/10.1038/s41429-021-00462-x
5. Alifano, P., Palumbo, C., Pasanisi, D., & Talà, A. (2015). Rifampicin-resistance, rpoB polymorphism and RNA polymerase genetic engineering. *Journal of Biotechnology*, *202*, 60377. https://doi.org/10.1016/j.jbiotec.2014.11.024
6. Andersson, D. I., Nicoloff, H., & Hjort, K. (2019). Mechanisms and clinical relevance of bacterial heteroresistance. *Nature Reviews Microbiology*, *17*(8), 4793496. https://doi.org/10.1038/s41579-019-0218-1
7. Andre, E., Goeminne, L., Cabibbe, A., Beckert, P., Kabamba Mukadi, B., Mathys, V., Gagneux, S., Niemann, S., Van Ingen, J., & Cambau, E. (2017). Consensus numbering system for the rifampicin resistance-associated rpoB gene mutations in pathogenic mycobacteria. *Clinical Microbiology and Infection*, *23*(3), 1673172. https://doi.org/10.1016/j.cmi.2016.09.006
8. Angulo, J., & Nieto, P. M. (2011). STD-NMR: application to transient interactions between biomolecules4a quantitative approach. *European Biophysics Journal*, *40*(12), 135731369. https://doi.org/10.1007/s00249-011-0749-5
9. Armianinova, D. K., Karpov, D. S., Kotliarova, M. S., & Goncharenko, A. V. (2022). Genetic Engineering in Mycobacteria. *Molecular Biology*, *56*(6), 8303 841. https://doi.org/10.1134/S0026893322060036
10. Artsimovitch, I., Vassylyeva, M. N., Svetlov, D., Svetlov, V., Perederina, A., Igarashi, N., Matsugaki, N., Wakatsuki, S., Tahirov, T. H., & Vassylyev, D. G. (2005). Allosteric Modulation of the RNA Polymerase Catalytic Reaction Is an Essential Component of Transcription Control by Rifamycins. *Cell*, *122*(3), 3513 363. https://doi.org/10.1016/j.cell.2005.07.014
11. Ates, L. S., van der Woude, A. D., Bestebroer, J., van Stempvoort, G., Musters, R. J. P., Garcia-Vallejo, J. J., Picavet, D. I., Weerd, R. van de, Maletta, M., Kuijl, C. P., van der Wel, N. N., & Bitter, W. (2016). The ESX-5 System of Pathogenic Mycobacteria Is Involved In Capsule Integrity and Virulence through Its Substrate PPE10. *PLOS Pathogens*, *12*(6), e1005696. https://doi.org/10.1371/journal.ppat.1005696
12. Aubry, A., Jarlier, V., Escolano, S., Truffot-Pernot, C., & Cambau, E. (2000). Antibiotic Susceptibility Pattern of *Mycobacterium marinum*. *Antimicrobial*

Agents and Chemotherapy, *44*(11), 313333136. https://doi.org/10.1128/AAC.44.11.3133-3136.2000
13. Aubry, A., Mougari, F., Reibel, F., & Cambau, E. (2017). *Mycobacterium marinum*. *Microbiology Spectrum*, *5*(2). https://doi.org/10.1128/microbiolspec.TNMI7-0038-2016
14. Bachmann, N. L., Salamzade, R., Manson, A. L., Whittington, R., Sintchenko, V., Earl, A. M., & Marais, B. J. (2020). Key Transitions in the Evolution of Rapid and Slow Growing Mycobacteria Identified by Comparative Genomics. *Frontiers in Microbiology*, *10*. https://doi.org/10.3389/fmicb.2019.03019
15. Bagheri, Y., Ali, A. A., & You, M. (2020). Current Methods for Detecting Cell Membrane Transient Interactions. *Frontiers in Chemistry*, *8*. https://doi.org/10.3389/fchem.2020.603259
16. Balaban, N. Q., Helaine, S., Lewis, K., Ackermann, M., Aldridge, B., Andersson, D. I., Brynildsen, M. P., Bumann, D., Camilli, A., Collins, J. J., Dehio, C., Fortune, S., Ghigo, J.-M., Hardt, W.-D., Harms, A., Heinemann, M., Hung, D. T., Jenal, U., Levin, B. R., … Zinkernagel, A. (2019). Definitions and guidelines for research on antibiotic persistence. *Nature Reviews Microbiology*, *17*(7), 4413 448. https://doi.org/10.1038/s41579-019-0196-3
17. Barletta, F., Otero, L., de Jong, B. C., Iwamoto, T., Arikawa, K., Van der Stuyft, P., Niemann, S., Merker, M., Uwizeye, C., Seas, C., & Rigouts, L. (2015). Predominant Mycobacterium tuberculosis Families and High Rates of Recent Transmission among New Cases Are Not Associated with Primary Multidrug Resistance in Lima, Peru. *Journal of Clinical Microbiology*, *53*(6), 185431863. https://doi.org/10.1128/JCM.03585-14
18. Barry, C. E., Boshoff, H., Dartois, V., Dick, T., Ehrt, S., Flynn, J., Schnappinger, D., Wilkinson, R. J., & Young, D. (2009). The spectrum of latent tuberculosis: rethinking the goals of prophylaxis. *Nat Rev Microbiol*, *7*(12), 8453855. https://doi.org/10.1038/nrmicro2236
19. Basavannacharya, C., Robertson, G., Munshi, T., Keep, N. H., & Bhakta, S. (2010). ATP-dependent MurE ligase in Mycobacterium tuberculosis: Biochemical and structural characterisation. *Tuberculosis*, *90*(1), 16324. https://doi.org/10.1016/j.tube.2009.10.007
20. Beltrame S, Latorraca M, & Moral M. (2014). *Enfermedades infecciosas-Tuberculosis*. https://bancos.salud.gob.ar/sites/default/files/2018-10/0000000049cnt-guia_de_diagnostico_tratamiento_y_prevencion_de_la_tuberculosis_2015.pdf
21. Benson, T. E., Walsh, C. T., & Hogle, J. M. (1996). The structure of the substrate-free form of MurB, an essential enzyme for the synthesis of bacterial cell walls. *Structure*, *4*(1), 47354. https://doi.org/10.1016/S0969-2126(96)00008-1
22. Bentley, S. D., Comas, I., Bryant, J. M., Walker, D., Smith, N. H., Harris, S. R., Thurston, S., Gagneux, S., Wood, J., Antonio, M., Quail, M. A., Gehre, F., Adegbola, R. A., Parkhill, J., & de Jong, B. C. (2012). The Genome of Mycobacterium Africanum West African 2 Reveals a Lineage-Specific Locus and Genome Erosion Common to the M. tuberculosis Complex. *PLoS Neglected Tropical Diseases*, *6*(2), e1552. https://doi.org/10.1371/journal.pntd.0001552

23. Berridge, M. V., Herst, P. M., & Tan, A. S. (2005). *Tetrazolium dyes as tools in cell biology: New insights into their cellular reduction* (pp. 1273152). https://doi.org/10.1016/S1387-2656(05)11004-7
24. Bespiatykh, D., Bespyatykh, J., Mokrousov, I., & Shitikov, E. (2021). A Comprehensive Map of Mycobacterium tuberculosis Complex Regions of Difference. *MSphere*, *6*(4). https://doi.org/10.1128/mSphere.00535-21
25. Bhakta, S., & Basu, J. (2002). Overexpression, purification and biochemical characterization of a class A high-molecular-mass penicillin-binding protein (PBP), PBP1∗ and its soluble derivative from Mycobacterium tuberculosis. *Biochemical Journal*, *361*(3), 6353639. https://doi.org/10.1042/bj3610635
26. Biet, F., Boschiroli, M. L., Thorel, M. F., & Guilloteau, L. A. (2005). Zoonotic aspects of *Mycobacterium bovis* and *Mycobacterium avium-intracellulare* complex (MAC). *Veterinary Research*, *36*(3), 4113436. https://doi.org/10.1051/vetres:2005001
27. Bishai, W. (1998). The Mycobacterium tuberculosis genomic sequence: anatomy of a master adaptor. *Trends in Microbiology*, *6*(12), 4643465. https://doi.org/10.1016/S0966-842X(98)01414-0
28. Bisson, G. P., Mehaffy, C., Broeckling, C., Prenni, J., Rifat, D., Lun, D. S., Burgos, M., Weissman, D., Karakousis, P. C., & Dobos, K. (2012). Upregulation of the Phthiocerol Dimycocerosate Biosynthetic Pathway by Rifampin-Resistant, *rpoB* Mutant Mycobacterium tuberculosis. *Journal of Bacteriology*, *194*(23), 644136452. https://doi.org/10.1128/JB.01013-12
29. Blasco, B., Chen, J. M., Hartkoorn, R., Sala, C., Uplekar, S., Rougemont, J., Pojer, F., & Cole, S. T. (2012). Virulence Regulator EspR of Mycobacterium tuberculosis Is a Nucleoid-Associated Protein. *PLoS Pathogens*, *8*(3), e1002621. https://doi.org/10.1371/journal.ppat.1002621
30. Boehme, C. C., Nicol, M. P., Nabeta, P., Michael, J. S., Gotuzzo, E., Tahirli, R., Gler, M. T., Blakemore, R., Worodria, W., Gray, C., Huang, L., Caceres, T., Mehdiyev, R., Raymond, L., Whitelaw, A., Sagadevan, K., Alexander, H., Albert, H., Cobelens, F., … Perkins, M. D. (2011). Feasibility, diagnostic accuracy, and effectiveness of decentralised use of the Xpert MTB/RIF test for diagnosis of tuberculosis and multidrug resistance: a multicentre implementation study. *The Lancet*, *377*(9776), 149531505. https://doi.org/10.1016/S0140-6736(11)60438-8
31. Boldrin, F., Provvedi, R., Cioetto Mazzabò, L., Segafreddo, G., & Manganelli, R. (2020). Tolerance and Persistence to Drugs: A Main Challenge in the Fight Against Mycobacterium tuberculosis. *Frontiers in Microbiology*, *11*. https://doi.org/10.3389/fmicb.2020.01924
32. Bosch, B., DeJesus, M. A., Poulton, N. C., Zhang, W., Engelhart, C. A., Zaveri, A., Lavalette, S., Ruecker, N., Trujillo, C., Wallach, J. B., Li, S., Ehrt, S., Chait, B. T., Schnappinger, D., & Rock, J. M. (2021). Genome-wide gene expression tuning reveals diverse vulnerabilities of M. tuberculosis. *Cell*, *184*(17), 4579-4592.e24. https://doi.org/10.1016/j.cell.2021.06.033
33. Bosserman, R. E., Nicholson, K. R., Champion, M. M., & Champion, P. A. (2019). A New ESX-1 Substrate in Mycobacterium marinum That Is Required

for Hemolysis but Not Host Cell Lysis. *Journal of Bacteriology*, *201*(14). https://doi.org/10.1128/JB.00760-18
34. Bottai, D., & Brosch, R. (2009). Mycobacterial PE, PPE and ESX clusters: novel insights into the secretion of these most unusual protein families. *Molecular Microbiology*, *73*(3), 3253328. https://doi.org/10.1111/j.1365-2958.2009.06784.x
35. Bouhss, A., Mengin-Lecreulx, D., Le Beller, D., & van Heijenoort, J. (1999). Topological analysis of the MraY protein catalysing the first membrane step of peptidoglycan synthesis. *Molecular Microbiology*, *34*(3), 5763585. https://doi.org/10.1046/j.1365-2958.1999.01623.x
36. Brauner, A., Fridman, O., Gefen, O., & Balaban, N. Q. (2016). Distinguishing between resistance, tolerance and persistence to antibiotic treatment. *Nature Reviews Microbiology*, *14*(5), 3203330. https://doi.org/10.1038/nrmicro.2016.34
37. Braunstein, M., Espinosa, B. J., Chan, J., Belisle, J. T., & R. Jacobs, W. (2003). SecA2 functions in the secretion of superoxide dismutase A and in the virulence of *Mycobacterium tuberculosis*. *Molecular Microbiology*, *48*(2), 4533464. https://doi.org/10.1046/j.1365-2958.2003.03438.x
38. Breitsprecher, D., Fung, P. A., & Tschammer, N. (2018). Improving biosensor assay development by determining sample quality with Tycho NT.6. *Nature Methods*, *15*(4), 2983298. https://doi.org/10.1038/nmeth.f.406
39. Broussard, G. W., & Ennis, D. G. (2007). Mycobacterium marinum produces long-term chronic infections in medaka: A new animal model for studying human tuberculosis. *Comparative Biochemistry and Physiology Part C: Toxicology & Pharmacology*, *145*(1), 45354. https://doi.org/10.1016/j.cbpc.2006.07.012
40. Burgos, H. L., O9Connor, K., Sanchez-Vazquez, P., & Gourse, R. L. (2017). Roles of Transcriptional and Translational Control Mechanisms in Regulation of Ribosomal Protein Synthesis in Escherichia coli. *Journal of Bacteriology*, *199*(21). https://doi.org/10.1128/JB.00407-17
41. Campbell, E. A., Korzheva, N., Mustaev, A., Murakami, K., Nair, S., Goldfarb, A., & Darst, S. A. (2001). Structural Mechanism for Rifampicin Inhibition of Bacterial RNA Polymerase. *Cell*, *104*(6), 9013912. https://doi.org/10.1016/S0092-8674(01)00286-0
42. Canetti, G., Froman, S., Grosset, J., Hauduroy, P., Langerova, M., Mahler, H. T., Meissner, G., Mitchison, D. A., & Sula, L. (1963). Mycobacteria: Laboratory Methods For Testing Drug Sensitivity And Resistance. *Bulletin of the World Health Organization*, *29*(5), 5653578.
43. Canetti, G., Rist, N., & Grosset, J. (1963). [Measurement of sensitivity of the tuberculous bacillus to antibacillary drugs by the method of proportions. Methodology, resistance criteria, results and interpretation]. *Revue de Tuberculose et de Pneumologie*, *27*, 2173272.
44. Catipovic, M. A., Bauer, B. W., Loparo, J. J., & Rapoport, T. A. (2019). Protein translocation by the SecA ATPase occurs by a power-stroke mechanism. *The EMBO Journal*, *38*(9). https://doi.org/10.15252/embj.2018101140
45. Caviedes, L., Delgado, J., & Gilman, R. H. (2002). Tetrazolium Microplate Assay as a Rapid and Inexpensive Colorimetric Method for Determination of

Antibiotic Susceptibility of Mycobacterium tuberculosis. *Journal of Clinical Microbiology*, *40*(5), 187331874. https://doi.org/10.1128/JCM.40.5.1873-1874.2002

46. Caviedes, L., Lee, T. S., Gilman, R. H., Sheen, P., Spellman, E., Lee, E. H., Berg, D. E., & Montenegro-James, S. (2000). Rapid, efficient detection and drug susceptibility testing of Mycobacterium tuberculosis in sputum by microscopic observation of broth cultures. The Tuberculosis Working Group in Peru. *Journal of Clinical Microbiology*, *38*(3), 120331208. https://doi.org/10.1128/JCM.38.3.1203-1208.2000
47. CDC MINSA. (2023, May 23). *Boletin epidemiológico*. https://www.dge.gob.pe/epipublic/uploads/boletin/boletin_202320_28_163316.pdf
48. Cepheid. (2020). *Xpert MTB/RIF* . https://www.cepheid.com/content/dam/www-cepheid-com/documents/package-insert-files/Xpert-MTB-RIF-SPANISH-Package-Insert-301-1404-ES-Rev-G.pdf
49. Cepheid. (2024). *Xpert MTB/RIF Ultra*. https://www.cepheid.com/en-GB/tests/tb-emerging-infectious-diseases/xpert-mtb-rif-ultra.html
50. Chandra, P., Grigsby, S. J., & Philips, J. A. (2022). Immune evasion and provocation by Mycobacterium tuberculosis. *Nature Reviews Microbiology*, *20*(12), 7503766. https://doi.org/10.1038/s41579-022-00763-4
51. Chang, Y. H., Labgold, M. R., & Richards, J. H. (1990). Altering enzymatic activity: recruitment of carboxypeptidase activity into an RTEM beta-lactamase/penicillin-binding protein 5 chimera. *Proceedings of the National Academy of Sciences*, *87*(7), 282332827. https://doi.org/10.1073/pnas.87.7.2823
52. Chen, H., He, X., Jiang, H.-W., Zheng, Y.-X., Zhang, H.-N., Wu, F.-L., Xu, Z.-W., Guo, S.-J., & Tao, S.-C. (2024). Elucidating the network interactions between 21 secreted <italic>Mycobacterium tuberculosis</italic> proteins and host proteins: the role of DnaK in enhancing <italic>Mtb</italic> survival via LDHB. *Acta Biochimica et Biophysica Sinica*. https://doi.org/10.3724/abbs.2024041
53. Chengalroyen, M. D., Beukes, G. M., Otwombe, K., Gordhan, B. G., Martinson, N., & Kana, B. (2022). The detection of mixed tuberculosis infections using culture filtrate and resuscitation promoting factor deficient filtrate. *Frontiers in Cellular and Infection Microbiology*, *12*. https://doi.org/10.3389/fcimb.2022.1072073
54. Clark, H. F., & Shepard, C. C. (1963). Effect of environmental temperatures on infection with *Mycobacterium marinum* (balnei) of mice and a number of poikilothermic species. *Journal of Bacteriology*, *86*(5), 105731069. https://doi.org/10.1128/jb.86.5.1057-1069.1963
55. Clay, H., Davis, J. M., Beery, D., Huttenlocher, A., Lyons, S. E., & Ramakrishnan, L. (2007). Dichotomous Role of the Macrophage in Early Mycobacterium marinum Infection of the Zebrafish. *Cell Host & Microbe*, *2*(1), 29339. https://doi.org/10.1016/j.chom.2007.06.004

56. Clinical and Laboratory Standards Institute. (2018). *CLSI supplement M62* (CLSI, Ed.; 1st ed.).
57. Cohen, T., Wilson, D., Wallengren, K., Samuel, E. Y., & Murray, M. (2011). Mixed-Strain *Mycobacterium tuberculosis* Infections among Patients Dying in a Hospital in KwaZulu-Natal, South Africa. *Journal of Clinical Microbiology*, *49*(1), 3853388. https://doi.org/10.1128/JCM.01378-10
58. Cole, S. T., Brosch, R., Parkhill, J., Garnier, T., Churcher, C., Harris, D., Gordon, S. V., Eiglmeier, K., Gas, S., Barry, C. E., Tekaia, F., Badcock, K., Basham, D., Brown, D., Chillingworth, T., Connor, R., Davies, R., Devlin, K., Feltwell, T., … Barrell, B. G. (1998). Deciphering the biology of Mycobacterium tuberculosis from the complete genome sequence. *Nature*, *393*(6685), 5373544. https://doi.org/10.1038/31159
59. Comas, I., Borrell, S., Roetzer, A., Rose, G., Malla, B., Kato-Maeda, M., Galagan, J., Niemann, S., & Gagneux, S. (2012). Whole-genome sequencing of rifampicin-resistant Mycobacterium tuberculosis strains identifies compensatory mutations in RNA polymerase genes. *Nature Genetics*, *44*(1), 1063110. https://doi.org/10.1038/ng.1038
60. Cook, G. M., Berney, M., Gebhard, S., Heinemann, M., Cox, R. A., Danilchanka, O., & Niederweis, M. (2009). *Physiology of Mycobacteria* (pp. 813319). https://doi.org/10.1016/S0065-2911(09)05502-7
61. Corso, G., Stark, H., Jing, B., Barzilay, R., & Jaakkola, T. (2022). *DiffDock: Diffusion Steps, Twists, and Turns for Molecular Docking*. ICLR. https://paperswithcode.com/paper/diffdock-diffusion-steps-twists-and-turns-for
62. Cosma, C. L., Swaim, L. E., Volkman, H., Ramakrishnan, L., & Davis, J. M. (2006). Zebrafish and Frog Models of *Mycobacterium marinum* Infection. *Current Protocols in Microbiology*, *3*(1). https://doi.org/10.1002/0471729256.mc10b02s3
63. Cowley, S., Ko, M., Pick, N., Chow, R., Downing, K. J., Gordhan, B. G., Betts, J. C., Mizrahi, V., Smith, D. A., Stokes, R. W., & Av-Gay, Y. (2004). The *Mycobacterium tuberculosis* protein serine/threonine kinase PknG is linked to cellular glutamate/glutamine levels and is important for growth *in vivo*. *Molecular Microbiology*, *52*(6), 169131702. https://doi.org/10.1111/j.1365-2958.2004.04085.x
64. Cristobal, S. (1999). Competition between Sec- and TAT-dependent protein translocation in Escherichia coli. *The EMBO Journal*, *18*(11), 298232990. https://doi.org/10.1093/emboj/18.11.2982
65. Das, S., Pettersson, B. M. F., Behra, P. R. K., Mallick, A., Cheramie, M., Ramesh, M., Shirreff, L., DuCote, T., Dasgupta, S., Ennis, D. G., & Kirsebom, Leif. A. (2018). Extensive genomic diversity among Mycobacterium marinum strains revealed by whole genome sequencing. *Scientific Reports*, *8*(1), 12040. https://doi.org/10.1038/s41598-018-30152-y
66. Davis, J. M., Clay, H., Lewis, J. L., Ghori, N., Herbomel, P., & Ramakrishnan, L. (2002). Real-Time Visualization of Mycobacterium-Macrophage Interactions Leading to Initiation of Granuloma Formation in Zebrafish Embryos. *Immunity*, *17*(6), 6933702. https://doi.org/10.1016/S1074-7613(02)00475-2

67. Dickman, K. R., Nabyonga, L., Kateete, D. P., Katabazi, F. A., Asiimwe, B. B., Mayanja, H. K., Okwera, A., Whalen, C., & Joloba, M. L. (2010). Detection of multiple strains of Mycobacterium tuberculosis using MIRU-VNTR in patients with pulmonary tuberculosis in Kampala, Uganda. *BMC Infectious Diseases*, *10*(1), 349. https://doi.org/10.1186/1471-2334-10-349
68. Dippenaar, A., Derendinger, B., Dolby, T., Beylis, N., van Helden, P. D., Theron, G., Warren, R. M., & de Vos, M. (2021). Diagnostic accuracy of the FluoroType MTB and MTBDR VER 2.0 assays for the centralized high-throughput detection of Mycobacterium tuberculosis complex DNA and isoniazid and rifampicin resistance. *Clinical Microbiology and Infection*, *27*(9), 1351.e1-1351.e4. https://doi.org/10.1016/j.cmi.2021.04.022
69. Donald, P. R., Diacon, A. H., Lange, C., Demers, A.-M., von Groote-Biddlingmeier, F., & Nardell, E. (2018). Droplets, dust and guinea pigs: an historical review of tuberculosis transmission research, 187831940. *The International Journal of Tuberculosis and Lung Disease*, *22*(9), 9723982. https://doi.org/10.5588/ijtld.18.0173
70. Dorman, S. E., Schumacher, S. G., Alland, D., Nabeta, P., Armstrong, D. T., King, B., Hall, S. L., Chakravorty, S., Cirillo, D. M., Tukvadze, N., Bablishvili, N., Stevens, W., Scott, L., Rodrigues, C., Kazi, M. I., Joloba, M., Nakiyingi, L., Nicol, M. P., Ghebrekristos, Y., … Xie, Y. (2018). Xpert MTB/RIF Ultra for detection of Mycobacterium tuberculosis and rifampicin resistance: a prospective multicentre diagnostic accuracy study. *The Lancet Infectious Diseases*, *18*(1), 76384. https://doi.org/10.1016/S1473-3099(17)30691-6
71. Dörr, T., Möll, A., Chao, M. C., Cava, F., Lam, H., Davis, B. M., & Waldor, M. K. (2014). Differential Requirement for PBP1a and PBP1b in *In Vivo* and *In Vitro* Fitness of Vibrio cholerae. *Infection and Immunity*, *82*(5), 211532124. https://doi.org/10.1128/IAI.00012-14
72. Dumas, E., Christina Boritsch, E., Vandenbogaert, M., Rodríguez de la Vega, R. C., Thiberge, J.-M., Caro, V., Gaillard, J.-L., Heym, B., Girard-Misguich, F., Brosch, R., & Sapriel, G. (2016). Mycobacterial Pan-Genome Analysis Suggests Important Role of Plasmids in the Radiation of Type VII Secretion Systems. *Genome Biology and Evolution*, *8*(2), 3873402. https://doi.org/10.1093/gbe/evw001
73. Dutta, N. K., Mehra, S., Didier, P. J., Roy, C. J., Doyle, L. A., Alvarez, X., Ratterree, M., Be, N. A., Lamichhane, G., Jain, S. K., Lacey, M. R., Lackner, A. A., & Kaushal, D. (2010). Genetic Requirements for the Survival of Tubercle Bacilli in Primates. *The Journal of Infectious Diseases*, *201*(11), 174331752. https://doi.org/10.1086/652497
74. Edoo, Z., Arthur, M., & Hugonnet, J.-E. (2017). Reversible inactivation of a peptidoglycan transpeptidase by a β-lactam antibiotic mediated by β-lactam-ring recyclization in the enzyme active site. *Scientific Reports*, *7*(1), 9136. https://doi.org/10.1038/s41598-017-09341-8
75. Eilertson, B., Maruri, F., Blackman, A., Guo, Y., Herrera, M., van der Heijden, Y., Shyr, Y., & Sterling, T. R. (2016). A novel resistance mutation in *eccC* $_5$ of the ESX-5 secretion system confers ofloxacin resistance in *Mycobacterium*

tuberculosis. *Journal of Antimicrobial Chemotherapy*, *71*(9), 241932427. https://doi.org/10.1093/jac/dkw168
76. El-Etr, S. H., Subbian, S., Cirillo, S. L. G., & Cirillo, J. D. (2004). Identification of Two *Mycobacterium marinum* Loci That Affect Interactions with Macrophages. *Infection and Immunity*, *72*(12), 690236913. https://doi.org/10.1128/IAI.72.12.6902-6913.2004
77. Famelis, N., Geibel, S., & van Tol, D. (2023). Mycobacterial type VII secretion systems. *Biological Chemistry*, *404*(7), 6913702. https://doi.org/10.1515/hsz-2022-0350
78. Farhat, M. R., Shapiro, B. J., Kieser, K. J., Sultana, R., Jacobson, K. R., Victor, T. C., Warren, R. M., Streicher, E. M., Calver, A., Sloutsky, A., Kaur, D., Posey, J. E., Plikaytis, B., Oggioni, M. R., Gardy, J. L., Johnston, J. C., Rodrigues, M., Tang, P. K. C., Kato-Maeda, M., … Murray, M. (2013). Genomic analysis identifies targets of convergent positive selection in drug-resistant Mycobacterium tuberculosis. *Nature Genetics*, *45*(10), 118331189. https://doi.org/10.1038/ng.2747
79. Feltcher, M. E., Gunawardena, H. P., Zulauf, K. E., Malik, S., Griffin, J. E., Sassetti, C. M., Chen, X., & Braunstein, M. (2015). Label-free Quantitative Proteomics Reveals a Role for the Mycobacterium tuberculosis SecA2 Pathway in Exporting Solute Binding Proteins and Mce Transporters to the Cell Wall*. *Molecular & Cellular Proteomics*, *14*(6), 150131516. https://doi.org/10.1074/mcp.M114.044685
80. Fernandez Do Porto, D. A., Monteserin, J., Campos, J., Sosa, E. J., Matteo, M., Serral, F., Yokobori, N., Benevento, A. F., Poklepovich, T., Pardo, A., Wainmayer, I., Simboli, N., Castello, F., Paul, R., Martí, M., López, B., Turjanski, A., & Ritacco, V. (2021). Five-year microevolution of a multidrug-resistant Mycobacterium tuberculosis strain within a patient with inadequate compliance to treatment. *BMC Infectious Diseases*, *21*(1), 394. https://doi.org/10.1186/s12879-021-06069-9
81. Filippova, E. V., Kieser, K. J., Luan, C. H., Wawrzak, Z., Kiryukhina, O., Rubin, E. J., & Anderson, W. F. (2016). Crystal structures of the transpeptidase domain of the Mycobacterium tuberculosis penicillin-binding protein PonA1 reveal potential mechanisms of antibiotic resistance. *FEBS Journal*, *283*, 220632218. https://doi.org/10.1111/febs.13738
82. Fishovitz, J., Hermoso, J. A., Chang, M., & Mobashery, S. (2014). Penicillin-binding protein 2a of methicillin-resistant *Staphylococcus aureus*. *IUBMB Life*, *66*(8), 5723577. https://doi.org/10.1002/iub.1289
83. Folkvardsen, D. B., Thomsen, V. Ø., Rigouts, L., Rasmussen, E. M., Bang, D., Bernaerts, G., Werngren, J., Toro, J. C., Hoffner, S., Hillemann, D., & Svensson, E. (2013). Rifampin Heteroresistance in Mycobacterium tuberculosis Cultures as Detected by Phenotypic and Genotypic Drug Susceptibility Test Methods. *Journal of Clinical Microbiology*, *51*(12), 422034222. https://doi.org/10.1128/JCM.01602-13

84. Galla, H.-J., & Hartmann, W. (1980). Excimer-forming lipids in membrane research. *Chemistry and Physics of Lipids*, *27*(3), 1993219. https://doi.org/10.1016/0009-3084(80)90036-5
85. Gallego-Parrilla, J. J., Severi, E., Chandra, G., & Palmer, T. (2024). Identification of novel tail-anchored membrane proteins integrated by the bacterial twin-arginine translocase. *Microbiology*, *170*(2). https://doi.org/10.1099/mic.0.001431
86. Gao, B., Wang, J., Huang, J., Huang, X., Sha, W., & Qin, L. (2019a). The dynamic region of the peptidoglycan synthase gene, Rv0050, induces the growth rate and morphologic heterogeneity in Mycobacteria. *Infection, Genetics and Evolution*, *72*(November), 86392. https://doi.org/10.1016/j.meegid.2018.12.012
87. Gao, B., Wang, J., Huang, J., Huang, X., Sha, W., & Qin, L. (2019b). The dynamic region of the peptidoglycan synthase gene, Rv0050, induces the growth rate and morphologic heterogeneity in Mycobacteria. *Infection, Genetics and Evolution*, *72*, 86392. https://doi.org/10.1016/j.meegid.2018.12.012
88. Gao, L., Guo, S., McLaughlin, B., Morisaki, H., Engel, J. N., & Brown, E. J. (2004). A mycobacterial virulence gene cluster extending RD1 is required for cytolysis, bacterial spreading and ESAT-6 secretion. *Molecular Microbiology*, *53*(6), 167731693. https://doi.org/10.1111/j.1365-2958.2004.04261.x
89. Gao, L., & Manoranjan, J. (2006). Laboratory Maintenance of *Mycobacterium marinum*. *Current Protocols in Microbiology*, *00*(1). https://doi.org/10.1002/9780471729259.mc10b01s00
90. Garnier, T., Eiglmeier, K., Camus, J.-C., Medina, N., Mansoor, H., Pryor, M., Duthoy, S., Grondin, S., Lacroix, C., Monsempe, C., Simon, S., Harris, B., Atkin, R., Doggett, J., Mayes, R., Keating, L., Wheeler, P. R., Parkhill, J., Barrell, B. G., … Hewinson, R. G. (2003). The complete genome sequence of *Mycobacterium bovis*. *Proceedings of the National Academy of Sciences*, *100*(13), 787737882. https://doi.org/10.1073/pnas.1130426100
91. GenoSreen. (2023). *Deeplex Myc-TB. User manual RUO*. https://www.genoscreen.fr/index.php?Itemid=371&id=200&lang=en&option=com_content&view=article
92. Getahun, M., Blumberg, H. M., Ameni, G., Beyene, D., & Kempker, R. R. (2022). Minimum inhibitory concentrations of rifampin and isoniazid among multidrug and isoniazid resistant Mycobacterium tuberculosis in Ethiopia. *PLOS ONE*, *17*(9), e0274426. https://doi.org/10.1371/journal.pone.0274426
93. Ghosh, P., Kim, A. I., & Hatfull, G. F. (2003). The Orientation of Mycobacteriophage Bxb1 Integration Is Solely Dependent on the Central Dinucleotide of attP and attB. *Molecular Cell*, *12*(5), 110131111. https://doi.org/10.1016/S1097-2765(03)00444-1
94. Gleeson, L. E., Sheedy, F. J., Palsson-McDermott, E. M., Triglia, D., O9Leary, S. M., O9Sullivan, M. P., O9Neill, L. A. J., & Keane, J. (2016). Cutting Edge: Mycobacterium tuberculosis Induces Aerobic Glycolysis in Human Alveolar Macrophages That Is Required for Control of Intracellular Bacillary Replication. *The Journal of Immunology*, *196*(6), 244432449. https://doi.org/10.4049/jimmunol.1501612

95. Global Tuberculosis Programme (GTB). (2021). *WHO consolidated guidelines on tuberculosis: module 3: diagnosis: rapid diagnostics for tuberculosis detection, 2021 update*. https://www.who.int/publications/i/item/who-consolidated-guidelines-on-tuberculosis-module-3-diagnosis---rapid-diagnostics-for-tuberculosis-detection
96. Global Tuberculosis Programme (GTB). (2022). Manual for selection of molecular WHO-recommended rapid diagnostic tests for detection of tuberculosis and drug-resistant tuberculosis. In *https://www.who.int/publications/i/item/9789240042575*. World Health Organization. https://www.who.int/publications/i/item/9789240042575
97. Goldstein, B. P. (2014). Resistance to rifampicin: a review. *The Journal of Antibiotics*, *67*(9), 6253630. https://doi.org/10.1038/ja.2014.107
98. Golemi-Kotra, D., Cha, J. Y., Meroueh, S. O., Vakulenko, S. B., & Mobashery, S. (2003). Resistance to β-Lactam Antibiotics and Its Mediation by the Sensor Domain of the Transmembrane BlaR Signaling Pathway in Staphylococcus aureus. *Journal of Biological Chemistry*, *278*(20), 18419318425. https://doi.org/10.1074/jbc.M300611200
99. Goosens, V. J., Monteferrante, C. G., & van Dijl, J. M. (2014). The Tat system of Gram-positive bacteria. *Biochimica et Biophysica Acta (BBA) - Molecular Cell Research*, *1843*(8), 169831706. https://doi.org/10.1016/j.bbamcr.2013.10.008
100. Gray, T. A., Clark, R. R., Boucher, N., Lapierre, P., Smith, C., & Derbyshire, K. M. (2016). Intercellular communication and conjugation are mediated by ESX secretion systems in mycobacteria. *Science*, *354*(6310), 3473350. https://doi.org/10.1126/science.aag0828
101. Gröschel, M. I., Sayes, F., Simeone, R., Majlessi, L., & Brosch, R. (2016). ESX secretion systems: mycobacterial evolution to counter host immunity. Nature Reviews Microbiology, 14(11), 6773691. https://doi.org/10.1038/nrmicro.2016.131
102. Gunawardena, H. P., Feltcher, M. E., Wrobel, J. A., Gu, S., Braunstein, M., & Chen, X. (2013). Comparison of the Membrane Proteome of Virulent Mycobacterium tuberculosis and the Attenuated Mycobacterium bovis BCG Vaccine Strain by Label-Free Quantitative Proteomics. Journal of Proteome Research, 12(12), 546335474. https://doi.org/10.1021/pr400334k
103. Hashish, E., Merwad, A., Elgaml, S., Amer, A., Kamal, H., Elsadek, A., Marei, A., & Sitohy, M. (2018). Mycobacterium marinum infection in fish and man: epidemiology, pathophysiology and management; a review. Veterinary Quarterly, 38(1), 35346. https://doi.org/10.1080/01652176.2018.1447171
104. Hervas-Stubbs, S., Majlessi, L., Simsova, M., Morova, J., Rojas, M.-J., Nouzé, C., Brodin, P., Sebo, P., & Leclerc, C. (2006). High Frequency of CD4 + T Cells Specific for the TB10.4 Protein Correlates with Protection against Mycobacterium tuberculosis Infection. Infection and Immunity, 74(6), 33963 3407. https://doi.org/10.1128/IAI.02086-05
105. Hess, B., Bekker, H., Berendsen, H. J. C., & Fraaije, J. G. E. M. (1997). LINCS: A linear constraint solver for molecular simulations. Journal of Computational

Chemistry, 18(12), 146331472. https://doi.org/10.1002/(SICI)1096-987X(199709)18:12<1463::AID-JCC4>3.0.CO;2-H
106. Hett, E. C., Chao, M. C., & Rubin, E. J. (2010). Interaction and modulation of two antagonistic cell wall enzymes of mycobacteria. PLoS Pathogens, 6(7), 13 14. https://doi.org/10.1371/journal.ppat.1001020
107. Hofmann-Thiel, S., van Ingen, J., Feldmann, K., Turaev, L., Uzakova, G. T., Murmusaeva, G., van Soolingen, D., & Hoffmann, H. (2008). Mechanisms of heteroresistance to isoniazid and rifampin of Mycobacterium tuberculosis in Tashkent, Uzbekistan. European Respiratory Journal, 33(2), 3683374. https://doi.org/10.1183/09031936.00089808
108. Howard, N. C., Marin, N. D., Ahmed, M., Rosa, B. A., Martin, J., Bambouskova, M., Sergushichev, A., Loginicheva, E., Kurepina, N., Rangel-Moreno, J., Chen, L., Kreiswirth, B. N., Klein, R. S., Balada-Llasat, J.-M., Torrelles, J. B., Amarasinghe, G. K., Mitreva, M., Artyomov, M. N., Hsu, F.-F., … Khader, S. A. (2018). Mycobacterium tuberculosis carrying a rifampicin drug resistance mutation reprograms macrophage metabolism through cell wall lipid changes. Nature Microbiology, 3(10), 109931108. https://doi.org/10.1038/s41564-018-0245-0
109. Ilghari, D., Lightbody, K. L., Veverka, V., Waters, L. C., Muskett, F. W., Renshaw, P. S., & Carr, M. D. (2011). Solution Structure of the Mycobacterium tuberculosis EsxG·EsxH Complex. Journal of Biological Chemistry, 286(34), 29993330002. https://doi.org/10.1074/jbc.M111.248732
110. Instituto Nacional de Salud. (2011). Susceptibilidad a drogas de Mycobacterium tuberculosis mediante observación microscopica (MODS). https://repositorio.ins.gob.pe/bitstream/handle/20.500.14196/1118/MODS.pdf?sequence=1&isAllowed=y
111. Jankute, M., Cox, J. A. G., Harrison, J., & Besra, G. S. (2015). Assembly of the Mycobacterial Cell Wall. Annual Review of Microbiology, 69(1), 4053423. https://doi.org/10.1146/annurev-micro-091014-104121
112. Jees Sebastian, Sharmada Swaminath, P. A. (2019). Reduced Permeability to Rifampicin by Capsular Thickening as a Mechanism of Antibiotic Persistence in Mycobacterium tuberculosis. BioRxiv. https://doi.org/https://doi.org/10.1101/624569
113. Jin, C., Wu, X., Dong, C., Li, F., Fan, L., Xiong, S., & Dong, Y. (2019). EspR promotes mycobacteria survival in macrophages by inhibiting MyD88 mediated inflammation and apoptosis. Tuberculosis, 116, 22331. https://doi.org/10.1016/j.tube.2019.03.010
114. Jumper, J., Evans, R., Pritzel, A., Green, T., Figurnov, M., Ronneberger, O., Tunyasuvunakool, K., Bates, R., Žídek, A., Potapenko, A., Bridgland, A., Meyer, C., Kohl, S. A. A., Ballard, A. J., Cowie, A., Romera-Paredes, B., Nikolov, S., Jain, R., Adler, J., … Hassabis, D. (2021). Highly accurate protein structure prediction with AlphaFold. Nature, 596(7873), 5833589. https://doi.org/10.1038/s41586-021-03819-2
115. Kargarpour Kamakoli, M., Sadegh, H. R., Farmanfarmaei, G., Masoumi, M., Fateh, A., Javadi, G., Rahimi Jamnani, F., Vaziri, F., & Siadat, S. D. (2017).

Evaluation of the impact of polyclonal infection and heteroresistance on treatment of tuberculosis patients. Scientific Reports, 7(1), 41410. https://doi.org/10.1038/srep41410

116. Kieser, K. J., Baranowski, C., Chao, M. C., Long, J. E., Sassetti, C. M., Waldor, M. K., Sacchettini, J. C., Ioerger, T. R., & Rubin, E. J. (2015). Peptidoglycan synthesis in Mycobacterium tuberculosis is organized into networks with varying drug susceptibility. Proceedings of the National Academy of Sciences, 112(42), 13087313092. https://doi.org/10.1073/pnas.1514135112
117. Kieser, K. J., Boutte, C. C., Kester, J. C., Baer, C. E., Barczak, A. K., Meniche, X., Chao, M. C., Rego, E. H., Sassetti, C. M., Fortune, S. M., & Rubin, E. J. (2015). Phosphorylation of the Peptidoglycan Synthase PonA1 Governs the Rate of Polar Elongation in Mycobacteria. PLoS Pathogens, 11(6), 1328. https://doi.org/10.1371/journal.ppat.1005010
118. Kim, D. H., Lees, W. J., Kempsell, K. E., Lane, W. S., Duncan, K., & Walsh, C. T. (1996). Characterization of a Cys115 to Asp Substitution in the Escherichia coli Cell Wall Biosynthetic Enzyme UDP-GlcNAc Enolpyruvyl Transferase (MurA) That Confers Resistance to Inactivation by the Antibiotic Fosfomycin †. Biochemistry, 35(15), 492334928. https://doi.org/10.1021/bi952937w
119. Koch, A., Mizrahi, V., & Warner, D. F. (2014). The impact of drug resistance on Mycobacterium tuberculosis physiology: what can we learn from rifampicin? Emerging Microbes & Infections, 3(1), 1311. https://doi.org/10.1038/emi.2014.17
120. Kowalska-Krochmal, B., & Dudek-Wicher, R. (2021). The Minimum Inhibitory Concentration of Antibiotics: Methods, Interpretation, Clinical Relevance. Pathogens, 10(2), 165. https://doi.org/10.3390/pathogens10020165
121. Kumar, D., Srivastava, B. S., & Srivastava, R. (1998). Genetic rearrangements leading to disruption of heterologous gene expression in mycobacteria: An observation with Escherichia coli β-galactosidase in Mycobacterium smegmatis and its implication in vaccine development. Vaccine, 16(11312), 121231215. https://doi.org/10.1016/S0264-410X(98)80121-7
122. Kumar, P., Arora, K., Lloyd, J. R., Lee, I. Y., Nair, V., Fischer, E., Boshoff, H. I. M., & Barry, C. E. (2012). Meropenem inhibits D,D-carboxypeptidase activity in Mycobacterium tuberculosis. Molecular Microbiology, 86(2), 3673381. https://doi.org/10.1111/j.1365-2958.2012.08199.x
123. Kurepina, N., Chudaev, M., Kreiswirth, B. N., Nikiforov, V., & Mustaev, A. (2022). Mutations compensating for the fitness cost of rifampicin resistance in Escherichia coli exert pleiotropic effect on RNA polymerase catalysis. Nucleic Acids Research, 50(10), 573935756. https://doi.org/10.1093/nar/gkac406
124. Lavollay, M., Arthur, M., Fourgeaud, M., Dubost, L., Marie, A., Veziris, N., Blanot, D., Gutmann, L., & Mainardi, J. L. (2008). The peptidoglycan of stationary-phase Mycobacterium tuberculosis predominantly contains cross-links generated by L,D-transpeptidation. Journal of Bacteriology, 190(12), 43603 4366. https://doi.org/10.1128/JB.00239-08
125. Lechevalier, M. P., Prauser, H., Labeda, D. P., & Ruan, J.-S. (1986). Two New Genera of Nocardioform Actinomycetes: Amycolata gen. nov. and

Amycolatopsis gen. nov. International Journal of Systematic Bacteriology, 36(1), 29337. https://doi.org/10.1099/00207713-36-1-29
126. Lee, M., Hesek, D., Suvorov, M., Lee, W., Vakulenko, S., & Mobashery, S. (2003). A Mechanism-Based Inhibitor Targeting the <scp>dd</scp> - Transpeptidase Activity of Bacterial Penicillin-Binding Proteins. Journal of the American Chemical Society, 125(52), 16322316326. https://doi.org/10.1021/ja038445l
127. Levine, S. R., & Beatty, K. E. (2021). Investigating β-Lactam Drug Targets in Mycobacterium tuberculosis Using Chemical Probes. ACS Infectious Diseases, 7(2), 4613470. https://doi.org/10.1021/acsinfecdis.0c00809
128. Li, G., Zhang, J., Guo, Q., Wei, J., Jiang, Y., Zhao, X., Zhao, L., Liu, Z., Lu, J., & Wan, K. (2015). Study of efflux pump gene expression in rifampicin-monoresistant Mycobacterium tuberculosis clinical isolates. The Journal of Antibiotics, 68(7), 4313435. https://doi.org/10.1038/ja.2015.9
129. Li, H. (2018). Minimap2: pairwise alignment for nucleotide sequences. Bioinformatics, 34(18), 309433100. https://doi.org/10.1093/bioinformatics/bty191
130. Lin, W., Mandal, S., Degen, D., Liu, Y., Ebright, Y. W., Li, S., Feng, Y., Zhang, Y., Mandal, S., Jiang, Y., Liu, S., Gigliotti, M., Talaue, M., Connell, N., Das, K., Arnold, E., & Ebright, R. H. (2017). Structural Basis of Mycobacterium tuberculosis Transcription and Transcription Inhibition. Molecular Cell, 66(2), 169-179.e8. https://doi.org/10.1016/j.molcel.2017.03.001
131. Lin, Z., Akin, H., Rao, R., Hie, B., Zhu, Z., Lu, W., Smetanin, N., Verkuil, R., Kabeli, O., Shmueli, Y., dos Santos Costa, A., Fazel-Zarandi, M., Sercu, T., Candido, S., & Rives, A. (2023). Evolutionary-scale prediction of atomic-level protein structure with a language model. Science, 379(6637), 112331130. https://doi.org/10.1126/science.ade2574
132. Los, F. C. O., Randis, T. M., Aroian, R. V., & Ratner, A. J. (2013). Role of Pore-Forming Toxins in Bacterial Infectious Diseases. Microbiology and Molecular Biology Reviews, 77(2), 1733207. https://doi.org/10.1128/MMBR.00052-12
133. Louw, G. E., Warren, R. M., Gey van Pittius, N. C., McEvoy, C. R. E., Van Helden, P. D., & Victor, T. C. (2009). A Balancing Act: Efflux/Influx in Mycobacterial Drug Resistance. Antimicrobial Agents and Chemotherapy, 53(8), 318133189. https://doi.org/10.1128/AAC.01577-08
134. Machowski, E. E., Senzani, S., Ealand, C., & Kana, B. D. (2014). Comparative genomics for mycobacterial peptidoglycan remodelling enzymes reveals extensive genetic multiplicity. BMC Microbiology, 14(1), 75. https://doi.org/10.1186/1471-2180-14-75
135. MacLean, E., Kohli, M., Weber, S. F., Suresh, A., Schumacher, S. G., Denkinger, C. M., & Pai, M. (2020). Advances in Molecular Diagnosis of Tuberculosis. Journal of Clinical Microbiology, 58(10). https://doi.org/10.1128/JCM.01582-19
136. Mahapatra, S., Crick, D. C., & Brennan, P. J. (2000). Comparison of the UDP-N-Acetylmuramate:l-Alanine Ligase Enzymes from Mycobacterium tuberculosis andMycobacterium leprae. Journal of Bacteriology, 182(23), 68273 6830. https://doi.org/10.1128/JB.182.23.6827-6830.2000

137. Majlessi, L., Rojas, M.-J., Brodin, P., & Leclerc, C. (2003). CD8 + -T-CellResponses of Mycobacterium-Infected Mice to a Newly Identified MajorHistocompatibility Complex Class I-Restricted Epitope Shared byProteins of the ESAT-6Family. Infection and Immunity, 71(12), 717337177. https://doi.org/10.1128/IAI.71.12.7173-7177.2003
138. Malenfant, J. H., & Brewer, T. F. (2021). Rifampicin Mono-Resistant Tuberculosis4A Review of an Uncommon But Growing Challenge for Global Tuberculosis Control. Open Forum Infectious Diseases, 8(2). https://doi.org/10.1093/ofid/ofab018
139. Manjunath, A., Thumu, S. C. R., Kumar, S., & Halami, P. M. (2021). Bacterial heteroresistance: an evolving novel way to combat antibiotics. Biologia, 76(10), 302933041. https://doi.org/10.1007/s11756-021-00820-y
140. Mankiewicz, E., & Liivak, M. (1975). Phage types of mycobacterium tuberculosis in cultures isolated from Eskimo patients. The American Review of Respiratory Disease, 111(3), 3073312. https://doi.org/10.1164/arrd.1975.111.3.307
141. Marion Merrell, S. A. (2023). Rifaldin . Ficha Tecnica. https://cima.aemps.es/cima/pdfs/es/ft/46028/FT_46028.html.pdf
142. Maurya, S., Jain, A., Rehman, M. T., Hakamy, A., Bantun, F., AlAjmi, M. F., Singh, V., Zehra, A., Khan, F., Haque, S., & Mishra, B. N. (2023). In Silico Identification of Novel Derivatives of Rifampicin Targeting Ribonuclease VapC2 of M. tuberculosis H37Rv: Rifampicin Derivatives Target VapC2 of Mtb H37Rv. Molecules, 28(4), 1652. https://doi.org/10.3390/molecules28041652
143. Mazars, E., Lesjean, S., Banuls, A.-L., Gilbert, M., Vincent, V., Gicquel, B., Tibayrenc, M., Locht, C., & Supply, P. (2001). High-resolution minisatellite-based typing as a portable approach to global analysis of Mycobacterium tuberculosis molecular epidemiology. Proceedings of the National Academy of Sciences, 98(4), 190131906. https://doi.org/10.1073/pnas.98.4.1901
144. McClure, W. R., & Cech, C. L. (1978). On the mechanism of rifampicin inhibition of RNA synthesis. The Journal of Biological Chemistry, 253(24), 894938956. http://www.ncbi.nlm.nih.gov/pubmed/363713
145. McDonough, J. A., Hacker, K. E., Flores, A. R., Pavelka, M. S., & Braunstein, M. (2005). The Twin-Arginine Translocation Pathway of Mycobacterium smegmatis Is Functional and Required for the Export of Mycobacterial β-Lactamases. Journal of Bacteriology, 187(22), 766737679. https://doi.org/10.1128/JB.187.22.7667-7679.2005
146. McNeil, M. B., Chettiar, S., Awasthi, D., & Parish, T. (2019). Cell wall inhibitors increase the accumulation of rifampicin in Mycobacterium tuberculosis. Access Microbiology, 1(1). https://doi.org/10.1099/acmi.0.000006
147. McNutt, A. T., Francoeur, P., Aggarwal, R., Masuda, T., Meli, R., Ragoza, M., Sunseri, J., & Koes, D. R. (2021). GNINA 1.0: molecular docking with deep learning. Journal of Cheminformatics, 13(1), 43. https://doi.org/10.1186/s13321-021-00522-2
148. McPherson, D. C., & Popham, D. L. (2003). Peptidoglycan Synthesis in the Absence of Class A Penicillin-Binding Proteins in Bacillus subtilis. Journal of

Bacteriology, 185(4), 142331431. https://doi.org/10.1128/JB.185.4.1423-1431.2003
149. Mehra, A., Zahra, A., Thompson, V., Sirisaengtaksin, N., Wells, A., Porto, M., Köster, S., Penberthy, K., Kubota, Y., Dricot, A., Rogan, D., Vidal, M., Hill, D. E., Bean, A. J., & Philips, J. A. (2013). Mycobacterium tuberculosis Type VII Secreted Effector EsxH Targets Host ESCRT to Impair Trafficking. PLoS Pathogens, 9(10), e1003734. https://doi.org/10.1371/journal.ppat.1003734
150. Merker, M., Blin, C., Mona, S., Duforet-Frebourg, N., Lecher, S., Willery, E., Blum, M. G. B., Rüsch-Gerdes, S., Mokrousov, I., Aleksic, E., Allix-Béguec, C., Antierens, A., Augustynowicz-Kopeć, E., Ballif, M., Barletta, F., Beck, H. P., Barry, C. E., Bonnet, M., Borroni, E., … Wirth, T. (2015). Evolutionary history and global spread of the Mycobacterium tuberculosis Beijing lineage. Nature Genetics, 47(3), 2423249. https://doi.org/10.1038/ng.3195
151. Meyerovich, M., Mamou, G., & Ben-Yehuda, S. (2010). Visualizing high error levels during gene expression in living bacterial cells. Proceedings of the National Academy of Sciences, 107(25), 11543311548. https://doi.org/10.1073/pnas.0912989107
152. Meza, J. C. (2010). Steepest descent. WIREs Computational Statistics, 2(6), 7193 722. https://doi.org/10.1002/wics.117
153. Miller, B. K., Zulauf, K. E., & Braunstein, M. (2017). The Sec Pathways and Exportomes of Mycobacterium tuberculosis. In Tuberculosis and the Tubercle Bacillus (pp. 6073625). ASM Press. https://doi.org/10.1128/9781555819569.ch28
154. Miotto, P., Tessema, B., Tagliani, E., Chindelevitch, L., Starks, A. M., Emerson, C., Hanna, D., Kim, P. S., Liwski, R., Zignol, M., Gilpin, C., Niemann, S., Denkinger, C. M., Fleming, J., Warren, R. M., Crook, D., Posey, J., Gagneux, S., Hoffner, S., … Rodwell, T. C. (2017). A standardised method for interpreting the association between mutations and phenotypic drug resistance in Mycobacterium tuberculosis. European Respiratory Journal, 50(6), 1701354. https://doi.org/10.1183/13993003.01354-2017
155. Mitarai, S., Kato, S., Ogata, H., Aono, A., Chikamatsu, K., Mizuno, K., Toyota, E., Sejimo, A., Suzuki, K., Yoshida, S., Saito, T., Moriya, A., Fujita, A., Sato, S., Matsumoto, T., Ano, H., Suetake, T., Kondo, Y., Kirikae, T., & Mori, T. (2012). Comprehensive Multicenter Evaluation of a New Line Probe Assay Kit for Identification of Mycobacterium Species and Detection of Drug-Resistant Mycobacterium tuberculosis. Journal of Clinical Microbiology, 50(3), 8843890. https://doi.org/10.1128/JCM.05638-11
156. Mohamadi M, T. N. and B. D. (2017). Quick protein binding analysis by label-free thermal shift analysis on the Tycho NT.6.
157. Mohammadi, T., van Dam, V., Sijbrandi, R., Vernet, T., Zapun, A., Bouhss, A., Diepeveen-de Bruin, M., Nguyen-Distèche, M., de Kruijff, B., & Breukink, E. (2011). Identification of FtsW as a transporter of lipid-linked cell wall precursors across the membrane. The EMBO Journal, 30(8), 142531432. https://doi.org/10.1038/emboj.2011.61

158. Molodtsov, V., Nawarathne, I. N., Scharf, N. T., Kirchhoff, P. D., Showalter, H. D. H., Garcia, G. A., & Murakami, K. S. (2013). X-ray Crystal Structures of the Escherichia coli RNA Polymerase in Complex with Benzoxazinorifamycins. Journal of Medicinal Chemistry, 56(11), 475834763. https://doi.org/10.1021/jm4004889
159. Mueller, E. A., Egan, A. J., Breukink, E., Vollmer, W., & Levin, P. A. (2019). Plasticity of Escherichia coli cell wall metabolism promotes fitness and antibiotic resistance across environmental conditions. ELife, 8. https://doi.org/10.7554/eLife.40754
160. Murphy, K. C., Nelson, S. J., Nambi, S., Papavinasasundaram, K., Baer, C. E., & Sassetti, C. M. (2018). ORBIT: a New Paradigm for Genetic Engineering of Mycobacterial Chromosomes. MBio, 9(6). https://doi.org/10.1128/mBio.01467-18
161. Nakayama, H., Kurokawa, K., & Lee, B. L. (2012). Lipoproteins in bacteria: structures and biosynthetic pathways. The FEBS Journal, 279(23), 424734268. https://doi.org/10.1111/febs.12041
162. Ng, K. C. S., Supply, P., Cobelens, F. G. J., Gaudin, C., Gonzalez-Martin, J., de Jong, B. C., & Rigouts, L. (2019). How Well Do Routine Molecular Diagnostics Detect Rifampin Heteroresistance in Mycobacterium tuberculosis? Journal of Clinical Microbiology, 57(11). https://doi.org/10.1128/JCM.00717-19
163. Ng, K. C. S., van Deun, A., Meehan, C. J., Torrea, G., Driesen, M., Gabriëls, S., Rigouts, L., André, E., & de Jong, B. C. (2018). Xpert Ultra Can Unambiguously Identify Specific Rifampin Resistance-Conferring Mutations. Journal of Clinical Microbiology, 56(9). https://doi.org/10.1128/JCM.00686-18
164. Nkatha Micheni, L., Deyno, S., & Bazira, J. (2022). Mycobacterium tuberculosis mixed infections and drug resistance in sub-Saharan Africa: a systematic review. African Health Sciences, 22(1), 5603572. https://doi.org/10.4314/ahs.v22i1.65
165. Nurwidya, F., Handayani, D., Burhan, E., & Yunus, F. (2018). Molecular Diagnosis of Tuberculosis. Chonnam Medical Journal, 54(1), 1. https://doi.org/10.4068/cmj.2018.54.1.1
166. Ohno, H., Koga, H., Kohno, S., Tashiro, T., & Hara, K. (1996). Relationship between rifampin MICs for and rpoB mutations of Mycobacterium tuberculosis strains isolated in Japan. Antimicrobial Agents and Chemotherapy, 40(4), 10533 1056. https://doi.org/10.1128/AAC.40.4.1053
167. Ohol, Y. M., Goetz, D. H., Chan, K., Shiloh, M. U., Craik, C. S., & Cox, J. S. (2010). Mycobacterium tuberculosis MycP1 Protease Plays a Dual Role in Regulation of ESX-1 Secretion and Virulence. Cell Host & Microbe, 7(3), 2103 220. https://doi.org/10.1016/j.chom.2010.02.006
168. Orgeur, M., Frigui, W., Pawlik, A., Clark, S., Williams, A., Ates, L. S., Ma, L., Bouchier, C., Parkhill, J., Brodin, P., & Brosch, R. (2021). Pathogenomic analyses of Mycobacterium microti, an ESX-1-deleted member of the Mycobacterium tuberculosis complex causing disease in various hosts. Microbial Genomics, 7(2). https://doi.org/10.1099/mgen.0.000505
169. Oxford University Hospitals. (2024). Mycobacterial culture. https://www.ouh.nhs.uk/microbiology/a-z/mycobacterial-culture.aspx

170. Paetzel, M., Karla, A., Strynadka, N. C. J., & Dalbey, R. E. (2002). Signal Peptidases. Chemical Reviews, 102(12), 454934580. https://doi.org/10.1021/cr010166y
171. Pajuelo, D., Tak, U., Zhang, L., Danilchanka, O., Tischler, A. D., & Niederweis, M. (2021). Toxin secretion and trafficking by Mycobacterium tuberculosis. Nature Communications, 12(1), 6592. https://doi.org/10.1038/s41467-021-26925-1
172. Pak, M. A., Markhieva, K. A., Novikova, M. S., Petrov, D. S., Vorobyev, I. S., Maksimova, E. S., Kondrashov, F. A., & Ivankov, D. N. (2023). Using AlphaFold to predict the impact of single mutations on protein stability and function. PLOS ONE, 18(3), e0282689. https://doi.org/10.1371/journal.pone.0282689
173. Pal, R., Bisht, M. K., & Mukhopadhyay, S. (2022). Secretory proteins of Mycobacterium tuberculosis and their roles in modulation of host immune responses: focus on therapeutic targets. The FEBS Journal, 289(14), 414634171. https://doi.org/10.1111/febs.16369
174. Pallen, M. J. (2002). The ESAT-6/WXG100 superfamily 3 and a new Gram-positive secretion system? Trends in Microbiology, 10(5), 2093212. https://doi.org/10.1016/S0966-842X(02)02345-4
175. Pang, Y., Lu, J., Wang, Y., Song, Y., Wang, S., & Zhao, Y. (2013a). Study of the Rifampin Monoresistance Mechanism in Mycobacterium tuberculosis. Antimicrobial Agents and Chemotherapy, 57(2), 8933900. https://doi.org/10.1128/AAC.01024-12
176. Pang, Y., Lu, J., Wang, Y., Song, Y., Wang, S., & Zhao, Y. (2013b). Study of the Rifampin Monoresistance Mechanism in Mycobacterium tuberculosis. Antimicrobial Agents and Chemotherapy, 57(2), 8933900. https://doi.org/10.1128/AAC.01024-12
177. Paradis-Bleau, C., Markovski, M., Uehara, T., Lupoli, T. J., Walker, S., Kahne, D. E., & Bernhardt, T. G. (2010). Lipoprotein Cofactors Located in the Outer Membrane Activate Bacterial Cell Wall Polymerases. Cell, 143(7), 111031120. https://doi.org/10.1016/j.cell.2010.11.037
178. Patru, M.-M., & Pavelka, M. S. (2010a). A Role for the Class A Penicillin-Binding Protein PonA2 in the Survival of Mycobacterium smegmatis under Conditions of Nonreplication. Journal of Bacteriology, 192(12), 304333054. https://doi.org/10.1128/JB.00025-10
179. Patru, M.-M., & Pavelka, M. S. (2010b). A Role for the Class A Penicillin-Binding Protein PonA2 in the Survival of Mycobacterium smegmatis under Conditions of Nonreplication. Journal of Bacteriology, 192(12), 304333054. https://doi.org/10.1128/JB.00025-10
180. Petersen, H. G. (1995). Accuracy and efficiency of the particle mesh Ewald method. The Journal of Chemical Physics, 103(9), 366833679. https://doi.org/10.1063/1.470043
181. Phyu, A. N., Aung, S. T., Palittapongarnpim, P., Htet, K. K. K., Mahasirimongkol, S., Aung, H. L., Chaiprasert, A., & Chongsuvivatwong, V. (2022). Distribution of Mycobacterium tuberculosis Lineages and Drug

Resistance in Upper Myanmar. Tropical Medicine and Infectious Disease, 7(12), 448. https://doi.org/10.3390/tropicalmed7120448

182. Pillay, S., Steingart, K. R., Davies, G. R., Chaplin, M., De Vos, M., Schumacher, S. G., Warren, R., & Theron, G. (2022). Xpert MTB/XDR for detection of pulmonary tuberculosis and resistance to isoniazid, fluoroquinolones, ethionamide, and amikacin. Cochrane Database of Systematic Reviews, 2022(5). https://doi.org/10.1002/14651858.CD014841.pub2
183. Posey, J. E., Shinnick, T. M., & Quinn, F. D. (2006). Characterization of the Twin-Arginine Translocase Secretion System of Mycobacterium smegmatis. Journal of Bacteriology, 188(4), 133231340. https://doi.org/10.1128/JB.188.4.1332-1340.2006
184. Prisic, S., Dankwa, S., Schwartz, D., Chou, M. F., Locasale, J. W., Kang, C.-M., Bemis, G., Church, G. M., Steen, H., & Husson, R. N. (2010). Extensive phosphorylation with overlapping specificity by Mycobacterium tuberculosis serine/threonine protein kinases. Proceedings of the National Academy of Sciences, 107(16), 752137526. https://doi.org/10.1073/pnas.0913482107
185. Pym, A. S., Brodin, P., Brosch, R., Huerre, M., & Cole, S. T. (2002). Loss of RD1 contributed to the attenuation of the live tuberculosis vaccines Mycobacterium bovis BCG and Mycobacterium microti. Molecular Microbiology, 46(3), 7093717. https://doi.org/10.1046/j.1365-2958.2002.03237.x
186. Rabanal J. (2020). Potenciales mutaciones compensatorias asociadas a la resistencia a rifampicina en Mycobacterium tuberculosis. Universidad Peruana Cayetano Heredia.
187. Randall, L. L., & Hardy, S. J. S. (2002). SecB, one small chaperone in the complex milieu of the cell. Cellular and Molecular Life Sciences, 59(10), 16173 1623. https://doi.org/10.1007/PL00012488
188. Raymond, J. B., Mahapatra, S., Crick, D. C., & Pavelka, M. S. (2005). Identification of the namH Gene, Encoding the Hydroxylase Responsible for the N -Glycolylation of the Mycobacterial Peptidoglycan. Journal of Biological Chemistry, 280(1), 3263333. https://doi.org/10.1074/jbc.M411006200
189. Raynaud, C., Guilhot, C., Rauzier, J., Bordat, Y., Pelicic, V., Manganelli, R., Smith, I., Gicquel, B., & Jackson, M. (2002). Phospholipases C are involved in the virulence of Mycobacterium tuberculosis. Molecular Microbiology, 45(1), 2033217. https://doi.org/10.1046/j.1365-2958.2002.03009.x
190. Rego, E. H., Audette, R. E., & Rubin, E. J. (2017). Deletion of a mycobacterial divisome factor collapses single-cell phenotypic heterogeneity. Nature, 546(7656), 1533157. https://doi.org/10.1038/nature22361
191. Renshaw, P. S., Lightbody, K. L., Veverka, V., Muskett, F. W., Kelly, G., Frenkiel, T. A., Gordon, S. V, Hewinson, R. G., Burke, B., Norman, J., Williamson, R. A., & Carr, M. D. (2005). Structure and function of the complex formed by the tuberculosis virulence factors CFP-10 and ESAT-6. The EMBO Journal, 24(14), 249132498. https://doi.org/10.1038/sj.emboj.7600732
192. Richardson, K., Bennion, O. T., Tan, S., Hoang, A. N., Cokol, M., & Aldridge, B. B. (2016). Temporal and intrinsic factors of rifampicin tolerance in

mycobacteria. Proceedings of the National Academy of Sciences, 113(29), 83023 8307. https://doi.org/10.1073/pnas.1600372113
193. Robinson, C., Matos, C. F. R. O., Beck, D., Ren, C., Lawrence, J., Vasisht, N., & Mendel, S. (2011). Transport and proofreading of proteins by the twin-arginine translocation (Tat) system in bacteria. Biochimica et Biophysica Acta (BBA) - Biomembranes, 1808(3), 8763884. https://doi.org/10.1016/j.bbamem.2010.11.023
194. Romano, G. E., Silva-Pereira, T. T., de Melo, F. M., Sisco, M. C., Banari, A. C., Zimpel, C. K., Soler-Camargo, N. C., & Guimarães, A. M. de S. (2022). Unraveling the metabolism of Mycobacterium caprae using comparative genomics. Tuberculosis, 136, 102254. https://doi.org/10.1016/j.tube.2022.102254
195. Rosenberg, O. S., Dovey, C., Tempesta, M., Robbins, R. A., Finer-Moore, J. S., Stroud, R. M., & Cox, J. S. (2011). EspR, a key regulator of Mycobacterium tuberculosis virulence, adopts a unique dimeric structure among helix-turn-helix proteins. Proceedings of the National Academy of Sciences, 108(33), 134503 13455. https://doi.org/10.1073/pnas.1110242108
196. Roy, S., Ghatak, D., Das, P., & BoseDasgupta, S. (2020). ESX secretion system: The gatekeepers of mycobacterial survivability and pathogenesis. European Journal of Microbiology and Immunology, 10(4), 2023209. https://doi.org/10.1556/1886.2020.00028
197. Rueden, C. T., Schindelin, J., Hiner, M. C., DeZonia, B. E., Walter, A. E., Arena, E. T., & Eliceiri, K. W. (2017). ImageJ2: ImageJ for the next generation of scientific image data. BMC Bioinformatics, 18(1), 529. https://doi.org/10.1186/s12859-017-1934-z
198. Ruiz, N. (2008). Bioinformatics identification of MurJ (MviN) as the peptidoglycan lipid II flippase in Escherichia coli. Proceedings of the National Academy of Sciences, 105(40), 15553315557. https://doi.org/10.1073/pnas.0808352105
199. Saelens, J. W., Sweeney, M. I., Viswanathan, G., Xet-Mull, A. M., Jurcic Smith, K. L., Sisk, D. M., Hu, D. D., Cronin, R. M., Hughes, E. J., Brewer, W. J., Coers, J., Champion, M. M., Champion, P. A., Lowe, C. B., Smith, C. M., Lee, S., Stout, J. E., & Tobin, D. M. (2022). An ancestral mycobacterial effector promotes dissemination of infection. Cell, 185(24), 4507-4525.e18. https://doi.org/10.1016/j.cell.2022.10.019
200. Saint-Joanis, B., Demangel, C., Jackson, M., Brodin, P., Marsollier, L., Boshoff, H., & Cole, S. T. (2006). Inactivation of Rv2525c, a Substrate of the Twin Arginine Translocation (Tat) System of Mycobacterium tuberculosis , Increases β-Lactam Susceptibility and Virulence. Journal of Bacteriology, 188(18), 66693 6679. https://doi.org/10.1128/JB.00631-06
201. Salentin, S., Schreiber, S., Haupt, V. J., Adasme, M. F., & Schroeder, M. (2015). PLIP: fully automated protein3ligand interaction profiler. Nucleic Acids Research, 43(W1), W4433W447. https://doi.org/10.1093/nar/gkv315
202. Sanchez-Padilla, E., Merker, M., Beckert, P., Jochims, F., Dlamini, T., Kahn, P., Bonnet, M., & Niemann, S. (2015). Detection of Drug-Resistant Tuberculosis by

Xpert MTB/RIF in Swaziland. New England Journal of Medicine, 372(12), 118131182. https://doi.org/10.1056/NEJMc1413930

203. Sander, P., Rezwan, M., Walker, B., Rampini, S. K., Kroppenstedt, R. M., Ehlers, S., Keller, C., Keeble, J. R., Hagemeier, M., Colston, M. J., Springer, B., & Böttger, E. C. (2004). Lipoprotein processing is required for virulence of Mycobacterium tuberculosis †. Molecular Microbiology, 52(6), 154331552. https://doi.org/10.1111/j.1365-2958.2004.04041.x
204. Sankey, N., Merrick, H., Singh, P., Rogers, J., Reddi, A., Hartson, S. D., & Mitra, A. (2023). Role of the Mycobacterium tuberculosis ESX-4 Secretion System in Heme Iron Utilization and Pore Formation by PPE Proteins. MSphere, 8(2). https://doi.org/10.1128/msphere.00573-22
205. Santi, I., Dhar, N., Bousbaine, D., Wakamoto, Y., & McKinney, J. D. (2013). Single-cell dynamics of the chromosome replication and cell division cycles in mycobacteria. Nature Communications, 4(1), 2470. https://doi.org/10.1038/ncomms3470
206. Santoshi, M., Tare, P., & Nagaraja, V. (2024). Nucleoid-associated proteins of mycobacteria come with a distinctive flavor. Molecular Microbiology. https://doi.org/10.1111/mmi.15287
207. Sardiñas, M., García, G., Rosarys Martínez, M., Díaz, R., & Mederos, L. M. (2016). Importancia del control de la calidad de la baciloscopia en los laboratorios de diagnóstico de tuberculosis. Revista Chilena de Infectología, 33(3), 2823286. https://doi.org/10.4067/S0716-10182016000300005
208. Sauvage, E., Kerff, F., Terrak, M., Ayala, J. A., & Charlier, P. (2008a). The penicillin-binding proteins: structure and role in peptidoglycan biosynthesis. FEMS Microbiology Reviews, 32(2), 2343258. https://doi.org/10.1111/j.1574-6976.2008.00105.x
209. Sauvage, E., Kerff, F., Terrak, M., Ayala, J. A., & Charlier, P. (2008b). The penicillin-binding proteins: Structure and role in peptidoglycan biosynthesis. FEMS Microbiology Reviews, 32(2), 2343258. https://doi.org/10.1111/j.1574-6976.2008.00105.x
210. Schubert, O. T., Mouritsen, J., Ludwig, C., Röst, H. L., Rosenberger, G., Arthur, P. K., Claassen, M., Campbell, D. S., Sun, Z., Farrah, T., Gengenbacher, M., Maiolica, A., Kaufmann, S. H. E., Moritz, R. L., & Aebersold, R. (2013). The Mtb Proteome Library: A Resource of Assays to Quantify the Complete Proteome of Mycobacterium tuberculosis. Cell Host & Microbe, 13(5), 6023612. https://doi.org/10.1016/j.chom.2013.04.008
211. Schulz, W., & Zillig, W. (1981). Rifampidn inhibition of RNA synthesis by destabilisation of DNA-RNA polymerase-oligonucleotide-complexes. Nucleic Acids Research, 9(24), 688936906. https://doi.org/10.1093/nar/9.24.6889
212. Scott, A. N., Menzies, D., Tannenbaum, T.-N., Thibert, L., Kozak, R., Joseph, L., Schwartzman, K., & Behr, M. A. (2005). Sensitivities and Specificities of Spoligotyping and Mycobacterial Interspersed Repetitive Unit-Variable-Number Tandem Repeat Typing Methods for Studying Molecular Epidemiology of Tuberculosis. Journal of Clinical Microbiology, 43(1), 89394. https://doi.org/10.1128/JCM.43.1.89-94.2005

213. Sebastian, J., Nair, R. R., Swaminath, S., & Ajitkumar, P. (2020). Mycobacterium tuberculosis Cells Surviving in the Continued Presence of Bactericidal Concentrations of Rifampicin in vitro Develop Negatively Charged Thickened Capsular Outer Layer That Restricts Permeability to the Antibiotic. Frontiers in Microbiology, 11. https://doi.org/10.3389/fmicb.2020.554795
214. Sensi, P. (1983). History of the Development of Rifampin. Clinical Infectious Diseases, 5(Supplement_3), S4023S406. https://doi.org/10.1093/clinids/5.Supplement_3.S402
215. Shaku, M., Ealand, C., Matlhabe, O., Lala, R., & Kana, B. D. (2020). Peptidoglycan biosynthesis and remodeling revisited (pp. 673103). https://doi.org/10.1016/bs.aambs.2020.04.001
216. Shea, J., Halse, T. A., Kohlerschmidt, D., Lapierre, P., Modestil, H. A., Kearns, C. H., Dworkin, F. F., Rakeman, J. L., Escuyer, V., & Musser, K. A. (2021). Low-Level Rifampin Resistance and rpoB Mutations in Mycobacterium tuberculosis: an Analysis of Whole-Genome Sequencing and Drug Susceptibility Test Data in New York. Journal of Clinical Microbiology, 59(4). https://doi.org/10.1128/JCM.01885-20
217. Shin, S. S., Modongo, C., Baik, Y., Allender, C., Lemmer, D., Colman, R. E., Engelthaler, D. M., Warren, R. M., & Zetola, N. M. (2018). Mixed Mycobacterium tuberculosis3Strain Infections Are Associated With Poor Treatment Outcomes Among Patients With Newly Diagnosed Tuberculosis, Independent of Pretreatment Heteroresistance. The Journal of Infectious Diseases. https://doi.org/10.1093/infdis/jiy480
218. Sia, J. K., & Rengarajan, J. (2019). Immunology of Mycobacterium tuberculosis Infections. Microbiology Spectrum, 7(4). https://doi.org/10.1128/microbiolspec.GPP3-0022-2018
219. Sirgel, F. A., Wiid, I. J. F., & van Helden, P. D. (2009). Measuring Minimum Inhibitory Concentrations in Mycobacteria (pp. 1733186). https://doi.org/10.1007/978-1-59745-207-6_11
220. Siu, G. K. H., Zhang, Y., Lau, T. C. K., Lau, R. W. T., Ho, P.-L., Yew, W.-W., Tsui, S. K. W., Cheng, V. C. C., Yuen, K.-Y., & Yam, W.-C. (2011). Mutations outside the rifampicin resistance-determining region associated with rifampicin resistance in Mycobacterium tuberculosis. Journal of Antimicrobial Chemotherapy, 66(4), 7303733. https://doi.org/10.1093/jac/dkq519
221. Sobkowiak, B., Glynn, J. R., Houben, R. M. G. J., Mallard, K., Phelan, J. E., Guerra-Assunção, J. A., Banda, L., Mzembe, T., Viveiros, M., McNerney, R., Parkhill, J., Crampin, A. C., & Clark, T. G. (2018). Identifying mixed Mycobacterium tuberculosis infections from whole genome sequence data. BMC Genomics, 19(1), 613. https://doi.org/10.1186/s12864-018-4988-z
222. Some, D., Amartely, H., Tsadok, A., & Lebendiker, M. (2019). Characterization of Proteins by Size-Exclusion Chromatography Coupled to Multi-Angle Light Scattering (SEC-MALS). Journal of Visualized Experiments, 148. https://doi.org/10.3791/59615
223. Sonnenkalb, L., Strohe, G., Dreyer, V., Andres, S., Hillemann, D., Maurer, F. P., Niemann, S., & Merker, M. (2021). Microevolution of Mycobacterium

tuberculosis Subpopulations and Heteroresistance in a Patient Receiving 27 Years of Tuberculosis Treatment in Germany. Antimicrobial Agents and Chemotherapy, 65(7). https://doi.org/10.1128/AAC.02520-20

224. Stinear, T. P., Seemann, T., Harrison, P. F., Jenkin, G. A., Davies, J. K., Johnson, P. D. R., Abdellah, Z., Arrowsmith, C., Chillingworth, T., Churcher, C., Clarke, K., Cronin, A., Davis, P., Goodhead, I., Holroyd, N., Jagels, K., Lord, A., Moule, S., Mungall, K., … Cole, S. T. (2008). Insights from the complete genome sequence of Mycobacterium marinum on the evolution of Mycobacterium tuberculosis. Genome Research, 18(5), 7293741. https://doi.org/10.1101/gr.075069.107
225. Stoop, E. J. M., Schipper, T., Rosendahl Huber, S. K., Nezhinsky, A. E., Verbeek, F. J., Gurcha, S. S., Besra, G. S., Vandenbroucke-Grauls, C. M. J. E., Bitter, W., & van der Sar, A. M. (2011). Zebrafish embryo screen for mycobacterial genes involved in the initiation of granuloma formation reveals a newly identified ESX-1 component. Disease Models & Mechanisms, 4(4), 5263536. https://doi.org/10.1242/dmm.006676
226. Stover, C. K., de la Cruz, V. F., Fuerst, T. R., Burlein, J. E., Benson, L. A., Bennett, L. T., Bansal, G. P., Young, J. F., Lee, M. H., Hatfull, G. F., Snapper, S. B., Barletta, R. G., Jacobs, W. R., & Bloom, B. R. (1991). New use of BCG for recombinant vaccines. Nature, 351(6326), 4563460. https://doi.org/10.1038/351456a0
227. Su, F., Cao, L., Ren, X., Hu, J., Tavengana, G., Wu, H., Zhou, Y., Fu, Y., Jiang, M., & Wen, Y. (2023). The mutation rate of rpoB gene showed an upward trend with the increase of MIRU10, MIRU39 and QUB4156 repetitive number. BMC Genomics, 24(1), 26. https://doi.org/10.1186/s12864-023-09120-y
228. Supply, P., Marceau, M., Mangenot, S., Roche, D., Rouanet, C., Khanna, V., Majlessi, L., Criscuolo, A., Tap, J., Pawlik, A., Fiette, L., Orgeur, M., Fabre, M., Parmentier, C., Frigui, W., Simeone, R., Boritsch, E. C., Debrie, A.-S., Willery, E., … Brosch, R. (2013). Genomic analysis of smooth tubercle bacilli provides insights into ancestry and pathoadaptation of Mycobacterium tuberculosis. Nature Genetics, 45(2), 1723179. https://doi.org/10.1038/ng.2517
229. Swaim, L. E., Connolly, L. E., Volkman, H. E., Humbert, O., Born, D. E., & Ramakrishnan, L. (2006). Mycobacterium marinum Infection of Adult Zebrafish Causes Caseating Granulomatous Tuberculosis and Is Moderated by Adaptive Immunity. Infection and Immunity, 74(11), 610836117. https://doi.org/10.1128/IAI.00887-06
230. Taniguchi, H., Aramaki, H., Nikaido, Y., Mizuguchi, Y., Nakamura, M., Koga, T., & Yoshida, S. (1996). Rifampicin resistance and mutation of the rpoB gene in Mycobacterium tuberculosis. FEMS Microbiology Letters, 144(1), 1033108. https://doi.org/10.1111/j.1574-6968.1996.tb08515.x
231. Tarashi, S., Fateh, A., Mirsaeidi, M., Siadat, S. D., & Vaziri, F. (2017). Mixed infections in tuberculosis: The missing part in a puzzle. Tuberculosis, 107, 1683 174. https://doi.org/10.1016/j.tube.2017.09.004
232. Taw, M. N., Boock, J. T., Sotomayor, B., Kim, D., Rocco, M. A., Waraho-Zhmayev, D., & DeLisa, M. P. (2022). Twin-arginine translocase component

TatB performs folding quality control via a chaperone-like activity. Scientific Reports, 12(1), 14862. https://doi.org/10.1038/s41598-022-18958-3

233. Tipper, D. J., & Strominger, J. L. (1965). Mechanism of action of penicillins: a proposal based on their structural similarity to acyl-D-alanyl-D-alanine. Proceedings of the National Academy of Sciences, 54(4), 113331141. https://doi.org/10.1073/pnas.54.4.1133
234. Tobin, D. M., & Ramakrishnan, L. (2008). Comparative pathogenesis of Mycobacterium marinum and Mycobacterium tuberculosis. Cellular Microbiology, 10(5), 102731039. https://doi.org/10.1111/j.1462-5822.2008.01133.x
235. Torrey, H. L., Keren, I., Via, L. E., Lee, J. S., & Lewis, K. (2016). High Persister Mutants in Mycobacterium tuberculosis. PLOS ONE, 11(5), e0155127. https://doi.org/10.1371/journal.pone.0155127
236. Trunkfield, A. E., Gurcha, S. S., Besra, G. S., & Bugg, T. D. H. (2010). Inhibition of Escherichia coli glycosyltransferase MurG and Mycobacterium tuberculosis Gal transferase by uridine-linked transition state mimics. Bioorganic & Medicinal Chemistry, 18(7), 265132663. https://doi.org/10.1016/j.bmc.2010.02.026
237. Tsukamura, M. (1983). Numerical Classification of 280 Strains of Slowly Growing Mycobacteria. Microbiology and Immunology, 27(4), 3153334. https://doi.org/10.1111/j.1348-0421.1983.tb00591.x
238. Tufariello, J. M., Chapman, J. R., Kerantzas, C. A., Wong, K.-W., Vilchèze, C., Jones, C. M., Cole, L. E., Tinaztepe, E., Thompson, V., Fenyö, D., Niederweis, M., Ueberheide, B., Philips, J. A., & Jacobs, W. R. (2016). Separable roles for Mycobacterium tuberculosis ESX-3 effectors in iron acquisition and virulence. Proceedings of the National Academy of Sciences, 113(3). https://doi.org/10.1073/pnas.1523321113
239. Ullah, N., Hao, L., Banga Ndzouboukou, J.-L., Chen, S., Wu, Y., Li, L., Borham Mohamed, E., Hu, Y., & Fan, X. (2021). Label-Free Comparative Proteomics of Differentially Expressed Mycobacterium tuberculosis Protein in Rifampicin-Related Drug-Resistant Strains. Pathogens, 10(5), 607. https://doi.org/10.3390/pathogens10050607
240. Valbuena, N., Letek, M., Ordóñez, E., Ayala, J., Daniel, R. A., Gil, J. A., & Mateos, L. M. (2007). Characterization of HMW-PBPs from the rod-shaped actinomycete Corynebacterium glutamicum : peptidoglycan synthesis in cells lacking actin-like cytoskeletal structures. Molecular Microbiology, 66(3), 6433 657. https://doi.org/10.1111/j.1365-2958.2007.05943.x
241. Vallejo V, P., Rodríguez D, J. C., Searle M, A., & Farga C, V. (2015). Ensayo Xpert MTB/RIF en el diagnóstico de tuberculosis. Revista Chilena de Enfermedades Respiratorias, 31(2), 1273131. https://doi.org/10.4067/S0717-73482015000200010
242. van der Woude, A. D., Stoop, E. J. M., Stiess, M., Wang, S., Ummels, R., van Stempvoort, G., Piersma, S. R., Cascioferro, A., Jiménez, C. R., Houben, E. N. G., Luirink, J., Pieters, J., van der Sar, A. M., & Bitter, W. (2014). Analysis of SecA2-dependent substrates in M ycobacterium marinum identifies protein

kinase G (PknG) as a virulence effector. Cellular Microbiology, 16(2), 2803295. https://doi.org/10.1111/cmi.12221
243. Volkman, H. E., Clay, H., Beery, D., Chang, J. C. W., Sherman, D. R., & Ramakrishnan, L. (2004). Tuberculous Granuloma Formation Is Enhanced by a Mycobacterium Virulence Determinant. PLoS Biology, 2(11), e367. https://doi.org/10.1371/journal.pbio.0020367
244. von Heijne, G. (1990). The signal peptide. The Journal of Membrane Biology, 115(3), 1953201. https://doi.org/10.1007/BF01868635
245. Walker, T. M., Miotto, P., Köser, C. U., Fowler, P. W., Knaggs, J., Iqbal, Z., Hunt, M., Chindelevitch, L., Farhat, M. R., Cirillo, D. M., Comas, I., Posey, J., Omar, S. V, Peto, T. E., Suresh, A., Uplekar, S., Laurent, S., Colman, R. E., Nathanson, C.-M., … Puyen, Z. M. (2022). The 2021 WHO catalogue of Mycobacterium tuberculosis complex mutations associated with drug resistance: a genotypic analysis. The Lancet Microbe, 3(4), e2653e273. https://doi.org/10.1016/S2666-5247(21)00301-3
246. Walpole, S., Monaco, S., Nepravishta, R., & Angulo, J. (2019). STD NMR as a Technique for Ligand Screening and Structural Studies (pp. 4233451). https://doi.org/10.1016/bs.mie.2018.08.018
247. Wan Nor Amilah, W. A. W., Mohammad Lukman, Y., Siti Suraiya, M. N., & Noor Izani, N. J. (2016). Direct tetrazolium microplate assay (TEMA) for rapid drug susceptibility test screening of Mycobacterium tuberculosis. Tropical Biomedicine, 33(4), 8143823.
248. Wang, J., Wang, W., Kollman, P., & Case, D. (2000). ANTECHAMBER: an accessory software package for molecular mechanical calculations. Journal of Chemical Information and Computer Sciences, JCISD. 222.
249. Wang, L., Asare, E., Shetty, A. C., Sanchez-Tumbaco, F., Edwards, M. R., Saranathan, R., Weinrick, B., Xu, J., Chen, B., Bénard, A., Dougan, G., Leung, D. W., Amarasinghe, G. K., Chan, J., Basler, C. F., Jacobs, W. R., & Tufariello, J. M. (2022). Multiple genetic paths including massive gene amplification allow Mycobacterium tuberculosis to overcome loss of ESX-3 secretion system substrates. Proceedings of the National Academy of Sciences, 119(8). https://doi.org/10.1073/pnas.2112608119
250. Wang, L., Campino, S., Phelan, J., & Clark, T. G. (2023). Mixed infections in genotypic drug-resistant Mycobacterium tuberculosis. Scientific Reports, 13(1), 17100. https://doi.org/10.1038/s41598-023-44341-x
251. Wang, X., Tang, B., Ye, Y., Mao, Y., Lei, X., Zhao, G., & Ding, X. (2017). Bxb1 integrase serves as a highly efficient DNA recombinase in rapid metabolite pathway assembly. Acta Biochimica et Biophysica Sinica, 49(1), 44350. https://doi.org/10.1093/abbs/gmw115
252. Wehrli, W. (1983). Rifampin: Mechanisms of Action and Resistance. Clinical Infectious Diseases, 5(Supplement_3), S4073S411. https://doi.org/10.1093/clinids/5.Supplement_3.S407
253. WHO. (2020a). Global tuberculosis report. https://apps.who.int/iris/bitstream/handle/10665/336069/9789240013131-eng.pdf

254. WHO. (2020b). WHO operational handbook on tuberculosis Module 4: Treatment (World Health Organization;, Ed.). WHO. https://iris.who.int/bitstream/handle/10665/332398/9789240006997-eng.pdf
255. WHO. (2022). Line probe assays for detection of drug-resistant tuberculosis: interpretation and reporting manual for laboratory staff and clinicians. https://www.who.int/publications/i/item/9789240046665
256. WHO. (2023a). Directrices unificadas de la OMS sobre la tuberculosis. Módulo 4: Tratamiento. Tratamiento de la tuberculosis farmacorresistente. Actualización del 2022. PAHO. https://doi.org/10.37774/9789275327869
257. WHO. (2023b). Global Tuberculosis Report 2023. https://www.who.int/publications/i/item/9789240083851
258. World Health Organization. (2016). The Use of Loop-Mediated Isothermal Amplification (TB-LAMP) for the Diagnosis of Pulmonary Tuberculosis: Policy Guidance. https://www.ncbi.nlm.nih.gov/books/NBK384520/#:~:text=TB%2DLAMP%20is%20a%20manual,signs%20and%20symptoms%20of%20TB.
259. Xu, G., Liu, H., Jia, X., Wang, X., & Xu, P. (2021). Mechanisms and detection methods of Mycobacterium tuberculosis rifampicin resistance: The phenomenon of drug resistance is complex. Tuberculosis, 128, 102083. https://doi.org/10.1016/j.tube.2021.102083
260. Yang, B. (1998). Relationship between antimycobacterial activities of rifampicin, rifabutin and KRM-1648 and rpoB mutations of Mycobacterium tuberculosis. Journal of Antimicrobial Chemotherapy, 42(5), 6213628. https://doi.org/10.1093/jac/42.5.621
261. Yoshida, M., Fukano, H., Miyamoto, Y., Shibayama, K., Suzuki, M., & Hoshino, Y. (2018). Complete Genome Sequence of Mycobacterium marinum ATCC 927 T , Obtained Using Nanopore and Illumina Sequencing Technologies. Genome Announcements, 6(20). https://doi.org/10.1128/genomeA.00397-18
262. Zetola, N. M., Shin, S. S., Tumedi, K. A., Moeti, K., Ncube, R., Nicol, M., Collman, R. G., Klausner, J. D., & Modongo, C. (2014). Mixed Mycobacterium tuberculosis Complex Infections and False-Negative Results for Rifampin Resistance by GeneXpert MTB/RIF Are Associated with Poor Clinical Outcomes. Journal of Clinical Microbiology, 52(7), 242232429. https://doi.org/10.1128/JCM.02489-13
263. Zhang, Y. J., Reddy, M. C., Ioerger, T. R., Rothchild, A. C., Dartois, V., Schuster, B. M., Trauner, A., Wallis, D., Galaviz, S., Huttenhower, C., Sacchettini, J. C., Behar, S. M., & Rubin, E. J. (2013). Tryptophan Biosynthesis Protects Mycobacteria from CD4 T-Cell-Mediated Killing. Cell, 155(6), 129631308. https://doi.org/10.1016/j.cell.2013.10.045
264. Zhao, G., Meier, T. I., Kahl, S. D., Gee, K. R., & Blaszczak, L. C. (1999). BOCILLIN FL, a Sensitive and Commercially Available Reagent for Detection of Penicillin-Binding Proteins. Antimicrobial Agents and Chemotherapy, 43(5), 112431128. https://doi.org/10.1128/AAC.43.5.1124
265. Zhu, J.-H., Wang, B.-W., Pan, M., Zeng, Y.-N., Rego, H., & Javid, B. (2018). Rifampicin can induce antibiotic tolerance in mycobacteria via paradoxical

changes in rpoB transcription. Nature Communications, 9(1), 4218. https://doi.org/10.1038/s41467-018-06667-3

266. Zhu, M., & Dai, X. (2018). On the intrinsic constraint of bacterial growth rate: M. tuberculosis 9s view of the protein translation capacity. Critical Reviews in Microbiology, 44(4), 4553464. https://doi.org/10.1080/1040841X.2018.1425672

Appendix index

Appendix III.7. *In silico* ligation of ponA1$_{234\text{-}820}$ -P631S in pET28a plasmid (a), nucleotide (b) and amino acid (c) sequence.

Appendix III.8. *In silico* ligation of *rpoB* from *M. tuberculosis* H37Rv in pET28a plasmid (a), nucleotide (b) and amino acid (c) sequence.

Appendix III.9 Zym media-5052 composition

Appendix III.10. Promotor evaluation by FACS in *M. smegmatis* (Source from Cohen-Gonsaud et al, 2021). *rpsTp* from *M. marinum* integrated in *M.smegmatis* evaluation.

Appendix III.11. ponA1 promoter sequence from *M. tuberculosis*, ponA1 *Mycobacterium tuberculosis* gene sequence and *in silico* representation of *M. tuberculosis* ponA1 promoter and gene ligated in pKM464 plasmid.

Appendix III.12 Generation of pKM464-ponA1p-ponA1g plasmid

Appendix III.13. EGFP nucleotide sequence

Appendix III.14. *In silico* ligation of ponA1p-EGFP in pKM464

Appendix III.15. *rpsTp* promotor sequence from *M. marinum*

Appendix III.16. *In silico* ligation of *rpsTp*-EGFP in pKM464

Appendix III.17. Cloning by Gibson assembly (Synthetic biology protocols-Montpellier-France).

Appendix III.18 Gibson assembly preparation (Synthetic biology protocols-Montpellier-France).

Appendix III.19. *In silico* ligation of *rpsTp*-ponA1 in pKM464.

Appendix III.20. *In silico* ligation of ponA1 in pMV361.

Appendix III.21. Antibiotic cassette replacement in pMV361-ponA1 to generate pMV361$_{ZEO}$-ponA1.

Appendix III.22. *In silico* ligation of *rpsTp*-ponA1-T34A in pKM464

Appendix III.23. *In silico* ligation of *rpsTp*-ponA1-T34D in pKM464.

Appendix III.24. *In silico* ligation of *rpsTp*-ponA1-Q365H in pKM464.

Appendix III.25. *In silico* ligation of *rpsTp*-ponA1-A516T in pKM464.

Appendix III.26. *In silico* ligation of *rpsTp*-ponA1-P631S in pKM464.

Appendix III.27. *In silico* ligation ponA1-T34A in $pMV361_{ZEO}$ and gene sequence.

Appendix III.28. *In silico* ligation ponA1-T34D in $pMV361_{ZEO}$ and gene sequence.

Appendix III.29. *In silico* ligation ponA1-Q365H in $pMV361_{ZEO}$ and gene sequence.

Appendix III.30. *In silico* ligation ponA1-A516T in $pMV361_{ZEO}$ and gene sequence.

Appendix III.31. *In silico* ligation ponA1-P631S in $pMV361_{ZEO}$ and gene sequence.

Appendix III.32. *In silico* ligation of *rpsT*-MMAR0069 in pKM464.

Appendix III.33. *In silico* ligation *MMAR_0069* in $pMV361_{ZEO}$ and *MMAR_0069* gene sequence.

Appendix III.34. Primers designed for cloning, site mutagenesis directed and Gibson assembly and sequence verification.

Appendix III.35 Metrics for molecular docking between PonA1 crystal transpeptidase 5CRF and penicillin (open form) by GNINA.

Appendix II.36 Metrics for molecular docking between PonA1 crystal transpeptidase 5CRF and penicillin (open form) by DiffDock

Appendix III.37. Metrics for molecular docking between PonA_WT_ESM against penicillin V by Diffdock.

Appendix III.38. Metrics for molecular docking between PonA1_WT-ESM and rifampicin.

Appendix III.39. STD_NMR assay titration for K_D determination between $PonA1_{234-820}$_WT and rifampicin

Appendix III.40. STD_NMR assay titration for KD determination between $PonA1_{234-820}$_Q365H and rifampicin.

Appendix III.41. STD_NMR assay titration for KD determination between $PonA1_{234-820}$_P631S and rifampicin.

Appendix chapter II

Identification of rifampicin heteroresistant tuberculosis infection through whole genome analysis of peruvian isolates

Katherine Vallejos-Sánchez[a,b], Diego A. Taquiri-Díaz[a], Omar A. Romero-Rodriguez[a], Ana Paula Vargas[a], Jorge Coronel[a], Arturo Torres[c], Jose L. Perez[a], Adiana Ochoa[a], Robert H. Gilman[d], Louis Grandjean[c]; Martin Cohen-Gonsaud[b], Mirko Zimic[a*], Patricia Sheen[a*]

[a]Laboratorio de Bioinformática, Biología Molecular y Desarrollos Tecnológicos. Laboratorios de Investigación y Desarrollo. Facultad de Ciencias e Ingeniería. Universidad Peruana Cayetano Heredia, Av. Honorio Delgado 430, San Martín de Porres 15102, Peru.

[b]Centre de Biologie Structurale, CNRS, INSERM, 29 rue de Navacelles, 34090 Montpellier, France.

[c] Department of Infection, Immunity and Inflammation, Institute of Child Health, University College London, WC1N 1EH, London, UK.

[d] International Health Department. Johns Hopkins School of Public Health, 615 N. Wolfe Street, Baltimore, MD 21205, USA.

This manuscript was submitted for peer-review to the Journal of Medical Microbiology. Minor changes have been introduced in the chapter below.

Author Contributions

Conceptualization, MZ, PS and KV ; methodology, KV and MZ, PS; investigation, KV, DT, OR, AO and JC; formal analysis, MZ, PS, DT, OR and KV; resources MZ and PS; data curation KV, DT, OR, AT, JP writing4original draft preparation, KV; writing4 review and editing MZ, LG, MCG, AT, RHG and PS. All authors have read and agreed to the published version of the manuscript.

Appendix II.1. Analysis of mutations in drug resistance-related genes in rifampicin-heteroresistant primary *M. tuberculosis* isolates using TBprofiler.

	Genes related to drug resistance					
StrainID	RIF	INH	PZA	EMB	STM	FQ
LI2174109	rpoC_c.1626C>G (1.00), rpoC_p.Pro1040Ala (0.79)	fabG1_c.-15C>T (0.73)	pncA_p.His51Arg (0.86)	-	gid_c.319dupG (0.19)	-
PLE-0891	rpoA_p.Thr187Pro (0.19), rpoC_c.1626C>G (1.00), rpoC_p.Ile832Val (0.48)	katG_p.Ala109Val (1.00)	-	-	-	-
PMFR-0719	rpoC_c.1626C>G (0.94)	fabG1_c.-15C>T (0.89)	-	-	-	-
PMFR-0732	rpoA_c.-88C>T (0.27), rpoA_c.-128C>T (0.22)	katG_p.Ser315Thr (1.00)	-	embB_p.Gly406Ser (1.00)	-	-
PMFR-0737	rpoC_c.-339T>C (0.99)	-	-	-	rpsL_p.Lys43Arg (1.00)	-
PMOP-0526	rpoC_c.1626C>G (1.00), rpoC_p.Pro1040Ala (0.75)	fabG1_c.-15C>T (0.73)	pncA_p.His51Arg (0.82)	embB_p.Met306Val (0.83)	-	-
PMOP-0618	rpoC_p.His525Gln (0.38), rpoC_p.Gly594Glu (1.00)	katG_p.Ser315Thr (1.00)	pncA_p.His57Arg (1.00)	embB_p.Met306Ile (1.00)	rpsL_p.Lys43Arg (1.00)	gyrA_p.Asp94Gly (1.00)
PSLM-0811	rpoA_c.-88C>T (0.25), rpoA_c.-128C>T (0.27)	fabG1_c.-17G>T (1.00), katG_p.Ser315Asn (0.99)	pncA_p.Ser104Arg (1.00)	embB_p.Met306Ile (1.00)	-	gyrA_p.Asp94Gly (1.00)
PSLM-0843	rpoC_c.1626C>G (1.00), rpoC_p.Glu1033Lys (0.25)	fabG1_c.-15C>T (1.00), inhA_p.Ile21Val (1.00)	pncA_p.His51Arg (1.00)	embB_p.Gly406Ala (1.00)	-	-
PTAN-0241	rpoC_c.1626C>G (1.00), rpoC_p.Arg741Ser (1.00)	katG_p.Ser315Thr (1.00)	-	-	gid_c.180delA (1.00)	-
28832_3#257	rpoC_c.1626C>G (1.00), rpoC_p.Pro1040Ala (0.64)	fabG1_c.-15C>T (0.63)	pncA_p.His51Arg (0.73)	-	-	-
28832_3#91	-	-	-	-	-	-
28832_4#246	rpoA_c.-74_-73insCAACCCA (0.25), rpoA_c.-88C>T (0.28), rpoA_c.-128C>T (0.19), rpoC_c.1626C>G (0.19)	katG_p.Ser315Thr (0.23)	pncA_p.Leu116Pro (0.25)	embB_p.Met306Ile (0.34)	-	-
28832_4#250	rpoC_c.1626C>G (0.82)	katG_p.Ser315Thr (0.70)	pncA_p.Leu116Pro (0.62)	embB_p.Met306Ile (0.80)	-	-

Abbr. RIF-Rifampicin, INH-Isoniazid, PZA-Pyrazinamide, EMB-Ethambutol, STM-Streptomycin, FQ-Fluoroquinolones, MXF-Moxifloxacin, OFX-Ofloxacin, LVX-Levofloxacin, CIP-Ciprofloxacin, AG-Aminoglycosides, AMK-Amikacin, KAN-Kanamycin, CAP-Capreomycin, ETH-Ethionamide, PAS-Para-aminosalicylic acid, CS-Cycloserine, LZD-Linezolid, BDQ-Bedaquiline, CFZ-Clofazimine, DLM-Delamanid.

Appendix II.1.(*continuation*…) Analysis of mutations in drug resistance-related genes in rifampicin-heteroresistant primary *M. tuberculosis* isolates using TBprofiler.

StrainID	Genes related to drug resistance					
	RIF	INH	PZA	EMB	STM	FQ
28889_1#38	rpoC_p.Gly594Glu (1.00), rpoC_p.Thr1230Ile (1.00)	katG_p.Ser315Thr (1.00)	pncA_p.Gln10Pro (1.00)	embB_p.Asp354Ala (1.00)	-	-
28889_1#95	rpoA_c.-88C>T (0.57)	katG_p.Ser315Thr (1.00)	-	embB_p.Gly406Ser (1.00)	-	-
29544_1#13	rpoC_p.Gly594Glu (0.92)	katG_p.Ser315Thr (0.19)	-	embB_p.Met306Ile (0.16)	-	-
29544_1#232	rpoC_p.Gly594Glu (1.00), rpoC_p.His767Pro (0.76)	fabG1_c.-15C>T (0.77), katG_p.Ser315Asn (0.79)	pncA_p.Leu4Trp (0.70)	embB_p.Gln497Lys (0.79)	gid_p.Tyr195* (0.79)	gyrA_p.Ser91Pro (0.77)
29544_1#316	rpoC_c.1626C>G (1.00)	katG_p.Ser315Thr (0.26)	pncA_p.Tyr103* (0.16)	embB_p.Asp354Ala (0.38)	-	-
29544_1#337	rpoC_c.1626C>G (1.00)	katG_p.Ser315Thr (0.42)	pncA_p.Tyr103* (0.35)	embB_p.Asp354Ala (0.52)	-	-
29544_1#6	rpoC_c.1626C>G (0.41), rpoC_p.Gly594Glu (0.39)	katG_p.Ser315Thr (0.50)	pncA_p.Gln10Arg (0.46)	embB_p.Tyr319Ser (0.50)	gid_p.Pro84Leu (0.56)	-
CA-0116	rpoC_c.-339T>C (1.00), rpoC_c.162G>C (1.00), rpoC_p.Ala172Val (1.00), rpoC_c.517C>A (1.00)	katG_p.Ser315Thr (1.00)	-	-	gid_p.Leu79* (1.00)	-

Abbr. RIF-Rifampicin, INH-Isoniazid, PZA-Pyrazinamide, EMB-Ethambutol, STM-Streptomycin, FQ-Fluoroquinolones, MXF-Moxifloxacin, OFX-Ofloxacin, LVX-Levofloxacin, CIP-Ciprofloxacin, AG-Aminoglycosides, AMK-Amikacin, KAN-Kanamycin, CAP-Capreomycin, ETH-Ethionamide, PAS-Para-aminosalicylic acid, CS-Cycloserine, LZD-Linezolid, BDQ-Bedaquiline, CFZ-Clofazimine, DLM-Delamanid.

Appendix II.1 (*continuation*…). Analysis of mutations in drug resistance-related genes in rifampicin-heteroresistant primary *M. tuberculosis* isolates using TBprofiler.

	Genes related to drug resistance						
StrainID	MXF	OFX	LVX	CIP	AG	AMK	KAN
LI2174109	-	-	-	-	-	-	-
PLE-0891	-	-	-	-	-	-	-
PMFR-0719	-	-	-	-	-	-	-
PMFR-0732	-	-	-	-	rrs_n.1401A>G (1.00)	rrs_n.1401A>G (1.00)	rrs_n.1401A>G (1.00)
PMFR-0737	-	-	-	-	-	-	-
PMOP-0526	-	-	-	-	-	-	-
PMOP-0618	gyrA_p.Asp94Gly (1.00)	gyrA_p.Asp94Gly (1.00)	gyrA_p.Asp94Gly (1.00)	gyrA_p.Asp94Gly (1.00)	rrs_n.1401A>G (1.00)	rrs_n.1401A>G (1.00)	rrs_n.1401A>G (1.00)
PSLM-0811	gyrA_p.Asp94Gly (1.00)	gyrA_p.Asp94Gly (1.00)	gyrA_p.Asp94Gly (1.00)	gyrA_p.Asp94Gly (1.00)	rrs_n.1401A>G (1.00)	rrs_n.1401A>G (1.00)	rrs_n.1401A>G (1.00)
PSLM-0843	-	-	-	-	-	-	eis_c.-10G>A (1.00)
PTAN-0241	-	-	-	-	-	-	-
28832_3#257	-	-	-	-	-	-	-
28832_3#91	-	-	-	-	-	-	-
28832_4#246	-	-	-	-	-	-	-
28832_4#250	-	-	-	-	-	-	-
28832_4#318	-	-	-	-	-	-	-
28889_1#38	-	-	-	-	-	-	-
28889_1#95	-	-	-	-	-	-	-
29544_1#13	-	-	-	-	-	-	-
29544_1#232	gyrA_p.Ser91Pro (0.77)	gyrA_p.Ser91Pro (0.77)	gyrA_p.Ser91Pro (0.77)	gyrA_p.Ser91Pro (0.77)	-	-	-
29544_1#316	-	-	-	-	-	-	-
29544_1#337	-	-	-	-	-	-	-
29544_1#6	-	-	-	-	-	-	-
CA-0116	-	-	-	-	-	-	-

Abbr. RIF-Rifampicin, INH-Isoniazid, PZA-Pyrazinamide, EMB-Ethambutol, STM-Streptomycin, FQ-Fluoroquinolones, MXF-Moxifloxacin, OFX-Ofloxacin, LVX-Levofloxacin, CIP-Ciprofloxacin, AG-Aminoglycosides, AMK-Amikacin, KAN-Kanamycin, CAP-Capreomycin, ETH-Ethionamide, PAS-Para-aminosalicylic acid, CS-Cycloserine, LZD-Linezolid, BDQ-Bedaquiline, CFZ-Clofazimine, DLM-Delamanid.

Appendix II.1 (*continuation*…). Analysis of mutations in drug resistance-related genes in rifampicin-heteroresistant primary *M. tuberculosis* isolates using TBprofiler.

	Genes related to drug resistance							
StrainID	CAP	ETH	PAS	CS	LZD	BDQ	CFZ	DLM
LI2174109	-	fabG1_c.-15C>T (0.73)	-	-	-	-	-	-
PLE-0891	-	-	-	-	-	-	-	-
PMFR-0719	-	fabG1_c.-15C>T (0.89)	-	-	-	-	-	-
PMFR-0732	rrs_n.1401A>G (1.00)	-	-	-	-	mmpR5_c.198dupG (1.00)	mmpR5_c.198dupG (1.00)	-
PMFR-0737	-	-	-	-	-	-	-	-
PMOP-0526	-	fabG1_c.-15C>T (0.73)	-	-	-	-	-	-
PMOP-0618	rrs_n.1401A>G (1.00)	-	-	ald_c.464delG (0.65)	-	-	-	-
PSLM-0811	rrs_n.1401A>G (1.00)	fabG1_c.-17G>T (1.00)	-	-	-	-	-	-
PSLM-0843	-	fabG1_c.-15C>T (1.00)	-	-	-	-	-	-
PTAN-0241	-	-	-	-	-	-	-	-
28832_3#257	-	fabG1_c.-15C>T (0.63)	-	-	-	-	-	-
28832_3#91	-	-	-	-	-	-	-	-
28832_3#91	-	-	-	-	-	-	-	-
28832_4#246	-	-	-	-	-	-	-	-
28832_4#250	-	-	-	-	-	-	-	-
28832_4#318	tlyA_p.Gly232Asp (0.77)	-	-	-	-	-	-	-
28889_1#38	-	-	-	-	-	-	-	-
28889_1#95	-	-	-	-	-	mmpR5_c.198dupG (1.00)	mmpR5_c.198dupG (1.00)	-
29544_1#13	-	-	-	-	-	-	-	-
29544_1#232	-	fabG1_c.-15C>T (0.77)	-	-	-	-	-	-
29544_1#316	-	-	-	-	-	-	-	-
29544_1#337	-	-	-	-	-	-	-	-
29544_1#6	-	-	-	-	-	-	-	-
CA-0116	-	-	-	-	-	-	-	-

Abbr. RIF-Rifampicin, INH-Isoniazid, PZA-Pyrazinamide, EMB-Ethambutol, STM-Streptomycin, FQ-Fluoroquinolones, MXF-Moxifloxacin, OFX-Ofloxacin, LVX-Levofloxacin, CIP-Ciprofloxacin, AG-Aminoglycosides, AMK-Amikacin, KAN-Kanamycin, CAP-Capreomycin, ETH-Ethionamide, PAS-Para-aminosalicylic acid, CS-Cycloserine, LZD-Linezolid, BDQ-Bedaquiline, CFZ-Clofazimine, DLM-Delamanid.

Appendix II.2. MODS indirect test for rifampicin-heteroresistant and susceptible clinical isolates selected for this study.

STRAIN ID	Genotypic status	MODS indirect*					
		Day 6			Day 14		
		Control No drug	INH (0,4 µg/mL)	RIF (1 µg/mL)	Control No drug	INH (0,4 µg/mL)	RIF (1 µg/mL)
1R	RIF heteroresistant	1	1	0	1	1	0**
2R	RIF heteroresistant	1	1	1	1	1	1
3R	RIF heteroresistant	1	0	0	1	1	1
4R	RIF heteroresistant	1	0	1	1	0	1
1S	susceptible	1	0	0	1	0	0
2S	susceptible	1	0	0	1	0	0
3S	susceptible	1	0	0	1	0	0
4S	susceptible	1	0	0	1	0	0
H37Rv	pan-sensitive	1	0	0	1	0	0
DM97	MDR	1	1	1	1	1	1

*Drugs susceptibility profile by MODS indirect 0= no growth; 1= growth.
**This isolate was susceptible by MODS from the sputum sample, but MDR by MTBseq and TBprofiler analysis. Additionally, this isolate grew on day 21, showing slow growth compared to the other isolates. Abbr. RIF=Rifampicin, INH=Isoniazid

Appendix II.3. Minimum inhibitory concentration determined by TEMA in Mtb clinical strains with rifampicin-heteroresistant and susceptible profiles selected for this study.

Strain ID	Genotypic status	INH (µg/mL)	RIF (µg/mL)	STM(µg/mL)	EMB(µg/mL)	CAP(µg/mL)	CIP(µg/mL)
1R	RIF heteroresistant	1	0.125	0.5	2	2	1
2R	RIF heteroresistant	>32	>16	0.25	16	2	0.25
3R	RIF heteroresistant	0.125	0.063	0.125	4	2	0.25
4R	RIF heteroresistant	0.125	0.063	>32	4	2	0.125
1S	susceptible	0.125	0.063	0.125	4	1	0.25
2S	susceptible	0.125	0.063	0.25	4	4	0.25
3S	susceptible	0.125	0.25	0.125	2	4	8
4S	susceptible	0.25	0.063	0,5	8	4	0.25
H37Rv	pan−sensitive	0.125	0.063	0.5	1	1	0.25
DM97	MDR	4	>16	2	8	1	0.25

MDR=multidrug resistant, RIF=Rifampicin, INH=Isoniazid, STM=Streptomycin, EMB=Ethambutol, CAP=Capreomycin, CIP=Ciprofloxacin.

Appendix data II.4. Agar-plate proportions method in selected Mtb clinical strains reactivated with rifampicin-heteroresistant and susceptible profiles selected for this study.

STRAIN ID	DR Genotypic status	APM (>0.01=R)*		
		RIF (1 µg/mL)	INH (1 µg/mL)	INH (0.2 µg/mL)
1R	RIF heteroresistant	Res (0.025)	Res (0.56)	Res (1.0)
2R	RIF heteroresistant	Res (0.85)	Res (0.8)	Res (0.91)
3R	RIF heteroresistant	Res (0.018)	Sus	Sus
4R	RIF heteroresistant	Res (0.53)	Sus	Sus
1S	susceptible	Sus	Sus	Sus
2S	susceptible	Sus	Sus	Sus
3S	susceptible	Sus	Sus	Sus
4S	susceptible	Sus	Sus	Res(0.2)
H37Rv	pan-sensitive	Sus	Sus	Sus
DM97	MDR	Res (1.0)	Res (1.0)	Res (1.0)

DR= Drug-resistant. (*) The proportion of resistance is described for the resistant strains.
Abbr. Res = resistant, Sus = susceptible, DR= Drug-resistant, RIF=Rifampicin, INH=Isoniazid.

Appendix chapter III

Appendix III.1. Nucleotide alignment between *ponA1* from Mtb H37Rv and *MMAR_0069* genes annotated in the genome of *M. tuberculosis* and *M. marinum*, respectively. Identity percentage 82.82%, evaluated by CLUSTAL O (1.2.4)

```
PONA1_MTB       -----------------------------------------------GTGGTGATCCTGTTGCCGATGGTCACCTTC      30
MMAR0069        GTGCGGCGGTCGGCCTACCTGGCCGCGGCGGTGGTCATCCTGCTGCCCATCGTCACCTTC      60
                                                 ***** ****** **** ** *********

PONA1_MTB       ACGATGGCCTACCTGATCGTCGACGTTCCCAAGCCAGGTGACATCCGTACCAACCAGGTC      90
MMAR0069        ACCATGGCCTACTTCATCGTCGATGTGCCAAGGCCGGGCGACATCCGCACCAATCAGGTG      120
                ** ********* * ******** ** ** * *** ** ******** ***** *****

PONA1_MTB       TCCACGATCCTTGCCAGCGACGGCTCGGAAATCGCCAAAATTGTTCCGCCCGAAGGTAAT      150
MMAR0069        TCCACGATCCTGGCTAGCGACGGCTCCGAGATCGCCAAGATCGTTCCCCCCGAAGGCAAT      180
                *********** ** *********** ** ******** ** ***** ******** ***

PONA1_MTB       CGGGTCGACGTCAACCTCAGCCAGGTGCCGATGCATGTGCGCCAGGCGGTGATTGCGGCC      210
MMAR0069        CGGGTCGACGTGAACCTCAGTCAGGTGCCCGAGCATGTCCGCGCCGCGGTCATCGCCGCC      240
                *********** ******** ********    ****** ***    ***** ** ** ***

PONA1_MTB       GAAGACCGCAATTTCTATTCGAATCCGGGATTCTCGTTCACCGGCTTCGCGCGGGCAGTC      270
MMAR0069        GAAGACCGCGGTTTCTACTCCAACCCGGGGTTCTCCTTCAGCGGCTTCGCGCGAGCGATA      300
                *********  ****** ** ** ***** ***** **** ************ **  *

PONA1_MTB       AAGAACAACCTGTTCGGCGGCGATCTGCAGGGCGGATCGACGATTACCCAGCAGTACGTC      330
MMAR0069        AAGAACAACTTGTTCGGCGGTGACCTGCAAGGCGGCTCCACGATCACCCAGCAATACGTC      360
                ********* ********** ** ***** ***** ** ***** ******** ******

PONA1_MTB       AAGAACGCGCTGGTCGGTTCCGCACAGCACGGGTGGAGCGGTCTGATGCGCAAGGCGAAA      390
MMAR0069        AAGAACGCGTTGGTCGGCTCGGCGCAACACGGGTGGAGCGGCCTGATGCGCAAGGCCAAG      420
                ********* ******* ** ** ** *************** *************** **

PONA1_MTB       GAATTGGTCATCGCGACGAAGATGTCGGGGGGAGTGGTCTAAAGACGATGTGCTGCAGGCG      450
MMAR0069        GAACTCGTCATCGCCACCAAGATGTCGGGGGGAGTGGTCCAAAGACGATGTCCTGCAGGCC      480
                *** * ******** ** ********************** ************ ********

PONA1_MTB       TATCTGAACATCATCTACTTCGGCCGGGGCGCCTACGGCATTTCGGCGGCGTCCAAGGCT      510
MMAR0069        TATCTCAACATCATCTACTTCGGCCGCGGCGCATACGGGATTTCGGCAGCGTCCAAGGCC      540
                ***** ********************* ***** ***** ******** ***********

PONA1_MTB       TATTTCGACAAGCCCGTCGAGCAGCTGACCGTTGCCGAAGGGGCGTTGTTGGCAGCGCTG      570
MMAR0069        TACTTCGACAAGCCGGTCGAGCAGCTCACCGTGTCGGAGGGAGCCTTGCTGGCGGCGTTG      600
                ** *********** *********** *****  * ** ** ** *** **** *** **

PONA1_MTB       ATTCGGCGGCCTTCGACGCTGGACCCGGCGGTCGACCCCGAAGGGGCCCATGCCCGCTGG      630
MMAR0069        ATTCGGCGGCCCTCCACGCTGGACCCGGCGGTGGATCCCGATGGGGCGCTGGCGCGCTGG      660
                *********** ** ***************** ** ***** ***** *  ** ******

PONA1_MTB       AATTGGGTACTCGACGGCATGGTGGAAACCAAGGCTCTCTCGCCGAATGACCGTGCGGCG      690
MMAR0069        AACTGGGTGCTCGACGGCATGGTGGATACCAAGGCGTTGTCCGCCAAAGACCGGGCCGAG      720
                ** ***** ***************** ********  * **  * ** ***** ** * *

PONA1_MTB       CAGGTGTTTCCCGAGACAGTGCCGCCCGATCTGGCCCGGGCAGAGAATCAGACCAAAGGA      750
MMAR0069        CAGGTATTTCCCAGGACCGTGCCGCCGGATCAAGCCCGCGCGGCCAACCAGACCACCGGG      780
                ***** ******  *** ******** ****  ***** ** *  ** *******  **

PONA1_MTB       CCCAACGGGCTGATCGAGCGGCAGGTGACAAGGGAGTTGCTCGAGCTGTTCAACATCGAC      810
MMAR0069        CCCAACGGGCTGATCGAACGCCAGGTCACCAAAGAGTTGTTGGAGCTGTTCAACATCGAT      840
                ***************** ** ***** ** *  ****** * *****************

PONA1_MTB       GAGCAGACCCTCAACACCCAGGGGCTGGTGGTCACCACCACGATTGATCCGCAGGCCCAA      870
MMAR0069        GAACAGACCCTGAACACGCAGGGGCTGCAAGTCACGACCACGATCGATGCCCAAGCGCAG      900
                ** ******** ***** *********    ***** ******** *** * ** ** **

PONA1_MTB       CGGGCGGCGGAGAAGGCGGTTGCGAAATACCTGGACGGGCAGGACCCCGACATGCGTGCC      930
MMAR0069        CAGGCGGCCGAAAAGGCGGTAGCGAAATACCTTGACGGGCAGGATCCCGAGATGCGGGCC      960
                * ****** ** ******** *********** *********** ***** ***** ***

PONA1_MTB       GCCGTGGTTTCCATCGACCCGCACAACGGGGCGGTGCGTGCGTACTACGGTGGCGACAAT      990
MMAR0069        GCGGTGGTCTCCATCGACCCGCACAACGGGGCCGTGCGCGCCTATTACGGCGGCGACAAC      1020
                ** ***** ********************** ***** ** ** ***** ********

PONA1_MTB       GCCAATGGCTTTGACTTCGCTCAAGCGGGATTGCAGACTGGATCGTCGTTTAAGGTGTTT      1050
MMAR0069        GCCAACGGGTTCGACTTCGCCCAGGCCGGGCTGCAGACGGGATCCTCGTTCAAGGTATTC      1080
                ***** ** ** ******** ** ** **  ******* ***** ***** ***** **

PONA1_MTB       GCTCTGGTGGCCGCCCTTGAGCAGGGGATCGGCCTGGGCTACCAGGTAGACAGCTCTCCG      1110
MMAR0069        GCCCTGGTGGCCGCCCTTGAACAGGGAATTGGCCTGGGCTATGACGTCGACAGTTCGCCA      1140
                ** ***************** ***** ** ************  * ** ***** ** **

PONA1_MTB       TTGACGGTCGACGGCATCAAGATCACCAACGTCGAGGGCGAGGGTTGCGGGACGTGCAAC      1170
MMAR0069        CTGACGGTGGACGGCATCAAGATCACCAATGTCGAAGGCGAGAGCTGCGGTACCTGCAAC      1200
                  ******* ******************** ***** ****** * ***** ** ******

PONA1_MTB       ATCGCCGAGGCGCTCAAAATGTCGCTGAACACCTCCTACTACCGGCTGATGCTCAAGCTC      1230
MMAR0069        ATCGCGCAGGCGCTCAAGATGTCGCTGAACACCTCCTACTACCGGCTGATGCTCAAACTG      1260
                *****  ********** ****************************************
```

```
PONA1_MTB       AACGGCGGCCCACAGGCTGTGGCCGATGCCGCGCACCAAGCCGGCATTGCCTCCAGCTTC       1290
MMAR0069        AAGGGCGGCCCGGAGGCCGTCGCCGACGCCGCGCACCAGGCCGGCATTGCCACCAGCTTC       1320
                ** ********  **** ** ***** ********** ************ ********

PONA1_MTB       CCGGGCGTTGCGCACACGCTGTCCGAAGATGGCAAGGGTGGACCGCCCAACAACGGGATC       1350
MMAR0069        CCGGGCGTGCCCCACACGCTGTCCGAGGACGGCAAGGGTGGACCGCCCAACAACGGGATT       1380
                ********  * ************** ** ******************************

PONA1_MTB       GTGTTGGGCCAGTACCAAACCCGGGTGATCGACATGGCATCGGCGTATGCCACGTTGGCC       1410
MMAR0069        GTGCTGGGCCAGTATCAGACCCGGGTGATCGACATGGCTTCGGCCTACGCCACGCTGGCC       1440
                *** ********** ** ******************** ***** ** ****** *****

PONA1_MTB       GCGTCCGGTATCTACCACCCGCCGCATTTCGTACAGAAGGTGGTCAGTGCCAACGGCCAG       1470
MMAR0069        GCATCCGGGATCTATCACCGGCCACACTTCGTGCAGAAGGTCGTCAACGCCGACGGCCGG       1500
                ** ***** ***** **** *** ** ***** ******** ****  *** ****** *

PONA1_MTB       GTCCTCTTCGACGCCAGCACCGCGGACAACACCGGCGATCAGCGCATCCCCAAGGCGGTA       1530
MMAR0069        GTTCTCTTCGACGCCTCCACCGAAGACAACACCGGTGACCAGCGCATCCCCAAGGCGGTA       1560
                ** ************  *****  *********** ** **********************

PONA1_MTB       GCCGACAACGTGACTGCGGCGATGGAGCCGATCGCAGGTTATTCGCGTGGCCACAACCTA       1590
MMAR0069        GCCGACAATGTCACCGCGGCAATGGAACCCATTGCCGGATATTCGCGGGGTCACAACCTG       1620
                ******** ** ** ***** ***** ** ** ** ** ******** ** ********

PONA1_MTB       GCGGGTGGGCGGGATTCGGCGGCCAAGACCGGCACTACGCAATTTGGTGACACCACCGCG       1650
MMAR0069        GCCGGCGGCCGGCCGTCGGCCTCCAAGACCGGCACGGTGCAGTTGGGCGACACCAGCGCC       1680
                ** ** ** ***   *****  *************   *** ** ** ******** ***

PONA1_MTB       AACAAAGACGCCTGGATGGTCGGGTACACGCCGTCGTTGTCTACGGCTGTGTGGGTGGGC       1710
MMAR0069        AACCGAGACGCCTGGATGGTCGGTTACACCCCGTCACTGTCGACGGCCGTGTGGGTGGGA       1740
                ***  ****************** ***** *****  **** ***** ***********

PONA1_MTB       ACCGTCAAGGGTGACGAGCCACTGGTAACCGCTTCGGGTGCAGCGATTTACGGCTCGGGC       1770
MMAR0069        ACGGTCAAGGGTGACGAGCCGTTGGTGACCGCCTCGGGCGCACCGATTTACGGCTCGGGC       1800
                ** *****************  **** ***** ***** *** ******************

PONA1_MTB       CTGCCGTCGGACATCTGGAAGGCAACCATGGACGGCGCCTTGAAGGGCACGTCGAACGAG       1830
MMAR0069        CTGCCGTCGGACATCTGGAAAGCCACCATGGACGGTGCATTGAAGGGCACCGAGGTCGAG       1860
                ******************** ** ************ ** ************    *  ****

PONA1_MTB       ACTTTCCCCAAACCGACCGAGGTCGGTGGTTATGCCGGTGTGCCGCCGCCGCCGCCGC--       1888
MMAR0069        AGCTTCCCCAAGCCCACCGAGATCGGCGGCTACGCCGGCGTGCCGGCACCGCCTCCACCT       1920
                *  ******** ** ****** **** ** ** ***** ****** * ***** ** *

PONA1_MTB       ----CGCCGGAGGTACCACCTTCGGAGACCGTCATCCAGCCCACGGTCGAAATTGCGCCG       1944
MMAR0069        CCACCGGAGGCGCCGCCGCCCTCGGAGACCGTCATCCAGCCCACGGTCGAAATAGCGCCC       1980
                    **  ** *   ** ** ********************************** *****

PONA1_MTB       GGGATTACCATCCCGATCGGTCCCCCGACCACCATTACCCTGGCGCCACCGCCCCCGGCC       2004
MMAR0069        GGGATCACGATTCCCGTCGGGCCGCCAACCACCATCACTCTTGCTCCCCCTCCGCCACCA       2040
                ***** ** ** **  **** ** ** ******** ** ** ** ** ** ** **  *

PONA1_MTB       CCGCCCGCTGCGACTCCCACGCCGCCGCCGTGA          2037
MMAR0069        GGGGCGCCACCCGCCGACAATCCGCCACCGTGA          2073
                  * *  *  *  *   **  ***** ******
```

Appendix III.2. Protein alignment between PonA1 versus MMAR_0069 annotated in the genome of *M. tuberculosis* and *M. marinum*, respectively. 91% identity, evaluated by CLUSTAL O (1.2.4).

```
PONA1-MTB       ----------MVILLPMVTFTMAYLIVDVPKPGDIRTNQVSTILASDGSEIAKIVPPEGN      50
MMAR_0069       MRRSAYLAAAVVILLPIVTFTMAYFIVDVPRPGDIRTNQVSTILASDGSEIAKIVPPEGN      60
                         :******:*******:*****:*****************************

PONA1-MTB       RVDVNLSQVPMHVRQAVIAAEDRNFYSNPGFSFTGFARAVKNNLFGGDLQGGSTITQQYV      110
MMAR_0069       RVDVNLSQVPEHVRAAVIAAEDRGFYSNPGFSFSGFARAIKNNLFGGDLQGGSTITQQYV      120
                ********** *** ********.*********:******:*********************

PONA1-MTB       KNALVGSAQHGWSGLMRKAKELVIATKMSGEWSKDDVLQAYLNIIYFGRGAYGISAASKA      170
MMAR_0069       KNALVGSAQHGWSGLMRKAKELVIATKMSGEWSKDDVLQAYLNIIYFGRGAYGISAASKA      180
                ************************************************************

PONA1-MTB       YFDKPVEQLTVAEGALLAALIRRPSTLDPAVDPEGAHARWNWVLDGMVETKALSPNDRAA      230
MMAR_0069       YFDKPVEQLTVSEGALLAALIRRPSTLDPAVDPDGALARWNWVLDGMVDTKALSAKDRAE      240
                ***********:**********************:** ***********:***** :***

PONA1-MTB       QVFPETVPPDLARAENQTKGPNGLIERQVTRELLELFNIDEQTLNTQGLVVTTTIDPQAQ      290
MMAR_0069       QVFPRTVPPDQARAANQTTGPNGLIERQVTKELLELFNIDEQTLNTQGLQVTTTIDAQAQ      300
                ****.***** *** ***.***********:****************** ****** ***

PONA1-MTB       RAAEKAVAKYLDGQDPDMRAAVVSIDPHNGAVRAYYGGDNANGFDFAQAGLQTGSSFKVF      350
MMAR_0069       QAAEKAVAKYLDGQDPEMRAAVVSIDPHNGAVRAYYGGDNANGFDFAQAGLQTGSSFKVF      360
                :***************:************************************************

PONA1-MTB       ALVAALEQGIGLGYQVDSSPLTVDGIKITNVEGEGCGTCNIAEALKMSLNTSYYRLMLKL      410
MMAR_0069       ALVAALEQGIGLGYDVDSSPLTVDGIKITNVEGESCGTCNIAQALKMSLNTSYYRLMLKL      420
                **************:******************.*******:*****************

PONA1-MTB       NGGPQAVADAAHQAGIASSFPGVAHTLSEDGKGGPPNNGIVLGQYQTRVIDMASAYATLA      470
MMAR_0069       KGGPEAVADAAHQAGIATSFPGVPHTLSEDGKGGPPNNGIVLGQYQTRVIDMASAYATLA      480
                :***:************:***** ************************************

PONA1-MTB       ASGIYHPPHFVQKVVSANGQVLFDASTADNTGDQRIPKAVADNVTAAMEPIAGYSRGHNL      530
MMAR_0069       ASGIYHRPHFVQKVVNADGRVLFDASTEDNTGDQRIPKAVADNVTAAMEPIAGYSRGHNL      540
                ****** ********.*:*:******* *********************************

PONA1-MTB       AGGRDSAAKTGTTQFGDTTANKDAWMVGYTPSLSTAVWVGTVKGDEPLVTASGAAIYGSG      590
MMAR_0069       AGGRPSASKTGTVQLGDTSANRDAWMVGYTPSLSTAVWVGTVKGDEPLVTASGAPIYGSG      600
                **** **:****.*:***:**:********************************** *****

PONA1-MTB       LPSDIWKATMDGALKGTSNETFPKPTEVGGYAGVPPPPPP--PEVPPSETVIQPTVEIAP      648
MMAR_0069       LPSDIWKATMDGALKGTEVESFPKPTEIGGYAGVPAPPPPPPEAPPPSETVIQPTVEIAP      660
                *****************. *:*******:******* ****      ***************

PONA1-MTB       GITIPIGPPTTITLAPPPPAPPAATPTPPP    678
MMAR_0069       GITIPVGPPTTITLAPPPPPGAPPADNPPP    690
                *****:**************      : .***
```

Appendix III.3. Nucleotide alignment between ponA1 from *M. tuberculosis* with –426 start site and *MMAR_0069* from *M. marinum* with -465 start site with respect to the sites annotated for these genes. Identity percentage 79.62%, evaluated by CLUSTAL O (1.2.4).

```
PONA1_426_MTB        GTGAATAGCGACGGGCGTCACCATCAG---------------------------------- 27
MMAR_0069-465        GTGAGTAACGAAGGGCGCCACCACCAGCCGCCCAGCGACGCTCGGGGCGGTCCAGCGGGC 60
                    **** ** *** ***** ***** ***
PONA1_426_MTB        -------------------------TCGTCCAGCGGCGCCCCGCGCGGGCCGGCGAATCCCGGCCAGCGT 72
MMAR_0069-465        GACGACATGGGCGGCCAATCCGGCAACGACGAACGGTCGCGTTCGGCGCCGGTTCCGCGT 120
                                  *** **  ** *   **   **   **   ** *  * ****
PONA1_426_MTB        GGTCAGGTTCCACCCGACGACAGACTGACCGCGATCCTCCCGCCGGTGACCGATGACCGA 132
MMAR_0069-465        CGTGCGGTTCCTCCCGACGACAGGATGACCACGATCATTCCTGCGGTGTCGGATCCTCGT 180
                     **  ****** ***********  ***** ***** * **  ***** * ***    **
PONA1_426_MTB        TCGGCTCCGCACGCGGACTCCATCGAGGCGGTCAAGGCCGCGCTCGACGGCGCGCCGCCG 192
MMAR_0069-465        TCAGCTCGCCACGCCGACCCGATCGAGGAAGTCAAGGCCGCCCTCGACAGTCCGCCCTCG 240
                    ** ****  ***** *** * *******  *********** ****** *  ****  **
PONA1_426_MTB        ATGCCCCCGCCGCGCGACCCGCTCGAGGAGGTCACGGCCGCGTTGGCCGCCCCGCCCGGT 252
MMAR_0069-465        GCGCCCCTGCAGCGTGATCAGCTCGATCAGGTCAAGGCCGCGCTCGACGCCCCGCCGACG 300
                      ***** ** *** ** * ******  ****** ******* * * *********
PONA1_426_MTB        AAACCGCCGCGGGGGGGATCAGC------------------TTGGTGGC---AGACGTCGC 291
MMAR_0069-465        CGGCCCATCCGCAGCCGGCGCGGCGGCGGTGGGCTTCCGCCCGATGGCGGGGCGCCTCCA 360
                       **    **  *    *                          * ****       * **
PONA1_426_MTB        CCACCGGGGCCGCCCGGGCCCCCCGGTTCGTCCGGACAGCCTGCCGGCCGGCTGCCCCAA 351
MMAR_0069-465        CCCGCGGGGCCCGCGGGGCCTTCAGGTCCAACAGGTCGCTCTCGCGCCCGGTCCCACCGG 420
                    **  *******  * *****  * *** *  * ** *   **  ** ****   * **
PONA1_426_MTB        CCGAGGGTGGACTTGCCCCGGGTCGGCCAGATCAACTGGAAATGGATACGGCGTTCGCTG 411
MMAR_0069-465        TCCACGACACAGCGCGACTGGCTGCGCCGGATCAACTGGAAATGGGTGCGGCGGTCGGCC 480
                     * * *    *       * ** *  *** ***************** * ***** ***
PONA1_426_MTB        TACCTCACCGCGGCGGTGGTGATCCTGTTGCCGATGGTCACCTTCACGATGGCCTACCTG 471
MMAR_0069-465        TACCTGGCCGCGGCGGTGGTCATCCTGCTGCCCATCGTCACCTTCACCATGGCCTACTTC 540
                    *****  ************* ****** **** ** ********** ********* *
PONA1_426_MTB        ATCGTCGACGTTCCCAAGCCAGGTGACATCCGTACCAACCAGGTCTCCACGATCCTTGCC 531
MMAR_0069-465        ATCGTCGATGTGCCAAGGCCGGGCGACATCCGCACCAATCAGGTGTCCACGATCCTGGCT 600
                    ******** ** ** * *** ** ******** ***** ***** ********** **
PONA1_426_MTB        AGCGACGGCTCGGAAATCGCCAAAATTGTTCCGCCCGAAGGTAATCGGGTCGACGTCAAC 591
MMAR_0069-465        AGCGACGGCTCCGAGATCGCCAAGATCGTTCCCCCCGAAGGCAATCGGGTCGACGTGAAC 660
                     *********** ** ******** ** ***** ******** ************** ***
PONA1_426_MTB        CTCAGCCAGGTGCCGATGCATGTGCGCCAGGCGGTGATTGCGGCCGAAGACCGCAATTTC 651
MMAR_0069-465        CTCAGTCAGGTGCCCGAGCATGTCCGCGCCGCGGTCATCGCCGCCGAAGACCGCGGTTTC 720
                     ***** ********    ****** ***    ***** ** ** *************  ****
PONA1_426_MTB        TATTCGAATCCGGGATTCTCGTTCACCGGCTTCGCGCGGGCAGTCAAGAACAACCTGTTC 711
MMAR_0069-465        TACTCCAACCCGGGGTTCTCCTTCAGCGGCTTCGCGCGAGCGATAAAGAACAACTTGTTC 780
                     ** ** ** ***** ***** **** ************ **  * ********* *****
PONA1_426_MTB        GGCGGCGATCTGCAGGGCGGATCGACGATTACCCAGCAGTACGTCAAGAACGCGCTGGTC 771
MMAR_0069-465        GGCGGTGACCTGCAAGGCGGCTCCACGATCACCCAGCAATACGTCAAGAACGCGTTGGTC 840
                     ***** ** ***** ***** ** ***** ******** *************** *****
PONA1_426_MTB        GGTTCCGCACAGCACGGGTGGAGCGGTCTGATGCGCAAGGCGAAAGAATTGGTCATCGCG 831
MMAR_0069-465        GGCTCGGCGCAACACGGGTGGAGCGGCCTGATGCGCAAGGCCAAGGAACTCGTCATCGCC 900
                    ** ** ** ** *************** *************** ** *** * ********
PONA1_426_MTB        ACGAAGATGTCGGGGGAGTGGTCTAAAGACGATGTGCTGCAGGCGTATCTGAACATCATC 891
MMAR_0069-465        ACCAAGATGTCGGGGGAGTGGTCCAAAGACGATGTCCTGCAGGCCTATCTCAACATCATC 960
                     ** ******************** *********** ******** ***** *********
PONA1_426_MTB        TACTTCGGCCGGGGCGCCTACGGCATTTCGGCGGCGTCCAAGGCTTATTTCGACAAGCCC 951
MMAR_0069-465        TACTTCGGCCGCGGCGCATACGGGATTTCGGCAGCGTCCAAGGCCTACTTCGACAAGCCG 1020
                    ************ ***** ***** ******** ************ ** ************
PONA1_426_MTB        GTCGAGCAGCTGACCGTTGCCGAAGGGGCGTTGTTGGCAGCGCTGATTCGGCGGCCTTCG 1011
MMAR_0069-465        GTCGAGCAGCTCACCGTGTCGGAGGGAGCCTTGCTGGCGGCGTTGATTCGGCGGCCCTCC 1080
                    ************ *****  * ** ** ** *** **** *** ************** **
PONA1_426_MTB        ACGCTGGACCCGGCGGTCGACCCCGAAGGGGCCCATGCCCGCTGGAATTGGGTACTCGAC 1071
MMAR_0069-465        ACGCTGGACCCGGCGGTGGATCCCGATGGGGCGCTGGCGCGCTGGAACTGGGTGCTCGAC 1140
                     ****************** ** ***** ***** *  ** ******** ***** ******
PONA1_426_MTB        GGCATGGTGGAAACCAAGGCTCTCTCGCCGAATGACCGTGCGGCGCAGGTGTTTCCCGAG 1131
MMAR_0069-465        GGCATGGTGGATACCAAGGCGTTGTCCGCCAAAGACCGGGCCGAGCAGGTATTTCCCAGG 1200
                     ************ ********  * **  * ** ***** ** * ****** ******  *
PONA1_426_MTB        ACAGTGCCGCCCGATCTGGCCCGGGCAGAGAATCAGACCAAAGGACCCAACGGGCTGATC 1191
```

```
MMAR_0069-465       ACCGTGCCGCCGGATCAAGCCCGCGCGGCCAACCAGACCACCGGGCCCAACGGGCTGATC  1260
                    ** ******** ****  ***** ** *  ** *******  ** ***************
PONA1_426_MTB         GAGCGGCAGGTGACAAGGGAGTTGCTCGAGCTGTTCAACATCGACGAGCAGACCCTCAAC 1251
MMAR_0069-465         GAACGCCAGGTCACCAAAGAGTTGTTGGAGCTGTTCAACATCGATGAACAGACCCTGAAC 1320
                      ** ** ***** ** *  ****** * ****************** ** ******** ***
PONA1_426_MTB         ACCCAGGGGCTGGTGGTCACCACCACGATTGATCCGCAGGCCCAACGGGCGGCGGAGAAG 1311
MMAR_0069-465         ACGCAGGGGCTGCAAGTCACGACCACGATCGATGCCCAAGCGCAGCAGGCGGCCGAAAAG 1380
                      ** *********   ***** ******** *** * ** ** ** * ****** ** ***
PONA1_426_MTB         GCGGTTGCGAAATACCTGGACGGGCAGGACCCCGACATGCGTGCCGCCGTGGTTTCCATC 1371
MMAR_0069-465         GCGGTAGCGAAATACCTTGACGGGCAGGATCCCGAGATGCGGGCCGCGGTGGTCTCCATC 1440
                      ***** ********** ********** ***** ***** ***** ***** ******
PONA1_426_MTB         GACCCGCACAACGGGGCGGTGCGTGCGTACTACGGTGGCGACAATGCCAATGGCTTTGAC 1431
MMAR_0069-465         GACCCGCACAACGGGGCCGTGCGCGCCTATTACGGCGGCGACAACGCCAACGGGTTCGAC 1500
                      ***************** ***** ** ** ***** ******** ***** ** ** ***
PONA1_426_MTB         TTCGCTCAAGCGGGATTGCAGACTGGATCGTCGTTTAAGGTGTTTGCTCTGGTGGCCGCC 1491
MMAR_0069-465         TTCGCCCAGGCCGGGCTGCAGACGGGATCCTCGTTCAAGGTATTCGCCCTGGTGGCCGCC 1560
                      ***** ** ** **  ******* ***** ***** ***** ** ** ************
PONA1_426_MTB         CTTGAGCAGGGGATCGGCCTGGGCTACCAGGTAGACAGCTCTCCGTTGACGGTCGACGGC 1551
MMAR_0069-465         CTTGAACAGGGAATTGGCCTGGGCTATGACGTCGACAGTTCGCCACTGACGGTGGACGGC 1620
                      ***** ***** ** ***********  * ** ***** ** **  ******* ******
PONA1_426_MTB         ATCAAGATCACCAACGTCGAGGGCGAGGGTTGCGGGACGTGCAACATCGCCGAGGCGCTC 1611
MMAR_0069-465         ATCAAGATCACCAATGTCGAAGGCGAGAGCTGCGGTACCTGCAACATCGCGCAGGCGCTC 1680
                      ************** ***** ****** * ***** ** ***********  ********
PONA1_426_MTB         AAAATGTCGCTGAACACCTCCTACTACCGGCTGATGCTCAAGCTCAACGGCGGCCCACAG 1671
MMAR_0069-465         AAGATGTCGCTGAACACCTCCTACTACCGGCTGATGCTCAAACTGAAGGGCGGCCCGGAG 1740
                      ** ************************************ ** ** ********  **
PONA1_426_MTB         GCTGTGGCCGATGCCGCGCACCAAGCCGGCATTGCCTCCAGCTTCCCGGGCGTTGCGCAC 1731
MMAR_0069-465         GCCGTCGCCGACGCCGCGCACCAGGCCGGCATTGCCACCAGCTTCCCGGGCGTGCCCCAC 1800
                      ** ** ***** ************ ************ ****************  * ***
PONA1_426_MTB         ACGCTGTCCGAAGATGGCAAGGGTGGACCGCCCAACAACGGGATCGTGTTGGGCCAGTAC 1791
MMAR_0069-465         ACGCTGTCCGAGGACGGCAAGGGTGGACCGCCCAACAACGGGATTGTGCTGGGCCAGTAT 1860
                      ********** ** ***************************** *** **********
PONA1_426_MTB         CAAACCCGGGTGATCGACATGGCATCGGCGTATGCCACGTTGGCCGCGTCCGGTATCTAC 1851
MMAR_0069-465         CAGACCCGGGTGATCGACATGGCTTCGGCCTACGCCACGCTGGCCGCATCCGGGATCTAT 1920
                      ** ********************** ***** ** ****** ******* ***** *****
PONA1_426_MTB         CACCCGCCGCATTTCGTACAGAAGGTGGTCAGTGCCAACGGCCAGGTCCTCTTCGACGCC 1911
MMAR_0069-465         CACCGGCCACACTTCGTGCAGAAGGTCGTCAACGCCGACGGCCGGGTTCTCTTCGACGCC 1980
                      **** *** ** ***** ******** ****  *** ****** *** ************
PONA1_426_MTB         AGCACCGCGGACAACACCGGCGATCAGCGCATCCCCAAGGCGGTAGCCGACAACGTGACT 1971
MMAR_0069-465         TCCACCGAAGACAACACCGGTGACCAGCGCATCCCCAAGGCGGTAGCCGACAATGTCACC 2040
                        *****  ************ ** ****************************** ** **
PONA1_426_MTB         GCGGCGATGGAGCCGATCGCAGGTTATTCGCGTGGCCACAACCTAGCGGGTGGGCGGGAT 2031
MMAR_0069-465         GCGGCAATGGAACCCATTGCCGGATATTCGCGGGGTCACAACCTGGCCGGCGGCCGGCCG 2100
                      ***** ***** ** ** ** ** ******** ** ******** ** ** ** ** ***
PONA1_426_MTB         TCGGCGGCCAAGACCGGCACTACGCAATTTGGTGACACCACCGCGAACAAAGACGCCTGG 2091
MMAR_0069-465         TCGGCCTCCAAGACCGGCACGGTGCAGTTGGGCGACACCAGCGCCAACCGAGACGCCTGG 2160
                      *****  **************    *** ** ** ******* *** ***  **********
PONA1_426_MTB         ATGGTCGGGTACACGCCGTCGTTGTCTACGGCTGTGTGGGTGGGCACCGTCAAGGGTGAC 2151
MMAR_0069-465         ATGGTCGGTTACACCCCGTCACTGTCGACGGCCGTGTGGGTGGGAACGGTCAAGGGTGAC 2220
                      ******** ***** *****  **** ***** ************ ** *************
PONA1_426_MTB         GAGCCACTGGTAACCGCTTCGGGTGCAGCGATTTACGGCTCGGGCCTGCCGTCGGACATC 2211
MMAR_0069-465         GAGCCGTTGGTGACCGCCTCGGGCGCACCGATTTACGGCTCGGGCCTGCCGTCGGACATC 2280
                      *****  **** ***** ***** *** ***********************************
PONA1_426_MTB         TGGAAGGCAACCATGGACGGCGCCTTGAAGGGCACGTCGAACGAGACTTTCCCCAAACCG 2271
MMAR_0069-465         TGGAAAGCCACCATGGACGGTGCATTGAAGGGCACCGAGGTCGAGAGCTTCCCCAAGCCC 2340
                      ***** ** ************ ** ************    *  *****  ******** **
PONA1_426_MTB         ACCGAGGTCGGTGGTTATGCCGGTGTGCCGCCGCCGCCGCCGC----------CGCCGGAGGTA 2325
MMAR_0069-465         ACCGAGATCGGCGGCTACGCCGGCGTGCCGGCACCGCCTCCACCTCCACCGGAGGCGCCG 2400
                      ****** **** ** ** ***** ****** * ***** ** *       **  ** *
PONA1_426_MTB         CCACCTTCGGAGACCGTCATCCAGCCCACGGTCGAAATTGCGCCGGGGATTACCATCCCG 2385
MMAR_0069-465         CCGCCCTCGGAGACCGTCATCCAGCCCACGGTCGAAATAGCGCCCGGGATCACGATTCCC 2460
                      ** ** ********************************* ***** ***** ** ** **
PONA1_426_MTB         ATCGGTCCCCCGACCACCATTACCCTGGCGCCACCGCCCCCGGCCCCGCCCGCTGCGACT 2445
MMAR_0069-465         GTCGGGCCGCCAACCACCATCACTCTTGCTCCCCCTCCGCCACCAGGGGCGCCACCCGCC 2520
                      **** ** ** ******** ** ** ** ** ** ** **  *   * *  *  *  *  *
PONA1_426_MTB         CCCACGCCGCCGCCGTGA   2463
MMAR_0069-465         GACAATCCGCCACCGTGA   2538
                        **  ***** ******
```

Appendix III.4. Protein alignment between ponA1 from *M. tuberculosis* with –426 start site and MMAR_0069 from *M. marinum* with -465 start site with respect to the sites annotated for these genes. Identity percentage 84.39 %, evaluated by CLUSTAL O (1.2.4).

```
PONA1-426          MNSDGRHHQSSSGAPRGPA---------------------------NPGQRGQVPPDDRLTAILPPVTDDR  44
MMAR_0069-465      MSNEGRHHQPPSDARGGPAGDDMGGQSGNDERSRSAPVPRRAVPPDDRMTTIIPAVSDPR  60
                   *.:*****  *.*  ***                  *  *  ******:*:*:* *:* *
PONA1-426          SAPHADSIEAVKAALDGAPPMPPPRDPLEEVTAALAAPPGKPPRGDQLGGRRR-------  97
MMAR_0069-465      SARHADPIEEVKAALDSPPSAPLQRDQLDQVKAALDAPPTRPIRSRRGGGGLPPDGGAPP  120
                   ** *** ** ******. *  *  ** *::*.*** *** :* *. : **
PONA1-426          PPGPPGPPGSSGQPAGRLPQPRVDLPRVGQINWKWIRRSLYLTAAVVILLPMVTFTMAYL  157
MMAR_0069-465      PAGPAGPSGPTGRSRARSHRSTTQRDWLRRINWKWVRRSAYLAAAVVILLPIVTFTMAYF  180
                   * ** ** * :*:  .*  :  .:   : :*****:*** **:********:*******:
PONA1-426          IVDVPKPGDIRTNQVSTILASDGSEIAKIVPPEGNRVDVNLSQVPMHVRQAVIAAEDRNF  217
MMAR_0069-465      IVDVPRPGDIRTNQVSTILASDGSEIAKIVPPEGNRVDVNLSQVPEHVRAAVIAAEDRGF  240
                   *****:****************************************** *** ********.*
PONA1-426          YSNPGFSFTGFARAVKNNLFGGDLQGGSTITQQYVKNALVGSAQHGWSGLMRKAKELVIA  277
MMAR_0069-465      YSNPGFSFSGFARAIKNNLFGGDLQGGSTITQQYVKNALVGSAQHGWSGLMRKAKELVIA  300
                   ********:*****:**********************************************
PONA1-426          TKMSGEWSKDDVLQAYLNIIYFGRGAYGISAASKAYFDKPVEQLTVAEGALLAALIRRPS  337
MMAR_0069-465      TKMSGEWSKDDVLQAYLNIIYFGRGAYGISAASKAYFDKPVEQLTVSEGALLAALIRRPS  360
                   ********************************************:*************
PONA1-426          TLDPAVDPEGAHARWNWVLDGMVETKALSPNDRAAQVFPETVPPDLARAENQTKGPNGLI  397
MMAR_0069-465      TLDPAVDPDGALARWNWVLDGMVDTKALSAKDRAEQVFPRTVPPDQARAANQTTGPNGLI  420
                   ********:** ***********:***** :*** ****.***** *** ***.******
PONA1-426          ERQVTRELLELFNIDEQTLNTQGLVVTTTIDPQAQRAAEKAVAKYLDGQDPDMRAAVVSI  457
MMAR_0069-465      ERQVTKELLELFNIDEQTLNTQGLQVTTTIDAQAQQAAEKAVAKYLDGQDPEMRAAVVSI  480
                   *****:****************** ****** ***:***************:********
PONA1-426          DPHNGAVRAYYGGDNANGFDFAQAGLQTGSSFKVFALVAALEQGIGLGYQVDSSPLTVDG  517
MMAR_0069-465      DPHNGAVRAYYGGDNANGFDFAQAGLQTGSSFKVFALVAALEQGIGLGYDVDSSPLTVDG  540
                   ************************************************:***********
PONA1-426          IKITNVEGEGCGTCNIAEALKMSLNTSYYRLMLKLNGGPQAVADAAHQAGIASSFPGVAH  577
MMAR_0069-465      IKITNVEGESCGTCNIAQALKMSLNTSYYRLMLKLKGGPEAVADAAHQAGIATSFPGVPH  600
                   *********.*******:*****************:***:************:*****  *
PONA1-426          TLSEDGKGGPPNNGIVLGQYQTRVIDMASAYATLAASGIYHPPHFVQKVVSANGQVLFDA  637
MMAR_0069-465      TLSEDGKGGPPNNGIVLGQYQTRVIDMASAYATLAASGIYHRPHFVQKVVNADGRVLFDA  660
                   ****************************************  ********.*:*:*****
PONA1-426          STADNTGDQRIPKAVADNVTAAMEPIAGYSRGHNLAGGRDSAAKTGTTQFGDTTANKDAW  697
MMAR_0069-465      STEDNTGDQRIPKAVADNVTAAMEPIAGYSRGHNLAGGRPSASKTGTVQLGDTSANRDAW  720
                   ** ********************************** **:****.*:***:**:***
PONA1-426          MVGYTPSLSTAVWVGTVKGDEPLVTASGAAIYGSGLPSDIWKATMDGALKGTSNETFPKP  757
MMAR_0069-465      MVGYTPSLSTAVWVGTVKGDEPLVTASGAPIYGSGLPSDIWKATMDGALKGTEVESFPKP  780
                   **************************** ***********************. *:****
PONA1-426          TEVGGYAGVPPPPPP--PEVPPSETVIQPTVEIAPGITIPIGPPTTITLAPPPPAPPAAT  815
MMAR_0069-465      TEIGGYAGVPAPPPPPPEAPPPSETVIQPTVEIAPGITIPVGPPTTITLAPPPPPGAPPA  840
                   **:******* ****     ********************:*************      :
PONA1-426          PTPPP        820
MMAR_0069-465      DNPPP        845
                    .***
```

Appendix III.5 *In silico* ligation of ponA1$_{234\text{-}820}$-WT in pET28a plasmid (a), nucleotide (b) and amino acid (c) sequence.

(a)

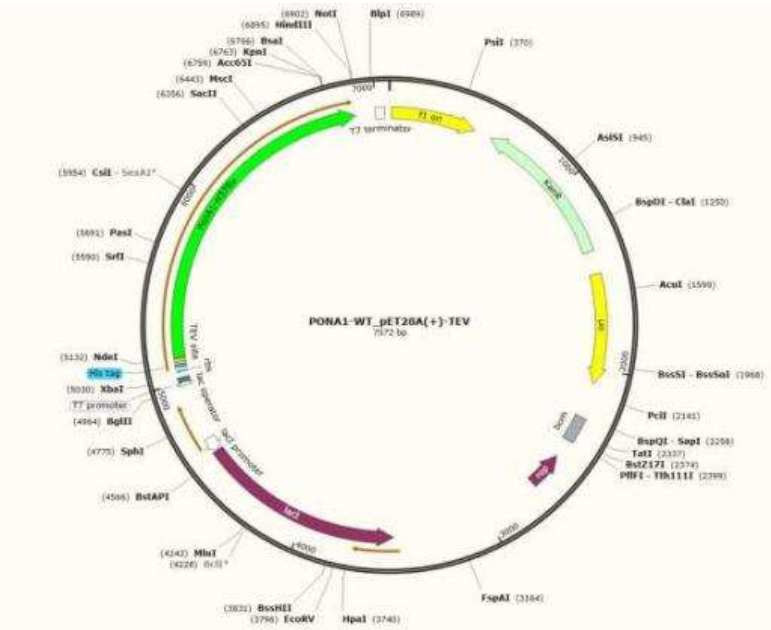

(b) PonA1$_{234\text{-}820}$_wt nucleotide sequence

ATGAACAACCTGTTCGGCGGCGATCTGCAGGGCGGATCGACGATTACCCAGCAGTACGTCAAGAACGCGCTGGTCGGTTCCGCACAGCA
CGGGTGGAGCGGTCTGATGCGCAAGGCGAAAGAATTGGTCATCGCGACGAAGATGTCGGGGGAGTGGTCTAAAGACGATGTGCTGCAG
GCGTATCTGAACATCATCTACTTCGGCCGGGGCGCCTACGGCATTTCGGCGGCGTCCAAGGCTTATTTCGACAAGCCCGTCGAGCAGCT
GACCGTTGCCGAAGGGGCGTTGTTGGCAGCGCTGATTCGGCGGCCTTCGACGCTGGACCCGGCGGTCGACCCCGAAGGGGCCCATGC
CCGCTGGAATTGGGTACTCGACGGCATGGTGGAAACCAAGGCTCTCTCGCCGAATGACCGTGCGGCGCAGGTGTTTCCCGAGACAGTGC
CGCCCGATCTGGCCCGGGCAGAGAATCAGACCAAAGGACCCAACGGGCTGATCGAGCGGCAGGTGACAAGGGAGTTGCTCGAGCTGTT
CAACATCGACGAGCAGACCCTCAACACCCAGGGGCTGGTGGTCACCACCACGATTGATCCGCAGGCCCAACGGGCGGCGGAGAAGGCG
GTTGCGAAATACCTGGACGGGCAGGACCCCGACATGCGTGCCGCCGTGGTTTCCATCGACCCGCACAACGGGGCGGTGCGTGCGTACT
ACGGTGGCGACAATGCCAATGGCTTTGACTTCGCTCAAGCGGGATTGCAGACTGGATCGTCGTTTAAGGTGTTTGCTCTGGTGGCCGCCC
TTGAGCAGGGGATCGGCCTGGGCTACCAGGTAGACAGCTCTCCGTTGACGGTCGACGGCATCAAGATCACCAACGTCGAGGGCGAGGG
TTGCGGGACGTGCAACATCGCCGAGGCGCTCAAAATGTCGCTGAACACCTCCTACTACCGGCTGATGCTCAAGCTCAACGGCGGCCCAC
AGGCTGTGGCCGATGCCGCGCACCAAGCCGGCATTGCCTCCAGCTTCCCGGGCGTTGCGCACACGCTGTCCGAAGATGGCAAGGGTGG
ACCGCCCAACAACGGGATCGTGTTGGGCCAGTACCAAACCCGGGTGATCGACATGGCATCGGCGTATGCCACGTTGGCCGCGTCCGGT
ATCTACCACCCGCCGCATTTCGTACAGAAGGTGGTCAGTGCCAACGGCCAGGTCCTCTTCGACGCCAGCACCGCGGACAACACCGGCGA
TCAGCGCATCCCCAAGGCGGTAGCCGACAACGTGACTGCGGCGATGGAGCCGATCGCAGGTTATTCGCGTGGCCACAACCTAGCGGGT
GGGCGGGATTCGGCGGCCAAGACCGGCACTACGCAATTTGGTGACACCACCGCGAACAAAGACGCCTGGATGGTCGGGTACACGCCGT
CGTTGTCTACGGCTGTGTGGGTGGGCACCGTCAAGGGTGACGAGCCACTGGTAACCGCTTCGGGTGCAGCGATTTACGGCTCGGGCCT
GCCGTCGGACATCTGGAAGGCAACCATGGACGGCGCCTTGAAGGGCACGTCGAACGAGACTTTCCCCAAACCGACCGAGGTCGGTGGT
TATGCCGGTGTGCCGCCGCCGCCGCCGCCGAGGTACCACCTTCGGAGACCGTCATCCAGCCCACGGTCGAAATTGCGCCGGGGA
TTACCATCCCGATCGGTCCCCCGACCACCATTACCCTGGCGCCACCGCCCCCGGCCCCGCCCGCTGCGACTCCCACGCCGTGA

(c) PonA1$_{234\text{-}820}$_wt amino acid sequence

MNNLFGGDLQGGSTITQQYVKNALVGSAQHGWSGLMRKAKELVIATKMSGEWSKDDVLQAYLNIIYFGRGAYGISAASKAYFDKPVEQLTVAEG
ALLAALIRRPSTLDPAVDPEGAHARWNWVLDGMVETKALSPNDRAAQVFPETVPPDLARAENQTKGPNGLIERQVTRELLELFNIDEQTLNTQG
LVVTTTIDPQAQRAAEKAVAKYLDGQDPDMRAAVVSIDPHNGAVRAYYGGDNANGFDFAQAGLQTGSSFKVFALVAALEQGIGLGYQVDSSPLT
VDGIKITNVEGEGCGTCNIAEALKMSLNTSYYRLMLKLNGGPQAVADAAHQAGIASSFPGVAHTLSEDGKGGPPNNGIVLGQYQTRVIDMASAY
ATLAASGIYHPPHFVQKVVSANGQVLFDASTADNTGDQRIPKAVADNVTAAMEPIAGYSRGHNLAGGRDSAAKTGTTQFGDTTANKDAWMVGY
TPSLSTAVWVGTVKGDEPLVTASGAAIYGSGLPSDIWKATMDGALKGTSNETFPKPTEVGGYAGVPPPPPPPEVPPSETVIQPTVEIAPGITIPIG
PPTTITLAPPPPAPPAATPTP*

Appendix III.6. *In silico* ligation of ponA1$_{234\text{-}820}$-Q365H in pET28a plasmid (a), nucleotide (b) and amino acid (c) sequence.

(a)

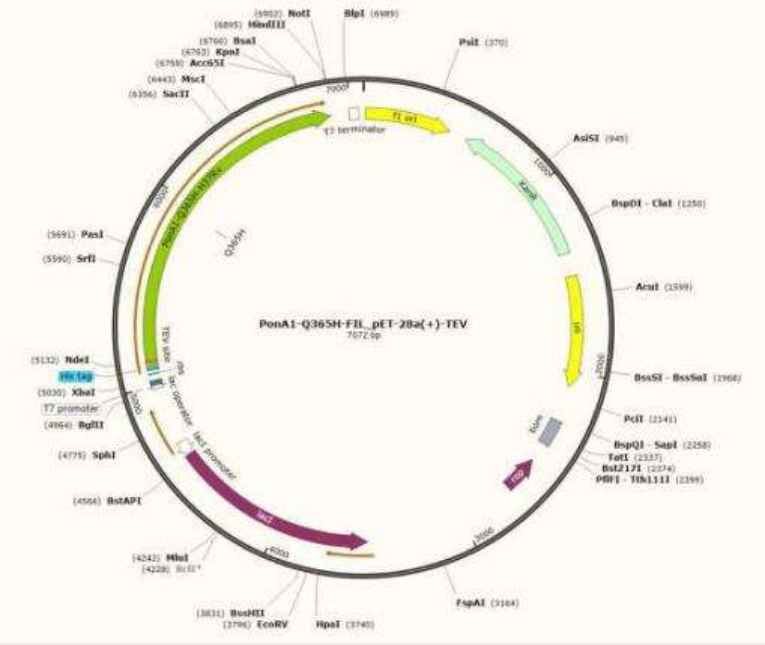

(b) ponA1_Q365H nucleotide sequence

ATGAACAACCTGTTCGGCGGCGATCTGCAGGGCGGATCGACGATTACCCAGCAGTACGTCAAGAACGCGCTGGTCGGTTCCGCACAGCACG
GGTGGAGCGGTCTGATGCGCAAGGCGAAAGAATTGGTCATCGCGACGAAGATGTCGGGGGAGTGGTCTAAAGACGATGTGCTGCAGGCGTA
TCTGAACATCATCTACTTCGGCCGGGGCGCCTACGGCATTTCGGCGGCGTCCAAGGCTTATTTCGACAAGCCCGTCGAGCAGCTGACCGTTG
CCGAAGGGGCGTTGTTGGCAGCGCTGATTCGGCGGCCTTCGACGCTGGACCCGGCGGTCGACCCCGAAGGGGCCCATGCCCGCTGGAATTG
GGTACTCGACGGCATGGTGGAAACCAAGGCTCTCTCGCCGAATGACCGTGCGGCGCAGGTGTTTCCCGAGACAGTGCCGCCCGATCTGGCCC
GGGCAGAGAATCAGACCAAAGGACCCAACGGGCTGATCGAGCGGCAGGTGACAAGGGAGTTGCTCGAGCTGTTCAACATCGACGAGCAGA
CCCTCAACACCCAGGGGCTGGTGGTCACCACCACGATTGATCCGCAGGCCCAACGGGCGGCGGAGAAGGCGGTTGCGAAATACCTGGACGG
GCAGGACCCCGACATGCGTGCCGCCGTGGTTTCCATCGACCCGCACAACGGGGCGGTGCGTGCGTACTACGGTGGCGACAATGCCAATGGCT
TTGACTTCGCTCAAGCGGGATTGCAGACTGGATCGTCGTTTAAGGTGTTTGCTCTGGTGGCCGCCCTTGAGCAGGGGATCGGCCTGGGCTACC
ATGTAGACAGCTCTCCGTTGACGGTCGACGGCATCAAGATCACCAACGTCGAGGGCGAGGGTTGCGGGACGTGCAACATCGCCGAGGCGCT
CAAAATGTCGCTGAACACCTCCTACTACCGGCTGATGCTCAAGCTCAACGGCGGCCCACAGGCTGTGGCCGATGCCGCGCACCAAGCCGGCA
TTGCCTCCAGCTTCCCGGGCGTTGCGCACACGCTGTCCGAAGATGGCAAGGGTGGACCGCCCAACAACGGGATCGTGTTGGGCCAGTACCAA
ACCCGGGTGATCGACATGGCATCGGCGTATGCCACGTTGGCCGCGTCCGGTATCTACCACCCGCCGCATTTCGTACAGAAGGTGGTCAGTGC
CAACGGCCAGGTCCTCTTCGACGCCAGCACCGCGGACAACACCGGCGATCAGCGCATCCCCAAGGCGGTAGCCGACAACGTGACTGCGGCG
ATGGAGCCGATCGCAGGTTATTCGCGTGGCCACAACCTAGCGGGTGGGCGGGATTCGGCGGCCAAGACCGGCACTACGCAATTTGGTGACA
CCACCGCGAACAAAGACGCCTGGATGGTCGGGTACACGCCGTCGTTGTCTACGGCTGTGTGGGTGGGCACCGTCAAGGGTGACGAGCCACT
GGTAACCGCTTCGGGTGCAGCGATTTACGGCTCGGGCCTGCCGTCGGACATCTGGAAGGCAACCATGGACGGCGCCTTGAAGGGCACGTCG
AACGAGACTTTCCCCAAACCGACCGAGGTCGGTGGTTATGCCGGTGTGCCGCCGCCGCCGCCGCCGGAGGTACCACCTTCGGAGACCGT
CATCCAGCCCACGGTCGAAATTGCGCCGGGGATTACCATCCCGATCGGTCCCCCGACCACCATTACCCTGGCGCCACCGCCCCCGGCCCCGC
CCGCTGCGACTCCCACGCCGTGA

(c) PonA1$_{234\text{-}820}$_Q365H amino acid sequence

MNNLFGGDLQGGSTITQQYVKNALVGSAQHGWSGLMRKAKELVIATKMSGEWSKDDVLQAYLNIIYFGRGAYGISAASKAYFDKPVEQLTVAE
GALLAALIRRPSTLDPAVDPEGAHARWNWVLDGMVETKALSPNDRAAQVFPETVPPDLARAENQTKGPNGLIERQVTRELLELFNIDEQTLNTQG
LVVTTTIDPQAQRAAEKAVAKYLDGQDPDMRAAVVSIDPHNGAVRAYYGGDNANGFDFAQAGLQTGSSFKVFALVAALEQGIGLGYHVDSSPLT
VDGIKITNVEGEGCGTCNIAEALKMSLNTSYYRLMLKLNGGPQAVADAAHQAGIASSFPGVAHTLSEDGKGGPPNNGIVLGQYQTRVIDMASAYA
TLAASGIYHPPHFVQKVVSANGQVLFDASTADNTGDQRIPKAVADNVTAAMEPIAGYSRGHNLAGGRDSAAKTGTTQFGDTTANKDAWMVGYT
PSLSTAVWVGTVKGDEPLVTASGAAIYGSGLPSDIWKATMDGALKGTSNETFPKPTEVGGYAGVPPPPPPPEVPPSETVIQPTVEIAPGITIPIGPPTTI
TLAPPPPAPPAATPTP*

Appendix III.7. *In silico* ligation of ponA1$_{234-820}$ -P631S in pET28a plasmid (a), nucleotide (b) and amino acid (c) sequence.

(a)

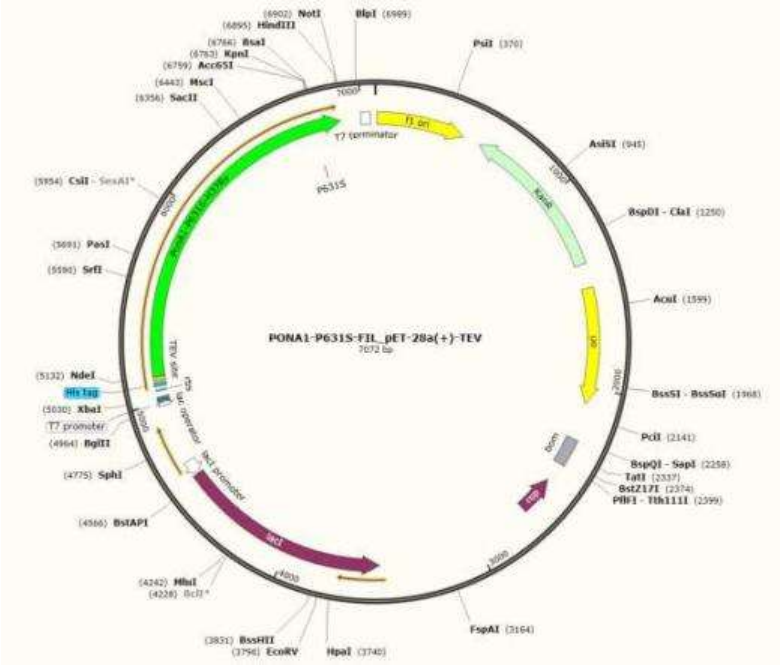

(b) ponA1$_{234-820}$_P631S nucleotide sequence

ATGAACAACCTGTTCGGCGGCGATCTGCAGGGCGGATCGACGATTACCCAGCAGTACGTCAAGAACGCGCTGGTCGGTTCCGCACAGCACG
GGTGGAGCGGTCTGATGCGCAAGGCGAAAGAATTGGTCATCGCGACGAAGATGTCGGGGGAGTGGTCTAAAGACGATGTGCTGCAGGCGTA
TCTGAACATCATCTACTTCGGCCGGGGCGCCTACGGCATTTCGGCGGCGTCCAAGGCTTATTTCGACAAGCCCGTCGAGCAGCTGACCGTTG
CCGAAGGGGCGTTGTTGGCAGCGCTGATTCGGCGGCCTTCGACGCTGGACCCGGCGGTCGACCCCGAAGGGGCCCATGCCCGCTGGAATTG
GGTACTCGACGGCATGGTGGAAACCAAGGCTCTCTCGCCGAATGACCGTGCGGCGCAGGTGTTTCCCGAGACAGTGCCGCCCGATCTGGCCC
GGGCAGAGAATCAGACCAAAGGACCCAACGGGCTGATCGAGCGGCAGGTGACAAGGGAGTTGCTCGAGCTGTTCAACATCGACGAGCAGA
CCCTCAACACCCAGGGGCTGGTGGTCACCACCACGATTGATCCGCAGGCCCAACGGGCGGCGGAGAAGGCGGTTGCGAAATACCTGGACGG
GCAGGACCCCGACATGCGTGCCGCCGTGGTTTCCATCGACCCGCACAACGGGGCGGTGCGTGCGTACTACGGTGGCGACAATGCCAATGGCT
TTGACTTCGCTCAAGCGGGATTGCAGACTGGATCGTCGTTTAAGGTGTTTGCTCTGGTGGCCGCCCTTGAGCAGGGGATCGGCCTGGGCTACC
AGGTAGACAGCTCTCCGTTGACGGTCGACGGCATCAAGATCACCAACGTCGAGGGCGAGGGTTGCGGGACGTGCAACATCGCCGAGGCGCT
CAAAATGTCGCTGAACACCTCCTACTACCGGCTGATGCTCAAGCTCAACGGCGGCCCACAGGCTGTGGCCGATGCCGCGCACCAAGCCGGCA
TTGCCTCCAGCTTCCCGGGCGTTGCGCACACGCTGTCCGAAGATGGCAAGGGTGGACCGCCCAACAACGGGATCGTGTTGGGCCAGTACCAA
ACCCGGGTGATCGACATGGCATCGGCGTATGCCACGTTGGCCGCGTCCGGTATCTACCACCCGCCGCATTTCGTACAGAAGGTGGTCAGTGC
CAACGGCCAGGTCCTCTTCGACGCCAGCACCGCGGACAACACCGGCGATCAGCGCATCCCCAAGGCGGTAGCCGACAACGTGACTGCGGCG
ATGGAGCCGATCGCAGGTTATTCGCGTGGCCACAACCTAGCGGGTGGGCGGGATTCGGCGGCCAAGACCGGCACTACGCAATTTGGTGACA
CCACCGCGAACAAAGACGCCTGGATGGTCGGGTACACGCCGTCGTTGTCTACGGCTGTGTGGGTGGGCACCGTCAAGGGTGACGAGCCACT
GGTAACCGCTTCGGGTGCAGCGATTTACGGCTCGGGCCTGCCGTCGGACATCTGGAAGGCAACCATGGACGGCGCCTTGAAGGGCACGTCG
AACGAGACTTTCCCCAAACCGACCGAGGTCGGTGGTTATGCCGGTGTGCCGCCGCCGCCGCCGTCGGAGGTACCACCTTCGGAGACCGT
CATCCAGCCCACGGTCGAAATTGCGCCGGGGATTACCATCCCGATCGGTCCCCCGACCACCATTACCCTGGCGCCACCGCCCCCGGCCCCGC
CCGCTGCGACTCCCACGCCGTGA

(c) PonA1$_{234-820}$_P631S amino acid sequence

MNNLFGGDLQGGSTITQQYVKNALVGSAQHGWSGLMRKAKELVIATKMSGEWSKDDVLQAYLNIIYFGRGAYGISAASKAYFDKPVEQLTVAE
GALLAALIRRPSTLDPAVDPEGAHARWNWVLDGMVETKALSPNDRAAQVFPETVPPDLARAENQTKGPNGLIERQVTRELLELFNIDEQTLNTQG
LVVTTTIDPQAQRAAEKAVAKYLDGQDPDMRAAVVSIDPHNGAVRAYYGGDNANGFDFAQAGLQTGSSFKVFALVAALEQGIGLGYQVDSSPLT
VDGIKITNVEGEGCGTCNIAEALKMSLNTSYYRLMLKLNGGPQAVADAAHQAGIASSFPGVAHTLSEDGKGGPPNNGIVLGQYQTRVIDMASAYA
TLAASGIYHPPHFVQKVVSANGQVLFDASTADNTGDQRIPKAVADNVTAAMEPIAGYSRGHNLAGGRDSAAKTGTTQFGDTTANKDAWMVGYT
PSLSTAVWVGTVKGDEPLVTASGAAIYGSGLPSDIWKATMDGALKGTSNETFPKPTEVGGYAGVPPPPPPSEVPPSETVIQPTVEIAPGITIPIGPPTTI
TLAPPPPAPPAATPTP*

Appendix III.8. *In silico* ligation of *rpoB* from *M. tuberculosis* H37Rv in pET28a plasmid (a), nucleotide (b) and amino acid (c) sequence.

(a)

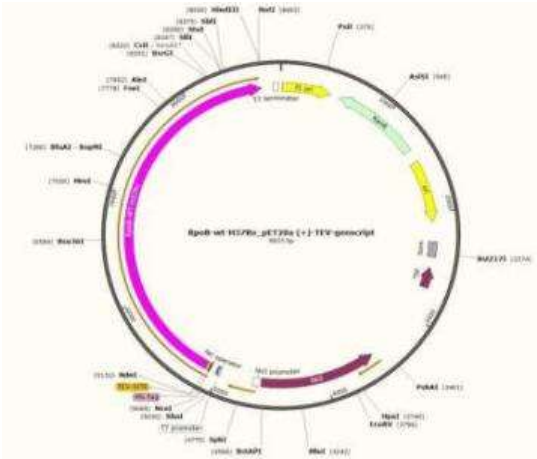

(b) rpoB nucleotide sequence

atgttggcagattcccgccagagcaaaacagccgctagtcctagtccgagtcgcccgcaaagttcctcgaataactccgtacccggagcgccaaaccgggtctccttcgctaagctgcgcgaaccacttgaggttccgg
gactccttgacgtccagaccgattcgttcgagtggctgatcggttcgccgcgctggcgcgaatccgccgccgagcggggtgatgtcaacccagtgggtggcctggaagaggtgctctacgagctgtctccgatcgagg
acttctccgggtcgatgtcgttgtcgttctctgaccctcgtttcgacgatgtcaaggcacccgtcgacgagtgcaaagacaaggacatgacgtacgcggctccactgttcgtcaccgccgagttcatcaacaacaacaccg
gtgagatcaagagtcagacggtgttcatgggtgacttcccgatgatgaccgagaagggcacgttcatcatcaacgggaccgagcgtgtggtggtcagccagctggtgcggtcgcccggggtgtacttcgacgagacc
attgacaagtccaccgacaagacgctgcacagcgtcaaggtgatcccgagccgcggcgcgtggctcgagtttgacgtcgacaagcgcgacaccgtcggcgtgcgcatcgaccgcaaacgccggcaaccggtcac
cgtgctgctcaaggcgctgggctggaccagcgagcagattgtcgagcggttcgggttctccgagatcatgcgatcgacgctggagaaggacaacaccgtcggcaccgacgaggcgctgttggacatctaccgcaag
ctgcgtccgggcgagcccccgaccaaagagtcagcgcagacgctgttggaaaacttgttcttcaaggagaagcgctacgacctggcccgcgtcggtcgctataaggtcaacaagaagctcgggctgcatgtcggcg
agcccatcacgtcgtcgacgctgaccgaagaagacgtcgtggccaccatcgaatatctggtccgcttgcacgagggtcagaccacgatgaccgttccgggcggcgtcgaggtgccggtggaaaccgacgacatcga
ccacttcggcaaccgccgcctgcgtacggtcggcgagctgatccaaaaccagatccgggtcggcatgtcgcggatggagcgggtggtccgggagcggatgaccacccaggacgtggaggcgatcacaccgcaga
cgttgatcaacatccggccggtggtcgccgcgatcaaggagttcttcggcaccagccagctgagccaattcatggaccagaacaacccgctgtcggggttgacccacaagcgccgactgtcggcgctggggcccgg
cggtctgtcacgtgagcgtgccgggctggaggtccgcgacgtgcacccgtcgcactacggccggatgtgcccgatcgaaaccccctgaggggcccaacatcggtctgatcggctcgctgtcggtgtacgcgcgggtc
aacccgttcgggttcatcgaaacgccgtaccgcaaggtggtcgacggcgtggttagcgacgagatcgtgtacctgaccgccgacgaggaggaccgccacgtggtggcacaggccaattcgccgatcgatgcggac
ggtcgcttcgtcgagccgcgcgtgctggtccgccgcaaggcgggcgaggtggagtacgtgccctcgtctgaggtggactacatggacgtctcgccccgccagatggtgtcggtggccaccgcgatgattcccttcct
ggagcacgacgacgccaaccgtgccctcatgggggcaaacatgcagcgccaggcggtgccgctggtccgtagcgaggccccgctggtgggcaccgggatggagctgcgcgcggcgatcgacgccggcgacgt
cgtcgtcgccgaagaaagcggcgtcatcgaggaggtgtcggccgactacatcactgtgatgcacgacaacggcacccggcgtacctaccggatgcgcaagtttgcccggtccaaccacggcacttgcgccaaccag
tgccccatcgtggacgcgggcgaccgagtcgaggccggtcaggtgatcgccgacggtccctgtactgacgacggcgagatggcgctgggcaagaacctgctggtggccatcatgccgtgggagggccacaacta
cgaggacgcgatcatcctgtccaaccgcctggtcgaagaggacgtgctcacctcgatccacatcgaggagcatgagatcgatgctcgcgacaccaagctgggtgcggaggagatcacccgcgacatcccgaacatc
tccgacgaggtgctcgccgacctggatgagcggggcatcgtgcgcatcggtgccgaggttcgcgacggggacatcctggtcggcaaggtcaccccgaagggtgagaccgagctgacgccggaggagcggctgct
gcgtgccatcttcggtgagaaggcccgcgaggtgcgcgacacttcgctgaaggtgccgcacggcgaatccggcaaggtgatcggcattcgggtgttttcccgcgaggacgaggacgagttgccggccggtgtcaac
gagctggtgcgtgtgtatgtggctcagaaacgcaagatctccgacggtgacaagctggccggccggcacggcaacaagggcgtgatcggcaagatcctgccggttgaggacatgccgttccttgccgacggcaccc
cggtggacattattttgaacacccacggcgtgccgcgacggatgaacatcggccagattttggagacccacctgggttggtgtgcccacagcggctggaaggtcgacgccgccaaggggttccggactgggccgc
caggctgcccgacgaactgctcgaggcgcagccgaacgccattgtgtcgacgccggtgttcgacggcgcccaggaggccgagctgcagggcctgttgtcgtgcacgctgcccaaccgcgacggtgacgtgctggt
cgacgccgacggcaaggccatgctcttcgacgggcgcagcggcgagccgttcccgtacccggtcacggttggctacatgtacatcatgaagctgcaccacctggtggacgacaagatccacgcccgctccaccggg
ccgtactcgatgatcacccagcagccgctgggcggtaaggcgcagttcggtggccagcggttcggggagatggagtgctgggccatgcaggcctacggtgctgcctacaccctgcaggagctgttgaccatcaagtc
cgatgacaccgtcggccgcgtcaaggtgtacgaggcgatcgtcaagggtgagaacatcccggagccgggcatccccgagtcgttcaaggtgctgctcaaagaactgcagtcgctgtgcctcaacgtcgaggtgctat
cgagtgacggtgcggcgatcgaactgcgcgaaggtgaggacgaggacctggagcgggccgcggccaacctgggaatcaatctgtcccgcaacgaatccgcaagtgtcgaggatcttgcgtaa

(b) RpoB amino acid sequence

MLADSRQSKTAASPSPSRPQSSSNNSVPGAPNRVSFAKLREPLEVPGLLDVQTDSFEWLIGSPRWRESAAERGDVNPVGGLEEVLYELSPIEDFSGSMSLSFSDP
RFDDVKAPVDECKDKDMTYAAPLFVTAEFINNNTGEIKSQTVFMGDFPMMTEKGTFIINGTERVVVSQLVRSPGVYFDETIDKSTDKTLHSVKVIPSRGAWLE
FDVDKRDTVGVRIDRKRRQPVTVLLKALGWTSEQIVERFGFSEIMRSTLEKDNTVGTDEALLDIYRKLRPGEPPTKESAQTLLENLFFKEKRYDLARVGRYKV
NKKLGLHVGEPITSSTLTEEDVVATIEYLVRLHEGQTTMTVPGGVEVPVETDDIDHFGNRRLRTVGELIQNQIRVGMSRMERVVRERMTTQDVEAITPQTLINI
RPVVAAIKEFFGTSQLSQFMDQNNPLSGLTHKRRLSALGPGGLSRERAGLEVRDVHPSHYGRMCPIETPEGPNIGLIGSLSVYARVNPFGFIETPYRKVVDGVVS
DEIVYLTADEEDRHVVAQANSPIDADGRFVEPRVLVRRKAGEVEYVPSSEVDYMDVSPRQMVSVATAMIPFLEHDDANRALMGANMQRQAVPLVRSEAPLV
GTGMELRAAIDAGDVVVAEESGVIEEVSADYITVMHDNGTRRTYRMRKFARSNHGTCANQCPIVDAGDRVEAGQVIADGPCTDDGEMALGKNLLVAIMPW
EGHNYEDAIILSNRLVEEDVLTSIHIEEHEIDARDTKLGAEEITRDIPNISDEVLADLDERGIVRIGAEVRDGDILVGKVTPKGETELTPEERLLRAIFGEKAREVRD
TSLKVPHGESGKVIGIRVFSREDEDELPAGVNELVRVYVAQKRKISDGDKLAGRHGNKGVIGKILPVEDMPFLADGTPVDIILNTHGVPRRMNIGQILETHLGW
CAHSGWKVDAAKGVPDWAARLPDELLEAQPNAIVSTPVFDGAQEAELQGLLSCTLPNRDGDVLVDADGKAMLFDGRSGEPFPYPVTVGYMYIMKLHHLVD
DKIHARSTGPYSMITQQPLGGKAQFGGQRFGEMECWAMQAYGAAYTLQELLTIKSDDTVGRVKVYEAIVKGENIPEPGIPESFKVLLKELQSLCLNVEVLSSD
GAAIELREGEDEDLERAAANLGINLSRNESASVEDLA-

Appendix III.9 Zym media-5052 composition

Stock solution	components
Zym	Tryptone 1% (v/w), yeast extract 0.5% (v/w)
50X M	1.25 M Na_2HPO_4, 1.25 M KH_2PO_4, 2.5 M NH_4Cl, 0.25 M Na_2SO_4
MgSO4 1M	$MgSO_4.7H_2O$.
50X 5052	Glycerol 25%(v/w), glucose 2.5% (v/w), α−lactose 10% (v/w).
Metal mix	50 mM FeCl3•6H2O; 20 mM CaCl2•2H2O; 10 mM MnCl2•4H2O;10 mM ZnSO4•7H2O; 2 mM CoCl2•6H2O 2 mM CuCl2•2H2O; 2 mM NiCl2•6H2O; 2 mM Na2MoO4•2H2O; 2 mM Na2SeO3; 2 mM H3BO3

From: https://www.elabprotocols.com

Appendix III.10. Promotor evaluation by FACS in *M. smegmatis* (Source from Cohen-Gonsaud et al, 2021). *rpsTp* from *M. marinum* integrated in *M.smegmatis* evaluation.

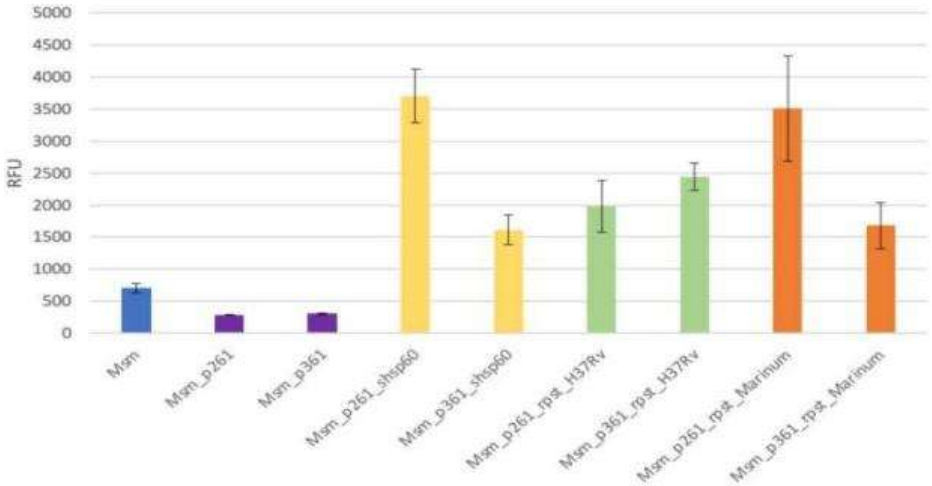

Appendix III.11. *ponA1* promoter sequence, *ponA1* gene sequence from *M. tuberculosis*and and *in silico* representation of *M. tuberculosis ponA1* promoter and gene ligated in pKM464 plasmid.

A. ponA1 *M. tuberculosis* promoter

TTGCGCAACTCGTAGCCATGCATCGGTGACTCGATCAACAGACCCAGGATGGCGAGCTCCAGCATCGAGTCACCTCCTTTTGTATGGCTTTTGAATGGCCGTTACGAC
GGTTCGACGCCTCGCGTCATCGTATCGCCTCGATATATTTGCGACAACATCACCGCGTCAAGACGGGTAGCTGACGTGCTTGATGGTGCCGTCACCTGCGAAAACGAG
GTATCCACCGCCGTAGTCGCTAGAGACATACAACGACAACGACAACGCAGCCGGCGTGGTGGGGTCCTTGACCGGTTCGACGATCAGGTACATGCTTTTGACGTCGG
ATTGTTTGAGGCCGAGGGTTTCCGGGGCGCCGCGCATGATGCCCACAGCGGTCTTCGCATCGAATTTGCTCAGGTCAACCACGGACACGTCGGCAATGCTCTTGGCGG
AACTGGTCGCATCGCCCCAGCCGCCGCGGTAGGTATACGCCAGGACTCGGCGGTCGTCCGCCGGGTCGACGCGATCGAGCGACGCATACTCCGGGTAGATCACCAGC
CGGTAGCCCATGGTGTCGCCGAACCGCTTGCGGGTCTGCTCCAGCAGGCCGGTGAGCCCGCCGAGGGAATGCAGCTGCCTGGGCGGGGTCAGCACCACGGGGGCGA
TCCCGTCGGGCTTTGCTCCGGGATCCGAGGTGAAGTCCAGCGGAGAGCGGGTGTTGCCGTACACGCCCCAGCCGATGCCGACGCCCAGCAGCACCGATGCGACAAAC
GCAGCGGCCAGCAAGCCCAACTCGGTGCGTTTCGCCCGCGATTTGAGCGCGGGCATTTGTGCGGGTGCGCTCTCGACCTGCAGGTCGGCCACCAGACGCTGCAGGTC
ACCTAGGGTCACAGCCTTGGTAGCTGCGCTGACGCGCTCCCGGTGTTCCTCCATCGAGAGCTCGCCGTCACGCAGGGCGTCGTCGAGAATCCGGCAGGCGTCCTGCC
GGTCGCTGTCTTTGGCGCGGGTTGCCGTCGATACTCCGCGCGCAAGGGGTGCGCCCAGCCACTTCGCCACAGGGACGATAGTAGGAGTCTGGCTGGGAATCTGAACT
CGATCCCGCCGTACCCGCGCAACAACGGCGCCGGTTGCGTATCGGTGGTGTGGATGGCGTCGTACTCTGGTCAGCGTGCGACTGCAGCGACAGGTAGTGGACTACAC
GCTACGGCGACGCTCCCTGCTGGCCGAGGTGTATTCGGGACGCACCGGTGTGTCGGAGGTGTGCGACGCCAACCCCTACCTGCTGCGCGCCGCGAAAGTTTCATGGGA
AGCCCAGCCGGGTCATCTGCCCGATCTGCCGCAAGGAGCAGCTCACACTGGTGTCGTGGGTGTTCGGCGAGCACCTCGGTGCGGTATCAGGGTCCGCGCGCACCGCC
GAAGAACTGATCCTGCTGGCGACCCGGTTCTCCGAGTTCGCGGTCCACGTGGTGGAGGTATGTCGAACCTGCAGTTGGAATCATCTGGTCAAGTCATACGTCCTGGGC
GCCGCACGTCCGGCACGCCCCCCTAGGGGGTCTGGCGGGACGCGGACGGCGCGCAACGGGGCCCGCACGGCCA

B. ponA1 *M. tuberculosis* gene

GTGAATAGCGACGGGCGTCACCATCAGTCGTCCAGCGGCGCCCCGCGCGGGCCGGCGAATCCCGGCCAGCGTGGTCAGGTTCCACCCGACGACAGACTGACCGCGA
TCCTCCCGCCGGTGACCGATGACCGATCGGCTCCGCACGCGGACTCCATCGAGGCGGTCAAGGCCGCGCTCGACGGCGCGCCGCCGATGCCCCCGCCGCGCGACCCG
CTCGAGGAGGTCACGGCCGCGTTGGCCGCCCCGCCCGGTAAACCGCCGCGGGGGGATCAGCTTGGTGGCAGACGTCGCCCACCGGGGCCGCCCGGGCCCCCCGGTTC
GTCCGGACAGCCTGCCGGCCGGCTGCCCCAACCGAGGGTGGACTTGCCCCGGGTCGGCCAGATCAACTGGAAATGGATACGGCGTTCGCTGTACCTCACCGCGGCGG
TGGTGATCCTGTTGCCGATGGTCACCTTCACGATGGCCTACCTGATCGTCGACGTTCCCAAGCCAGGTGACATCCGTACCAACCAGGTCTCCACGATCCTTGCCAGCG
ACGGCTCGGAAATCGCCAAAATTGTTCCGCCCGAAGGTAATCGGGTCGACGTCAACCTCAGCCAGGTGCCGATGCATGTGCGCCAGGCGGTGATTGCGGCCGAAGAC
CGCAATTTCTATTCGAATCCGGGATTCTCGTTCACCGGCTTCGCGCGGGCAGTCAAGAACAACCTGTTCGGCGGCGATCTGCAGGGCGGATCGACGATTACCCAGCA
GTACGTCAAGAACGCGCTGGTCGGTTCCGCACAGCACGGGTGGAGCGGTCTGATGCGCAAGGCGAAAGAATTGGTCATCGCGACGAAGATGTCGGGGGAGTGGTCT
AAAGACGATGTGCTGCAGGCGTATCTGAACATCATCTACTTCGGCCGGGGCGCCTACGGCATTTCGGCGGCGTCCAAGGCTTATTTCGACAAGCCCGTCGAGCAGCT
GACCGTTGCCGAAGGGGCGTTGTTGGCAGCGCTGATTCGGCGGCCTTCGACGCTGGACCCGGCGGTCGACCCCGAAGGGGCCCATGCCCGCTGGAATTGGGTACTCG
ACGGCATGGTGGAAACCAAGGCTCTCTCGCCGAATGACCGTGCGGCGCAGGTGTTTCCCGAGACAGTGCCGCCCGATCTGGCCCGGGCAGAGAATCAGACCAAAGG
ACCCAACGGGCTGATCGAGCGGCAGGTGACAAGGGAGTTGCTCGAGCTGTTCAACATCGACGAGCAGACCCTCAACACCCAGGGGCTGGTGGTCACCACCACGATT
GATCCGCAGGCCCAACGGGCGGCGGAGAAGGCGGTTGCGAAATACCTGGACGGGCAGGACCCCGACATGCGTGCCGCCGTGGTTTCCATCGACCCGCACAACGGGG
CGGTGCGTGCGTACTACGGTGGCGACAATGCCAATGGCTTTGACTTCGCTCAAGCGGGATTGCAGACTGGATCGTCGTTTAAGGTGTTTGCTCTGGTGGCCGCCCTTG
AGCAGGGGATCGGCCTGGGCTACCAGGTAGACAGCTCTCCGTTGACGGTCGACGGCATCAAGATCACCAACGTCGAGGGCGAGGGTTGCGGGACGTGCAACATCGC
CGAGGCGCTCAAAATGTCGCTGAACACCTCCTACTACCGGCTGATGCTCAAGCTCAACGGCGGCCCACAGGCTGTGGCCGATGCCGCGCACCAAGCCGGCATTGCCT
CCAGCTTCCCGGGCGTTGCGCACACGCTGTCCGAAGATGGCAAGGGTGGACCGCCCAACAACGGGATCGTGTTGGGCCAGTACCAAACCCGGGTGATCGACATGGC
ATCGGCGTATGCCACGTTGGCCGCGTCCGGTATCTACCACCCGCCGCATTTCGTACAGAAGGTGGTCAGTGCCAACGGCCAGGTCCTCTTCGACGCCAGCACCGCGG
ACAACACCGGCGATCAGCGCATCCCCAAGGCGGTAGCCGACAACGTGACTGCGGCGATGGAGCCGATCGCAGGTTATTCGCGTGGCCACAACCTAGCGGGTGGGCG
GGATTCGGCGGCCAAGACCGGCACTACGCAATTTGGTGACACCACCGCGAACAAAGACGCCTGGATGGTCGGGTACACGCCGTCGTTGTCTACGGCTGTGTGGGTGG
GCACCGTCAAGGGTGACGAGCCACTGGTAACCGCTTCGGGTGCAGCGATTTACGGCTCGGGCCTGCCGTCGGACATCTGGAAGGCAACCATGGACGGCGCCTTGAAG
GGCACGTCGAACGAGACTTTCCCCAAACCGACCGAGGTCGGTGGTTATGCCGGTGTGCCGCCGCCGCCGCCGCCGCCGAGGTACCACCTTCGGAGACCGTCATCCA
GCCCACGGTCGAAATTGCGCCGGGGATTACCATCCCGATCGGTCCCCCGACCACCATTACCCTGGCGCCACCGCCCCCGGCCCCGCCCGCTGCGACTCCCACGCCGCC
GCCGTGA

C. pKM464-ponA1p-ponA1g plasmid *in silico* representation

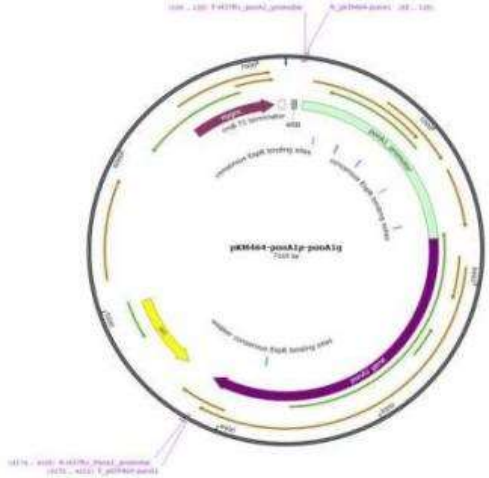

Appendix III.12. Generation of pKM464-*ponA1p*-ponA1 plasmid

Plasmid construction

Genomic DNA from Mtb H37Rv was used to amplify the region spanning 51663 to 55699 with primers F-H37Rv_ponA1_promoter 59-CCAGCAGGCCGGTCAGCCTC-39 and R-H37Rv_ponA1_promoter 59-AGATGTTGCTGCTTTGGGACAG-39. The reaction employed Q5 High-Fidelity 2X Master Mix (New England Biolabs), 10 µM of each primer, and 10 ng of genomic DNA from Mtb H37Rv was used as a template. PCR conditions included an initial denaturation at 98°C for 30 seconds, followed by thirty cycles of 98°C for 10 seconds, 70°C for 20 seconds, and 72°C for 2 minutes, with a final extension at 72°C for 2 minutes and a hold at 12°C. The second step was to amplify the pKM464 with the primers F_pKM464-ponA1 59- GTCCCAAAGCAGCAACATCTTgcggccgctagcggtaccag-39 and R_pKM464-ponA1 59- GAGGCTGACCGGCCTGCTGGactagtgcatgctctagactc-39. The reaction employed Q5 High-Fidelity 2X Master Mix, 10 µM of each primer, and 10 ng of pKM464 plasmid was used as a template. PCR conditions included an initial denaturation at 98°C for 30 seconds, followed by thirty cycles of 98°C for 10 seconds, 70°C for 20 seconds, and 72°C for 1 minute, with a final extension at 72°C for 2 minutes and a hold at 12°C.

The plasmid pKM464-ponA1p-ponA1 was generated by amplifying the plasmid pKM464 with cohesive ends producing fragments of 3122 bp (A). The *ponA1p* and *ponA1* gene were also amplified from Mtb H37Rv producing fragments of 4087 bp (B). Following GA, the constructs were transformed in *E. coli* DH5α cells, yielding 686 CFU for the assembled reaction versus 23 CFU for the open plasmid ligation control. The efficiency of the competent cells was approximately 10^6 for all assays (C). Verification was conducted by PCR colony using One Taq polymerase with primers F-H37Rv_ponA1_promoter and R-H37Rv_ponA1_promoter. The conditions were as follows: an initial denaturation at 94°C for 5 minutes, followed by thirty cycles of 94°C for 30 seconds, 65°C for 30 seconds, and 68°C for 4 minutes, ending with a final extension at 68°C for 5 minutes and a hold at 12°C. Two clones were sequenced and the analysis showed deletion in the P630 and P631.

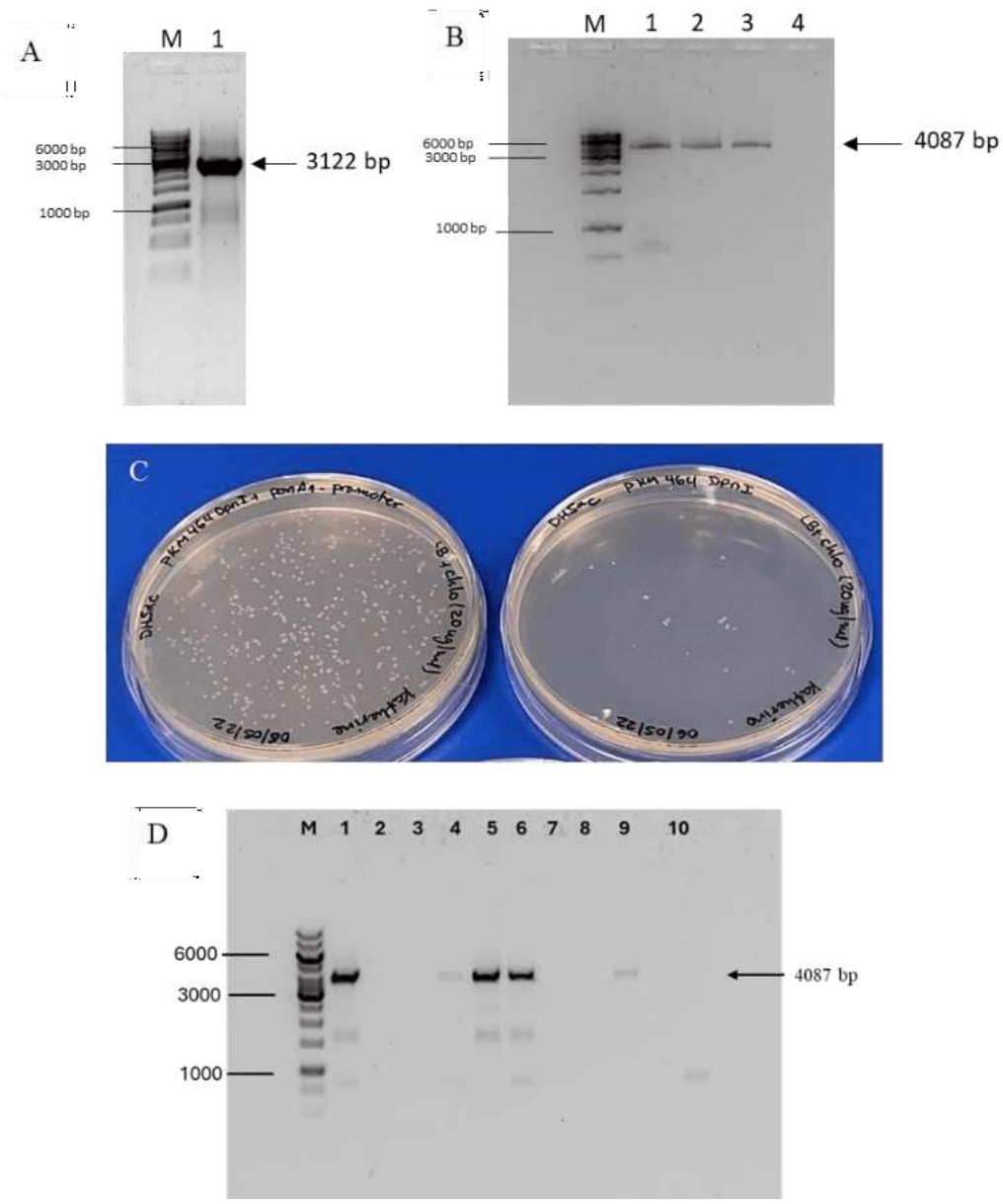

Clonation of pKM464-ponA1p-ponA1g and transformation in *E. coli* DH5α A.pKM464 plasmid amplification. B. ponA1p-ponA1g PCR amplification from *M. tuberculosis* H37Rv. Line 1-4 Temperature gradient (66-68-70-72°C, respectively). C. Heat-shock transformation in *E coli.* Positive (left) and negative (right) transformation plates. D. ponA1p-ponA1 g 4087 bp fragment cloned in pKM464. Line 1-8 clones D1-D8, line 9 positive control with DNAg from Mtb H37Rv, line 10 Negative control. (M) Ladder GeneRuler 1Kb. Agarose gel at 0.8 % in TAE 1X.

***ponA1* directed mutagenesis**

The following conditions were used for the point modification of residues P630-P631: Q5 High-Fidelity 2X Master Mix, 10 µM of each primer, and 10 ng of pKM464-ponA1p-ponA1g as the template and two fragments were generated.

For the fragment I amplification, primers F-H37Rv_ponA1_promoter 59-CCAGCAGGCCGGTCAGCCTC-39 and R-P630-P631-ponA1 59-GTCTCCGAAGGTGGTACCTCCGGCGGCGGCGGCGGCGGCGGCACACC-39 were used. The PCR cycle consisted of an initial denaturation at 98°C for 30 seconds, followed by thirty cycles of 98°C for 10 seconds, 72°C for 2 minutes 20 seconds, with a final extension at 72°C for 2 minutes and storage at 12°C.

To the amplification of the fragment II F-P630-P631-ponA1 59-GAGGTACCACCTTCGGAGAC-39 and R_pKM464-ponA1 59-GAGGCTGACCGGCCTGCTGGactagtgcatgctctagactc-39 were used. The PCR cycle consisted of an initial denaturation at 98°C for 30 seconds, followed by thirty cycles of 98°C for 10 seconds, 62°C for 20 seconds and 72°C for 1 minute 39 seconds, with a final extension at 72°C for 2 minutes and storage at 12°C. Clones9 verification was performed with F-pKM464-int 59-CTTCGCCCGCGAACTGCTC-39 and R_pKM464-int 59-CGGAGCCTATGGAAAAACGCCAGC-39.

Two fragments were generated from plasmid pKM464-ponA1p-ponA1g for gene correction to the *ponA1* wild-type form of Mtb H37Rv (B-C), gel purification was performed for both fragments. 350 CFU in the positive cloning plate, 11 and 61 CFU in the autoligation plate growth (D-left to right). The clone in line 3 (codified as 5.2) was sent for sequencing, getting the wild type sequence (E).

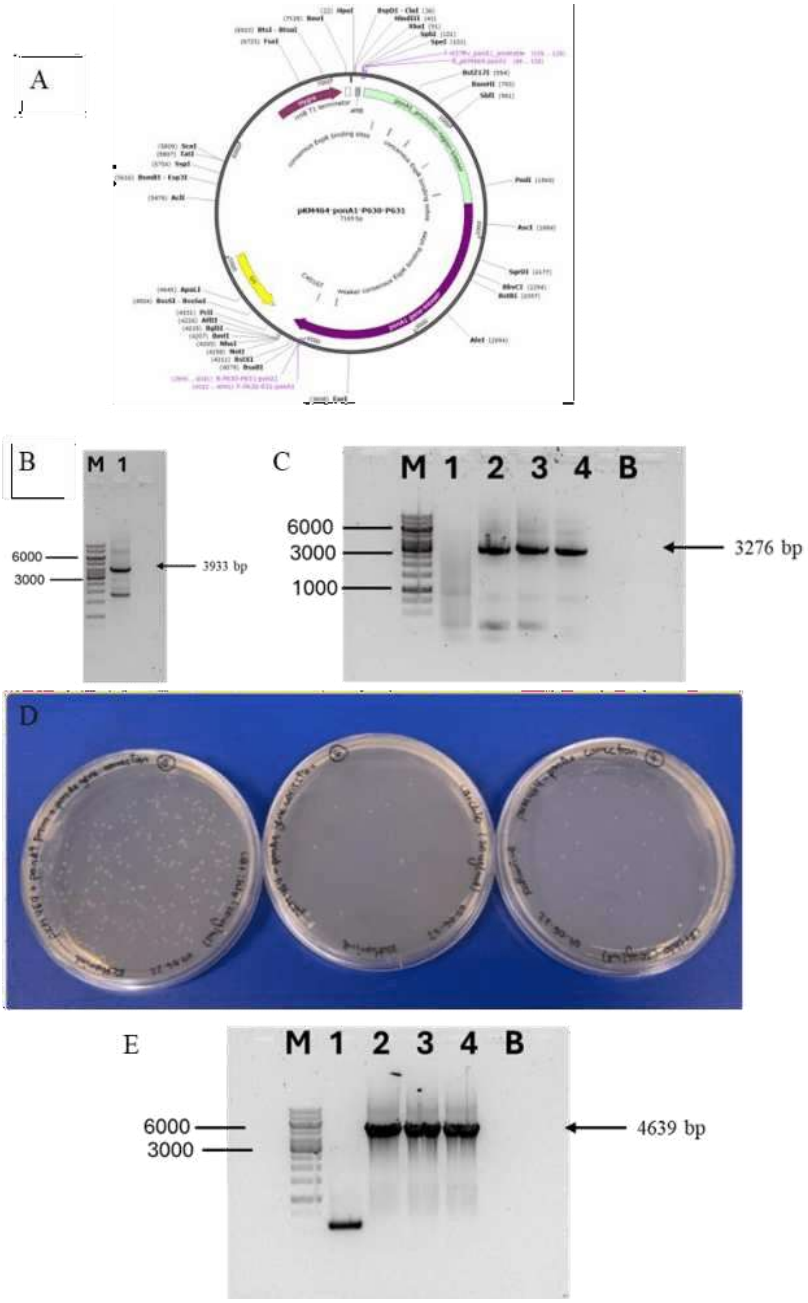

***ponA1* PCR directed mutagenesis in pKM464-*ponA1p-ponA1* transformed in *E. coli* DH5α** A. *In silico* representation and primers disposition to *ponA1* gene directed mutagenesis of the residues P630-P631. B.Electrophoresis for fragment I amplified with F-H37Rv_ponA1_promoter and R-P630-P631-ponA1. C. Electrophoresis for fragment II amplified with F-P630-P631-ponA1 and R_pKM464-ponA1. Temperature gradient was performed between 56-58-60-62°C from line 1 to 4, respectively. D. *E. coli* DH5α transformants in the LB plate. Left. Two fragments assembled; middle and right plates are autoligated controls for each fragment. E. PCR colony with primers F-pKM464-int and R_pKM464-int., Line 1 Negative control with plasmid pKM464, line 2-4 clones evaluation. (B) negative control. (M) marker 1 kb GeneRuler.

Appendix III.13. EGFP nucleotide sequence

ATGGTGTCGAAGGGCGAGGAGCTGTTCACCGGCGTCGTGCCCATCCTGGTCGA
GCTGGACGGCGACGTGAACGGCCACAAGTTCAGCGTCTCGGGCGAGGGCGAG
GGCGACGCGACCTACGGCAAGCTGACCCTGAAGTTCATCTGCACCACCGGCAA
GCTGCCGGTCCCCTGGCCGACCCTGGTGACCACCCTGACCTACGGCGTGCAGTG
TTTCTCGCGGTACCCCGACCACATGAAGCAGCACGACTTCTTCAAGAGCGCGAT
GCCGGAGGGCTACGTCCAGGAGCGCACCATCTTCTTCAAGGACGACGGCAACT
ACAAGACCCGGGCCGAGGTCAAGTTCGAGGGCGACACCCTGGTGAACCGCATC
GAGCTGAAGGGCATCGACTTCAAGGAAGACGGCAACATCCTGGGCCACAAGCT
GGAGTACAACTACAACTCGCACAACGTCTACATCATGGCGGACAAGCAGAAGA
ACGGCATCAAGGTGAACTTCAAGATCCGCCACAACATCGAGGACGGCAGCGTC
CAGCTGGCCGACCACTACCAGCAGAACACCCCCATCGGCGACGGCCCCGTCCT
GCTGCCGGACAACCACTACCTGAGCACCCAGTCGGCGCTGAGCAAGGACCCGA
ACGAGAAGCGGGACCACATGGTCCTGCTGGAGTTCGTGACCGCCGCGGGCATC
ACCCTGGGCATGGACGAGCTGTACAAG

Appendix III.14. *In silico* ligation of *ponA1p*-EGFP in pKM464

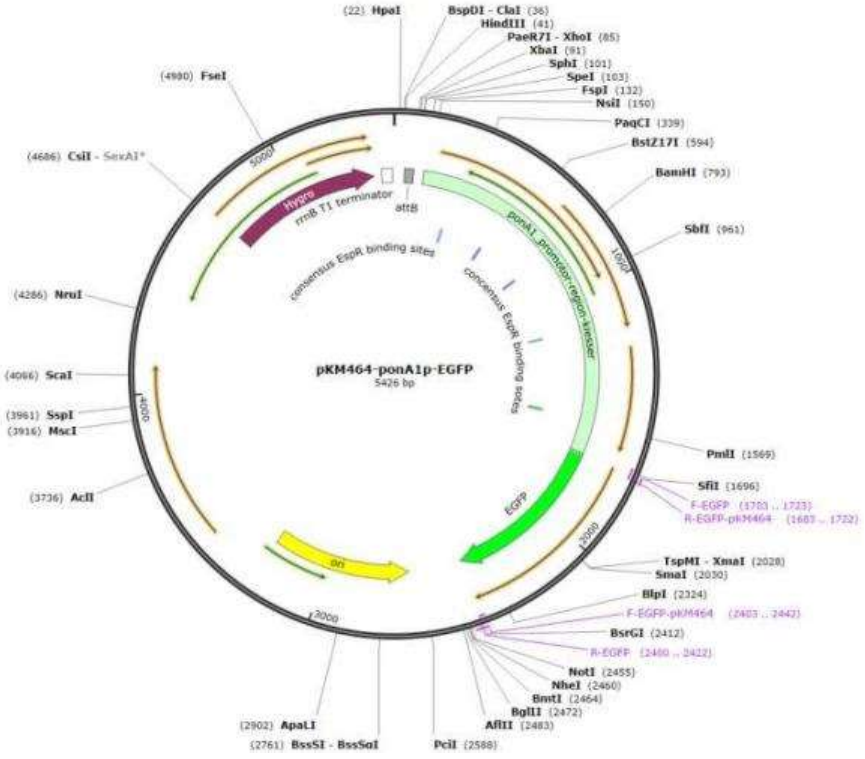

Appendix III.15. *rpsTp* sequence from *M. marinum*

ACGtcttttgggtgaaaacgtaaccgactGATAACCTgagcactcgctgtcgggtgtcaaggtcacccgagcaaccacc
gagcagactttaaggaactaacgcGTGGCCAACATCAAGTCGCAGCAAAAGCGCAACCGCAC
CAACAGC

Appendix III.16. *In silico* ligation of *rpsTp*-EGFP in pKM464

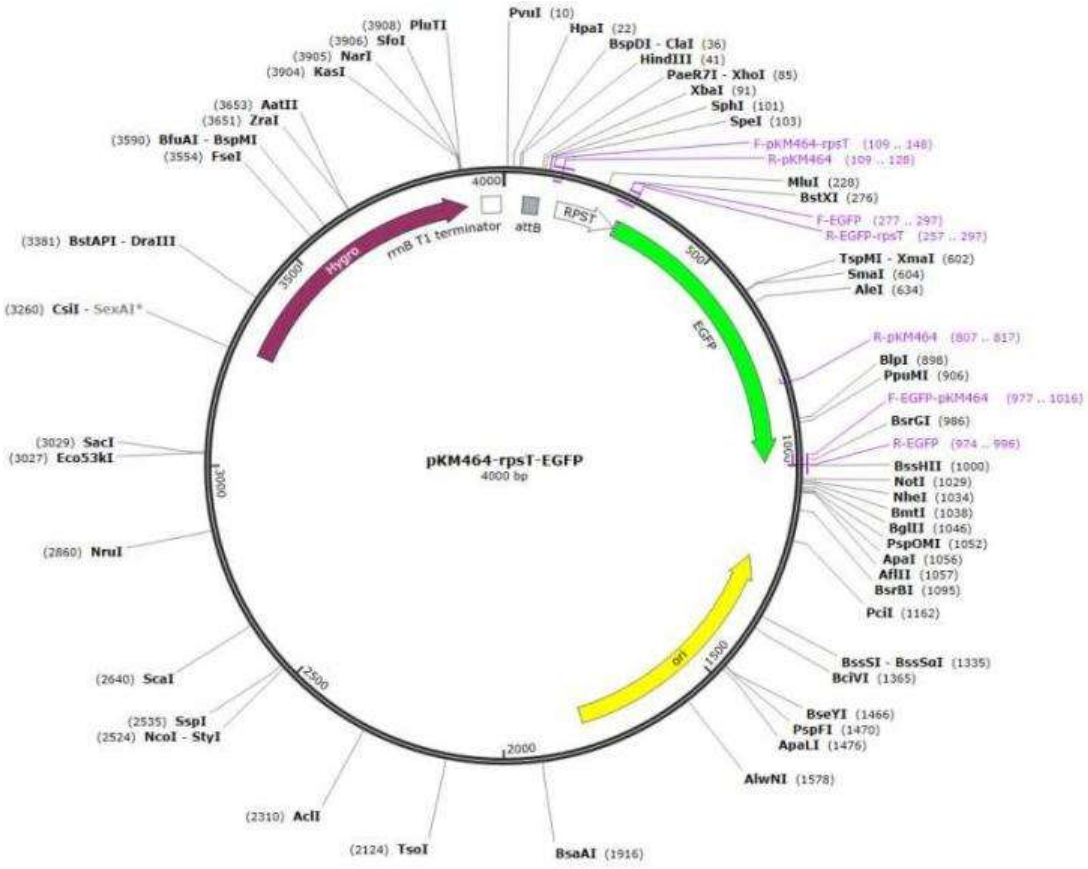

Appendix III.17. Cloning by Gibson assembly (Synthetic biology protocols-CBS-Montpellier-France).

This protocol involves different steps, from the design of primers, PCR with Q5, DpnI digestion, PCR clean up, Gibson assembly reaction, transformation and verification by sequencing.
The PCR reaction must be performed with Q5, with specific conditions for each couple of primers.

DpnI digestion:

Add 1¼L DpnI in a 17.5 ¼L PCR tube from Q5, mix well by pipetting up and down so that your solution is homogeneous and glycerol is not in the bottom of the tube. Incubate 1h at 37°C and 10min at 80°C, finally hold at 12°.

PCR clean-up

It is performed with Monarch PCR & DNA clean-up (NEB catalog #T1030S), manufacturer instructions were followed. DNA concentration is verified with nanodrop.

Gibson assembly

Components

- 2X Gibson Assembly Mix (see Gibson Assembly Mix protocol)
- Insert fragment(s) from PCR
- Vector fragment (after PCR, DpnI and clean-up).
- Ultrapure water
- Thermo-cycler at 50°C

Protocol

Calculate the volume of insert and vector to mix in the Gibson Assembly reaction. For 2 fragment assembly (one insert and one vector), the optimum is to mix 100 ng of vector with 3 times more insert in mole, and for more than 2 fragment assembly, 100 ng of vector with same quantity of each insert in mole. The total volume of insert(s) and vector have to be 10¼L or less, if the calculated total volume is higher, the quantity of vector can be reduced up to 50ng and the volume of insert calculated accordingly.
Then, mix the vector and insert(s) fragments according to previously calculated proportions with 10 ¼L of the Gibson Assembly Mix and adjust the total volume of the reaction to 20 ¼L with water. As negative control of assembly, mix the vector alone in the same proportion than previously with 10¼L of Gibson Assembly Mix and adjust the total volume of the reaction to 20 ¼L with water. Place the reactions at 50°C during one hour and for better conservation incubate the reaction for 10 minutes at 80°C.

Transformation

Thaw gently competent cells on ice (aliquot of 100¼L), one tube per Gibson assembly reaction (do not forget negative controls). Sultrily, add 10¼L of the Gibson Assembly reaction (keep cells on ice). Incubate 30 minutes on ice and heat-shock cells at 42°C during 45seconds (in water bath). Then, put back on ice after heat-shock (2 to 5minutes) and immediately add 900 ¼L pre-warmed SOC (37°C) (rich medium). Incubate cells at 37°C with agitation during at least 30min and centrifuge cells at 4000rpm during 1 to 2 minutes, remove

800 ¼L of supernatant and plate the rest. Finally, incubate at 37°C overnight in appropriate agar with antibiotics.

Colony PCR

For each cloning, perform colony PCR from different colonies (between 3-5), for each colony PCR, pick one colony and re-suspend it in 10 ¼L of sterile water (in PCR tube). Pre-mix the One-Taq master mix, primers and water for the corresponding number of reactions.

Mix 9 µL of the pre-mix with 1 ¼L of the re-suspended colony and run the PCR. On the other hand, keep the colony re-suspended in water at 4°C, to use afterward to inoculate the culture for plasmid extraction. Finally, run an agar electrophoresis for verification and image it.

Plasmid extraction

For the colony PCR with the corresponding fragment size, mix 5¼L of the re-suspended colony in water in 5mL of LB for high copy plasmid or 10mL for low copy plasmid in a 50 mL falcon. Place the culture at 37°C with agitation overnight. From the overnight culture, perform a strick of each culture in a petri dish with the appropriate antibiotic for further glycerol stock (Plate at 37°C overnight, and stored at 4°C), centrifuge the culture (5 minutes at 5000 rpm) and perform plasmid extraction according to protocol from Monarch Plasmid Miniprep kit (NEB catalog # T1010S).

Sequencing and glycerol stock

Send the plasmid extracted with appropriate primers to verify the sequence cloned. After verification, inoculate 2 mL of LB with appropriate antibiotic with the selected colony and culture at 37°C. Mix 1.2 mL of culture with 300 µL of 50% glycerol (10 % glycerol). Storage t -80°C with appropriate label.

Appendix III.18. Gibson assembly preparation (Synthetic biology protocols-CBS-Montpellier-France).

Gibson Assembly Mix preparation

Materials

- 1,5mL Microtubes
- PCR tubes

To prepare the 5X Isothermal solution (ISO 5X):

- Tris-HCl pH 7.5 solution 1M (on bench)
- PEG-8000 (Common powders in the JB9s lab)
- MgCl2 solution 1M (on bench)
- DTT 1M (common -20°C in GA Mix preparation Box)
- dNTP Mix 10mM (common -20°C in GA Mix preparation Box)
- NAD 100mM (aliquots in common -20°C in GA Mix preparation Box or powder of B-Nicotinamide
adenine dinucleotide sodium sulfate with common powders in the JB9s lab)
- dd H2O

To prepare the Gibson Assembly Mix 2X solution:

- ISO 5x (common -20°C in GA Mix preparation Box)
- T5 exonucelase (10 U/µL) (common -20°C in GA Mix preparation Box)
- Taq DNA ligase (40 U/µL) (common -20°C in GA Mix preparation Box)
- Phusion DNA polymerase (2U/µL) (common -20°C in GA Mix preparation Box)
- dd H2O Protocol

Protocol

5X isothermal reaction buffer.

Preparation for 10mL final solution

Components	Final Conc	10 mL final
Tris–HCl pH 7.5	500 mM	5 mL
PEG–8000	50%	2.5 g
Vortex		
$MgCl_2$	50 mM	500 µL
DTT	50 mM	500 µL
dNTP Mix	1 mM	1 mL
NAD	5 mM	500 µL
ddH_2O		Qsp 10 mL

The 5X isothermal reaction buffer has to be aliquot in 1 mL.

2X Gibson assembly mix

	X2	X2
Final volume (uL)	1000	1500
ISO 5X (uL)	300,8	451,2
T5 exonuclease (10U/ul)	0,6	0,9
Taq DNA ligase (40U/ul)	150,4	225,6
Phusion DNA polymerase (2U/ul)	18,8	28,2
ddH_2O	529,4	794,1

The Gibson assembly 2X mix has to be aliquot in 10 µL in PCR tubes on a rack and storage at -20°C. When it is freeze put all tubes in a box.

Appendix III.19. *In silico* ligation of *rpsTp*-ponA1 in pKM464.

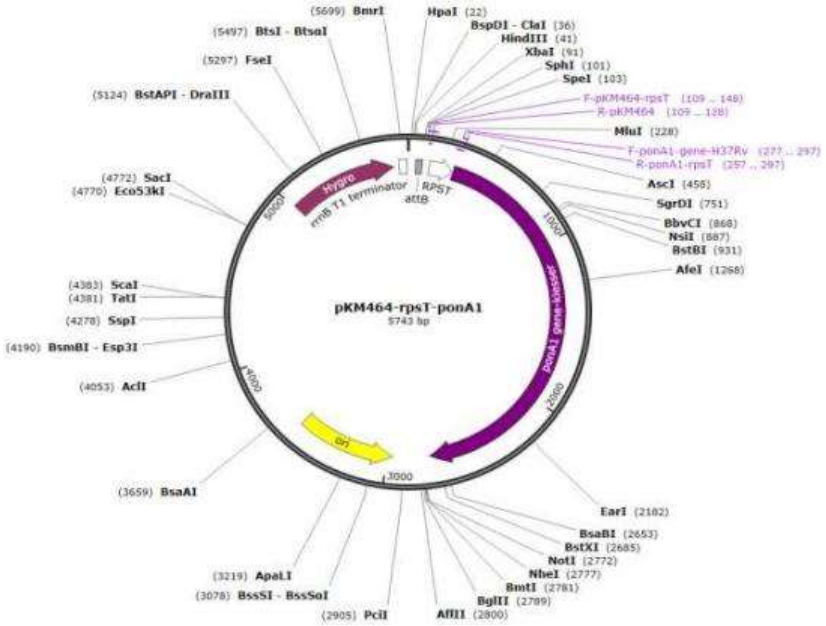

Appendix III.20. *In silico* ligation of *ponA1* in pMV361.

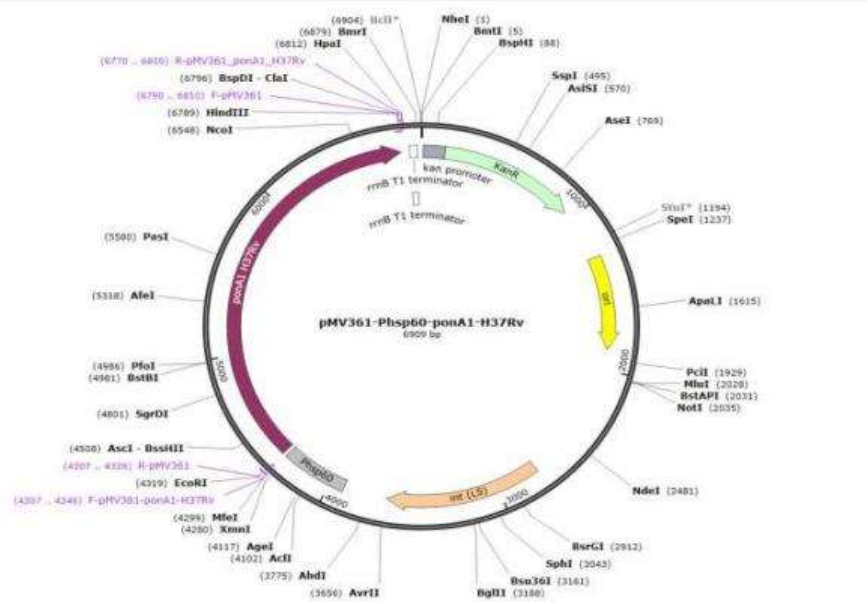

Appendix III.21. Antibiotic cassette replacement in pMV361-ponA1 to generate pMV361$_{ZEO}$-ponA1.

A. sequence of EM7 promoter
gttgacaattaatcatcggcatagtatatcggcatagtataatacgac

B. Sequence of the Bleo gene
Atggccaagttgaccagtgccgttccggtgctcaccgcgcgcgacgtcgccggagcggtcgagttctggaccgaccg
gctcgggttctcccgggacttcgtggaggacgacttcgccggtgtggtccgggacgacgtgaccctgttcatcagcgc
ggtccaggaccaggtggtgccggacaacaccctggcctgggtgtgggtgcgcggcctggacgagctgtacgccgag
tggtcggaggtcgtgtccacgaacttccgggacgcctctgggccggccatgaccgagatcggcgagcagccgtggg
ggcgggagttcgccctgcgcgacccggccggcaactgcgtgcacttcgtggccgaggagcaggactga

C. *In silico* cloning of ponA1 from H37Rv in pMV361-ZEO. Disposition of primers used for cloning and verification process by sequencing.

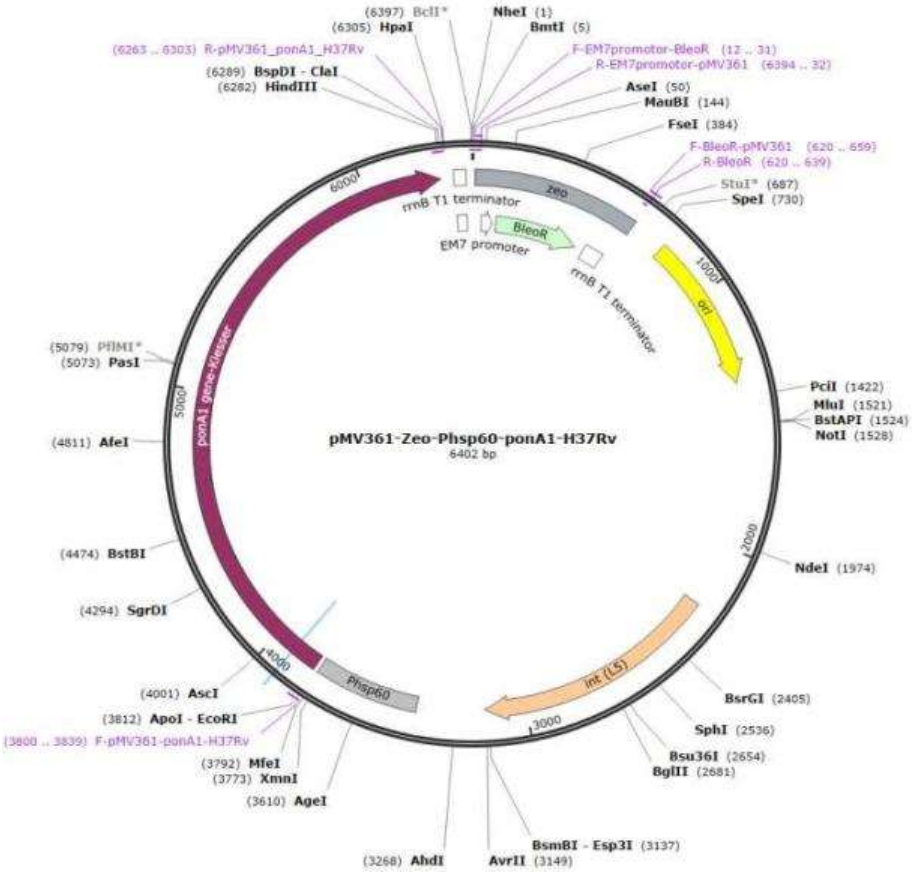

Appendix III.22. *In silico* ligation of *rpsTp*-ponA1-T34A in pKM464.

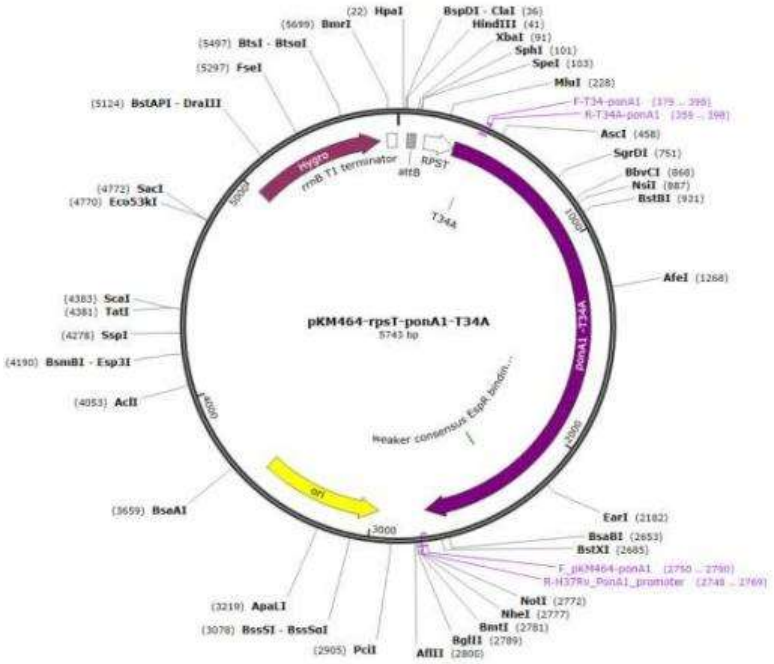

Appendix III.23. *In silico* ligation of *rpsTp*-ponA1-T34D in pKM464.

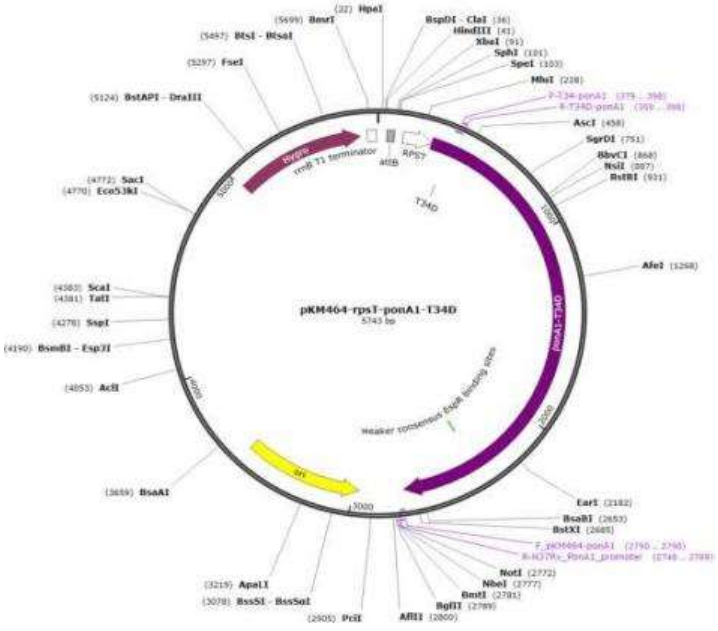

Appendix III.24. *In silico* ligation of *rpsTp*-ponA1-Q365H in pKM464.

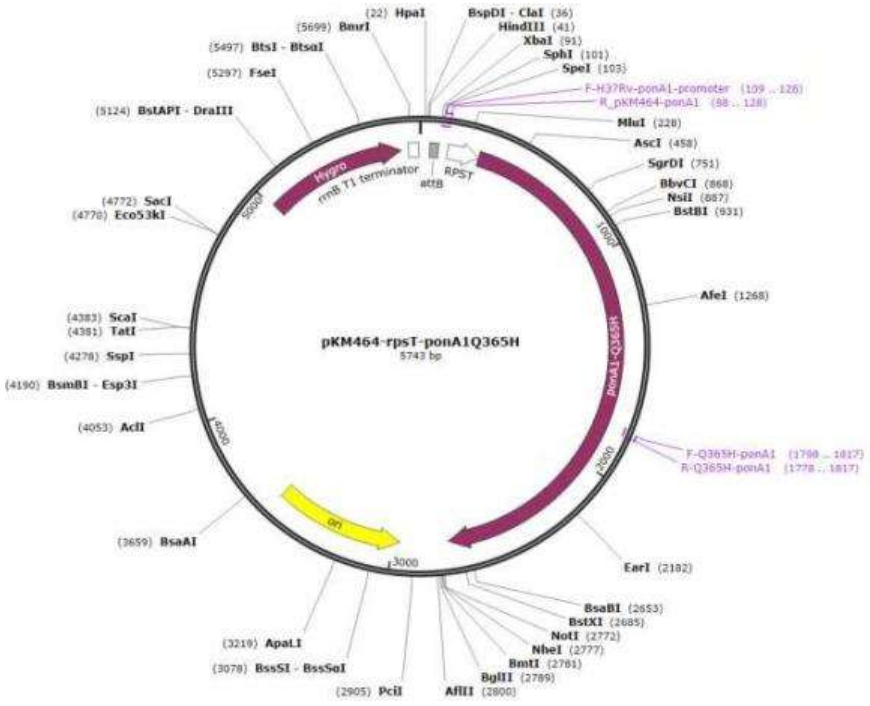

Appendix III.25. *In silico* ligation of *rpsTp*-ponA1-A516T in pKM464.

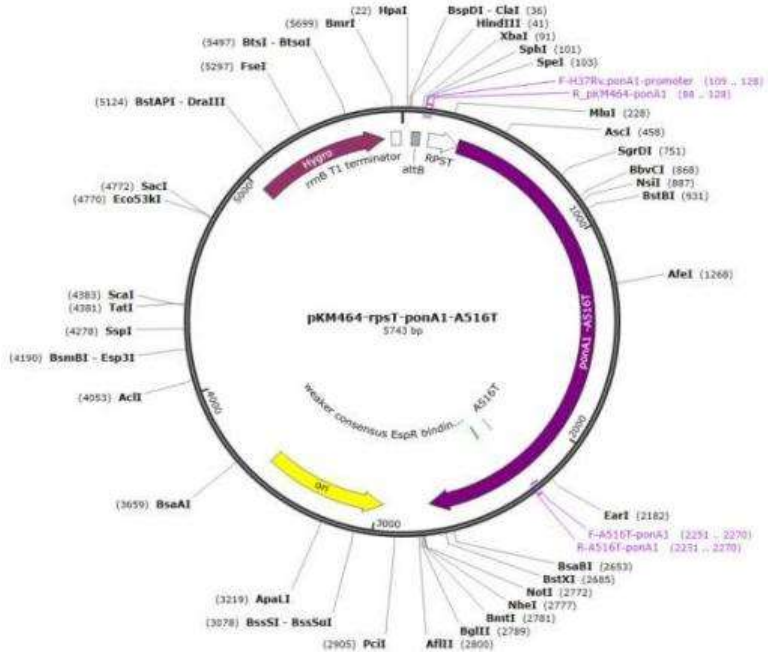

Appendix III.26. *In silico* ligation of *rpsTp*-ponA1-P631S in pKM464.

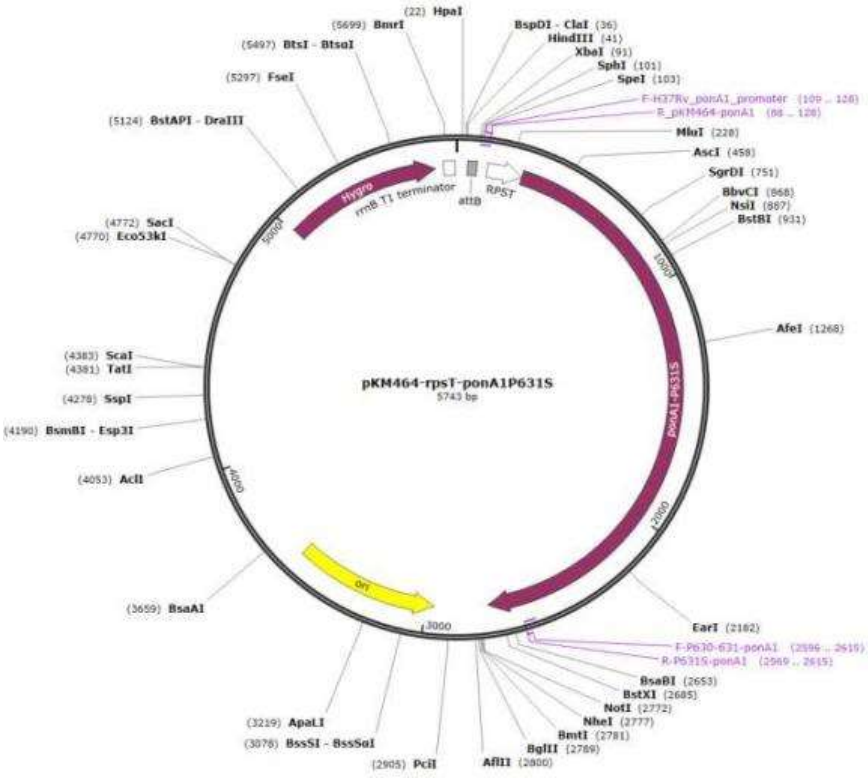

Appendix III.27. *In silico* ligation ponA1-T34A in pMV361$_{ZEO}$ and gene sequence.

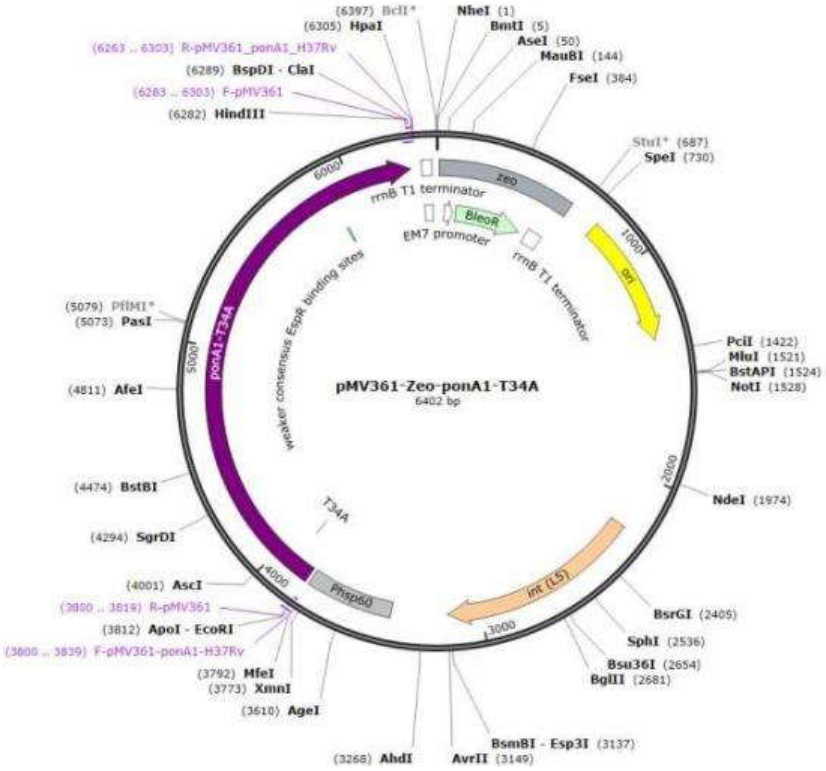

gtgaatagcgacgggcgtcaccatcagtcgtccagcggcgccccgcgcgggccggcgaatcccggccagcgtggtcaggttccacccgacgacagactggccgcgatcctc
ccgccggtgaccgatgaccgatcggctccgcacgcggactccatcgaggcggtcaaggccgcgctcgacggcgcgccgccgatgcccccgccgcgcgacccgctcgagg
aggtcacggccgcgttggccgccccgcccggtaaaccgccgcgggggatcagcttggtggcagacgtcgcccaccggggccgcccgggccccccggttcgtccggaca
gcctgccggccggctgccccaaccgagggtggacttgccccgggtcggccagatcaactggaaatggatacggcgttcgctgtacctcaccgcggcggtggtgatcctgttgc
cgatggtcaccttcacgatggcctacctgatcgtcgacgttcccaagccaggtgacatccgtaccaaccaggtctccacgatccttgccagcgacggctcggaaatcgccaaaat
tgttccgcccgaaggtaatcgggtcgacgtcaacctcagccaggtgccgatgcatgtgccgccaggcggtgattgcggccgaagaccgcaatttctattcgaatccgggattctcg
ttcaccggcttcgcgcgggcagtcaagaacaacctgttcggcggcgatctgcagggcggatcgacgattacccagcagtacgtcaagaacgcgctggtcggttccgcacagca
cgggtggagcggtctgatgcgcaaggcgaaagaattggtcatcgcgacgaagatgtcgggggagtggtctaaagacgatgtgctgcaggcgtatctgaacatcatctacttcgg
ccggggcgcctacggcatttcggcggcgtccaaggcttatttcgacaagcccgtcgagcagctgaccgttgccgaaggggcgttgttggcagcgctgattcggcggccttcgac
gctggacccggcggtcgaccccgaaggggcccatgcccgctggaattgggtactcgacggcatggtggaaaccaaggctctctcgccgaatgaccgtgcggcgcaggtgttt
cccgagacagtgccgcccgatctggcccgggcagagaatcagaccaaaggacccaacgggctgatcgagcggcaggtgacaagggagttgctcgagctgttcaacatcgac
gagcagaccctcaacacccaggggctggtggtcaccaccacgattgatccgcaggcccaacgggcggcggaggaaggcggttgcgaaatacctggacgggcaggaccccg
acatgcgtgccgccgtggtttccatcgacccgcacaacggggcggtgcgtgcgtactacggtggcgacaatgccaatggctttgacttcgctcaagcgggattgcagactggat
cgtcgtttaaggtgtttgctctggtggccgcccttgagcaggggatcggcctgggctaccaggtagacagctctccgttgacggtcgacggcatcaagatcaccaacgtcgaggg
cgagggttgcgggacgtgcaacatcgccgaggcgctcaaaatgtcgctgaacacctcctactaccggctgatgctcaagctcaacggcggcccacaggctgtggccgatgcc
gcgcaccaagccggcattgcctccagcttcccgggcgttgcgcacacgctgtccgaagatggcaagggtggaccgcccaacaacgggatcgtgttgggccagtaccaaaccc
gggtgatcgacatggcatcggcgtatgccacgttggccgcgtccggtatctaccacccgccgcatttcgtacagaaggtggtcagtgccaacggccaggtcctcttcgacgcca
gcaccgcggacaacaccggcgatcagcgcatccccaaggcggtagccgacaacgtgactgcggcgatggagccgatcgcaggttattcgcgtggccacaacctagcgggtg
ggcgggattcggcggccaagaccggcactacgcaatttggtgacaccaccgcgaacaaagacgcctggatggtcgggtacacgccgtcgttgtctacggctgtgtgggtggg
caccgtcaagggtgacgagccactggtaaccgcttcgggtgcagcgatttacggctcgggcctgccgtcggacatctggaaggcaaccatggacggcgccttgaagggcacg
tcgaacgagactttccccaaaccgaccgaggtcggtggttatgccggtgtgccgccgccgccgccgccgccggaggtaccaccttcggagaccgtcatccagcccacggtcg
aaattgcgccggggattaccatcccgatcggtcccccgaccaccattaccctggcgccaccgcccccggcccgcccgctgcgactcccacgccgccgccgtga

Appendix III.28. *In silico* ligation ponA1-T34D in pMV361$_{ZEO}$ and gene sequence.

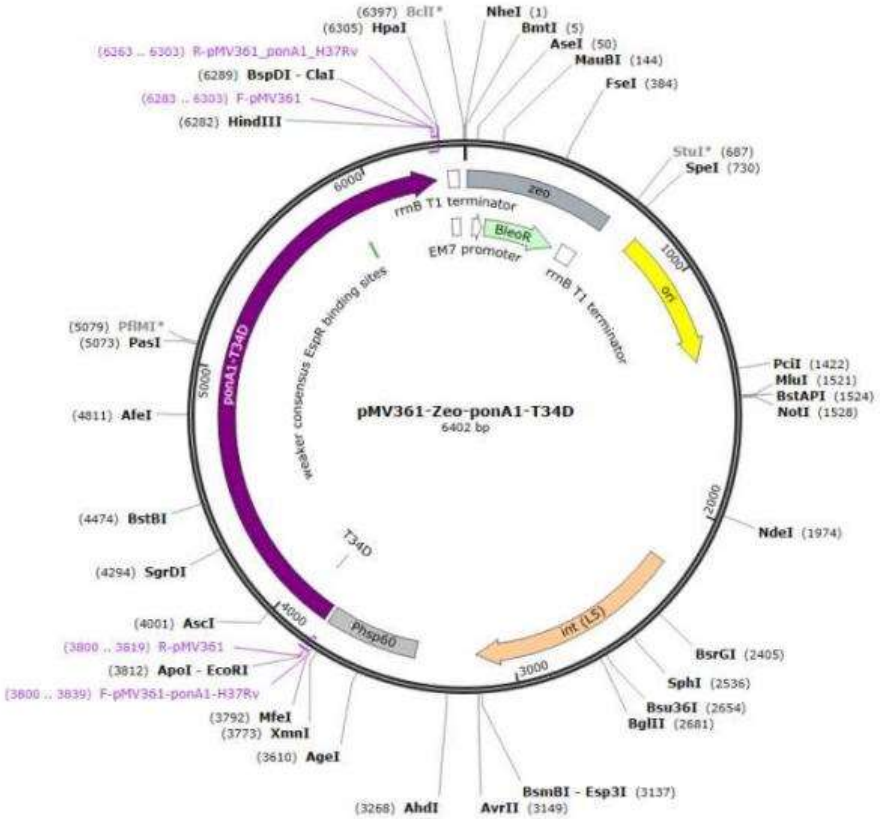

gtgaatagcgacgggcgtcaccatcagtcgtccagcggcgccccgcgcgggccggcgaatcccggccagcgtggtcaggttccacccgacgacagactggacgcgatcctc
ccgccggtgaccgatgaccgatcggctccgcacgcggactccatcgaggcggtcaaggccgcgctcgacggcgcgccgccgatgcccccgccgcgcgacccgctcgagg
aggtcacggccgcgttggccgccccgcccggtaaaccgccgcgggggggatcagcttggtggcagacgtcgcccaccggggccgcccgggccccccggttcgtccggaca
gcctgccggccggctgccccaaccgagggtggacttgccccgggtcggccagatcaactggaaatggatacggcgttcgctgtacctcaccgcggcggtggtgatcctgttgc
cgatggtcaccttcacgatggcctacctgatcgtcgacgttcccaagccaggtgacatccgtaccaaccaggtctccacgatccttgccagcgacggctcggaaatcgccaaaat
tgttccgcccgaaggtaatcgggtcgacgtcaacctcagccaggtgccgatgcatgtgcgccaggcggtgattgcggccgaagaccgcaatttctattcgaatccgggattctcg
ttcaccggcttcgcgcgggcagtcaagaacaacctgttcggcggcgatctgcagggcggatcgacgattacccagcagtacgtcaagaacgcgctggtcggttccgcacagca
cgggtggagcggtctgatgcgcaaggcgaaagaattggtcatcgcgacgaagatgtcgggggagtggtctaaagacgatgtgctgcaggcgtatctgaacatcatctacttcgg
ccggggcgcctacggcatttcggcggcgtccaaggcttatttcgacaagcccgtcgagcagctgaccgttgccgaaggggcgttgttggcagcgctgattcggcggccttcgac
gctggacccggcggtcgaccccgaaggggcccatgcccgctggaattgggtactcgacggcatggtggaaaccaaggctctctcgccgaatgaccgtgcggcgcaggtgttt
cccgagacagtgccgcccgatctggcccgggcagagaatcagaccaaaggacccaacgggctgatcgagcggcaggtgacaagggagttgctcgagctgttcaacatcgac
gagcagaccctcaacacccaggggctggtggtcaccaccacgattgatccgcaggcccaacgggcggcggagaaggcggttgcgaaatacctggacgggcaggaccccg
acatgcgtgccgccgtggtttccatcgacccgcacaacggggcggtgcgtgcgtactacggtggcgacaatgccaatggctttgacttcgctcaagcgggattgcagactggat
cgtcgtttaaggtgtttgctctggtggccgcccttgagcaggggatcggcctgggctaccaggtagacagctctccgttgacggtcgacggcatcaagatcaccaacgtcgaggg
cgagggttgcgggacgtgcaacatcgccgaggcgctcaaaatgtcgctgaacacctcctactaccggctgatgctcaagctcaacggcggcccacaggctgtggccgatgcc
gcgcaccaagccggcattgcctccagcttcccgggcgttgcgcacacgctgtccgaagatggcaagggtggaccgcccaacaacgggatcgtgttgggccagtaccaaaccc
gggtgatcgacatggcatcggcgtatgccacgttggccgcgtccggtatctaccacccgccgcatttcgtacagaaggtggtcagtgccaacggccaggtcctcttcgacgcca
gcaccgcggacaacaccggcgatcagcgcatccccaaggcggtagccgacaacgtgactgcggcgatggagccgatcgcaggttattcgcgtggccacaacctagcgggtg
ggcgggattcggcggccaagaccggcactacgcaatttggtgacaccaccgcgaacaaagacgcctggatggtcgggtacacgccgtcgttgtctacggctgtgtgggtggg
caccgtcaagggtgacgagccactggtaaccgcttcgggtgcagcgatttacggctcgggcctgccgtcggacatctggaaggcaaccatggacggcgccttgaagggcacg
tcgaacgagactttccccaaaccgaccgaggtcggtggttatgccggtgtgccgccgccgccgccgccgccggaggtaccaccttcggagaccgtcatccagcccacggtcg
aaattgcgccggggattaccatcccgatcggtcccccgaccaccattaccctggcgccaccgcccccggccccgcccgctgcgactcccacgccgccgccgtga

Appendix III.29. *In silico* ligation ponA1-Q365H in pMV361$_{ZEO}$ and gene sequence.

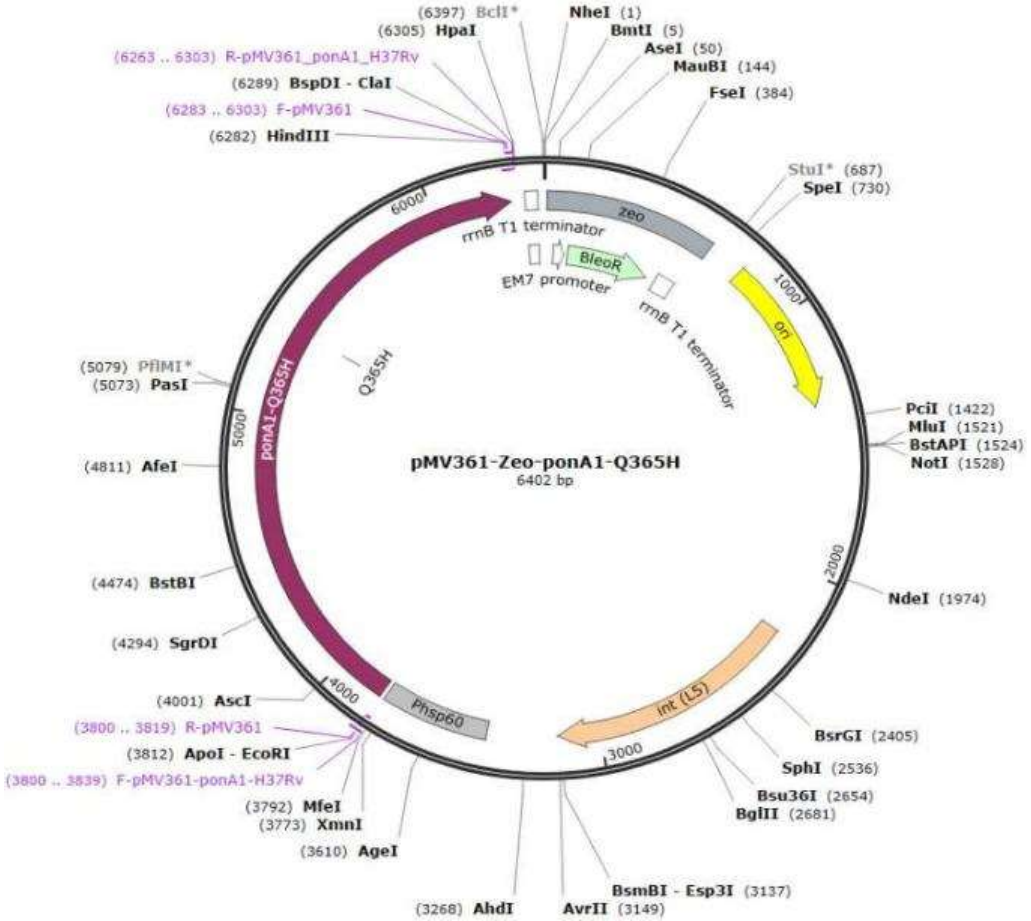

gtgaatagcgacgggcgtcaccatcagtcgtccagcggcgccccgcgcgggccggcgaatcccggccagcgtggtcaggttccacccgacgacagactgaccgcgatcctc
ccgccggtgaccgatgaccgatcggctccgcacgcggactccatcgaggcggtcaaggccgcgctcgacggcgcgccgccgatgcccccgccgcgcgacccgctcgagg
aggtcacggccgcgttggccgccccgcccggtaaaccgccgcgggggggatcagcttggtggcagacgtcgcccaccggggccgcccgggccccccggttcgtccggaca
gcctgccggccggctgccccaaccgagggtggacttgccccgggtcggccagatcaactggaaatggatacggcgttcgctgtacctcaccgcggcggtggtgatcctgttgc
cgatggtcaccttcacgatggcctacctgatcgtcgacgttcccaagccaggtgacatccgtaccaaccaggtctccacgatccttgccagcgacggctcggaaatcgccaaaat
tgttccgcccgaaggtaatcgggtcgacgtcaacctcagccaggtgccgatgcatgtgcgccaggcggtgattgcggccgaagaccgcaatttctattcgaatccgggattctcg
ttcaccggcttcgcgcgggcagtcaagaacaacctgttcggcggcgatctgcagggcggatcgacgattacccagcagtacgtcaagaacgcgctggtcggttccgcacagca
cgggtggagcggtctgatgcgcaaggcgaaagaattggtcatcgcgacgaagatgtcgggggagtggtctaaagacgatgtgctgcaggcgtatctgaacatcatctacttcgg
ccggggcgcctacggcatttcggcggcgtccaaggcttatttcgacaagcccgtcgagcagctgaccgttgccgaaggggcgttgttggcagcgctgattcggcggccttcgac
gctggacccggcggtcgaccccgaaggggcccatgcccgctggaattgggtactcgacggcatggtggaaaccaaggctctctcgccgaatgaccgtgcggcgcaggtgttt
cccgagacagtgccgcccgatctggcccgggcagagaatcagaccaaaggacccaacgggctgatcgagcggcaggtgacaagggagttgctcgagctgttcaacatcgac
gagcagaccctcaacacccaggggctggtggtcaccaccacgattgatccgcaggcccaacgggcggcggagaaggcggttgcgaaatacctggacgggcaggaccccg
acatgcgtgccgccgtggtttccatcgacccgcacaacggggcggtgcgtgctactacggtggcgacaatgccaatggctttgacttcgctcaagcgggattgcagactggat
cgtcgtttaaggtgtttgctctggtggccgcccttgagcaggggatcggcctgggctaccatgtagacagctctccgttgacggtcgacggcatcaagatcaccaacgtcgaggg
cgagggttgcgggacgtgcaacatcgccgaggcgctcaaaatgtcgctgaacacctcctactaccggctgatgctcaagctcaacggcggcccacaggctgtggccgatgcc
gcgcaccaagccggcattgcctccagcttcccgggcgttgcgcacacgctgtccgaagatggcaagggtggaccgcccaacaacgggatcgtgttgggccagtaccaaaccc
gggtgatcgacatggcatcggcgtatgccacgttggccgcgtccggtatctaccacccgccgcatttcgtacagaaggtggtcagtgccaacggccaggtcctcttcgacgcca
gcaccgcggacaacaccggcgatcagcgcatccccaaggcggtagccgacaacgtgactgcggcgatggagccgatcgcaggttattcgcgtggccacaacctagcgggtg
ggcgggattcggcggccaagaccggcactacgcaatttggtgacaccaccgcgaacaaagacgcctggatggtcgggtacacgccgtcgttgtctacggctgtgtgggtggg
caccgtcaagggtgacgagccactggtaaccgcttcgggtgcagcgatttacggctcgggcctgccgtcggacatctggaaggcaaccatggacggcgccttgaagggcacg
tcgaacgagactttccccaaaccgaccgaggtcggtggttatgccggtgtgccgccgccgccgccgccgccggaggtaccaccttcggagaccgtcatccagcccacggtcg
aaattgcgccggggattaccatcccgatcggtcccccgaccaccattaccctggcgccaccgcccccggccccgcccgctgcgactcccacgccgccgccgtga

Appendix III.30. *In silico* ligation ponA1-A516T in pMV361$_{ZEO}$ and gene sequence.

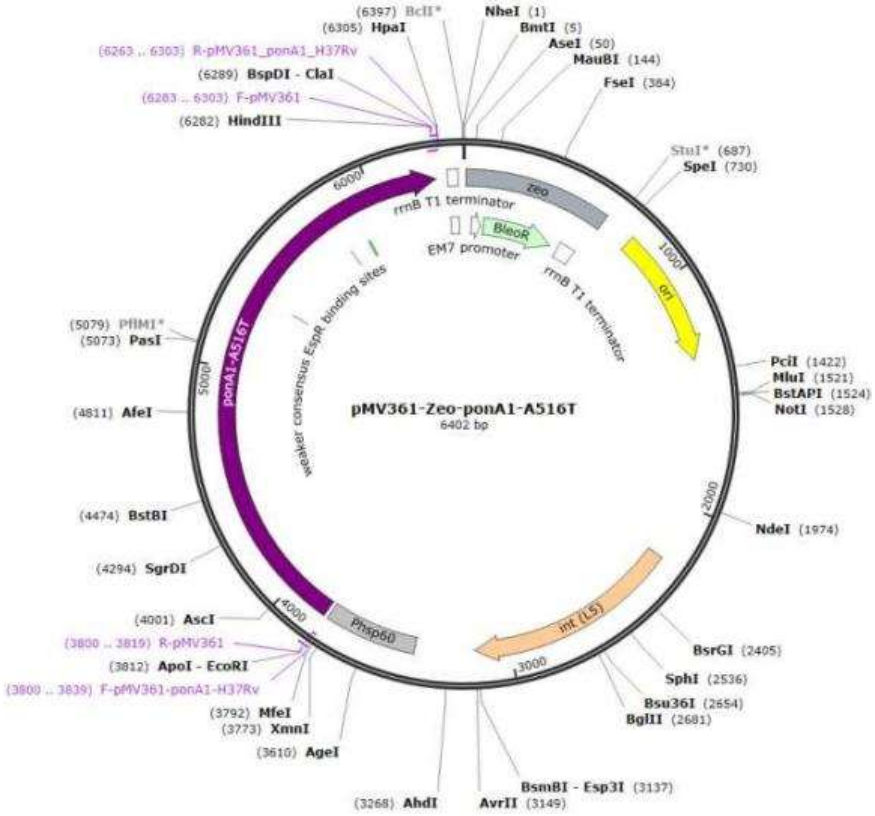

gtgaatagcgacgggcgtcaccatcagtcgtccagcggcgccccgcgcgggccggcgaatcccggccagcgtggtcaggttccacccgacgacagactgaccgcgatcctc
ccgccggtgaccgatgaccgatcggctccgcacgcggactccatcgaggcggtcaaggccgcgctcgacggcgcgccgccgatgcccccgccgcgcgacccgctcgagg
aggtcacggccgcgttggccgccccgcccggtaaaccgccgcgggggggatcagcttggtggcagacgtcgcccaccggggccgcccgggccccccggttcgtccggaca
gcctgccggccggctgccccaaccgagggtggacttgccccgggtcggccagatcaactggaaatggatacggcgttcgctgtacctcaccgcggcggtggtgatcctgttgc
cgatggtcaccttcacgatggcctacctgatcgtcgacgttcccaagccaggtgacatccgtaccaaccaggtctccacgatccttgccagcgacggctcggaaatcgccaaaat
tgttccgcccgaaggtaatcgggtcgacgtcaacctcagccaggtgccgatgcatgtgcgccaggcggtgattgcggccgaagaccgcaatttctattcgaatccgggattctcg
ttcaccggcttcgcgcgggcagtcaagaacaacctgttcggcggcgatctgcagggcggatcgacgattacccagcagtacgtcaagaacgcgctggtcggttccgcacagca
cgggtggagcggtctgatgcgcaaggcgaaagaattggtcatcgcgacgaagatgtcgggggagtggtctaaagacgatgtgctgcaggcgtatctgaacatcatctacttcgg
ccggggcgcctacggcatttcggcggcgtccaaggcttatttcgacaagcccgtcgagcagctgaccgttgccgaaggggcgttgttggcagcgctgattcggcggccttcgac
gctggacccggcggtcgaccccgaaggggcccatgcccgctggaattgggtactcgacggcatggtggaaaccaaggctctctcgccgaatgaccgtgcggcgcaggtgttt
cccgagacagtgccgcccgatctggcccgggcagagaatcagaccaaaggacccaacgggctgatcgagcggcaggtgacaagggagttgctcgagctgttcaacatcgac
gagcagaccctcaacacccaggggctggtggtcaccaccacgattgatccgcaggcccaacgggcggcggagaaggcggttgcgaaatacctggacgggcaggaccccg
acatgcgtgccgccgtggtttccatcgacccgcacaacggggcggtgcgtgcgtactacggtggcgacaatgccaatggctttgacttcgctcaagcgggattgcagactggat
cgtcgtttaaggtgtttgctctggtggccgcccttgagcaggggatcggcctgggctaccaggtagacagctctccgttgacggtcgacggcatcaagatcaccaacgtcgaggg
cgagggttgcgggacgtgcaacatcgccgaggcgctcaaaatgtcgctgaacacctcctactaccggctgatgctcaagctcaacggcggcccacaggctgtggccgatgcc
gcgcaccaagccggcattgcctccagcttcccgggcgttgcgcacacgctgtccgaagatggcaagggtggaccgcccaacaacgggatcgtgttgggccagtaccaaaccc
gggtgatcgacatggcatcggcgtatgccacgttggccgcgtccggtatctaccacccgccgcatttcgtacagaaggtggtcagtgccaacggccaggtcctcttcgacgcca
gcaccgcggacaacaccggcgatcagcgcatccccaaggcggtagccgacaacgtgactacggcgatggagccgatcgcaggttattcgcgtggccacaacctagcgggtg
ggcgggattcggcggccaagaccggcactacgcaatttggtgacaccaccgcgaacaaagacgcctggatggtcgggtacacgccgtcgttgtctacggctgtgtgggtggg
caccgtcaagggtgacgagccactggtaaccgcttcgggtgcagcgatttacggctcgggcctgccgtcggacatctggaaggcaaccatggacggcgccttgaagggcacg
tcgaacgagactttccccaaaccgaccgaggtcggtggttatgccggtgtgccgccgccgccgccgccgccggaggtaccaccttcggagaccgtcatccagcccacggtcg
aaattgcgccggggattaccatcccgatcggtcccccgaccaccattaccctggcgccaccgccccggccccgcccgctgcgactcccacgccgccgccgtga

Appendix III.31. *In silico* ligation ponA1-P631S in pMV361$_{ZEO}$ and gene sequence.

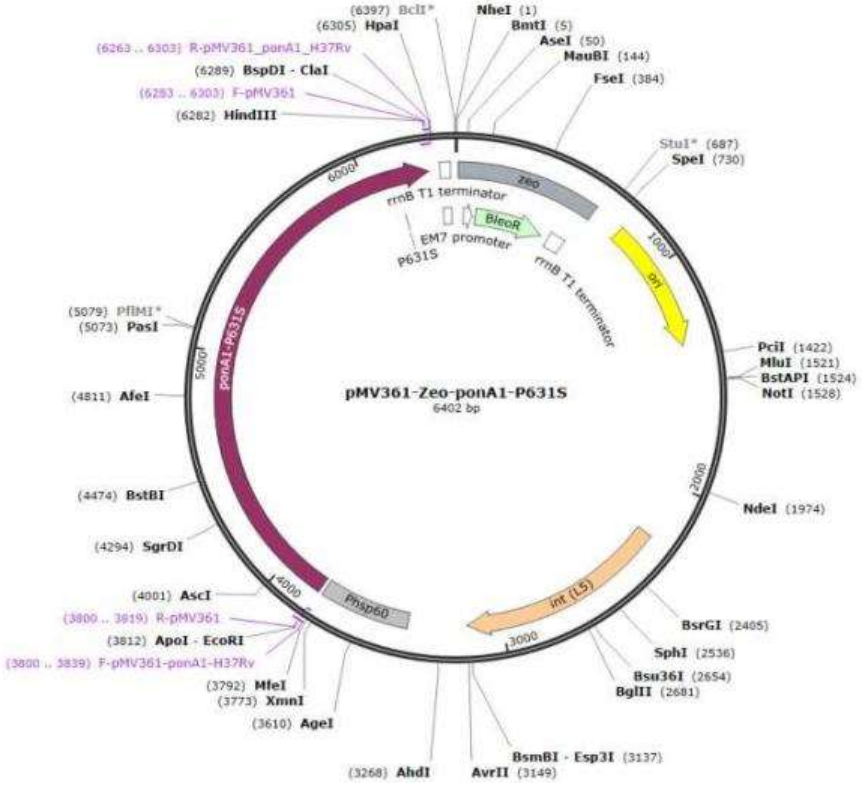

gtgaatagcgacgggcgtcaccatcagtcgtccagcggcgccccgcgcgggccggcgaatcccggccagcgtggtcaggttccacccgacgacagactgaccgcgatcctc
ccgccggtgaccgatgaccgatcggctccgcacgcggactccatcgaggcggtcaaggccgcgctcgacggcgcgccgccgatgcccccgccgcgcgacccgctcgagg
aggtcacggccgcgttggccgccccgcccggtaaaccgccgcgggggggatcagcttggtggcagacgtcgcccaccggggccgcccgggccccccggttcgtccggaca
gcctgccggccggctgccccaaccgagggtggacttgccccgggtcggccagatcaactggaaatggatacggcgttcgctgtacctcaccgcggcggtggtgatcctgttgc
cgatggtcaccttcacgatggcctacctgatcgtcgacgttcccaagccaggtgacatccgtaccaaccaggtctccacgatccttgccagcgacggctcggaaatcgccaaaat
tgttccgcccgaaggtaatcgggtcgacgtcaacctcagccaggtgccgatgcatgtgcgccaggcggtgattgcggccgaagaccgcaatttctattcgaatccgggattctcg
ttcaccggcttcgcgcgggcagtcaagaacaacctgttcggcggcgatctgcagggcggatcgacgattacccagcagtacgtcaagaacgcgctggtcggttccgcacagca
cgggtggagcggtctgatgcgcaaggcgaaagaattggtcatcgcgacgaagatgtcgggggagtggtctaaagacgatgtgctgcaggcgtatctgaacatcatctacttcgg
ccggggcgcctacggcatttcggcggcgtccaaggcttatttcgacaagcccgtcgagcagctgaccgttgccgaaggggcgttgttggcagcgctgattcggcggccttcgac
gctggacccggcggtcgaccccgaaggggcccatgcccgctggaattgggtactcgacggcatggtggaaaccaaggctctctcgccgaatgaccgtgcggcgcaggtgttt
cccgagacagtgccgcccgatctggcccgggcagagaatcagaccaaaggacccaacgggctgatcgagcggcaggtgacaagggagttgctcgagctgttcaacatcgac
gagcagaccctcaacacccaggggctggtggtcaccaccacgattgatccgcaggcccaacgggcggcggagaaggcggttgcgaaatacctggacgggcaggaccccg
acatgcgtgccgccgtggtttccatcgacccgcacaacggggcggtgcgtgcgtactacggtggcgacaatgccaatggctttgacttcgctcaagcgggattgcagactggat
cgtcgtttaaggtgtttgctctggtggccgcccttgagcaggggatcggcctgggctaccaggtagacagctctccgttgacggtcgacggcatcaagatcaccaacgtcgaggg
cgagggttgcgggacgtgcaacatcgccgaggcgctcaaaatgtcgctgaacacctcctactaccggctgatgctcaagctcaacggcggcccacaggctgtggccgatgcc
gcgcaccaagccggcattgcctccagcttcccgggcgttgcgcacacgctgtccgaagatggcaagggtggaccgcccaacaacgggatcgtgttgggccagtaccaaaccc
gggtgatcgacatggcatcggcgtatgccacgttggccgcgtccggtatctaccacccgccgcatttcgtacagaaggtggtcagtgccaacggccaggtcctcttcgacgcca
gcaccgcggacaacaccggcgatcagcgcatccccaaggcggtagccgacaacgtgactgcggcgatggagccgatcgcaggttattcgcgtggccacaacctagcgggtg
ggcgggattcggcggccaagaccggcactacgcaatttggtgacaccaccgcgaacaaagacgcctggatggtcgggtacacgccgtcgttgtctacggctgtgtgggtggg
caccgtcaagggtgacgagccactggtaaccgcttcgggtgcagcgatttacggctcgggcctgccgtcggacatctggaaggcaaccatggacggcgccttgaagggcacg
tcgaacgagactttccccaaaccgaccgaggtcggtggttatgccggtgtgccgccgccgccgccgtcggaggtaccaccttcggagaccgtcatccagcccacggtcga
aattgcgccggggattaccatcccgatcggtccccgaccaccattaccctggcgccaccgcccccggccccgcccgctgcgactcccacgccgccgccgtga

Appendix III.32. *In silico* ligation of *rpsTp*-MMAR0069 in pKM464.

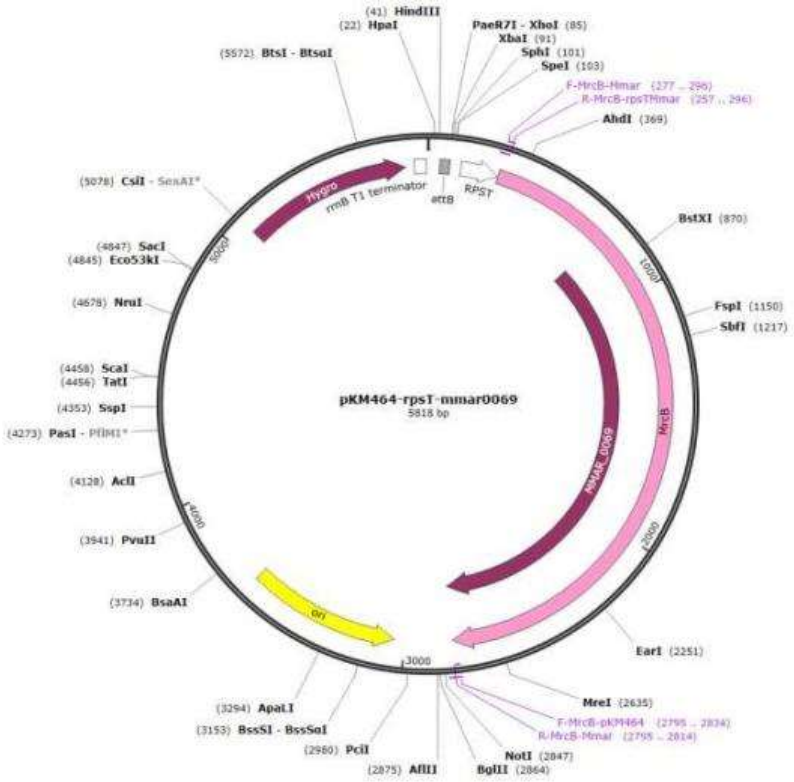

Appendix III.33. *In silico* ligation *MMAR_0069* in pMV361$_{ZEO}$, and *MMAR_0069* gene sequence.

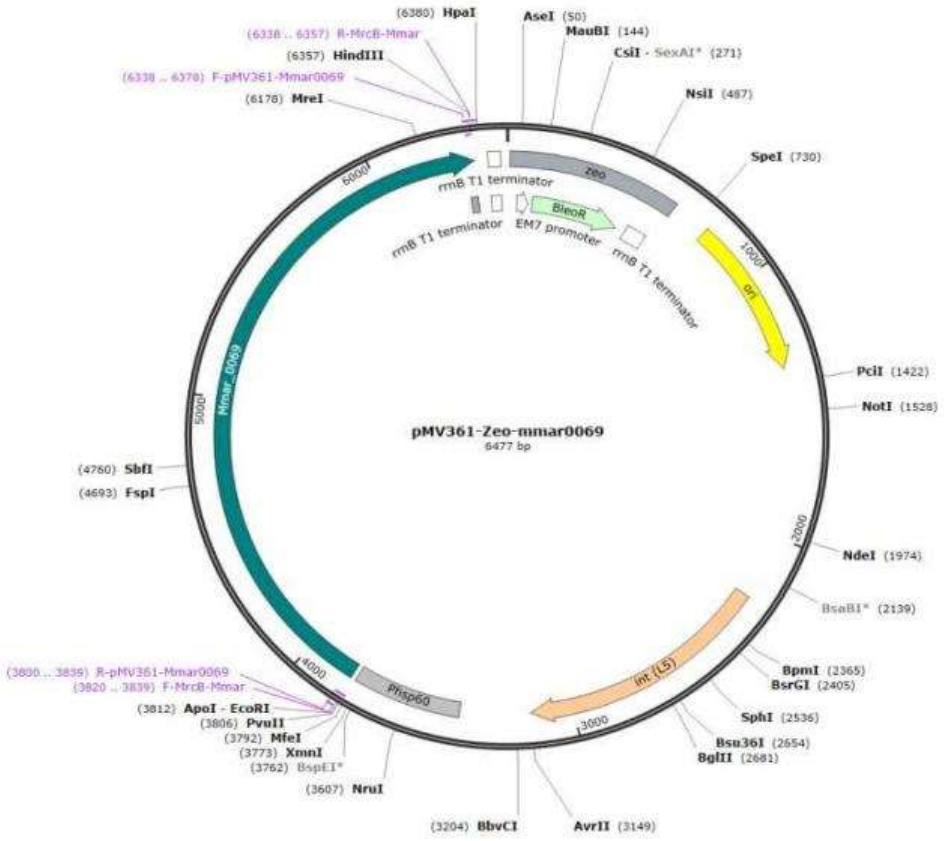

gtgagtaacgaagggcgccaccaccagccgcccagcgacgctcggggcggtccagcgggcgacgacatgggcggccaatccggcaacgacgaacggtcgcgttcggcg
ccggttccgcgtcgtgcggttcctcccgacgacaggatgaccacgatcattcctgcggtgtcggatcctcgttcagctcgccacgccgacccgatcgaggaagtcaaggccgcc
ctcgacagtccgccctcggcgcccctgcagcgtgatcagctcgatcaggtcaaggccgcgctcgacgcccgccgacgcggcccatccgcagccggcgcggcggcggtgg
gcttccgcccgatggcggggcgcctccacccgcggggcccgcggggccttcaggtccaacaggtcgctctcgcgcccggtcccaccggtccacgacacagcgcgactggct
gcgccggatcaactggaaatgggtgcggcggtcggcctacctggccgcggcggtggtcatcctgctgcccatcgtcaccttcaccatggcctacttcatcgtcgatgtgccaagg
ccgggcgacatccgcaccaatcaggtgtccacgatcctggctagcgacggctccgagatcgccaagatcgttccccccgaaggcaatcgggtcgacgtgaacctcagtcaggt
gcccgagcatgtccgcgccgcggtcatcgccgccgaagaccgcggtttctactccaacccggggttctccttcagcggcttcgcgcgagcgataaagaacaacttgttcggcgg
tgacctgcaaggcggctccacgatcacccagcaatacgtcaagaacgcgttggtcggctcggcgcaacacgggtggagcggcctgatgcgcaaggccaaggaactcgtcatc
gccaccaagatgtcgggggagtggtccaaagacgatgtcctgcaggcctatctcaacatcatctacttcggccgcggcgcatacgggatttcggcagcgtccaaggcctacttcg
acaagccggtcgagcagctcaccgtgtcggagggagccttgctggcggcgttgattcggcggccctccacgctggacccggcggtggatcccgatggggcgctggcgcgct
ggaactgggtgctcgacggcatggtggataccaaggcgttgtccgccaaagaccgggccgagcaggtatttcccaggaccgtgccgccggatcaagcccgcgcggccaacc
agaccaccgggcccaacgggctgatcgaacgccaggtcaccaaagagttgttggagctgttcaacatcgatgaacagaccctgaacacgcaggggctgcaagtcacgaccac
gatcgatgcccaagcgcagcaggcggccgaaaaggcggtagcgaaatacctgacgggcaggatcccgagatgcgggccgcggtggtctccatcgacccgcacaacgggg
ccgtgcgcgcctattacggcggcgacaacgccaacgggttcgacttcgcccaggccgggctgcagacgggatcctcgttcaaggtattcgccctggtggccgcccttgaacag
ggaattggcctgggctatgacgtcgacagttcgccactgacggtggacggcatcaagatcaccaatgtcgaaggcgagagctgcggtacctgcaacatcgcgcaggcgctcaa
gatgtcgctgaacacctcctactaccggctgatgctcaaactgaagggcggcccggaggccgtcgccgacgccgcgcaccaggccggcattgccaccagcttcccgggcgtg
ccccacacgctgtccgaggacggcaagggtggaccgcccaacaacgggattgtgctgggccagtatcagacccgggtgatcgacatggcttcggcctacgccacgctggcc
gcatccgggatctatcaccggccacacttcgtgcagaaggtcgtcaacgccgacggccgggttctcttcgacgcctccaccgaagacaacaccggtgaccagcgcatccccaa
ggcggtagccgacaatgtcaccgcggcaatggaacccattgccggatattcgcggggtcacaacctggccggcggccggccgtcggcctccaagaccggcacggtgcagtt
gggcgacaccagcgccaaccgagacgcctggatggtcggttacaccccgtcactgtcgacggccgtgtgggtgggaacggtcaagggtgacgagccgttggtgaccgcctc
gggcgcaccgatttacggctcgggcctgccgtcggacatctggaaagccaccatggacggtgcattgaagggcaccgaggtcgagagcttccccaagcccaccgagatcgg
cggctacgccggcgtgccggcaccgcctccacctccaccggaggcgccgccgccctcggagaccgtcatccagcccacggtcgaaatagcgcccgggatcacgattcccgt
cgggccgccaaccaccatcactcttgctccccctccgccaccaggggcgccacccgccgacaatccgccaccgtga

Appendix III.34. Primers designed for cloning, site mutagenesis directed and Gibson assembly and sequence verification.

Primer name	primer sequence
F−Mmar−Rv0050−orbit	CGCACCTGCAGTTGGAATCACCTG
R−Mmar−Rv0050−orbit	CGATCAGCGCGTGGCGG
R_pKM464−int	CGGAGCCTATGGAAAAACGCCAGC
F−pKM464−int	CTTCGCCCGCGAACTGCTC
R−H37Rv_ponA1_promoter	AGATGTTGCTGCTTTGGGACAG
F−H37Rv_ponA1_promoter	CCAGCAGGCCGGTCAGCCTC
F_pKM464−ponA1	GTCCCAAAGCAGCAACATCTTGCGGCCGCTAGCGGTACCAG
R_pKM464−ponA1	GAGGCTGACCGGCCTGCTGGACTAGTGCATGCTCTAGACTC
F−EGFP	ATGGTGTCGAAGGGCGAGGAG
R−EGFP	TTACTTGTACAGCTCGTCCATGC
F−EGFP−pKM464	TGGACGAGCTGTACAAGTAACCGGCGCGCTGTCCCAAAGC
R−EGFP−pKM464	TCCTCGCCCTTCGACACCATTGGCCGTGCGGGCCCCGTTG
F−pKM464−rpsT	CCAGCAGGCCGGTCAGCCTCACGTCTTTTGGGTGAAAACG
R−pKM464	GAGGCTGACCGGCCTGCTGG
R−EGFP−rpsT	CTCCTCGCCCTTCGACACCATGCTGTTGGTGCGGTTGCGCT
F−ponA1−gene−H37Rv	GTGAATAGCGACGGGCGTCAC
R−ponA1−rpsT	GTGACGCCCGTCGCTATTCACGCTGTTGGTGCGGTTGCGCT
F−P630−P631−ponA1	GAGGTACCACCTTCGGAGAC
R−P630−P631−ponA1	GTCTCCGAAGGTGGTACCTCCGGCGGCGGCGGCGGCGGCGGCACACC
R−pMV361	TCGAATTCTGCAGCTGGATC
F−pMV361	AGCTTATCGATGTCGACGTAG
F−pMV361−ponA1−H37Rv	GATCCAGCTGCAGAATTCGAGTGAATAGCGACGGGCGTCA
R−pMV361−ponA1−H37Rv	CTACGTCGACATCGATAAGCTTCACGGCGGCGGCGTGGGAG
F−pMV361−rpsT−Mmar	TTCCCGCCAGAAATCTAGACACGTCTTTTGGGTGAAAACG
R−pMV361−prom−exch	GTCTAGATTTCTGGCGGGAAC
F−pMV361−ponA1prom	GTTCCCGCCAGAAATCTAGACTTGCGCAACTCGTAGCCATG
R−P631S−ponA1	GTCTCCGAAGGTGGTACCTCCGACGGCGGCGGCGGCGGCGGCACACC
F−Q365H−ponA1	GTAGACAGCTCTCCGTTGAC
R−Q365H−ponA1	GTCAACGGAGAGCTGTCTACATGGTAGCCCAGGCCGATCC
F−MrcB−Mmar	GTGAGTAACGAAGGGCGCCA
R−MrcB−rpsTMmar	TGGCGCCCTTCGTTACTCACGCTGTTGGTGCGGTTGCGCT
R−MrcB−Mmar	TCACGGTGGCGGATTGTCGG
F−MrcB−pKM464	CCGACAATCCGCCACCGTGACCGGCGCGCTGTCCCAAAGC
R−MrcB−ponA1p−H37Rv	GTGGCGCCCTTCGTTACTCACTGGCCGTGCGGGCCCCGTT
F−MrcB−2	AATACGTCAAGAACGCGTTG
R−MrcB−2	GCCGCTCCACCCGTGCTGC
F−MMAR_0069	GTGCGGCGGTCGGCCTACCT
R−MMAR_0069−RPST	AGGTAGGCCGACCGCCGCACGCTGTTGGTGCGGTTGCGCT
F−T34−ponA1	GCGATCCTCCCGCCGGTGAC
R−T34D−ponA1	GTCACCGGCGGGAGGATCGCGTCCAGTCTGTCGTCGGGTG
R−T34A−ponA1	GTCACCGGCGGGAGGATCGCGGCCAGTCTGTCGTCGGGTG
R−pMV361−Mmar0069	TGGCGCCCTTCGTTACTCACTCGAATTCTGCAGCTGGATC
F−pMV361−Mmar0069	CCGACAATCCGCCACCGTGAAGCTTATCGATGTCGACGTAG

Appendix III.34. Primers designed for cloning, site mutagenesis directed and Gibson assembly and sequence verification (...continuation).

Primer name	primer sequence
F−A516T−ponA1	GCGATGGAGCCGATCGCAGG
R−A516T−ponA1	CCTGCGATCGGCTCCATCGCCGTAGTCACGTTGTCGGCTA
F−EM7promotor−BleoR	GCCCGTCATCGTCAACGCCT
R−BleoR	TTCGCAACGTTCAAATCCGC
F−BleoR−pMV361	GCGGATTTGAACGTTGCGAACCAACCGTGGCTCCCTCACT
R−EM7promoter−pMV361	CAGGCGTTGACGATGACGGGCAGGTGGCTAGCTGATCACCG
F−pMV361−Mmar0069	GATCCAGCTGCAGAATTCGAGTGAGTAACGAAGGGCGCCAC
R−pMV361−Mmar0069	TACGTCGACATCGATAAGCTTCACGGTGGCGGATTGTCGG
F−ponA1−H37Rv−MTB	GTGAATAGCGACGGGCGTCACCATCAG
R−ponA1−H37Rv−MTB	TCACGGCGGCGGCGTGG
F−H37Rv−ponA1−gen−1	GTGAATAGCGACGGGCGTCAC
F−H37Rv−ponA1−gen−2−2360	TCCAAGGCTTATTTCGACAAGCCC
R−H37Rv−ponA1−gen−2687	ACAACGCCCCTTCGGCAAC
F−H37Rv−PonA1−gen−3−3460	CAACGGGATCGTGTTGGGCCA
R−H37Rv−ponA1−gen−4	GTGTTGAGGGTCTGCTCGTCG
R−H37Rv−ponA1−gen5	GGCGACGTCTGCCACCAAGC
R−H37Rv_ponA1_promoter	AGATGTTGCTGCTTTGGGACAG
F−H37Rv−ponA1−prom−882	AGCGGCCAGCAAGCCC
R−H37Rv−ponA1−prom−945	ACCCGCACAAATGCCCG
R−H37Rv−ponA1−prom−1702	TGGCCGTGCGGGCCC
Verif_Gg_PMV_Fw	GACCATTTACGGGTCTTGTTGT
Verif_GgPMV_Rv	TGGCAGTCGATCGTACGCTA

Appendix III.35. Metrics for molecular docking between PonA1 crystal transpeptidase 5CRF and penicillin V (open form) by GNINA.

Mode	affinity (kacl/mol)	RMSD (Å)
1	-7.85	8.84
2	-8.58	3.67
3	-7.80	4.37
4	-7.16	10.33
5	-7.08	8.77
6	-6.92	11
7	-6.87	6.6
8	-7.42	4.99
G	-7.04	8.47

Appendix II.36. Metrics for molecular docking between PonA1 crystal transpeptidase 5CRF and penicillin (open form) by DiffDock

Mode	DiffDock_confidence	RMSD (Å)
1	0.13	1.68
2	0.09	1.85
3	-0.19	2.04
4	-0.2	3.1
5	-0.21	2.97
6	-0.29	2.11
7	-0.29	2.73
8	-0.34	2.61
G	-0.4	3.02

Appendix III.37. Metrics for molecular docking between PonA_WT_ESM against penicillin V by Diffdock.

Mode	DiffDock_confidence
1	-0.28
2	-0.59
3	-0.73
4	-0.6
5	-0.47
6	-0.63
7	-0.55
8	-0.67
G	-0.44

Appendix III.38. Metrics for molecular docking between PonA1_WT-ESM and rifampicin.

Mode	DiffDock_confidence
1	-1.98
2	-2.57
3	-2.53
4	-1.92
5	-2.39
6	-2.08
7	-1.78
8	-2.48
G	-1.92

Appendix III.39. STD_NMR assay titration for K_D determination between $PonA1_{234-820}$**_WT and rifampicin.**

[lig](mM)	STD-AFmax	dSTD-AFmax	ksat(s-1)	dksat(s-1)	STD-AF0	dSTD-AF0
0.075	0.27	0.01	2.37	0.51	0.64	0.13
0.150	0.46	0.03	2.02	0.58	0.93	0.18
0.300	0.72	0.02	2.37	0.39	1.70	0.10
0.600	1.28	0.04	1.92	0.22	2.46	0.07
1.200	2.24	0.12	1.98	0.47	4.44	0.15

Pic(ppm)	Alpha_STD	dAlpha_STD	Kd(mM)	dKd(mM)
6.82	8.13	5.24	0.49	0.71
6.22	9.63	6.13	1.45	1.45
2.89	994.40	146767.31	352.30	52148.32
1.89	992.64	99007.29	351.78	35189.82
1.72	8.97	2.60	1.64	0.72
1.65	10.80	9.37	1.77	2.29
1.23	20.95	17.62	3.38	3.63
1.05	9.54	8.31	1.32	1.86
0.81	5.31	1.59	0.95	0.51
0.46	2.73	0.79	0.22	0.19

Appendix III.40. STD_NMR assay titration for KD determination between PonA1$_{234-820}$**_Q365H and rifampicin.**

[lig](mM)	STD-AFmax	dSTD-AFmax	ksat(s-1)	dksat(s-1)	STD-AF0	dSTD-AF0
0.044	0.18	0.01	1.95	0.44	0.35	0.14
0.088	0.32	0.01	2.34	0.42	0.75	0.11
0.175	0.56	0.03	2.26	0.57	1.27	0.15
0.350	0.94	0.05	2.06	0.53	1.95	0.16
0.700	1.63	0.09	2.20	0.55	3.58	0.15
1.400	3.10	0.20	1.88	0.50	5.83	0.16

Pic(ppm)	Alpha_STD	dAlpha_STD	Kd(mM)	dKd(mM)
6.83	19.77	5.89	1.85	0.85
6.22	16.69	16.65	2.82	3.87
2.89	10.20	4.45	2.37	1.48
1.90	37.26	21.19	10.46	6.61
1.65	14.52	5.10	2.10	1.09
1.24	18.09	5.14	2.50	1.01
1.05	22.58	13.29	3.75	2.85
0.81	4.92	0.87	0.86	0.29
0.47	4.86	2.80	0.51	0.68

Appendix III.41. STD_NMR assay titration for KD determination between PonA1$_{234-820}$_P631S and rifampicin.

[lig](mM)	STD-AFmax	dSTD-AFmax	ksat(s-1)	dksat(s-1)	STD-AF0	dSTD-AF0
0.063	0.23	0.01	3.02	1.10	0.69	0.21
0.125	0.42	0.02	2.27	0.52	0.96	0.14
0.250	0.73	0.03	2.25	0.48	1.65	0.13
0.500	1.26	0.02	2.28	0.22	2.87	0.06
1.000	2.27	0.08	2.37	0.39	5.38	0.10
2.000	4.37	0.23	2.22	0.55	9.70	0.15

Pic(ppm)	Alpha_STD	dAlpha_STD	Kd(mM)	dKd(mM)
6.80	15.86	6.69	1.46	1.13
2.89	7443.55	3715269.90	1980.16	989204.35
1.90	7426.05	2503722.10	1967.66	663982.85
1.65	40.67	25.05	6.42	4.92
1.24	16.41	4.28	2.21	0.93
1.05	24.83	3.51	4.54	0.86
0.81	7.86	2.16	1.54	0.76
0.46	24.65	75.19	6.07	23.31

Additional Research contributions

This section presents extra contributions to papers during my PhD that fall outside the main manuscript's scope.

2020 *Mycobacterium tuberculosis* ribosomal protein S1 (RpsA) and variants with truncated C-terminal end show absence of interaction with pyrazinoic acid. **Katherine Vallejos-Sánchez** , Juan M Lopez, Ricardo Antiparra , Emily Toscano , Harry Saavedra , Daniela E Kirwan , L M Amzel , R H Gilman , Helena Maruenda, Patricia Sheen , Mirko Zimic. . Sci Rep. 2020 May 20;10(1):8356. doi: 10.1038/s41598-020-65173-z.

2020 Immunological detection of pyrazine-2-carboxylic acid for the detection of pyrazinamide resistance in Mycobacterium tuberculosis. Edgar A. Florentini, Noelia Angulo, Robert H. Gilman, Roberto Alcántara, Elisa Roncal, Ricardo Antiparra, Emily Toscano, **Katherine Vallejos**, Danni Kirwan, Mirko Zimic, Patricia Sheen. PLoS ONE 15(11): e0241600. https://doi.org/10.1371/journal.pone.0241600.

2021 Development and pre-clinical evaluation of NewCastle disease virus-vectored SARS-CoV-2 intranasal vaccine candidate. Manolo Fernandez Díaz, Ricardo Choque-Guevara, Katherine Calderon1, Aldo Rojas-Neyra1, Vikram N. Vakharia3, Andres AgurtoArteaga, Angela Montalvan, Astrid Poma-Acevedo, Dora Rios-Matos, Luis TatajeLavanda, María de Grecia Cauti-Mendoza, Norma Perez-Martinez, Gisela Isasi-Rivas,Manuel Criollo-Orozco, Miryam Palomino, Henri Bailón, Yacory Sernaque-Aguilar, Freddy Ygnacio-Aguirre, Doris VillanuevaPérez, Edison Huaccachi-Gonzalez, Elmer Delgado-Ccancce, Ricardo Montesinos-Millan, Kristel Gutiérrez-Manchay, Katherine Pauyac-Antezana, Ingrid Ramirez-Ortiz, Stefany Quiñones-Garcia, Yudith Cauna-Orocollo, **Katherine Vallejos-Sánchez**, Julio Ticona, Angela A. Rios-Angulo, Dennis Núñez-Fernández, Mario I. Salguedo-Bohorquez, Mirko Zimic, Manolo Fernández Sánchez, Paquita García, Eliana Icochea, Luis Guevara, for the COVID-19 Working Group in Perú. BioRxiv preprint doi: https://doi.org/10.1101/2021.03.07.434276; this version posted March 8, 2021.

2021 Comprehensive virtual screening of 4.8k flavonoids reveals novel insights in allosteric inhibition of SARS-CoV-2 Mpro. Gabriel Jiménez-Avalos, A. Paula Vargas- Ruiz, Nicolás E. Delgado-Pease, Gustavo E. Olivos-Ramirez, Patricia Sheen, Manolo Fernández-Díaz, Miguel Quiliano, Mirko Zimic & **COVID-19 Working Group in Perú**. Scientific Reports, (2021) 11:15452. https://doi.org/10.1038/s41598-021-94951-6

2021 A recombinant SARS-CoV-2 RBD antigen expressed in insect cells elicits immunogenicity and confirms safety in animal models. Ricardo Choque-Guevara, Astrid Poma-Acevedo,Ricardo Montesinos-Millán, Dora Rios-Matos, Kristel Gutiérrez-Manchay, Angela Montalvan, Stefany Quiñones-Garcia, Maria de Grecia Cauti-Mendoza, Andres Agurto-Arteaga, Ingrid Ramirez-Ortiz, Manuel Criollo-Orozco, Edison Huaccachi-Gonzales, Yomara K. Romero Lázaro, Norma Perez-Martinez,Gisela Isasi-Rivas, Yacory Sernaque-Aguilar, Doris Villanueva-Pérez, **Katherine Vallejos-Sánchez**, Manolo Fernández-Sánchez, Luis Guevara, Manolo Fernández-Díaz, MirkoZimic, for the COVID-19 Working Group in Perú. https://doi.org/10.1101/2021.11.26.470043doi:bioRxiv preprint.

2022 Squalene in oil-based adjuvant improves the immunogenicity of SARS-CoV-2 RBD and confirms safety in animal models. Ricardo Choque-Guevara1, Astrid Poma-AcevedoID1, Ricardo Montesinos-Milla´ n1,Dora Rios-Matos1, Kristel Gutie´ rrez-Manchay1, Angela Montalvan-Avalos1,Stefany Quiñones-Garcia1,2, Maria de Grecia Cauti-Mendoza1,2, Andres Agurto-ArteagaID1, Ingrid Ramirez-Ortiz1, Manuel Criollo-Orozco1, Edison Huaccachi-Gonzales1,Yomara K. Romero2, Norma Perez-Martinez1, Gisela Isasi-Rivas1, Yacory Sernaque-Aguilar1, Doris Villanueva-Pe´ rez1, Freddy Ygnacio1, **Katherine Vallejos-SanchezID2**,Manolo Fernandez-Sanchez1, Luis A. Guevara-Sarmiento1, Manolo Ferna´ ndez-Dı´az1,Mirko ZimicID1,2*, for the COVID-19 Working Group in Peru. PloS ONE 17(8) :e0269823.

2023 Quantitative 1H nuclear magnetic resonance assay for the rapid detection of pyrazinamide resistance in Mycobacterium tuberculosis from sputum samples. Juan M Lopez, Mirko Zimic, **Katherine Vallejos**, Diego Sevilla, Mariella Quispe-Carbajal, Elisa Roncal, Joseline Rodriguez, Jhojailith Rodriguez, Ricardo Antiparra, Hector Arteaga, Robert H Gilman, Helena Maruenda and Patricia Sheen. Journal of clinical microbiology. Volume 61. https://doi.org/10.1128/jcm.01522-22.

2023 Identification of virulence factors and antibiotic resistance in Salmonella enterica subsp. enterica serovar Javiana (FARPER-220) isolated from broiler chickens. Luis Tataje-Lavanda , Doris Villanueva-Pérez 9, Angela Montalván-Avalos, **Katherine Vallejos-Sánchez** , Mirko Zimic-Peralta, Manolo Fernández-Sánchez, Manolo Fernández-Díaz https://journals.asm.org/doi/10.1128/mra.00327-23